A BIOANALYTICAL APPROACH TO FORENSIC BODY FLUID IDENTIFICATION & AGE DETERMINATION

Charlotte-Maria Ruth Orphanou

A thesis submitted in partial fulfilment of the requirement of Staffordshire University for the degree of Doctor of Philosophy in the subject of Forensic & Crime Science

July 2015

Non est ad astra mollis e terris via

ABSTRACT

Human blood, saliva, semen and vaginal secretions are the main body fluids encountered at crime scenes. In the "Live-Time" era of forensic science it has become evident that the current challenge in the examination of body fluids is that non-destructive screening methods of greater specificity are required for body fluid identification compared to the presumptive tests currently utilised. Further to this, a method suitable for routine application is strongly sought after to determine the age of body fluid stains as it could enable police forces to make informed decisions regarding the relevance of forensic biological evidence recovered from crime scenes. The focus of this research was to investigate the use of analytical techniques (ATR-FTIR spectroscopy and protein analyses; SDS-PAGE and the Bradford assay) in the application of robust confirmatory body fluid identification and age determination. The findings of this research demonstrated that human blood, saliva, semen and vaginal secretions could successfully be detected and differentiated from one another when analysed with ATR-FTIR spectroscopy, based on the unique spectral pattern and combination of peaks corresponding to macromolecule groups, and SDS-PAGE, based on separation patterns of various proteins within each of the body fluids. Direct ATR-FTIR spectroscopic examination of blood and vaginal secretion stains enabled successful detection and identification in stains aged up to 18 months and 6 months, respectively. In contrast, stains of saliva and semen aged up to 18 months and 9 months, respectively, could not be detected when directly analysed. However, when the stains were extracted with a simple water-based method, all four body fluids could be detected. Age determination analysis with ATR FTIR spectroscopy demonstrated that peak intensities and ratios were not appropriate variables to discriminate between body fluids stains and extracts. Successful detection of extracted blood, semen and vaginal secretion stains aged up to 7 days was also achieved with SDS-PAGE, although saliva stains were not detected when extracted. The age of extracted samples appeared to have no impact on the detection of the proteins. Furthermore, comparison of average total protein yield obtained with the Bradford assay from aged extracted body fluid stains demonstrated no correlation with protein concentration and sample age for any of the body fluids examined. Overall, this research has demonstrated the successful application of both ATR-FTIR spectroscopy and SDS-PAGE for the identification of human body fluids. ATR-FTIR spectroscopy in particular has reproducibly demonstrated detection and identification of body fluids, which has great potential to be utilised in the routine screening of biological evidence due to its quick and robust application within forensic science.

ACKNOWLEDGEMENTS

I would sincerely like to thank the following people for their help and support during the research and production of this thesis.

Firstly, I would like to thank my supervisors; Laura Walton-Williams and Harry Mountain, and my project advisor; John Cassella. The last four years have been a very interesting journey, there have been up's and down's but you have always provided me with the support and encouragement to give me the confidence to see this through to the end. Without you this would not have been possible and I can't thank you enough.

Many thanks go to Dr. Alan Harper at Keele University's Institute of Science and Technology for Medicine for allowing me to store my samples at their premises under their Human Tissue Licence. Without access to licenced storage this research wouldn't have been able to go ahead.

My sincerest gratitude is extended to the Chartered Society of Forensic Sciences (formerly the Forensic Science Society) for awarding me the Research Scholarship in 2011 and 2012. This funding has been invaluable, allowing me to develop my research and attend conferences to promote my work. This gratitude is also extended to the Royal Masonic Trust for Girls and Boys who have awarded me funding to support my living costs during part of my PhD and enable me develop as a person both in and outside of my studies.

Many thanks also go to all the academic and technical staff of the School of Sciences at Staffordshire University who have offered me guidance and support during this PhD journey. All of your expertise has contributed to this thesis and for that I am so very grateful.

Lastly, but by no means least, I would like to thank my dear family, friends and Adam for always being there, being patient with me (particularly during the writing stage) and being my cheerleaders. Your love and support has played the biggest part in this journey and I hope I've made you proud.

TABLE OF CONTENTS

LIST OF EQUATIONS

LIST OF FIGURES

LIST OF TABLES

1. INTRODUCTION

The National Crime Survey reported that over 1.3 million violent and sexual offences were recorded in 2013/14 (Great Britain, Office of National Statistics, 2014). It would not be uncommon for human body fluids to be encountered at these types of crime scenes. The most frequently encountered body fluids at scenes of crime are blood, saliva, semen and vaginal secretions and these body fluids can play an important role within criminal investigations. The presence of these body fluids has significant forensic value as the identity of the person who deposited the body fluid can be determined with the use of deoxyribonucleic acid (DNA) profiling. DNA profiling has had a profound impact on the investigation of crime, allowing individuals of interest to be questioned, or potentially be eliminated as a suspect. However, a limitation of DNA profiling is that it cannot determine the source of the body fluid, or when it was deposited at a crime scene.

When considering DNA profiling as part of a criminal investigation, the source of the DNA can be as relevant to the context of the crime as the DNA profile itself. However, some sources of DNA encountered at crime scenes may not be as obvious as others, especially when body fluid stains are present. Due to the variability in the visual appearance of body fluids some sources may not be easily identified. Blood has a characteristic red colour that can easily be distinguished from other key body fluids. However, saliva, semen, and vaginal secretions can be much more difficult to see due to their creamy-white, or colourless appearance. An important aspect to consider is that stains present at a crime scene may appear similar in likeness to body fluid stains, but in fact be a stain from a non-biological source. To address this issue, the application of presumptive tests allows investigators to test suspect stains and fluids to detect the presence of particular body fluids (Virkler & Lednev, 2009a). When presumptive tests have been carried out, the potential source of the body fluid is indicated and this can provide context that may or may not be relevant to the crime. However, presumptive tests are not confirmatory and often subject to false positive or negative results. Therefore, a more robust and definitive identification method of body fluids would provide confidence in stating the DNA source of biological evidence.

Knowing when a body fluid stain was deposited can add more value to evidence than merely being able to detect the presence of body fluids alone. The ability to determine the age of body fluids is of great significance, especially in an era where “live-time” forensics is in high demand (Great Britain, Association of Chief Police Officers. 2013). Police forces want to be

able to determine "Who? What? When? Where? and How?" quickly and efficiently when investigating crime. The potential to determine the time since deposition, or age, of body fluid stains could provide a chronological order of events, which in turn will allow evidence analysis prioritisation. Age determination of body fluids could place individuals at the crime scene at identifiable points of time, which is an advantage for investigating police officers. This could provide intelligence information which highlights people of interest, as well as eliminate people who are not of relevance to the case, or potentially link offender groups and crime scenes. In addition to these benefits, determining the age of body fluids could support or refute a suspect's alibi. Within the investigation of crime it is not unusual for suspects to be dishonest about why their body fluids were found at a crime scene. Age determination of body fluids has the potential to establish whether a body fluid stain is the same age as the crime, or whether it was deposited before or after the crime took place.

1.1 BODY FLUID COMPOSITION

Body fluids comprise of biological and chemical components that can be analysed to provide information at varying levels of identification. There are various types of analysis that can be applied to blood, saliva, semen and vaginal secretions. However, from a forensic perspective the main analyses are presumptive testing, which indicate the presence of particular body fluids (Jackson & Jackson, 2008) and DNA profiling, which confirms the identity of the individual who deposited the body fluid (Bremmer et al. 2012). In order to apply appropriate analysis techniques, the composition of the key body fluids need to be understood.

1.1.1 BLOOD

The average volume of blood within the human body is approximately 5 litres (Pallister, 1994). The composition of blood is both fluid and cellular. Plasma accounts for around 55% of total blood volume and is an electrolytic, yellow fluid that suspends the cellular material. Within the plasma a variety of proteins are abundant which aid in the haemostasis of blood as a whole (Moore et al. 2010). The main plasma proteins are fibrinogen, albumin and transferrin. Fibrinogen is a substrate involved in the coagulation of blood (Krebs, 1950). Its role lies in the stopping of blood flow at points of injury. Fibrinogen works alongside proteins

such as thrombin and tissue factor, to convert to fibrin which clots at injury sites (Gray et al. 2012). Albumin and transferrin belong to the transport protein family and play roles independent of each other. Albumin has a significant role in maintaining the homeostasis of osmotic pressure within the blood vessels (Hankins, 2006) as well as facilitating a non-specific role in nutrient and waste transport within blood. Transferrin has a more specific transport role as it is a high affinity to bind to iron (Moore et al. 2010; Pallister, 1994). Particularly, transferrin binds to iron in its ferric state (Fe^{+3}) and transports it directly into bone marrow to ensure that iron levels in the blood are non-toxic (Chung, 1984). Other plasma proteins to note are the immunoglobulin's (Ig) A, D, E, G and M. These are antibodies that are produced in specific response to foreign antigens within the blood system (Knight, 2013).

The remaining approximate 45% of blood comprises of a range of cells, namely red blood cells, white blood cells and platelets (Li, 2008). Each of these cellular components play differing roles within blood. Red blood cells (RBC's), also termed erythrocytes, are the most abundant cell within the cellular make up and their primary function lies in the delivery of oxygen to tissues within the body from the lungs (Pallister, 1994). The discoid and biconcave shape of RBC's is complimentary to its primary function as it allows the cells to be flexible and travel through the smallest of capillaries within the body. This flexibility is in part due to the RBC's not containing a nucleus, which accommodates the high saturation of an oxygen binding protein called haemoglobin (Hb) within the RBC (Figure 1.1). Haemoglobin is a red pigmented globular protein which gives blood its characteristic colour. It comprises of four globin chains, two alpha (α) and two beta (β), each of which have a haem group attached and there is thought to be approximately 640 million molecules of haemoglobin per RBC (Moore et al. 2010; Pallister, 1994).

White blood cells (WBC's), also called leukocytes, can be categorised into five types; basophils, eosinophils, neutrophils, monocytes and lymphocytes. All WBC's contain a nucleus and have roles within the immune system (Moore et al. 2010). The neutrophils, eosinophils and basophils all contain granules within their cytoplasm and therefore are classed as granulocytes. Granulocytes tend to have irregular shaped nuclei and vary in granule morphology. Basophils cytoplasmic granules are large, these WBC's are vital in responding to anaphylactic, inflammatory and hyper-sensitivity reactions. Eosinophil can also be characterised by large granules present within the cytoplasm, although these WBC's tackle parasitic infection and act to reduce allergic reactions. In contrast, neutrophils' cytoplasm contains granules that appear fine and their function lies in bacterial and fungal infection defence (Pallister, 1994). It is the variation of the granules within the granulocytes that

enables differentiation between the basophils, eosinophils and neutrophils at a microscopic level (Pallister, 1994), demonstrated in Figure 1.2 (a-c).

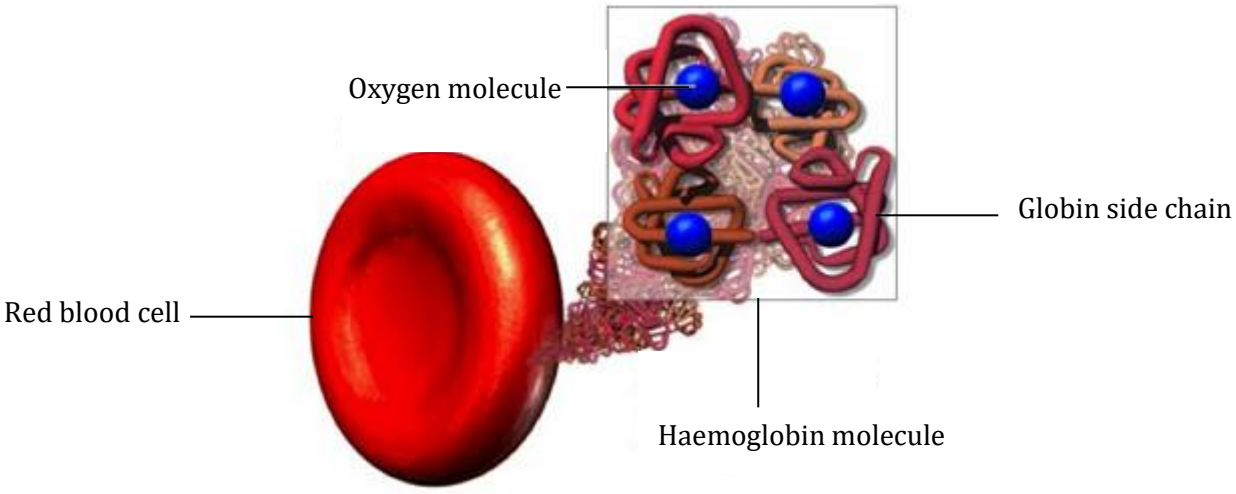

Figure 1.1: Example of haemoglobin protein structure within a red blood cell (University of Malta, 2010).

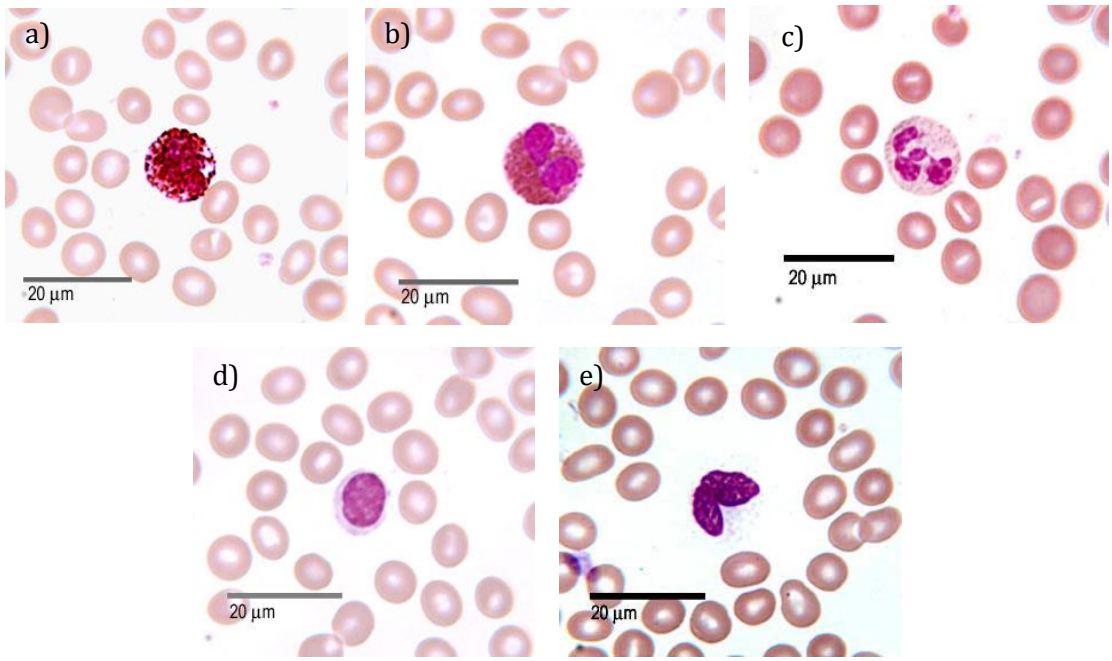

Figure 1.2: The white blood cells; a) basophil, b) eosinophil, c) neutrophil, d) lymphocyte & e) monocyte (University of Leeds, 2013).

The two other WBC types are lymphocytes and monocytes (Figure 1.2d & e) and these are classed as mononuclear leukocytes due the cells containing a single nucleus and the general absence of cytoplasmic granules (Moore et al. 2010). Lymphocytes are the most abundant of

the mononuclear leukocytes and are distinguishable by their small size and nucleus that fills almost the whole of the cell. There are a variety of lymphocytes, each with specific roles in the defence of immunity. Monocytes, on the other hand, are large WBC's that contain smaller, kidney shaped nuclei and are involved in the processing and removal of aged RBC's and other cellular debris within the blood stream (Pallister, 1994). Further information on the functions of any of the WBC's can be found in Moore et al. (2010) and Pallister (1994).

The final cellular component of whole blood is platelets, or thrombocytes, which are small discs present in the highest abundance of the all the cellular components. Platelets do not contain a nucleus, but instead contain many granules which are essential in the platelets role of haemostasis, which is the ceasing of bleeding. To maintain haemostasis, platelets aggregate to form a plug at injury sites preventing blood loss, whilst ensuring the fluidity of the blood as a whole (Moore et al. 2010).

1.1.2 SALIVA

Saliva is a water based fluid comprised of bacteria and the secretions of the major and minor salivary glands and gingival crevicular fluid within the mouth. The major salivary glands are made up of the sublingual, submandibular and parotid which are found in the floor of the mouth. Whereas, the minor salivary glands are located at various positions within the mouth including the lower lip and pharynx (Humphrey & Williamson, 2001). The average human saliva production is 1-1.5 litres per day and can be categorised into unstimulated and stimulated saliva. Unstimulated, or continuous saliva, is the natural constant flow of saliva when the mouth is at rest. Stimulated saliva is produced in response to stimuli, such as food, and accounts for approximately 80-90% of saliva production (Schenkels et al. 1995).

The composition of saliva is a complex mixture of proteins and electrolytes within water, with water accounting for 99% of the body fluid (de Almeida et al. 2008). The remaining 1% of saliva has five main components; electrolytes, immunoglobulins, proteins, enzymes and nitrogenous products. These components all play roles within the maintenance of a healthy oral mucosa and vary in the quantity present at any one time. The electrolytes present within saliva include sodium, potassium, calcium, and magnesium and each electrolyte has different functions. For example, bicarbonates and phosphates aid the nitrogenous product urea in maintaining salivary pH levels and buffering, whereas calcium acts as a lubricant to protect the teeth from wear (Humphrey & Williamson, 2001).

Proteins present within saliva come in many forms, including immunoglobulins, enzymes, mucins and glycoproteins, which have diverse functions. These include antibacterial protection, as well as controlling regulations of specific processes involved in the protection of the teeth. Some of the most abundant proteins are lysozyme, α-amylase, proline-rich proteins and histatins, amongst others (de Almeida, et al. 2008; Schenkels et al. 1995). The immunoglobulins present in saliva are secretory IgA, IgG and IgM. Secretory IgA is the most abundant of the immunoglobulins and is predominant in maintaining oral immunity from bacteria, viruses and acting as an antibody for bacterial antigens. Mucins are key in supporting the immunoglobulins in oral bacterial defence, and alongside this provide the greatest lubrication component for the mouth (Humphrey & Williamson, 2001).

1.1.3 SEMEN

The average semen ejaculate of a healthy male is between 2-5 ml in volume (Owen & Katz, 2005). Semen is a complex fluid and cellular mixture produced by a variety of different glands within the male reproductive organs (Li, 2008; Owen & Katz, 2005). The cellular part of semen comprises predominately of one cell type, spermatozoa (Figure 1.3). Spermatozoa, or sperm, are the reproductive cells that carry the genetic material vital for sexual reproduction. The structure of spermatozoa is quite basic and can be defined into three key regions; the head, which contains the chromosome packed nucleus and an acrosomal cap containing enzymes vital for fertilisation, the midpiece, or body, which consists mostly of mitochondria that provide the necessary energy for motility, and the tail, or flagellum, which enables the sperm to move (Li, 2008; Strachan & Read, 2011).

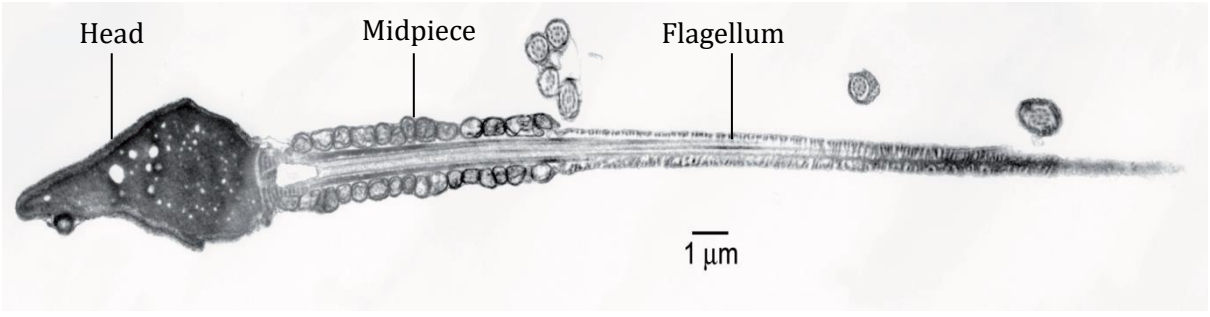

Figure 1.3: Human sperm cell (Barratt et al. 2009).

The fluid part of semen, known as seminal fluid, is more complex and is not considered as homogeneous upon initial ejaculation (Owen & Katz, 2005). Its main function is to provide a protective and nutrient rich environment for spermatozoa after ejaculation (Huang et al.

2011) and the content is indicative of the male reproductive glands function (Edwards et al. 1981). A variety of glandular secretions contribute to the protein-rich seminal fluid in differing volumes. It is thought that 5% of seminal fluid originates from the bulbourethral (Cowper's) gland which is the main source of mucin, one of a few highly abundant proteins present in seminal fluid (Pilch & Mann, 2006).

Approximately 15-30% of seminal fluid originates from the prostate which contains the highly abundant proteins acid phosphatase, prostate-specific antigen and albumin. Acid phosphatase (AP) is predominantly produced by the prostate and is a key protein within semen as it is optimised to withstand acidic environments, such as the vagina (Li, 2008). Prostate-specific antigen (PSA) is specifically a product of the epithelia within the prostate and its function lies in the liquefaction of whole semen post ejaculation by hydrolysing semenogelin, a coagulation protein (Li, 2008). Albumin is a water soluble protein that is also found in blood, but the concentrations of albumin in seminal fluid are much higher, with approximately one third of the seminal fluid protein content being albumin (Owen & Katz, 2005). Its main role within seminal fluid is to filter out cholesterol from spermatozoa membranes (Pilch & Mann, 2006). Other components of prostate seminal fluid include proteases involved in the liquefaction of whole semen, citric acid, calcium, and magnesium (Owen & Katz, 2005; World Health Organisation, 2010).

Of the remaining 75-80% of seminal fluid, 5% is produced from a collection of glands, including the epididymis and testis, and contributes a predominately sperm-rich fluid (Eliasson, 1965). The highest contribution of seminal fluid comes from the seminal vesicles, which produce approximately 60-75% of total seminal fluid and is where the majority of the proteins found in semen are derived from (Li, 2008; Owen & Katz, 2005). The seminal vesicles are responsible for the coagulation factors and high fructose concentration that occur upon the ejaculation of semen. The fructose within seminal fluid originates specifically from the seminal vesicles and is necessary as a source of energy to the spermatozoa, with an average concentration of 272 mg/100 ml. In addition to fructose, glucose also provides an energy source for spermatozoa and can be found at lower concentrations of 102 mg/100 ml (Owen & Katz, 2005). The coagulation factors of whole semen are a product of the seminal vesicles, whereby upon ejaculation semen forms into a gelatinous substance to trap the spermatozoa. In vivo, the gelatinous substance liquefies within 5 minutes, although in vitro this liquefaction can take up to 30 minutes to complete (World Health Organisation, 2010). The proteins involved in the coagulation of semen include fibronectin and semenogelin I and II (Pilch & Mann, 2006). Other proteins found in seminal fluid produced by the seminal

vesicles are lactoferrin, ascorbic acid and flavin (Li, 2008; Owen & Katz, 2005; Pilch & Mann, 2006).

1.1.4 VAGINAL SECRETIONS

Vaginal secretions are often termed as mucus, fluid or discharge and are a white/cream, highly viscous fluid produced from cervical and vaginal glands, such as the Bartholin's glands (Marques et al. 2011). It is thought that the average quantity of vaginal secretions produced per day is approximately 6 g, with 0.5-0.75 g present in the vagina at any one point, and the viscosity of vaginal secretions varies during the menstrual cycle due to changes in hormone levels (Chiriboga et al. 1998b; Shaw et al. 2007). In a dry state, vaginal secretions are heterogeneous in composition (Sikirzhytskaya et al. 2012).

The primary function of vaginal secretions is to protect against infection as the genitals of females are often susceptible to microbial and bacterial pathogens. To prevent infection, the vaginal secretions contain antibacterial/microbial properties in the form of proteins. There are various proteins involved in vaginal defence against microbes and viruses, some of which include secretory IgA and IgG, lysozyme, defensin, acid phosphatase and amylase (Marques et al. 2011; Shaw et al. 2007; Virkler & Lednev, 2009a; Zegels et al. 2009).

In addition to proteins, components such as shed epithelial cells, blood cells, urea and transudate from plasma and vaginal mucosa are present in whole vaginal secretions (Chiriboga et al. 1998a; Sikirzhytskaya et al. 2012; Virkler & Lednev, 2009a; Zegels et al. 2009). Glycogenated squamous epithelial cells are an abundant component of vaginal secretions. These are the sloughed, or shed, cells from the lining of the cervix which do not contain a nucleus. However, they do contain large amounts of glycogen, the concentration of which varies dependent upon the menstrual cycle (Chiriboga et al. 1998b). These cells are a main component of vaginal secretions due to the constant regeneration of epithelial cells within the cervix. Figure 1.4 demonstrates this regeneration process, which has a clear structure of many different layers of epithelial cells. The different layers represent the level of maturity the epithelial cells have reached. At the bottom of this structure lie the parent cells that are constantly and rapidly dividing to produce new, daughter, epithelial cells. These daughter epithelia are found in the parabasal cell layer of the cervix wall and are still in a state of growth and development. This results in the production of more daughter cells. As the daughter cells mature, the concentration of glucose present in the cells increases and they begin to migrate towards the cervix surface, into the intermediate layer. The cells become

differentiated from their parent parabasal cells during maturation and when full maturity is reached they migrate into the superficial layer on the cervix surface (Chiriboga et al. 1998b). Here, the cells are highly glycogenated and contain large amounts of cytoplasm in comparison to their parent cells in the basal layer of epithelia. As these cells are exposed on the surface of the cervix, they are vulnerable to pathogens. This regeneration system prevents the epithelia in the superficial layer from dividing, allowing them to provide a protective barrier to the younger cells. Within a short time period, usually a few days, the superficial cells die and slough off from the cervix wall into the vaginal secretions, resulting in the high abundance of epithelial cells within the fluid (Chiriboga et al. 1998b).

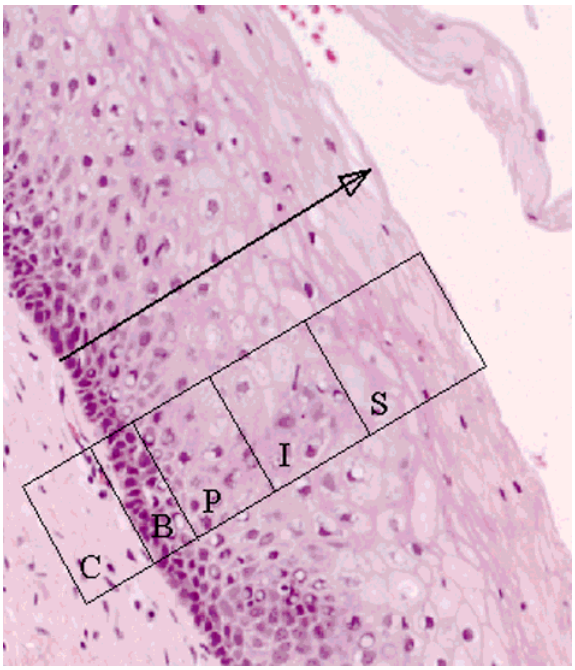

Figure 1.4: Tissue section of normal human cervical epithelium demonstrating the different layers of epithelial cells within the cervix: "C" connective tissue (stroma) layer, "B" basal cell layer, "P" parapbasal cell layer, "I" intermediate layer and "S" superficial layer. The arrow indicates the direction of cell maturation (Chiriboga et al. 1998b).

Some of the protein components within vaginal secretions are common amongst other body fluids, as can be seen in the earlier discussed body fluid compositions; namely, lysozyme, which is present in semen and saliva; amylase, which is present in saliva in much higher concentrations; albumin and immunoglobulins IgA and IgG, which are also found in blood, saliva, and semen. Additionally, acid phosphatase, predominantly found in semen and is commonly used as an indicator for the presence of semen. However, the relative quantities of vaginal acid phosphatase are much lower than those found in semen (Al-Garawi et al. 2012). The remaining key components of vaginal secretions are urea and acetic, citric and lactic acids (Virkler & Lednev, 2009a).

1.2 FORENSIC BODY FLUID IDENTIFICATION

When fluids and stains are encountered at crime scenes, the initial analysis of the potential evidence is to determine whether the fluid or stain is of biological origin. Once this has been presumptively indicated, evidential samples thought to contain biological material are then sent for further analysis on a priority basis. The ability to confirm the origin of a body fluid and determine the time since deposition has been a long sought after process within the forensic and criminal investigation community. Blood, saliva, semen and vaginal secretions are often key pieces of evidence at crime scenes involving violence and sexual motives. There has been and still is, a demand for more sensitive, specific, and non-destructive methods of body fluid identification and age determination (Association of Chief Police Officers, 2013). This demand has been ever increasing in the last decade, although research has been ongoing since the 1990's (Inoue et al. 1992).

Body fluid identification is well established within the investigation of crime and an array of presumptive and confirmatory tests have been used for many years to indicate or identify evidence that contains biological material. Such tests include Kastle-Meyer (KM) and ABAcard® Hematrace® for blood (Tobe et al. 2007), Phadebas® Forensic Press test for saliva (Hedman et al. 2008) and AP and PSA, or p30, or the detection of semen (Hochmeister et al. 1999; Raju & Iyengar, 1964). To date, there is no presumptive or confirmatory test routinely utilised in vaginal secretion detection. However, as time and technology has progressed there has been little development of traditional methods and as crime and criminals are becoming more intelligent, the techniques employed to identify body fluids need to become more sophisticated. Within the last decade a surge of research has been reported looking at new, innovative techniques to definitively identify body fluids. These techniques focus primarily on genetics (Haas et al. 2008; Wang et al. 2013), proteins (Yang et al. 2013) and spectroscopy (Virkler & Lednev 2008).

1.2.1 BIOLOGICAL APPROACHES

1.2.1.1 DNA

DNA profiling has revolutionised criminal investigations since its development in 1985 by Sir Alec Jeffreys, as the identity of the individual, or individuals, who deposited body fluids or

other biological material at crime scenes can be determined (Butler, 2010). However, that is the limit of its application within forensic investigation. DNA profiling can only identify the donor, it cannot provide confirmation of the source of the DNA, such as tissue or fluid, nor when it was deposited. Yet, the exploration of epigenetics, which is the study of heritable changes in gene expression not caused by differences in DNA sequence (Strachan & Read, 2011), has led to an alternative approach to forensic body fluid identification. In particular, research into DNA methylation assays has been recently documented. DNA methylation is the addition of methyl (CH_3) to the C5 position of cytosine in regions containing a cytosine nucleotide next to a guanine nucleotide. This is often referred to as a CpG dinucleotide (Strachan & Read, 2011). It is believed that DNA methylation prevents gene expression and that different tissues exhibit different methylation patterns (Frumkin et al. 2011). It is the methylation patterns of forensically relevant tissues that have been investigated as a means to provide definitive sample identification.

Frumkin et al. (2011) first reported this approach, whereby samples of blood, menstrual blood, saliva, semen, skin, urine and vaginal secretions were analysed. All samples underwent standard DNA analysis (extraction, quantification, PCR amplification and capillary electrophoresis (Butler, 2010)), with the addition of a *HhaI* endonuclease digestion after DNA quantification. *HhaI* digestion cleaves DNA at the recognition sequence of GCGC in unmethylated DNA (Frumkin et al. 2011). The addition of this step enabled the identification of appropriate loci that exhibit differential methylation patterns within the body fluids. A panel of 15 loci were selected and analysed on a total of 50 body fluid samples and the obtained methylation levels were calculated as quantifiable ratios to produce a likelihood score. The results demonstrated that each body fluid type had distinct methylation patterns and all 50 samples were correctly identified. Frumkin et al. (2011) further reported a semen detection assay that could be integrated into standard DNA profiling. Two specific loci were included within the PCR element of analysis, one of which would be successfully amplified if semen was present, the other would not. The results demonstrated that the integrated semen identification assay could successfully differentiate between semen and non-semen samples. Ma et al. (2013) followed on the investigation into DNA methylation as a method to identification body fluids with a similar method to Frumkin et al. (2011). Samples of blood, saliva, semen and vaginal secretions were analysed and Ma et al. (2013) reported that the methylation patterns observed within blood samples and other body fluids samples were obviously different. Six tissue specific differentially methylated regions were identified as blood specific, although no tissue specific differentially methylated regions could be identified for any of the other body fluids tested (Ma et al. 2013).

Wasserstrom et al. (2013) further developed the method utilised by Frumkin et al. (2011) to produce a semen identification assay kit that can be integrated fully into DNA analysis and look to replace semen detection using standard microscopy. Routine methods were carried out, including the *HhaI* digestion and a total of eight loci were incorporated to identify semen. Three of those loci acted as controls to ensure that PCR amplification and *HhaI* digestion were successful. The remaining five loci (L3-7) were differentially methylated regions that were identified as expressing unique patterns within semen and non-semen samples (Wasserstrom et al. 2013). L3 and L4 were expected to exhibit low or absent peaks in semen, but high peaks in non-semen samples, whereas L5-7 exhibited high peaks in semen and low peaks in non-semen samples. Software data analysis of the detected methylated DNA was developed into a program that only produced an output if PCR and digestion were successful and if semen or non-semen could be identified. If any of these criteria were not met, the analysis was aborted and no output was obtained (Wasserstrom et al. 2013). To test the validity of the semen identification assay, 33 casework samples obtained from sexual assault investigations were blind tested. Half of each sample was analysed by the research group, the other half were analysed microscopically by the local authority. Full concordance between the assay and microscopy results was observed, whereby 5 of the 33 samples were identified as semen, 21 as non-semen and 7 were aborted (Wasserstrom et al. 2013). These results were significant as it demonstrated that the semen identification assay of methylated DNA could successfully be utilised within forensic casework.

The benefits of DNA methylation as a method of forensic body fluid identification are evident in the research conducted by Frumkin et al. (2011), Ma et al. (2013) and Wasserstrom et al. (2013). Firstly, integration into standard DNA protocols utilised within forensic investigation has been successful. This means that no expensive reagents, equipment or specialist training is required to conduct DNA methylation analysis. This is highly advantageous as it opens up new avenues of potential analysis to investigating police officers that are not costly or time consuming, but in fact are complimentary and simultaneous. Additionally, Frumkin et al. (2011), Ma et al. (2013) and Wasserstrom et al. (2013) have all demonstrated that the method requires little to no sample consumption as the input DNA required for DNA methylation assaying can be utilised directly from the DNA extract. Furthermore, DNA methylation has been demonstrated to identify differential methylation patterns than can distinguish between blood (Ma et al. 2013) and semen (Wasserstrom et al. 2013). However, DNA methylation has also demonstrated that loci with differential methylation patterns have not been established to enable the identification of other body fluids such as menstrual blood, saliva and vaginal secretions. As this is a relatively new forensic application, further research

is required to ensure the validity of the technique. Until tissue specific methylated DNA loci are determined for all key body fluids and these are found to have no overlap in differential methylation patterns, DNA methylation is not an appropriate tool to be utilised routinely in the identification of body fluids.

1.2.1.2 RNA

One of the first documented developments of a more sensitive, specific and definitive body fluid identification method was conducted by Juusola & Ballantyne (2003) who reported the exploration of messenger RNA (mRNA). Messenger RNA is a type of RNA that relays genetic coding from DNA molecules to ribosomal proteins for gene expression in a process known as transcription and translation (Juusola & Ballantyne, 2003). Specific genes can be expressed in specific tissues and not others which enables differentiation between body fluids and tissues. The process of RNA analysis involves up to six steps, demonstrated in Figure 1.5. Juusola & Ballantyne (2003) made use of tissue specific gene expression and developed a multiplex assay that could detect mRNAs that appeared as specific and/or abundant to blood, saliva and semen. Total RNA was successfully extracted from these body fluids and mRNA gene markers were established from the reverse transcription-polymerase chain reaction (RT-PCR). In particular, housekeeping genes glyceraldehyde 3-phosphate dehydrogenase (GAPDH), β-actin and S15 were all detected in blood, saliva and semen samples. To determine the sensitivity of the technique, differing volumes of input total RNA for the RT-PCR reaction were investigated and Juusola & Ballantyne (2003) stated that as little as 160 picograms (pg) of total RNA from a bloodstain could successfully detect S15.

To assess the utilisation of mRNA analysis for specific body fluid identification, mRNA markers for saliva were investigated as no confirmatory test for saliva is currently available (Juusola & Ballantyne, 2003). Five gene markers were selected that displayed restricted expression in salivary glands; statherin (STATH), histatin 3 (HTN3) and basic salivary proline-rich protein 1, 2, 3 (PRB1, PRB2, PRB3). These markers were successfully detected in saliva stains. To ensure specificity, blood and semen stains were also analysed with the salivary mRNA marker multiplex and no cross-reactivity was observed.

The results reported by Juusola & Ballantyne (2003) were perceived as the foundations to the development of genetic analysis within forensic science to definitively identify body fluids in parallel with routinely utilised DNA procedures. Many research groups have since built upon these methods to identify many more tissue specific mRNA markers that have successfully discriminated between single and mixed body fluid samples. These developments have been

incorporated into routine protocols so that simultaneous extraction and analysis of mRNA and DNA can be carried out on the same sample.

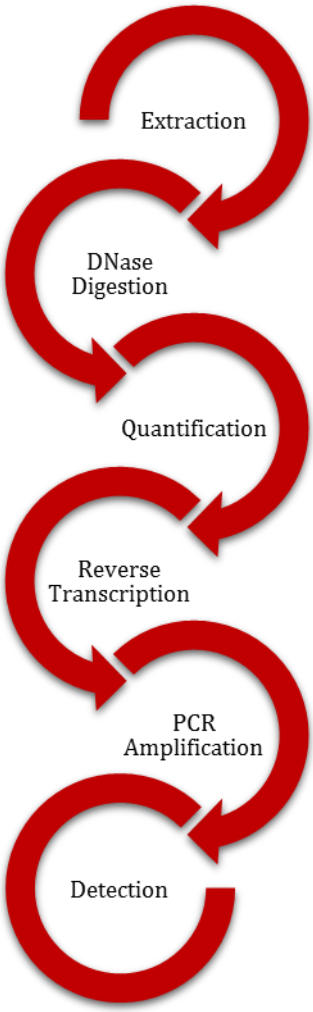

Figure 1.5: Overview of the steps involved in the analysis of RNA.

Table 1.1 and Table 1.2 contain a comprehensive list of the most frequently used mRNA markers within body fluid identification that have been published to date. The range of mRNA markers that have been identified as exhibiting specific and/or abundant expression within blood, menstrual blood, saliva, semen, skin and vaginal secretions is indicative of the sensitivity and specificity of the technique. On occasion, cross-reactivity has been observed in mRNA expression in non-target body fluids. Examples of this include detection of skin markers LOR and CDSN detection in menstrual blood and vaginal secretions (Van den Berge et al. 2014) and vaginal secretion marker MUC4 detection in saliva (Nussbaumer et al. 2006; Haas et al. 2009; Richard et al. 2012) and menstrual blood (Fang et al. 2006). However, often

the detection levels of mRNA marker expression in non-target tissues were lower than the tissue-specific markers present in comparison to expression in their respective target tissues.

Table 1.1: Gene markers utilised in the identification of housekeeping genes, menstrual blood & blood using mRNA analysis.

mRNA Gene Marker	Body Fluid Target	Description	Reference
18S rRNA	Housekeeping	Ubiquitously expressed ribosomal RNA (rRNA).	Haas et al. (2009); Lindenbergh et al. (2013); Nussbaumer et al. (2006); Sakurada et al. (2009); Van den Berge et al. (2014)
β-actin	Housekeeping	Ubiquitously expressed gene involved in cell growth and migration.	Juusola & Ballantyne (2003); Lindenbergh et al. (2013); Van den Berge et al. (2014)
Glyceraldehyde 3-phosphate dehydrogenase (GAPDH)	Housekeeping	Ubiquitously expressed gene involved in glycolysis and gluconeogenesis.	Haas et al. (2009); Juusola & Ballantyne (2003); Lindenbergh et al. (2013); Sakurada et al. (2009); Van den Berge et al. (2014)
Ubiquitin conjugating enzyme (UCE)	Housekeeping	Roles lies in ubiquitination, leading proteins to degradation.	Fleming & Harbison (2010); Haas et al. (2014)
Matrix metalloproteinase 7, 10, 11 (MMP7, MMP10, MMP11)	Menstrual blood	Involved in epithelia renewal during menstruation.	Fleming & Harbison (2010); Haas et al. (2008, 2009, 2014); Juusola & Ballantyne (2005); Lindenbergh et al. (2013); Richard et al. (2013); Van den Berge et al. (2014)
Adhesion molecule (AMICA1)	Blood	Inducer for adhesion to endothelial cells. Found in leukocytes.	Lindenbergh et al. (2013); Van den Berge et al. (2014); Zubakov et al. (2008)

Aminolevulinate synthase 2 (ALAS2)	Blood	Erythroid specific mitochondrial enzyme. First protein in the haem biosynthetic pathway.	Hass et al. (2011b, 2012); Richard et al. (2013)
Ankyrin 1	Blood	Erythrocyte membrane protein. Provides primary link between membrane skeleton and plasma membrane.	Fang et al. (2006); Haas et al. (2011b, 2012)
β-spectrin	Blood	Protein component unit of erythrocyte membrane.	Alverarez et al. (2004); Haas et al. (2008, 2009, 2011a, 2011b, 2012); Juusola & Ballantyne (2005);
CD3 gamma molecule (CD3G)	Blood	Role lies in coupling antigen recognition to several intracellular signal-transducing pathways. Part of T-cell receptor CD3 complex.	Hass et al. (2011b, 2012)
Gamma polypeptide (CD93)	Blood	Acts as mediator during phagocytosis. Expressed in leukocytes.	Lindenbergh et al. (2013); Sakurada et al. (2009); Van den Berge et al. (2014)
Glycophorin A (GlycoA)	Blood	Sialoglycoprotein of human erythrocyte membrane.	Fleming & Harbison (2010)
Haemoglobin α & β (HBA, HBB)	Blood	Subunits of haemoglobin molecules.	Haas et al. (2009, 2011a, 2011b, 2012); Nussbaumer et al. (2006); Park et al. (2013); Sakurada et al. (2009); Van den Berge et al. (2014)
Porphobilinogen deaminase (PBGD)	Blood	Third enzyme in haem biosynthesis pathway.	Haas et al. (2008, 2009, 2011a, 2011b, 2012); Juusola & Ballantyne (2005);

Table 1.2: Gene markers utilised in the identification of saliva, semen, skin & vaginal secretions using mRNA analysis.

mRNA Gene Marker	Body Fluid Target	Description	Reference
Basic salivary proline-rich protein 1, 2, 3 & 4. (PRB1, PRB2 & PRB3, PRB4)	Saliva	Defense against ingested polyhydroxylated phenols.	Fang et al. (2006); Juusola & Ballantyne (2003);
Histatin1 & 3 (HTN1, HTN3)	Saliva	Non-immune defense in oral cavity.	Alverarez et al. (2004); Fleming & Harbison (2010); Haas et al. (2008, 2009, 2013); Juusola & Ballantyne (2003); LIndenbergh et al. (2013); Park et al. (2013); Richard et al. (2013); Sakurada et al. (2009); Van den Berge et al. (2014)
Mucin 7 (MUC7)	Saliva	Glycoprotein facilitator of oral bacterial clearance and aids in chewing, swallowing and speech.	Haas et al. (2013)
Statherin (STATH)	Saliva	Inhibitor of calcium phosphate salt precipitation.	Fleming et al. (2010); Haas et al. (2008, 2009, 2013); Juusola & Ballantyne (2003, 2005); Richard et al. (2013); Sakurada et al. (2009); Van den Berge et al. (2014)
Prostate specific antigen (PSA) (also known as kallikrein 3, KLK)	Semen (seminal fluid)	Produced by prostate epithelia. Hydrolyses semenogelins during the liquefaction of ejaculated semen.	Haas et al. (2013); Nussbaumer et al. (2006);
Protamine 1 & 2 (PRM1, PRM 2)	Semen (spermatozoa)	DNA binding protein involved in sperm chromatin condensation.	Alverarez et al. (2004); Fleming & Harbison (2010); Haas et al. (2008, 2009, 2013); Juusola & Ballantyne (2005); Lindenbergh et al. (2013); Park et al. (2013); Richard et al. (2013); Sakurada et al. (2009); Van den Berge et al. (2014)

Semenogelin 1 & 2 (SEMG1, SEMG2)	Semen (seminal fluid)	Coagulation proteins involved in the ejaculation of semen.	Haas et al. (2013); Lindenbergh et al. (2013); Sakurada et al. (2009); Van den Berge et al. (2014)
Transglutaminase 4 (TGM4)	Semen (seminal fluid)	Catalyses irreversible cross-links of glutamine residues to peptide-bound lysines or primary amines.	Fang et al. (2006); Fleming & Harbison (2010); Haas et al. (2013); Richard et al. (2013)
Corneodesmosin (CDSN)	Skin	Involved in the shedding of outer membrane skin layers.	Lindenbergh et al. (2013)
Loricrin (LOR)	Skin	Component of cornified cell envelope found in terminally differentiated epidermal cells.	Lindenbergh et al. (2013)
Cytochrome P450 (CYP2B7P1)	Vaginal secretions	Catalyst in organic substance oxidization.	Van den Berge et al. (2014)
Estrogen receptor 1 (ESR1)	Vaginal secretions	Transcription factor involved in hormone and DNA binding.	Fang et al. (2006)
Human beta-defensin 1 (HBD1)	Vaginal secretions	Antimicrobial peptide found in urogenital epithelia.	Haas et al. (2008, 2009); Juusola & Ballantyne (2005); Lindenbergh et al. (2013); Sakurada et al. (2009); Van den Berge et al. (2014)
Mucin 4 (MUC 4)	Vaginal secretions	Membrane that defends epithelia within the reproductive tract and spans the mucin of the endocervix.	Alverarez et al. (2004); Haas et al. (2008, 2009); Juusola & Ballantyne (2005); Lindenbergh et al. (2013); Nussbaumer et al. (2006); Richard et al. (2013); Sakurada et al. (2009); Van den Berge et al. (2014)

One of the most recent published reports into the use of mRNA analysis in body fluid identification investigated the value of this technique within forensics. Specifically, the interpretation of forensically challenging samples, whereby estimates of the number and gender of donors, cell types present and association of donors was assessed across nine laboratories (Van den Berge et al. 2014). Each laboratory received the same sample set consisting of two parts. Part One involved ten numbered complementary DNA (cDNA) samples labelled 1-10 as single source body fluids. Within this sample set water and a

mixture of vaginal secretions and blood samples were included. Part Two involved four complex stains of which the origins were unknown (Table 1.3). Three categories of scoring were established; 'observed', 'sporadically observed' and 'not observed'. A multiplex containing 19 tissue specific mRNA markers was utilised during the analysis and all nine laboratories successfully analysed the stains (Lindenbergh et al. 2013; Van den Berge et al. 2014). The results obtained from Part One of the investigation should have generated a total of 208 cell type specific peaks for the samples analysed at both 0.5 µl and 2.0 µl cDNA input. However, across the nine participating laboratories only 109 and 161 peaks were observed in the 0.5 µl and 2.0 µl samples, respectively. The decreased detection of tissue specific peaks can be explained by marker dropout of vaginal secretion marker HBD1 and blood marker AMICA1, in addition to false positives as a result of marker drop-in from non-target mRNAs (Van den Berge et al. 2014). Part Two results reported that only 15% of the observed markers in the complex stains were attributed to false positive observations. 'Sporadically observed' marker peaks accounted for 13% of the interpretation of observed scores and 'not observed' scores for 21%.

Table 1.3: Complex stains used in Part Two of Van den Berge et al. (2014) study.

Stain Number	Description
1	Saliva collected from two donors and deposited on to a cotton swab.
2	Mixed menstrual and circulatory blood sample collected from different donors and deposited at 5µl on to fleece with an additional 50 µl of circulatory blood deposited on top of the dried stain.
3	Linen with skin rubbings on each side from different donors with 1 µl 100-fold dilute bloodspots deposited from one donor around the linen and areas near the bloodspots cut.
4	Nail clippings subjected to skin and vaginal secretion contact from a different donor and 1 µl of azoospermic semen (different donor).

Van den Berge et al. (2014) stated that the interpretation of number and gender of donors and association of donors was not appropriate with the profiling data obtained from each laboratory as great variation was observed. The interpretation of stain two was particularly challenging as the mRNA profile demonstrated high detection levels for menstrual blood compared to circulatory blood, whereas the DNA profile demonstrated almost half of the

relative fluorescence units (rfu) weight were contributed by the circulatory blood donor. Additionally, Van den Berge et al. (2014) reported that the scoring of 'sporadically observed' was utilised to reduce the number of false positive identifications. However, when scores of 'not observed' were given laboratories suggested that the lack of mRNA marker observation could be a result of cell types present in levels below detection or of unknown source rather than particular cell types being absent from the sample. This should be borne in mind in the analysis of evidential samples.

It can be seen from the research that has been conducted on mRNA analysis as a method of body fluid identification that it is highly reproducible. Over a ten year period, the only changes to the methods of conducting mRNA profiling have been developments in technology that have made the previous method redundant. Examples of this include mRNA detection with capillary electrophoresis rather than gel electrophoresis (Haas et al. 2008), or improved chemistries applied during the extraction process. Additionally, mRNA analysis has been demonstrated as highly sensitive and specific as many research groups have reported different gene markers as potential candidates for tissue specific body fluid identification, alongside markers already determined. The large range of mRNA markers already established as specific to and/or abundant in particular body fluids will enable the development of commercial multiplex kits that can be used to definitively identify body fluids. The ability to perform both singleplex and multiplex assays on samples of total RNA as small as 0.5µl is advantageous as it can be applied to unknown samples for mRNA detection of single or numerous body fluids in a single reaction (Hanson et al. 2012). This results in minimal sample consumption with maximum information obtained. Another benefit to consider is that the technique has already been incorporated into routine protocols utilised in DNA sample preparation and analysis. Therefore, the equipment required for mRNA analysis will already be available within forensic laboratories.

However, in addition to the benefits of mRNA analysis, there are limitations evident. Firstly, it is a destructive technique, therefore if mRNA profiling is unsuccessful upon initial analysis no further subsequent analyses can be carried out on the original sample. Additionally, difficulties in profile interpretation were evident amongst the research groups, with many stating that cross-reactivity was observed within some of the results, most of which could be accounted for. However, the more complex a sample is, the more difficult the interpretation of resulting mRNA profiles and discrepancies will be (Van den Berge et al. 2014). At present, there are no validated guidelines in place for mRNA profiling interpretation which means that no objective conclusions can be drawn. Van den Berge et al. (2014) openly discussed this limitation, whereby different conclusions were obtained from nine different laboratories in

regards to four body fluid samples. Until validated guidelines are in place to ensure that mRNA analysis data is interpreted in a consistent and uniform manner, it is not appropriate for application to forensic analysis of body fluid identification.

In addition to mRNA, the analysis of microRNA (miRNA) as a technique for forensic body fluid identification has been investigated (Hanson et al. 2009). MicroRNA is a class of small, noncoding ribonucleic acids that are typically no larger than 25 base pairs in length (Wang et al. 2012). The role of miRNA lies in post-transcription gene regulation and miRNAs are thought to be more stable than mRNA (Omelia et al. 2013). The rationale behind the investigation into miRNA for forensic application was that body fluid identification should be feasible due to differential expression of miRNAs within forensically relevant body fluids (Hanson et al. 2009). Samples of blood were collected and deposited on to cotton and samples of menstrual blood, saliva, semen and vaginal secretions were collected with cotton swabs. Initial analysis involved the identification of candidate miRNA markers from the 452 human miRNAs known, based on high expression levels observed within the body fluids (Hanson et al. 2009). MicroRNA analysis utilised similar methods to traditional mRNA analysis (Figure 1.5).

Initial results demonstrated that no truly body fluid specific miRNAs were identified. However, some miRNAs exhibited higher abundance and observable differences in expression amongst the body fluids. To validate potential candidate miRNA markers a small nuclear RNA, U6b, was utilised as a reference gene to normalise the expression observed. Candidates whose expression was higher than U6b expression within individual body fluids, but lower than U6b in others, were defined as potential strong markers (Hanson et al. 2009). Ten candidate markers were determined, all of which were detectable within the five body fluids. However, analysis with two-dimensional scatter plots demonstrated that the expression observed within each of the body fluid miRNA markers was significantly different from one another due to differential expression (Hanson et al. 2009).

Developments to establish more body fluid specific miRNA markers have been undertaken by a number of research groups, with no definitive candidate markers determined to date. Table 1.4 details the documented possible miRNA candidates for the forensic identification of blood, menstrual blood, saliva, semen and vaginal secretions. Like the mRNA markers, there are many potential candidates to be utilised in the identification of body fluids. The most promising miRNA candidate markers that could be utilised for definitive identification appear to be miR451 for blood and miR205 for saliva.

Table 1.4: MicroRNA candidate markers suggested for body fluid identification.

Body Fluid Target	miRNA Candidate	Reference	Body Fluid Target	miRNA Candidate	Reference
Blood	miR16*	Hanson et al (2009); Petersen et al. (2013) Wang et al. (2012, 2013)	Saliva	miR205*	Hanson et al. (2009); Omelia et al. (2013); Petersen et al. (2013); Wang et al. (2012); Williams et al. (2013)
	miR20a	Zubakov et al. (2010)		miR208b	Zubakov et al. (2010)
	miR106a	Zubakov et al. (2010)		miR518c	Zubakov et al. (2010)
	miR144*	Zubakov et al. (2010)		miR583	Zubakov et al. (2010)
	miR185*	Zubakov et al. (2010)		miR658	Hanson et al. (2009)
	miR451*	Hanson et al. (2009); Omelia et al. (2013); Petersen et al. (2013); Williams et al. (2013);	Semen	miR10 a & b	Hanson et al. (2009); Zubakov et al. (2010)
	miR486*	Petersen et al. (2013); Wang et al. (2013)		miR135 a & b	Hanson et al. (2009); Zubakov et al. (2010)
Menstrual blood	miR412	Hanson et al. (2009)		miR507	Zubakov et al. (2010)
	miR214	Wang et al. (2013)		miR888	Wang et al. (2013)
Vaginal secretions	miR124a	Hanson et al. (2009)		miR891a	Wang et al. (2013); Williams et al. (2013); Zubakov et al. (2010)
	miR372	Hanson et al. (2009)		miR943	Zubakov et al. (2010)
	miR617	Williams et al. (2013)			

*Expression detected in other body fluids

However, many of the results obtained from the research groups have not been demonstrated as reproducible, as different miRNA markers have been reported amongst the research groups, as well as different methodologies adopted. Additionally, some of these candidate markers have exhibited high expression within body fluids other than the target. For example, miR451 has been reported as highly expressed within menstrual blood, as well as in blood (Hanson et al. 2009; Omelia et al. 2013) and miR144 has shown high expression in menstrual blood in addition to lower, but still detectable expression levels in saliva and semen (Zubakov et al. 2010).

One of the most interesting methodologies adopted within the investigation of miRNA for forensic body fluid identification was reported by Omelia et al. (2013), whereby a comparison was conducted between miRNA recovery from DNA and RNA extraction methods. Omelia et al. (2013) stated that during standard DNA extraction, all washes and supernatants are retained along with the final extract in order to adhere to Crown Prosecution Service (CPS) guidelines. Therefore, it would not be surprising to find miRNAs within these samples. Candidate miRNA markers, miR451a (blood) and miR205 (saliva), were utilised to target expression within blood and saliva samples from six donors. Half of the samples were subjected to DNA extraction, the remaining half were subjected to RNA extraction followed by RT real time PCR. The results obtained identified that samples extracted with standard DNA methods recovered greater miRNA than samples extracted with RNA methods (Omelia et al. 2013). Particularly, the final extract of DNA contained the majority of detectable miRNA when compared to the eluted washings and supernatants retained from the process. Additionally, Omelia et al. (2013) reported that miRNA expression from the two candidate markers demonstrated a significant difference amongst the blood and saliva samples, which supports the use of miR451a and miR205 as blood and saliva specific markers, respectively.

The benefit to consider for the utilisation of miRNA to identify body fluids is that is it more stable than RNA, which suggests that it may be appropriate for application on degraded samples. In addition, analysis can be conducted with the same methods used in traditional DNA and RNA analysis. This is particularly advantageous as it demonstrates that current protocols are appropriate for miRNA analysis and that additional equipment and consumables/kits are not required. However, the lack of inconsistent and reproducible results within documented literature exhibits the immaturity of miRNA analysis as a technique to identify body fluids for forensic purposes. Much further development is needed to establish appropriate candidate markers that can be compiled into a multiplex assay for routine analysis. In order for miRNA analysis to be applied within forensic investigation, candidate markers must be selected that have specific or very high expression, as minimum,

within individual body fluids with no cross reactivity with other body fluids. These markers must also demonstrate reproducible expression to confirm body fluid specificity.

1.2.1.3 PROTEIN

Van Steendam et al. (2013) and Yang et al. (2013) took a different biological approach and investigated the use of proteomics with mass spectrometry as a potential application for body fluid identification. Mass spectrometry is a highly sensitive separation technique that is utilised to measure the molecular mass of the components within a given sample (Yang et al. 2013). It is often coupled with chromatographic techniques to obtain high resolution spectra of separated sample components. In its application within proteomics, which is the large-scale study of proteins (Strachan & Read, 2011), mass spectrometry effectively sequences proteins by producing spectra with mass measurements of fragmented peptides (Yang et al. 2013). In particular, both Van Steendam et al. (2013) and Yang et al. (2013) reported the use of mass spectrometry to establish biomarkers within body fluids that could be utilised to determine source identification.

Van Steendam et al. (2013) analysed cotton swabs containing blood, faeces, menstrual blood, nasal secretions, saliva, semen, urine and vaginal secretions with high performance liquid chromatography (HPLC) electrospray ionisation time of flight (ESI Q-TOF) mass spectrometry (MS) and tandem mass spectrometry (MS/MS). HPLC is a high pressured liquid separation technique that is often utilised within analytical chemistry and forensic science in order to determine the size of molecular components within heterogeneous samples (Langford et al. 2005). ESI Q-TOF is a soft ionisation technique that creates highly charged molecules that have little to no fragmentation (Altuntaş et al. 2010). This involves simultaneous peptide desalting and separation which results in greater sequencing of peptides within the sample based on molar mass (University College London, 2010). In addition to the neat samples, a series of dilution factors, ranging from 1:2 to 1:1,000,000, and forensic casework samples from rape cases were included in the analysis (Van Steendam et al. 2013). All samples were air dried and presumptively tested with routinely utilised tests, including benzidine for blood, Phadebas® for saliva and acid phosphatase (AP) and prostate specific antigen (PSA) for semen. This was included in the investigation so that limit of detection comparisons could be made between current methods and MS. Following presumptive testing, samples were extracted and analysed with HPLC ESI Q-TOF MS and MS/MS.

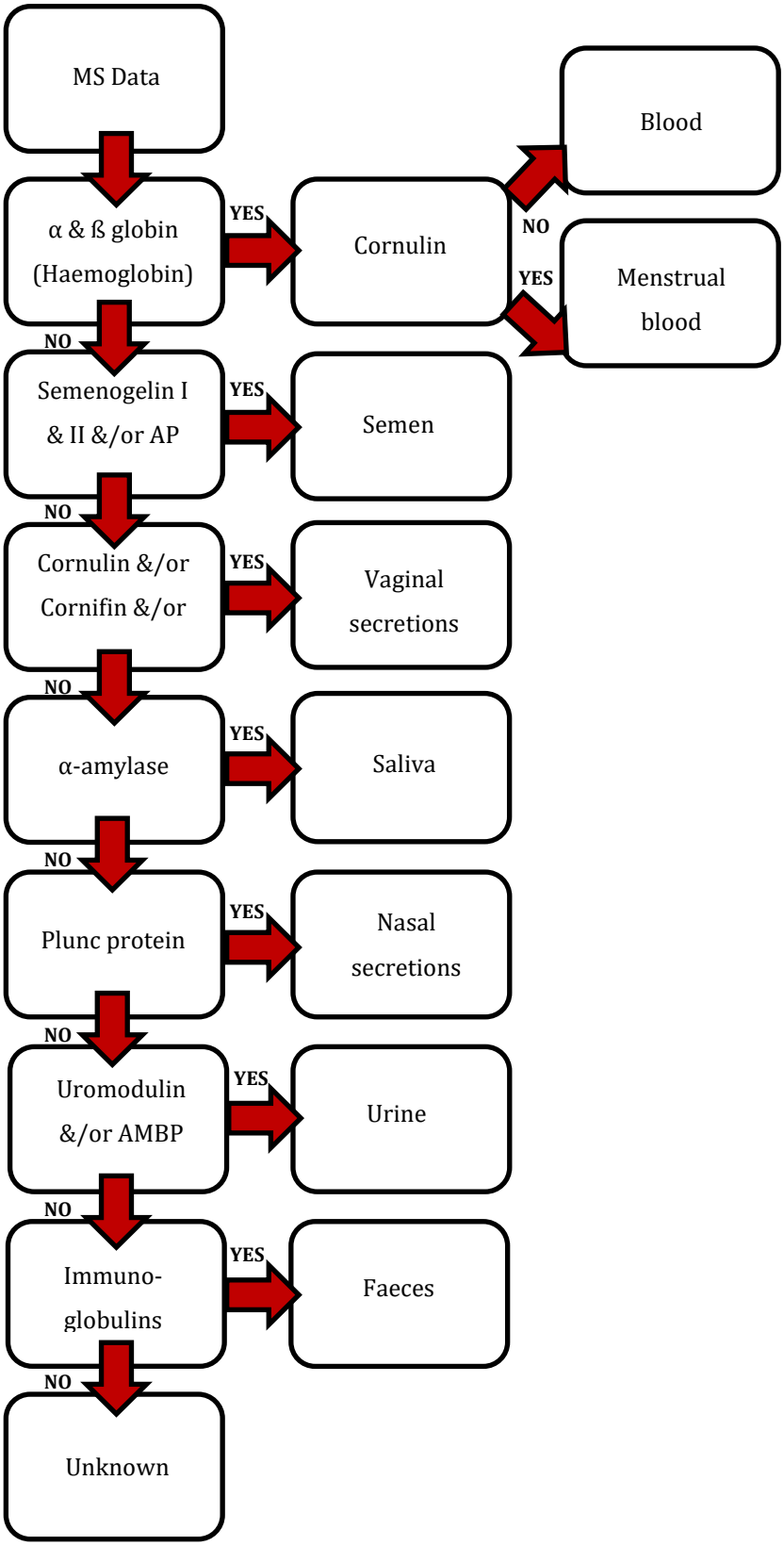

Figure 1.6: "Decision tree" utilised to identify body fluids by HPLC ESI Q-TOF MS, MS/MS (adapted from Van Steendan et al. (2013)).

Van Steendam et al. (2013) selected peptides that appeared to be specific to, or highly abundant within, each body fluid as biomarkers to determine sample identity. There were

some shared biomarkers selected for some of the body fluids, although the presence of a combination of biomarkers and subsequent absence of others enabled identifications to be made. To validate the method of HPLC ESI Q-TOF MS, MS/MS to identify body fluids, Van Steendam et al. (2013) developed a "decision tree" which confirmed the body fluid source based on the presence or absence of the selected biomarkers (Figure 1.6). Fifteen blind samples of body fluids were analysed with the use of the "decision tree", all of which were correctly identified. Additionally, all of the forensic casework samples were successfully analysed with MS, in which blood, semen and/or vaginal secretions were detected. Van Steendam et al. (2013) also reported that MS demonstrated comparable or greater sensitivity than the presumptive tests included in the analyses. Of the blood dilution factors, MS demonstrated a sensitivity of 1:100,000, whereas benzidine had a maximum sensitivity of 1:10,000. For saliva and semen dilutions MS sensitivity was observed up to 1:1000 and 1:100,000 respectively, although the presumptive equivalents have a limit of detection of 1:100 for both Phadebas® and AP, and 1:100,000 for PSA (Van Steendam et al. 2013).

Yang et al. (2013) made use of an alternative variation of MS analysis. Specifically, high performance liquid chromatography matrix-assisted laser desorption/ionisation tandem time of flight mass spectrometry and tandem mass spectrometry (HPLC MALDI-TOF/TOF MS and MS/MS) was utilised in body fluid identification for forensic purposes. MALDI-TOF is vaporisation technique, whereby the sample of interest is mixed with a matrix which absorbs ultra violet light. The matrix then heats rapidly, causing the matrix and sample to vaporise (Shimadzu, 2014). It is the amount of time taken for the molecule containing vapour to reach the detector that is quantified. Small and highly charged molecules reach the detector faster than large, low charged molecules. The time at which molecules reach the detector is representative of a mass to charge ratio and gives the process its name, time of flight (Shimadzu, 2014).

The proteomes of blood, saliva and semen were analysed and compared with published values in literature in order to identify multiple biomarkers that could be utilised for identification purposes (Yang et al. 2013). In addition to neat body fluids, diluted samples of up to 10,000-fold (blood), 1,000-fold (semen) and 100-fold (saliva) were deposited to assess the sensitivity of the technique. Diluted mixed samples at a ratio of 5µl neat body fluid to 5µl of dilute body fluid were also included in the study. The dilution mixtures examined were blood to diluted saliva (1:10), and saliva to diluted blood (1:5,000). Samples were then subjected to protein extraction, quantification and HPLC MALDI-TOF/TOF MS and MS/MS (Yang et al. 2013). The biomarkers selected were required to demonstrate a confidence level of greater than, or equal to 95% and a false positive ratio of equal to, or less than 5%. At these

levels of confidence, Yang et al. (2013) reported 59, 48 and 77 unique proteins in blood, semen and saliva, respectively. Of these, the specificity and abundance criteria identified four biomarkers for blood, five for saliva and eight for semen. The biomarkers that were considered to be the most distinct and abundant, relative to each body fluid, were observed to be α and ß globin (blood), α-amylase (saliva) and semenogelins I and II (semen). The presence of these biomarkers in conjunction with the remaining, less abundant biomarkers for each body fluid enabled successful identification of the body fluids in as little as approximately 2ng blood and semen and 10ng of saliva. Yang et al. (2013) also stated that the limit of detection for the blood:saliva mixture was observed at a 1:1 ratio. However, for saliva:blood mixtures, the limit of detection was observed at 1:2,000. This extreme difference in detection limits was perceived to be due to the vast difference in protein content and abundance between blood and saliva.

There are many benefits associated with the use of mass spectrometry in the identification of body fluids and these are evident within the research of both Van Steendam et al. (2013) and Yang et al. (2013). Firstly, MS has provided an alternative sequencing method that can be applied to proteins and allows discrimination between samples to a similar, if not equal, standard as DNA sequencing (Edwards et al. 2005). Van Steendam et al. (2013) and Yang et al. (2013) have both demonstrated that blood, saliva and semen can be distinguished from one another based on biomarkers that are specific and abundant to each body fluid. Both research groups identified the same specific proteins within blood, saliva and semen which demonstrates the reproducibility of the technique. Additionally, Van Steendam et al. (2013) reported that combinations of common proteins observed within numerous body fluids can still allow for fluid and materials of a biological nature to be differentiated. The use of MS as a method of body fluid identification is also advantageous in that it is not limited to application for specific body fluids. Any sample material can be analysed by the same method, which highlights the accuracy and specificity of the technique. The origin of forensic evidence is often unknown, whether it is biological or non-biological. Therefore, a technique that can be appropriately utilised to confirm the identity of unknown samples is highly desirable and MS has the potential to provide this. In comparison to routine presumptive and confirmatory body fluid identification tests, MS has demonstrated that it can detect low levels of diluted material to the same or greater sensitivity as current methods and is able to identify mixed sample contributions when present in different volumes. This is beneficial as it removes the ambiguity of whether forensic evidence contains biological material, as well identify if more than one body fluid component is present in a forensic sample. This therefore allows police officers to make informed decisions about which samples require further testing.

It is evident that there are many benefits to MS as a technique to identify body fluids within a forensic context. However, there are limitations that do not favour the technique. Van Steendam et al. (2013) openly stated that MS is not yet appropriate for routine analysis within forensic investigations as the current procedure is time consuming and results are not obtained in a timely manner. As quick, reliable methods are sought for direct analysis at crime scenes or immediately thereafter, MS still requires development to ensure that analysis time is reduced. Additionally, the equipment required to carry out MS analysis is expensive. Van Steendam et al. (2013) and Yang et al. (2013) both utilised MS coupled with HPLC and specific ionisation techniques, all of which may not be found in a typical laboratory and requires specialist training to utilise.

The biological approaches that have been explored to date in the identification of body fluids have shown that analysis of nucleic acids and proteins can provide highly sensitive and specific detection methods. The similarities between mRNA, miRNA and DNA methylation techniques are demonstrated in their ability to be incorporated into current DNA analysis protocols successfully. This presents potential options to forensic investigators as to which method could be applied to biological evidence without requiring additional resources or time. Messenger RNA analysis has held the forefront of forensic body fluid identification and a vast number of body fluid specific mRNA markers have been identified that have the potential to be incorporated into a validated multiplex assay. Movements have also been made to devise guidelines for mRNA profiling interpretation to definitively identify body fluids. MicroRNA has also demonstrated high levels of specificity and is thought to be more stable that mRNA due to its small size, which could indicate its applicability to degraded evidential samples. However, miRNA is still in its development stage as there has been little reproducibility within the candidate markers that could be utilised to distinguish between body fluids. Much more research is required before miRNA can be incorporated into forensic analysis protocols. This can also be said for DNA methylation techniques. To date, there are only three noteworthy publications investigating the use of DNA methylation within a forensic body fluid identification context. The lack of knowledge in the area highlights the vulnerability of the DNA methylation technique and therefore is not considered appropriate for routine application at present.

As the methods utilised for all three biological approaches to body fluid identification are strikingly similar, it is difficult to suggest the most appropriate technique. Based on the level of research and development that has been conducted within mRNA analysis, it is evident that this technique is most appropriate for routine application. However, due the similarities between the three methods it does raise the question as to why three nucleic acid methods

are necessary for forensic body fluid identification. A combined analysis of the three approaches may be the next development to consider in nucleic acid body fluid identification. However, the development of next generation DNA sequencing (NGS) may render these genetic applications for forensic identification as redundant (Yang et al. 2014) In contrast to the nucleic acid methods described, mass spectrometry enables the differentiation between known proteins by molecular weights in a manner reflective of DNA sequencing which highlights the high level of accuracy and sensitivity of the technique. When comparing mass spectrometry with the nucleic acid methods there are similarities in that it is the cost and sampling time that limit the techniques as methods of determining body fluid source. Additionally, mass spectrometry is not a technique that could be integrated into current forensic DNA protocols as it is a completely separate technique. Specific instrumentation and many intricate sample preparation steps are required for mass spectrometry analysis, therefore specific reagents and equipment are essential in order to obtain accurate data.

1.2.2 CHEMICAL APPROACHES

It can be seen that the use of genetic material, such as DNA and RNA, has been extensively explored as confirmatory methods in the identification of body fluids within a forensic context. Alongside these biological approaches, chemical approaches have also been explored to offer alternative methods of identifying the origin of biological material in a confirmatory manner.

1.2.2.1 RAMAN SPECTROSCOPY

Raman spectroscopy was one of the first traditionally chemically based techniques reported to have been successfully applied in body fluid identification (McLaughlin et al. 2013; McLaughlin & Lednev, 2014; Sikirzhytskaya et al. 2012; Sikirzhytski et al. 2012; Virkler & Lednev, 2008, 2009c, 2010a, 2010b). Raman spectroscopy is a vibrational spectroscopic technique which relies upon the inelastic scattering of light, whereby an exchange of energy takes place when photons collide with molecules within a sample when subjected to light radiation (Banwell & McCash, 1994). Unique chemical fingerprints can be obtained from Raman spectroscopy as the vibrational excitation modes of photons are emitted from a sample are collected and compiled in to a spectrum of peaks (Banwell & McCash, 1994).

Within a forensic context, Raman spectroscopy is often utilised in the analysis of chemicals, drugs and cosmetics (Virkler & Lednev, 2008). Virkler & Lednev (2008) initially reported the potential use of Raman spectroscopy as a non-destructive method of identifying body fluids.

Blood, saliva, semen, sweat and vaginal secretions were deposited on to aluminium foil covered microscope slides and air dried before analysis within the near infrared (NIR) region of the electromagnetic spectrum. Various different areas of each dried stain were analysed due to the presumed heterogeneous nature of body fluids. The Raman spectra obtained from each of the body fluids consisted of peaks representative of vibrational stretches and bends of the biological components present within the samples (Figure 1.7).

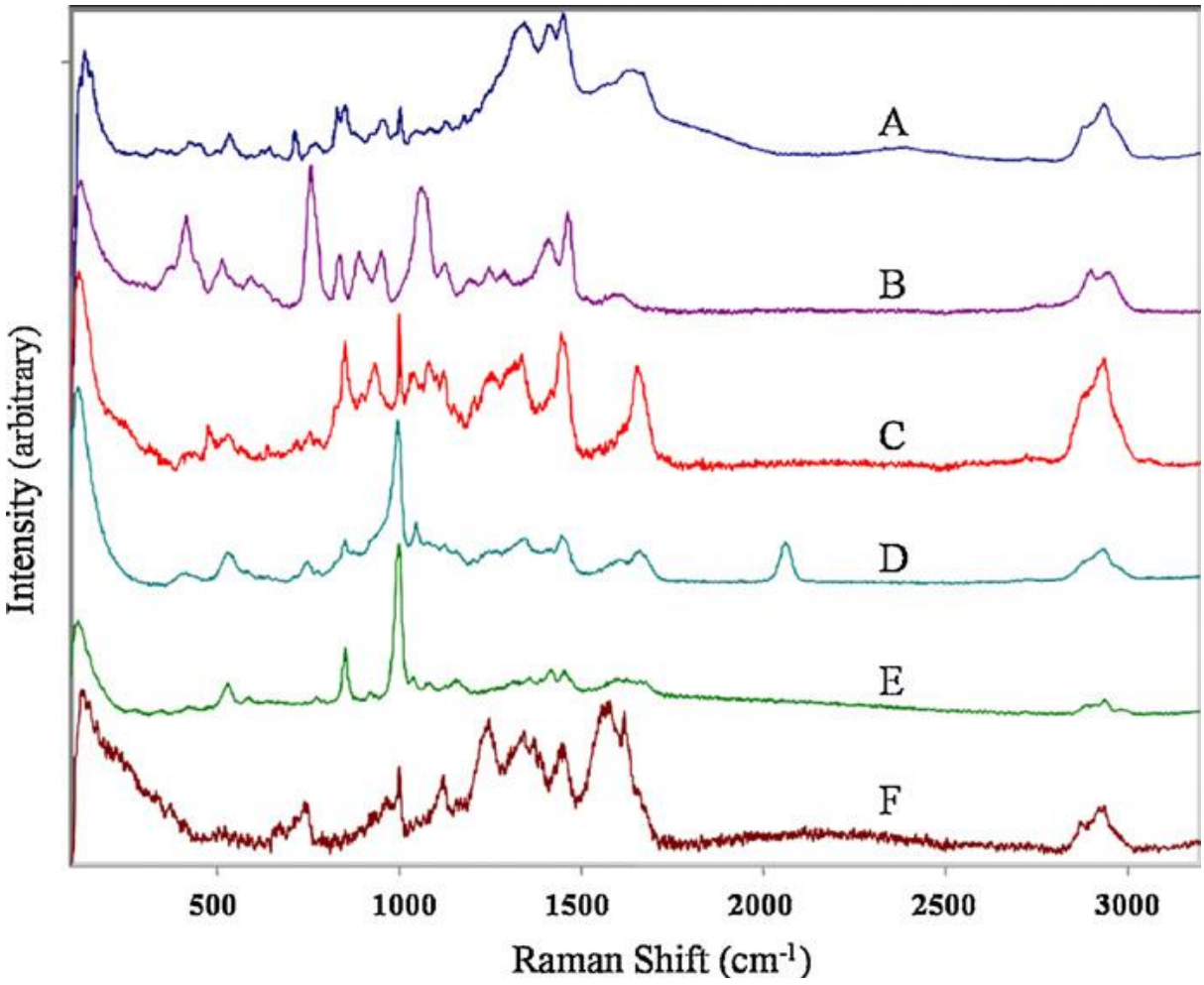

Figure 1.7: Raman spectra of body fluids as reported by Virkler & Lednev (2008); a) human semen, b) canine semen, c) vaginal secretions, d) saliva, e) sweat & f) blood.

Virkler & Lednev (2008) reported that there were common peaks and components observed between the spectra obtained from body fluids. Albumin was observed in blood and semen sample spectra, lysozyme was present in the Raman spectra for saliva, semen and vaginal secretion samples, and urea and lactate were observed in semen, sweat and vaginal secretion samples. Blood samples could be differentiated from the remaining samples due to the dominance of haemoglobin, which contributed 95% of the dried red blood cells weight (Virkler & Lednev, 2008). Saliva samples could be differentiated from the other body fluids

based on the strong peaks observed representative of amide I, phenylalanine and thiocyanate (Virkler & Lednev, 2008). It was not unexpected for common biological components, such as proteins, to be present within each of the different body fluids. However, the combination of shared and unique peaks for each body fluid allowed for the samples to be distinguished from one another (Virkler & Lednev, 2008).

Development from these reported findings led to the production of "spectroscopic signatures" for blood (McLaughlin & Lednev 2014; Virkler & Lednev, 2009b, 2010b), saliva (Virkler & Lednev, 2010a), semen (Virkler & Lednev, 2009c) and vaginal secretions (Sikirzhytskaya et al. 2012) for confirmatory body fluid identification (Sikirzhytski et al. 2010, 2012). Table 1.5 demonstrates the components observed within the spectra for the designated signature samples that appeared to be unique to each body fluid. These components were identified and used for comparison measurements with the remaining body fluid samples (Sikirzhytski et al. 2010). The incorporation of baseline fluorescence slope and horizontal lines to the unique components identified resulted in the spectroscopic signature for blood, saliva and semen (McLaughlin & Lednev 2014; Virkler & Lednev, 2009c, 2010a, 2010b; Sikirzhytski et al. 2010, 2012). The remaining samples of each body fluid were linearly fitted with their respective signature to assess how closely samples from different donors matched. Statistical analysis confirmed the quality of the fit at 99% confidence levels for each sample compared to the spectroscopic signature (Sikirzhytski et al. 2010). Alongside this, each body fluid was compared with the spectroscopic signature of a different body fluid. For example, blood spectra were compared with the spectroscopic signatures of saliva and semen to demonstrate the poor "goodness-of-fit" (Virkler & Lednev, 2010b). All four studies reported that poor "goodness-of-fit" values were obtained for samples compared to spectroscopic signatures of different body fluids (Sikirzhytski et al. 2010).

The Raman spectroscopic signatures of blood and semen were further investigated by Sikirzhytski et al. (2012) in the application of detecting blood and semen mixtures of various ratios and dilutions, ranging from 5:95 to 98.4:1.6. Initial results stated that all the spectra obtained from mixtures were dominated by blood characteristics and all mixtures with 50% or more blood present demonstrated no Raman peaks for the semen component. Additionally, low concentrations of either body fluid within the mixtures could not be distinguished from the neat spectroscopic signatures. Approximately 40% of spectra obtained from neat blood or semen were misclassified as mixtures and high concentrated blood mixtures were reported as indistinguishable from one another. Advanced statistical classification demonstrated that the limit of detection for blood and semen concentrations in a mixture was 5% and 25%, respectively (Sikirzhytski et al. 2012).

Table 1.5: Unique spectral components utilised in the development of Raman spectroscopic signatures for blood, saliva, semen & vaginal secretions.

Body Fluid Signature	Component Number	Component Identification	Reference
Blood	1	Haemglobin & derivatives.	Virkler & Lednev (2010b)
Blood	2	Unknown.	McLaughlin & Lednev (2014)
Saliva	1	Amide I – representative of whole saliva.	Virkler & Lednev (2010a)
Saliva	2	A saccharide & acetate.	Virkler & Lednev (2010s)
Saliva	3	Arginine & free amino acids.	Virkler & Lednev (2010a)
Semen	1	Tyrosine.	Virkler & Lednev (2009c)
Semen	2	Amide I & II	Virkler & Lednev (2009c)
Semen	3	Spermine phosphate hexahydrate (SPH).	Virkler & Lednev (2009c)
Vaginal secretions	1	Lactic acid, urea & proteins.	Sikirzhytskaya et al. (2012)
Vaginal secretions	2	Lactic acid, urea & proteins.	Sikirzhytskaya et al. (2012)
Vaginal secretions	3	N-C=O bending and CN stretching of urea.	Sikirzhytskaya et al. (2012)

In addition to the development of spectroscopic signatures of body fluids utilising Raman spectroscopy, the effect of substrate interference in bloodstain identification has been examined. Substrates examined include; aluminium foil coated microscope slides, glass microscope slides, cotton, denim, dry wall and plastic cutlery (Boyd et al. 2011; McLaughlin et al. 2013). The results demonstrated by Boyd et al. (2011) reported that bloodstains deposited on to aluminium foil coated and glass microscope slides yielded full haemoglobin characteristic peaks when analysed directly. However, the spectra obtained from bloodstains

deposited on to fabrics were dominated by the presence of substrate peaks. Reconstitution of the bloodstains from their respective substrates via a water-based extraction enabled full haemoglobin characteristic spectra to be obtained from the samples, with no substrate contamination (Boyd et al. 2011).

In contrast, McLaughlin et al. (2013) stated that all the Raman spectra obtained were dominated by the substrate, with no blood characteristics distinguishable. However, after substrate subtraction, full blood characteristic spectra were observed for samples deposited on to glass, tile and cotton Bloodstains deposited on denim spectra exhibited very strong fluorescence from indigo dye and even after subtraction, no blood characteristic peaks could be observed. The application of the Vancouver Raman Algorithm, an algorithm utilised to remove broad fluorescence (McLaughlin et al. 2013), to the blood on denim spectra resulted in the observation of several blood characteristics. Statistical analysis confirmed the high quality matches of the blood spectra to the reference blood spectrum after subtraction of the deposition substrates. Additionally, McLaughlin et al. (2013) reported that comparisons with the spectroscopic signature of blood as developed by Virkler & Lednev (2010b) demonstrated very good overlap with blood samples subtracted from cotton and glass substrates, although blood samples subtracted from denim and tile substrates did not overlap well.

The evident benefits of the utilisation of Raman spectroscopy in the identification of body fluids are that it is non-destructive to the sample, relatively small volumes of material can be analysed in depth and no sample preparation is required, therefore direct analysis can take place. However, the most important benefit observed in the use of Raman spectroscopy is its demonstrated specificity and reproducibility. Blood, saliva, semen and vaginal secretions have all been analysed against the spectroscopic signatures of the other body fluids and have statistically confirmed poor goodness-of-fit. Furthermore, bloodstains deposited on to various substrates have also exhibited overlap with the spectroscopic signature of blood. This is hugely advantageous within a forensic context as it demonstrates that it is possible for these to be utilised as library reference spectra. This could then be incorporated into spectral comparison software utilised on Raman spectrometers, which would prevent each prospective laboratory having to develop their own spectroscopic signatures. This ensures standardisation and consistency in the Raman spectroscopic analysis of blood, saliva, semen and vaginal secretion samples within different laboratories.

Another benefit to consider is that Raman spectroscopy has been demonstrated to successfully obtain blood characteristic spectra from a number of interfering substrates. Two

very different methods have been utilised to overcome the interference of background substrates and both methods have produced positive results. Particularly, the research conducted by Boyd et al. (2011) highlights that a reconstitution method can successfully extract bloodstains from substrates and not hinder subsequent analysis. This is advantageous within a forensic context as it has demonstrated that bloodstains can be extracted in a simple process that does not impact on the sample itself or extract material from the substrate upon which the blood is deposited. The simplicity of this extraction is not only beneficial for Raman spectroscopy analysis, but it also ensures that DNA, RNA or even protein extractions can be conducted on the same sample as no chemicals or reagents have been added that could hinder these further analyses. On the contrary, McLaughlin et al. (2013) demonstrated that an instrumental approach that makes use of simple subtraction of spectra can also produce spectra containing only blood characteristic peaks. This presents itself as a benefit as it provides evidence that direct analysis and manipulation of the spectral output can be conducted to identify bloodstains. This means that no sample preparation is required and the analysis method remains non-destructive. The method utilised by Boyd et al. (2011) could complement the method utilised by McLaughlin et al. (2013) if direct analysis and subtraction was unsuccessful on bloodstain evidence.

However, in light of the benefits demonstrated in literature of the application of Raman spectroscopy for body fluid identification, there are also limitations that need to be considered. Firstly, it was not possible to yield good quality spectra that were comparable to the spectroscopic signature of blood when bloodstains on denim were examined. This suggests that the examination of body fluid stains on coloured backgrounds could be problematic when utilising Raman spectroscopy. Therefore, this limits the scope of application for biological analysis with Raman spectroscopy as both spectral subtraction and direct analysis appear inadequate to enable confident bloodstain identification. Another limitation evident from the literature is that Raman spectroscopy may not be appropriate for the analysis of mixed body fluid stains. The high variability reported by Sikirzhytski et al. (2012) within the classification of neat and mixed blood and semen samples resulted in misclassification of neat blood and semen stains by approximately 40%. Alongside this, it was only after advanced statistical analysis could the limit of detection be determined for blood and semen components within stains. This is a large limitation for the application of Raman spectroscopy in the analysis of biological mixtures as it weakens the ability to conduct this analysis on unknown body fluid mixtures, a routine sample type in biological evidence. Furthermore, the limit of detection of 5% and 25% for blood and semen contributions, respectively, could only be determined after advanced statistical analysis. This requires

specialised knowledge of statistics in order to interpret the results and explain the findings in a manner that a court could understand.

1.2.2.2 FOURIER TRANSFORM INFRARED SPECTROSCOPY

It has been stated that the use of FTIR is not appropriate for forensic applications as only general chemical component information can be obtained from the spectra (De Wael et al. 2008). However, FTIR is frequently utilised within biomedicine (Barth, 2007; Chittur, 1998; Kazarian & Chan, 2006). Furthermore, Elkins (2011) produced a comprehensive report into the use of FTIR as a technique to identify biological materials from a forensic perspective. Attenuated total reflectance Fourier Transform infrared (ATR-FTIR) spectroscopy is a configuration of FTIR, whereby light is internally reflected between two mediums, one of a high refractive index, namely the internal reflection element (IRE), and one of a low refractive index, the sample (Kazarian & Chan, 2013). The reduction in light intensity over a distance is measured as light penetrates a sample in the form of an evanescent wave (Kazarian & Chan, 2013). Upon light reflection, the measurements are processed by FTIR and a spectrum is produced of sample component vibrations.

Elkins (2011) examined human samples of blood, earwax, faeces, fingernails, hair, nasal mucus, saliva, semen, tears, urine and vaginal secretions. Alongside these samples, comparisons were made with cosmetic and food stuffs which could be mistaken for biological materials, including barbeque sauce, lipstick, mayonnaise, Vaseline and yogurt. Further comparisons were made with standard protein samples of bovine haemoglobin, bovine serum albumin and α-amylase. All samples were deposited on to cotton cloth and air dried prior to analysis. As expected, many of the biological materials analysed had common peaks observed which corresponded to proteins. In particular, amides I-III, which are representative of the secondary structures of proteins (Garidel & Schott, 2006a), methyl and methylene groups (CH_3 and CH_2, respectively) and O-H stretch bonds often contributed to the infrared (IR) spectra obtained for many of the biological materials analysed (Elkins, 2011). However, despite the observed common component peaks, all of the biological materials could be differentiated from one another and from the cosmetic and food samples. This was demonstrated in the relative peak intensities and overall combination of peaks observed, particularly in the fingerprint region of the IR spectrum. The fingerprint region of the IR spectrum is indicative of the energy absorptions of molecular components that are often unique to the sample. Therefore, the peaks observed within the fingerprint region can be utilised in the process of sample identification (Garidel & Schott, 2006a). A full

comprehensive breakdown of the spectral components identified for each of these biological materials can be found in Elkins (2011).

Elkins (2011) also reported that the standard protein samples exhibited strong amide I peaks, as anticipated, which were comparable with the amide I peaks observed within the blood and saliva spectra. However, within the fingerprint region of each standard protein sample, significant differences were observed. This further demonstrates the differentiation between biological materials which can aid in identification utilising ATR-FTIR. A key benefit to consider for the application of ATR-FTIR in biological material identification is that it can discriminate between biological materials that contain common components, such as proteins. The peaks observed within the fingerprint region in particular, can enable comparisons to be made between samples which can confirm or exclude the material source. This highlights the specificity of the technique which is advantageous for routine application within the investigation of crime. The specificity of ATR-FTIR as an identification technique was also demonstrated in the comparison of biological and non-biological samples where no common component peaks were observed (Elkins, 2011).

Other benefits to consider are those that are common place amongst spectroscopic techniques. These include the robust nature of the analysis which allows for the potential of portable ATR-FTIR instruments, the non-destructive analysis of samples, a highly desirable requirement in the forensic analysis of crime scene evidence, and the simplicity of the technique. The output from ATR-FTIR spectroscopic analysis is available in minutes after sample analysis and the spectral information obtained can be compared with instrumental libraries immediately or at a later date. A limitation that is evident in the methodology adopted by Elkins (2011) is that the volume of sample analysed for all the biological and non-biological materials was not stated. Therefore, the potential sensitivity of the technique cannot be inferred. In addition, no details of sample numbers or repeats were given which means it is not possible to comment on the reproducibility of the analysis, nor whether any consideration needs to be made regarding inter and intra sample variation.

It is evident that a variety of chemical based techniques have been investigated as potential methods to confirm the identity of forensic body fluids. The main techniques addressed are ATR-FTIR and Raman spectroscopy. ATR-FTIR and Raman spectroscopy have shared advantages in that the analyses are non-destructive, reproducible, and discriminatory as well as demonstrating specificity at a molecular level. The spectroscopic techniques yield spectral information that is unique to the sample being analysed, which can determine characteristics specific and/or abundant to body fluids. In particular, Raman spectroscopic signatures have

been developed for blood, saliva, semen and vaginal secretions which have been successfully demonstrated to confirm body fluid source and have the potential to be validated as reference spectra in routine forensic analysis. Additionally, ATR-FTIR and Raman spectroscopy are robust and can provide spectra in minutes, with no sample preparation required. This makes spectroscopy a desirable technique to explore for the identification of body fluids within a forensic context.

1.3 FORENSIC BODY FLUID AGE DETERMINATION

The ability to determine the time since deposition, or age of a body fluid is keenly sought after within forensic and criminal investigations today. There have been a small number of published articles discussing new and innovative methods of estimating the age of bloodstains in particular. Some of these methods focus on biological approaches involving mRNA (Anderson et al. 2011; Bauer et al. 2003), whereas others make use of chemical techniques to measure oxidative and decomposition changes that occur to haemoglobin within bloodstains (Edelman et al. 2012a; Fujita et al. 2005).

1.3.1 BIOLOGICAL APPROACHES

1.3.1.1 RNA

As discussed in Section 1.2.1.2, ribonucleic acid (RNA) has been explored in detail in the identification of biological materials within a forensic context. Bauer et al. (2003) were one of the first to develop the method of RNA analysis further, in the application of determining bloodstain age. In particular, two RNA methods were examined; semi-quantitative duplex reverse transcriptase polymerase chain reaction (RT-PCR) with an internal standard and competitive RT-PCR with an external standard. Semi-quantitative duplex RT-PCR takes advantage of the underrepresented complimentary DNA (cDNA) sequences toward the 5' end of cDNA, which are produced by degraded mRNA fragments (Bauer et al. 2003). Competitive RT-PCR is utilised as a control method to ensure PCR specificity and monitor reverse transcriptase (RT) efficiency and ribonuclease contamination (Bauer et al. 2003).

Samples of whole blood were deposited on to cotton cloth and placed at room temperature in a darkened room for up to 5 years. Additional blood samples that had been aged to 8 and 15 years were also included in the investigation. A total of 106 bloodstains were utilised which examined the RNA degradation as a time-wise correlation. Of these 106 samples, 16 samples were exposed to different environmental conditions, namely light exposure, darkness and incubation at 37°C with 100% humidity. These samples were exposed to the different environmental conditions for up to 2 months to allow comparisons to be made with the aged bloodstains. The RNA components selected as markers for the amplification of the aged bloodstains were β-actin for semi-quantitative duplex RT-PCR analysis and cyclophilin,

derived from mice, for competitive RT-PCR analysis. Both β-actin and cyclophilin are considered as ubiquitously expressed housekeeping genes found in all tissue types (Bauer et al. 2003). The relative ratios of the expression peak areas of β-actin and cyclophilin were utilised to estimate bloodstain age.

The results demonstrated that there was sufficient RNA present in all the aged bloodstains over the 15 year period for full analysis to be carried out. Bauer et al. (2003) reported an increase in the relative peak area ratios for both β-actin and cyclophilin which demonstrated a correlation with the increase in sample age. Samples analysed with the β-actin mRNA marker demonstrated a significant difference in bloodstains aged up to 8 months when compared to bloodstains aged for longer than 41 months. Additionally, bloodstains aged to 96 and 180 months were significantly different from all other aged bloodstains. However, analysis with the cyclophilin marker demonstrated significant differences only between samples aged up to 59 months and those aged to 96 and 180 months (Bauer et al. 2003). Comparisons between the long term aged bloodstain samples and those subjected to environmental conditions were unsuccessful. The quantities of RNA recovered from bloodstains incubated at 37°C with 100% humidity were insufficient for full analysis to be carried out (Bauer et al. 2003). Bloodstains exposed to direct sunlight exhibited no significant differences over the 2 month period to indicate sample age.

The results reported by Bauer et al. (2003) were the first of a number of developments in the age determination of body fluid stains, particularly bloodstains, with RNA analysis. A number of research groups have examined various ribosomal and messenger RNA ratios in order to determine whether there is a correlation between RNA abundance and body fluid stain age. Table 1.6 provides an overview of the reported literature in this area to date. The method of RNA analysis utilised by these different groups was typically reverse transcription real time PCR (RT qPCR), although traditional RT-PCR with electrophoresis detection was utilised by Kohlmeier & Schneider (2012) and Setzer et al. (2008). Based on the literature exploring the use of RNA analysis for age determination it is evident there are a number of benefits to this approach. Firstly, RNA analysis has demonstrated that it can be utilised on a range of different body fluids and tissues, including hair. This is due to the selection of RNA markers that are ubiquitously expressed in all cell types (Anderson et al. 2005, 2011; Bauer et al. 2003; Hampson et al. 2011; Qi et al. 2013; Simard et al. 2012). This is highly advantageous as it demonstrates that the technique is not limited to the analysis of a particular body fluid type, therefore it would be appropriate for application to forensic samples which are often of an unknown source. In addition to utilising housekeeping RNA markers, Setzer et al. (2008) demonstrated that tissue specific mRNA markers have the potential to provide an estimation

of body fluid stain age as well as body fluid identification. However, the selection of appropriate tissue specific markers requires further exploration.

Table 1.6: Overview of the literature investigating the age determination of body fluids with RNA.

Research Group	mRNA Marker	Ageing Period	Key Findings
Anderson et al. (2005)	18S rRNA & β-actin	150 days	Bloodstains examined. Ratio of 18S:β-actin demonstrated a linear relationship with sample age. The ratio appeared to increase with the increase in sample age due to 18S remaining stable across all aged samples and β-actin decreasing. Bloodstains aged 96 & 180 months were could be clearly distinguished from all younger bloodstains.
Anderson et al. (2011)	18S rRNA & β-actin in three varying amplicons	120 days	Bloodstains examined. All three amplicon ratios decreased over time, with the largest amplicon demonstrating the greatest decrease. Ratios could distinguish fresh bloodstains from 6 day aged samples, 6 day aged samples from 30 day aged and some 30 day aged bloodstains from those aged to 90 days. None of the 120 day aged bloodstains were successfully amplified.
Bauer et al. (2003)	β-actin & cyclophilin	5 years, plus 8 & 15 year old samples	Bloodstains examined and exposed to various environmental conditions. Sufficient RNA recovered for amplification across all the aged samples. β-actin marker peak areas were significantly different in bloodstains aged up to 8 months than bloodstains aged 41 months or older. Cyclophilin marker peak areas only demonstrated significant differences in samples aged to 59 months or older.
Hampson et al. (2011)	18S rRNA & β-actin	90 days	Examined RNA ratio in aged hair samples with two multiplexes. 18S demonstrated stable up to 45 days, but decreased in older samples. β-actin demonstrated a decrease in yield that correlated with the increase in sample age. Hair samples aged 60 days and older not distinguishable from one another.
Kohlmeier & Schneider (2012)	β-haemoglobin & β-spectrin	23 years	Bloodstains aged to 23 years only. DNA and RNA successfully recovered and amplified from all samples. β-haemoglobin detected in all bloodstains, but β-spectrin not detected in any samples.
Qi et al. (2013)	18S rRNA & β-actin	28 days	Bloodstains examined. 18S was stable over time, whereas β-actin increased. Gender differences in 18S:β-actin ratio observed, with females exhibiting greater ratios than males, but females yielded lower amounts of RNA than males.

Setzer et al. (2008)	S15 rRNA, β-spectrin, porphobilinogen (blood), histatin 3, statherin (saliva), protamine 1 & 2 (semen), ,mucin 4 (vaginal secretions)	547 days	Blood, saliva, semen and vaginal secretion samples exposed to different environmental conditions. All of the aged body fluids demonstrated increase in total RNA when exposed to wet conditions. S15 exhibited the most variation in detection of the different sample ages; S15 detected in bloodstains aged up to 547 days when exposed to room temperature, 90 days in outside, wet conditions and only 30 days in outside dry conditions. In semen stains, S15 was detected up to day 90 at room temperature, day 1 in outside, wet and day 7 in outside dry conditions. Body fluid specific markers varied vastly amongst the sample ages and environmental conditions.
Simard et al. (2012)	3 assays: 18S & cyclophilin A, 18S & GAPDH, 18S & β-actin	169 days	Blood, saliva and semen stains examined. Blood and semen yielded sufficient RNA for amplification at all sample ages. Saliva, did not. No correlation in ratio components over time demonstrated in any of the assays, although individually the markers demonstrated a correlation. Bloodstains aged to 14 days could be distinguished from younger samples. Semen stains aged up to 29 days distinguishable from samples aged older than 56 days.

Another benefit to consider is the reproducibility of the technique itself. The method originally reported by Anderson et al. (2005, 2011) for the age determination of bloodstains was replicated and further developed by Hampson et al. (2011) and Simard et al. (2012) with its application to hair, saliva, semen and vaginal secretions. It was found that the results correlated even though different biological samples were examined, which further supports the potential utilisation within forensic biological analysis.

The benefits of RNA analysis for age determination purposes are clear, although there are limitations that should be considered, such as the large variability in RNA yield and detection over time. Various different storage conditions, as well as sample ages, were explored and it is evident that storage conditions have a direct impact on the integrity of body fluid stains, with severely decreased detection of RNA markers in samples exposed to outside conditions. This limits the potential application of RNA age determination analysis to any biological evidence recovered from crime scenes that have been exposed to outside elements. A further limitation to consider was the large associated error with the age estimations. Different research groups stated different error margins, where documented, whereby aged hair samples could only be distinguished if they were two months old or older (Hampson et al. 2011), and bloodstains 4-5 years or older could be distinguished from stains aged less than 4-

5 years (Bauer et al., 2003). Such large variation and inconsistency in age determinations demonstrates how RNA analysis requires further development before being implemented into forensic case work for age determination purposes. Alongside this, RNA analyses are complex and time consuming as the method requires much sample preparation and intricate analyses to be carried out before any usable results can be obtained in relation to age estimation. Additionally, this often involves expensive kits to prepare the samples and there is a high risk of contamination if sample handling is not carried out carefully.

The most recent report of age determination with RNA investigated the method developed by Anderson et al. (2005, 2011) to determine whether gender related differences could be observed within bloodstains aged over a short time period (Qi et al. 2013). Whole blood was collected from 16 donors, 8 male and 8 female, which was then deposited in volumes of 10 µl on cotton cloth. One cotton cloth was used per donor, although multiple bloodstains were deposited on to the cotton. Each cotton sheet was exposed to normal room temperature conditions, whereby humidity, light levels and fluctuations in temperature were not controlled. Samples were aged from 0 to 28 days prior to analysis by RNA extraction and RT-qPCR of rRNA 18S and mRNA β-actin expression ratios (Qi et al. 2013). The results demonstrated similar findings to those obtained by Anderson et al. (2005, 2011), whereby stable critical threshold (Ct) values for 18S were observed across the 28 days period, and Ct values for β-actin exhibited an increase with sample age. This therefore resulted in an increase in the 18S:β-actin expression ratio which correlated with the increase in bloodstain age. Qi et al. (2013) reported that gender related differences were observed only in the expression ratios and yield of RNA in the aged bloodstains. Particularly, the 18S:β-actin ratio was on average greater in female donated stains than male donated stains. However, the yield of RNA from female donated bloodstains was lower than male donated stains.

The results reported by Qi et al. (2013) further support the findings of the various research groups detailed in Table 1.6. It is evident that this RNA technique is robust and reproducible as the results reported correlate with those reported by Anderson et al. (2005, 2011). This is highly beneficial for the application of RNA analysis in bloodstain age determination as it demonstrates that consistent results can be obtained from this analysis. An additional benefit to consider is that the gender of the individual who deposited the bloodstain could be indicated from this age determination method, if DNA profiling is unsuccessful, based on the yield and expression ratio of the RNA markers. However, the gender differences reported by Qi et al. (2013) contradict those found by Anderson et al. (2005) who stated that no significant gender differences were observed. A limitation associated with the methodology utilised by Qi et al. (2013) lies in the short term ageing of samples. To establish whether

gender differences affect the age estimation of bloodstains, a wide range of short and long term ageing should be addressed to ensure that the gender differences observed were not a result of chance. Additionally, a repeat study of male and female donors from different ethnicities could have been utilised to examine whether comparisons can be made based on gender alone, or whether the results reported by Qi et al. (2013) were only observable in the Chinese Han population.

The review of the literature on biological approaches for the determination of the age of body fluids has further reinforced the suggestion that RNA analysis is an appropriate technique to consider in the analysis of body fluids within a forensic context. It can be seen from the extensive research in not only body fluid identification, but also age determination, that RNA analysis does meet the expectations of a method that is sensitive and tissue specific enough to definitively identify and estimate biological stain age since deposition. However, there are still inconsistencies in the results documented by numerous research groups. Particularly, no agreement has been observed in the selection of RNA markers to utilise as suitable candidates to measure changes in mRNA ratios over time. Where agreement is evident, the results differ amongst the research groups. It also needs to be taken into consideration that large error margins have been documented within the age estimation of body fluids. The inconsistencies and associated errors demonstrates that the use of mRNA analysis to determine body fluid age is not yet reproducible or reliable, which limits its adoption into forensic investigation within the near future. Furthermore, genetic analyses are expensive to carry out and involve complex sample preparation and data interpretation steps. These are disadvantaging to the prospect of application in the field as quick, efficient, simple methods are desired in the quest to establish a method for the age determination of body fluids.

1.3.2 CHEMICAL APPROACHES

1.3.2.1 HIGH PERFORMANCE LIQUID CHROMATOGRAPHY

The use of RNA methods has dominated the biological analysis aspect of determining body fluid age. However, a range of chemical techniques have also been explored in the quest to estimate the age of bloodstains. One of the first reported developments in the age determination of bloodstains using a chemical technique involved the use of HPLC (Inoue et al. 1992). HPLC, as described in Section 1.2.2, is a quantitative separation technique which is frequently utilised in the analysis of biological samples (Strachan & Read, 2011), although in

a forensic context it is typically utilised in the analysis of chemicals, such as drugs and poisons.

Inoue et al. (1992) deposited samples of whole blood on to filter paper which were air dried and stored under two conditions; fluorescent light and darkness, at three temperatures; 4°C, room temperature and 37°C. These samples were then stored up to one year before extraction and application to a HPLC column. The expected peaks of α-globin and haem, components of haemoglobin (Lehmann & Carrell, 1969), were observed and the corresponding peak areas demonstrated a decrease in size over time. However, an unidentified peak, labelled "X", at the retention time of five minutes was present in all samples, with the exception of fresh blood, and demonstrated an increase peak area over time. The ratio between the "X" peak and haem peak strongly correlated in a linear fashion with the bloodstains at all the analysed sample ages, regardless of sample storage conditions.

Following on from this research, Andrasko (1997) developed the HPLC method by comparing the method utilised by Inoue et al. (1992), referred to as system A, with a more sophisticated column system, system B. Blood samples were deposited onto cotton and filter paper which were stored at 0°C, room temperature and 37°C. These samples were stored up to one year for system A analysis and up to 60 days for system B analysis, prior to water extraction and analysis. The findings from system A analysis replicated those reported by Inoue et al. (1992). The unidentified peak "X" was present in dried blood samples, but not fresh, and the "X":haem ratio increased with sample age. The findings from system B analysis identified a further two peaks of interest, named accordingly as "Y" and "Z". "X", "Y" and "Z" were thought to be decomposition products of blood components. Andrasko (1997) reported that peaks "X" and "Y" were detectable at the retention times of 4.9 minutes and 9.9 minutes, respectively, when analysed at 220 nm. Peak "Z" was detectable at 6.3 minutes when analysed at 395 nm. The ratio of "X":haem and "Z":haem demonstrated the same exponential to linear increase correlating with sample age as stated by Inoue et al. (1992). This finding was reported for each of the temperature conditions examined. Ratios of the "X":"Y" and "Z":"Y" peaks also increased with bloodstain age. The "Y" peak appeared constant as after the first two days, the peak area of "Y" remained unchanged. However, this is based upon one analysis.

The benefits of the HPLC technique investigated by Inoue et al. (1992) and Andrasko (1997) are that it is reproducible and relatively easy to carry out. The results obtained by Inoue et al. (1992) have been successfully replicated and developed upon by Andrasko (1997) which indicates that HPLC has the potential to be utilised as a temperature independent method of determining bloodstain age. However, there are a number of limitations. Firstly, only small

sample numbers were used and few repeats were carried out. Larger sampling and repeat numbers are essential when establishing new applications of methods as they demonstrate that the findings are reliable and reproducible. In addition, only small volumes of extracted bloodstains were analysed due to the protein heavy components within blood which can impact on column separation and cause contamination during analysis (Andrasko, 1997). Alternative extraction methods could be utilised, although this may produce different results from those obtained by Inoue et al. (1992) and Andrasko (1997). Another limitation to be considered from both investigations was that the peaks utilised in determining time since deposition were not formally identified. Peak "X" (Inoue et al. 1992 & Andrasko, 1997) and "Y" and "Z" (Andrasko, 1997) were only detailed as decomposition products. Therefore, it cannot be confident that these peaks only appear in blood samples. Neither research group carried out comparative analysis on substrates known to have an appearance similar to blood once dried, or known to produce false positive results during presumptive testing. Also, it was not investigated whether the peaks of interest appear in any other body fluids, such as saliva or semen.

1.3.2.2 ELECTRON PARAMAGNETIC RESONANCE SPECTROSCOPY

As time and technology has progressed, the focus of techniques to determine bloodstain age has been directed towards spectroscopy. Since 2005, a variety of different spectroscopic methods have been applied in the pursuit of determining a method suitable for robust and routine use in the age estimation of bloodstains. Fujita et al. (2005) reported the use of electron paramagnetic resonance (EPR) spectroscopy in estimating bloodstain age when samples were aged to 775 days. EPR spectroscopy is a technique that detects unpaired electrons (Moore, 1968) and has been utilised within a multitude of disciplines. Fujita et al. (2005) made use of EPR spectroscopy to establish the time since deposition based on the denaturation of haemoproteins. Blood samples were deposited on to filter paper and gauze and were stored in quartz tubes under fluorescent light at 20°C and 25°C, darkness at 20°C and 40°C and direct sunlight.

The results obtained demonstrated signals corresponding to a variety of ferric (Fe^{3+}) species. The key species of interest were ferric haem species (g6), ferric non-haem species (g4), low-spin ferric haem species (H) and free radicals (R) (Fujita et al. 2005). The signals varied for each of the species over time and particularly in the older samples where the g4 signal increased, the H signal decreased and the g6 and R signals remained constant. This corresponds with ferric haem products decomposing to non-haem ferric products (g4) as sample age increases. High spin irons and radicals remained stable, in comparison to the low-

spin irons (H), as sample age increased. Based on these intensities, a ratio of the low-spin iron (H) to non-haem iron (g4) demonstrated a correlation with sample age over time with 25% error range. With this error range in mind, the approximate estimation for bloodstains aged to 133 days was 129 days ± 26, 432 days was estimated as 488 days ± 97 and 698 days was estimated as 835 days ± 236. When examining the effect of light and increased temperature on the bloodstains overtime, the ratio varied vastly suggesting that increased light exposure and temperatures can increase species decomposition, therefore making age estimation even less accurate.

Benefits to consider for this method of analysis include its non-destructive nature, which allows for additional analyses, such as DNA profiling, to be carried out. It has also demonstrated specificity, as specific haemoproteins were identified and the level of their denaturation could be measured. This highlights the potential for EPR spectroscopy to be utilised as an identification method for bloodstains. However, the major limitation of the method reported by Fujita et al. (2005) was the large error associated with estimating bloodstain age. In the investigation of crime, police forces want to know every minutia of event details, including specific timings where possible. An estimation of age error rate of 25% is not adequate in determining when bloodstains were deposited as it provides a possible margin as wide as a number of months.

1.3.2.3 ATOMIC FORCE MICROSCOPY FORCE SPECTROSCOPY

A different spectroscopic approach was taken by Strasser et al. (2007) which made use of atomic force microscopy (AFM) force spectroscopy. AFM is a form of scanning probe microscopy which enables the detection of atomic scale features on insulating surfaces (Blanchard, 1996). AFM force spectroscopy involves the probe coming into contact with the sample and being retracted to record the interaction measurements (JPK Instruments, 2014). In the research by Strasser et al. (2007), AFM force spectroscopy was utilised to measure age related changes in the elasticity of red blood cells (RBC's). Blood samples were deposited on to glass slides and were aged up to 31 days.

The results determined that no morphological changes took place between 1-31 days within the bloodstains when imaged with AFM. However, when coupled with force spectroscopy, AFM demonstrated that the elasticity of the erythrocytes decreased in correlation with sample age in bloodstains that were analysed immediately after drying, aged to 30 hours and 31 days. The benefits of AFM force spectroscopy are highlighted in its capability to image the sample at a very high resolution, up to 0.01 nm (Blanchard, 1996), at the same time as probing the bloodstains in a non-destructive manner. This allows for the maximum amount of

complimentary data, AFM measurements and high resolution images, to be obtained during analysis, as well as further analyses to be carried out if necessary. However, the limitation of AFM spectroscopy as a technique to determine the age of bloodstains is that is has low reliability. Strasser et al. (2007) openly discussed this limitation, stating that the results produced a high standard deviation and that the elasticity changes observed within the red blood cells could be due to the age of the blood cells. As RBC's have a lifespan of approximately 120 days, the elasticity and viscosity of each cell decreases with in vivo age (Strasser et al. 2007). Therefore, the observed decrease of RBC elasticity ex vivo could be a consequence of the RBC's point in their life cycle. A limitation to consider regarding the experimental methodology adopted by Strasser et al. (2007) is that only three time intervals were examined for bloodstain analysis with AFM force spectroscopy. RBC elasticity measurements taken at more frequent time intervals could have provided more data to show any potential correlation between elasticity decreases ex vivo and sample age.

1.3.2.4 NEAR-INFRARED SPECTROSCOPY

The use of visible spectroscopy in the age determination of bloodstains was first reported in the investigation of near-infrared (NIR) spectroscopy to examine the oxidative changes in the haemoglobin (Hb) fractions, deoxyhaemoglobin (deoxyHb) and methaemoglobin (metHb), over time (Botonjic-Sehic et al. 2009). NIR spectroscopy makes use of vibrational signals produced by molecules within the 680-3000 nm range of the electromagnetic spectrum (Workman, 2005). It is the bending and stretching vibrations of the functional groups –CH, -NH and –OH that provide measurements enabling a spectrum of bands or peaks to be produced (Edelman et al. 2012). Only a proportion of the NIR region was utilised by Botonjic-Sehic et al. (2009) which ranged from 1100-2500 nm. Human blood samples were deposited on to glass and gauze and then aged at room temperature for up to one month. Spectral measurements were taken periodically and spectra obtained within the first hour appeared to be dominated by bands representative of water.

Spectra obtained after one hour of ageing demonstrated bands within the 1800-2500 nm region and a single broad band between 1460-1860 nm. The broad band area increased exponentially during the first 50 hours of ageing, then reduced to a gradual increase from 50-300 hours, before reaching its maximum band area at approximately 500 hours. This band was representative of metHb, the oxidised counterpart of deoxyHb, which cannot bind oxygen efficiently ex vivo. Instead, metHb binds to water molecules (Botonjic-Sehic et al. 2009). The increase in the 1460-1860 nm band over time was indicative of the increase in metHb within the bloodstains. Cross validation of the 1460-1860 nm band areas over time of

three aged bloodstains determined a prediction standard error of 2.3 hours over 590 hours. This demonstrated that NIR spectroscopy has the potential to provide relatively accurate estimations of bloodstain ages.

Edelman et al. (2012) developed upon the work published by Botonjic-Sehic et al. (2009) by exploring the typical features of bloodstains detectable with NIR spectroscopy and quantitatively comparing these with spectral components detailed in literature. In particular, blood deposited onto coloured cotton backgrounds was examined using NIR spectroscopy to estimate bloodstain age. A comparative study was conducted with five different coloured cotton substrates (black, blue, green, red and white) upon which three bloodstains were deposited. The coloured background samples were aged to 28 days and the white cotton background samples were aged up to 77 days. Edelman et al. (2012) demonstrated that NIR spectroscopy could successfully identify all of the bloodstains deposited on coloured cotton backgrounds. However, the estimation of bloodstain age on coloured backgrounds was less successful. Using a partial least squared model, training sets from each of the bloodstains on the coloured backgrounds were produced to test each stain on each background. Bloodstains aged to short time intervals could be predicted with 8.9% error, although as the sample age increased, the accuracy of age prediction decreased. This was demonstrated for all of the bloodstains on all five different coloured backgrounds.

Botonjic-Sehic et al. (2009) and Edelman et al. (2012) both highlighted that NIR spectroscopy can successfully identify bloodstain components. It was highlighted that in comparison to other discussed techniques, NIR spectroscopy has a relatively low error prediction rate when estimating bloodstain age. Both of these benefits are of significance to the forensic community as NIR spectroscopy has shown great potential to provide confirmatory and complimentary intelligence information from bloodstains. In addition, NIR spectroscopy, like most spectroscopic techniques, has the potential to be portable, allowing analysis to be carried out directly at a crime scene. There is little to no sample preparation required when utilising NIR and it is a non-destructive method, which allows for further analyses to be carried out on the samples. The limitations demonstrated by Botonjic-Sheic et al. (2009) and Edelman et al. (2012) are demonstrated in the small sampling and ageing variables. Limited sample numbers were investigated within both research groups, which could account for the decrease in accuracy in age estimation as sample age increased. Alongside this, only short term ageing was performed, with the maximum sample age of approximately 2.5 months. In order to successfully predict bloodstain age, multiple repeats of a variety of short term and long term ages need to be explored.

1.3.2.5 ULTRA VIOLET/VISIBLE SPECTROSCOPY

Hanson & Ballantyne (2010) made use of ultra violet/visible (UV/Vis) spectrophotometry for the estimation of bloodstain age. UV/Vis spectrophotometry is also known as electronic spectroscopy (Housecroft & Constable, 2006). This form of spectroscopy detects energy absorption from the transition of molecules between energy levels within the UV/Vis region of the electromagnetic spectrum (Kemp 1991). Hanson & Ballantyne (2010) investigated the absorption spectral profile of haemoglobin in aged bloodstains. Bloodstains were prepared from aliquots of 50 µl of whole blood on to cotton cloth and aged at room temperature up to one year. Additional samples exploring the effects of temperature (-20°C, 4°C and 37°C) and humidity (50-90%) were deposited and aged up to one week. A set of bloodstains were also deposited on to cotton and subjected to three different environmental conditions which mimicked potential crime scenes; a rooftop, back seat of a car and a boot of a car. All mock scene samples were aged up to one week. When bloodstain samples were aged to the desired time interval, samples were subjected to extraction and UV/Vis spectrophotometry (Hanson & Ballantyne, 2010). Three peaks of interest were identified within all bloodstains analysed, namely the Soret band at approximately 410 nm, beta (β) globin at 541 nm and alpha (α) globin at 574 nm.

The results indicated that differences were observable in the UV/Vis spectra of the aged bloodstains. In particular, these differences were variation in the maximum absorption (λmax) of the Soret band (λmax_{Soret}), absorbance of β-Hb and α-Hb ratio and their comparisons with the minimum absorption (λmin) observed at 560 nm (Hanson & Ballantyne, 2010). However, these differences in absorption over time demonstrated no relationship with sample age. On the contrary, the position of the λmax_{Soret} was observed to shift towards the blue end of the UV/Vis spectrum in correlation with the increase in bloodstain age. Therefore, bloodstains could be differentiated from each other to indicate sample age based on the position of the λmax_{Soret}. The observed λmax_{Soret} shift towards a smaller wavelength is known as hypsochromic, or blue, shift (Kemp, 1991). The effect of increased humidity on the λmax_{Soret} demonstrated that as sample age increased, the hypsochromic shift decreased, with no shift observed in bloodstains exposed to 90% humidity. Hanson & Ballantyne (2010) also reported that as the exposure temperature increased, the hypsochromic shift was observed to increase rapidly in correlation with sample age. However, bloodstains exposed to -20°C demonstrated no significant change in the λmax_{Soret} across all the sample ages examined. This suggests that storage at -20°C halts the kinetic reaction that causes the variation in λmax_{Soret} over time. The bloodstain samples exposed to rooftop environmental conditions exhibited the greatest hypsochromic shift in the

λmax_{Soret}. However, samples could still be differentiated between from 15 minutes up to 7 days. The samples that were exposed to car environments (back seat and boot) were expected to demonstrate an even greater shift in the λmax_{Soret} than the rooftop samples, due to exposure to high temperatures. Contrastingly, these samples demonstrated a shift that lay between the bloodstains exposed to 37°C and the bloodstains exposed to the rooftop environment (Hanson & Ballantyne, 2010).

Hanson et al. (2011) developed the use of UV/Vis spectrophotometry in the age determination of bloodstains further with the examination of bloodstains deposited upon a variety of substrates. Whole blood was aliquoted in volumes of 50 µl on to cotton, denim, paper and polyester prior to ageing up to 3 months at 4°C, 22°C and 37°C. The results from this investigation demonstrated that the substrate upon which blood was deposited had no significant impact on the hypsochromic shift observed in the λmax_{Soret} of aged bloodstains. Additionally, the results correlated with those obtained from the earlier study (Hanson & Ballantyne, 2010) whereby the hypsochromic shift in the λmax_{Soret} increased with exposure to increased temperatures (Hanson et al. 2011). A benefit that can be perceived from the technique investigated by Hanson & Ballantyne (2010) and Hanson et al. (2011) is that substrates upon which bloodstains are deposited, such as paper and denim, do not hinder the analysis of age estimation. This is beneficial if the method is to be adopted for routine forensic analysis as bloodstains encountered at crimes scenes can be present on many different substrate types. Therefore, the application of UV/Vis spectrophotometry would not be limited to analysing bloodstains recovered from particular substrates. Hanson & Ballantyne (2010) reported that the mock case samples could be differentiated between each time interval and compared with the standard room temperature, aged samples. This is evident as a benefit to the application of UV/Vis spectrophotometry as it suggests that estimation of bloodstains can be predicted, if storage conditions of the sample are known. However, there are limitations to consider within the reported method. Firstly, this method requires sample preparation before any analysis can be carried out which is destructive to the original bloodstain and carries the risk of sample contamination if samples aren't handled appropriately. In addition, a full complement of calibration measures of bloodstain standards of known age and environmental conditions are required before any before biological evidence could be analysed.

1.3.2.6 DIFFUSE REFLECTANCE SPECTROSCOPY

Bremmer et al. (2011) took the age determination of bloodstains in a different spectroscopic direction with the use of diffuse reflectance spectroscopy (DRS). DRS is a technique routinely

utilised within medicine to determine the optical properties of tissues and fluids with a non-specular reflection of light (Bremmer et al. 2011). In this particular investigation, the fractions of haemoglobin (oxyhaemoglobin (HbO_2), methaemoglobin (metHb) and hemichrome (HC)) were quantified with multi-component spectral fits in order to assess the changes of these fractions over time. Forty bloodstains were deposited on to a single cotton cloth and aged up to 60 days, with a total of 1412 reflectance spectra obtained in the wavelength range 350-1050 nm. Initial measurements demonstrated that all haemoglobin present in the bloodstains was in the HbO_2 form. The level of HbO_2 was then observed to decrease as it converted to metHb and subsequently HC. Bremmer et al. (2011) described the rate of conversion of HbO_2 to its counterparts, metHb and HC, as rapid in the first ten days, with a substantial decline in conversion rate after ten days. This suggests that all the available HbO_2 had been auto-oxidised to metHb and subsequently denatured into the HC fraction (Marrone & Ballantyne, 2009). The quantity of metHb compared to HC remained lower, which also suggests the denaturation process to be rapid. The estimations of bloodstain age had a wide error margin. A margin of 1.5-6 days was predicted for a 3 day aged stain, 6-16 days predicted for a 12 day aged stain and a 25-55 day margin predicted for a 35 day aged bloodstain. Bremmer et al. (2011) stated that DRS could be useful in the age estimation of bloodstains under controlled conditions, although they also recognised that the variation that naturally occurs biologically can procure uncertainty within the measurements in age estimation.

The research conducted by Bremmer et al. (2011) was expanded upon by Li et al. (2011) with the underlying basis focusing on the exploration of haemoglobin fractions relative to bloodstain age. However, Li et al. (2011) made use of reflectance spectroscopy coupled with a microspectrophotometer (MSP) attachment. The method also incorporated data pre-processing to ensure the baseline shift did not affect the measurements, as well as selection techniques to minimise the variation between samples of the same age and increase discrimination between samples of differing ages. A total of three equine bloodstains were deposited on to white tile and aged up to 37 days. Measurements obtained consisted of the ratio between the bloodstain spectra and the white tile spectra. Ten measurements were recorded as datasets for each bloodstain. A further ten measurements were taken from only one bloodstain as a standard to test against the data sets. In comparison to the standard measurements, the spectral measurements obtained from the same bloodstain resulted in 100% accuracy in age estimation. However, when spectral measurements from different bloodstains were compared with the standard measurements, the accuracy in age estimation decreased to just 37.3%. Li et al. (2011) explain this dramatic decrease in accuracy as a result

of the white tile substrate not being flat when observed under MSP, causing spectral distortions.

The benefits of the DRS technique employed by Bremmer et al. (2011) and the reflectance spectroscopy with MSP utilised by Li et al. (2011) are demonstrated in their low cost and non-destructive applications. An additional benefit of the technique utilised by Li et al. (2011) is that MSP reflectance spectroscopy can be applied to bloodstain samples of any size. Therefore it is not limited to situations where analysis can only be carried out on bloodstains in high abundance. However, in this instance more limitations were evident when comparing the experimental methodologies adopted by both research groups. Bremmer et al. (2011) took only single measurements from the centre of each bloodstain upon each time interval analysis, whereas it is best practice to take multiple measurements from various different points within each bloodstain. This then allows for any potential intra-sample variation to be examined and accounted for, which could potentially highlight biological variations. In contrast, Li et al. (2011) took multiple measurements from various positions on the same bloodstains, but only used a total of three bloodstains. The decrease observed by Li et al. (2011) could also be a result of inter-sample variation. This could impact upon the estimation of age in bloodstains of differing ages when the training set is composed of measurements from only one bloodstain and then subsequently used for comparison. A further limitation that is applicable to both investigations is that in order to undertake this method to determine bloodstain age, a full understanding of reaction rates for each of the haemoglobin fractions is required. Additionally, knowledge of appropriate pre-processing and specific statistical analyses are required to be able to interpret the data generated from age determination analysis. Therefore specialist training would be necessary before any analysis could take place.

1.3.2.7 HYPERSPECTRAL IMAGING

Edelman et al. (2012a) continued exploring spectroscopic techniques as a method to estimate the age of bloodstains with hyperspectral imaging. Hyperspectral imaging makes use of specialised cameras that process information within the electromagnetic spectrum. It combines traditional spectroscopy and imaging, allowing spectral and spatial analysis to be carried out simultaneously (Edelman et al. 2012a). The fractions of Hb within bloodstains aged up to 200 days were investigated to determine whether a correlation between Hb fraction behaviour and time since deposition could be used to estimate bloodstain age. The region of the electromagnetic spectrum utilised was 500-800 nm to allow for the camera and light source to perform at their optimum (Edelman et al. 2012a). A reference bloodstain was

deposited on white cotton and imaged daily up to one month, followed by monthly analysis up to 200 days. The measurements collected from the reference stain acted as a training set for unknown samples to be tested against. A further five sets of bloodstains were obtained from different donors and deposited on white cotton before ageing to 0.1 (2.4 hours), 2, 15, 40 and 200 days. A simulated crime scene containing the aged bloodstains was analysed with the hyperspectral imager and estimations of absolute and relative age were conducted.

The results demonstrated that hyperspectral imaging could successfully distinguish between the Hb fractions of HbO_2, metHb and HC. As expected, the concentration of HbO_2 decreased as sample age increased, metHb concentration initially increased before decreasing and HC increased as sample age increased. The test sample bloodstains within the simulated crime scene were correctly assigned to the appropriate age, with the exception of the bloodstains aged 0.1 days which were assigned as 2 day old stains. When estimating absolute and relative age of bloodstains, Edelman et al. (2012a) reported that absolute error increased in correlation with sample age and the relative error margin was 13.4%. With this error margin in mind, a bloodstain aged to 2.8 days was estimated to be 2.2-4 days old.

The use of hyperspectral imaging in the age determination of bloodstains was developed further by Li et al. (2013), with the inclusion of spectral processing and feature selection already developed by the authors (Li et al. 2011). The subject of this method development also focused on the oxidative conversion of HbO_2 to its counterpart's, metHb and HC. The hyperspectral imaging analysis was conducted within the 500-600 nm range of the visible reflectance spectrum using a liquid crystal tuneable filter (LCTF) coupled with a complementary metal oxide semi-conductor (CMOS) camera (Li et al. 2013). Two equine bloodstains were deposited and smeared on to white paper and aged up to 30 days. A further two human bloodstains were deposited and smeared on to white paper and aged up to 21 hours. All bloodstains were stored at 30°C with 40% humidity in between analyses.

For both the equine and human bloodstains, one stain was utilised as a training set for the spectral processing and the other as a test set. A total of 310 measurements over 30 days were taken from each equine bloodstain. The measurements comprised of 5x5 pixel squares within the bloodstain spectral images which were extracted for processing and statistical analysis using a linear discriminate analysis model (LDA). Ratio measurements at 550 nm and 520 nm showed an increase and decrease, respectively, over time which correlated with the kinetics of HbO_2 and HC (Li et al. 2013). LDA analysis of the spectral images produced a correct classification rate (CCR) of 60.7% ±1.17 days, whereby the equine bloodstain test set data predicted age was the same as the actual bloodstain age. The LDA analysis CCR for the

human bloodstain test set was 94.6% ±0.09 hours. Li et al. (2013) reported that the LDA model was most accurate when ageing bloodstains up to seven days old and could be appropriate for analysis of bloodstains aged less than 14 days. However, as the bloodstain age increased, the accuracy of the LDA model, and therefore the accuracy in predicted age, decreased.

The primary benefit of hyperspectral imaging as a technique to determine bloodstain age is that it can simultaneously document and provide spectral data for bloodstains *in situ*. This enables complementary analysis to be carried out in any processing environment, whether that is at a crime scene or in a laboratory. As hyperspectral imaging is a spectroscopic technique, it has the additional benefits of no sample preparation and a non-destructive nature. The results presented by Edelman et al. (2012a) and Li et al. (2013) demonstrated that hyperspectral imaging can successfully differentiate and measure the fractions of Hb within dried bloodstains. Therefore, this technique could be appropriate as a confirmatory test for the presence of blood at crime scenes and upon evidential items.

A limitation of this technique is the high cost associated with the imager. Both Edelman et al. (2012a) and Li et al. (2013) reported error margins associated with the analysis, both of which were observed to increase with sample age. The cost associated with purchasing the equipment to carry out the technique is outweighed by the reliability of the method due to the rate of error associated with the analysis within an estimation context. Alongside this limitation, both research groups utilised only a very small number of bloodstains. Edelman et al. (2012a) has an advantage over Li et al. (2013) as a total of 6 different donors provided blood samples, although the number of bloodstains produced from each donor was not detailed. However, Li et al. (2013) investigated only 4 bloodstains in total, two of which were not human in origin. In order to address the potential variation produced within and between bloodstains, a great sample number of bloodstains should be investigated to ensure results are reliable.

It is evident from the literature that a plethora of typically chemistry-based techniques have been researched in order to establish a robust methodology for the age estimation of bloodstains. Spectroscopic methods have led the development in this research area, with traditional and coupled techniques being explored. Spectroscopic methods have common benefits to their application for age determination, in that little, or no sample preparation is required to analyse bloodstains. This maintains the integrity of bloodstains as biological evidence as additional analyses can be carried out without removing part of the sample or destroying it. The non-destructive nature of spectroscopic methods is hugely advantageous

within forensic and criminal investigations as the maximum amount of information can be obtained from bloodstain evidence, even from very small sample sizes. Furthermore, spectroscopic methods are thoroughly robust and have the potential to be portable, allowing for analysis of bloodstains to be carried out directly at crime scenes.

The limitations observed in the literature discussed lie more in the methodologies adopted by the research groups, rather than the methods utilised. For example, none of the chemical techniques discussed were examined in their application to estimate stain age of body fluids other than blood. This appears to be as a disadvantage as it limits the application of these spectroscopic techniques to age prediction of blood based evidence only. Additionally and most importantly, none of the techniques discussed could predict bloodstain age without a relatively large margin of error. This self presents a great limitation to the methods described as within forensic and criminal investigation accuracy and reliability are essential. The ability to identify a narrow window of time since deposition is the primary goal in age determination research. Therefore techniques that have a large error associated with them will not be suitable for development for routine analysis.

1.3.3 OTHER APPROACHES

In addition to the biological and chemical methods discussed above, there are other alternative methods of determining bloodstain age that are worthy of note. Arany & Ohtani, (2011) investigated a biochemical approach when investigating the age of bloodstains utilising aspartic acid racemization (AAR). Aspartic acid is a non-essential amino acid found within peptides and proteins which has two configuration forms, “L” or “D” (Pfeiffer et al. 1995). Racemization is a process that converts the configuration of living amino acids from “L” to “D” when no physiological renewal has taken place. This enables a ratio of “D”:”L” to be determined which can provide an indication as to when a biological sample was last regenerated, or living (Pfeiffer et al. 1995). Aspartic acid racemization has been successfully used within forensic science as a method of determining cadaver age from samples of tooth, bone and cartilage (Yekkala et al. 2006). Arany & Ohtani (2011) looked into the applicability of AAR as a method of estimating bloodstain age.

A bloodstain standard was produced from approximately 5ml of human blood that had been subjected to drying and pulverisation to form a powder. Total amino acid fraction measurements were carried out on the powdered blood and a series of heating experiments took place. Experimental samples of blood aged between one month and 20 years were

preserved on glass slides and stored at room temperature. All of the blood standards and experimental samples were derivatised prior to analysis with gas chromatography and the "D":"L" ratio of AAR was determined from the chromatograph peak areas. Arany & Ohtani (2011) analysed the results with an Arrhenius equation to determine the aspartic acid rate constant from racemization residues within the blood samples. A statistically significant correlation was identified between the rate of racemization within the blood samples and sample age, which demonstrated an increase over time. The authors also observed that the findings produced were similar to those obtained from protein fraction racemization carried out on tooth and bone tissues in chronological age estimation. This is one of the key benefits of the age estimation method adopted by Arany & Ohtani (2011) as it has produced comparable findings with an already established method utilised in a different context.

AAR has also demonstrated that is has the potential to not only be appropriate for the age estimation of bloodstains, but also other body fluid stains. This is advantageous in comparison to the previously discussed chemical techniques as none demonstrated applicability to any other body fluid type except blood. A limitation openly discussed by the authors was that only a small sample size was utilised within the investigation, despite ranging a large time frame. The inclusion of multiple samples of multiple ages would have strengthened the findings reported. Another limitation to consider for the AAR method is the in depth sample preparation involved. Not only do blood standards need to be produced, but samples must undergo derivatisation before separation analysis with gas chromatography. This is destructive to the sample and inevitably time consuming.

More recently, Thanakiatkrai et al. (2013) investigated an alternative approach to determining bloodstain age with the use of smartphones and digital imaging. The main focus of this research again exploited the oxidative reaction that occurs to haemoglobin within blood outside of the body. As the process of Hb decomposition occurs, the colour of blood and bloodstains converts from its characteristic bright red to brown. The brown colour is indicative of the HC fraction of Hb (Marrone & Ballantyne, 2009). Thanakiatkrai et al. (2013) examined whether this bloodstain colour change could be quantitatively detected with digital imaging. Blood samples were collected from four individual donors and deposited in volumes of 50 µl for analysis at various conditions. Specifically, the variables investigated were; type of smartphone (iPhone 4, iPad 2 and Samsung Galaxy S+), temperature (-20°C, 4°C and 25°C), humidity (30% and 50%), light exposure (direct sunlight, fluorescent light and darkness), the presence of anticoagulant (ethylenediaminetetraacetic acid (EDTA), heparin, none) and substrate type (denim, filter paper, glass, gypsum board, leather and white cotton). All of the samples utilised were aged up to 6 months. Upon sample analysis, 5 images of each

bloodstain were taken and the colour values of ten randomly selected pixels were pooled and averaged before analysis against four colour models with statistical analysis. The colour values termed as magenta (M) and saturation (S) showed the greatest correlation with sample age out of the four colour models. As bloodstain age increased, the M and S values decreased in a linear logarithmic decay pattern that mirrored the conversion of HbO_2 to HC.

Thanakiatkrai et al. (2013) reported that samples aged to six weeks and older did not demonstrate any further decrease in the M value. Highly accurate age predictions were obtained from bloodstains aged up to one day. However, the accuracy of age prediction decreased as samples grew older. In a comparison of smartphones, it was shown that iPhone 4 and iPad 2 devices were not suitable to estimate bloodstain age due to fluctuations observed within the M values obtained. The Samsung Galaxy S+ smartphone had the least fluctuations in M values and gave a 95% confidence interval in sample age predictions. As expected, temperature, humidity and light exposure impacted the colour change. In particular, Thanakiatkrai et al. (2013) found that after an hour of exposure to fluorescent light and darkness, bloodstain samples could not be distinguishable. Alongside this, the substrate type also affected the correlation of M values with sample age. It was reported that light coloured substrates demonstrated a high correlation, whereas dark substrates, such as denim, glass and gypsum board, had a very poor correlation. Overall, an age prediction error rate of 12% was observed in bloodstains aged up to 42 days.

Benefits to consider for the application of smartphones and digital analysis in the estimation of bloodstain age are that it is simple, cheap, rapid and portable. Nowadays, most people own a smartphone (Heggestuen, 2013), therefore it is highly likely that this method could be adopted routinely within forensic and criminal investigations. The concept of a method to determine bloodstain age, *in situ* and on a mobile device, is what police forces are looking for in today's "live-time" era (Association of Chief Police Officers. 2013) as it enables intelligence information to be produced quickly and efficiently. No specialist training would be required and it could easily be incorporated into the standard operating procedures of crime scene investigation. However, there are limitations to this technique. First of all, Thanakiatkrai et al. (2013) highlighted than iPhone 4 and iPad 2 were unsuitable for predicting bloodstain age due to the fluctuations of the M value. Approximately 51 million iPhones and 26 million iPads were sold in the period between October and December 2013 (Etherington, 2014). Therefore there is a possibility that iPhones and iPads are already utilised by police forces and forensic scientists during criminal investigations, but these would not be deemed as suitable to utilise in age determination analysis. This issue could be overcome with the constant improvement in smartphone technology, or with the development of an application that can be used on any

smartphone, whereby images from an appropriate camera could be uploaded to the application and the analysis is then undertaken. Another aspect of this methodology that proves as a limitation is that age estimation could only be predicted with 12% error rate in bloodstains aged to a maximum of 42 days. The article reports that samples were aged up to six months, which equates to approximately 182 days. Therefore only 23% of the aged dataset were successfully predicted.

The other methods discussed here demonstrate the vast range of possible avenues that have been explored in the age determination of body fluids. It is imperative to be aware of alternative analyses that can aid in age determination and both aspartic acid racemisation (AAR) and the use of smartphones and digital imaging have demonstrated proof-of-concept. However, little development has since been conducted within either area that has been reported. Additionally, comparisons with the well-established RNA and spectroscopic approaches highlight that there is a great requirement for age estimation techniques to be accurate and reproducible. It is evident that neither AAR nor smartphones and digital imaging have the capabilities of achieving these characteristics without further development and validation.

1.4 THE RESEARCH QUESTIONS

1.4.1 SIGNIFICANCE OF THE RESEARCH & ORIGINAL CONTRIBUTION TO KNOWLEDGE

The Silverman Report (Silverman, 2011) recommendations have changed the face of forensic science and the way in which forensic research is conducted. It has actioned police forces and forensic practitioners to address the challenges faced in the investigation of crime, in addition to recognising the value in collaboration between each other, academic institutions and other external partners. As a result of the Silverman Report recommendations, the Forensic Science Special Interest Group (ForSci SIG) was formed and a challenges database was set up. This database contains the current challenges in areas of forensic science and crime scene investigation that need to be addressed in order to evolve with current and future technologies and science that can be utilised in the investigation of crime (Technology Strategy Board, 2011). This research can be considered as addressing some of the body fluid analysis challenges stated by the ForSci SIG in areas of identification, such as:

- "Can we develop non-destructive screening methods?"
- "Can we improve the specificity of body fluid identification?"

In addition to improving the analysis of body fluid identification, there is an evident niche to be filled in the accurate determination of the age of body fluids since their deposition. At present, there is no official documentation, such as the Silverman Report or the Live-Time Forensics document (Association of Chief Police Officers, 2013), that states the requirement to establish how old body fluid stains are when encountered at crime scenes. However, often in serious crime there are instances where the inclusion or exclusion of evidence can be justified if it was known how old body fluid stains were. A conversation with A. Coombes of Derbyshire Police on Tuesday 7th October 2014 described the murder of a male in a property where four people, including the victim, were residents. Blood spatter was concentrated to the primary location where the body was found, although blood spatter was also present in a fine mist by the front door where no activity related to the crime was evident. The investigating officer had to justify the exclusion of the blood spatter as evidence due to the inconsistency of its location in relation to the crime. However, A. Coombes stated that if it was possible to determine whether that particular blood spatter was older than the other blood spatter at the crime scene, the decision to exclude it would have been objective rather than subjective.

The case explained above and the number of publications that have sought to address this area of forensic investigation demonstrates how great the need is to be able to determine the age of body fluid stains and how imperative it is for the method to be accurate. The findings from this research could contribute to both of these key development areas of forensic and criminal investigation. It is also hoped that the statistical approach to reinforce the significance of the findings can aid in the future progression of incorporating better body fluid identification and age determination protocols into routine forensic analysis.

1.4.2 JUSTIFICATION OF METHODS

The techniques employed during this research were attenuated total reflectance Fourier Transform Infrared (ATR-FTIR) spectroscopy and protein analysis involving sodium dodecyl sulphate polyacrylamide gel electrophoresis (SDS-PAGE). The rationale behind the choice of ATR-FTIR spectroscopy as a method to identify body fluids and determine body fluid age lies in the benefits associated with the technique, as discussed throughout Section 1.2. Of all the spectroscopic techniques, the least focus has been directed at ATR-FTIR spectroscopy as a tool for biological analysis within forensic science. However, ATR-FTIR spectroscopy has been demonstrated as a diagnostic tool within the biomedical science profession (Jackson & Mantsch, 1995; Kazarian & Chan, 2006; Ollesch et al. 2013; Wood et al. 1998). It is for these reasons that the application of ATR-FTIR spectroscopy to body fluid identification and age determination was investigated.

The rationale for the choice of protein analysis involving SDS-PAGE as a method to identify body fluids and determine body fluid age is that it is not commonly utilised within forensic science. Protein analysis with mass spectrometry has shown potential as a method of definitively identifying body fluids for forensic purposes. However, the cost involved in analysis using mass spectrometry and the sample preparation required lends itself as unsuitable within forensic science. However, SDS-PAGE has been demonstrated as a complementary technique to mass spectrometry in the detection and separation of proteins within biomedicine (Nicholson et al. 2005; Vitorino et al. 2004) which results in a simpler and more cost effective approach. Therefore, it is for these reasons why the application of protein analysis involving SDS-PAGE as an investigative biological analysis for forensic evidence is to be explored in body fluid identification and age determination.

1.4.3 AIMS & OBJECTIVES

The aims of this research are:

- To investigate the use of alternative forensic techniques in the application of body fluid identification in order to establish a robust, confirmatory and cost effective method.
- To establish a suitable technique that can be utilised to determine the age of body fluid samples since deposition as currently there is no routinely utilised method within forensic investigation.

In order to address these aims, the following objectives were addressed:

- To explore the use of ATR-FTIR spectroscopy as a non-destructive technique to successfully distinguish body fluids from one another in order to determine body fluid stain source.
- To examine the applicability of ATR-FTIR spectroscopy as a technique to determine the age of body fluid stains that had been aged for pre-determined time intervals up to 18 months.
- To assess the use of protein analysis involving SDS-PAGE as a detection technique to successfully distinguish body fluids from one another in order to determine body fluid stain source.
- To study the applicability of protein analysis involving SDS-PAGE as a technique to determine the age of body fluid stains that had been aged for pre-determined time intervals up to 7 days.
- To compare the success of ATR-FTIR spectroscopy and protein analysis involving SDS-PAGE in the definitive identification of body fluids and age determination.

2. FOURIER TRANSFORM INFRARED SPECTROSCOPY I:

INTRODUCTION, MATERIALS & METHODS

2.1 INTRODUCTION

Fourier transform infrared (FTIR) spectroscopy is routinely utilised within forensic science in the analysis of drugs, chemicals, paints and fibres (Bartick, 2002). However, its application to biological evidence has not been well documented within the forensic community. This chapter provides an introduction to the background of FTIR spectroscopy, the previous applications with body fluid samples and the methodology utilised within this research.

2.1.1 VIBRATIONAL SPECTROSCOPY

2.1.1.1 ELECTROMAGNETIC RADIATION

Electromagnetic radiation is an energy form that consists of electric and magnetic oscillating motions that move perpendicular to one another and to the direction of travel (Figure 2.1). Electromagnetic radiation is often considered as waves of differing frequencies and lengths travelling at the same speed in a vacuum (Levine, 1995).

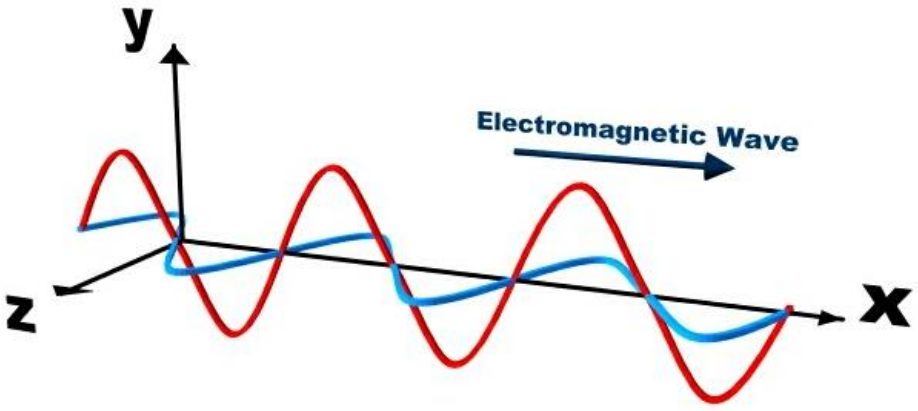

Figure 2.1: Example of electromagnetic radiation demonstrating the electric oscillating wave (red) and magnetic oscillating wave (blue) (Swinburne University of Technology, 2014).

The wavelength (λ) of the electromagnetic radiation wave is the distance between the peaks of the same orientation, which can also be described as one full oscillation. The frequency (ν) of the electromagnetic radiation wave refers to the number of oscillations that occur per unit of time and is commonly reported in units of s^{-1}, which defines the frequency unit as one reciprocal second of one hertz (Hz) (Levine, 1995). The time taken for one complete wavelength cycle to travel past a given time unit is inversely proportional to 1/ν. To determine the frequency of electromagnetic radiation the following equation can be utilised:

$$\nu = \frac{c}{\lambda} \qquad \textit{(Equation 2.1)}$$

where c is the constant, referring to the speed of the wave, which is equal to the speed of light. Within infrared spectroscopy, the detection of electromagnetic radiation waves is often recorded as wavenumber ($\tilde{\nu}$) units which are reciprocals of wavelengths that can be calculated by:

$$\tilde{\nu} = \frac{1}{\lambda} \qquad \textit{(Equation 2.2)}$$

The wavenumber of electromagnetic radiation waves are commonly expressed as cm^{-1} as it refers to the number of wave cycles within 1 cm (Griffths & De Haseth, 2007; Levine, 1995). Electromagnetic radiation encompasses a range of different energies, or wavelengths, which can be characterised by specific frequencies and wavelengths. The range of electromagnetic radiation is separated into differing regions that correspond to specific wavelength ranges (Figure 2.2). Electromagnetic radiation of low energy has long wavelengths with low amplitude, whereas electromagnetic radiation of high energy has short wavelengths of high amplitude (Crowe & Bradshaw, 2010). Spectroscopy is an analytical tool that makes use of the electromagnetic spectrum to investigate chemical components. Infrared spectroscopy in particular, utilises electromagnetic radiation to measure behavioural changes of molecules within the infrared region. The behavioural changes correspond to molecular vibrations which have absorbed the infrared radiation (Banwell & McCash, 1994). The infrared region itself can be further separated into three spectral ranges; near (12,500-4000 cm^{-1}), mid (4000-400 cm^{-1}) and far infrared (400-10 cm^{-1}). The most utilised region of infrared radiation is the mid-infrared, particularly in biological and biomedical applications (Garidel & Schott, 2006a).

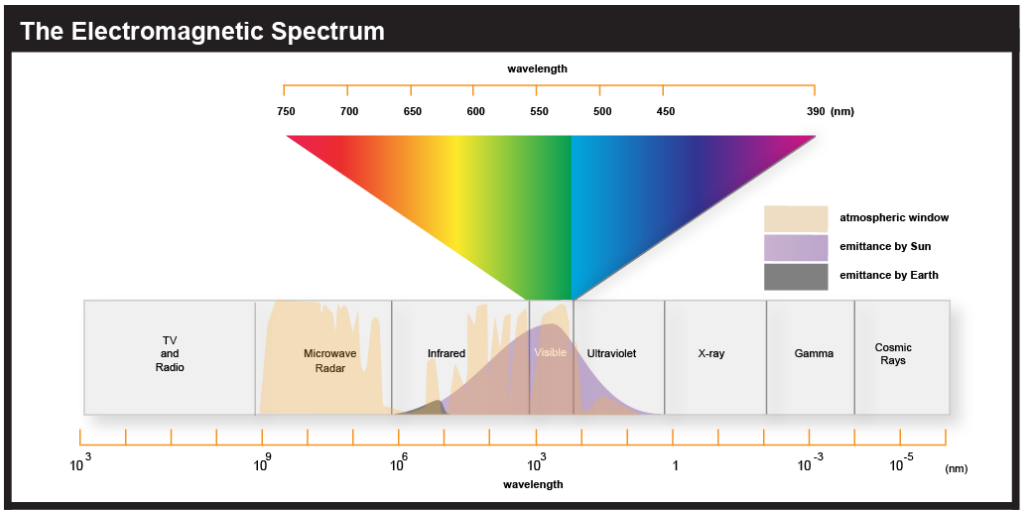

Figure 2.2: Example of the electromagnetic spectrum (The Pennsylvania State University, 2014).

2.1.1.2 INFRARED VIBRATIONAL SPECTROSCOPY

Vibrational spectroscopy can be categorised into two techniques; FTIR spectroscopy and Raman spectroscopy. Each of these techniques irradiate samples with light from different regions of the electromagnetic spectrum to observe the spectral characteristics of different components that have absorbed the energy (Crowe & Bradshaw, 2010). Raman makes use of monochromatic light within the visible, near-infrared and near-ultraviolet regions of the electromagnetic spectrum, whereas FTIR utilises light from the infrared region (Housecroft & Constable, 2006). Infrared spectroscopy in particular, detects the energy absorptions of chemical bonds that vibrate at specific wavelengths or frequencies when irradiated with infrared light (Crowe & Bradshaw, 2010). The vibrations of covalent bonds between molecules refer to slight movements across the molecules that result in a change in dipole moment. It is the change in dipole moment that gives rise to observable infrared spectra as the vibrational frequency interacts with the radiation (Banwell & McCash, 1994). The vibrations of molecules can vary from the simple motion of diatomic coupled atoms to complex polyfunctional molecules where each atom is in motion (Griffiths & De Haseth, 2007).

The number of vibrational modes any given molecule can have can be determined by a simple calculation; a molecule of N atoms has 3N degrees of freedom which refer to the position of each atom within three perpendicular axes (x, y and z). This, in essence, fixes the atoms in place, allowing the molecule to move around in three-dimensional space as a whole. Translational movement, that is the shifting of the molecule within space, makes use of three of the degrees of freedom. Rotational movement, the movement of a molecule about an axis,

takes a further three degrees of freedom. Both translational and rotational motion occurs across the x, y and z axes. The only remaining motion that a molecule can make is vibration and the number of vibrational modes for a non-linear (Eq. 2.3) and linear molecule (Eq. 2.4) can be determined as:

$$Non\text{-}Linear\ Molecule\ Vibrational\ modes = 3N - 6 \qquad (Equation\ 2.3)$$

$$Linear\ Molecule\ Vibrational\ modes = 3N - 5 \qquad (Equation\ 2.4)$$

Linear molecules have one less degree of freedom due to there being no rotational motion along the bond axis of the molecule itself, which is observable in infrared spectra (Banwell & McCash, 1994; Griffiths & De Haseth, 2007). This is due to there being no change in dipole moment when a linear molecule rotates along this axis.

There are several variations of bond vibrations, known as vibrational modes and Banwell & McCash (1994) define a vibrational mode as the motion of atoms within a molecule that all oscillate at the same frequency and pass through equilibrium positions simultaneously. Within infrared vibrational spectroscopy only three main vibrational modes are encountered; symmetric stretching, symmetric bending and asymmetric stretching (Figure 2.3). Symmetric bending and stretching vibrations within molecules can be described as those that do not change if the molecule is rotated 180° (Banwell & McCash, 1994). Specifically, a symmetric stretching vibration involves alternating stretching or compression of the molecular bonds. When the stretch vibration is symmetric, it is often infrared inactive, in that it is not detectable as there is no change in the dipole moment of the molecule (Griffiths & De Haseth, 2007). A symmetric bending vibration is a result of equal change in the angle of the molecular bonds. An asymmetric stretching vibration is described as one where the oscillation of the atoms within the molecule become opposite, or antiphase, to its original position when rotated 180°. In particular, this refers to the motion of one bond stretching whilst another compresses and vice versa (Banwell & McCash, 1994). Both symmetrical bending and asymmetrical stretching vibrational modes are infrared active as there are periodical alterations to the dipole moments of the molecules.

The frequency of each vibrational mode differs between the symmetry and vibration type. Symmetric vibrations have the higher frequency of the two symmetries, of which symmetric stretch vibrations have the highest. This is due to the motion requiring more energy than the other vibrational modes and is often labelled as ν_1. Symmetric bending vibrations have a lower frequency than symmetric stretches and are noted as ν_2. Asymmetric stretching

vibrations have the lowest frequency of the vibrational modes and are termed ν_3 (Banwell & McCash, 1994).

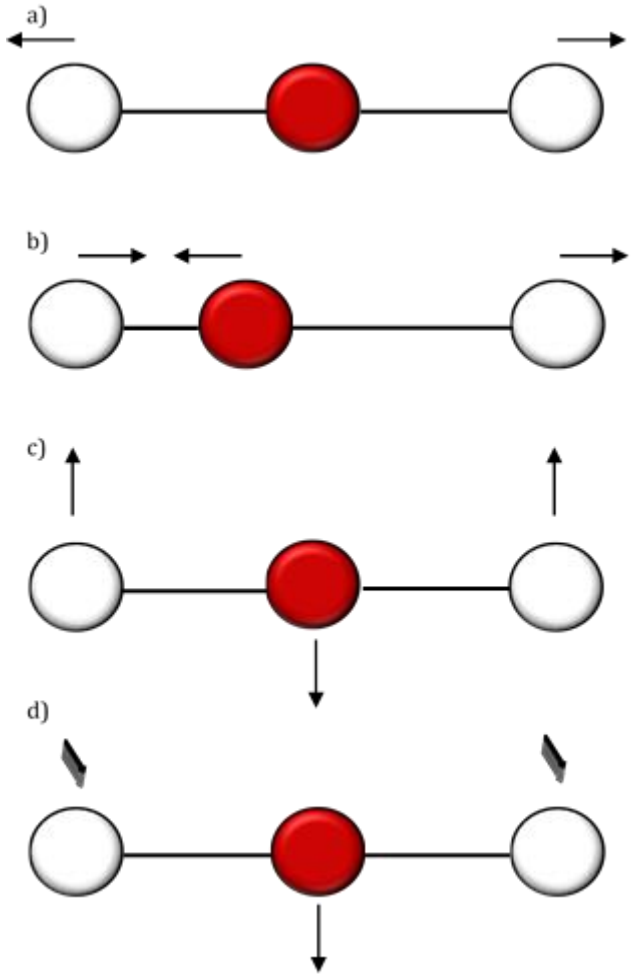

Figure 2.3: Vibrational modes of covalent bonds, a) symmetric stretching, b) asymmetric stretching, c) symmetric bending in plane & d) symmetric bending out of plane.

There are two types of bending modes, in plane and out of plane and these are only encountered within linear molecules. In plane refers to the motion of all the atoms within the molecule bending in the same dimension, whereas out of plane bending is where some of the atoms bend in a different dimension to the rest of the bending atoms. For example, Figure 2.3d demonstrates an out of plane bend with the two outer atoms bending perpendicular to the innermost molecule which is bending downwards. Except for the direction of the bending motion, both in plane and out of plane bending vibrations are identical, although are considered as separate molecular motions. These types of vibrations are referred to as degenerate and give linear molecules an additional vibrational mode (Banwell & McCash, 1994; Griffiths & De Haseth, 2007).

As the vibrational modes of molecules exhibit different frequencies, they therefore exhibit different vibrational energies which are constrained to a discreet number of frequencies, or quantized. The atoms within a molecule become displaced from their equilibrium position when the bond length is compressed or extended, much like the motion of a spring (Banwell & McCash, 1994). The harmonic oscillating motion of a bond can be approximated by Hooke's law (Eq. 2.5), where *F* is the force, *k* is the force constant and *x* is the bond displacement.

$$F = -kx \qquad \textit{(Equation 2.5)}$$

The potential energy of each harmonic oscillation is a function of atomic displacement and for any vibrational mode the vibrational energy state (V_{iv}) can be determined by:

$$V_{iv} = h\nu_i \, (\nu_i + ½) \qquad \textit{(Equation 2.6)}$$

where h is the Planck's constant, ν_i is the fundamental frequency of the vibrational modes and ν_i is the vibrational quantum number of the ith mode (ν_i = 0, 1, 2…) (Griffiths & De Haseth, 2007). The vibrational energy states and transitions for atoms in harmonic oscillation can be seen in Figure 2.4a. Within infrared spectroscopy, the transition of vibrational modes from ground state (ν_i = 0) to the first excited state (ν_i = 1) occurs within the mid-infrared region and creates a change in dipole moment. However, molecules do not follow harmonic oscillation and atomic displacement is anharmonic (Figure 2.4b) (Banwell & McCash, 1994; Griffiths & De Haseth, 2007). This is due to there being a point at which a bond will break when it is stretched and the molecule disassociates into atoms. Any bond stretch that is less than 10% of the bond length will demonstrate harmonic oscillation, whereas a vibrational motion that causes a stretch greater than 10% of the bond length causes the molecule to behave in a more complicated manner (Banwell & McCash, 1994). Anharmonic oscillation enables the transition of atoms between vibrational frequencies at levels greater than ±1. Depending on the vibrational mode, all atoms within a molecule can exhibit displacement to the same level, or only a small number of atoms will exhibit vigorous displacement.

The vibrational modes of covalent bonded molecules can be categorised as either skeletal or group vibrations (Banwell & McCash, 1994). Skeletal vibrational modes are those that experience large displacement of many atoms and can be utilised to distinguish between compounds of similar structure. The frequency of such vibrations are often observed in the 1400-1700 cm^{-1} range of the mid-infrared spectrum (Griffiths & De Haseth, 2007). Group vibrational modes of molecules only feature the large displacement of atoms, whereas the rest of the molecule remains stationary. This enables the observation of specific functional

groups of a molecule within specific regions of the infrared spectrum based on the frequency at which these vibrational modes displace atoms (Banwell & McCash, 1994).

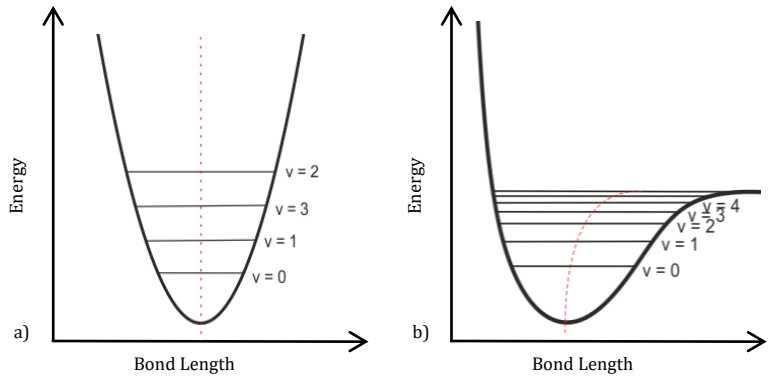

Figure 2.4: Harmonic (a) & anharmonic (b) oscillation of the vibrational energies of atoms within a molecule (adapted from University of Liverpool, 2013).

The vibrational motion of functional groups allows molecules to be distinguished from one another, even if they contain the same or similar functional groups. These vibrational modes tend to be independent from the overall molecular structure and can be observed on either side of the skeletal vibrations. It is seldom possible to assign specific spectral peaks to specific vibrational modes. However, an atomic change within the molecule can produce a different vibrational frequency, therefore a different characteristic peak is observed within the representative spectra. These minor changes to molecular composition are referred to as fingerprint peaks and they are often observed within the 1500-400 cm^{-1} region of the infrared spectrum. They are named so, as structural moieties and molecules can be recognised based on these alterations within the infrared spectra and the overall spectra are absolutely characteristic of the sample as a whole (Banwell & McCash, 1994; Housecroft & Constable, 2006).

2.1.1.3 FTIR INSTRUMENTATION

The development of the Fourier transformation (FT) by Jean Baptise Joseph Fourier in the early 1800's has led to being one of the most ubiquitous mathematical tools utilised within science in the current age (Thummalapalli, 2010). FT is a mathematical process that can resolve complex waves of energy into frequency components and is often incorporated into digital algorithms within computer software to enable the visualisation of molecular component vibrations, such as with FTIR spectroscopy (Banwell & McCash, 1994). The basic instrumentation of a FTIR spectrometer consists of a light source, Michelson interferometer, sampling area and a detector. The light source is often a helium-neon (HeNe) laser which has

a known frequency of approximately 5 kHz and is the source of the incident beam of infrared radiation that is utilised to examine the vibrational components within samples under analysis. The incident beam is split into two by the interferometer, which is composed of a beam splitter and two mirrors, one of which is fixed and the other moves in a back and forth motion at a constant velocity (Garidel & Schott, 2006; Griffiths & De Haseth, 2007).

The beam splitter is an infrared transparent plate that is coated in a reflective material which reflects only 50% of the incident beam directed towards each mirror. Upon the return reflection from each mirror, the incident beams travels back to the beam splitter and is recombined to a single beam before travelling to the detector. As one of the mirrors is moving, the optical path distance, also referred to as the optical path difference, travelled by both mirrors is either identical or different. Upon reflection of the incident beam from both the fixed and moving mirror to the beam splitter, the relative optical path difference can be determined by the observation of constructive and destructive interference (Banwell & McCash, 1994). Constructive interference is evident when the optical path difference is zero or when both beams are in phase, demonstrating that the path difference is an integral number of wavelengths. This interference type is observed by the presence of high amplitude peaks, whereas destructive interference is observed by the presence of low or diminished amplitude. This is due to the optical path difference of both incident beams being half-integral numbers of wavelengths and the two beams being out of phase from one another (Banwell & McCash, 1994; Griffiths & De Haseth, 2007). It is the recombined incident beam of infrared radiation that is directed on to the sample within the sampling area directly from the beam splitter. After sample interaction, the beam passes on to the detector and the intensity of the incident beam is measured which indicates the optical path difference for the moving mirror (Garidel & Schott, 2006a). The most common detectors utilised in FTIR spectrometers are deuterated triglycine sulphate (DTGS) and mercury cadmium telluride (MCT).

Based on the intensity of the incident beam after sample interaction, the transmittance, that is the proportion of the infrared radiation passed through the sample, can be determined by Beer-Lambert's Law (Griffiths & De Haseth, 2007). The basis of Beer-Lambert's Law is that absorption intensity is dependent on the amount of sample present for any given compound and that the absorbance (A) of radiation by a sample is related to transmittance (T):

$$A = -\log (T) \qquad \textit{(Equation 2.7)}$$

The transmittance of radiation from any given sample is expressed as the ratio of the intensity of the radiation emerging from the sample (I) to the intensity of the initial radiation (I_0) (Housecroft & Constable, 2006):

$$A = log \frac{I_0}{I} \qquad (Equation\ 2.8)$$

Often in FTIR spectroscopy, the samples are contained within a cell or pellet of known dimensions. Utilising Beer-Lambert's Law, the radiation absorption can be determined based on the molar coefficient of the sample component (ε), which is a property independent of the sample compound concentrations, the path length (l) of the radiation through the cell in dm^3 mol^{-1} cm^{-1} and the concentration (c) of the sample in units of mol dm^{-3} (Banwell & McCash, 1994; Housecroft & Constable, 2006):

$$A = log \frac{I_0}{I} = \varepsilon\ c\ l \qquad (Equation\ 2.9)$$

2.1.1.4 ATTENUATED TOTAL REFLECTANCE FTIR SPECTROSCOPY

Attenuated total reflectance FTIR (ATR-FTIR) spectroscopy has overtaken the traditional transmission mode as the most widely utilised technique of infrared spectroscopy. The application of ATR-FTIR spectroscopy is practiced in many scientific areas for the analysis of chemical and biological systems within biomedicine, chemistry, forensic science and pharmaceuticals (Jackson et al. 1997; Szafarska et al. 2009; Wartewig & Neubert, 2005; Zeng et al. 2014). The increased application of ATR-FTIR spectroscopy is due to there being little or no sample preparation required, unlike transmission FTIR spectroscopy. This is advantageous as it enables the analysis of samples in any phase; solid, semi-solid, liquid and adsorbed on to a substrate (Garidel & Schott, 2006a).

ATR-FTIR spectroscopy differs from transmission FTIR spectroscopy as the radiation of infrared light does not penetrate through a sample. Instead, it is internally reflected when a sample is placed in contact with an internal reflection element (IRE), enabling the spectrum of the sample surface to be observed. Internal reflection of infrared light is a result of Snell's law (Eq. 2.10) whereby the incident angle (θ_1) at which radiation is passed between two materials of different refractive indices is refracted (θ_2) (Griffiths & De Haseth, 2007).

$$n_i\ sin\ \theta_1 = n_2\ sin\ \theta_2 \qquad (Equation\ 2.10)$$

The material with the higher refractive index is the IRE and is referred to as the optically dense material (n_i). It is the higher refractive index material in which the infrared radiation travels through, therefore the material of the IRE must be transparent to infrared radiation (Banwell & McCash, 1994). The material with the lower refractive index is the sample and is referred to as the optically rare material (n_2) (Griffiths & De Haseth, 2007). When the angle of

incident radiation reaches the critical angle (θ_c), or is greater than θ_c, the beam of infrared light will reflect internally in the material of the higher refractive index and the reflection angle of the infrared light will equal that of the angle of incidence (Garidel & Schott, 2006a). During this process, an evanescent wave is produced by the electromagnetic field of photons. This field extends into the optically rare sample rather than the IRE, as the wave travels perpendicular to the direction of radiation. The decay of the evanescent wave as it extends into the sample is exponential with the increase in distance from the optically dense IRE and its rate of decay is dependent of the radiation wavelength (Griffiths & De Haseth, 2007). The depth of penetration (d_p) of the evanescent wave is the distance at which it can interact with the optically rare sample effectively. This can be approximated by the distance from the IRE where the evanescent wave strength decays exponentially from its intensity from the IRE surface (Griffiths & De Haseth, 2007). The depth of penetration can be calculated based upon the refractive index of the optically dense and rare materials, the angle of incidence and the wavelength (λ) of the radiation (Eq. 2.11). The depth of penetration ranges between instruments and IREs, although the typical range is between 0.2-5 μm (Garidel & Schott, 2006a; Kazarian & Chan, 2006).

$$d_p = \frac{\lambda}{2\,\pi\, n_1 \sqrt{\sin^2\theta - (n_2 / n_1)^2}} \qquad \textit{(Equation 2.11)}$$

The actual depth of penetration of infrared radiation into a sample varies from that of the calculated value, as the calculated value is, at best, an approximation of the effective depth of penetration (d_e). The value of effective penetration depth is the sample thickness when analysed by transmission spectroscopy that is required to correspond to the absorption in ATR-FTIR spectroscopy (Griffiths & De Haseth, 2007).

The IREs utilised in ATR-FTIR spectroscopy allow multiple internal reflections to occur based on their geometry and take the form of either a parallelpiped or trapezoidal prism (Figure 2.5). The infrared radiation beam enters the prism at a 90° angle which minimises the loss of reflection as the beam enters and exits the IRE (Griffiths & De Haseth, 2007). Multiple internal reflections within the IRE improve the sensitivity of the technique as the absorption of vibrating components is increased, although the depth of penetration does not alter. The increase in absorption improves the quality of the ATR spectra obtained for minor components within a sample (Griffiths & De Haseth, 2007).

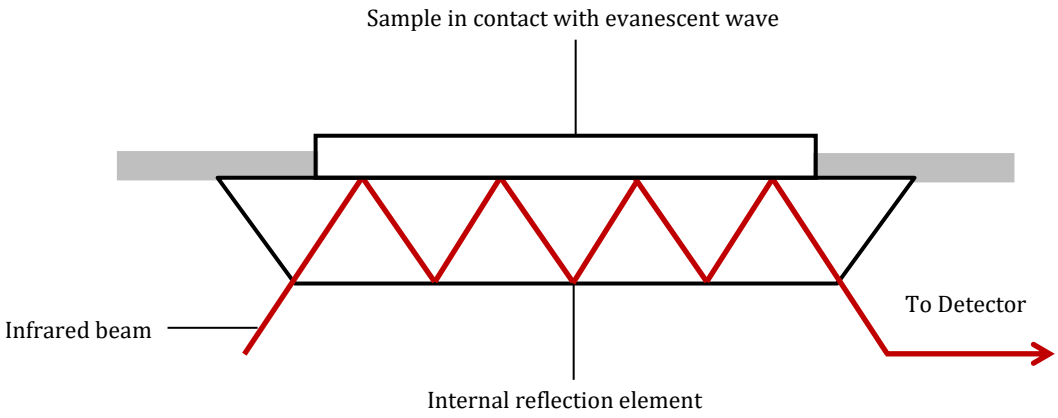

Figure 2.5: Example of trapezoidal ATR-FTIR internal reflection of infrared radiation.

The IRE is often referred to as a crystal and it should have a critical angle as high as possible when in contact with the sample in order to achieve internal reflection. The most common IRE materials are zinc selenide (ZeSe) and germanium (Ge), although diamond and silicon have been demonstrated to have practical uses in protecting the IRE from damage and when utilising ATR-microscopy, respectively (Griffiths & De Haseth, 2007). Most organic materials have a refractive index of 1.5, therefore based on this refractive index the critical angles can be determined for the IRE materials (Table 2.1).

Table 2.1: Most common ATR internal reflective element refractive index & critical angle when $n_1 = 1.5$ (Griffiths & De Haseth, 2007).

IRE Material	RI (n_1)	Critical Angle (θ_c)
Diamond	2.41	40
Germanium	4.00	22
Silicon	3.41	26
Zinc selenide	2.40	40

Unlike transmission spectroscopy, ATR-FTIR spectroscopy can analyse samples in their neat state, therefore samples do not require any preparation and the technique is non-destructive. This enables samples to be analysed *in situ* and in vitro, in some cases, leaving the sample effectively unaltered (Jackson et al. 1997). This technique provides an ideal alternative to sample preparation methods that affect the morphology of samples through grinding or melting, such as would be utilised during transmission spectroscopy. As a result, the spectra

obtained from ATR-FTIR spectroscopy are representative of the structural characteristics of samples that have not undergone morphological alteration (Griffiths & De Haseth, 2007).

When analysing samples with ATR-FTIR spectroscopy, complete contact must be made between the sample and the IRE in order for the resulting spectrum to be representative of the sample only. Any contaminant or impurity that has contact with the IRE, or is present within the depth of penetration of infrared radiation will be detected and will be present within the spectrum produced from the analysis scan (Griffiths & De Haseth, 2007). To overcome this, many ATR accessories include a clamp, or anvil, to secure samples in place during analysis, which is of particular use when analysing samples in powdered form. However, if the sample does not cover the IRE completely, the rubber padding on the bottom of the anvil will also be detected and represented within the resulting sample spectrum (Griffiths & De Haseth, 2007). Therefore, it is important that the sample is large enough to cover the IRE and that sufficient contact between the sample of interest and the IRE is maintained during analysis to avoid spectral interference from the atmosphere or contaminating substrates.

2.1.2 PREVIOUS APPLICATIONS WITH BODY FLUIDS

FTIR spectroscopy is routinely utilised within biomedicine for diagnostic purposes. It has been well documented that FTIR spectroscopy offers a non-invasive, quick and thorough alternative to traditional clinical analyses for the detection of diseases, such as cancers and diabetes, and drug delivery (Coutts-Lendon et al. 2003; Gazi et al. 2003; Scott et al. 2010). The FTIR spectroscopic analysis of biological samples enables the characterisation of specific molecules, functional groups and biochemical composition within given environments as a whole. This further enables spectral differences to be distinguished between tissue and cell types that may contain the same or similar vibrational frequencies (Wood et al. 1998). There is an abundance of literature spanning specific disease detection and diagnosis from human and animal cells, tissues and fluids (Huleihel et al. 2005; Ollesch et al. 2013). However, within the scope of this research area, the particular interest of biological FTIR spectroscopy lies in its application to human body fluids, specifically blood, saliva, semen and vaginal secretions, and their components.

Blood is incredibly useful within the clinical diagnosis of illness and disease as its cellular components can reflect any pathological or physiological changes present within tissues (Kanagathara et al. 2011). Various studies have been documented identifying spectral

components that can be utilised to differentiate between the blood of healthy individuals and the blood of individuals with particular diseases (Huleihel et al. 2005; Mostaço-Guidolin & Bachmann, 2011; Sitole et al. 2014). Gunasekaran & Sankari (2004) examined the FTIR spectra of healthy blood serum samples compared to blood serum samples recovered from individuals with high levels of glucose, cholesterol, urea and thyroid hormones. The spectral characteristics of the healthy and abnormal blood samples contained the same components, with particular dominance from protein absorptions. However, at a quantitative level spectral differences were observed in the relative concentrations of the absorption peaks (Gunasekaran & Sankari (2004). The examination of spectral differences was carried out at four intensity ratio parameters which corresponded to specific vibrational mode absorptions of glucose, lipid methyl groups, lipid phosphate and proteins. The ratios determined for blood serum samples of high glucose levels were higher than that of the healthy blood sera, whereas the remaining abnormal samples exhibited ratios lower than those determined for healthy blood samples. The results obtained by Gunasekaran & Sankari, (2004) demonstrate that, although the absorption features of healthy and abnormal blood spectra are similar, quantitative measurements can be obtained and utilised in the screening for abnormal levels of glucose, cholesterol, urea and thyroid hormones. This could then indicate the requirement of further clinical analysis to confirm diagnosis.

Work conducted by Mostaço-Guidolin & Bachmann (2011) further demonstrates how blood constituents can be examined with FTIR spectroscopy to differentiate between healthy peripheral blood mononuclear cells (PBMCs) and human leukaemia T-cells based on changes within biochemical markers. Again, the spectral characteristics of the healthy and diseased samples shared common absorptions corresponding to the key cellular components, such as lipids, nucleic acids and proteins. However, displacement was observed within almost all of the absorptions, with leukemic T-cells shifting in wavenumber. In order to verify the peak displacements, internal standards were selected to normalise the spectra. Peak area ratios were then determined to assess the score associated with particular macromolecules in relation to each other. Particularly, Mostaço-Guidolin & Bachmann (2011) utilised ratios of protein:protein, protein:DNA, protein:lipids and lipids:DNA, for which the scores obtained for leukemic T-cells were significantly higher than those obtained for the healthy PBMCs. The peak displacement observed, in combination with the peak area ratios, enabled differentiation between the healthy and diseased samples. These results demonstrate that FTIR spectroscopy can play a significant role in the identification of biochemical injury which can be utilised to assist clinical diagnosis of disease.

The collection of blood samples is often commented as being invasive and requires specially trained phlebotomists to obtain volumes adequate for clinical analysis. Saliva has, in recent years, been seen as an alternative body fluid which can be tested for diagnosis of diseases such as diabetes (Yoon et al. 2004). Scott et al. (2010) examined the potential detection of diabetes in saliva utilising FTIR spectroscopy. As diabetes is considered as multifactorial, FTIR spectroscopy is an ideal tool for analysis as the whole of the molecular content of a sample is examined and therefore comparisons can be made between healthy and diabetic saliva samples to identify any disease specific alterations in the obtained spectra. Scott et al. (2010) reported that variation was observed between saliva spectra of healthy and diabetic samples, with alterations observed in the protein components, amide I and II, the lipid ester group and carboxyl bands. These alterations enabled a training and test set to be analysed by linear discriminant analysis (LDA) where 100% sensitivity, specificity and predictive values were obtained for the training set and 90.9% sensitivity and 88.2% accuracy values were obtained for the test set (Scott et al. 2010).

The successful differentiation between healthy and diabetic saliva samples with FTIR spectroscopy has highlighted the universal application of the technique to varying body fluids, as well as demonstrating potential as a screening tool prior to clinical testing for diabetes. The scope of FTIR spectroscopic analysis of body fluids for biomedical application does not focus solely on the complete molecular composition of the samples, but also can be utilised to examine specific spectral features that can be characteristic of particular disease or health state. An example of this is the research conducted by Schultz et al. (1996), whereby the quantification of thiocyanate levels in human saliva was explored to establish the degree at which oral cellular debris and food affect thiocyanate detection. Thiocyanate is present in the mouth as an antibacterial agent and increased levels in saliva have been connected to smoking. It has been found to absorb within the infrared spectrum in a region where no other salivary components absorb (Schultz et al. 1996). FTIR spectra were recorded for saliva prior to and after centrifugation to determine the component of saliva where thiocyanate is most detectable. Schultz et al. (1996) reported that after centrifugation, very low levels of thiocyanate were detectable in the pellet with FTIR spectroscopy, whereas higher levels were observed in the supernatant. Additionally, dialysis of the salivary pellet yielded no thiocyanate absorption at all, suggesting that it is only loosely bound to salivary components. Further comparative analysis demonstrated that the peak area of the thiocyanate absorption peak correlated with the concentration of thiocyanate anions in saliva and that salivary levels of thiocyanate expression follow a circadian rhythm. The results reported by Schultz et al.

(1996) also highlight the specificity of the technique in detecting a body fluid compound that has no observed overlap from other molecular vibrations.

From an alternative biomedical perspective, FTIR spectroscopy can also provide insight into the assessment of male fertility. Traditionally, computer assisted semen analysis (CASA) and light microscopy are utilised to determine the morphology and motility of spermatozoa (Gilany et al. 2014). However, FTIR spectroscopy has been demonstrated as an alternative tool that has the potential to provide diagnosis of human reproduction dysfunction. Barcot et al. (2007) examined the FTIR spectra of seminal fluid and spermatozoa separately to establish the spectral characteristics contributed from each component of semen. As with all the body fluids, spectral characteristics were observed that corresponded to abundant categories of macromolecules. However, the position and shape of the associated peaks varied between body fluids, therefore tissue and cell types could be differentiated. The peaks observed for the nucleic acid vibrations in the spermatozoa spectra demonstrated the most variation in comparison to the seminal fluid spectra. This was believed to be a result of spermatozoa DNA being very different from cellular DNA and in order to verify this, a peak area ratio was developed (Barcot et al. 2007). A comparison with blood and cervical cell spectra confirmed that the nucleic acid peak area ratio of spermatozoa spectra could be utilised to distinguish between these fluids. Further differences observed between the spermatozoa and seminal fluid spectra were the peak intensity ratios of phospholipids, with spermatozoa yielding a ratio much lower than the seminal fluid, and the observed reduction in peaks within the fingerprint region of the seminal plasma infrared spectrum (Barcot et al. 2007). To assess the motility of spermatozoa with FTIR spectroscopy, a ratio of the relative volume of nucleic acid content to protein content was examined. A linear relationship was observed, whereby increased DNA but low protein content resulted in better motility and decreased DNA and high protein content resulted in reduced motility. The results demonstrated by Barcot et al. (2007) highlight the usefulness of FTIR spectroscopy outside of disease diagnosis and its potential for application as a corroborative technique to those traditionally utilised in the assessment of male fertility.

Within FTIR spectroscopic analysis of biological samples, it is important to be aware of the potential incorrect assignment of molecular components, especially when numerous cell types are present within the sample. Wood et al. (1998) considered this potential limitation in the spectroscopic screening of cervical tissue for malignancies. Cytological smears from the cervical area contain an abundance of different cell types, including endo and ecto cervical epithelia, erythrocytes, leukocytes and thrombocytes, bacteria, semen and on occasion the synthetic threads and bristles from the sampling implement. Wood et al. (1998) examined the

infrared spectra of all the possible cell types and contaminants that may be present in a cervical smear, in addition to malignant cervical cells and how the spectral characteristics vary from those of healthy cervical cells. The findings reported that healthy and abnormal endocervical cell spectra showed no obvious variation, although healthy endocervical and ectocervical cells could be differentiated from one another. Ectocervical cell spectra also differed from the abnormal cell spectra, with the abnormal cell spectra exhibiting an increased intensity of the amide II peak in comparison to the healthy ectocervical cell spectra (Wood et al. 1998). An overlap in spectral characteristics was observed in leukocyte spectra and abnormal cell spectra, particularly in the phosphodiester region. However, the peak intensities observed in the leukocyte spectra were reduced compared to the abnormal cell peak intensities. Erythrocyte spectra also demonstrated an overlap in the phosphodiester region, with reduced glycogen band intensity, although erythrocytes could be readily distinguished from the cervical cells based on the spectral characteristics corresponding to phosphates. Overall, Wood et al. (1998) reported that many of the cell types and potential contaminants analysed exhibited overlap in the obtained FTIR spectra. However, the overall combination of characteristic peaks, as well as the peak intensities of these characteristics enabled each of the samples to be differentiated from one another.

It has been demonstrated here that it is important to be aware of all the possible contributors to a biological sample and to ensure that correct spectral assignment is made so that misdiagnosis is avoided. Additional research into the utilisation of FTIR spectroscopy of cells located from the vagina undertaken by Chiriboga et al. (1997) focused on the differentiation of the various cervical cell types which could aid in the screening of abnormal cervical cell diagnosis. Chiriboga et al. (1997) examined the spectral differences between basal layer and superficial layer squamous epithelia and columnar epithelia originating from the exocervix and endocervix, respectively. Squamous epithelia are mature cells which migrate to the surface layer prior to surface exfoliation. These cells are often highly glycogenated and this was observed within the FTIR spectra of these cells. It was possible to differentiate the mature, superficial squamous cells from both the basal layer squamous cells and the columnar cells, which both lacked the characteristic glycogen peak (Chiriboga et al. 1997). Columnar cells could still be differentiated from the basal layer squamous cell spectra due to a distinctive broad peak and weak shoulder peak which were representative of mucus. Chiriboga et al. (1997) suggested that the observation of what appears to be basal layer squamous epithelia within a sample of exfoliated cervical cells could indicate an underlying abnormality. This highlights the importance of understanding where spectral characteristic

differences are exhibited in samples with similar molecular components and how these can be utilised to determine whether further clinical analysis is required.

It can be seen from the variety of research discussed that FTIR spectroscopy has far reaching applications within biomedical research. The main benefit that can be perceived it is that FTIR spectroscopy is an ideal tool for screening samples prior to any costly and complex clinical analysis. This would allow the quicker processing of pre-diagnostic tests and would ensure that resources weren't wasted as only samples that appear abnormal will be taken forward for further testing. Additionally, the research areas discussed have demonstrated that FTIR spectroscopy is not just a qualitative analysis, but with the application of appropriate ratios and statistical analysis, quantitative measurements can be obtained that correlate with the concentration of the molecular components of interest. The clear benefits here indicate the potential for appropriate application of FTIR spectroscopy within the forensic analysis of body fluids in order to establish the body fluid source or sample age.

2.2 MATERIALS & METHODS

2.2.1 SAMPLE COLLECTION & STORAGE

Human blood, saliva, semen and vaginal secretions were the body fluids examined within this research. All samples were collected from healthy volunteers who had provided full consent prior to any samples donated.

Blood samples were collected using the finger prick method using an Accu-Chek Safe-T-Pro Plus lancet (Roche, Australia). The blood was collected directly with an automatic pipette, ready for analysis or blood deposition.

Saliva samples were collected in sterile, screw-top tubes. Participants were asked to not eat or drink anything, with the exception of water at least one hour before providing saliva samples. Saliva was then obtained from "spitting" into the tube.

Semen samples were collected by self-masturbation at 7 day intervals to ensure consistency in the composition of semen across all samples. The samples were deposited in to sterile, screw-top tubes.

Vaginal secretion samples were collected using a Softcup (Venkataraman et al. 2005). Participants were asked to wear the Softcup for a minimum of one hour prior to donating samples. Upon removal, the Softcup was placed into a sterile beaker and two collection methods were utilised to obtain the vaginal secretions from the collection vessel. A sterile, small spatula was used to scrape all the secretions around the Softcup into a pool at the bottom most part of the 'cup'. The vaginal secretions could then be aliquoted via automatic pipette. Alternatively, when the vaginal secretions were too viscous in composition to be collected in their neat state, 200 µl of sterile, double distilled water (diH_2O) was added to the Softcup and thoroughly mixed with the vaginal secretions. This allowed the vaginal secretions to be aliquoted for analysis.

Samples were collected for two types of analysis; identification using neat body fluids and age determination whereby the body fluids were deposited on to sterile, 100% white cotton cloth. For identification analysis, body fluid samples were collected and deposited in a single volume of 20 µl on to the analysis stage. Samples collected for age determination analysis were deposited on to the cotton substrate in volumes of 20 µl for blood, semen and vaginal secretion samples and aliquots of 100 µl were deposited for saliva samples. The cotton was

contained within sterile petri dishes, which were consequently placed into evidence cardboard boxes (33 x 24 x 4.5 cm). Each cardboard box held 8 samples, and all boxes were placed into storage in a dry, secure environment at room temperature in accordance with the Human Tissue Act (2004).

Within the Human Tissue Act (2004) it states that body fluids cannot be stored in their whole state for longer than 48 hours without the appropriate Human Tissue Licence. In order to age samples of body fluids older than 48 hours, storage of samples took place at The Institute of Science and Technology in Medicine (ISTM) at Keele University, under the licence number 12349, as Staffordshire University does not hold a Human Tissue Licence. A Human Tissue Authority human cell log proforma was completed for all body fluid samples that were deposited for age determination. This ensured the continuity of all samples.

2.2.2 ATR-FTIR ANALYSIS

All samples were analysed using the Nicolet 380 Fourier Transform Infrared (FTIR) Spectrometer with a Smart Orbit, diamond crystal attenuated total reflectance (ATR) accessory and EZ Omnic (v7.4) software (Thermo Nicolet Corporation, United States of America).

Instrument diagnostics were run prior to any sample analysis which included a desiccant test, performance test and diagnostic checks of the interferrogram, laser, voltage and current. Following diagnostic checks, an atmospheric background scan was run initially to ensure instrument was working correctly and then background scans were run where appropriate, depending on whether identification or age determination analysis was being carried out. The ATR-FTIR stage was cleaned with diH_2O in between background scans and individual samples.

All samples were scanned 32 times per analysis at 4 cm^{-1} resolution within the 400-4000 cm^{-1} infrared region. The measurement format utilised was %Reflectance with data spacing at 1.929 cm^{-1}.

FTIR spectroscopy was used to produce a chemical “fingerprint” of the biological materials to identify common peaks that could be utilised to determine identity and age based on the biological and chemical components within each body fluid. Different analytical approaches were undertaken for body fluid identification analysis and age determination analysis. The methodologies for these analyses are detailed below (Sections 2.2.2.1 and 2.2.2.2).

2.2.2.1 IDENTIFICATION METHOD

Blood, saliva, semen and vaginal secretions were analysed with ATR-FTIR in their neat state, with no background substrate upon which the sample was deposited. All body fluid samples were collected fresh and analysed immediately where possible. An aliquot of 20 µl of a fresh body fluid sample was deposited directly on to the clean ATR-FTIR analysis stage. ATR-FTIR measurement scans were performed upon immediate deposition on to the analysis stage. Following immediate analysis, further ATR-FTIR scans were carried out at pre-determined time intervals until the sample was completely dry. The pre-determined time intervals utilised for all neat identification analyses were; 10, 20, 30, 45 and 60 minutes, 2, 3, 4 and 5 hours after deposition. The sample remained on the analysis stage until the measurement scan at 5 hours was completed and due to this atmospheric background scans could not be obtained during analysis. Instead, a background scan was performed prior to the deposition of the neat body fluid for every sample. The background scan was then saved and used as a specified background throughout the sample analysis. The spectra obtained from each of the analyses were assigned peak information relating to peak position and intensity.

2.2.2.2 AGE DETERMINATION METHOD

Blood, saliva, semen and vaginal secretion samples utilised for age determination analysis were analysed with ATR-FTIR in a dried state. In particular, each body fluid sample was deposited onto cotton and then placed in to storage for pre-determined time intervals to allow the samples to age. Specific pre-determined time intervals were utilised for age determination analysis and differing time intervals were examined for each body fluid type. Table 2.2 provides an overview of the time intervals investigated.

Table 2.2: Overview of ageing timescale for blood, saliva, semen & vaginal secretion samples.

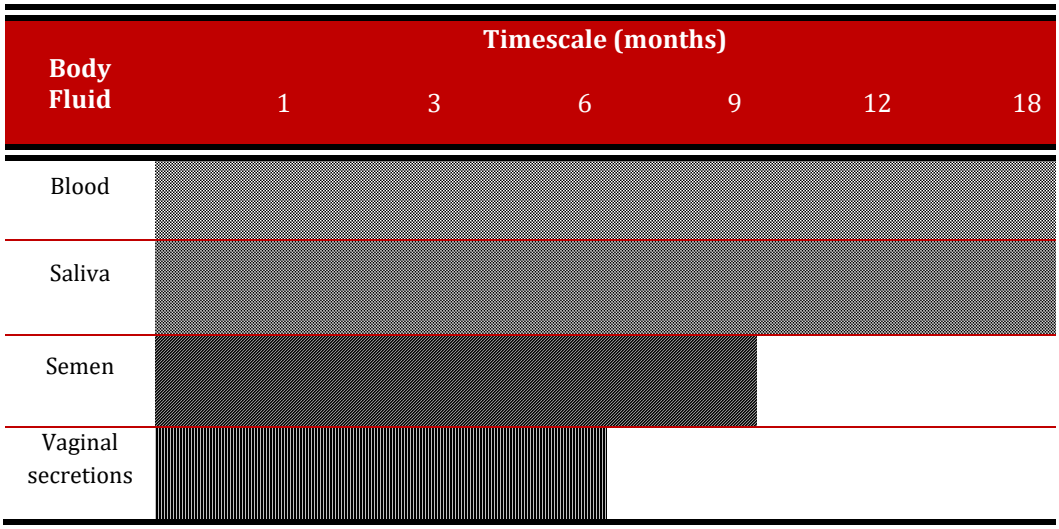

The specific pre-determined time intervals utilised for the ageing of blood and saliva samples were; 24 hours, 48 hours, 3, 4, 5, 6, 7, 14, 21 days, 1, 2, 3, 6, 12 and 18 months. Semen samples were aged for; 24 hours, 48 hours, 3, 4, 5, 6, 7, 14, 21 days, 1, 2, 3, 6, 8 and 9 months. Vaginal secretion samples were aged for; 24 hours, 48 hours, 3, 4, 5, 6, 7, 14, 21 days, 1, 2, 3, 4, 5 and 6 months.

ATR-FTIR analysis was conducted on the body fluid samples when the samples had aged to the desired time interval. Two methods of analysis were utilised for aged samples, direct and extracted. For direct analysis, the dried body fluid stain on a cotton sample was placed on to the clean analysis stage and secured with the anvil. ATR-FTIR measurement scans were completed in five different areas of the sample (Figure 2.6), one of which was an area of the cotton substrate known to not contain any of the body fluid. Atmospheric background scans were performed before and in between samples and the analysis stage was cleaned with diH_2O.

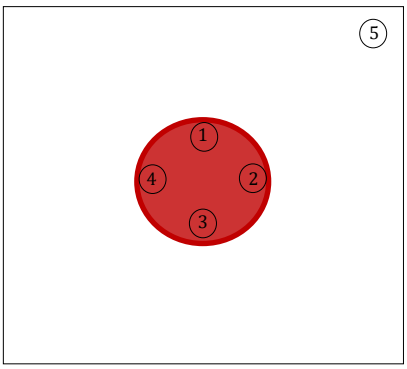

Figure 2.6: Example of analysis points within a dried body fluid stain deposited on cotton, such as blood.

Extracted analysis involved the dried body fluid stain being cut from the cotton and placed into a sterile Eppendorf tube. A volume of 100 µl of diH_2O was added to the tube, followed by vortexing for two minutes. This process was repeated once and the cotton removed. The sample extract was then analysed as per the identification method, in that a 20 µl aliquot of the extract was placed on to the clean ATR-FTIR analysis stage and measurement scans were carried out immediately, followed by scans at 10, 20, 30, 45 and 60 minutes. In circumstances where the sample had not dried within 45 minutes, an additional measurement scan was performed at 75 minutes after deposition. As the sample could not be removed during the analysis time, an atmospheric background scan was run prior to extract deposition and then saved and utilised as a specific background. For both direct and extracted analysis, the spectra obtained from each of the analysis points were assigned peak information relating to peak position and intensity.

2.2.3 STATISTICAL TOOLS

All statistical analysis of data was carried out with Microsoft Excel and IBM SPSS Statistics (v22). Simple statistical techniques were utilised in order to establish whether differences could be identified within the body fluid spectra that could enable discrimination with ATR-FTIR.

Body fluid identification analysis examined ratios of peak intensities corresponding to specific macromolecules commonly identified within all four body fluids (Table 3.11). This was to establish whether neat, stain and extracted blood, saliva, semen and vaginal secretion spectra could be discriminated from each other. Where multiple donors were examined in the bloodstain identification data, statistical analysis consisted of; the Kolmogorov-Smirnov (KS) test for normal distribution, the Kruskal-Wallis test (non-parametric) to identify differences in the peak frequency data, and pair-wise comparative follow up analysis to identify where significant differences (at a p value of < 0.05), if any, were amongst the peak frequencies between the donors.

Age determination analysis of the body fluid spectra utilised both peak frequency and peak ratio comparisons to assess whether discrimination could be achieved between the different sample ages examined.

3. FOURIER TRANSFORM INFRARED SPECTROSCOPY II:

BODY FLUID IDENTIFICATION RESULTS & DISCUSSION

ATR-FTIR spectroscopy is a physiochemical analytical technique that has been widely used within biomedical science to examine and identify biomolecule components and structures. All human tissues, cells and body fluids contain biomolecules which can be differentiated from one another by their unique structures (Olsztynska-Janus et al. 2012; Petibois et al. 2001a). FTIR and ATR-FTIR spectroscopic techniques produce spectra containing bands, or peaks, representative of the vibrations of structural bonds and functional groups within biological samples. The positioning of the peaks are specific to particular interactions with molecular bonds and provide specific information relating to the biochemical composition (Movasaghi et al. 2008). Therefore, the spectra produced are unique to the sample type.

Neat analysis of blood, saliva, semen and vaginal secretions utilising ATR-FTIR spectroscopy was conducted in order to determine the vibrational spectra of each body fluid and the detectable components present within each body fluid type when examined in the infrared region of the electromagnetic spectrum. Spectral analysis of biological samples, such as body fluids, can be divided into three major modes (Figure 3.1). These modes are; lipids, which absorb within the 3000-2800 cm^{-1} region of the infrared spectrum; proteins, which absorb within 1700-1600 cm^{-1} and 1560-1500 cm^{-1}; and nucleic acids which absorb within the 1250-1000 cm^{-1} region (Olsztynska-Janus et al. 2012). Peaks within these regions can then be assigned to specific components relevant to the sample type and the observation of any additional peaks can be utilised to characterise the biological material. For all forensic body fluid identification analyses, a 'wet-to-dry' approach was undertaken. This involved placing the body fluid sample in its neat state directly on to the analysis stage of the FTIR instrument and performing measurement scans as the sample dried *in situ* (Section 2.2.2.1). The peaks observed from the measurements collected upon immediate analysis after deposition and over a period of 5 hours demonstrated the peaks of interest that could be attributed to the body fluid only, as no interfering substrates or solutions were introduced to the sample. For

all four body fluid types, ATR-FTIR measurement scans of the wet samples produced spectra that were representative of water (Figure 3.2).

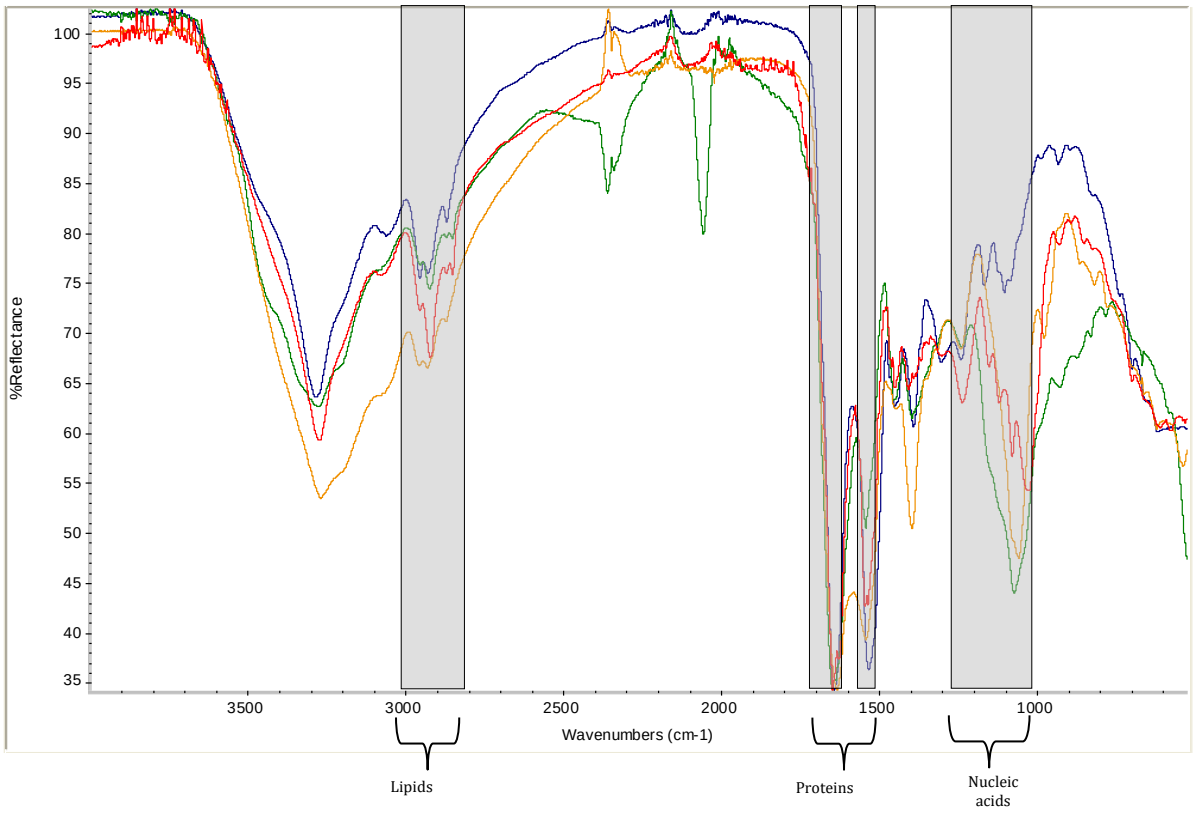

Figure 3.1: Example of FTIR spectral regions for the major vibrational modes of lipids, proteins & nucleic acids in biological samples.

The 'wet-to-dry' approach was utilised in order to determine the spectra of each body fluid type both in wet (liquid) and dry (solid) states. It is evident in the ATR-FTIR spectra of the wet body fluids in Figure 3.2, that when the samples are in a liquid state no characteristic peaks are detectable to enable differentiation between the body fluids. This is due to water being a strong absorber within the infrared region, with peaks representative of O-H stretching and H bonded O-H bending vibrations at approximately 3300 cm^{-1} and 1640 cm^{-1} respectively, which dominate the body fluid spectrum (Chittur, 1998). This limitation of FTIR spectroscopy is well documented and has been deemed problematic as the 1640 cm^{-1} region of water absorption overlaps with the protein absorption region, therefore masking any protein absorptions that may be present within the sample (Hassler et al. 2011; Kong & Yu, 2007). However, in the investigation of protein structure, the addition, or presence of water within a sample is preferable to alternative solutes, such as deuterium oxide (D_2O). In particular, D_2O can cause a shift in the protein absorption peaks observed in FTIR spectra, as

well as altering the secondary structures of the proteins within the sample (Kong & Yu, 2007).

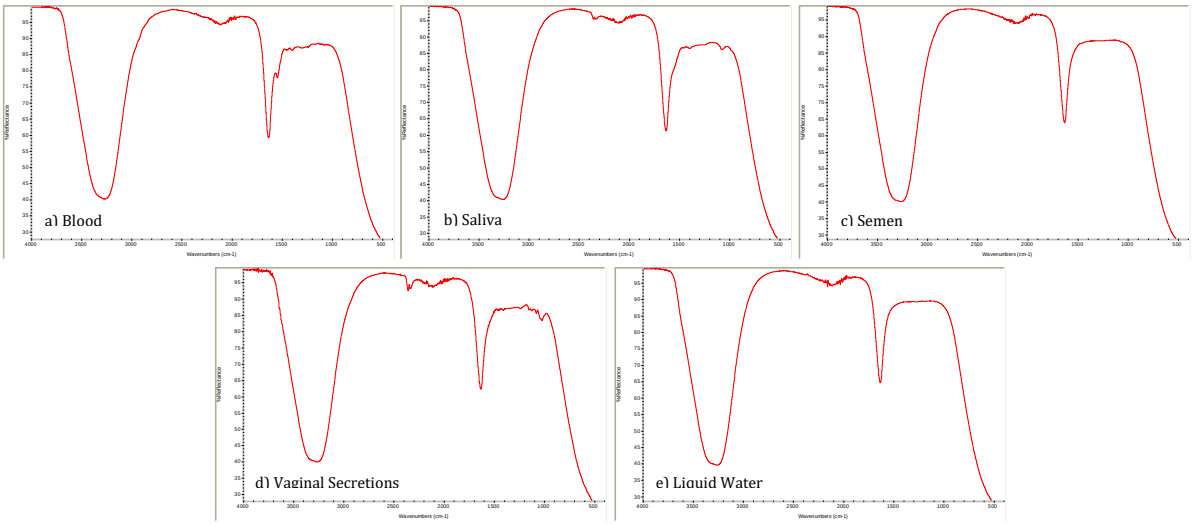

Figure 3.2: FTIR spectra of neat body fluids when wet; a) blood, b) saliva, c) semen, d) vaginal secretions & e) liquid water.

When the body fluid samples had dried and the liquid content had evaporated, the ATR-FTIR spectra contained peaks that were representative of the appropriate sample components. The position of the peaks observed were utilised to identify the biological components and functional groups present and the combination of peaks observed allowed for each body fluid type to be distinguished from one another (Figure 3.3).

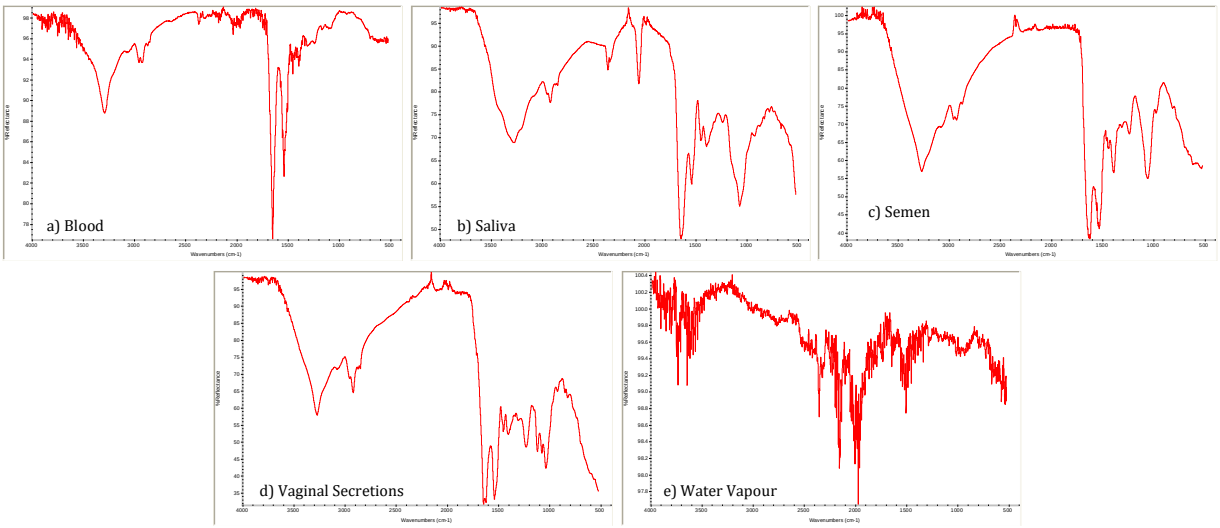

Figure 3.3: ATR-FTIR spectra of neat body fluids when dry; a) blood, b) saliva, c) semen, d) vaginal secretions & e) water vapour.

The width of the spectral peaks observed within an infrared spectrum can be categorised as broad or narrow, depending of the wavenumber range in which each peak is observed (Coates, 2000; Larson, 2013). A broad peak is one where a peak is observed across wide range of wavenumbers, such as the peaks positioned at approximately 3300-3200 cm^{-1} in the four body fluid spectra demonstrated in Figure 3.3. A narrow peak is defined by the narrow range of wavenumbers in which a peak is observed. For example, the peaks observed at approximately the 1650 cm^{-1} region of the infrared spectra for all four body fluids in Figure 3.3. These same peaks can also be categorised as strong peaks as their peak intensities are the greatest observed in all four spectra. The intensity of the infrared spectral peaks varies across a spectrum and can be categorised as strong, medium or weak (Coates, 2000; Larson, 2013). A medium or weak peak intensity is observed in peaks which demonstrate smaller peak intensities compared to strong peaks, with weak peaks demonstrating the smallest in the spectrum. An example of weak peaks are the small peaks observed at approximately 1300 cm^{-1} in the blood spectrum of Figure 3.3a. The strength of the spectral peak intensity representing a given sample are indicative of the change in dipole moment that has occurred during analysis. The more intense, or strong, a peak is within an infrared spectrum, the greater the change in dipole moment across the vibrating molecule when irradiated with infrared light (Larson, 2013).

3.1 BLOOD

Figure 3.4 demonstrates an ATR-FTIR spectrum obtained from a blood sample that had been dried *in situ* on the ATR-FTIR analysis stage for five hours. Table 3.1 provides an overview of the identified blood components that result in the presence of these peaks at the particular wavenumbers (cm^{-1}). A total of 45 measurements were taken from five individual 20µl aliquots of neat blood, taken directly from the finger.

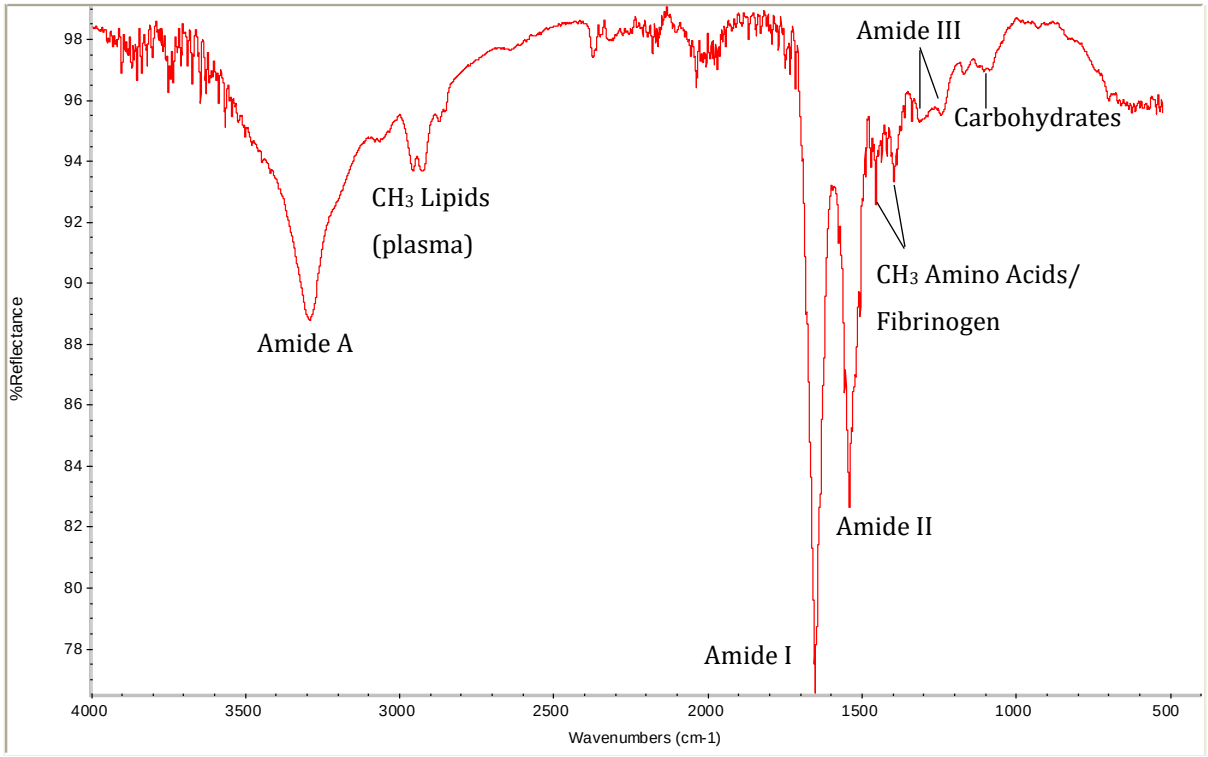

Figure 3.4: ATR-FTIR spectrum of neat blood air dried in situ at 5 hours.

The peak positioned at 3292 cm^{-1} is a broad peak which corresponds to amide A and is categorised as a medium peak. The two narrow peaks positioned at approximately 1650 cm^{-1} and 1540 cm^{-1} are categorised as strong peaks as they are the most intense peaks observed within the spectrum. These peaks correspond to amide I and amide II respectively. The remaining peaks observed are categorised as weak peaks due their low peak intensities. These peaks were identified as corresponding to plasma lipids (2956 cm^{-1}), amino acids, lipids and proteins (1456 cm^{-1}), fibrinogen and amino acid side groups (1395 cm^{-1}), amide III (1286-1320 cm^{-1}) and carbohydrates, such as glucose (1250-925 cm^{-1}).

Table 3.1: ATR-FTIR peak component identification for blood.

Wavenumber (cm^{-1})	Component Identification	Vibrational Mode	Reference
3292	Amide A	H bonded O-H stretching, N-H symmetric stretching	Garidel & Schott (2006b); Gunasekaran & Sankari (2004); Kanagathara et al. (2011)
2956	Methyl stretches of lipids in plasma	C-H stretching	Kanagathara et al. (2011); Movasaghi et al. (2008); Olsztynska-Janus et al. (2012)
1651	Amide I (α helix)	C=O stretching	Gajjar et al. (2013); Garidel & Schott (2006b); Huang et al. (2011); Kanagathara et al. (2011); Olsztynska-Janus et al. (2012)
1540	Amide II	N-H bending coupled to C-N stretching	Gajjar et al. (2013); Garidel & Schott (2006b); Kanagathara et al. (2011); Olsztynska-Janus et al. (2012)
1456	Methyl bending of amino acids, lipids & proteins	Asymmetric CH_3 bending	Gunasekaran & Sankari (2004); Kanagathara et al. (2011); Movasaghi et al. (2008)
1395	Fibrinogen/Amino acid side groups	Symmetric CH_3 bending	Gunasekaran & Sankari (2004); Movasaghi et al. (2008)
1220-1350	Amide III	C-N stretching	Movasaghi et al. (2008)
1250-925	Carbohydrates (glucose)	C-O symmetric stretching	Gunasekaran & Sankari (2004); Kanagathara et al. (2011)

Amide peaks represent polypeptide repeat units within proteins and amino acids which produce nine characteristic peaks when analysed with infrared spectroscopy. These nine

amide peaks are termed as amide A, B, I-VII, although only amides I-III have been reported as useful in the investigation of protein secondary structure (Hering & Haris, 2009; Kong & Yu, 2007). The amide peaks present within the ATR-FTIR spectra for neat blood samples are indicative of the secondary structure of proteins present, which can be identified based on the peak position within the spectrum (Hering & Haris, 2009) (Table 3.2). The secondary structure of proteins refers to the conformation taken by the polypeptide chains of the proteins (Branden & Tooze, 1991). Within the blood samples, four amides were identified, namely amide A, I, II and III. Amide A arises predominantly from N-H symmetric stretching vibrations in the region 3310-3270 cm^{-1}, although a peak in this region can also be attributed to H bonded O-H stretching vibrations when the blood is in a liquid state. The amide A peak can be attributed to a number of possible components that are found in blood, including carbohydrates and lipids, although it is thought that the amide A peak in neat blood corresponds to proteins (Olsztynska-Janus et al. 2012). Information regarding the protein structure cannot be obtained from the amide A peak as it comprises of a NH group which is insensitive to protein backbone conformation (Barth, 2007).

Table 3.2: Protein secondary structure assignment based on amide I peak frequency in IR spectra (Barth, 2007; Garidel & Schott, 2006b; Hering & Haris, 2009).

Secondary Structure Assignment	Amide I Frequency (cm^{-1})	Amide II Frequency (cm^{-1})
β-sheet	1620-1640 1670-1695	1530-1550* 1510-1530†
Unordered	1640-1650	-
α-helix	1648-1660	-
β-turns	1662-1686	-

*parallel, †anti-parallel

The amide I peak provides the most information regarding the protein secondary structure as it is often the most sensitive and intense peak observed in the infrared spectra of organic molecules and it occurs in the 1700-1600 cm^{-1} region (Garidel & Schott, 2006b; Olsztynska-Janus et al. 2012). Approximately 80% of the vibrational mode associated with the amide I peak originates from C=O stretches corresponding to the peptide-linked backbone of proteins. The remaining 20% arises from N-H bending and C-N stretching vibrations (Olsztynska-Janus et al. 2012). Each conformation of protein secondary structures has a unique geometry with different hydrogen bonding patterns. As a result, the varying secondary structures of proteins produce peaks at different vibrational frequencies within

infrared spectra, which enables identification of these structures (Table 3.2) (Barth, 2007; Garidel & Schott, 2006b; Hering & Haris, 2009). In neat blood ATR-FTIR spectra, the amide I peak position, or frequency, is located at 1651 cm^{-1} on average, which indicates that the dominant protein secondary structure can be defined as α-helical.

Due to the vast range of proteins present within blood it is difficult to specifically assign proteins as contributors to the amide I peak. The differing secondary structures amongst proteins present in blood would all contribute to the amide I peak observed, resulting in an overlap in the amide I region. However, particular proteins can be stated as contributing to the overall amide I peak based on comparisons with some of the most abundant proteins present in blood. Direct ATR-FTIR spectroscopy comparisons were carried out with human serum albumin (HSA) and haemoglobin (Figure 3.5), as well as comparisons with amide I frequencies stated in literature for other proteins present in blood. The average vibrational frequencies observed for amide I peaks in neat blood, HSA and haemoglobin were 1651 cm^{-1}, 1645 cm^{-1} and 1645 cm^{-1}, respectively. It is evident that neither of these proteins can be wholly attributed to the amide I peak observed at 1651 cm^{-1} in blood based on the peak frequencies, although both can be stated as contributing to the amide I peak based on the shape of the amide I peaks demonstrated in all three spectra (Figure 3.5).

The amide I frequency observed in the neat blood spectra suggest that HSA could be the major contributor to the amide peak. The secondary structure of HSA is known to be predominantly α-helical, with only 10% of the structure comprised of β-turns (Hassler et al. 2011). Therefore, the frequency observed within the neat blood spectra correlates with the secondary structure and the observed amide I peak frequency of HSA. Additionally, as HSA is a key component of whole blood, with a concentration of approximately 40 mg/ml and contributing 45% of the protein mass of blood plasma, it is reasonable to assign the amide I peak in neat blood to that of HSA (Hassler et al. 2011; Petibois et al. 2001).

It could also be suggested that haemoglobin is a major contributor to the amide I peak observed in the neat blood spectra. This is due to there being approximately 640 million molecules of haemoglobin per RBC, with an average haemoglobin concentration of 13 mg/ml of whole blood (Hawkins et al. 1954; Moore et al. 2010). The frequency of the amide I peak observed in the ATR-FTIR spectrum of haemoglobin differs from the frequency observed in the neat blood by 6 cm^{-1}. As the average haemoglobin amide I frequency was observed at 1645 cm^{-1}, this suggests an unordered secondary structure for the protein (Table 3.2).

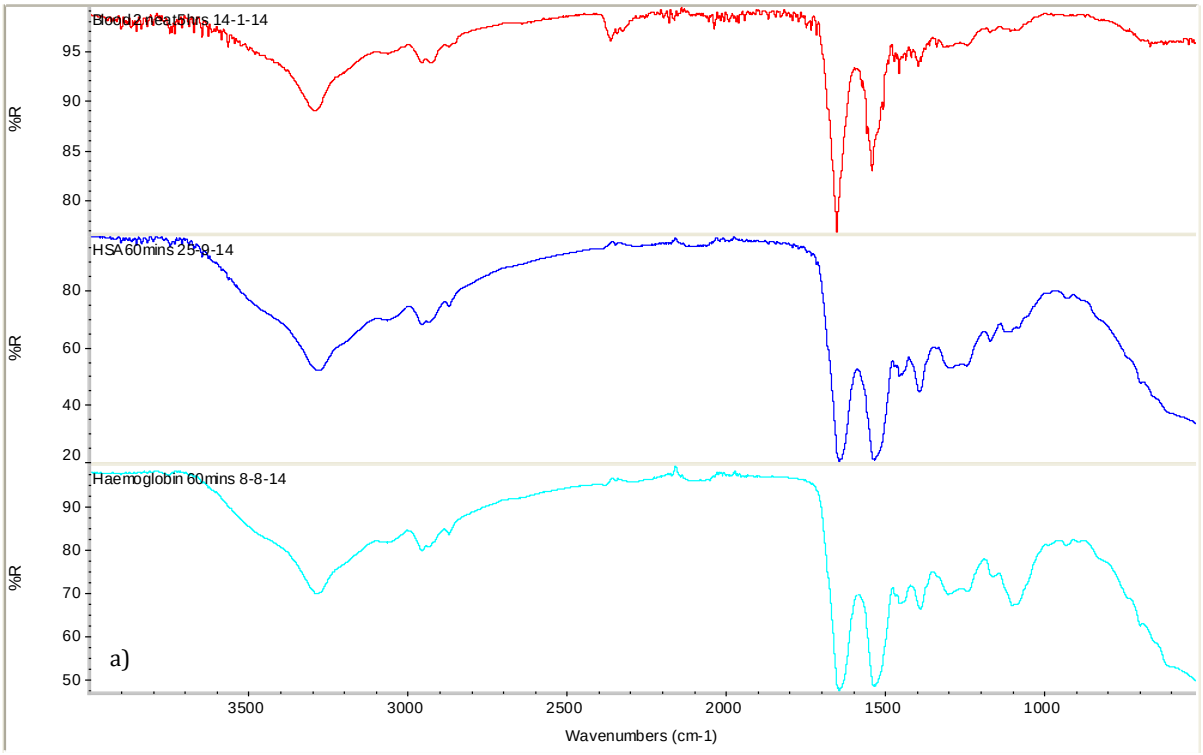

Figure 3.5: ATR-FTIR stacked spectra comparison of neat blood (red), HSA (blue) & haemoglobin (turquoise).

However, it is well understood that the true secondary structure of haemoglobin molecules comprises of 75-85% α-helix and 15-25% unordered (Dong et al. 1990). Previous literature reported that the amide I frequency observed in FTIR spectra of haemoglobin lies at approximately 1650 cm^{-1}, which correlates with the amide I frequency observed in the neat blood spectra studied here (Dong et al. 1990; Kong & Yu, 2007; Olsztynska-Janus et al. 2012). The adjustment observed in the average haemoglobin amide I peak could be due to hydrogen bonding interference in the same region causing a shift in peak frequency (Garidel & Schott, 2006b).

Comparisons between the neat blood, HSA and haemoglobin ATR-FTIR spectra further support the suggestion that both proteins are major contributors to the amide I peak. It is evident that the peak conformation of the amide I regions are a near match. The spectra also demonstrate that the pattern produced by the peaks and their relative positions observed within the HSA and haemoglobin spectra are reflected in the neat blood spectrum. Therefore, it can be stated that both HSA and haemoglobin are the dominant macromolecules detected in the ATR-FTIR spectroscopic analysis of neat blood.

The amide II peak is often the second most intense peak observed within the FTIR spectra of samples containing proteins and in the neat blood samples is observed within the 1557-

1507 cm^{-1} region, with an average frequency of 1541 cm^{-1}. The vibrational mode that gives rise to the amide II peak is a combination of in-plane N-H bending (40-60%) and C-N stretching (18-40%), with small contributions from in-plane C=O bending and C-C stretching vibrations (Garidel & Schott, 2006b; Kong & Yu, 2007; Olsztynska-Janus et al. 2012).

Like the amide I peak, information regarding protein secondary structure can be yielded from the frequency of amide II peaks. Strong amide II peaks observed in the 1550-1530 cm^{-1} range of the infrared spectrum can be attributed to parallel β-sheet secondary structures, whereas weak amide II peaks with frequencies between 1530-1510 cm^{-1} are thought to arise from antiparallel β-sheet structures (Pelton & McLean, 2000). However, assigning particular structural conformations to specific proteins is difficult due to the number of functional groups contributing to the amide II peak frequency (Jackson & Mantsch, 1995). It is only upon physical match comparisons that suggestions can be made as to the proteins that contribute to the amide II frequency. Figure 3.5 demonstrates that both HSA and haemoglobin exhibit peaks within the amide II frequency, therefore it is possible to suggest that both of these key blood proteins contribute to the amide II peak observed in the neat blood ATR-FTIR spectra.

The amide III peak within the neat blood spectra is the weakest of all the amides detected, with a peak frequency typically observed within the spectral region of 1320-1286 cm^{-1} (Movasaghi et al. 2008). A number of vibrational modes give rise to the observation of an amide III peak, with the dominant modes arising from C-N stretches coupled to in-plane N-H bends and weaker contributions from in-plane C=O bending and C-C stretching vibrations (Barth, 2007; Hering & Haris, 2009). Information relating to the secondary structure of the proteins present within a sample can also be determined by this amide when examined in addition to the amide I peak, although its relation to secondary structure is not fully understood (Jackson & Mantsch, 1995; Pelton & McLean, 2000). The vibrational modes associated with amide III occur in a region of the infrared spectrum where various other vibrational modes belonging to other biological components produce absorption/transmission peaks (Jackson & Mantsch, 1995). This particular region is also associated with vibrations that can be attributed to CH_2 bending vibrations from amino acid side chains, which can overlap with the amide III peak. Alongside this, the spectral region of amide III is not as well defined as the characteristic regions of amide I and II due to the various possible proteins within a sample having various vibrational modes. These factors overall result in a characteristically weak amide III peak compared to amide I, II and A peaks.

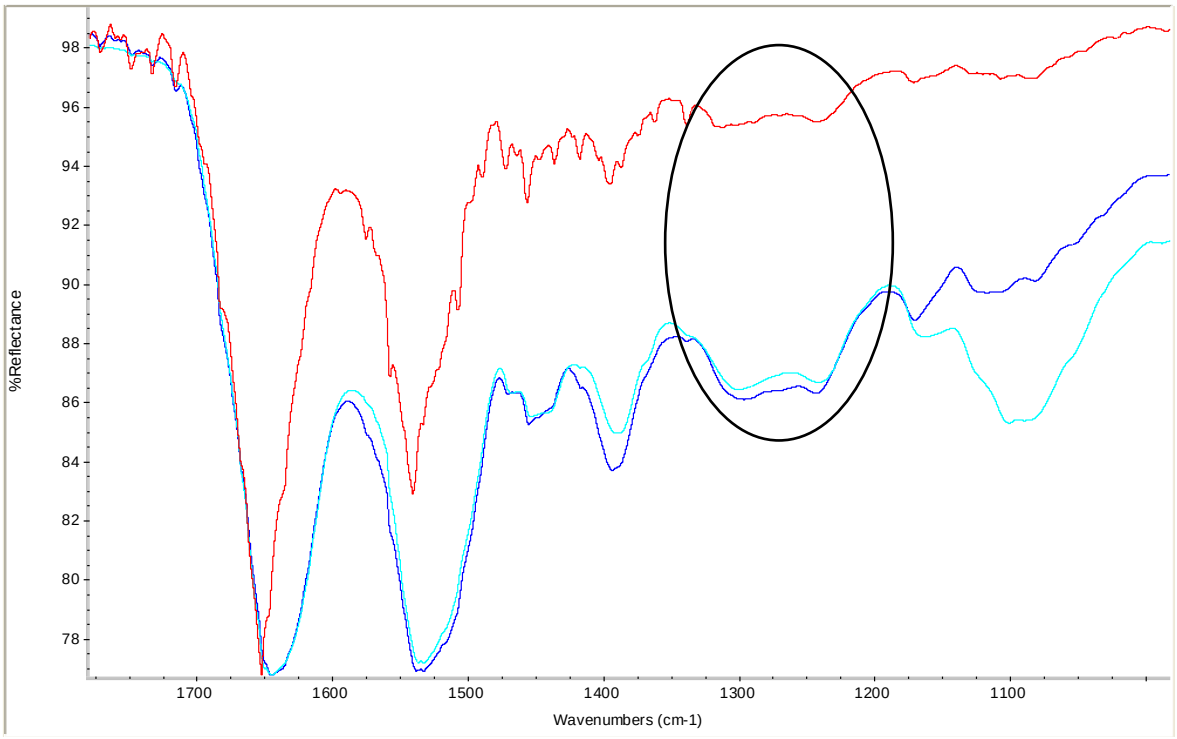

Figure 3.6: Example of the typical "W" shape of the amide III peak (circled) in relation to the amide I & II peaks in the ATR-FTIR spectra of neat blood (red), HSA (blue) & haemoglobin (turquoise).

As can be seen in Figure 3.6, the amide III peak observed within the neat blood spectra has a distinct "W" shape, with an average frequency typically detected at 1306 cm^{-1} for the left apex of the peak. This correlates with the amide III frequency in the FTIR spectroscopic analysis of blood reported by Gunasekaran & Sankari (2004), Kanagathara et al. (2011) and Mostaço-Guidolin & Bachmann (2011). As little protein secondary structure information can be confidently yielded from the frequency/frequencies of amide III vibrations, it is difficult to assign specific proteins as potential contributors. However, comparisons with literature have suggested that plasma proteins, transferrin and α_1-acid glycoprotein produce peaks within the amide III region (Petibois et al. 2001). Additionally, a comparison between the spectra of neat blood, HSA and haemoglobin demonstrates that the same distinct "W" shape peak is observed at the same vibrational frequency region of amide III (Figure 3.6), suggesting that HSA and haemoglobin are the dominant contributors to the amide III peak in neat blood.

The remaining peaks observed within the neat blood spectra are predominately weak peaks. These can be categorised by their frequencies into specific macromolecule groups, although specific components of blood are more difficult to assign to these peaks. The peak observed at 2956 cm^{-1} between the amide A and amide I peak can be attributed to the methyl (CH_3) groups in lipids with an asymmetric stretching vibrational mode (Olsztynska-Janus et al. 2012; Petibois et al. 2001b). The two small, narrow peaks positioned in between amide II and

amide III, observed at 1456 cm^{-1} and 1395 cm^{-1}, originate from vibrational modes belonging to proteins and amino acids. It is a combination of asymmetric and symmetric bending of methyl (CH_3) groups and COO^- stretching, particularly in the amino acids, vibrational modes that give rise to these characteristically small, sharp and narrow peaks (Gunasekaran & Sankari, 2004; Kanagathara et al. 2011; Mostaço-Guidolin & Bachmann, 2011). Proteins that are known to fall within the 1456-1395 cm^{-1} FTIR spectral region include fibrinogen, haptoglobin, IgG, IgA and IgM (Olsztynska-Janus et al. 2012). However, it was not possible to assign any one of these proteins specifically to the peaks observed within the neat blood spectra.

The final peak observed within the ATR-FTIR spectra of neat blood can be found within the low frequency range of the spectrum in the fingerprint region. This weak and broad peak, observed within the 1250-925 cm^{-1} frequency range, corresponds with a region typically associated with carbohydrates, such as sugar moieties. Within blood spectra, this peak can be attributed to glucose arising from vibrational modes consisting of symmetric C-O and C-C stretches (Gunasekaran & Sankari, 2004; Mostaço-Guidolin & Bachmann, 2011; Petibois et al., 1999). However, this particular region of the infrared spectrum also produces peaks representative of phosphodiester bonds within nucleic acids, lipid phosphates, both of which exhibit PO_2 stretching vibrations, and amino acids corresponding to C-N symmetric stretching vibrations (Gunasekaran & Sankari, 2004; Kanagathara et al. 2011; Mostaço-Guidolin & Bachmann, 2011; Olsztynska-Janus et al. 2012).

The results obtained from the ATR-FTIR spectroscopic analysis of neat blood samples correlate with those reported by various research groups. Much of the literature that examines the FTIR spectroscopic analysis of blood focuses on identifying regions of the spectrum where differences can be recognised in relation to specific diseases, such as HIV/AIDS (Sitole et al. 2014), leukaemia (Mostaço-Guidolin & Bachmann, 2011) and diabetes (Gunasekaran & Sankari, 2004). A key element to the results obtained by these research groups was the comparison of diseased blood FTIR spectra with normal, or healthy, blood spectra. All of the peak frequencies and relative shapes obtained in the results reported here demonstrate the same or very similar peak frequencies and shapes as those observed within literature. This highlights that the spectral pattern of peaks produced from blood samples is consistent and reproducible regardless of ethnicity, age, degree of health or gender. This is advantageous as it demonstrates the potential for a blood reference spectrum to be validated and incorporated into spectral libraries within FTIR instruments.

3.1.1 IDENTIFICATION OF BLOODSTAINS: ON COTTON

As body fluids encountered at crime scenes are often in the form of dry stains deposited on surfaces, it was important to determine whether bloodstains could be detected with ATR-FTIR spectroscopy when the stain is deposited on to a substrate. In this instance cotton was used as it is one of the most abundant materials utilised in textiles (WWF, 2014). The characterisation of the ATR-FTIR spectrum of neat blood and its components provided a reference for which comparisons could be made with the ATR-FTIR spectra of bloodstains on cotton, indicating the areas of the spectrum mostly likely to exhibit peaks that correspond to the components of blood. Figure 3.7 demonstrates the typical ATR-FTIR spectrum produced from a dried bloodstain on cotton that has been aged for 24 hours. A total of 510 measurements were taken from 128 bloodstains deposited on cotton.

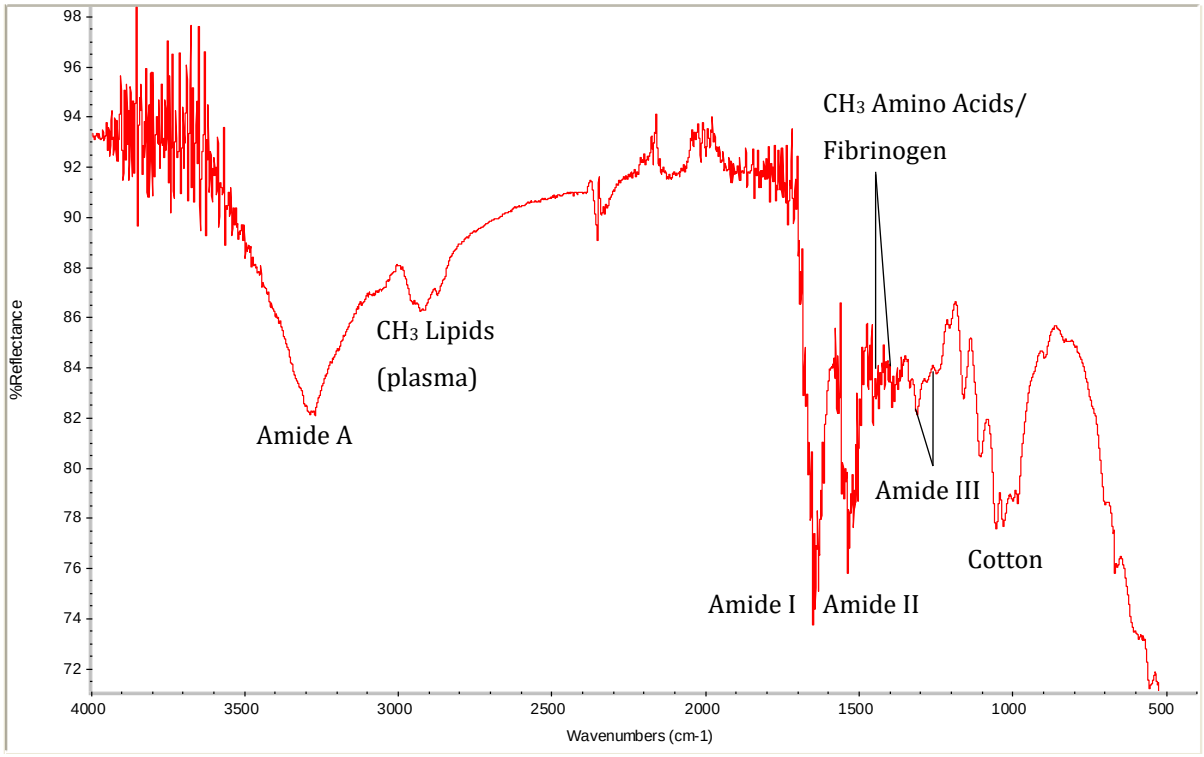

Figure 3.7: ATR-FTIR spectrum of a bloodstain on cotton aged for 24 hours.

Based on the characteristic peaks observed within the spectra for neat blood (Table 3.1), it is evident that within the 3500-1200 cm^{-1} frequency range of the bloodstain on cotton spectra that the peaks observed correspond with the biological components exhibited in blood. The amide A, I, II and III and plasma lipid methyl group peaks are clearly present in peak position and shape, although the amide I and II peaks do not appear as clearly defined as they do in the neat blood spectra. This could be due to atmospheric water vapour interference which is known to overlap with the protein region of the infrared spectrum (Garidel & Schott, 2006b).

Alternatively, the interference could be attributed to an overlap between the blood and cotton within the same region of the spectrum. The lower frequency methyl groups attributed to amino acid side chains and proteins, present at approximately 1456 cm^{-1} and 1395 cm^{-1}, also exhibit undefined peaks, unlike their neat blood spectra counterparts. Again, the interference demonstrated here could be due to an overlap between the blood and cotton peaks within the same frequency region, as demonstrated in Figure 3.8.

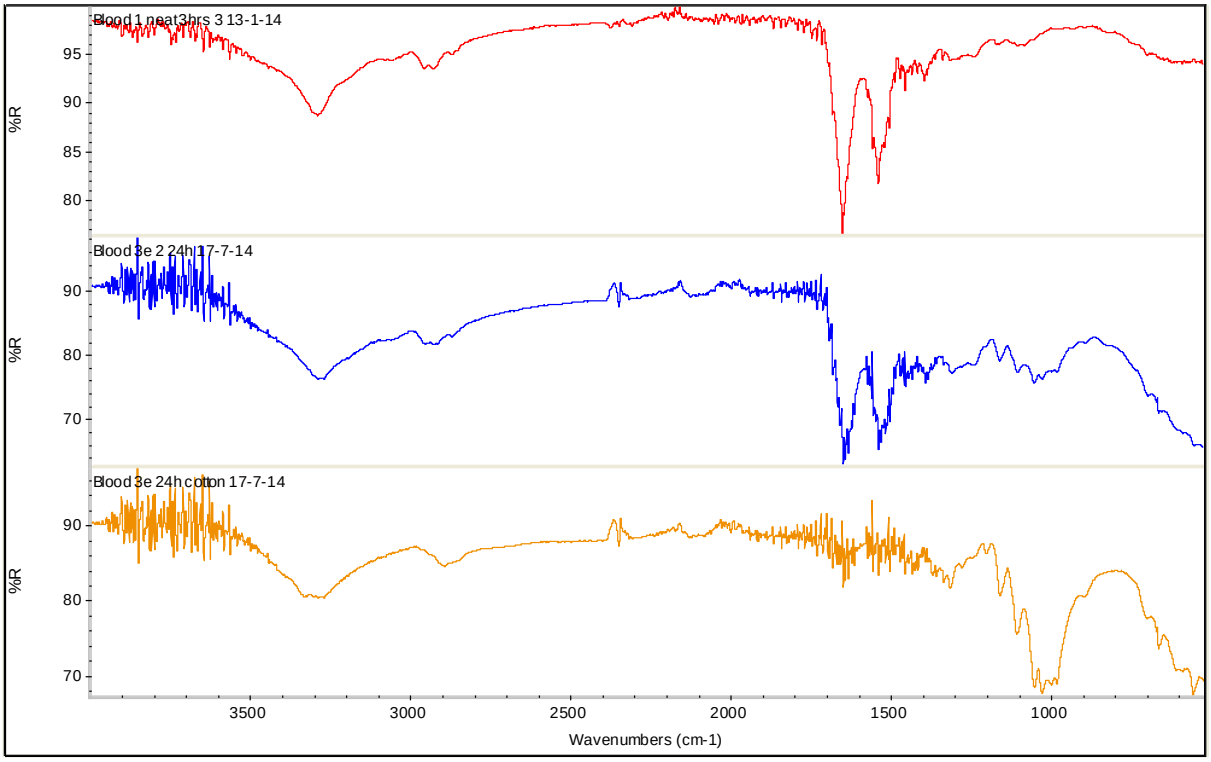

Figure 3.8: Comparison of ATR-FTIR spectra of neat blood (blue), bloodstain on cotton aged for 24 hours (red) & cotton (orange).

The pattern of the cotton spectrum is visibly different from that produced from blood, although towards the higher frequencies similar peaks were observed due to the occurrence of vibrations from common functional groups, such as C-H, O-H, C=C stretches (Housecroft & Constable, 2006). For example, in the 3500-2800 cm^{-1} region of the bloodstain and cotton overlay spectra (Figure 3.8) similar peaks were observed for both the bloodstain and cotton that can be attributed to O-H and CH_3 stretching vibrations (approximately 3270 and 2895 cm^{-1}, respectively). However, the overall shapes and sizes of these peaks did not match which suggests that although the vibrations originate from the same functional groups, the components containing these functional groups were not the same. As the frequency decreases across the spectrum, it can be seen that there is a region containing what appears to be noise (2050-1350 cm^{-1}). The noise exhibited here can be most likely attributed to the

absorption of water by the cotton as the quantity of protein typically found in cotton is often too low to give rise to a peak, which would appear within this region (Arrowsmith, 2013; Chung et al. 2004; Li et al. 2010). Noise is also evident in the 4000-3500 cm^{-1} region, which is also likely to be attributed to water adsorption by the cotton as these particular regions are known to exhibit H bonded O-H vibrations.

The most distinct peaks observed within the cotton spectrum lie in the fingerprint region (1500-650 cm^{-1}), where the more complex and low frequency vibrational modes are exhibited. The main feature of the cotton spectra is a strong, broad peak composed of a number of smaller apexes and two distinct shoulders observed in between 1200-800 cm^{-1}. The frequencies of each shoulder were 1160 cm^{-1}, which originates from an asymmetric bridge of C-O-C stretching in cellulose, and 1108 cm^{1}, relating to vibrations from asymmetrical in-plane ring stretching of glucose (Chung et al. 2004; Li et al. 2010). The apex points of the peak were located at 1053, 1029, 1000 and 983 cm^{1}, which arise from the asymmetrical in-plane ring stretching of glucose (1053 cm^{-1}) and C-O stretching vibrations (1029, 1000 and 983 cm^{1}) (Chung et al. 2004).

When compared to the spectra of neat blood the only overlap expected in this region between the cotton and a bloodstain would correspond to the glucose peak, although in the blood spectra this appeared as a very weak broad peak. As demonstrated in both Figure 3.7 and Figure 3.8, the strong broad peak of the 1200-800 cm^{-1} region in the cotton spectrum has overlapped the weak broad peak of glucose in the blood spectrum. This was not surprising, given the relatively high peak intensity exhibited by the cotton peak compared to the relatively low intensity of the blood glucose peak. However, this observed overlap of the cotton peaks within the bloodstain on cotton spectra varies across measurements, with some bloodstain on cotton spectra demonstrating spectral patterns almost comparable to those produced from neat blood samples (Figure 3.8). There are a number of possible explanations for this occurrence, such as the distribution of the bloodstain across the sample may not be homogeneous and the amount of contact between the sample and internal reflection element (IRE). The heterogeneous distribution of a bloodstain may be as a result of the "coffee-ring effect", whereby when a liquid, such as blood, is deposited on to a substrate and begins to dry, the edges become secured to the substrate. As the fluid then evaporates, the edges of the stain are fixed in place, which results in the fluid flattening, forcing the fluid toward the edges (Lerner, 2014). This theory suggests that the thickness of a stain varies across its circumference, therefore the edges of bloodstains may be thicker than the middle of the stain. As a result, if measurements were made near the edge of the bloodstain, the vibrational

modes detected in the ATR-FTIR spectra are more likely to originate from the blood rather than the cotton and the spectrum may contain few peaks attributable to the cotton.

Another possible explanation for the variation observed between the overlap of characteristic cotton peaks and the blood glucose peak could be due to the amount of contact between the sample and the IRE. An anvil with approximately 200 lbs of pressure was applied to secure the stained cotton samples in place prior to analysis. If the anvil was not secured tight enough, the evanescent wave of infrared light may penetrate more of the cotton aspect of the sample than the blood component as full contact may not be achieved. Additionally, if the sample area containing blood does not cover the entirety of the IRE, the resulting spectrum produced will represent the dominant functional groups relating to both cotton, from the area containing no blood, and the bloodstain.

A distinct difference between the ATR-FTIR spectra of bloodstains on cotton and neat blood is the overall quality. For neat blood samples, the spectra exhibit clear, distinctive peaks that can be easily attributed to specific vibrational modes and functional groups (Figure 3.4). Noise within the neat blood spectra predominantly occurs as the drying time reaches five hours. This is due to the blood drying on a non-absorbent surface, causing the blood sample to crack. As a result, complete contact between the sample and analysis stage is no longer maintained and atmospheric interference is detected within the ATR-FTIR spectra. However, the peaks observed are not generally affected by this and exhibit an average maximum peak intensity of approximately 70% for the strongest peaks (amide I). The intensity measurements recorded from an FTIR spectrum are recorded as a percentage and descend from 100%, therefore the lower the intensity percentage for a peak, the stronger the peak is within the spectrum. Figure 3.9 displays the average peak intensities for the amide peaks, which were the most characteristic peaks observed across all the spectra, within neat blood samples and bloodstains on cotton samples.

It is evident from the bar graph that there appears to be a small difference between the peak intensities of the amide peaks of neat blood and bloodstains, although overall the peak intensities observed within both sample types appear to be consistent. In contrast, the standard deviation of the average intensity for the neat blood samples was much greater than the standard deviation of the bloodstains on cotton. This is due to the peak intensities of the initial dry spectra of neat blood samples, which were typically obtained after one or two hours drying *in situ* on the IRE, exhibiting a greater peak intensity compared to the peak intensities exhibited by the dry spectra obtained at hours two/three to five. For example, the maximum peak intensity of the strongest peak in the first dry spectrum obtained for a neat

blood sample after one hour, where adsorption to the IRE was strongest, was approximately 47%. In contrast, the remaining dry spectra obtained at the hourly intervals up to five hours from the same blood sample exhibited maximum peak intensities of approximately 77%.

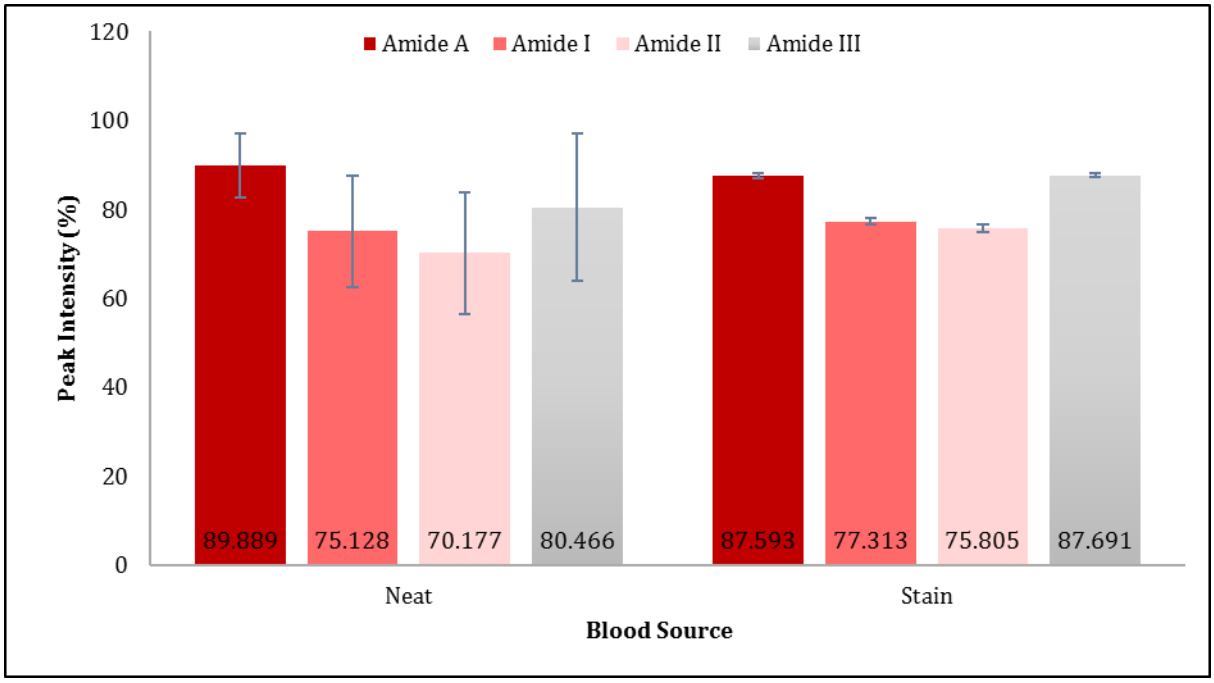

Figure 3.9: Bar graph comparison of peak intensity across the amide peaks within neat blood samples & bloodstains on cotton.

There are two possible explanation for this difference in peak intensity within the neat blood samples. Firstly, the variation in the maximum peak intensity may be due to the sample concentration changing during the drying process, suggesting that although spectra were obtained with peaks correlating to blood in frequency, shape and size, the samples were not completely dry when these measurements were taken (Hughes et al. 2014). The second explanation may be due to the cracking and lifting of the blood samples from the IRE, which caused a reduction in adsorption to the IRE and as a result, the intensity of the spectral peaks decreased. This apparent decrease in the maximum peak intensity was not observed within bloodstain on cotton measurements. However, all the bloodstain samples were dry prior to analysis.

Often, when body fluid stains are recovered from crime scenes, it is not known when the stain was deposited. The stain may be a result of the circumstances surrounding the crime, or could have been left at the scene days, weeks, or months prior to the crime. In order to ensure that bloodstains could be successfully identified utilising ATR-FTIR spectroscopy, regardless of how old the stains were, a series of bloodstains were collected from three individual donors, two female and one male, and then deposited on to cotton and placed into storage to

age from 24 hours up to 18 months. Across all the aged bloodstain samples, the characteristic peaks associated with the biological components of neat blood were exhibited and distinguishable from the characteristic peaks associated with cotton. However, some spectra appeared to exhibit the blood peaks with greater quality than others. Comparisons between the average relative frequencies of each of the blood characteristic peaks for each donor and the donors pooled together demonstrated that little variation appeared to be observed (Table 3.3).

Table 3.3: Average peak frequencies for the blood characteristic peaks exhibited in bloodstains deposited by three donors & the pooled data.

Donor	Glucose		Amide III	Fibrinogen /Amino acid side chains	CH_3 Amino Acids	Amide II	Amide I	CH_3 Lipids	Amide A
1	1104.62 ± 1.32	1160.71 ± 0.49	1311.28 ± 1.06	1392.56 ± 0.07	1454.80 ± 0.15	1537.89 ± 0.52	1650.84 ± 0.04	2921.18 ± 9.36	3273.56 ± 6.23
2	1103.99 ± 1.01	1161.23 ± 0.89	1310.14 ± 2.51	1392.55 ± 0.06	1454.77 ± 0.14	1537.88 ± 0.14	1650.78 ± 0.50	2932.15 ± 12.78	3275.21 ± 7.49
3	1104.45 ± 1.05	1160.76 ± 0.53	1311.12 ± 1.39	1392.55 ± 0.20	1454.75 ± 0.27	1538.03 ± 2.05	1650.83 ± 0.11	2924.31 ± 11.14	3275.49 ± 7.67
Pooled	1104.35 ± 1.17	1160.91 ± 0.70	1310.84 ± 1.84	1392.55 ± 0.12	1457.77 ± 0.19	1537.93 ± 1.19	1650.82 ± 0.30	2925.94 ± 12.11	3274.73 ± 7.18

To ascertain whether there were any significant differences between the bloodstain peak frequencies of individual donors a Kolmogorov-Smirnov (KS) test was carried out to determine whether the data was normally distributed. The blood peaks utilised within the KS test excluded the glucose peaks due to a lack of confidence in attributing the peak position to that of blood rather than the cotton. Peak frequencies corresponding to amide III, fibrinogen/amino acid side chains, methyl groups of amino acids, amide II, amide I, methyl groups of lipids and amide A were all included in the KS test. It was demonstrated that all of the peak frequencies from all three donors was not normally distributed. As a result, only non-parametric tests could be explored in the further statistical analysis of the data.

The non-parametric test utilised in the further statistical analysis of bloodstains from three individual donors was the Kruskal-Wallis test. This particular non-parametric test examines the data from multiple groups, in this instance multiple donors, to identify differences

between the peak frequency data (Field, 2013). Differences are determined by ranking of the data, regardless of group, which are then reassigned to the relevant group and the ranks added together. The sum of the group ranks enables the calculation of the test statistic, *H*, which is defined by the degrees of freedom distributed from chi-square distributions (Field, 2013; Ho, 2014). Overall, the Kruskal-Wallis *H* scores demonstrated that there were significant differences between each of the donors at each of the blood peak frequencies.

Pairwise comparative follow-up analysis of the Kruskal-Wallis test highlighted that significant differences could be found between the donors at specific blood peak frequencies, although the significant differences found were not consistent across the three donors. Figure 3.10 demonstrates the output diagrams associated with the Kruskal-Wallis test follow-up analysis. Each donor is indicated by their respective number (1, 2 or 3) and the average rank within each group is displayed. Coloured connecting lines between the donor points show where the significant differences were; black connecting lines demonstrate no significant difference, yellow and mustard lines demonstrate a significant difference. The *H* scores obtained in the follow up analysis are representative of the difference between the average ranks between the donors. These scores are then divided by their respective standard errors to convert them in to *z*-scores, which have exact *p*-values to take into account the number of analyses carried out across the data set and results in an adjusted significance value (Field, 2013). In this instance, a total of seven tests were completed to obtain the adjusted significance values, which were observed for each donor and the pooled donor data in Table 3.4 and Figure 3.10.

Pairwise comparisons demonstrated the most significant differences between donor one and donor two, where a significant difference was obtained at all of the peak frequencies except at amide A. Significant differences between donors one and three were observed at peak frequencies corresponding to amide A, I, II and methyl groups of amino acids, whereas at the remaining peak frequencies no significant difference was found. The least amount of significant differences across the blood peak frequencies was observed in pairwise comparisons between donors two and three, with significant differences only observed at methyl groups of lipids and amide III frequencies. The variation observed in the significant differences between donor one and donor two could be due to donor one being female and donor two being male. However, this seems unlikely as it does not explain why fewer significant differences were obtained between donors two and three, as donor three was also female. Amongst the various research groups who have reported on the FTIR spectroscopic analysis of blood, differences between blood samples from males and females have not been

stated, therefore it is expected that gender should not influence the frequencies at which the characteristic peaks of blood are observed.

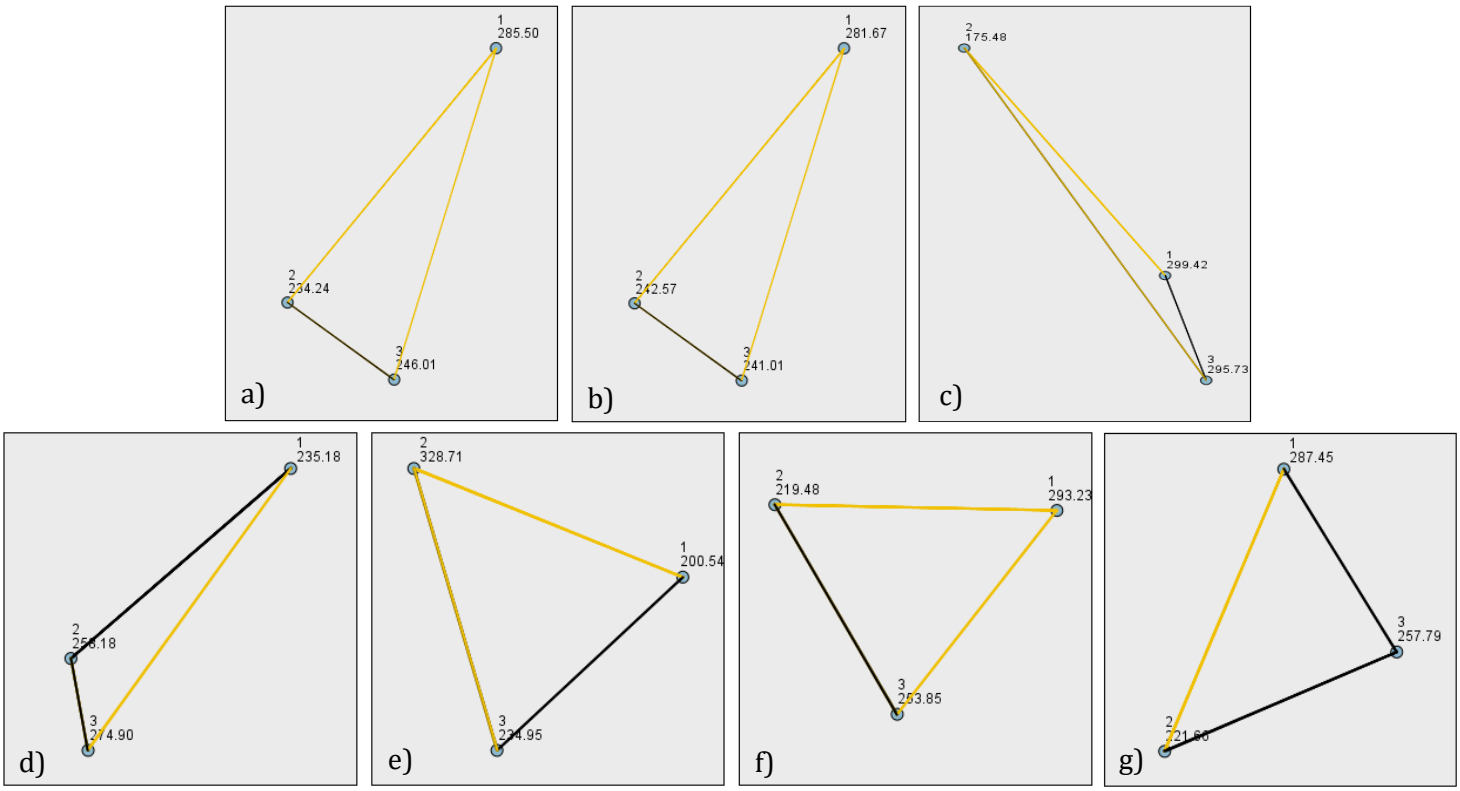

Figure 3.10: Pairwise comparisons between donors at each blood peak frequency; a) amide II, b) methyl groups of amino acids, c) amide III, d) amide A, e) methyl groups of lipids, f) amide I & g) fibrinogen/amino acid side chains.

Table 3.4: Adjusted significance values obtained from pairwise comparative follow-up analysis of the Kruskal-Wallis test for bloodstain peak frequencies from three individual donors.

Peak	Donor 1:2	Donor 1:3	Donor 2:3
Amide A	0.431	0.042*	0.900
CH_3 Lipids	0.000*	0.099	0.000*
Amide I	0.000*	0.043*	0.098
Amide II	0.003*	0.043*	1.000
CH_3 Amino Acids	0.039*	0.035*	1.000
Fibrinogen/Amino Acid Side Chains	0.000*	0.197	0.074
Amide III	0.000*	1.000	0.000*

* significant, based on a significance level of 0.05.

It is possible that the significant differences identified by the pairwise comparisons of the Kruskal-Wallis test were a result of the variation in peak frequencies at the various peaks examined across the 510 measurements obtained (Table 3.3). However, these significant differences did not influence the peak identification within any of the samples, and therefore it was evident that differences in donor did not hinder the identification of bloodstains.

3.1.2 IDENTIFICATION OF BLOODSTAINS: EXTRACTED

As previously mentioned in Section 3.1.1, some of the ATR-FTIR spectra obtained from the analysis of bloodstains on cotton from individual donors were of poor quality compared to others. The samples analysed within this investigation were known to be free of other known contaminants as they were stored within petri dishes in boxes. However within the investigation of crime, recovered biological evidence will seldom be in such good condition with little contamination. If such evidence was to be directly analysed with ATR-FTIR spectroscopy, it is likely that the resulting spectrum would contain characteristic peaks representative of the substrate upon which the biological evidence was found, the biological material itself, such as blood, and any contaminants that may be present. This could result in an inconclusive determination of whether blood was identified on the evidence. A way to overcome this issue was to examine whether the bloodstains deposited on to cotton could be successfully extracted from the substrate and then produce a characteristic blood spectrum when analysed with ATR-FTIR spectroscopy.

A total of 306 measurements were taken from 51 extracted samples in a "wet-to-dry" analysis, across the bloodstains on cotton samples that had been aged from 24 hours to 7 days, 12 and 18 months following direct analysis. Of the 306 measurements, 102 reflected the spectra of dry blood and 204 yielded spectra representative of water, as demonstrated in Figure 3.2a. A simple sterile, distilled water (diH_2O) extraction procedure was carried out on the bloodstains (Section 2.2.2.2) in order to maintain the integrity of the samples, as well as keeping the protocol user-friendly. For all samples aged up to 7 days, the bloodstains were successfully washed from the cotton into the diH_2O, resulting in a red liquid extract. However, the 12 and 18 month old bloodstains did not appear to wash off from the cotton very well, if at all, as can be seen in Figure 3.11. A possible explanation is that as the samples have aged, the various proteins and constituents in blood, such as haemoglobin and iron, have embedded themselves within the cotton weave forming a hydrophobic bond with the substrate, therefore staining the cotton and making it difficult to remove with a pH neutral

solute and vortexing (Smith & Olson, 2002). It may be possible to achieve better extraction of the older bloodstains with stronger solutes and mixing methods, although these techniques could degrade the components within the bloodstains, including DNA. The effect of such extractions was not explored as part of this research.

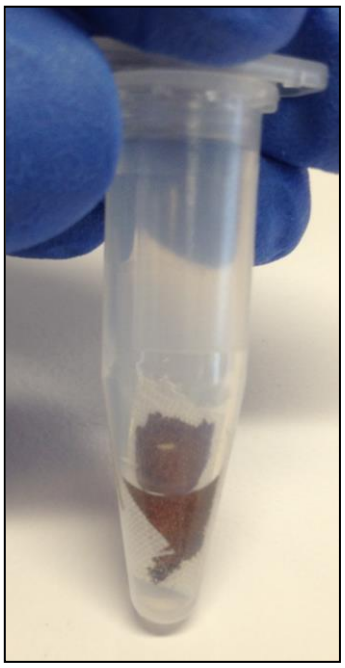

Figure 3.11: Eighteen month old bloodstain extract sample which has undergone four minutes of vortexing.

As the sample extracts were in a liquid form, ATR-FTIR spectroscopic analysis was conducted in the same manner as the neat blood samples (Sections 2.2.2.1 & 2.2.2.2), although measurements were only taken typically up to one hour, when the sample had dried, rather than up to five. Figure 3.12 demonstrates the typical spectra obtained from the extracted bloodstains aged up to 7 days (red) in comparison to the bloodstain on cotton (blue) and a cotton blank (turquoise) spectrum obtained from the same sample prior to extraction.

It is evident that the overall quality of the spectrum is excellent, with clearly defined peaks that are comparable with the peaks observed within neat blood spectra. The peak frequencies that correspond to the nine characteristic blood peaks were observed within the extracted sample spectra (24 hours – 7 day samples), with no apparent peaks that could be attributed to cotton. This demonstrates that the simple water extraction technique applied to the bloodstains was sufficient to extract the stain from the cotton without also extracting any contaminating cotton components. This is highly advantageous for forensic purposes as it offers an alternative analysis method in determining the presence of blood if poor quality spectra were obtained when analysing directly from the substrate. It also has the potential to

be utilised as a method for extracting bloodstains from substrates other than cotton, which is of great benefit within the forensic investigation of biological evidence. Another benefit of the water extraction method is that is does not remove or destroy any of the components within the blood which may be useful for further analysis, such as DNA profiling. From a forensic perspective, this is ideal as it does not rule out any potential further analysis that may be required to provide further intelligence within a case.

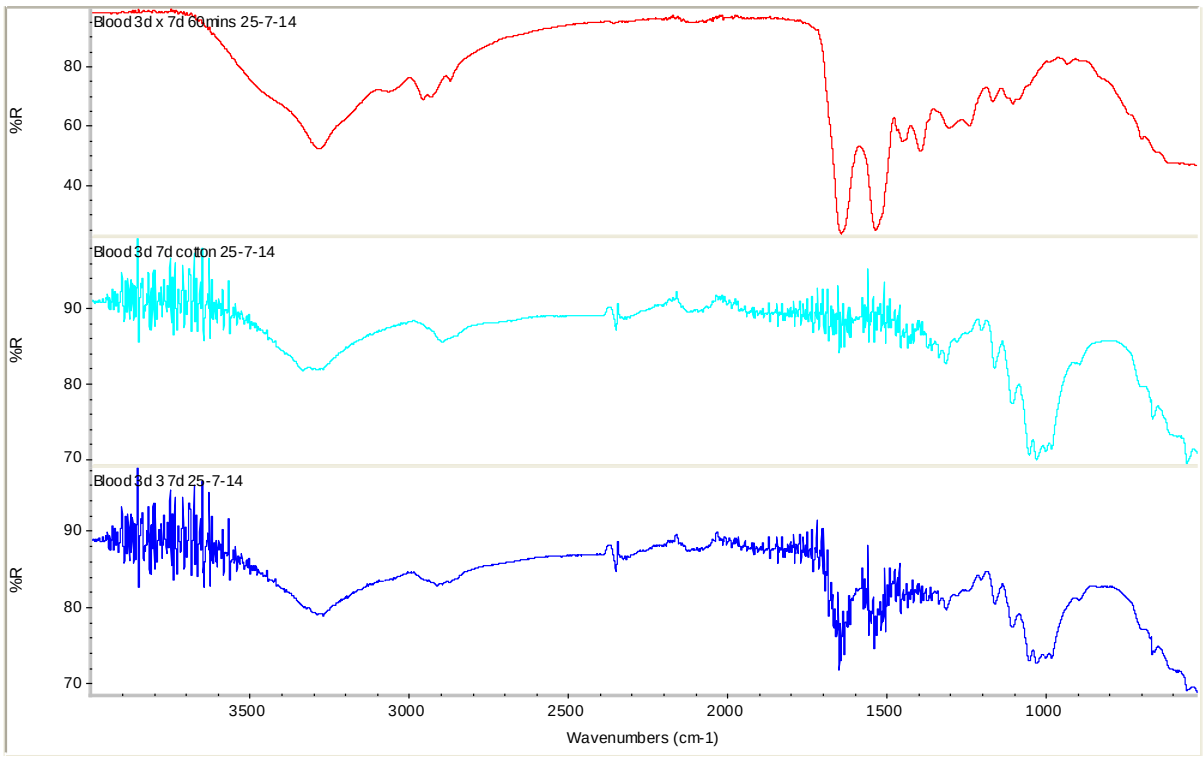

Figure 3.12: Example ATR-FTIR spectra from an extracted bloodstain (red), cotton blank (turquoise) & bloodstain on cotton (blue) from the same sample that had been aged for seven days.

Figure 3.13 provides an overview of the peak frequencies observed across all the variations of blood samples examined. The specific peak frequencies observed within the extracted bloodstain spectra that had been aged from 24 hours to 7 days were comparable with those obtained from both neat blood spectra and the bloodstain on cotton spectra from the same and different samples. This further demonstrates the reliability of ATR-FTIR spectroscopy as a technique to identify blood from various sample preparations. Consistent spectra were obtained that enabled successful comparison and peak assignment to blood component vibrational modes in samples that reflect how bloodstain evidence may be present at crime scenes.

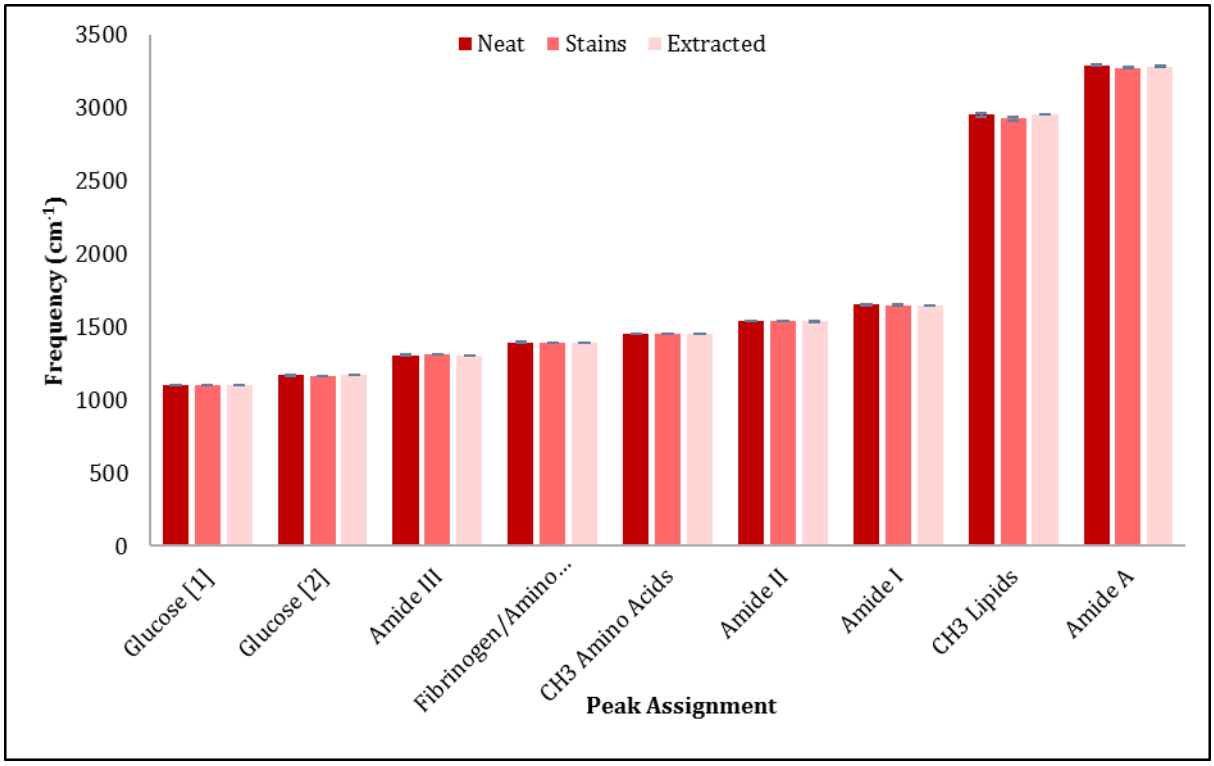

Figure 3.13: Bar graph comparing the average peak frequencies observed in the spectra of neat, stained & extracted blood.

The ATR-FTIR analysis of sample extracts from the older bloodstains (12 and 18 months) demonstrated considerably greater variation in the quality of the spectra produced, as well as greatly reduced peak intensity and confidence in peak assignment. Figure 3.14 demonstrates the extremes of variation of the spectra obtained from 12 and 18 month old bloodstain extracts in comparison with the typical spectra obtained from the 24 hour to 7 day old bloodstain extracts. Some spectra demonstrated comparable peaks corresponding to blood, whereas others demonstrated increased noise, lack of peak definition and a reduction in peak number. This was a direct result of the poor extraction of the bloodstains from the cotton substrate during the washing and vortexing procedure, where the stain was still evident on the cotton (Figure 3.11).

The spectra obtained from 12 month old bloodstain extracts were overall of better quality compared to the spectra obtained from the 18 month old bloodstain extracts. However, when compared with the extracted bloodstains that had been aged up to seven days, there is a noticeable decrease in the spectral profile quality for both the 12 and 18 month aged samples. Upon visual inspection, the 12 month extract blood samples had an increase in noise across the spectra, particularly within the 4000-3500 cm^{-1} and 2500-1650 cm^{-1} regions. This noise is likely to be a result of water vapour as the bloodstains were extracted with this solute.

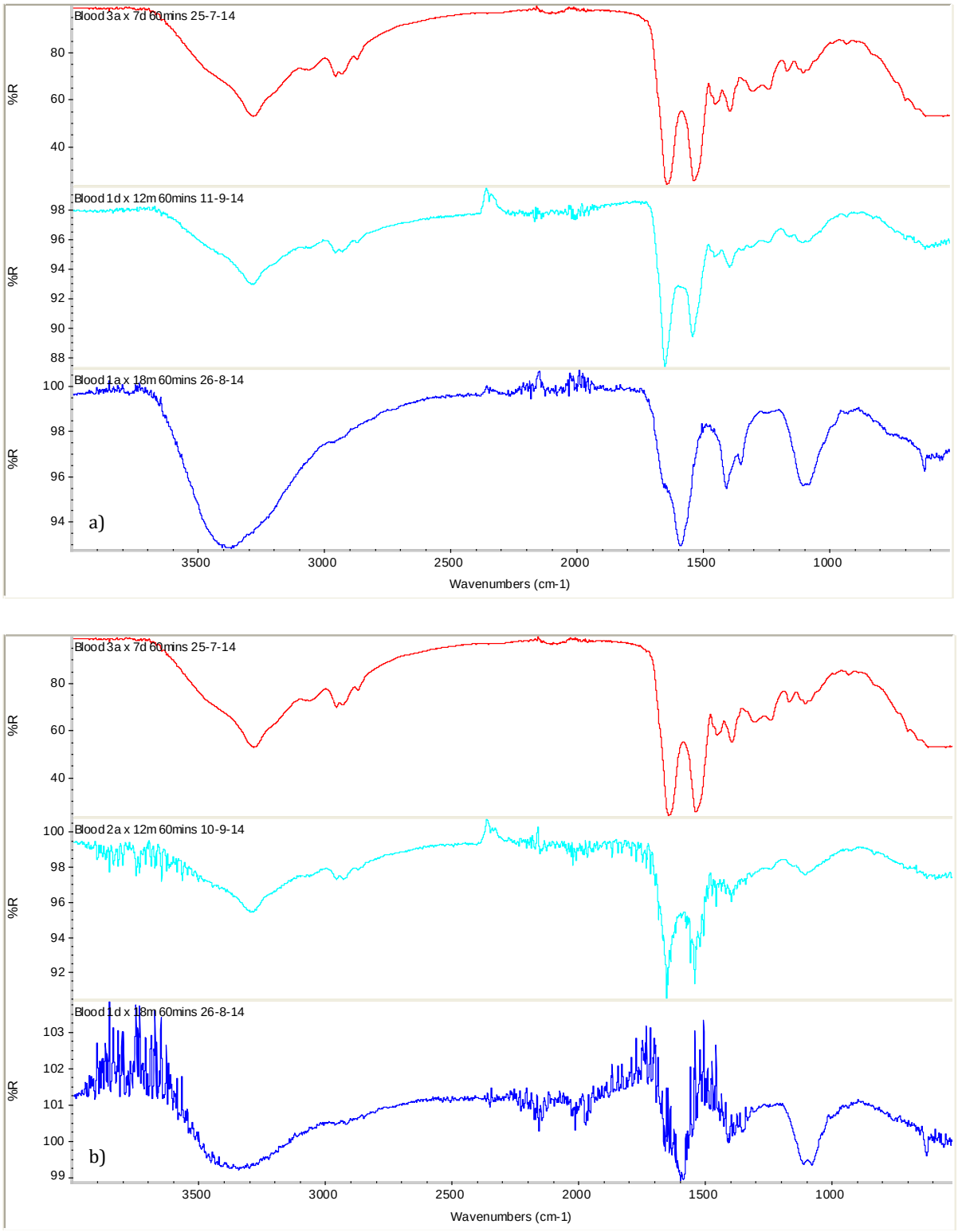

Figure 3.14: ATR-FTIR spectra demonstrating the extreme variation observed from extracted bloodstains that were aged to 7 days (red), 12 months (turquoise) & 18 months (blue); a) exhibits the best spectra obtained from each sample age, b) exhibits the worst spectra obtained from each sample age.

An additional observation of the spectra was the decreasing quality in the overall appearance of the peaks, which appeared to be less well-defined. In particular, the weak peaks, such as glucose, amide III, fibrinogen/amino acid side chains and methyl groups of amino acids, became much more difficult to distinguish and accurately assign an identification. However, in some of the extract spectra from bloodstains of 12 months it was possible to yield a spectrum that appeared comparable to the younger bloodstain extracts and the neat blood spectra (Figure 3.14a).

The spectra obtained from the extracts of the 18 months bloodstains had the poorest overall quality, with a clear reduction in the number of peaks observed and low maximum peak intensities across the spectra (Figure 3.14, blue). Particular features of the 18 month aged bloodstain extract spectra were the loss of peaks that are expected within blood spectra and the distinct widening and merging of other peaks. Comparison of the peaks observed within the 18 month bloodstain extracts with the peak components expected in blood spectra (Table 3.1) highlights that the peaks corresponding to the methyl groups of lipids (2956 cm^{-1}), methyl groups of amino acids and proteins (1456 cm^{-1}) and amide III (1220-1350 cm^{-1}) were no longer present. The blood characteristic peaks that were observed within the 18 month old extracted bloodstains appeared visibly different than would be expected. The peaks corresponding to amide A (3292 cm^{-1}) and glucose (1250-925 cm^{-1}) appear broader and stronger than their counter parts observed in the younger bloodstain extracts, bloodstains on cotton and neat blood spectra.

The alteration in the peak size and shape for amide A can be associated with the increased contribution of water in the sample, due to the poor extraction of the bloodstain from the cotton. As water was utilised as the washing solute, the main component of the sample extract was therefore water. Unlike the 24 hour to 7 day bloodstain extracts, the extract solution was near colourless, suggesting that the red blood cells had not successfully dissociated from the cotton into the solute. As haemoglobin appears as the dominant contributor to the ATR-FTIR spectra of blood (Figure 3.5), it is unsurprising that fewer characteristic blood peaks were observed within the 18 month bloodstain extract spectra and that there was an increase in the detection of water in the regions associated with O-H vibrational modes within the dry sample spectra. The increased peak corresponding to glucose vibrational modes may be a result of the absence of dominant proteins within the sample (Petibois et al. 1999; Shen et al. 2003). As observed within the spectra of the younger bloodstain extracts and the neat blood, the glucose peak was typically weak and this may be due to the concentration of glucose within the blood being much lower compared to the concentration of overall proteins. However, if these dominant proteins are tightly bound to

the cotton in 18 month old bloodstains, to the extent that the bloodstain does not dissociate during the washing aspect of extraction then these would be left behind on the cotton (Smith & Olson, 2002). Any cellular material such as nucleic acids and carbohydrates that may not be as tightly bound to the stained substrate could therefore dissociate from the cotton, enabling the observation of stronger peaks in resulting ATR-FTIR spectra.

An interesting peak observation within the spectra of extracted bloodstains aged 18 months was the apparent merging of the amide I and II peaks, with one apex occurring at approximately 1600 cm^{-1} (Figure 3.14, blue), rather than the typically exhibited narrow, strong peaks adjacent to one another. This phenomenon was observed within all the spectra obtained from extracted 18 month old bloodstains and could also be a result of the proteins adhering securely to the cotton, whereby reduced concentrations of proteins were present in the extracts. It is possible that the observed peak within the protein region of the infrared spectrum is representative of the proteins present within blood that are not strongly associated with the red blood cells (RBCs). RBC's contain strong binding agent's haemoglobin and iron that cause blood to stain (Smith & Olson, 2002), therefore if the RBCs did not dissociate from the cotton during extraction, the proteins present within the extract are unlikely to be those found in erythrocytes.

The peak frequency observed for the merged amide peak lies in between the amide I and amide II characteristic regions, which makes peak assignment more difficult. Assessment of the distribution of the peak, suggests the protein contributor could correspond more to an amide II vibrational mode than amide I, although this is merely a suggestion as there are no reports in literature for this merging of the amide peaks being observed previously in blood spectra. However, the peak may not be representative of protein at all, as a peak frequency of approximately 1600 cm^{-1} can be attributed to the C=N and N-H functional groups of cytosine and adenine, respectively, within DNA (Movasaghi et al. 2008). Based on these observations, it is possible to state that samples of extracted bloodstains that have been aged from 24 hours to 7 days and 12 months can successfully produce ATR-FTIR spectra that contain the characteristic peaks expected in samples of neat blood. However, the extraction of the stain physically from the cotton is poor when the bloodstains have been aged for a year or longer. In particular, the ATR-FTIR spectra yielded from 18 month old bloodstain extracts contained fewer comparable peak frequencies within the overall profile that could be definitively identified as originating from blood.

3.1.3 FORENSIC APPLICATION

The characterisation of ATR-FTIR spectral peaks obtained from blood demonstrated here correlate with those reported by a number of research groups (Gajjar et al. 2013; Gunasekaran & Sankari, 2004; Kanagathara et al. 2011; Mostaço-Guidolin & Bachmann, 2011; Olsztynska-Janus et al. 2012; Petibois et al. 2001a; Sitole et al. 2014). The reproducibility of ATR-FTIR spectroscopy has been highlighted within this investigation as neat blood samples, bloodstains deposited onto cotton and extracted bloodstains have produced comparable spectra containing the characteristic peaks attributable to vibrational modes exhibited by components within blood. Significant differences were detected amongst individual donors of bloodstains, although this significance is likely to have been a result of the variation in frequency across the dataset, as the average peak frequencies and intensities observed within neat blood and bloodstains were consistent, regardless of donor. In addition, ATR-FTIR spectroscopy has demonstrated that characteristic blood peaks can be detected and assigned to bloodstains on cotton that have been stored for up to 18 months, as well as successfully extracted from stains aged up to 12 months.

These findings are hugely beneficial within a forensic context as it demonstrates the potential of ATR-FTIR spectroscopy to be utilised as a confirmatory technique for the detection of blood. Currently, presumptive tests, such as Kastle-Meyer (KM) and luminol, and confirmatory tests, such as ABAcard® Hematrace®, are routinely utilised within forensic investigations for the detection of blood. These particular blood tests rely on the presence of haemoglobin to induce a reaction which suggests or confirms the presence blood. ATR-FTIR spectroscopy has demonstrated successfully that a dominant component detected within blood samples is haemoglobin (Figure 3.5), therefore the level of protein specificity exhibited by ATR-FTIR spectroscopy is parallel with these blood detection tests. A limitation of such presumptive tests is that they are subject to false positives due to the oxidative reaction which causes a colour change and the result is often very subjective, reducing the perceived reliability of the tests (Tobe et al. 2007). Additionally, luminol, KM and the ABAcard® Hematrace® have relatively short shelf lives of 1-2 hours, 9-12 months and twenty months, respectively (National Forensic Science Technology Centre, 2007; Omaha Police Department Crime Laboratory, 2003; Scenesafe, 2010).

ATR-FTIR spectroscopic analysis of blood has advantages over these routine presumptive and confirmatory tests in that no reagents are utilised in order to determine the presence of blood, the spectra obtained is objective and that there is no shelf life associated with its use. Particularly, once the instrument has been purchased, there are no additional kits, reagents

or accessories required to conduct analysis, which maintains the integrity of samples during analysis, in addition to keeping analysis costs down. It is these characteristics that are desirable in techniques utilised within the investigation of crime. ATR-FTIR spectroscopy offers a confirmatory alternative to fallible reaction-based tests, whereby the analysis is not limited to the detection of one body fluid, such as blood. The spectral output from the analysis is also objective; either the sample analysed is blood, as indicated by the specific characteristic peaks of blood, or it is not. The ability to carry out library searches on the instrument to compare the unknown sample with known spectra enables initial screening to determine qualitatively whether the sample is blood. This can then be quantitatively confirmed by examining and assigning the peak frequencies observed. A disadvantage that ATR-FTIR spectroscopy has compared to confirmatory blood identification tests is that it cannot distinguish between human and non-human blood (De Wael et al. 2008), which may prove challenging within the investigation of crime. However, the results obtained and discussed here demonstrate that ATR-FTIR spectroscopy is a suitable technique to identify blood.

3.2 SALIVA

Figure 3.15 demonstrates an ATR-FTIR spectrum obtained from a saliva sample that had been dried *in situ* on the ATR-FTIR analysis stage for five hours. Table 3.5 provides an overview of the identified saliva components that result in the presence of these peaks at the particular wavenumbers (cm^{-1}). A total of 45 measurements were taken from five individual 20µl aliquots of neat saliva collected in a sterile tube via spitting.

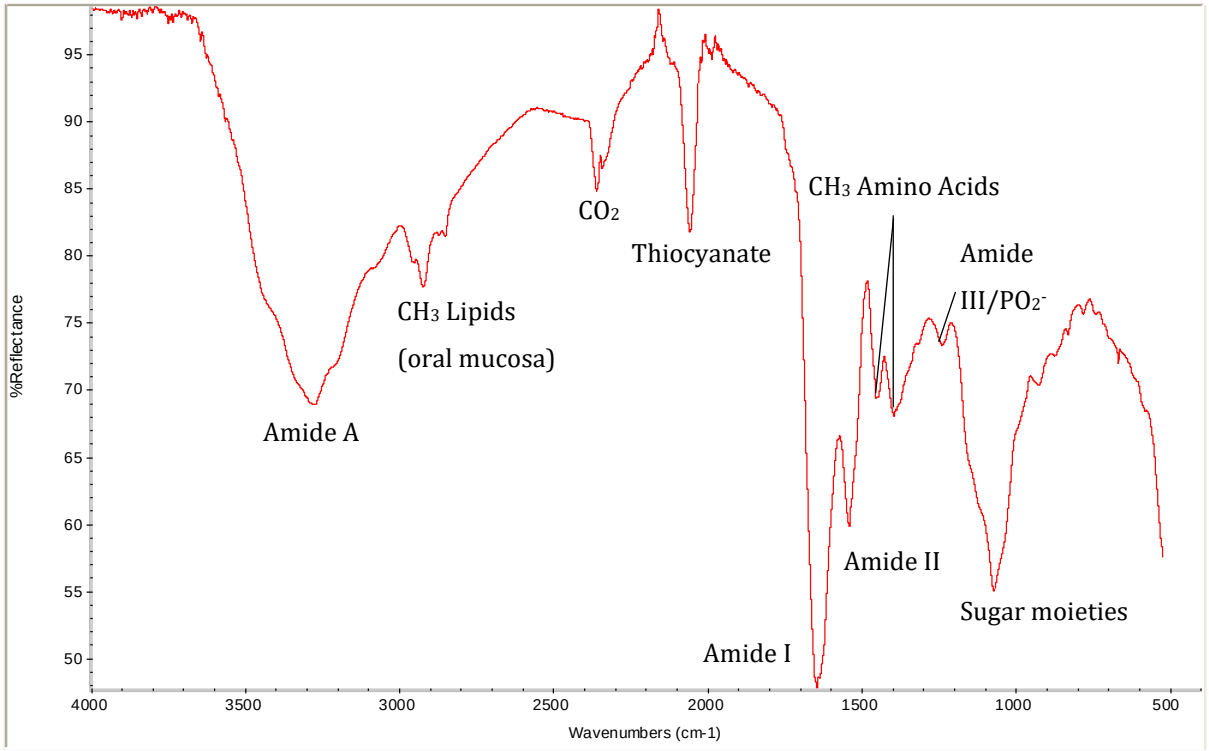

Figure 3.15: ATR-FTIR spectrum of neat saliva air dried in situ at 5 hours.

The peak positioned at 3273 cm^{-1} is a broad, strong peak which corresponds to amide A. The narrow peak observed at approximately 2057 cm^{-1} is categorised as a medium peak which is attributed to thiocyanate anions. The two narrow peaks positioned at approximately 1649 cm^{-1} and 1543 cm^{-1} are categorised as a strong amide I peak and a medium amide II peak, respectively. As echoed in the blood spectra (Figure 3.4), the amide I peak is also the most intense peak observed within the saliva spectrum. The final dominant peak observed at approximately 1075 cm^{-1} within the neat saliva spectrum corresponds to sugar moieties.

Table 3.5: ATR-FTIR peak component identification for saliva.

Wavenumber (cm^{-1})	Component Identification	Vibrational Mode	Reference
3282	Amide A	H bonded OH stretching, NH stretching	Garidel & Schott (2006b); Khaustova et al. (2010)
2926, 2850	Methylene stretches of lipid acyls in oral mucosa	Asymmetric & symmetric CH_2 stretching	Khaustova et al. (2010); Scott et al. (2010); Yoshida & Yoshida, (2004)
2059	Thiocyanate anions (SCN^-)	CN stretching	Schultz et al. (1996); Scott et al. (2010); Shaw & Mantsch, (2006)
1645	Amide I (α helix)	C=O stretching	Garidel & Schott (2006b); Khaustova et al. (2010); Movasaghi et al. (2008); Scott et al. (2010); Sultana et al. (2011)
1544	Amide II	NH bending coupled to CN stretching	Garidel & Schott (2006b); Khaustova et al. (2010); Movasaghi et al. (2008); Scott et al. (2010); Sultana et al. (2011)
1452	Methylene bending of amino acid side chains of proteins & lipids	Asymmetric CH_2 bending	Ahmed & Mantsch (1994); Khaustova et al. (2010); Scott et al. (2010)
1393	Amino acid protein side chains	Symmetric CH_2 bending	Khaustova et al. (2010); Scott et al. (2010); Sultana et al. (2011)
1239	Amide III/Phospholipids	CN stretching, asymmetric PO_2^- stretching	Arrondo & Goñi (1998); Movasaghi et al. (2008); Sultana et al. (2011)
1080-950	Sugar moieties (glycosylation)	CH_2OH groups, CO stretching and bending of COH groups, symmetric PO_2^- stretching.	Ahmed & Mantsch (1994); Khaustova et al. (2010); Scott et al. (2010); Sultana et al. (2011)

The remaining peaks observed are categorised as weak peaks due their low peak intensities. These peaks were identified as corresponding to lipid acyls of oral mucosa (2924 cm^{-1}), methylene groups of amino acid side chains in proteins and lipids (1452 cm^{-1}), amino acid side groups (1396 cm^{-1}), amide III/phospholipids (1320-1286 cm^{-1}) and sugar moieties, such as glucose, glycosylated proteins, and phosphate groups within nucleic acids (1080-950 cm^{-1}). The peak observed at approximately 2342 cm^{-1}, present in some spectra but not all, corresponds to carbon dioxide interference (Gerakines et al. 1995). This peak has also been observed within semen and vaginal secretion samples, but is not considered as a contributing peak to the identification of any of the overall body fluid spectra.

It is evident that there are a number of common peak frequencies, and therefore common biological components present within the spectra of neat saliva and neat blood. This is not surprising given that many of the corresponding functional groups are abundant across biological samples in general (Khaustova et al. 2010). However, it is the peak frequency and shape observed that can enable characterisation of some of the common peaks to body fluid specific components. The common peaks observed in both neat saliva and blood were amide A, I, II and III and methyl/methylene groups within amino acid side chains of proteins and lipids (Table 3.1 & Table 3.5). Amide A and III correspond to protein components, although cannot provide conformational information like amide I and II peaks, as stated in Section 3.1.

In order to establish whether any of the peaks observed within the spectra of neat saliva could be assigned to specific biological components, direct comparisons of two of the most common proteins often detected in saliva, α-amylase and lysozyme, were carried out. The amide peaks are specifically associated with proteins within a sample, therefore it was logical to determine whether α-amylase or lysozyme could be attributed as contributors to the amide A, I and II peaks of neat saliva spectra. The amide A peak (~3282 cm^{-1}) within the neat saliva spectra is categorised as a strong, broad peak, much like the amide A peak observed within the spectra of blood. The functional groups responsible for the amide A vibration within neat saliva originate from the same groups which give rise to the amide A blood peak (CH, NH and OH stretching vibrations). However, the biological components that are attributable to this peak, namely proteins (Sultana et al. 2011), will differ across the two body fluids based on their composition. It is evident from Figure 3.16 that the ATR-FTIR spectra of lysozyme and α-amylase differ from one another vastly, although it is possible to ascertain where each protein could be contributing to the peaks observed within the neat saliva spectra. The average peak frequencies observed within the neat saliva spectra for amide A, I and II were 3282, 1645 and 1544 cm^{-1}, respectively. Lysozyme exhibited very similar peak frequencies for the same amide peaks, observed at frequencies 3282, 1638 and 1530 cm^{-1},

respectively, which appeared as strong peaks throughout the spectra. However, α-amylase exhibited only two of the amide peaks; a strong amide A peak (3292 cm^{-1}) and a weak amide I peak (1641 cm^{-1}). Comparisons between the spectra in Figure 3.16 demonstrate that lysozyme could be a major contributor to the amide peaks of neat saliva based on the peak frequencies, the shape of the peaks and the general spectral pattern observed.

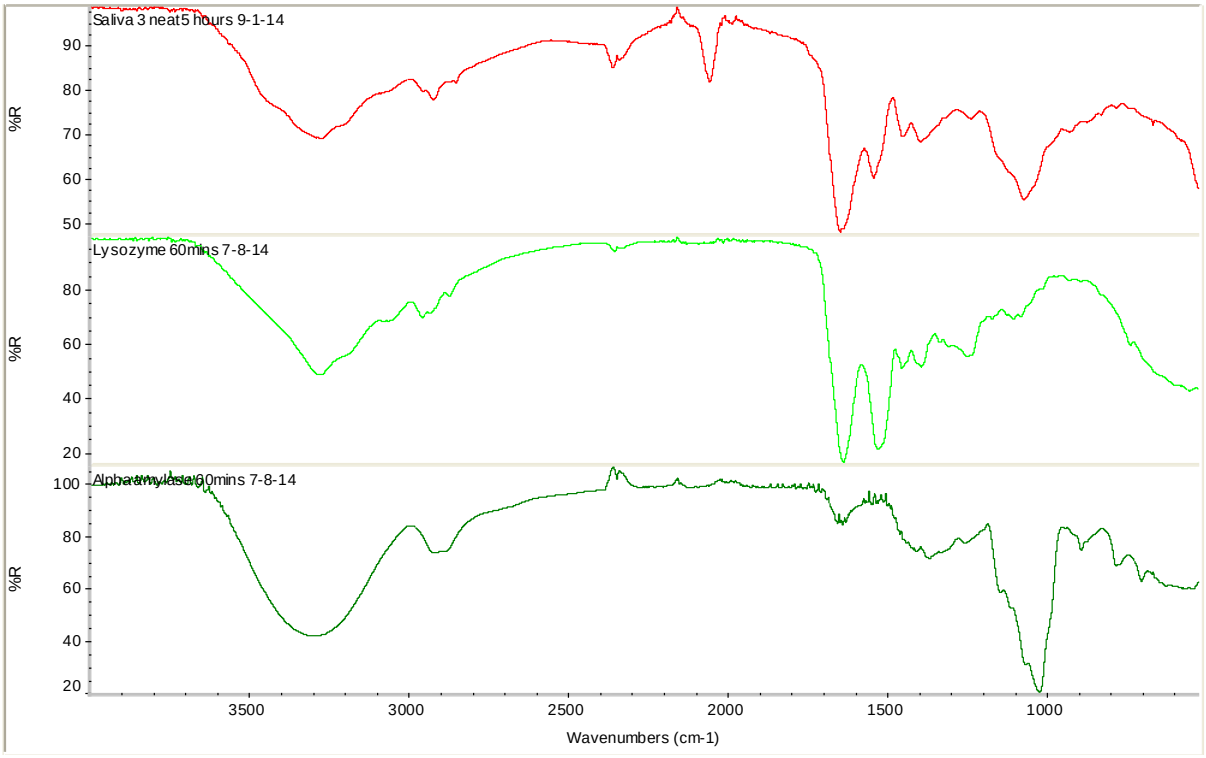

Figure 3.16: ATR-FTIR stacked spectra comparisons of neat saliva (red), lysozyme (green) & α-amylase (dark green).

The amide A peak of the α-amylase spectra exhibited a very different appearance compared to the amide A peak of both neat saliva and lysozyme. The overall appearance was a strong, broad peak, which is typical of the ATR-FTIR spectra of α-amylase (Ernest et al. 2013), whereas in the neat saliva and lysozyme spectra the peak is much more defined and considered as a medium intensity peak. This suggests that α-amylase may not be a major contributor to the spectral profile of neat saliva, although lysozyme may contribute to the amide A peak in neat saliva spectra.

The amide I peak observed within neat saliva, with an average peak frequency of 1645 cm^{-1}, was the strongest peak. This suggests that the dominant protein secondary structure within saliva is unordered (Table 3.2), although this structure contrasts with the altered α-helix secondary structure assignment stated by Scott et al. (2010) for the amide I peak. The average amide II peak frequency observed across the neat saliva spectra was 1544 cm^{-1}

which corresponds with a β-sheet protein secondary structure (Table 3.2). Due to the complex nature of saliva, it is much more difficult to assign specific proteins to the amide I and II peaks, as less than 1% of the body fluid contains protein based molecules, such as glycoproteins, enzymes, immunoglobulins and mucins (Humphrey & Williamson, 2001). The amide I peak observed in the lysozyme spectra is comparable with those observed within the neat spectra, although the peak frequencies vary. The protein secondary structure of lysozyme equates to 40% α-helix, 27% β-turn, 19% β-sheet and 14% unordered (Calabrò & Magazù, 2012; Kong & Yu, 2007). However, in the neat saliva spectra, the average peak frequency obtained for amide I suggests an unordered secondary structure is most abundant across the protein constituents. The average peak frequencies observed for the amide II peak within both neat saliva and lysozyme do not correspond well, both visually and in relation to the protein secondary structure, which suggests that the lysozyme was not the dominant contributor to this particular peak. However, it is possible to suggest that lysozyme may be attributed to the peak in combination with various other proteins present within neat saliva. One other protein found in saliva that could contribute to the amide I peak could be proline-rich proteins (PRPs), which typically exhibit an amide I peak at approximately 1655 cm^{-1} (Elangovan et al. 2007).

In contrast to the lysozyme spectrum, the α-amylase spectrum does not appear to exhibit any strong peaks within the amide I and II region, although a weak peak was observed at approximately 1641 cm^{-1} (Figure 3.16). As α-amylase is an abundant protein within saliva, this observation initially seemed unusual, given that the secondary structure of this protein comprises of three domains, consisting predominantly of β-structures, followed by α-helical structures (Ramasubbu et al. 2005; UniProt, 2014). However, there are two families of α-amylase; family "A" consisting of glycosylated proteins (that is, the α-amylase molecules have sugar moiety chain attachments) (Snider, 2014), and family "B" which are α-amylase molecules which are not glycosylated (Ramasubbu et al. 1996). It is possible that the A family of α-amylase was the dominant protein present within the α-amylase examined, resulting in only a weak peak within the amide region. This suggestion was supported by the observation of the strongest peak at approximately 1024 cm^{-1} within the α-amylase spectrum, which falls within the sugar moiety region, therefore it is probable that the sugar moiety peak observed corresponds to family "A" α-amylase molecules. The sugar moiety region of the infrared spectrum typically extends from 1180-950 cm^{-1}, whereby peaks corresponding specifically to carbohydrates such as glucose, glycogen and glycosylated proteins are exhibited (Scott et al. 2010). When compared to the sugar moiety peak observed within the neat saliva spectra, the peak frequencies vary drastically, therefore it is unlikely that α-amylase is a major

contributor to this particular peak. However, when the sugar moiety region of the ATR-FTIR spectra of neat saliva and α-amylase were overlapped, it was evident that the widths of each peak were comparable, although the apex of each peak does not lie at the same frequency (Figure 3.17). Based on this, it could be stated that the peak observed typically at 1073 cm^{-1} in the spectra of neat saliva can be attributed to glycosylated α-amylase, as well as other sugar moieties present in saliva.

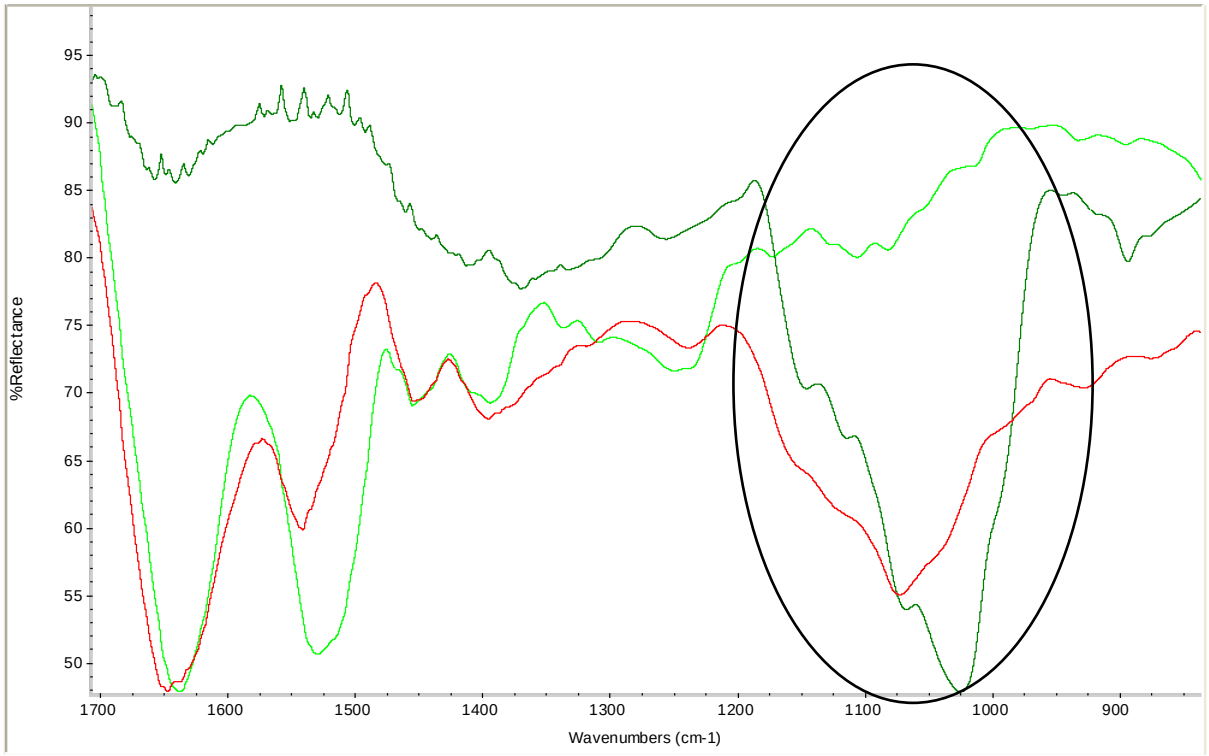

Figure 3.17: Overlay spectra demonstrating the overlap (circled) of the sugar moiety peaks in neat saliva (red) & the glycosylated protein peak in α-amylase (dark green) (very weak peak also observed in the sugar region within the lysozyme spectrum (green)).

The amide III peak observed within the spectra of neat saliva appears as weak and narrow, with an average peak frequency exhibited at 1239 cm^{-1}. Unlike the amide III peak observed within the neat blood spectra, there is no characteristic "W" shape exhibited (Figure 3.6), which indicates that different proteins give rise to the amide III peak in saliva. As can be seen in Figure 3.16, α-amylase does not exhibit any peaks within the typical amide III region. However, the lysozyme spectrum does exhibit a similar, weak peak with an average peak frequency of 1250 cm^{-1} that correlates with an amide III vibration. These particular peaks arise from asymmetric and symmetric C-O-C vibrations that correspond to phospholipid constituents of proteins, which span the 1250-925 cm^{-1} region of the infrared spectrum (Khaustova et al. 2010; Sultana et al. 2011).

The majority of the remaining peaks observed within the neat saliva spectra are also categorised as weak peaks. At the high frequency end of the spectrum, the relatively narrow peak observed at 2926 cm^{-1}, with a small shoulder exhibited at approximately 2852 cm^{-1}, corresponds to methylene groups on lipid acyls with symmetric and asymmetric stretching vibrational modes, respectively (Khaustova et al. 2010; Scott et al. 2010; Sultana et al. 2011). Two small, narrow peaks, positioned in between amide II and amide III, with peak frequencies 1452 cm^{-1} and 1393 cm^{-1}, also correspond to the bending of methylene groups, although these particular vibrations arise from amino acid side chains and proteins, which are comparable with the similar peak appearance and frequencies observed within the neat blood spectra (Figure 3.4) (Kanagathara et al. 2011; Movasaghi et al. 2008; Sultana et al. 2011).

The peak observed at approximately 2060 cm^{-1} within the spectra of neat saliva can be attributed to the anion thiocyanate (SCN^-) (Figure 3.18). This peak arises specifically from the C-N stretching vibrational mode and it is of significance to the spectra of neat saliva as it appears in a region that is typically free from any peak absorption from biological samples (Schultz, et al. 1996; Scott et al. 2010).

Thiocyanate is known to be present in saliva, serum and urine in relatively low concentrations, although in samples of blood and urine the thiocyanate concentration is often too low to be detected with ATR-FTIR spectroscopy (Glatz et al. 2001; Schultz et al. 1996). However, in saliva samples the thiocyanate peak typically exhibits a medium-to-weak intensity which varies between samples. The variation observed is a result of physiological, environmental and genetic factors (Glatz et al. 2001; Tsuge et al. 2000). The presence of thiocyanate is related to its antibacterial role, whereby it is oxidised by salivary peroxidases to hypothiocyanate, which acts as a potent salivary antibacterial agent (de Almeida et al. 2008; Schultz et al. 1996; Scott et al. 2010). Thiocyanate levels within saliva can increase as a result of poor health, such as colds and smoking habits, causing an increase in antibacterial activity within the mouth. Thiocyanate levels can also be increased due to the intake of glucosinolate-containing vegetables and thiocyanate-containing dairy products. These factors, singularly or in combination impact on the variation in thiocyanate peak intensity observed within neat saliva spectra (de Almeida et al. 2008; Schultz et al. 1996; Scott et al. 2010).

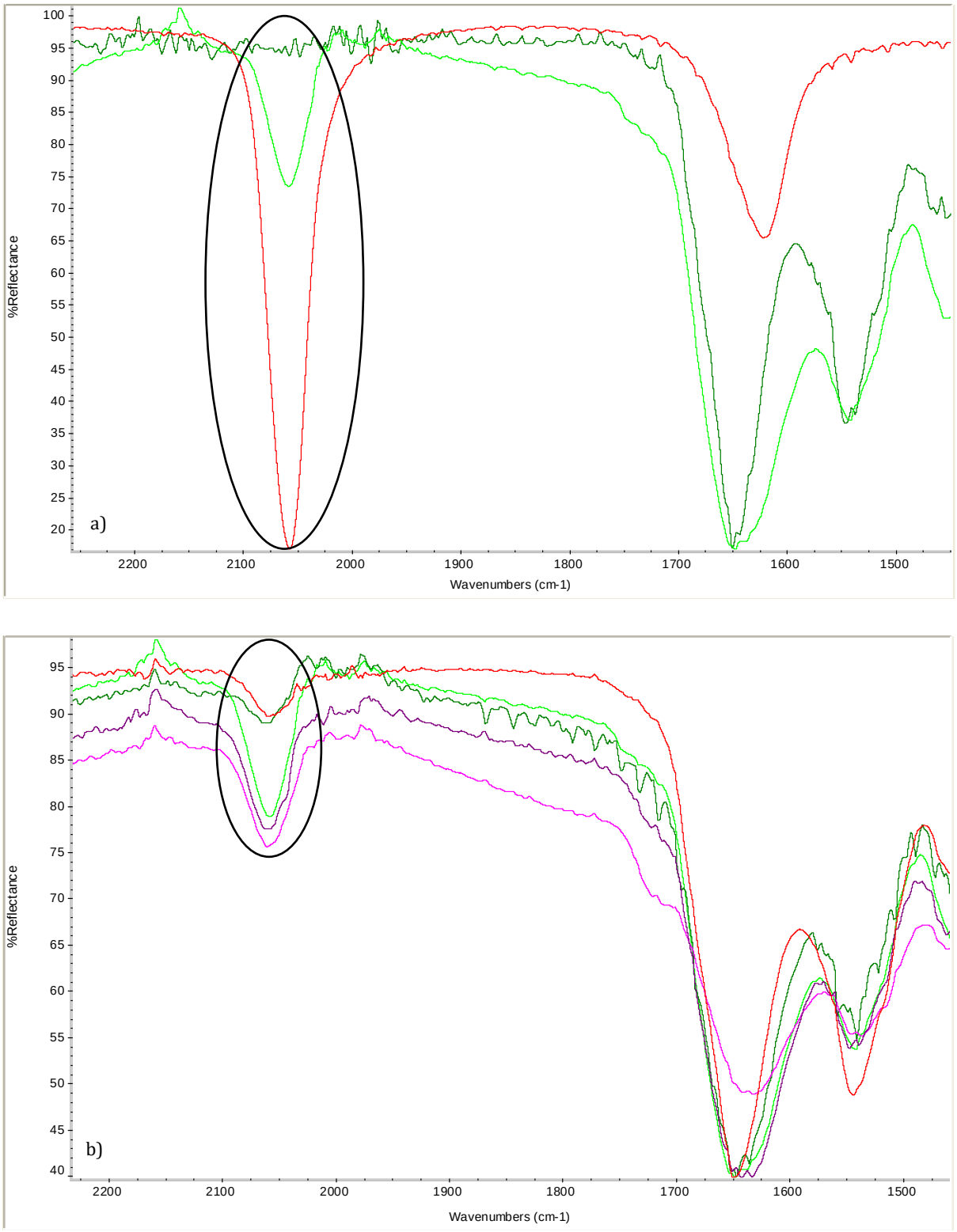

Figure 3.18: a) Overlay spectra demonstrating the correspondence in the thiocyanate peak (circled) observed in potassium thiocyanate (red) with neat saliva (green) & extracted saliva (dark green); b) overlay of the thiocyanate peaks observed across five different saliva samples.

The results obtained from the ATR-FTIR spectroscopic analysis of neat saliva samples correlate with those reported by a number of research groups (Khaustova et al. 2010; Schultz et al. 1996; Scott et al. 2010; Shaw & Mantsch, 2006; Sultana et al. 2011). As with much of the literature examining body fluids with infrared spectroscopy, the saliva specific literature identifies and examines differences within the spectra of saliva obtained from healthy individuals compared to individuals of differing health states, such as during pregnancy (Sultana et al. 2011), sufferers of diabetes (Scott et al. 2010) or when stressed (Khaustova et al. 2010). The relative peak frequencies and characteristic peak shapes were comparable across the literature with that obtained in this research. This demonstrates the reproducibility of a characteristic spectral pattern that can be obtained from neat saliva, with only obvious variation observed within the thiocyanate peak. These findings are a reflection of those obtained for the neat blood spectra and provide additional support for the development of a validated body fluid reference infrared spectral library to be incorporated into FTIR instruments, which would allow comparisons to be automated, resulting in faster confirmation of particular body fluids.

3.2.1 IDENTIFICATION OF SALIVA STAINS: ON COTTON

When neat saliva is encountered at crime scenes, it is not always clearly visible as it is a colourless fluid. However, when saliva is present in the form of a dried stain, the identification of saliva can be even more difficult. Section 3.2 demonstrated that ATR-FTIR spectroscopy could successfully be utilised to characterise the spectrum of neat saliva. However, as stated in Section 3.1.1, it is important to ascertain whether body fluids can be successfully detected and identified when deposited on to cotton. Figure 3.19 demonstrates the typical ATR-FTIR spectrum yielded from a dried saliva stain on cotton that has been aged for 24 hours. A total of 460 measurements were taken from 92 saliva stains on cotton collected from one donor.

It is evident from the spectrum produced that there were no characteristic saliva peaks observed when saliva was deposited on cotton. The peaks observed throughout the spectrum were representative of the cotton substrate as demonstrated in Figure 3.20, where the 24 hour aged saliva stain on cotton is exhibited in green and the cotton blank obtained from the same sample is in orange. The spectrum of neat saliva has also been included (red) to demonstrate where the saliva peaks were expected to be observed within the spectrum. Saliva stains from three individual donors which were aged from 24 hours to 18 months, and

of varying volumes (20-500 µl) were examined to determine whether any of these variables would enable better detection of salivary components within the ATR-FTIR spectra. However, across all the samples analysed, none exhibited peaks that could be attributed to the biological components of saliva (Table 3.5).

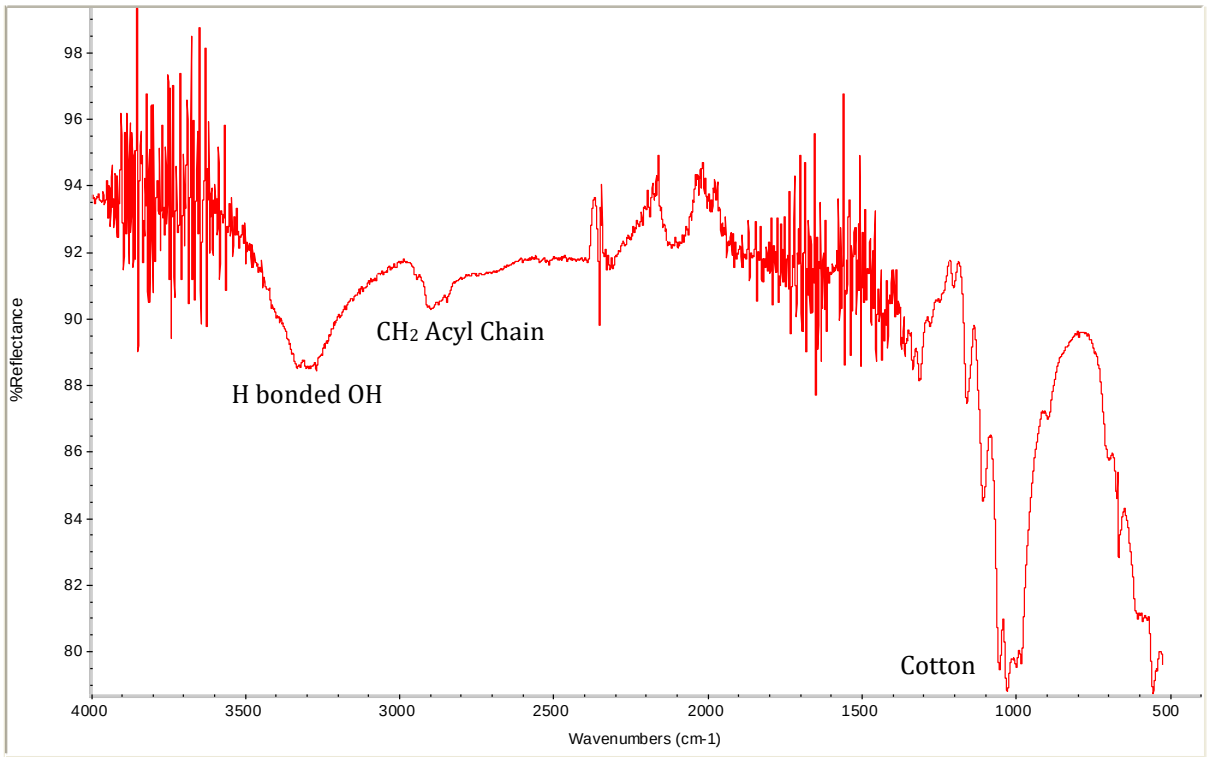

Figure 3.19: ATR-FTIR spectrum of a saliva stain on cotton aged for 24 hours.

These results were surprising when considering the volumes of saliva that were tested. To examine the limit of detection for saliva stains on cotton, swatches measuring approximately 2x2 cm were prepared prior to any sample deposition. Cotton swatches of 4x4 cm were typically utilised for any body fluid deposition. However, smaller swatches were utilised in this instance to determine whether a smaller absorbance area would allow for better detection of saliva peaks when analysed due to an expected higher concentration present across the cotton overall. For saliva aliquots of 20 µl and 50 µl, the cotton was not saturated, but widespread absorption was evident as soon as the fluid was deposited. For saliva aliquots of 100-500 µl, the cotton was completely saturated with the sample, with some overflowing from the cotton into the petri dish for the larger volumes. This would suggest that there should be adequate salivary components throughout the cotton substrate due to complete saturation. However, for all of the volumes of saliva depositions analysed no characteristic saliva peaks were observed within the resulting spectra (Figure 3.21).

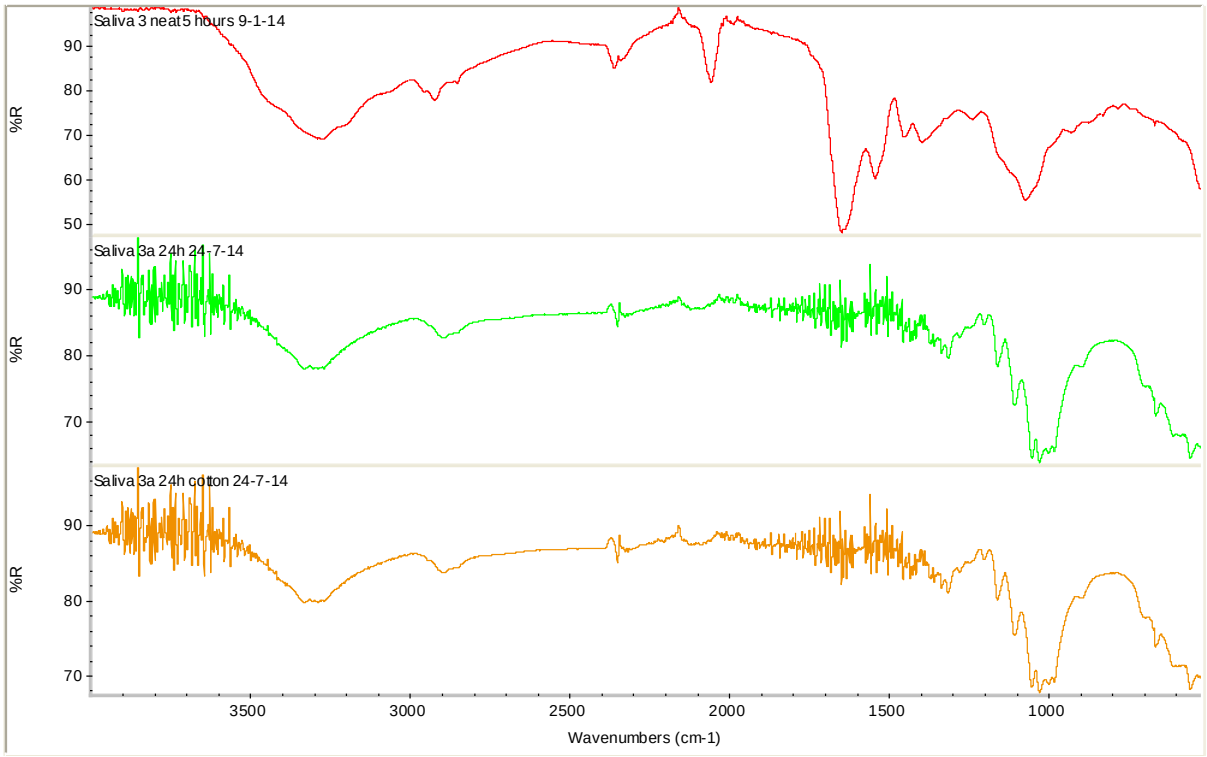

Figure 3.20: ATR-FTIR overlay spectra of saliva stain on cotton aged for 24 hours (green), cotton blank from the same sample (orange) & neat saliva (red).

There are a number of possible explanations as to why saliva stains on cotton were not detected when analysed with ATR-FTIR spectroscopy. Firstly, as the body fluid itself is colourless, it is possible that it could not be differentiated from the cotton substrate due to the saliva appearing as transparent. This would result in the evanescent wave of infrared light passing the salivary component vibrating molecules and transferring the energy from these molecules to the cotton component vibrating molecules. Therefore, it is only the vibrational modes detected from the cotton substrate when the infrared light is transmitted to the detector (Sahu, 2007). Another possible explanation could be that the saliva itself experiences widespread absorption by the cotton, therefore the areas examined on the cotton substrate have a low concentration of salivary constituents which results in the dominance of the cotton components overlapping any salivary components that may be detectable in the obtained ATR-FTIR spectra.

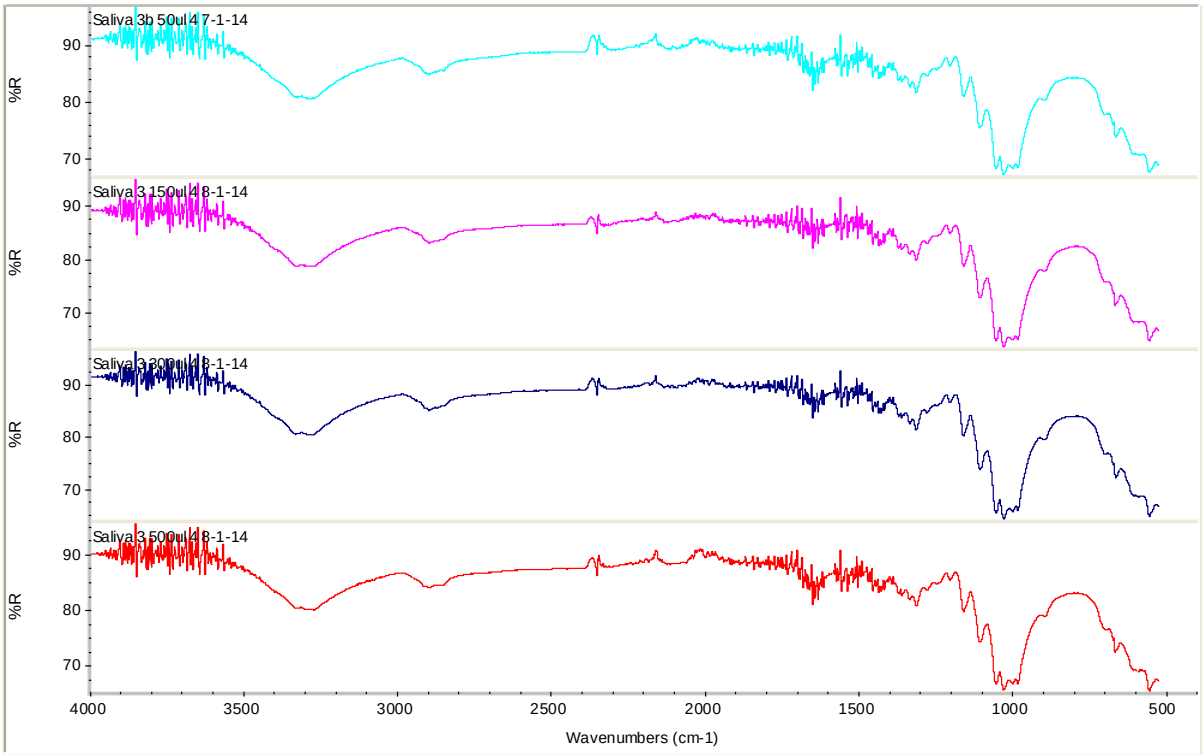

Figure 3.21: Example spectra of saliva stains on cotton deposited at volumes of; 50 µl (turquoise), 150 µl (pink), 300 µl (dark blue) & 500 µl (red).

As no characteristic saliva peaks were evident on samples deposited on cotton, no comparisons could be made with the spectra of neat saliva in regards to the maximum peak intensity and overall quality observed. This is a clear limitation of the method which demonstrates that direct analysis with ATR-FTIR spectroscopy is not appropriate for biological samples that appear colourless when deposited on to a substrate. Within a forensic context, this limits the application of biological analysis with ATR-FTIR spectroscopy to only samples that can be visibly distinguished from the deposition substrate, i.e. bloodstains.

3.2.2 IDENTIFICATION OF SALIVA STAINS: EXTRACTED

The issue of saliva stains being undetectable when analysed with ATR-FTIR spectroscopy was examined to determine whether sample extraction, as carried out on bloodstains on cotton (Section 2.2.2.2 & 3.1.2), could be utilised to successfully obtain a characteristic saliva spectrum. Prior to analysing any aged saliva stains, it was necessary to determine the limit of detection when extracting the saliva from the cotton. Saliva aliquots of 20 µl, 50 µl and 100 µl were deposited on to cotton and air dried for up to a maximum of 24 hours. Each sample was then extracted and analysed with ATR-FTIR spectroscopy as per the “wet-to-dry” procedure.

Figure 3.22 demonstrates the ATR-FTIR spectra obtained for each extracted aliquot. Initial observations of the three spectra indicate that a poor quality spectrum was obtained from the extracted 20 µl saliva stain (red), where lots of noise and atmospheric interference was observed. The only peaks observed that could be attributed to the characteristic peaks of saliva were the asymmetric and symmetric stretching vibrations of methylene groups of lipid acyls in oral mucosa (~2919 cm^{-1} & 2850 cm^{-1}) and sugar moieties (~1114 cm^{-1}). Any of the remaining characteristic peaks expected to be observed within saliva were masked by the noise interference across the spectrum. The maximum peak intensity observed for the strongest peak within the 20 µl extract was approximately 98%. As intensity measurements descend from 100%, this demonstrates the weakness of the peaks overall within the saliva extract sample, as well as provides an indication of how few biological components were successfully extracted from the cotton.

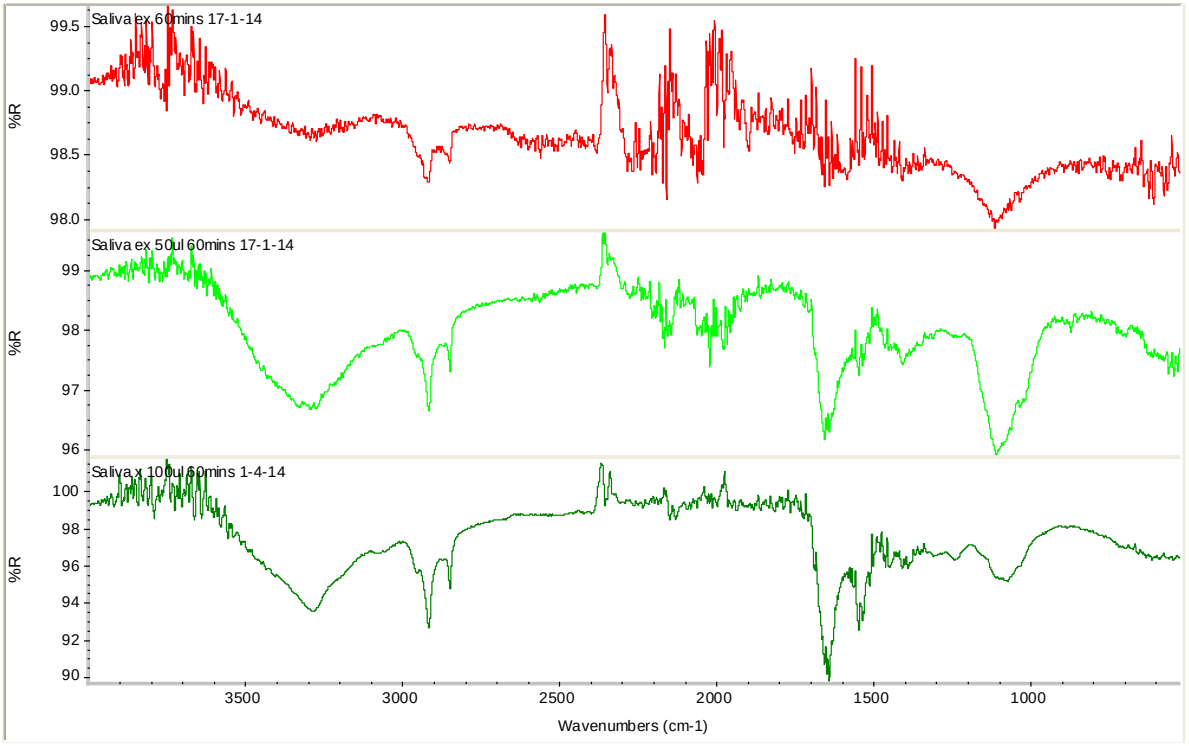

Figure 3.22: ATR-FTIR spectra comparisons of 20 µl (red), 50 µl (green) & 100 µl (dark green) extracted saliva stains.

Improvements across the spectrum were observed for the extracted 50 µl saliva stain (Figure 3.22, green), whereby the noise had reduced and appeared more confined to the water absorption regions. Additionally, more defined peaks were evident which could be attributed to corresponding saliva peaks by comparison of the peak frequencies (Table 3.5). Namely, amide A (3293 cm^{-1}), the methylene groups of lipid acyls doublet (2917 cm^{-1} & 2849 cm^{-1}), amide I (1649 cm^{-1}), very weak amide II (1547 cm^{-1}), methylene groups of amino acids and

proteins (1452 cm^{-1}) and the sugar moiety (1110 cm^{-1}) peaks were detected. The only peaks not evident within the 50 µl extract were thiocyanate and amide III/phospholipids. This may be a result of the noise exhibited within the 2400-1700 cm^{-1} region masking any potential thiocyanate peak and as amide III was typically a weak peak in the spectra of neat saliva it was therefore not detected in this extract (Figure 3.15). The maximum peak intensity observed for the strongest peak within the 50 µl saliva extract was approximately 96%, which is an improvement in peak strength across the spectrum compared to the 20 µl saliva extract but it is generally still very poor. When compared to the maximum peak intensity exhibited within the spectra of neat saliva (~48%), a near 50% decrease in intensity was observed in the 50 µl extract. However, the spectral pattern observed, the combination of peaks and peak frequencies enabled comparisons to be made to establish the presence of saliva.

The spectrum obtained for the 100 µl saliva extract (Figure 3.22, dark green) demonstrated the best overall quality from all of the saliva extracts examined. It is evident that the spectral peaks exhibit clear definition with good resolutions and there was a further reduction in noise interference observed across the spectrum. All of the characteristic saliva peaks, with the exception of thiocyanate, were observed within the 100 µl extracted spectrum, although the peak strength appeared to have decreased within the 1450-950 cm^{-1} region, with a noticeable difference in peak strength observed in the sugar moiety peak. This particular peak ordinarily exhibits a strong peak within the spectra of both neat and extracted saliva samples, although within the 100 µl extract spectrum, this peak appears uncharacteristically weak. As saliva is a body fluid comprised of a complex, heterogeneous mixture of constituents, it is possible that this particular aliquot of saliva did not contain as many sugar moieties as previous depositions.

The absence of the thiocyanate peak from the extracted saliva spectra was unexpected as typically the peak intensity observed was equal to or greater than the peak intensities of the methylene groups, both high and low frequency peaks, amino acid side chains and amide III/phospholipid peaks. It has been well documented that thiocyanate is present in saliva in relatively small amounts and typically the thiocyanate peak is categorised as relatively narrow and weak, but is considered as unique to the spectra of saliva (Scott et al. 2010; Shaw & Mantsch, 2006; Shultz et al. 1996). It is possible that during the extraction process the thiocyanate did not disassociate from the cotton substrate effectively, therefore it was sparsely distributed throughout the saliva extract and not detectable when analysed with ATR-FTIR spectroscopy. The absence of the thiocyanate peak within saliva stain extract

spectra does not hinder the potential for these samples to be identified as saliva, although the specificity is reduced to some degree.

A distinct difference within the extracted sample spectra of all three saliva aliquots compared to the neat saliva spectra was the increased peak intensity and general presence of the methylene groups of lipid acyls (~2920 cm^{-1} & ~2850 cm^{-1}). Within the neat saliva spectra (Figure 3.15), these particular peaks were relatively weak in comparison to the amide peaks. However, within the extracted saliva spectra (Figure 3.22) the same peaks appear as one of the strongest peaks across the spectrum with comparable peak intensities to those observed amongst the amide A and I peaks. The apparent increase in peak intensity of the methylene groups of lipid acyl peaks within extracted saliva spectra may have been due to the aggregation of these molecules during the extraction procedure. Lipid acyl residues contain a hydrophobic backbone, which makes them insoluble molecules when interfaced with water and typically produce peaks within the high frequency end of the infrared spectrum (~2920 cm^{-1} & ~2850 cm^{-1}) (Arrondo & Goñi, 1998; Defagó et al. 2011). As no interaction takes place between the lipid acyls and the extraction solution, the aggregated molecules remain as independent entities within the overall extraction sample, which may have resulted in greater detection of these molecules once the water had evaporated during analysis.

Assessment of the spectral quality obtained from the various saliva extracts demonstrated that depositing 100 µl of starting material enabled ATR-FTIR spectra to be obtained that exhibited the characteristic peaks attributable to those of neat saliva with the least amount of variability. Therefore, it can be suggested that the limit of detection for the use of ATR-FTIR spectroscopic analysis on extracted saliva stains is appropriate for a stain that is representative of approximately 100 µl of saliva. However, stains representative of approximately 50 µl or greater could potentially still yield characteristic salivary peaks. As a result of the limit of detection analysis for extracted saliva samples, any subsequent saliva samples that were prepared for ageing purposes were deposited in volumes of 100 µl, unless otherwise stated.

A total of 378 measurements were taken from 63 extracted samples in a “wet-to-dry” analysis across saliva stains on cotton that had been aged from 24 hours to 7 days, 14 days to 6 months and 18 months (20 µl saliva depositions). Of the 378 measurements, 138 reflected the spectra of a dry sample and 240 yielded spectra representative of water, as demonstrated in Figure 3.2b. Across all of the sample ages that were extracted, peaks were obtained that corresponded with some of the characteristic peaks of neat saliva, although there was

significantly greater variation observed in the extracted saliva spectra compared to the extracted spectra of the other body fluids analysed. Figure 3.23 demonstrates a good quality spectrum obtained from an extracted 3 day aged saliva stain (red) in comparison to the ATR-FTIR spectrum of the same saliva sample on cotton prior to extraction (green) and a cotton blank (dark green). It is evident that the extraction of the saliva stain from this particular sample had been successful, with clearly defined peaks across the spectrum which were comparable to the characteristic peaks of neat saliva spectra. In contrast, it is evident that none of the saliva associated peaks were detectable when the same saliva stain was initially analysed directly from the cotton. The spectra produced from the saliva stain on cotton and the cotton blank exhibit a near identical spectral pattern, further supporting that saliva was not detectable when deposited on to cotton and analysed directly with ATR-FTIR spectroscopy.

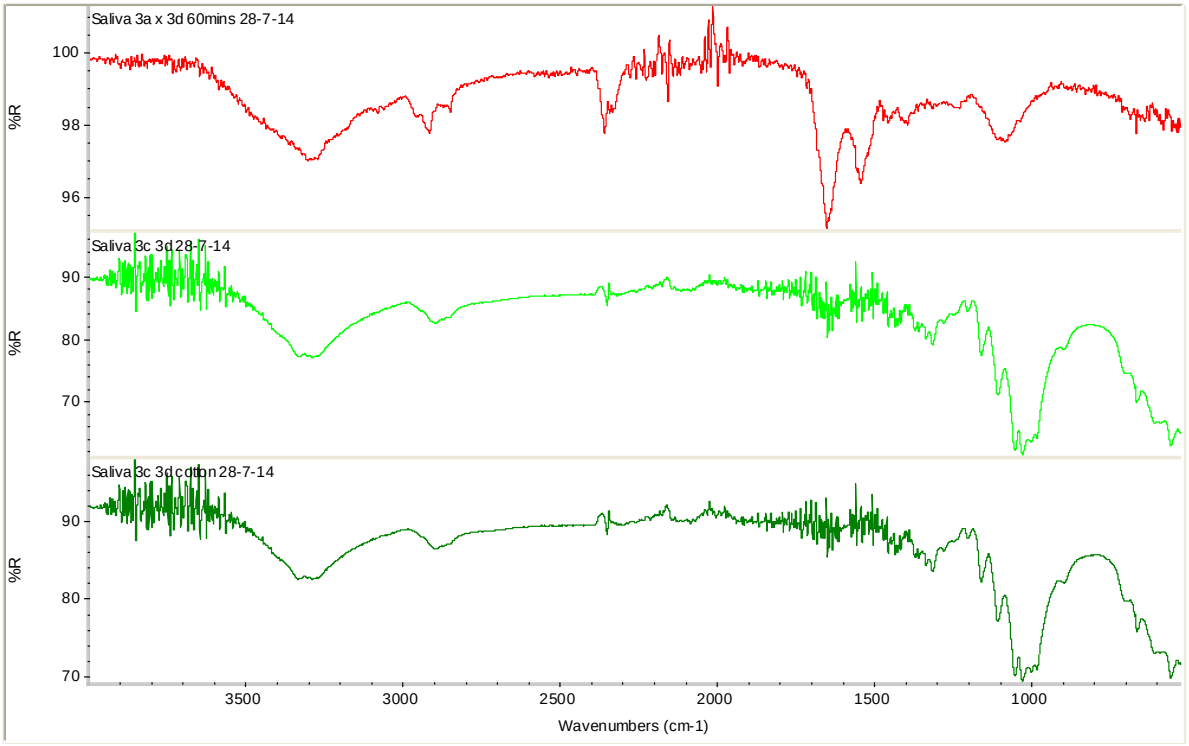

Figure 3.23: Example ATR-FTIR spectra from an extracted saliva stain (red), saliva stain on cotton (green) & a cotton blank (dark green), all from the same sample that had been aged for 3 days.

The spectrum for the extracted aged saliva stain observed in Figure 3.23 provides an example of the more successful extractions of saliva stains. However, not all of the spectra were consistent in regards to the reproducibility of good quality spectra from extracted saliva stains. This was not a result of the limitations of the technique, but more so of the challenge of analysing a body fluid that is comprised of 99% water (de Almeida et al. 2008). There was great variation across the spectra regarding the spectral quality, whereby some of the sample

extracts exhibited all of the corresponding saliva peaks, where others contained great levels of atmospheric interference from water vapour and carbon dioxide. Figure 3.24 demonstrates the variation in spectral quality across four different aged saliva stain extracts.

Observations from the spectra displayed in Figure 3.24a, c, e & g demonstrate that saliva stains aged from 24 hours up to 18 months could successfully be extracted and yield a good quality ATR-FTIR spectrum with the method developed in this research. Assessment of the observed peak frequencies, peak combination and the overall spectral pattern allowed for each of these samples to be identified as originating from saliva. In direct contrast to these good quality spectra, approximately 40% of the extracted saliva samples produced very poor quality spectra, whereby atmospheric interference dominated the spectra and only limited distinguishable peaks were observed where the frequencies could be compared to those of known saliva peaks (Figure 3.24 b, d, f & h).

The regions of the infrared spectra that appeared to suffer most from this interference were 4000-3100 cm^{-1} and 2400-1200 cm^{-1}, where excessive noise was abundant. It is likely that this noise is due the presence of atmospheric water vapour (Figure 3.3e). The peaks that were present could be compared to the characteristic saliva peaks by assessing the peak frequencies at which they occur. However, the fewer peaks that were present, the less confidence there was in the successful determination of the sample as saliva. As a result, these samples were excluded from any comparative and statistical analysis. As approximately 60% of the dry measurements obtained from the extracted saliva spectra contained spectral patterns equivalent to those of neat saliva, comparisons could be made between the average peak frequencies observed for both datasets. Figure 3.25 provides an overview of the variation in peak frequency between neat saliva and extracted saliva spectra. It is evident that the variation in peak frequency between the neat saliva and extracted saliva was minimal, which demonstrates consistency in the peak frequencies associated with the biological components of saliva when examined with ATR-FTIR spectroscopy. These findings support those obtained for blood samples, as discussed in Section 3.1.2, which further highlights the potential for this technique to be utilised for the examination of biological evidence.

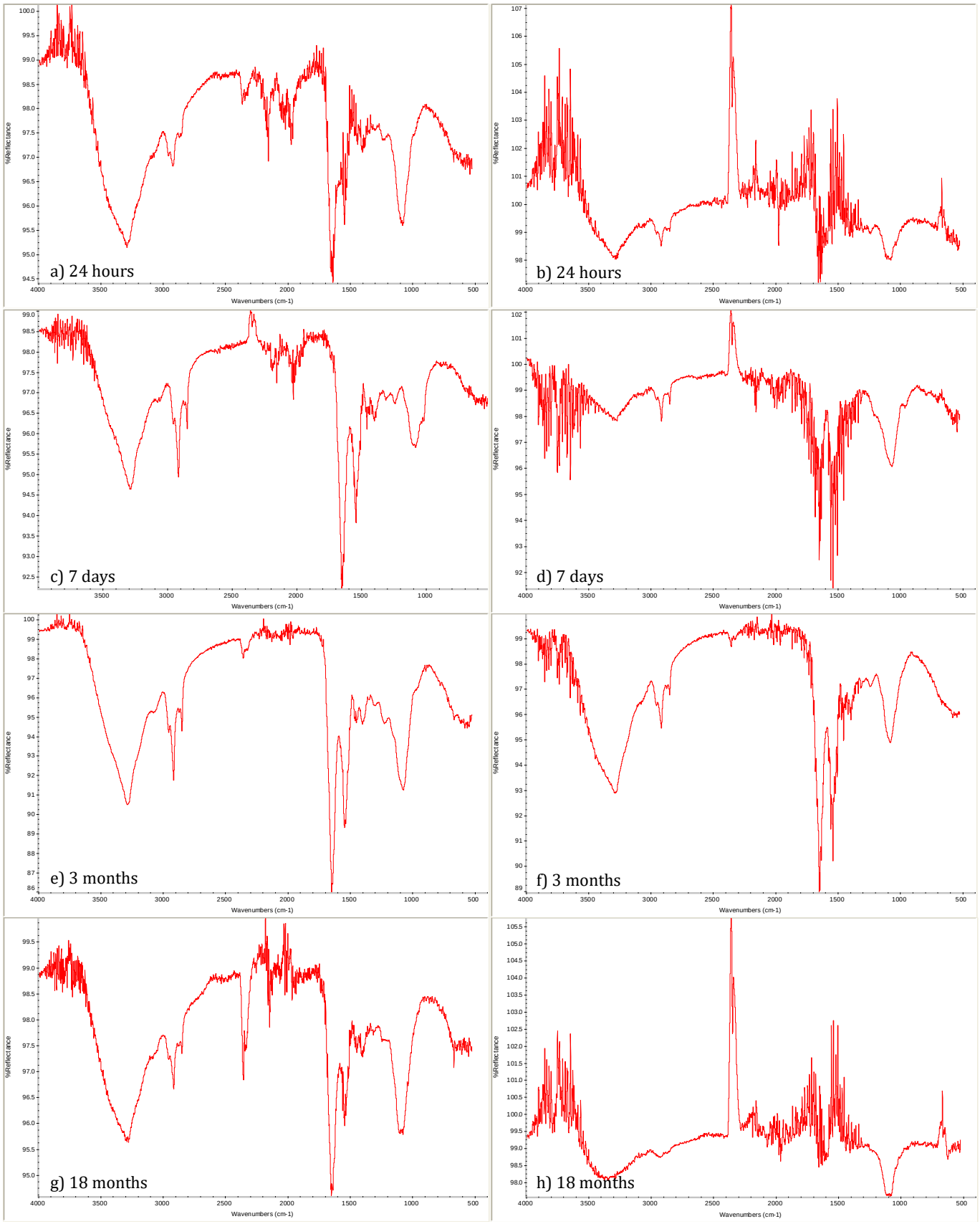

Figure 3.24: Examples of good & poor quality ATR-FTIR spectra obtained from aged saliva stains; a) good quality, 24 hours, b) poor quality 24 hours, c) good quality, 7 days, d) poor quality, 7 days, e) good quality, 3 months, f) poor quality, 3 months, g) good quality, 18 months, h) poor quality, 18 months.

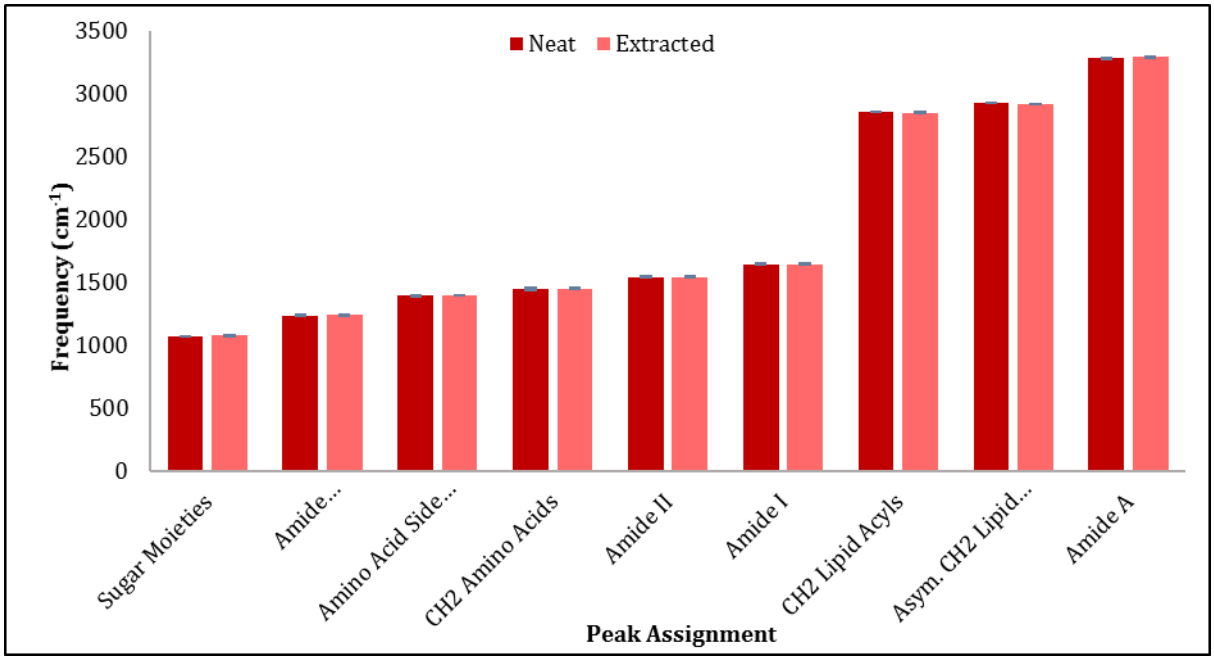

Figure 3.25: Bar graph comparing the average peak frequencies observed in the spectra of neat & extracted saliva.

The spectra obtained from saliva stains that had been aged prior to extraction, for various time periods, did not demonstrate any particular relationship between the sample age and the overall quality of spectra produced. However, the 18 month saliva stain extracts exhibited the greatest number of poor quality spectra across the various sample ages, with seven out of eight samples producing spectra that were not fit for comparison. These samples were prepared with 20 µl of saliva, rather than 100 µl, as the extent of the limit of detection for saliva extract samples had not been explored when these samples were placed into storage. Therefore, it was anticipated that these extracts would be of poor quality. Conversely, one of the eight samples did yield good quality spectra that enabled comparisons of the peak frequencies to be made with the characteristic peaks of neat saliva (Figure 3.24g). This demonstrates that it is possible for saliva stains, which comprise approximately 20 µl of saliva and have been aged for 18 months, to be successfully extracted and analysed with ATR-FTIR spectroscopy, as well as highlights the challenges associated with such a dilute body fluid.

The variation observed across the extracted saliva stain samples can be attributed to a number of possible factors. Firstly, as saliva stains are frequently transparent, depending on the substrate upon which the stain is present, it was often difficult to guarantee that the area of cotton utilised in extraction was the precise site of initial deposition. Therefore, the area undergoing extraction may not contain the whole of the stained area which would result in a

poorer quality spectrum due to less salivary cellular material present. In an attempt to prevent such an occurrence, the area in which the sample was deposited was targeted for extraction preparation. A way to overcome this issue could be to search the cotton substrate prior to extraction with an alternative light source (ALS) and then mark around the stained area to visualise stain location (Vandenberg & van Oorschot, 2006). This would ensure that the whole of the stain is prepared for extraction and would increase the maximum potential of saliva recovery during extraction. Other factors to consider that could affect the variability in saliva stain extraction are the wide-spread distribution of saliva components within the stain which may result in a low concentration of the biological constituents, and the overall nature of saliva as a complex, yet very dilute body fluid.

3.2.3 FORENSIC APPLICATION

Saliva is notoriously one of the most difficult body fluids to screen for and identify as amylase, the key protein utilised in the presumptive testing of saliva, is not saliva-specific or is consistently produced in all individuals. Additionally, there are no confirmatory tests currently available (Olsén et al. 2011). The results obtained in this investigation have demonstrated that ATR-FTIR spectroscopy has the potential to be utilised as a robust technique to provide definitive identification of saliva. The characterisation of ATR-FTIR spectral peaks from saliva demonstrated here are consistent with those reported by a number of research groups (Khaustova et al. 2010; Schultz et al. 1996; Scott et al. 2010; Shaw & Mantsch, 2006; Sultana et al. 2011). Reproducible spectra were obtained from samples of neat saliva and aged saliva stains extracted from cotton, although the quality of the extracted spectra was variable across the sample range. Nevertheless, the good quality spectra from extracted saliva stains enabled comparisons of the peak frequencies with those associated with the specific vibrational modes exhibited by components within neat saliva. Direct ATR-FTIR spectroscopic analysis was not successful in detecting salivary components when present on cotton, although the ability to obtain comparable saliva spectra from extracts provides a further analysis option.

These findings are of benefit to the forensic and criminal investigation community as there is a need for the development of a better method to identify the presence of saliva that is objective, definitive, does not result in the occurrence of false negatives/positives, nor consume or destroy most of the evidential sample. Currently, the only widely utilised presumptive test available for the detection of saliva is the Phadebas® Forensic Press test

which is a chemical assay that produces a blue colour change in the presence of amylase (Hedman et al. 2008, 2011; Olsén et al. 2011). The test itself makes use of a starch-dye complex on filter paper, whereby the dye is released in the presence of amylase. ATR-FTIR spectroscopy has demonstrated successfully that saliva-specific α-amylase can be attributed to a specific peak within the spectra of saliva (Figure 3.16), whereas the Phadebas® Forensic Press test is known to provide positive results from other body fluids which contain low levels of amylase, such as semen (Olsén et al. 2011). Further limitations of the Phadebas® Forensic Press test include a maximum reaction time of 40 minutes for a positive indication of saliva, of which the interpretation is subjective and invasive transfer of the blue dye onto the substrate suspected to contain a saliva stain and therefore the biological stain itself (Hedman et al. 2008).

ATR-FTIR spectroscopic analysis of saliva has many advantages over the Phadebas® Forensic Press test, in that it is non-invasive as only water is added to the sample for the extraction. The sample is not exhausted for the analysis; the "wet-to-dry" analysis utilises only 20 µl of an extract of approximately 300 µl, ensuring that there is a sufficient volume of evidential material left for further analysis to be carried out. The spectra obtained from saliva analysis are body fluid specific, therefore a definitive identification can be made regarding the sample origin, as well as establishing an identification of the sample if it is not saliva. Alongside these benefits in comparison to the Phadebas® Forensic Press test, ATR-FTIR spectroscopy is reproducible, robust and cost-effective, as discussed in Section 3.1.3. Overall, it can be stated that ATR-FTIR spectroscopy is a suitable technique to identify saliva.

3.3 SEMEN

Figure 3.26 demonstrates an ATR-FTIR spectrum obtained from a semen sample that had been dried *in situ* on the ATR-FTIR analysis stage for five hours. Table 3.6 provides an overview of the identified semen components that result in the presence of these peaks at the particular wavenumbers (cm^{-1}). A total of 44 measurements were taken from five individual 20 µl aliquots of neat semen.

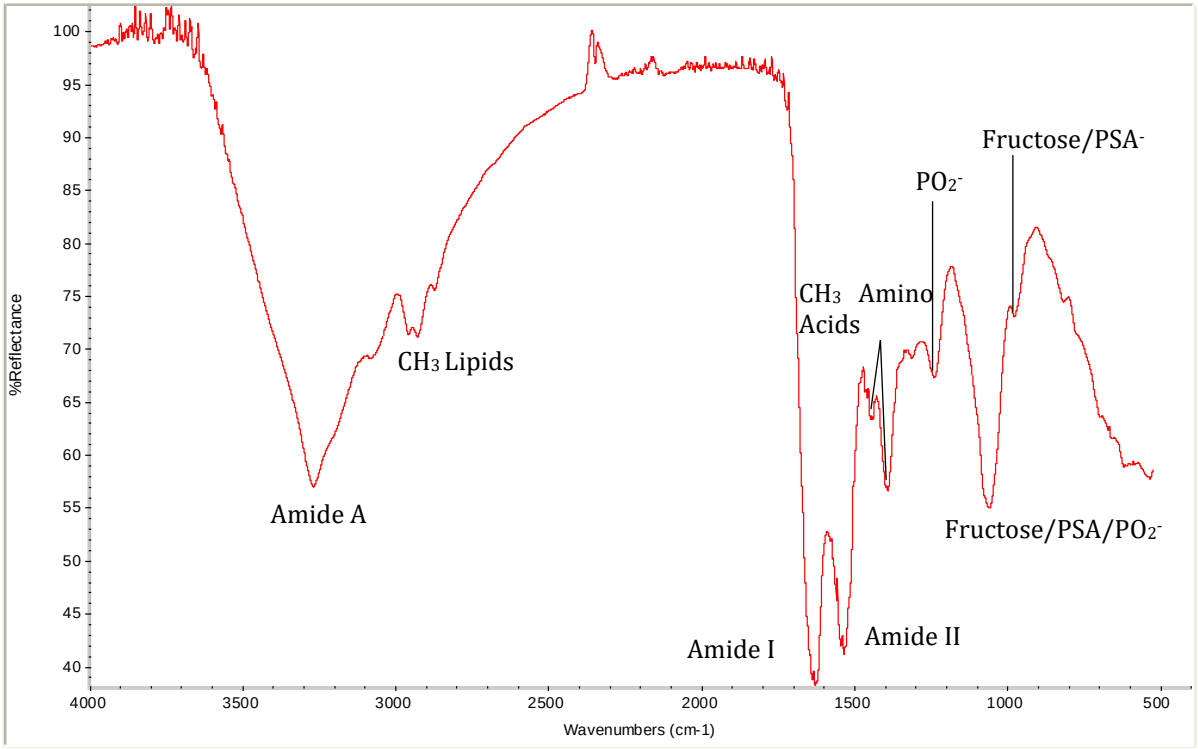

Figure 3.26: ATR-FTIR spectrum of neat semen air dried at 5 hours.

The strong peaks observed within the neat semen spectra were observed at peak frequencies of 1625 cm^{-1} and 1540 cm^{-1}, which were attributed to amide I and amide II, respectively. The medium strength peaks observed had peak frequencies of: 3273 cm^{-1}, corresponding to amide A; 1400 cm^{-1}, indicative of symmetric methyl bends in the amino acid side chains of proteins and 1059 cm^{-1} which most likely arise from the sugars within the semen, such as glucose and fructose. However, the 1059 cm^{-1} peak may also be attributed to the sugar phosphate groups within DNA and RNA (Movasaghi et al. 2008; Olsztynska-Janus et al. 2012) and sugar moieties within glycoproteins, such as prostate specific antigen (PSA). The remaining peaks observed within the spectra of neat semen were weak, exhibiting peak frequencies at 2941, 1450, 1240 and 980 cm^{-1} which could be attributed to methyl stretches

within lipids, asymmetric methyl bends in amino acid side chains of proteins, nucleic acid phosphates and seminal plasma, respectively. All of the peaks observed within the neat spectra of semen could be categorised as narrow, with the exception of amide A which demonstrated a broad peak shape.

Table 3.6: ATR-FTIR peak component identification for semen.

Wavenumber (cm^{-1})	Component Identification	Vibrational Mode	Reference
3268	Amide A	H bonded OH stretching, NH symmetric stretching	Garidel & Schott (2006b); Movasaghi et al. (2008)
2950	Methyl groups of lipids	CH_3 stretching	Movasaghi et al. (2008)
1625	Amide I (β sheets)	C=O stretching	Garidel & Schott (2006b); Barcot et al. (2007) Movasaghi et al. (2008)
1540	Amide II	NH bending coupled to CN stretching	Garidel & Schott (2006b); Movasaghi et al. (2008); Wood et al. (1998)
1450, 1393	Methyl bending of amino acid protein side chains	Asymmetric & symmetric CH_3 bending	Barcot et al, (2007); Wood et al. (1998)
1240	Nucleic acid phosphate	Asymmetric PO_2^- stretching.	Barcot et al, (2007); Garidel & Schott (2006b); Movasaghi et al. (2008)
1059, 980	Fructose & prostate specific antigen (PSA)	CH_2OH groups, CO stretching and bending of COH groups.	Barcot et al (2007); Movasaghi et al. (2008); Olsztynska-Janus et al. (2012)

As seen in the ATR-FTIR spectra of both neat blood and saliva (Figure 3.4 & Figure 3.19), there were also common biological components within the neat semen sample that could be attributed to particular vibrational modes arising from proteins, methyl groups and sugars. However, as stated in Section 3.2, it is the overall spectral pattern and the specific peak frequencies that are utilised to assign these common macromolecules to body fluid specific components. For instance, within the neat semen spectra amides A, I and II were detected,

although very different peak shapes were produced for the amide I and II corresponding to semen than those in blood and saliva (see Section 3.5, Figure 3.50 for example).

The literature currently available that has examined human semen, seminal fluid or spermatozoa with infrared spectroscopy is rather limited, with only three relevant reports since 1998, compared to the literature available for the identification of other body fluids (Barcot et al. 2007; Elkins, 2011; Wood et al. 1998). The most comprehensive report of the characterisation of human semen with FTIR spectroscopy was by Barcot et al. (2007), which examined the spectra of seminal fluid and spermatozoa independently. This report and other literature on the FTIR analysis of generic biological components (Garidel & Schott, 2006b; Movasaghi et al. 2008; Olsztynska-Janus et al. 2012) enabled the attribution of specific functional groups and biological components to the peaks observed within the spectra of neat semen within this research.

To ensure that peak assignments were as accurate and comparable with literature as possible, it was important to determine which particular peaks arose from the seminal fluid or spermatozoa component of whole semen. To separate whole semen into its two basic constituents, a sample of approximately 200 µl was micro-centrifuged at 14,800 rpm (16,162 x g) for 15 minutes which created a dense pellet of cellular material, predominantly spermatozoa, and a liquid layer of seminal fluid (Barcot et al. 2007). Subsequent ATR-FTIR spectroscopic analysis of each constituent was conducted independently as per the "wet-to-dry" method (Section 2.2.2.1), until dried, with an aliquot of 20 µl. Figure 3.27 demonstrates the ATR-FTIR spectra obtained for seminal fluid (pink) and spermatozoa (purple) in comparison to neat semen (red).

It is evident that there were similarities across the spectra for both the cellular and fluid components of semen. There was no apparent dominance from either the seminal fluid or spermatozoa to the overall contribution of the neat semen spectra as the exhibited peak frequencies and the overall spectral patterns were clearly comparable. However, the most observable difference between the seminal fluid and spermatozoa spectra was the definition of the amide I and II peaks. The seminal fluid spectra exhibited a shallow furrow between these protein peaks, whereas a deeper furrow and differing peak strengths were evident in the spermatozoa amide I and II peaks.

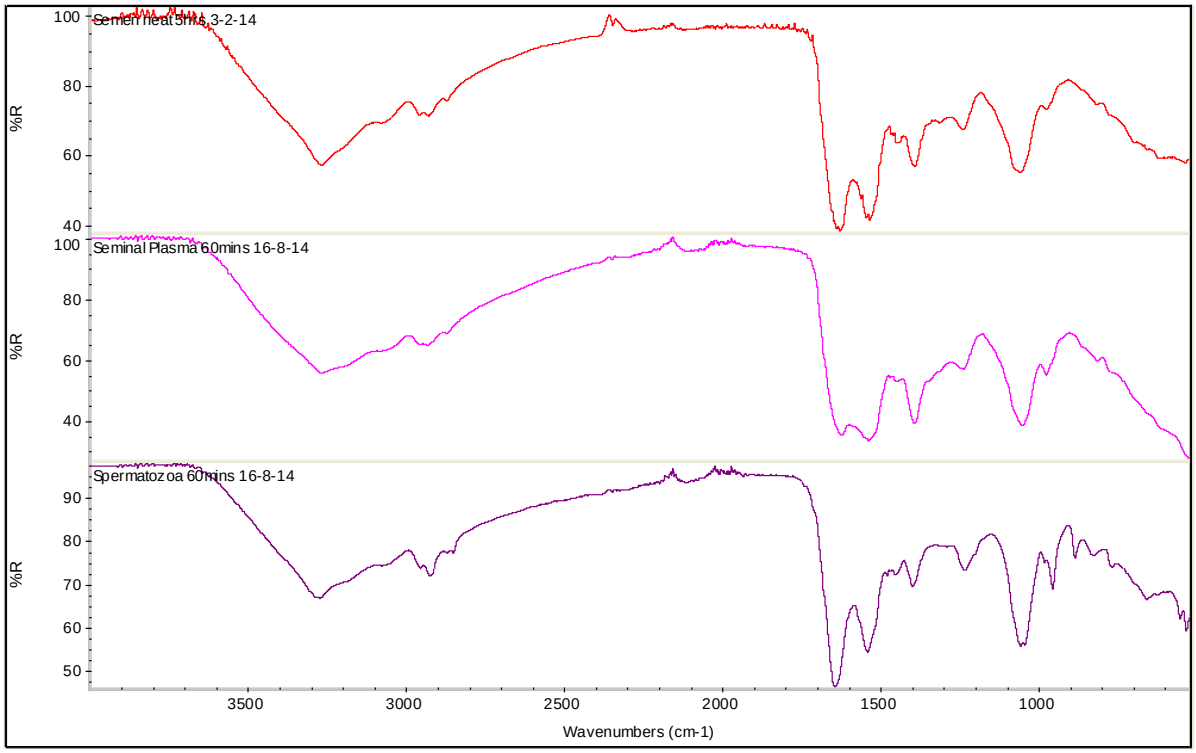

Figure 3.27: ATR-FTIR spectra comparisons of neat semen (red), seminal fluid (pink) & spermatozoa pellet (purple).

Comparison with the neat semen spectrum demonstrates that the amide I and II peaks are likely to arise from both the cellular and fluid constituents, as the furrow appears deeper than that observed in the seminal fluid spectrum, but shallower than that in the spermatozoa spectrum. In the recovery of semen evidence from a crime scene, the sample is most likely to contain both cellular and seminal fluid components, with the exception of azoospermic semen. Therefore, based on these observations and the potential application to forensic evidence, the spectra of neat semen as a whole was utilised to assign biological components and functional groups to each of the peaks, rather than considering the seminal fluid and spermatozoa pellet spectra separately.

The amide peaks were a common component across all four of the body fluids examined, although it was possible to attribute the key amide peaks to particular proteins. In the spectra of neat semen, the amide A peak observed (~3268 cm^{-1}) could not be specifically characterised based on the protein secondary structure due to the N-H group vibration which masks any structurally-specific vibrations (Barth, 2007). However, the amide A peak most likely corresponds to proteins (Movasaghi et al, 2008). The vibrational modes that give rise to the amide A peak originate from the same functional groups as the amide A peaks within blood and saliva, namely C-H, N-H and O-H stretching vibrations (Garidel & Schott, 2006b). It must be borne in mind that the amide A peak is not the most reliable peak to provide

component information within biological samples spectra as the same region is susceptible to peaks attributed to water absorption (Movasaghi et al, 2008).

In contrast, the amide I and II peaks can provide conformation-specific information regarding the dominant proteins contributing to the peaks and therefore comparisons can be made with known proteins within semen (Olsztynska-Janus et al. 2012). The vibrational modes that give rise to the amide I peak in the neat semen spectra were C=O stretches, whereas N-H bends coupled to C-N stretches are characteristic of the amide II peak (Garidel & Schott, 2006a). These same vibrational modes contribute to amide I and II peaks observed in blood and saliva. The average amide I peak frequency observed within the neat semen spectra was 1625 cm^{-1}, which is indicative of a β-sheet protein secondary structure (Table 3.2). This varies from the amide I peak frequency stated by Barcot et al. (2007), 1657 cm^{-1}, which suggests an α-helix conformation. However, the amide I and II peak frequencies were only reported for the spermatozoa spectra. The average peak frequency exhibited for amide II in the neat semen spectra was 1540 cm^{-1}, suggesting a parallel β-sheet conformation. This varies only slightly from the amide II peak reported by Barcot et al. (2007), 1547 cm^{-1}, although this peak frequency was only stated for the amide II peak corresponding to spermatozoa. Comparisons with the amide I peak frequencies observed in the spermatozoa pellet and seminal fluid spectra (Figure 3.27), 1645 and 1622 cm^{-1}, respectively, suggest that the dominant contributor to the amide I peak in neat semen was seminal fluid. The amide II average peak frequencies observed within the spermatozoa pellet (1541 cm^{-1}) and seminal fluid (1538 cm^{-1}) did not vary much from the frequency observed within the neat semen spectra, therefore both the cellular and fluid components appear to contribute to this particular peak.

It is well known that seminal fluid is a complex, heterogeneous mixture upon ejaculation which contains a variety of proteins and enzymes, all of which could contribute to the amide I and II peak vibrations (Owen & Katz, 2005). To establish the potential contributors to the amide I, and subsequently the amide II peak, direct comparisons were made with three of the most abundant proteins and enzymes in seminal fluid, namely acid phosphatase (AP), albumin (HSA) and prostate specific antigen (PSA) (Figure 3.28). Initial observations of the spectra corresponding to AP, albumin and PSA demonstrate that both AP and albumin could be contributors to the amide I and II peaks observed within neat semen spectra. Distinct, narrow peaks were evident for the amide I and II peaks in both proteins which exhibited average peak frequencies of 1631 and 1537 cm^{-1} (AP) and 1645 and 1536 cm^{-1} (albumin).

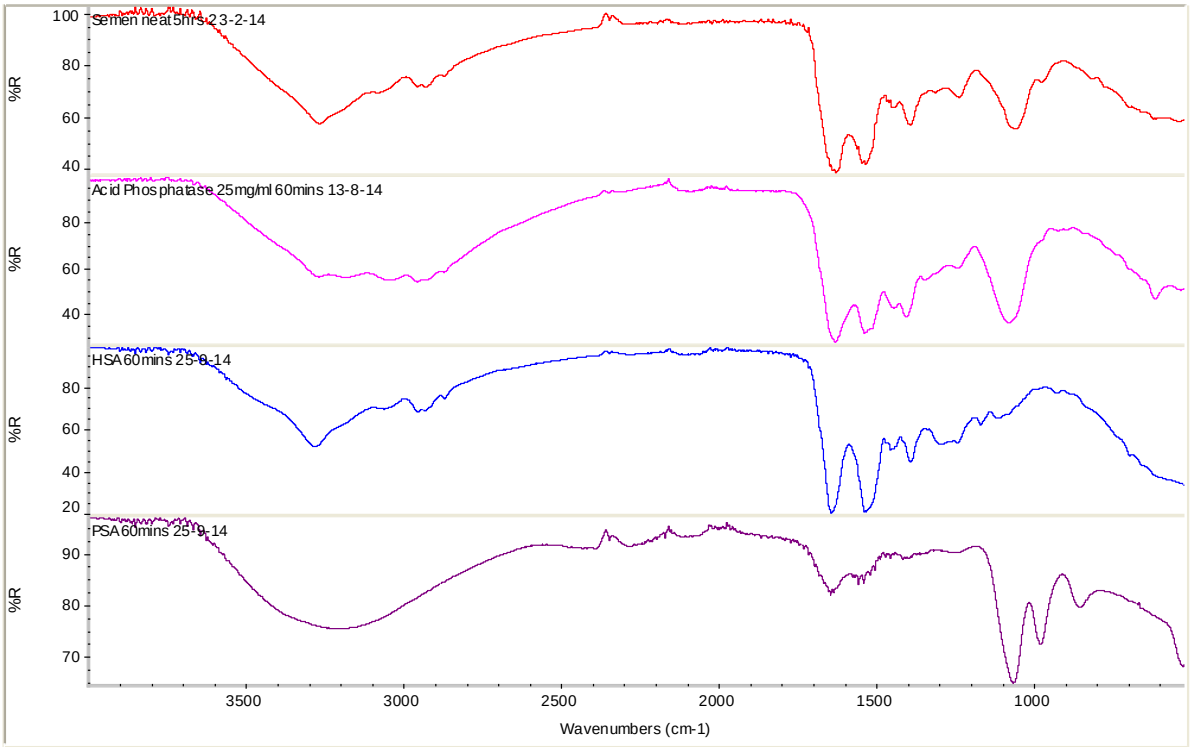

Figure 3.28: ATR-FTIR spectra comparison; neat semen (red), acid phosphatase (pink), albumin (blue) & prostate specific antigen (purple).

Comparisons between the spectra of neat semen and AP (Figure 3.28, red & pink) demonstrate that the amide I and II peaks exhibit the same peak shape. The secondary structure of AP is known to comprise of a number of different conformations and has been reported to produce six independent amide I peaks when examined with FTIR spectroscopy (Bem & Ostrowski, 2001). However, one of the amide I peaks of AP was observed at 1627 cm^{-1}, which corresponds with a β-sheet secondary structure and with the amide I frequency demonstrated in the spectra of neat semen. These findings suggest that AP is a dominant contributor to the amide I peak exhibited in neat semen.

Upon comparison of the amide I and II peaks between the spectra of neat semen and albumin (Figure 3.28 red & blue) it is evident that there is overlap between the amide peaks within this region. However, the furrow in between the amide I and II peak in albumin is much deeper than the furrow observed within the neat semen. As discussed in Section 3.1, albumin has a secondary structure that comprises of approximately 90% α-helices and 10% β-turns (Hassler et al. 2011), which does not correspond with the secondary structure suggested by the amide I peak frequency in the neat semen spectra. However, the amide II peak frequency of albumin does correspond with its counterpart in neat semen. Therefore, it could be suggested that albumin is not a dominant component contributing to the amide I peak in neat semen, although it could be a dominant contributor to the amide II peak observed.

When comparing the ATR-FTIR spectra of PSA to that of neat semen (Figure 3.28, red & purple), the initial observation that can be made is that the spectrum varies drastically from the spectra of AP and albumin. In relation to the amide region, it may be possible for PSA to contribute to the amide I and II peaks within neat semen as peaks within this particular region were evident in the PSA spectrum. However, these peaks were not strong and exhibited a relatively broad peak width across the protein region, with no distinct separation of the amide I and II peaks and increased noise levels. The average peak frequencies observed for the amide I and II peaks within the PSA spectra were 1635 and 1558 cm^{-1}, respectively. At these frequencies the amide I peak does correspond with the amide I peak in neat semen, although the amide II peak does not. It could be suggested that PSA is a weak contributor to the amide I and II peaks observed within neat semen, although it is not a dominant component in comparison to AP and albumin.

The proteins and enzymes analysed here are some of the most abundant proteins within human semen, although AP, albumin and PSA all originate from the prostate, which produces only 15-30% of seminal fluid. Therefore, it is possible that the amide I and II peaks could arise from proteins that are attributable to the seminal vesicles, which accounts for 60-75% of seminal fluid (Owen & Katz, 2005). Such proteins could be semenogelin I and II, particularly semenogelin I which is known to have a secondary structure that comprises predominantly of β-sheets, followed by α-helices (Malm et al. 2007). With this secondary structure, an amide I peak would be expected within the frequency range exhibited by the amide I peak of neat semen and therefore semenogelin I could also be suggested as a contributor.

The remainder of the peaks observed within the spectra of neat semen were of medium or weak strength and were assigned to peak frequency-specific macromolecule groups. At the high frequency end of the spectrum, in between amide A and amide I, a small peak is exhibited (~2950 cm^{-1}) which corresponds to the methyl group stretches attributed to lipids within semen. This characteristic peak was also observed within both the spermatozoa pellet and seminal fluid spectra, which demonstrates that lipids were present in both components. However, the peak appeared more distinct within the spectrum of the spermatozoa pellet. This was not surprising as spermatozoa have a plasma lipid membrane which is key in the process of fertilisation (James et al. 1999; Lenzi et al. 1996). Therefore it is probable that the peak corresponding to methyl groups in lipids originates from the lipid membrane of spermatozoa. Comparisons of the methyl groups of lipids peak in the AP and albumin spectra with the neat semen spectrum demonstrate that these proteins could be suggested as

contributors to this particular peak based on the characteristic shape of the peak that was observed in both protein spectra.

Further along the infrared spectrum, in the low frequency region, two peaks observed within the 1390-1450 cm^{-1} region also correspond to the bending of the CH_3 functional group. Specifically, these peaks can be attributed to the asymmetric and symmetric bending of methyl groups attached to amino acids side chains in proteins (Barcot et al. 2007; Wood et al. 1998). The stronger of the two peaks demonstrated a typical peak frequency of 1395 cm^{-1}, which corresponds with the symmetric vibration, whereas the peak observed at approximately 1450 cm^{-1} corresponds to the asymmetric vibrations and appears as a weak shoulder to the 1395 cm^{-1} peak. Inspection of the spectra of seminal fluid and the spermatozoa pellet (Figure 3.27) demonstrates that both peaks were detectable in seminal fluid, but only the symmetric bending peak was detected within the spermatozoa pellet. Upon comparison of the protein and enzyme spectra (Figure 3.28), the methyl groups of amino acid side chains in proteins peaks were observed within the AP and albumin spectra (Figure 3.29), but were absent in the PSA spectrum. It is evident that the methyl group peaks corresponding to amino acid side chains in proteins in both the neat semen and AP spectra share the same characteristic peak shape, which suggests that AP is a dominant contributor to these peaks when observed in semen spectra. Interestingly, within the neat semen and albumin spectra there was a distinct overlap between the methyl bending peaks which also suggest that this particular protein is a main contributor that gives rise to these peaks in neat semen.

One of the weakest peaks observed within the neat semen spectra corresponds to the phosphate groups attached to the nucleic acids which are the functional group that produce the peak typically exhibited at 1240 cm^{-1} (Barcot et al. 2007; Movasaghi et al. 2008). This particular region of the infrared spectrum, ranging from 1350-1220 cm^{-1}, often experiences overlap between phosphate group and amide III vibrations. Within the spectra of blood and saliva, the peaks observed at approximately 1240 cm^{-1} were assigned to amide III. However, within the neat semen spectra the equivalent peak corresponds to the nucleic acid phosphates, as an amide III peak would be expected within the 1260-1290 cm^{-1} region due to the α-helix conformation of human spermatozoa (Barcot et al. 2007). Examination of the nucleic acid phosphate peak within the spectra of seminal fluid (~1233 cm^{-1}) and spermatozoa pellet (~1239 cm^{-1}) (Figure 3.27) demonstrate that this peak exhibits a stronger intensity in the spermatozoa pellet spectrum, which correlates with the peak phosphate vibrations. Comparison of the average peak frequencies observed across these two spectra also supports the assignment of nucleic acid phosphates to the 1240 cm^{-1} peak. It is likely that

the peak observed within the seminal fluid arises from an overlap of amide III and phospholipid vibrations (Barcot et al. 2007; Movasaghi et al. 2008).

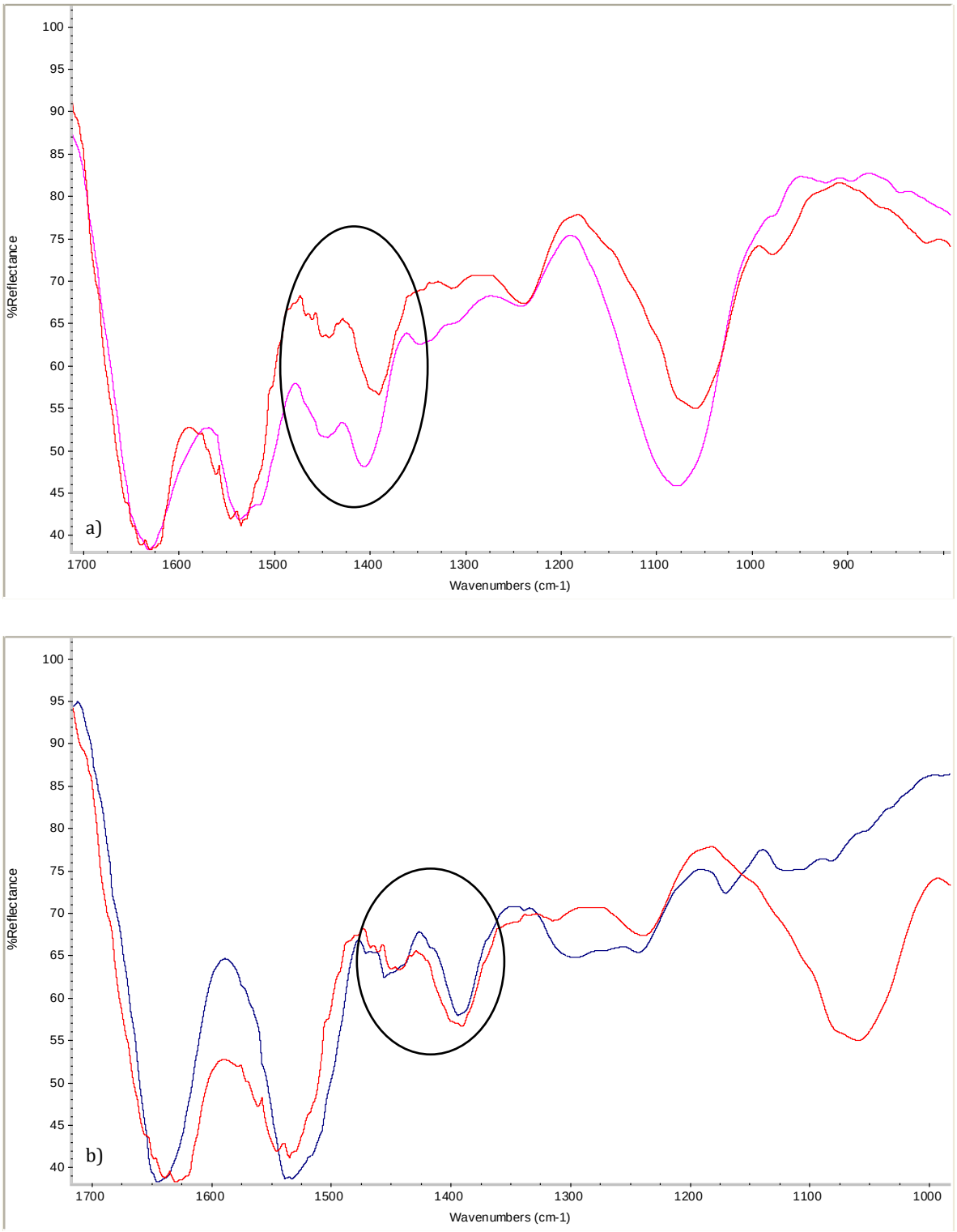

Figure 3.29: ATR-FTIR spectra comparison of the methyl groups of amino acid side chains in neat semen (red) &; a) AP (pink) & b) albumin (blue).

One of the strongest peaks observed within the neat spectra of semen can be attributed to three possible biological components based on an average peak frequency of 1059 cm^{-1}. The three components suggested were fructose, nucleic acids and PSA, all of which are abundant within semen. Fructose is one of the main components within seminal fluid as it provides a vital energy source for spermatozoa (Owen & Katz, 2005). Direct comparison of the ATR-FTIR spectrum of fructose with neat semen (Figure 3.30a) demonstrated that there was a distinct overlap between the peaks within the 1060-1020 cm^{-1} region, with the dominant peak of the fructose spectrum exhibiting a frequency of 1056 cm^{-1}. However, it is also documented that nucleic acids produce peaks within this region of the infrared spectrum (Barcot et al. 2007; Movasaghi et al. 2008). Barcot et al. (2007) reported that peaks corresponding to nucleic acids within spermatozoa were typically observed at two frequencies, 1087 and 966 cm^{-1}, whereas in seminal fluid these peaks demonstrated a shift to 1081 and 980 cm^{-1}. Comparisons with the seminal fluid and spermatozoa pellet spectra demonstrate that the peaks observed at 1054 and 1059 cm^{-1}, respectively, do not support the suggestion that they arise from nucleic acids.

Interestingly, it is probable that the peak observed at approximately 1059 cm^{-1} also arises from prostate specific antigen (PSA). An average peak frequency of 1066 cm^{-1} was observed within the PSA ATR-FTIR spectra, which would not ordinarily be considered as an accurate component assignment based on the 7 cm^{-1} difference. However, when the spectra of neat semen and PSA were overlapped, the entirety of the 1059 cm^{-1} peak falls within the breadth of the corresponding PSA peak. The presence of such a dominant peak within the PSA spectrum at 1066 cm^{-1} was not surprising as PSA is a glycoprotein (Vermassen et al. 2012); that is, the PSA proteins have sugar moiety side chains which give rise to a distinctive peak in the sugar moiety region of the infrared spectrum instead of, or in addition to, amide peaks. Based on these observations, the major contributors to the 1059 cm^{-1} peak within neat semen spectra can be suggested as both fructose and PSA (Figure 3.30b).

The final, relatively weak peak observed at 980 cm^{-1} in the neat semen spectra also seems to correspond to both fructose and PSA. The peak appears as a shoulder to the strong peak at 1059 cm^{-1} in both the neat semen and the seminal fluid spectra, whereas in the spectra of spermatozoa the peak exhibits a different frequency (~957 cm^{-1}) which represents the DNA of spermatozoa (Barcot et al. 2007). In the spectra of AP and albumin this peak shoulder was not observed (Figure 3.28), which demonstrates that neither of these semen components act as contributors to this particular peak. However, in the spectra of fructose and PSA this shoulder appears as a distinct peak with a medium/strong intensity and an average peak frequency of 977 and 981 cm^{-1}, respectively.

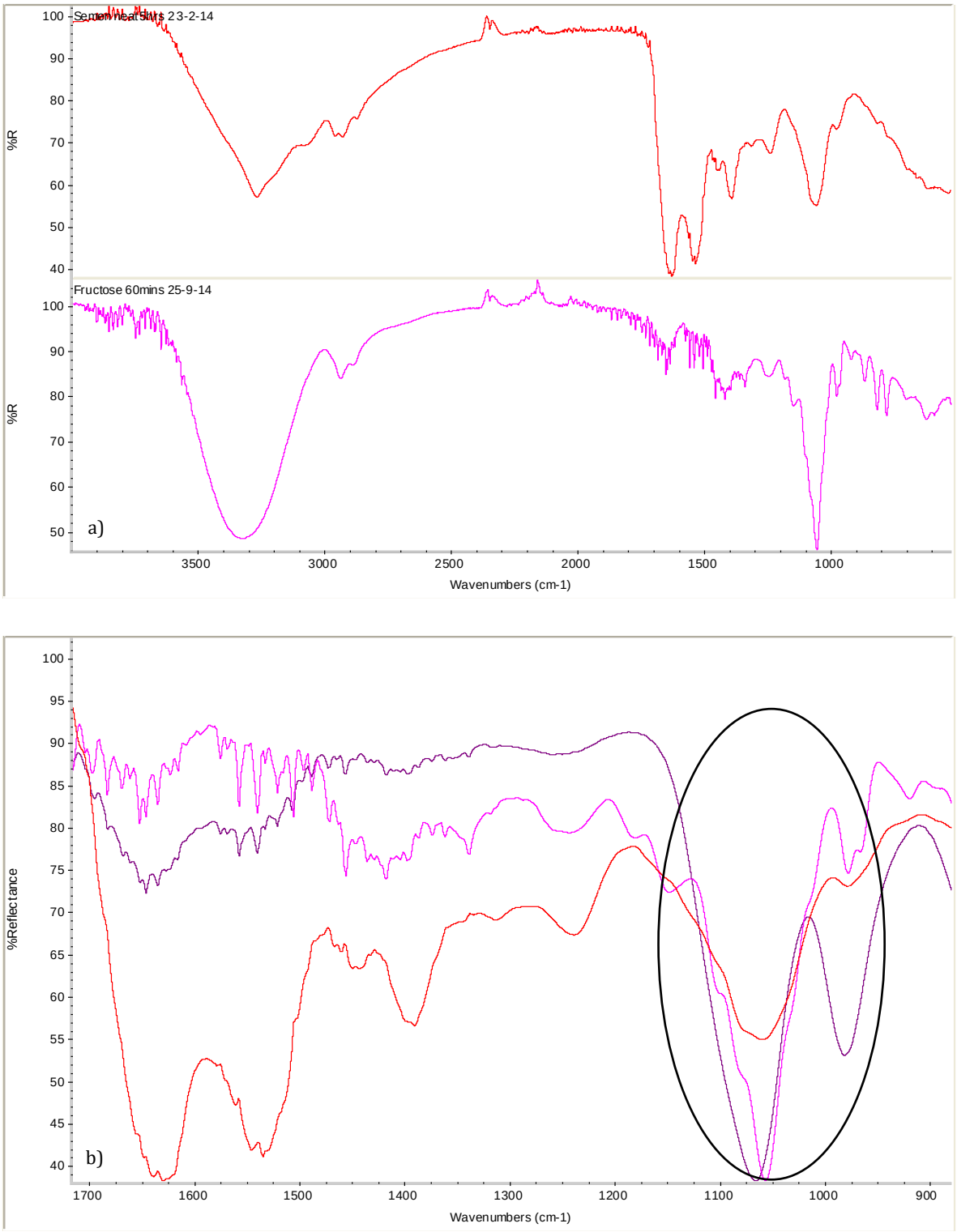

Figure 3.30: ATR-FTIR spectra comparison of; a) neat semen (red) and fructose (pink) & b) the sugar moiety peak in neat semen (red), fructose (pink) & PSA (purple) at approximately 980 cm^{-1}.

Barcot et al. (2007) reported the observation of a peak at 980 cm^{-1} within the seminal fluid spectra which could only be suggested as arising from seminal fluid, rather than a specific component within semen. As seminal fluid contains both fructose and PSA, this statement

seems feasible. However, as there was no literature available to support this suggestion, it could not be confirmed that this peak arises specifically from seminal fluid. To date there is still no literature that can support the claim by Barcot et al. (2007). However, the findings observed in the comparison between the spectra of neat semen, fructose and PSA (Figure 3.30) demonstrate that both components are the major contributors to the peak observed at 980 cm^{-1} in neat semen.

The results obtained from the ATR-FTIR spectroscopic analysis of neat semen samples and its fluid and cellular constituents mostly correlate with those obtained by Barcot et al. (2007). However, there is a lack of semen-specific FTIR spectroscopy-based literature available at present, which initially made accurate peak identification more difficult. Many of the peaks observed could be attributed to abundant macromolecule types across all biological materials, although the specific spectral pattern, peak shapes and frequencies enabled the assignment of specific components that exist within semen. Functional groups and peak assignments stated in literature supported the findings obtained from direct comparisons with the most abundant proteins and enzymes in semen, as well as establishing the fructose and PSA-specific peaks present within semen which has been previously unreported. Overall, these findings demonstrate the unique spectrum of semen, which has the potential to be utilised within forensic science as a definitive identification technique. These results also support the notion for a validated database of body fluid reference spectra, as demonstrated in the results obtained for neat blood and saliva.

3.3.1 IDENTIFICATION OF SEMEN STAINS: ON COTTON

Semen stains recovered from crime scenes may or may not be physically visible, depending on the substrate upon which the stain is deposited. The ability to confirm the presence of semen on forensic evidence is important in the investigation of sexual assault and rape cases, as clothing, and more specifically underwear, is one of the most prevalent items of biological evidence. Therefore, it was necessary to determine whether semen stains on cotton could successfully be detected with ATR-FTIR spectroscopy. Sections 3.1.1 and 3.2.1 demonstrated that bloodstains could successfully be detected and identified when deposited on cotton, although saliva stains could not. Figure 3.31 demonstrates the typical ATR-FTIR spectra obtained from a dried semen stain on cotton that has been aged for 24 hours. A total of 495 measurements were taken from 99 semen stains on cotton from one donor.

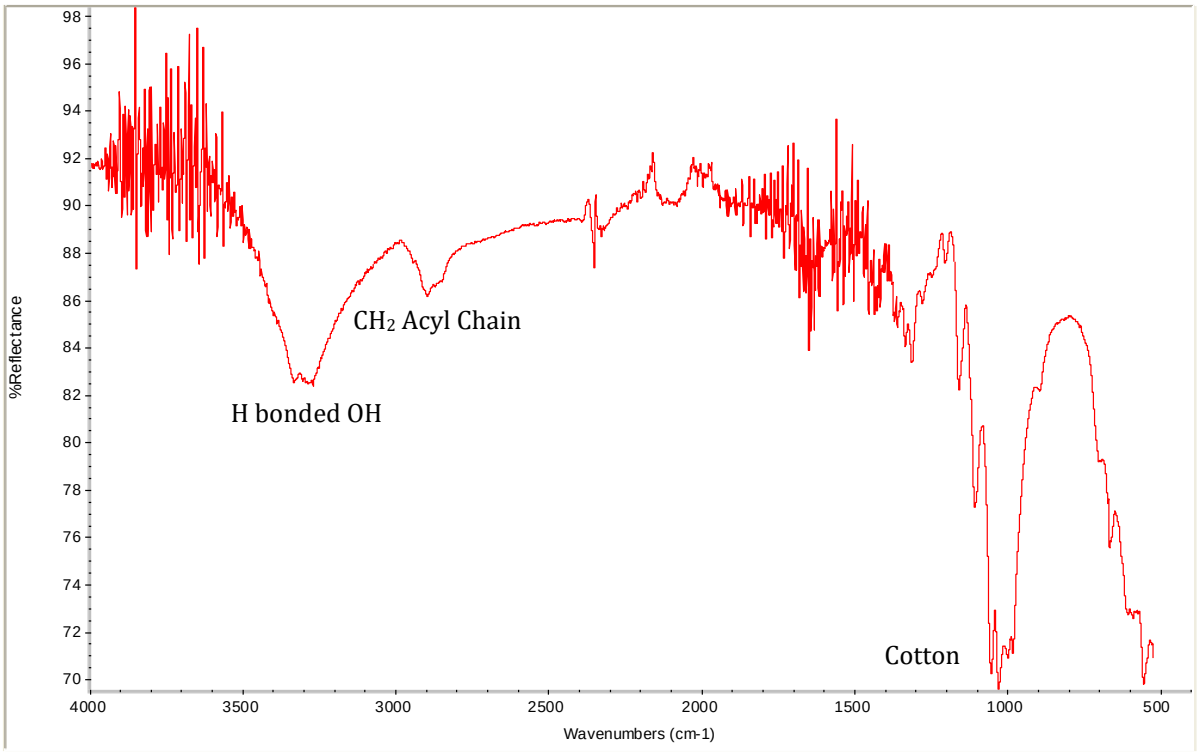

Figure 3.31: ATR-FTIR spectrum of a semen stain on cotton aged for 24 hours.

It is evident from the spectrum produced that there were no characteristic semen peaks observed when direct analysis of a semen stain dried on to cotton was conducted. The peaks observed throughout the spectrum were representative of the cotton substrate, as demonstrated in Figure 3.32 which exhibits the spectra of a 24 hours aged semen stain on cotton (pink), a cotton blank obtained from the same sample (orange) and neat semen (red). The inclusion of the neat semen spectrum demonstrates where the characteristic semen peaks would be expected if detection on cotton had been successful. Semen from one donor was deposited on to cotton, placed into storage to age from 24 hours to 9 months and were then examined to determine whether the stain age affected the detection of semen on cotton. Across all 99 samples, none of the ATR-FTIR spectra yielded peaks that could be attributed to the biological components of semen.

The results obtained mirror those yielded from the direct ATR-FTIR spectroscopic analysis of saliva stains (Section 3.2.1), whereby the body fluid stain was not detectable when deposited on cotton. As discussed in Section 3.2.1, there are various reasons for this such as; the colour of the semen appearing as transparent to the infrared radiation compared to the cotton substrate (Sahu, 2007), or the low concentration of semen constituents in the areas of the stains analysed. The limit of detection of semen stains on cotton with direct ATR-FTIR spectroscopic analysis was not investigated as it was anticipated that, despite the semen stain

being visible to the naked eye, it would still appear as "transparent" against the cotton substrate when analysed with ATR-FTIR spectroscopy due to its pale yellow/brown colour.

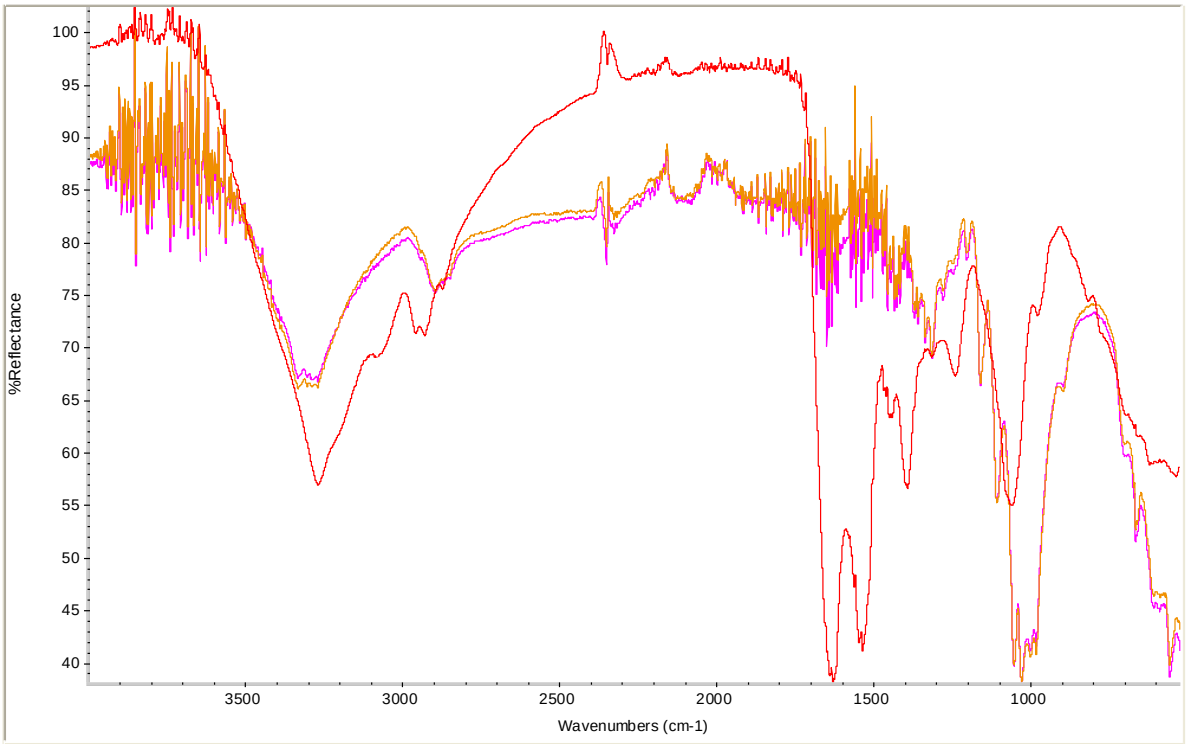

Figure 3.32: ATR-FTIR overlay spectra of a semen stain on cotton aged for 24 hours (pink), cotton blank (orange) & neat semen (red).

As no characteristic semen peaks were evident within the spectra of semen stains deposited on cotton, comparisons of maximum peak intensity and spectral quality could not be made to the spectra of neat semen. This demonstrates that ATR-FTIR spectroscopy is not an appropriate technique for semen identification when suspected stains are analysed directly from white cotton substrates.

3.3.2 IDENTIFICATION OF SEMEN STAINS: EXTRACTED

The extraction, and subsequent ATR-FTIR spectroscopic analysis, of blood and saliva stains from cotton successfully demonstrated that spectra can be obtained that are representative of each body fluid (Sections 3.1.2 & 3.2.2). In order to assess whether the water extraction method could also be applied to semen stains, the limit of detection was examined regarding the volume of semen utilised to produce a stain that was detectable when extracted from the cotton. Semen aliquots of 20 µl, 50 µl and 100 µl were deposited on to cotton, air dried for up to 24 hours, extracted and then analysed with ATR-FTIR spectroscopy as per the "wet-to-dry"

procedure. Figure 3.33 demonstrates the ATR-FTIR spectra obtained for each extracted aliquot. It is evident that the spectra for each aliquot were comparable, with little to no noise observed and clear, distinct peaks which could be attributed to the characteristic peaks within the spectra of neat semen with little observable variability (Figure 3.26 & Table 3.6).

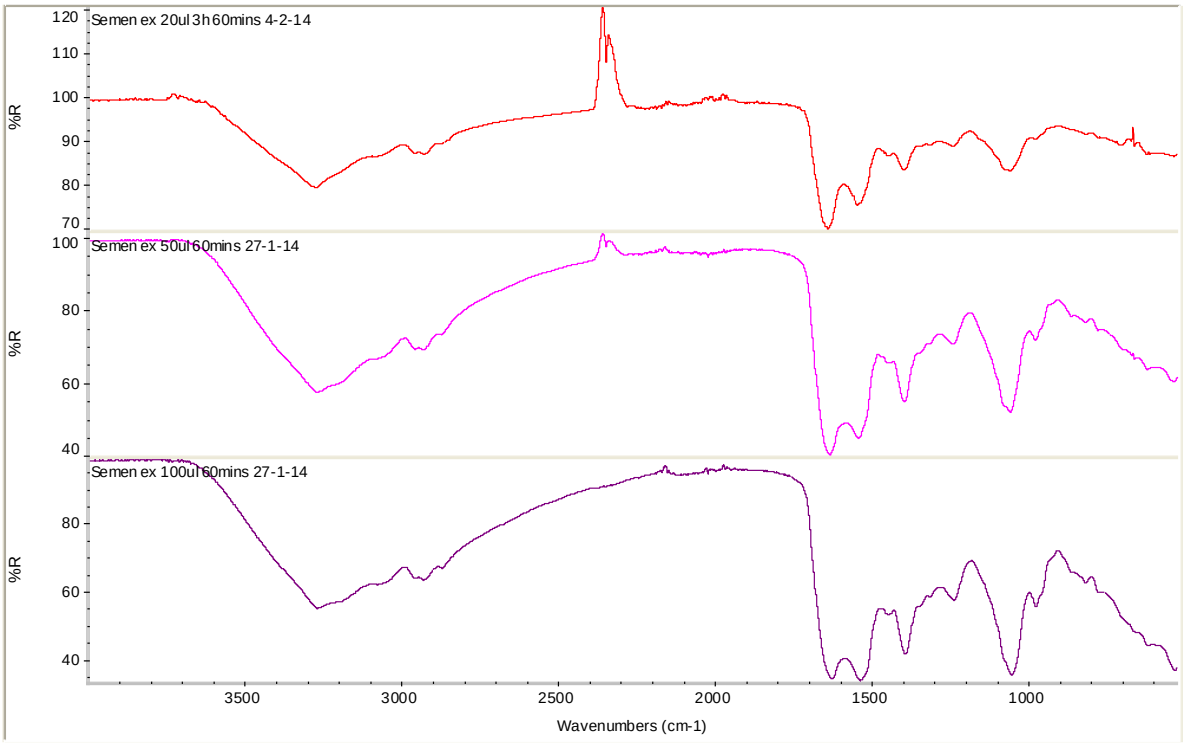

Figure 3.33: ATR-FTIR spectra comparisons of 20 µl (red), 50 µl (pink) & 100 µl (purple) extracted semen stains.

The only apparent peak that was not attributable to the semen was a negative peak observed at approximately 2350 cm^{-1} in the 20 µl and 50 µl extracted spectra. This peak was a result of carbon dioxide (CO_2) interference, possibly in the form of a trapped air bubble within the dried sample, and therefore can be overlooked in this instance (Gerakines et al. 1995). However, it was important to be able to correctly identify this peak to ensure that mischaracterisation could be avoided. The only observable difference between the spectra of various stain aliquots was that the maximum peak intensity was greater for the strongest peaks in the 50 µl and 100 µl spectra, approximately 40% and 35%, respectively, than the 20 µl spectrum (maximum peak intensity ~70%). However, this had no visible impact on the appearance of the peaks independently or collectively. The stain representative of 20 µl of semen could yield an excellent quality spectrum, if the CO_2 peak is disregarded. Therefore, it could be suggested that to yield a spectrum comparable to that of neat semen from an extracted stain, a deposition volume of 20 µl or greater is desirable. As a result of these

findings, any subsequent semen samples that were prepared for ageing purposes were deposited in volumes of 20 µl.

A total of 594 measurements were taken from 99 extracted samples in a "wet-to-dry" analysis of semen stains on cotton that had been aged from 24 hours to 9 months. Of the 594 measurements, 198 reflected the spectra of a dry sample and 369 yielded spectra representative of water (Figure 3.2c). Figure 3.34 demonstrates the typical spectra obtained from the extracted semen stains (red), semen stains on cotton (pink) and a cotton blank (purple). The extracted semen in this example had been aged up to one month prior to extraction, although the spectra obtained from all of the time periods examined demonstrated comparable spectral quality.

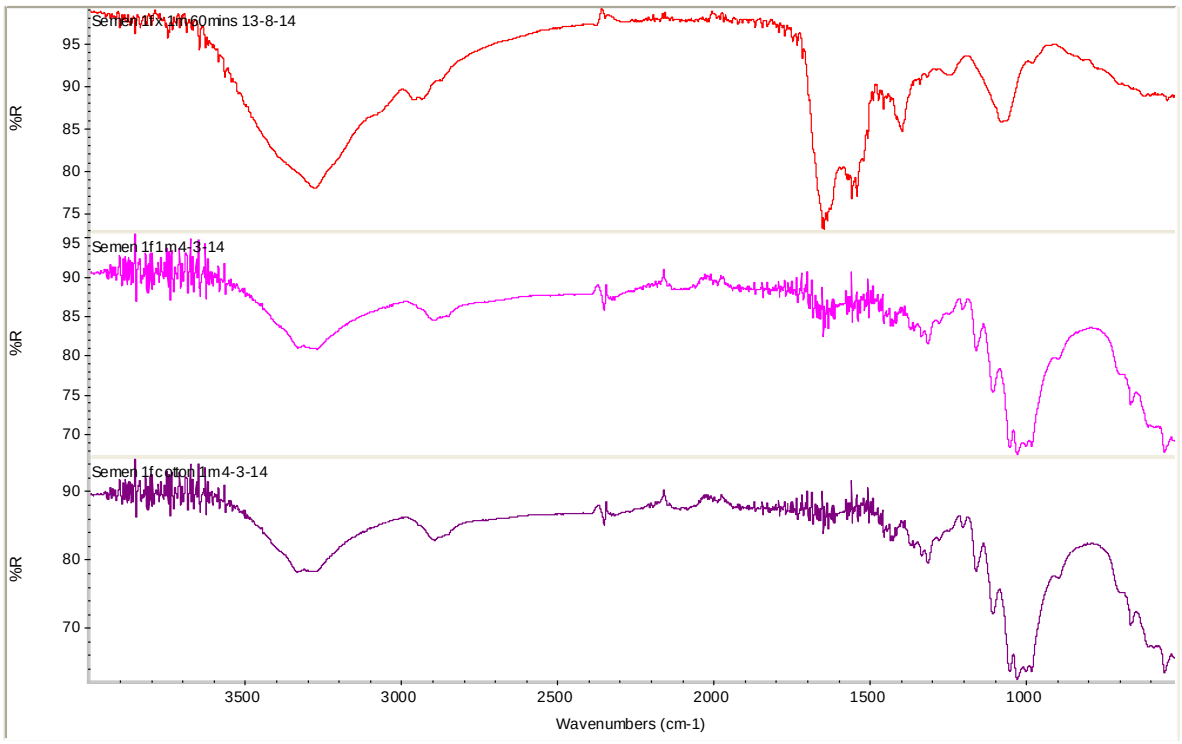

Figure 3.34: Example of ATR-FTIR spectra from an extracted semen stain (red), semen stain on cotton (pink) & cotton (blank) from the same sample that had been aged for one month.

The peak frequencies that correspond to the nine characteristic semen peaks were observed within the extracted semen spectra across all the sample ages (24 hours to 9 months), with no apparent peaks that could be attributed to cotton. However, the typically weak peaks, such as 1450 and 980 cm^{-1}, were frequently less distinct compared to the limit of detection extracted semen and the neat semen spectra (Figure 3.35). This may be due to a relatively low concentration of amino acid side chains in proteins and PSA that give rise to these particular peaks within the extract aliquots examined, although this does not hinder the

characterisation of spectra as semen. Other peaks within the aged extracted semen spectra that appear less well defined were amide I and II; within the neat semen and limit of detection extracted spectra the amide I and II exhibit clear apexes with a clear, but shallow furrow between the two protein peaks. Whilst in some, but not all, of the extracted aged semen spectra, the furrow appears to merge into the amide II peak, which subsequently appears as a shoulder to the amide I peak rather than an independent peak, as demonstrated in Figure 3.36[*1*].

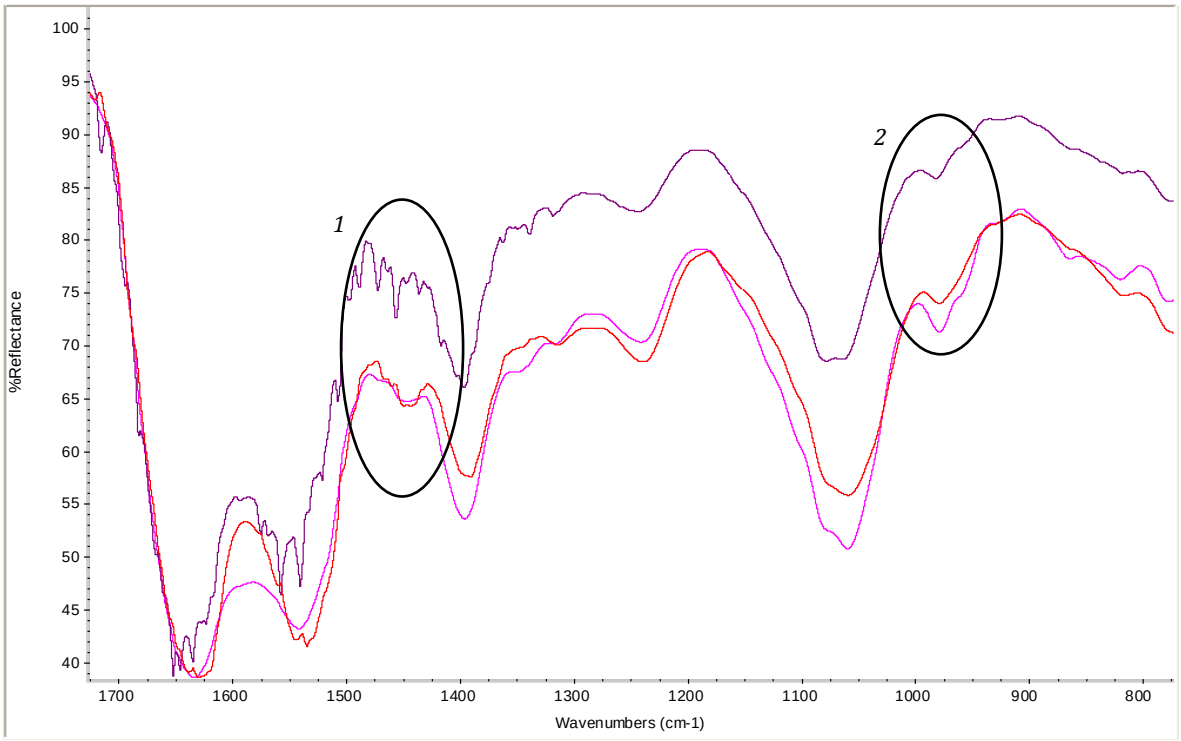

Figure 3.35: Overlay ATR-FTIR spectra demonstrating the loss of distinction in the weak peaks; 1450 cm^{-1} [1] & 980 cm^{-1} [2], within the extracted aged semen (purple) compared to the limit of detection extracted semen (pink) & neat semen (red).

The extraction spectra demonstrate that the simple water extraction method was sufficient to extract the semen from the cotton without recovering any cotton contamination, which corresponds with the results obtained from the extraction of bloodstains from cotton (Section 3.1.2). These findings further highlight the potential application of such a simple, neutral extraction method to forensic biological evidence which can enable the definitive identification of body fluids, and in this instance the specific identification of semen. Table 3.7 provides an overview of the variation in peak frequency between neat semen and extracted semen spectra. It is evident that the average peak frequencies of extracted semen spectra were higher than those for the corresponding peaks within neat semen, with the fructose/PSA/nucleic acid phosphate and amide peaks exhibiting the greatest difference in

average peak frequency. For the amide peaks, the shift in peak frequency is likely to be due to the interference from the water extraction solute as these regions of the infrared spectra typically exhibit peaks attributable to water absorption (Movasaghi et al, 2008). However, it is also possible that during the extraction procedure the proteins that predominantly give rise to an amide II peak may be tightly bound to the cotton substrate, and therefore do not dissociate into the extract solution. The shift observed within the fructose/PSA/nucleic acid phosphate region suggests that the peak corresponds specifically to the symmetric stretching of nucleic acid phosphates, as opposed to fructose and/or PSA (Movasaghi et al, 2008). However, upon comparison of the overlay of this particular peak in the spectra of neat semen (Figure 3.36[*2*]) and extracted aged semen it is evident that the peak formation is near identical, with only a slight shift in the peak apex observed. It is based on this observation that it can be stated as fructose and PSA acting as the dominant contributors to this peak rather than nucleic acid phosphates.

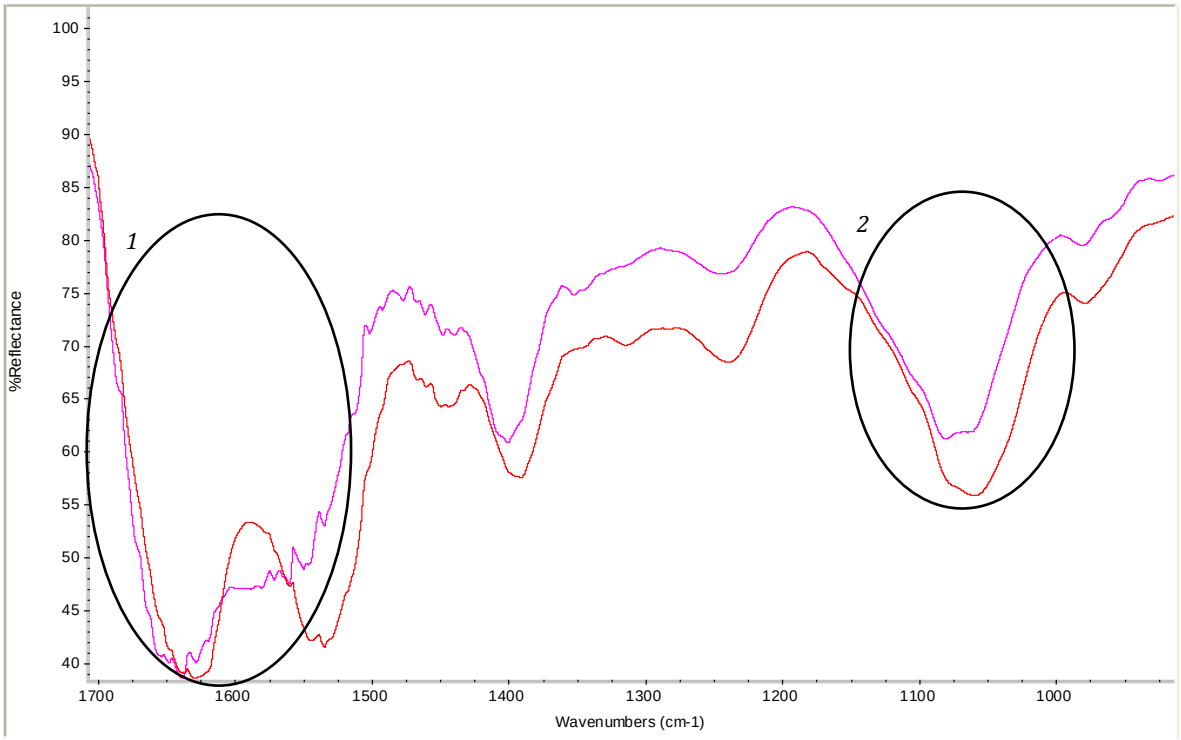

Figure 3.36: Comparison of the ATR-FTIR spectra of neat semen (red) & a 2 month old extracted semen stain (pink); [1] Example of the poor definition of the amide II, which appears as a shoulder of the amide I peak within some of the extracted aged semen spectra, [2] Overlay of fructose/PSA peaks in neat semen & extracted aged semen.

Table 3.7: Comparison table of the average peak frequencies observed across the spectra obtained from neat semen & extracted semen stains.

Semen Source	Fructose /PSA		PO_2^-	CH_3 Amino Acids	CH_3 Amino Acids [2]	Amide II	Amide I	CH_3 Lipids	Amide A
Neat	980.00 ± 2.63	1058.55 ± 5.03	1241.33 ± 2.14	1393.10 ± 1.92	1450.24 ± 5.24	1540.68 ± 4.79	1625.01 ± 5.06	2950.34 ± 14.59	3268.53 ± 2.1
Extracted	981.22 ± 2.8	1075.65 ± 7.94	1245.98 ± 2.45	1399.23 ± 1.92	1451.89 ± 7.43	1551.86 ± 12.58	1643.86 ± 5.64	2959.22 ± 6.92	3276.61 ± 3.54

The spectra yielded from the extracted semen stains that had been aged did not exhibit any particular variation in spectral quality that could correlate with the sample age. Unlike the oldest extracted bloodstains, the semen stains appeared to wash completely from the cotton during the extraction procedure. However, as extracts of semen stains aged up to 9 months were analysed, it is not possible to determine whether older semen stains may have been more difficult to extract. In comparison to the saliva stains extracts, the semen stains were visible with the naked eye, therefore the exact area of the stain could be targeted for removal and extraction, whereas there was an element of estimation required in the removal and extraction of saliva stains. These findings demonstrate that good quality spectra which exhibit peaks characteristic of semen can be successfully obtained from extracted semen stains up to nine months old, which are comprised of approximately 20 µl of semen and do not encounter the limitations faced in the extraction of blood and saliva stains.

3.3.3 FORENSIC APPLICATION

Semen is one of the most important body fluids when investigating crimes involving sexual assault or abuse. The characterisation of semen, seminal fluid and a spermatozoa pellet by ATR-FTIR spectroscopy have correlated with the only known literature to date that reports on the infrared spectra of the fluid and cellular constituents of semen (Barcot et al. 2007). Direct comparisons with a number of known biological components within semen, such as acid phosphatase (AP), prostate specific antigen (PSA), albumin and fructose, enabled accurate and specific peak assignment across the spectra. In particular, it was possible to specifically assign PSA to two peaks within the spectra of semen and seminal fluid which has not been previously reported. Reproducible spectra were obtained from extracted aged semen stains on cotton that were characteristic of neat semen. However, direct ATR-FTIR

spectroscopic analysis of semen stains on cotton could not detect semen components deposited on to a cotton substrate.

These findings are advantageous within a forensic context as it further supports the application of ATR-FTIR spectroscopy as a method to identify body fluids in a confirmatory and non-invasive manner. Currently there are a number of chemical tests utilised in forensic investigations that detect the presence of semen, namely: the acid phosphatase (AP) test which is presumptive (Raju & Iyengar, 1964); the prostate specific antigen (PSA, or p30) assay (Hochmeister et al. 1999), the Florence Iodine choline test (Hardinge et al. 2013) and spermatozoa detection with microscopy which are confirmatory (Li, 2008). However, for ease of use, the AP and PSA tests are routinely used. The AP test is an enzymatic test which produce a colour change in the presence of phenol; particularly, AP reacts with α-naphthyl phosphate when in the presence of zinc double salt which produces a purple colour (Jackson & Jackson, 2011). As AP is not specific to semen, the presumptive test is susceptible to false positive reactions not just from other body fluids, such as vaginal secretions, but any substance containing free phenols (Raju & Iyengar, 1964). The time in which a colour change can take place varies depending on the concentration, and on a sample to sample basis, which results in a level of subjectivity as to whether a positive reaction has been yielded. The PSA assay is much more reliable as it is an immunological test which makes use of monoclonal anti-human PSA antibodies conjugated with dye (Hochmeister et al. 1999). In the presence of human PSA a complex is formed which migrates towards a further group of polyclonal anti-human PSA antibodies which results in an observable line, indicating the presence of seminal fluid. In order for a positive reaction to be determined, two lines must be observed within the assay, one in the “test” region and one in the “control” region. Only then can a sample be confirmed as seminal fluid. However, the PSA can be subject to false negative results as a result of the “high dose hook effect”, whereby an excess in PSA can produce a negative result (Hochmeister et al. 1999).

ATR-FTIR spectroscopy has many advantages over the AP test, in that it is objective, no chemical reagents are added during analysis which could alter the original sample, the result is immediate and there is no susceptibility to false positive or false negative reactions. In comparison to the PSA assay, ATR-FTIR spectroscopy offers an alternative confirmatory method that can also provide spectral information regarding the evidential sample if semen is not detected. However, an added benefit is that ATR-FTIR spectroscopy is not affected by excess biological or chemical components within a sample and therefore there is no risk of “high dose hook effect”. The results obtained and discussed here demonstrate that reproducible spectra can be produced from semen, seminal fluid, spermatozoa pellet and

extracted semen stains aged up to nine months. The spectra yielded are unique to this body fluid, when compared to the spectra obtained from blood and saliva, which highlights the suitability of ATR-FTIR spectroscopy as a technique to identify semen and its constituents.

3.4 VAGINAL SECRETIONS

Figure 3.37 demonstrates an ATR-FTIR spectrum obtained from a vaginal secretion sample that had been dried *in situ* on the ATR-FTIR analysis stage for five hours. Table 3.8 provides an overview of the identified vaginal secretion components that result in the presence of these peaks at the particular wavenumber frequencies (cm^{-1}). A total of 40 measurements were taken from five individual 20 µl aliquots of neat vaginal secretions collected with a Softcup.

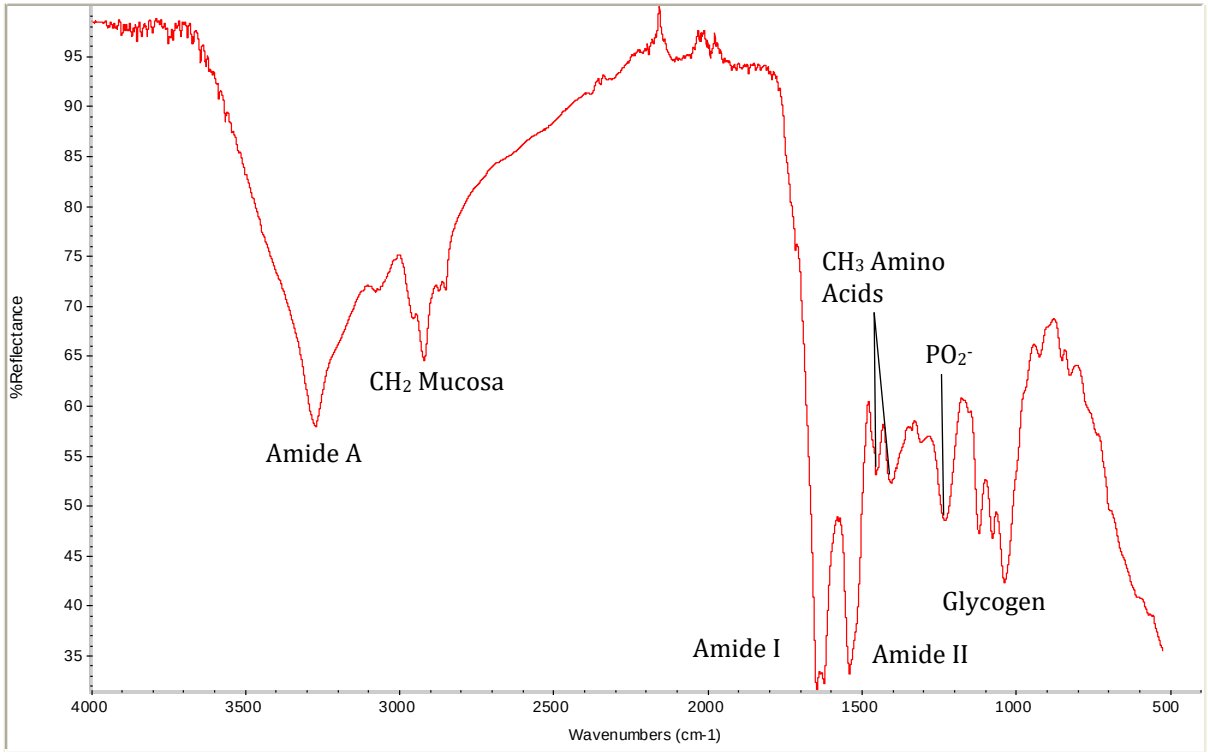

Figure 3.37: ATR-FTIR spectrum of neat vaginal secretions air dried for 5 hours.

The peak positioned at 3274 cm^{-1} is a broad, medium intensity peak that corresponds to amide A. The strongest and narrowest peaks observed within the neat vaginal secretions spectra are attributed to amide I and II, with peak frequencies of 1641 and 1542 cm^{-1}, respectively. The final dominant peak was observed in the 1126-1034 cm^{-1} region and can be categorised as a broad, medium intensity peak. There are three apexes within this peak, all of which are representative of glycogen. The remaining peaks within the spectra are categorised as medium or weak peaks as they do not exhibit such strong intensities as the four dominant peaks. These peaks were identified as corresponding to methylene stretches of vaginal

mucosa (2923 cm^{-1}), methyl bending of proteins (1457 and 1406 cm^{-1}) and nucleic acid phosphates (1232 cm^{-1}).

Table 3.8: ATR-FTIR peak component identification for vaginal secretions.

Wavenumber (cm^{-1})	Component Identification	Vibrational Mode	Reference
3274	Amide A	H bonded OH stretching	Elkins (2011): Garidel & Schott (2006b); Movasaghi et al. (2008)
2923	Methylene stretches vaginal mucosa	CH_2 stretching	Elkins (2011); Movasaghi et al. (2008)
1641	Amide I (unordered)	C=O stretching	Wong et al. (1991); Wood et al. (1998)
1542	Amide II	NH bending coupled to CN stretching	Movasaghi et al. (2008); Wong et al. (1991); Wood et al. (1998)
1454, 1406	Methyl stretches of amino acid side chains in proteins	Asymmetric & symmetric CH_3 bending	Wong et al. (1991); Wood et al. (1998)
1233	Nucleic acid phosphate (PO_2^-)	Asymmetric PO_2^- stretching	Wong et al. (1991); Wood et al. (1998)
1127-1030	Glycogen from human epithelial cells	CH_2OH groups, C-O stretching and bending of COH groups, symmetric PO_2^- stretching.	Chiriboga et al. (1998a); Elkins (2011); Wood et al. (1998); Wong et al. (1991)

As biological materials comprise the same generic macromolecule constituents, it was not surprising that many of the components identified within the ATR-FTIR spectra of neat vaginal secretions were also observed within the spectra of neat blood, saliva and semen. However, the overall spectral pattern produced by the component vibrations, as well as the peak frequencies enabled the characterisation of each peak to specific functional groups within vaginal secretions. Of all the peak assignments in the neat vaginal secretions spectra, only those attributed to glycogen were not observed within the three other body fluids investigated.

As discussed in Section 3.1, the amide peaks are representative of the polypeptide repeats of proteins and exhibit characteristic peaks when analysed with infrared spectroscopy. Their abundance across the neat vaginal secretions spectra was evident in the strength of the amide A, I and II peaks and based on the peak frequencies observed for amides I and II, secondary structure information corresponding to the dominant protein contributors can be determined (Hering & Harris, 2009). Different functional groups give rise to the different amide peaks; amide A is a result of C-H, N-H and O-H stretching vibrations, amide I arises predominantly from C=O stretches with small N-H bends and C-H stretches, whereas amide II originates from a combination of N-H bending, and C-N stretching with weak contributions from coupled C=O bending and C-C stretching vibrations (Garidel & Schott, 2006a; Olsztynska-Janus et al. 2012). As the N-H functional group within amide A is not protein backbone specific, no secondary structure information can be derived from the presence of this peak (Barth, 2007). However, the peak frequency of amide I within the neat spectra of vaginal secretions suggests that the dominant proteins within the sample comprise of an unordered secondary structure. The amide II peak frequency suggests the protein secondary structure consists of β-sheet conformation (Table 3.2).

Vaginal secretions are heterogeneous in nature and consist of many biological components, many of which are present within other body fluids. In particular, the proteins amylase and lysozyme, predominantly found in saliva, and acid phosphatase (AP), which is abundant in semen, are known to exist within vaginal secretions, although in levels that are lower than saliva and semen (Adams & Wraxall, 1974; Carboni et al. 2014; Virkler & Lednev, 2009; Zegels et al. 2009). As each of these proteins produce specific ATR-FTIR spectra, it was possible to make comparisons with the spectra of neat vaginal secretions in order to assess whether any of these proteins can be attributed to the amide I and II peaks (Figure 3.38). An average peak frequency of 1641 cm^{-1} was observed for amide I and 1542 cm^{-1} for amide II in neat vaginal secretions, whereas the typical peak frequencies for amide I and II in lysozyme, amylase and AP were 1638 and 1530 cm^{-1}, 1641 cm^{-1}, and 1627 and 1537 cm^{-1}, respectively. Based on peak frequency alone, it could be suggested that AP does not contribute to the amide I peak in neat vaginal secretions, whereas both lysozyme and amylase do. However, observation of the spectral patterns of each protein and the neat vaginal secretions demonstrates that it is more probable that AP is the dominant protein contributing to both the amide I and II peaks as the peak conformation is near identical (Figure 3.38). AP has been reported as producing six distinct peaks within the amide I region of the infrared spectrum, one of which exhibits a peak frequency at 1642 cm^{1} (Bem & Ostrowski, 2001), which correlates with the amide I frequency observed in the neat vaginal secretion spectra.

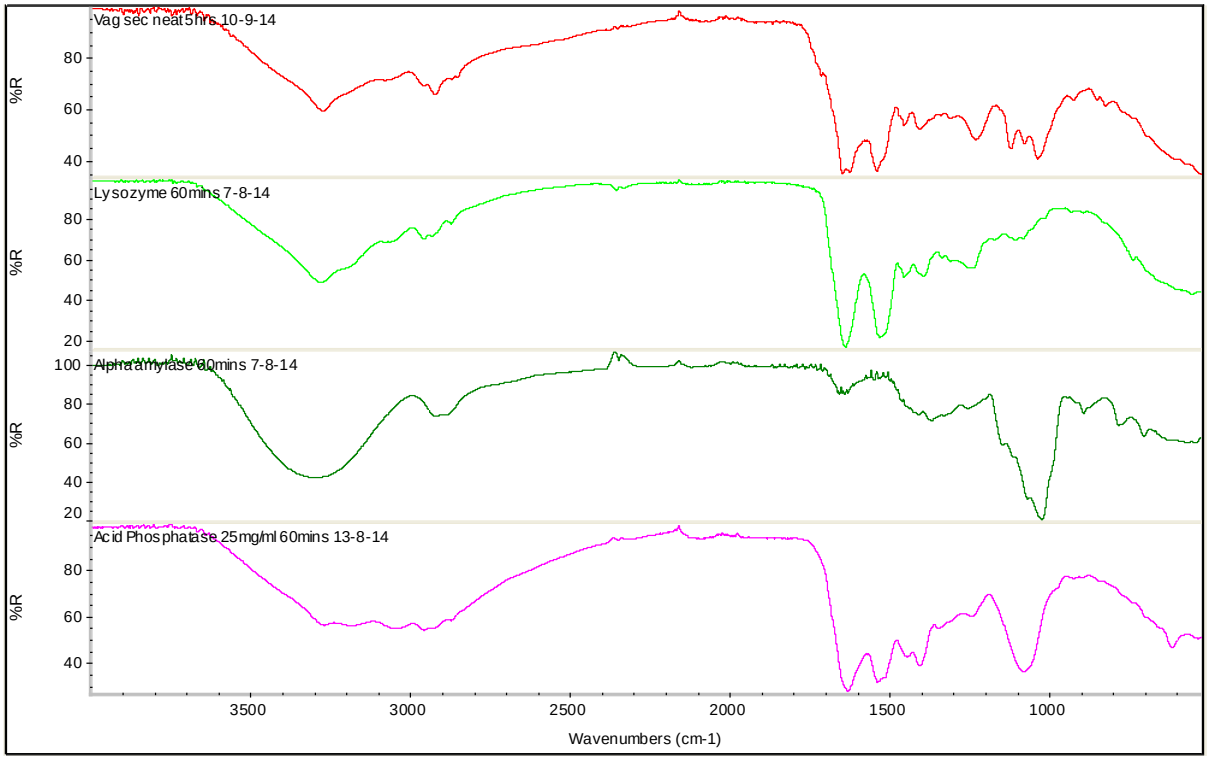

Figure 3.38: ATR-FTIR spectra comparison of neat vaginal secretions (red), lysozyme (green), amylase (dark green) & acid phosphatase (pink).

The spectral patterns observed between neat vaginal secretions and lysozyme (Figure 3.38) demonstrates that it too could be a contributor to the amide I and II peaks of neat vaginal secretions. However, a deep furrow lies between the amide I and II peaks which does not correspond with the furrow observed between the amide I and II peaks in the neat vaginal secretions spectra. Based on these observations, lysozyme can be stated as a potential contributor to these peaks, although the contribution is likely to be less than that of AP. In contrast, it is evident from the spectra of amylase and neat vaginal secretions (Figure 3.38) that amylase only exhibits one relatively weak peak in the amide I region, as seen in the ATR-FTIR spectral comparison with neat saliva (Figure 3.16). Therefore, it is unlikely that the amylase components contribute to the peak corresponding to amide I in this instance.

The glycogen peaks within the spectra of neat vaginal secretions were very distinct, not only from the other peaks across the spectrum, but also from other sugar and sugar moiety peaks exhibited in this region across the other body fluids investigated. Typically, pure glycogen spectra exhibit a strong, broad peak with three apexes arising at 1151, 1078 and 1028 cm^{-1} from the vibrational modes C-O, C-C and C-O-H deformation (Chiriboga et al. 1998). The presence of glycogen within vaginal secretions is due to the abundance of sloughed cervical and endometrial epithelial cells. The cervix and endometria continuously regenerate epithelia

and during the maturation process these cells accumulate glycogen within the cytoplasm. Upon cell exfoliation, the epithelia comprise of large volumes of glycogen, which subsequently gives rise to characteristic peaks within the sugar moiety region of the infrared spectrum. Within the neat vaginal secretions spectra, the average peak frequencies observed for the glycogen peaks were 1127, 1079 and 1036 cm^{1}, which do not fully correspond with the peak frequencies reported for glycogen. However, comparisons with comprehensive spectral interpretations of biological materials suggest that glycogen can be attributed to the particular peak frequencies observed in these vaginal secretion samples (Movasaghi et al. 2008).

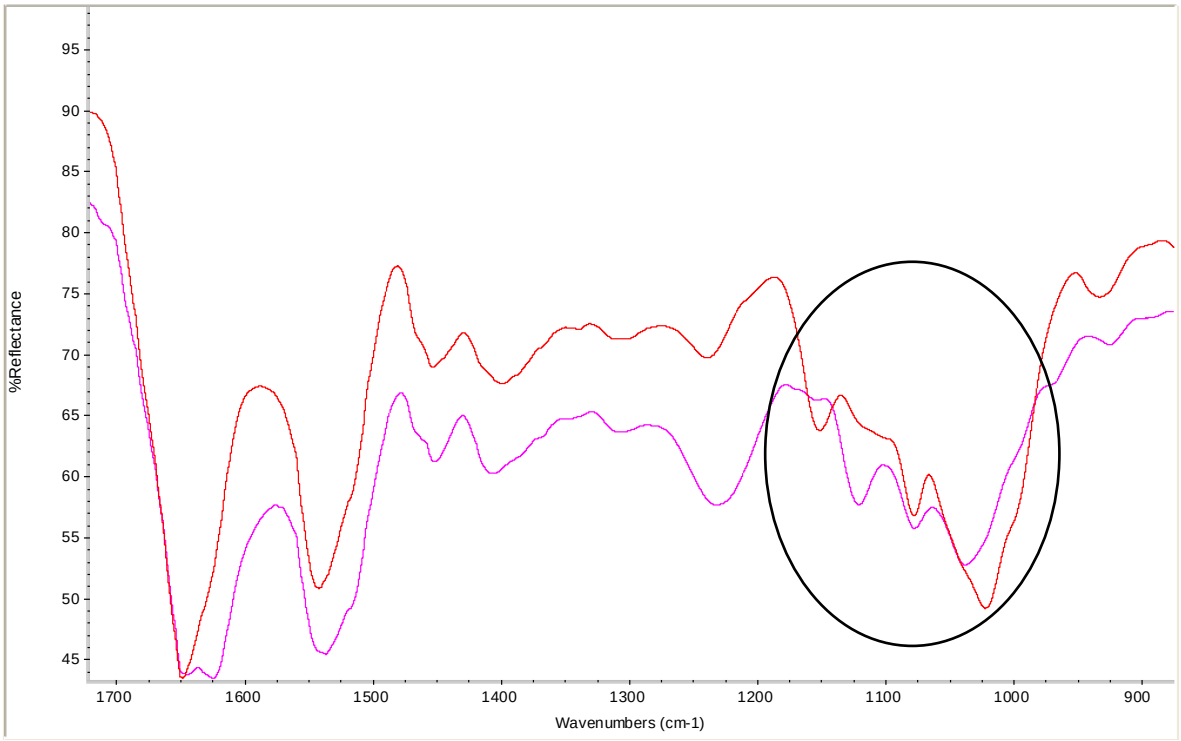

Figure 3.39: Overlay spectra demonstrating the variation of the glycogen peaks (circled) within vaginal secretions collected during the follicular phase (red) & the luteal phase (pink).

An interesting observation across the neat vaginal secretions spectra was that one sample of the five exhibited a different conformation in the glycogen peaks compared to the other samples (Figure 3.39). It is evident that a strong, narrower peak represents the glycogen component, rather than a medium, broad peak. The apexes of the peak also exhibit a different conformation as they appear more as shoulders rather than as independent apexes. The typical peak frequency reported for glycogen is 1024 cm^{-1}, which corresponds to the strongest apex of the glycogen peak across all the neat vaginal secretions spectra (Taylor et al. 2011; Wong et al. 1991; Wood et al. 1998). The peak frequencies observed in the glycogen region of this particular sample were 1151, 1078 and 1022 cm^{-1}, which correlate better with

the pure glycogen frequencies for all three apexes. A possible explanation for this difference in the glycogen peaks is that this particular sample was collected approximately four days after menstruation, during the follicular phase. The concentration of glycogen within cervical and endometrial epithelia varies throughout the menstrual cycle as it is influenced by hormones (Chiriboga et al. 1998). Particularly, levels of glycogen are expected to be higher in the luteal phase, that is the stage between ovulation and menses, when the epithelia migrate towards the tissue surface and fill with glycogen in response to progesterone (Merck Sharp & Dohme Corporation, 2014). As this particular sample was collected within the follicular phase where epithelial proliferation occurs, it is likely that the glycogen concentration in the vaginal secretion sample collected differed from the remaining samples which were typically collected during the luteal phase.

The remaining peaks observed within the neat vaginal secretions spectra were predominantly weak in comparison to the amide and glycogen peaks. At the high frequency end of the spectrum, the characteristic peaks of symmetric methylene stretching vibrations within lipids were observed. The peak shape and frequency of this functional group exhibits the same peak shape and frequency as the methylene group observed within the saliva spectra which corresponds specifically to oral mucosa (Figure 3.40). It is well documented that the mucosal cells of the oral cavity and vagina share many similar attributes (van der Bijl et al. 1997; Squier & Brogden, 2011), therefore it was not surprising that the frequency and composition of the methylene lipid peak was near identical. Based on these observations, it can be stated that the lipids within the mucosal epithelial cells of vaginal secretions give rise to the characteristic peak at 2923 cm^{-1}.

The two small, narrow peaks, with peak frequencies of 1454 and 1406 cm^{-1} correspond to the asymmetric deformation and symmetric bending of methyl (CH_3) groups within proteins (Wong et al. 1991; Wood et al. 1998). These two peaks were ubiquitous across the body fluid spectra due to their non-specific characterisation to proteins. However, the peak frequencies vary for each of the body fluids. The final peak observed within the neat vaginal secretions spectra was exhibited at 1233 cm^{-1} and was attributed to the asymmetric stretching of nucleic acid phosphate groups. Overlap between nucleic acid phosphate and amide III frequently occurs within this region of the infrared spectrum, although the position of the amide III peak is influenced by the secondary structure of the proteins that contribute to the amide I peak and would be typically observed within the 1290-1260 cm^{-1} region (Wong et al. 1991). Overlap with collagen also occurs in the nucleic acid phosphate region, although this peak exhibits a frequency of 1240 cm^{-1}, which does not correlate with the average frequency yielded for this peak in the neat vaginal secretions spectra (Wood et al. 2004).

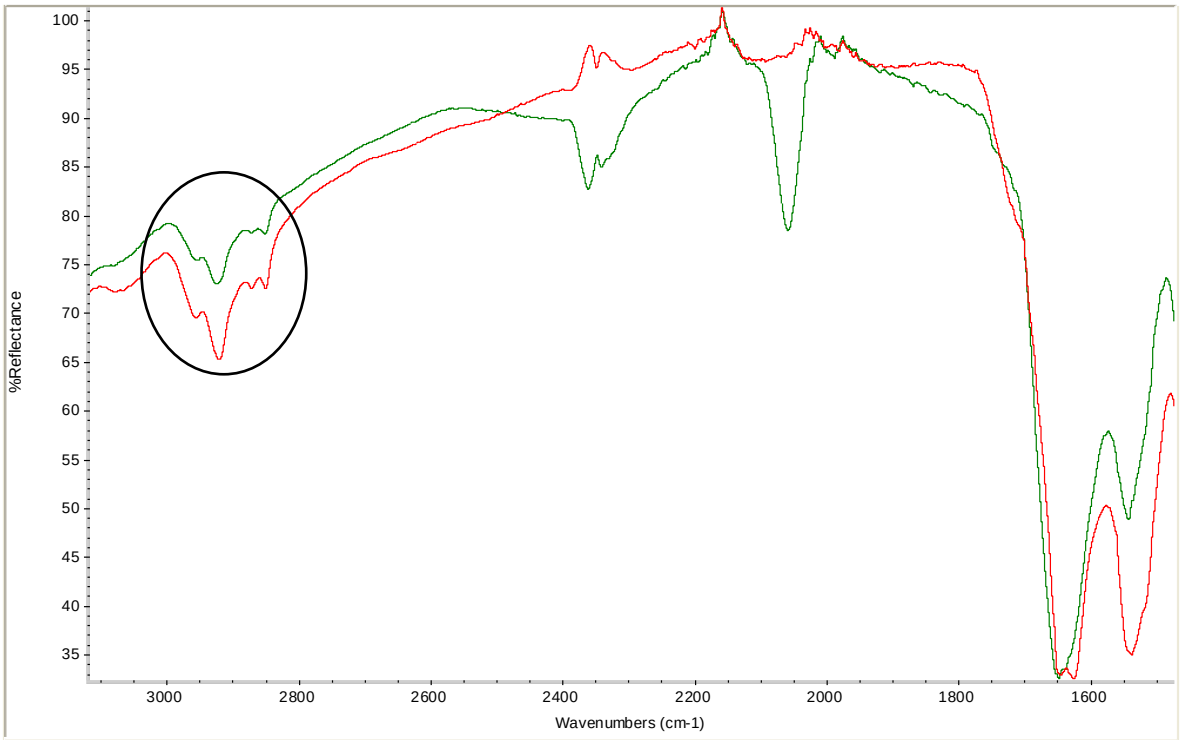

Figure 3.40: Overlay of the methylene lipid mucosa peaks in neat vaginal secretions (red) & neat saliva (green).

As mentioned earlier, one of the neat vaginal secretion samples exhibited a different glycogen peak composition in comparison to the four other vaginal secretions samples, as it was collected during the follicular phase of the menstrual cycle rather than the luteal phase. A comparison of the dry spectra obtained from the follicular phase sample with the luteal phase vaginal secretions demonstrates that there were also observable differences in other areas of the spectra (Figure 3.41); namely, the peak strength of nucleic acid phosphate (1233 cm^{-1}) vibration, which appear to be extremely weak. Additionally, the amide I and II peaks, 1641 and 1542 cm^{-1} respectively, exhibit a much deeper furrow than typically exhibited within the neat vaginal secretions spectra. As it was known that this particular sample was collected approximately four days after menstruation, it is possible that red blood cells were present within the sample, which would cause the dominant contributor to the amide I and II peaks to be haemoglobin and result in the change in amide I and II peak appearance. Figure 3.41b (circled [*1*]) demonstrates an overlap between both variations of the neat vaginal secretions spectra and haemoglobin at the amide I and II peaks. The furrow that separates the amide I and II peaks in vaginal secretions in the luteal phase is typically shallow, whereas in the follicular phase this furrow has deepened. It is evident that the furrow of the follicular phase vaginal secretions sample matches the furrow observed within the spectrum of haemoglobin (Figure 3.41b, circled [*1*]). This supports the suggestion that haemoglobin is the major

protein contributor to the amide I and II peaks of the follicular phase neat vaginal secretions sample, rather than acid phosphatase.

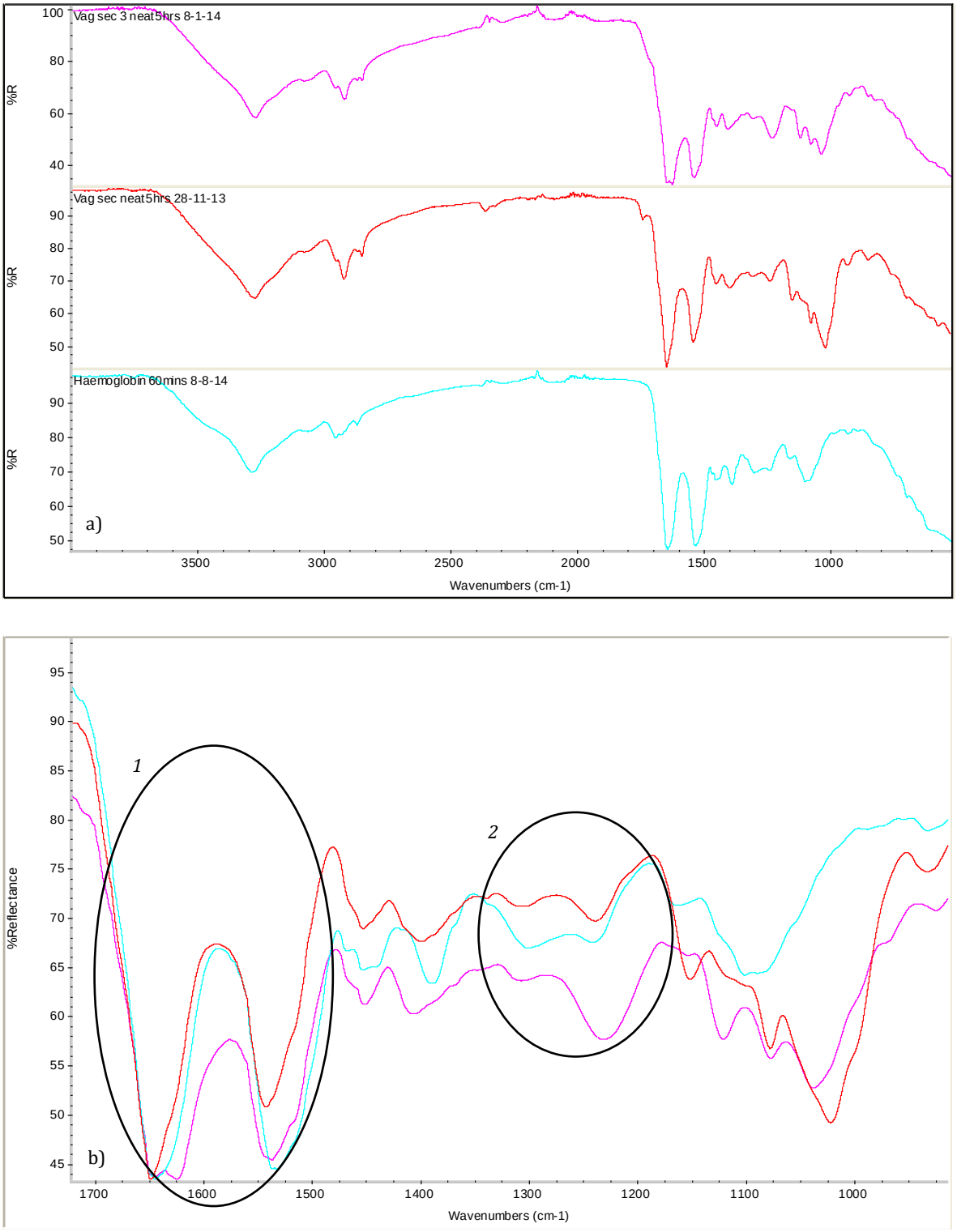

Figure 3.41: Comparison of neat vaginal secretions collected a) during follicular phase (red), luteal phase (pink) & haemoglobin (turquoise); b) amide I & II [1] & nucleic acid phosphate [2] circled.

The peak frequencies observed within the spectra obtained from the vaginal secretions samples collected during the follicular phase varied at some peaks when compared to the peak frequencies of the luteal phase vaginal secretions spectra (Table 3.9). The greatest difference was observed in the glycogen peak, with the highest and lowest frequency apexes exhibiting a difference of 11.67 and 20.72 cm^{-1}, respectively. This observation was not surprising if the distinct difference in glycogen peak conformation between the follicular and luteal phase spectra were considered (Figure 3.39). Despite the large difference at these peak frequencies, both fall within the frequency range that is attributed to glycogen vibrations (Movasaghi et al. 2008). The difference in peak frequency observed at the amide I peak (1652 cm^{-1}) can be attributed to the potential increase in haemoglobin molecules within red blood cells during the follicular phase. The correlation between the amide I frequency of haemoglobin and that observed within the follicular vaginal secretions spectra supports this suggestion (Dong et al. 1990; Olsztynska-Janus et al. 2012). Frequency differences were also exhibited at the nucleic acid phosphate (5.90 cm^{-1}) and the lower frequency methyl bending of amino acid side chains in proteins (5.10 cm^{-1}), although the average peak frequencies exhibited at these peaks within both the follicular and luteal phase vaginal secretion spectra fall within their respective regions. The remaining characteristic vaginal secretion peaks exhibited only very small frequency differences between follicular and luteal phase samples.

Table 3.9: Average peak frequencies & frequency difference observed within vaginal secretion samples collected during the follicular & luteal phases of the menstrual cycle.

Menstrual Phase	Glycogen$^-$			PO_2^-	CH_3 Amino Acids of Proteins		Amide II	Amide I	CH_2 Lipids	Amide A
Follicular	1021.78 ± 0.18	1077.73 ± 0.09	1151.42 ± 0.12	1239.76 ± 0.23	1400.22 ± 1.2	1453.22 ± 0.33	1542.58 ± 0.65	1648.56 ± 0.44	2922.90 ± 0.15	3275.47 ± 0.97
Luteal	1038.29 ± 1.17	1078.51 ± 0.87	1122.12 ± 0.86	1231.42 ± 1.34	1407.43 ± 1.85	1454.18 ± 1.16	1542.01 ± 2.06	1639.34 ± 10.09	2922.88 ± 1.39	3273.19 ± 0.95
Frequency Difference	11.67	0.55	20.72	5.90	5.10	0.47	0.40	6.52	0.01	1.61

The results obtained from the ATR-FTIR spectroscopic analysis of neat vaginal secretions correlate with those reported by various research groups for the various components within this body fluid (Chiriboga et al. 1998; Wong et al. 1991; Wood et al. 1998, 2004). Much of the literature examines the FTIR spectroscopic analysis of cervical cells, as opposed to vaginal secretions as a fluid. However, as sloughed cervical epithelia are an abundant component of vaginal secretions, the literature enabled comparisons to be made and peaks to be assigned.

Where it was not possible to utilise literature to characterise the spectral peaks observed, comparison with known protein constituents were carried out to ascertain peak identifications. All of the peak frequencies and relative shapes obtained in the results here demonstrate the same or very similar peak frequencies as those observed in literature and direct comparisons. These findings highlight that the spectrum of neat vaginal secretions is reproducibly characterised by specific peaks that correspond to a combination of common and vaginal secretion specific biological components.

3.4.1 IDENTIFICATION OF VAGINAL SECRETION STAINS: ON COTTON

Vaginal secretion stains recovered at crime scenes may not be distinctly visible due to the cream/white colouring of the fluid. The substrate upon which the stain is deposited could also affect the visibility of the stain. On light coloured substrates, close visual examination may be required to identify the presence of a stain, whereas dark coloured substrates may enhance the stain visibility. Due to the colouring of vaginal secretion stains, which are similar to that of semen, it is important within forensic investigations to able to distinguish between vaginal secretions and semen. ATR-FTIR spectroscopy has demonstrated that bloodstains can successfully be detected and identified when deposited on to cotton (Section 3.1.1), although neither saliva nor semen could be (Sections 3.2.1 & 3.3.1). Figure 3.42 demonstrates the typical ATR-FTIR spectra obtained from a dried vaginal secretion stain on cotton that had been aged for 24 hours. A total of 315 measurements were taken from 63 vaginal secretion stains from one donor.

It is evident that the peaks exhibited in the spectrum of a vaginal secretion stain correspond with the characteristic peaks observed within the spectra for neat vaginal secretions (Table 3.8). No characteristic peaks attributable to the cotton substrate were evident in the spectrum demonstrated in the dried vaginal secretion stain in Figure 3.42. However, due to the small sampling area, it was not always possible to obtain such good quality spectra from the vaginal secretion stains. Figure 3.43 demonstrates the typical appearance of a vaginal secretion stain deposited on to cotton. It can be seen that the stain consists of two elements; the outer “coffee ring” and the concentrated inner stain. The outer “coffee ring” stain was barely visible (Figure 3.43b outer circle) and demonstrates the area in which the fluid component of the vaginal secretions spread across, and was absorbed into, the substrate. The inner stain was more visible against the cotton and demonstrates the concentrated area in which the highly viscous component of the vaginal secretions spread across the cotton

(Figure 3.43b, inner circle). When ATR-FTIR spectroscopic analysis was carried out in the outer circle region of the stain, the resulting spectra did not exhibit any peaks that were characteristic of vaginal secretions. Instead, the resulting spectra was representative of the cotton substrate only (Figure 3.44, green). The inner circle area of the stain produced spectra containing peaks that were characteristic of vaginal secretions (Figure 3.42 & Figure 3.44, red).

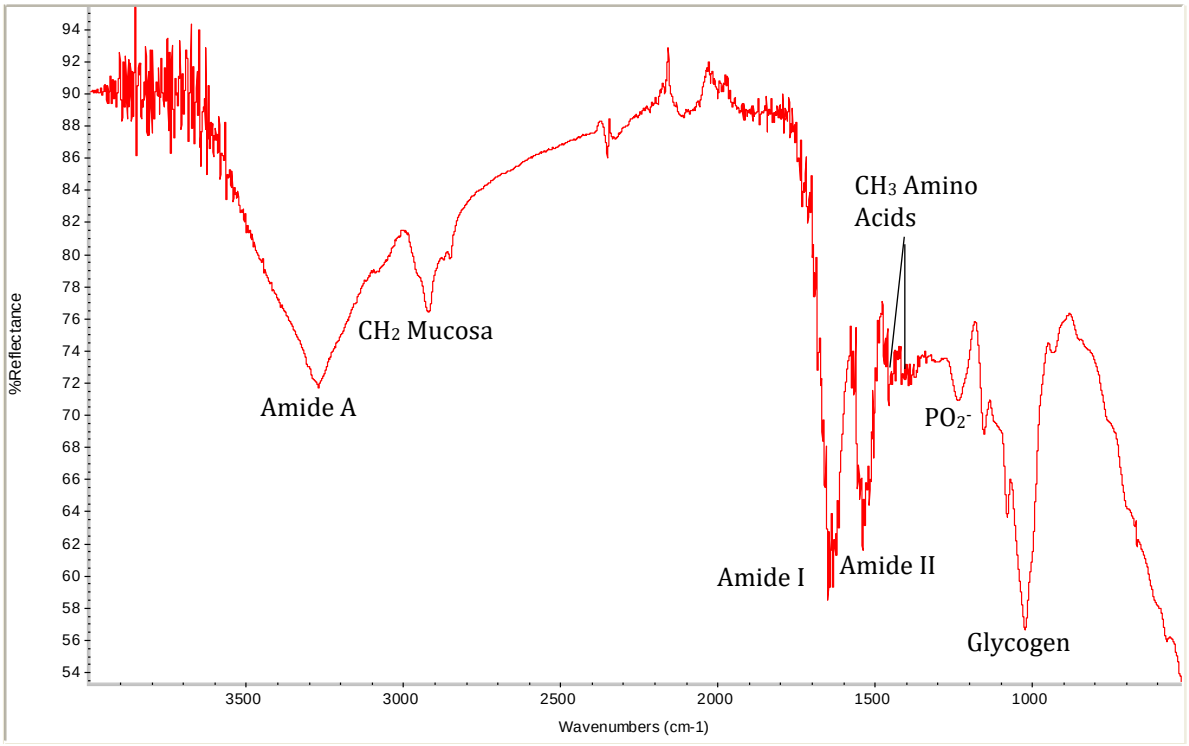

Figure 3.42: ATR-FTIR spectrum of a vaginal secretions stain on cotton aged for 24 hours.

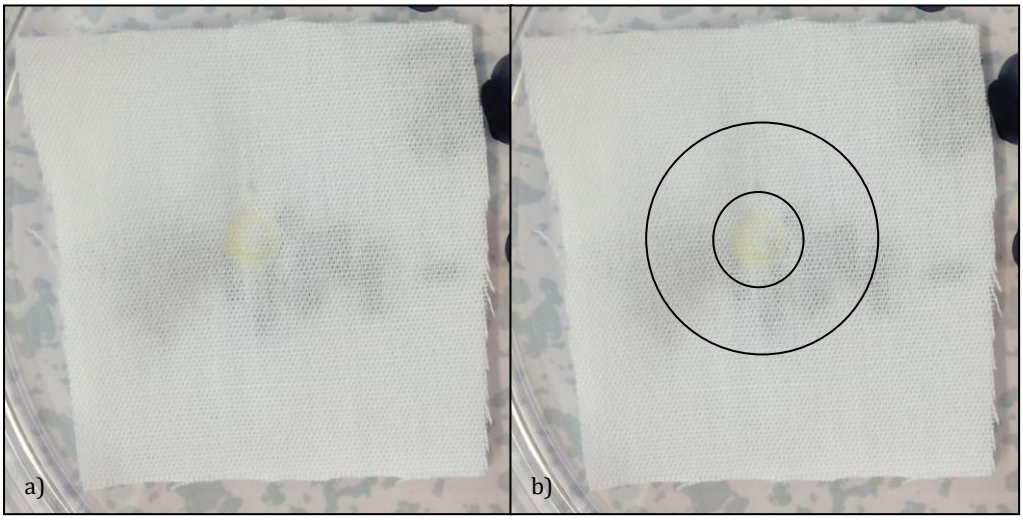

Figure 3.43: a) typical vaginal secretion stain deposited onto 4x4 cm cotton, b) stain regions highlighted; "coffee ring" outer circle & concentrated material inner circle.

As a result, the area of the vaginal secretion stains analysed with ATR-FTIR spectroscopy was limited to the inner circle area in order for vaginal secretion identification to be determined. Of the 252 measurements that were taken from the stain (excluding the 63 cotton blank measurements) 12% were of poor quality, whereby the cotton substrate dominated the spectra rather than the vaginal secretion stain. This was due to the area of the concentrated inner stain not completely covering the internal reflective element (IRE) during analysis. Consequently, these spectra were not included in any comparative or statistical analysis.

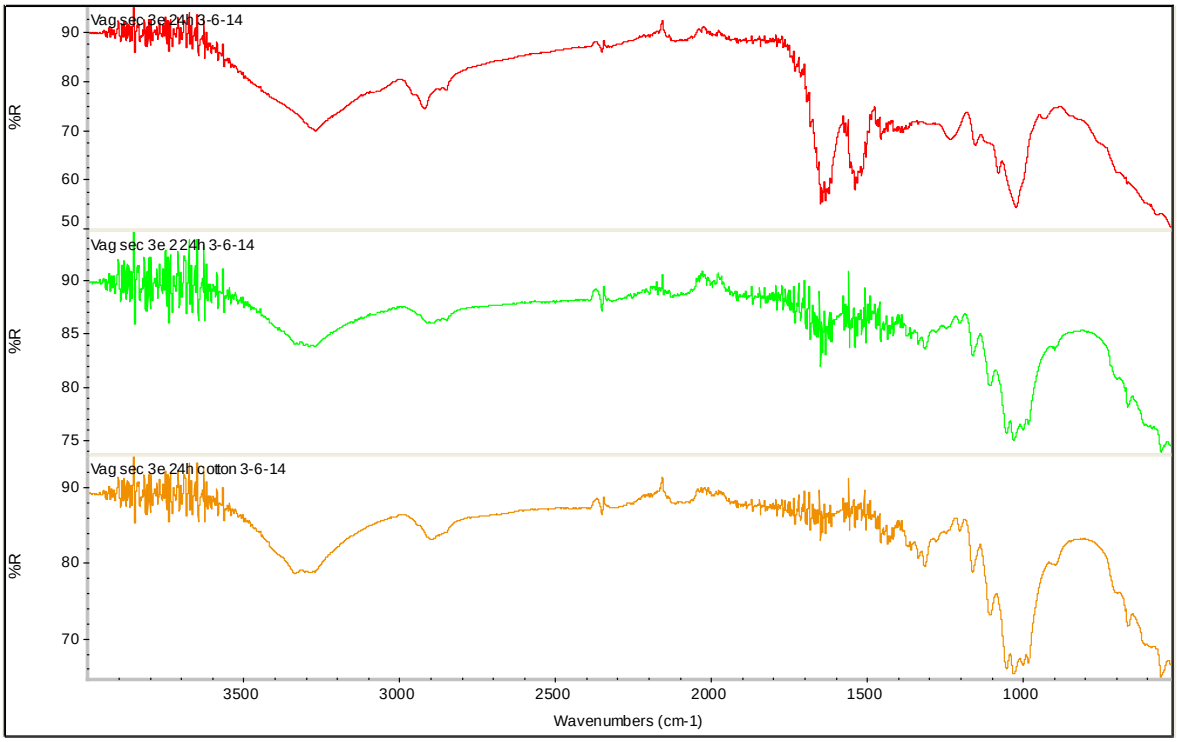

Figure 3.44: Example ATR-FTIR spectrum of a vaginal secretion stain analysed within the outer circle area of the stain (green) compared to the spectrum from analysis of the inner stain (red) & cotton blank (orange).

The spectra produced from the vaginal secretion stains were representative of the follicular phase of the menstrual cycle, rather than the luteal phase, as demonstrated in Figure 3.42. This was indicated by the deep furrow between the amide I and II peaks and the distinct narrow and strong glycogen peak. Additionally, the average peak frequencies obtained for the vaginal secretion stains exhibited very little variation from those exhibited by the ATR-FTIR spectra of the follicular phase vaginal secretion sample. The quality of the vaginal secretion stain spectra were comparable to that of the neat vaginal secretions spectra, although atmospheric and cotton interference did impact on the spectral quality across the sample set. Particularly, the characteristically weak peaks of methyl groups in amino acid protein side chains and nucleic acid phosphate were less clearly defined, and due to their weak

appearance, it was sometimes difficult to identify the peak apex from the noise interference. This was also observed within the amide I and II peaks (Figure 3.45) and was due to the 2000-1300 cm^{-1} region of the cotton spectra overlapping the peak absorptions of the body fluid.

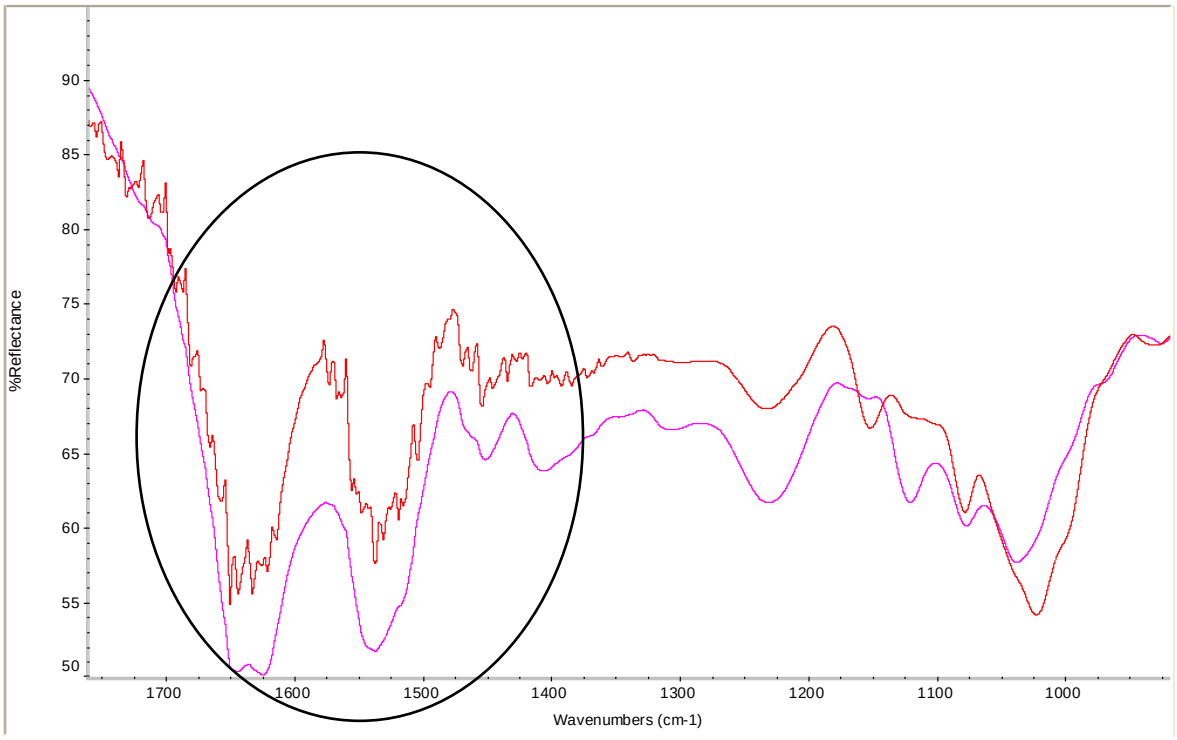

Figure 3.45: Example of the noise interference affecting the spectral quality of the amide I & II & methyl amino acids of proteins peaks (circled) within some of the vaginal secretion stains on cotton (red) compared to the amide I & II & methyl amino acids of proteins peaks within neat vaginal secretions (pink).

The interference exhibited within some of the vaginal secretion stain spectra did not appear to affect the peak intensities, with an average maximum peak intensity of approximately 71% observed for the strongest peaks, namely amide I and glycogen. Comparison with the average maximum peak intensity within the neat vaginal secretions spectra (~37%) demonstrates a maximum intensity difference of approximately 40% between the neat samples and stains on cotton. Figure 3.46 displays the average peak intensities for the amide and glycogen peaks, which were the most distinct peaks observed across the spectra, within neat and deposited stains of vaginal secretions.

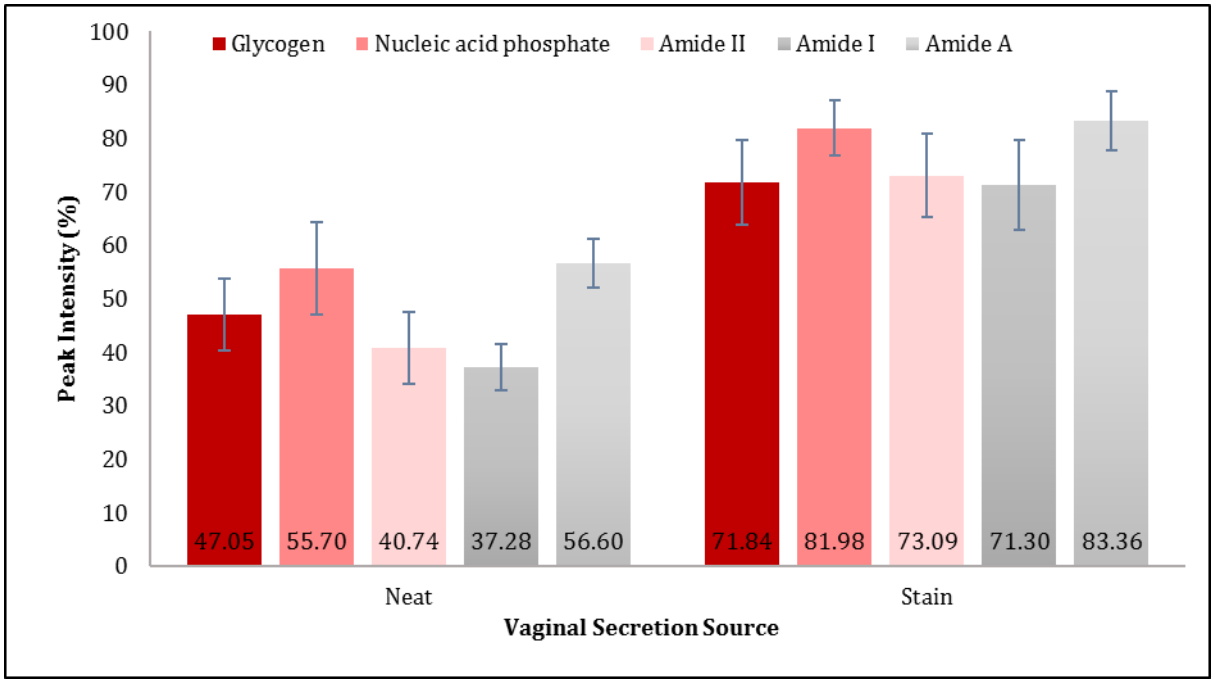

Figure 3.46: Bar graph comparison of peak intensity for the amide & glycogen peaks within the neat vaginal secretion & vaginal secretion stains on cotton spectra.

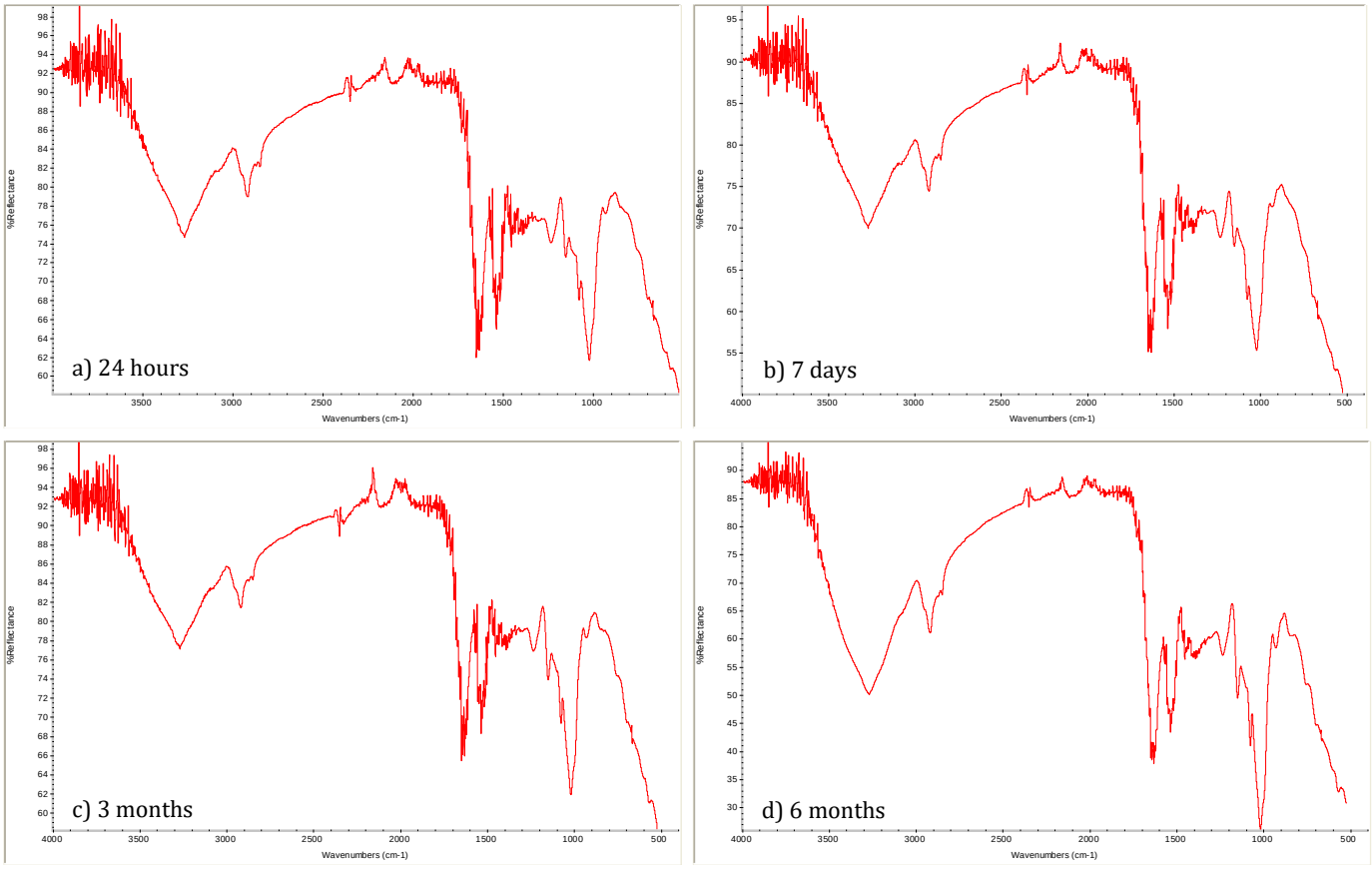

Figure 3.47: Examples of the vaginal secretion stain spectra aged to a) 24 hours, b) 7 days, c) 3 months & d) 6 months.

Peak intensity measurements when in %Reflectance or transmission analysis modes are recorded in percentages descending from 100%, therefore, the lower the peak intensity, the stronger the peak. It is evident from the bar graph that the peak intensities yielded from neat vaginal secretion samples were much stronger than those obtained from vaginal secretion stains. However, the standard deviation from the average peak intensities for amide and glycogen peaks within both sample types were similar (±4-8%) within the spectra of the two sample types. This demonstrates that the variation exhibited in peak intensity across neat and dried stains of vaginal secretions fell within a consistent percentage at each peak, regardless of the overall average intensity.

Often, when body fluid stains are encountered at crime scenes it is not known how long ago the stain was deposited, which means that the relevance of the stain to the investigation could be ambiguous. In order to determine whether sample age affected the quality of vaginal secretion stain spectra, the stain samples analysed were aged from 24 hours to six months prior to analysis. Across all of the spectra that yielded characteristic peaks indicative of vaginal secretions there appeared to be no correlation between spectral quality and the age of the sample. Spectra that were obtained from a six month old sample were comparable with spectra yielded from a one month or 24 hour old sample (Figure 3.47). This demonstrates that ATR-FTIR spectroscopy can successfully be utilised to identify vaginal secretion stains.

3.4.2 IDENTIFICATION OF VAGINAL SECRETIONS STAINS: EXTRACTED

The ATR-FTIR spectroscopic analysis of vaginal secretion stains on cotton demonstrates that it is possible to yield a spectrum that is comparable with that obtained from neat vaginal secretions (Figure 3.37). The extraction of vaginal secretion stains was also explored, as previous applications to blood, saliva and semen stains have demonstrated to be successful and yield better spectra than those obtained from direct analysis of the stain on cotton (Sections 3.1.2, 3.2.2 & 3.3.2). A total of 378 measurements were taken from 63 samples utilising the “wet-to-dry” extraction method on vaginal secretion stains that had been aged from 24 hours to 6 months. Of the 378 measurements, 138 reflected the spectra of a dry sample and 240 yielded spectra representative of water (Figure 3.2d). When deposited on to cotton, the vaginal secretions produced a stain comprising of an outer “coffee-ring” and a concentrated area of the viscous material (Figure 3.43). During the “wet-to-dry” extraction procedure, both parts of the stain were removed from the cotton to ensure that all possible biological material was included in the extraction. Due to the viscous nature of the

concentrated inner stain, it was possible to scrape this from the cotton into the extraction solute during the second addition of sterile, distilled water, which was then thoroughly mixed. The resulting sample extracts were then analysed with ATR-FTIR spectroscopy. Figure 3.48 demonstrates the typical spectra obtained from the extracted vaginal secretion stains (red), in comparison to the directly analysed vaginal secretion stain on cotton (green) and the cotton blank (pink) obtained from the same 14 day aged sample.

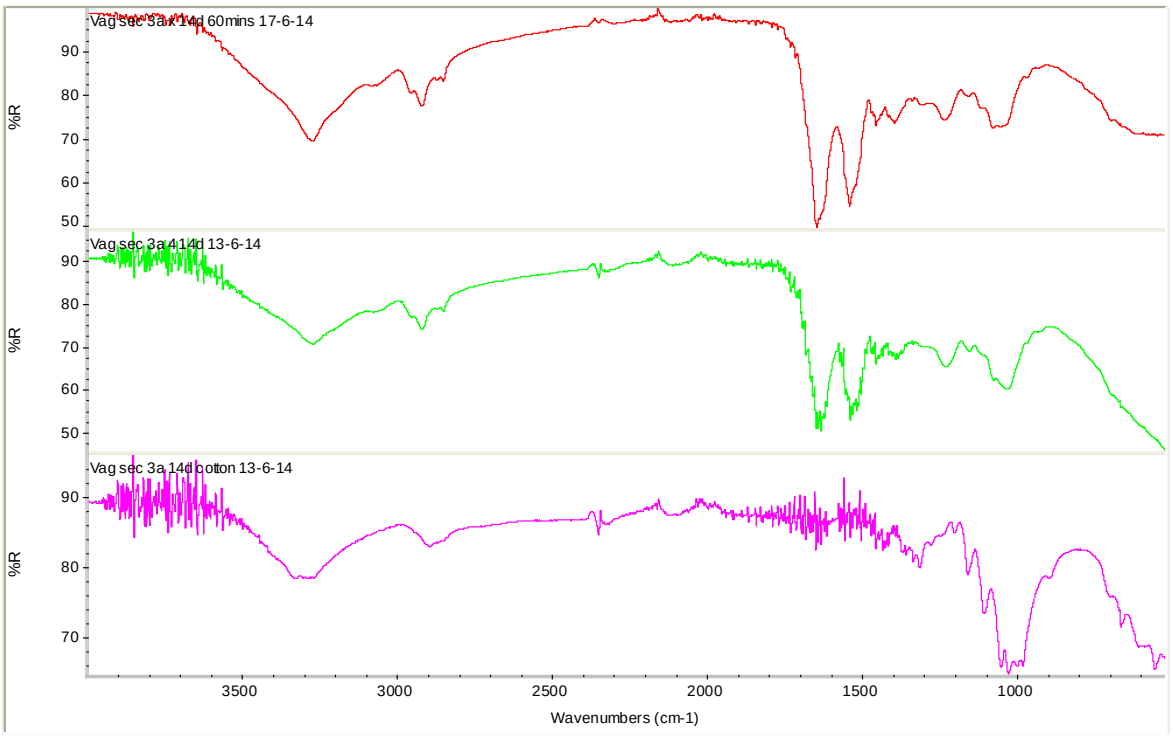

Figure 3.48: Example of ATR-FTIR spectra from an extracted vaginal secretion stain (red), vaginal secretion stain on cotton (green) & cotton blank (pink).

It is evident from the extracted vaginal secretions spectrum that the overall quality is excellent in terms of clearly defined peaks that were comparable with the peaks observed within neat vaginal secretions (Table 3.8). The peak frequencies that correspond to the ten characteristic vaginal secretion peaks were observed within the extracted spectra across the various sample ages (24 hours to 6 months), with no apparent contamination from the cotton substrate. The clarity of the extracted vaginal secretion spectra is due to the inclusion of the concentrated viscous material within the extract solute. As this cellular material is scraped from the cotton into the extract solute during extraction, this material was abundant when each sample extract was aliquoted for ATR-FTIR analysis. Therefore, the majority of resulting spectra exhibited characteristic peaks that were almost identical to those of neat vaginal secretion spectra. However, the typically clearly defined glycogen peak and its apexes were

frequently observed as less distinct when compared to its appearance within the neat and stain vaginal secretions spectra (Figure 3.49).

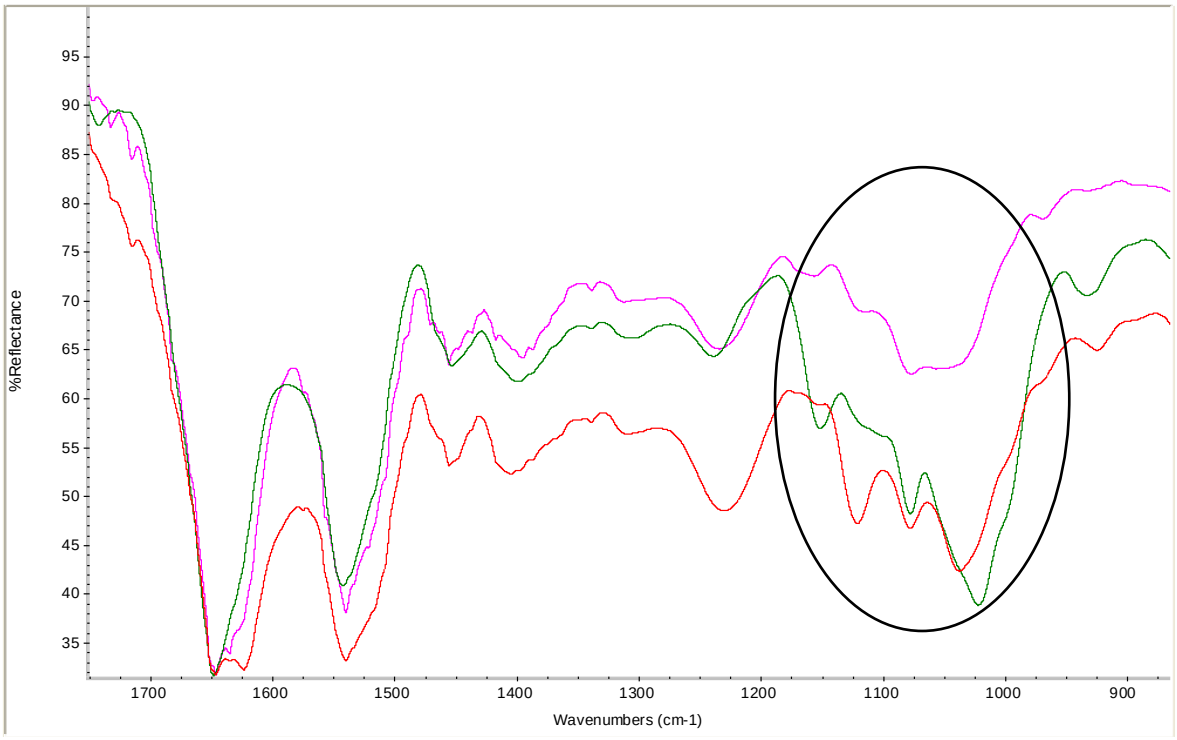

Figure 3.49: Comparison of glycogen peaks (circled) exhibited in the neat vaginal secretion spectra when collected during follicular (green) and luteal phase (red) of the menstrual cycle and the extracted vaginal secretion spectra (pink).

The lack of distinction of the glycogen peak within some of the extracted vaginal secretion stain spectra made the attribution of the menstrual phase (follicular or luteal) difficult to confirm. However, it was still possible to determine that the peaks corresponded to the glycogen-rich epithelial cells within vaginal secretions. A possible explanation as to why the glycogen peak demonstrated such variation within the extracted spectra is the reduced concentration of glycogen present within the extracted samples compared to the stains and neat vaginal secretions. The glycogen within vaginal secretions predominantly arise from the sloughed epithelial cells of the endometrium and cervix, although free glycogen has also been described within this body fluid (Mirmonsef et al. 2014). If the glycogen-containing epithelia did not dissociate from the cotton substrate adequately during the extraction process, the concentration of glycogen present within the extract would be reduced and therefore result in a less defined peak with shifted apexes. It is also possible that the aliquots of the vaginal secretion stain extracts examined did not contain high concentrations of glycogen and therefore only weak, broad peaks were exhibited. The remainder of the peaks observed within the extracted vaginal secretions spectra were consistent with the characteristic peaks

of neat vaginal secretions, which demonstrates that the simple water extraction procedure was sufficient to extract vaginal secretions from cotton without substrate contamination. Additionally, the spectra yielded were directly comparable to those produced from neat vaginal secretions which is highly advantageous for application within forensic investigations.

Table 3.10 provides an overview of the differences in peak frequency observed between vaginal secretions in the neat, stain or extracted form. It is evident that there is little difference exhibited within the average peak frequencies of the vaginal secretion characteristic peaks across the three sample types, with the exception of two of the glycogen apexes. The vast difference exhibited in the average peak frequencies that correspond to glycogen across the neat, stain and extracted vaginal secretions was not surprising due to the differences in peak conformation across and within the three sample types. As the glycogen peak is located within the fingerprint region of the infrared spectrum, any changes in the biological components, or their concentration, would result in peak conformational changes within the spectrum. Based on the average peak frequencies demonstrated in Table 3.10, the strongest glycogen apex demonstrates a spectral range of 1036-1025 cm^{-1}, whereas the weakest of the apexes demonstrates a spectral range of 1153-1127 cm^{-1} within the three sample types. This is as a result of the glycogen peak exhibiting vast variability in its appearance, although it could also be a result of an overlap with other biological components comprising of sugars or sugar moieties, such as amylase (Figure 3.38).

Table 3.10: Comparison table of the average peak frequencies observed across the spectra obtained from vaginal secretions as neat, stains & extracted.

Vaginal Secretions Source	**Glycogen$^-$**			**PO_2^-**	**CH_3 Amino Acids of Proteins**		**Amide II**	**Amide I**	**CH_2 Lipids**	**Amide A**
Neat	1035.81 ± 6.07	1078.39 ± 0.85	1126.51 ± 10.62	1232.67 ± 3.26	1409.67 ± 3.14	1454.08 ± 1.10	1542.10 ± 1.92	1640.73 ± 9.87	2922.88 ± 1.28	3273.53 ± 1.25
Stain	1024.62 ± 4.84	1078.01 ± 0.29	1153.03 ± 1.72	1233.33 ± 1.64	1394.78 ± 4.27	1454.69 ± 0.14	1545.82 ± 4.38	1644.41 ± 0.73	2919.96 ± 1.26	3270.93 ± 0.17
Extract	1034.96 ± 6.85	1078.83 ± 0.76	1141.87 ± 17.06	1236.12 ± 2.02	1402.10 ± 1.05	1453.63 ± 1.93	1540.44 ± 2.75	1647.10 ± 4.19	2922.33 ± 0.92	3275.33 ± 1.92

With the exception of the glycogen apexes, little difference was observed in the peak frequencies between neat, stains and extracted vaginal secretions which demonstrates consistency within the appearance of peaks associated with the biological components of vaginal secretions when examined with ATR-FTIR spectroscopy. These findings correlate

with those obtained for blood, saliva and semen, which add further strength to the application of this technique for body fluid identification.

The spectra obtained from the extracted vaginal secretions that had been aged up to six months did not exhibit any changes in spectral appearance or quality that could be associated with the increase in sample age prior to extraction. For all the sample ages examined, the vaginal secretions successfully washed from the cotton into the extraction solute, unlike the oldest bloodstains that were extracted. However, the age of the oldest bloodstains extracted was 18 months, whereas the oldest vaginal secretion stains extracted were only six months old. Therefore, it is not possible to determine whether vaginal secretion stains of the same age would have been difficult to extract, although the concentrated viscous material could be physically removed after the first washing step. This was not possible in any of the other body fluids investigated and suggests that this may allow for successful extraction, and subsequent ATR-FTIR spectroscopic analysis of vaginal secretions stains that are older than six months. Based on these observations, it is possible to state that extracted vaginal secretion stains aged from 24 hours to 6 months can successfully yield ATR-FTIR spectra that contain the characteristic peaks expected in samples of neat vaginal secretions, regardless of the phase of the menstrual cycle, without the limitations encountered in the extraction of blood and saliva.

3.4.3 FORENSIC APPLICATION

Vaginal secretions offer a challenge within forensic investigations as their appearance can be similar to that of semen. Its presence can yield positive reactions from presumptive tests designed for saliva and semen, due to the shared composition of amylase and acid phosphatase. However, the characterisation of ATR-FTIR spectral peaks obtained from vaginal secretions demonstrated here correlate with literature that has examined the FTIR spectroscopic analysis of vaginal secretion constituents (Chiriboga et al. 1998, 1997; Wong et al. 1991; Wood et al. 1998, 2004). Direct comparisons with known vaginal secretion constituents also allowed the specific attribution of proteins to particular peaks; acid phosphatase, haemoglobin, lysozyme and amylase. The reproducibility of this technique was exhibited in the production of comparable spectra from vaginal secretions in their neat form, as stains on cotton and when extracted from cotton. These findings are of benefit to the forensic science community as there are currently no presumptive or confirmatory test available for the identification of vaginal secretions.

ATR-FTIR spectroscopy has demonstrated that vaginal secretions-specific spectra can be obtained not only from neat samples of the body fluid, but also from stains when analysis is carried out directly, or when the stain is extracted from the substrate. This highlights the versatility of the technique in the application of vaginal secretion identification, as well as demonstrating reliability. As no reagents were utilised within the spectroscopic analysis, the original samples were not exhausted and further analysis can be conducted on the sample extracts. Additionally, ATR-FTIR spectroscopy offers a universal, yet specific technique that can be utilised to identify vaginal secretions, as well as potentially establish the phase of the menstrual cycle during which the vaginal secretions were deposited. However, it must be borne in mind that if vaginal secretion samples are deposited close to the beginning or end of menses, the dominance of red blood cells, and thus haemoglobin, could result in a spectrum that indicates the presence of blood, rather than vaginal secretions. It would require subjective interpretation to determine the origin of the sample based on the overall combination and appearance of peaks present within the spectrum. Overall, it can be stated that ATR-FTIR spectroscopy is a suitable technique to identify vaginal secretions.

3.5 BODY FLUID IDENTIFICATION: COMPARISON

The results discussed in the previous sections (3.1-3.4) demonstrate that ATR-FTIR spectroscopy can successfully yield spectra that obtain characteristic peaks attributable to biological components within blood, saliva, semen and vaginal secretions, independently. Each of these body fluids have demonstrated different spectral patterns, despite comprising of peaks originating from common macromolecules. However, in order to recommend the utilisation of ATR-FTIR spectroscopy as a method of body fluid identification, the similarities and differences between the typical spectra of each body fluid must be identified. Figure 3.50 exhibits an overlay of the neat spectra of blood (red), saliva (green), semen (pink) and vaginal secretions (purple). The regions of the spectrum where different macromolecule groups were typically expressed are circled.

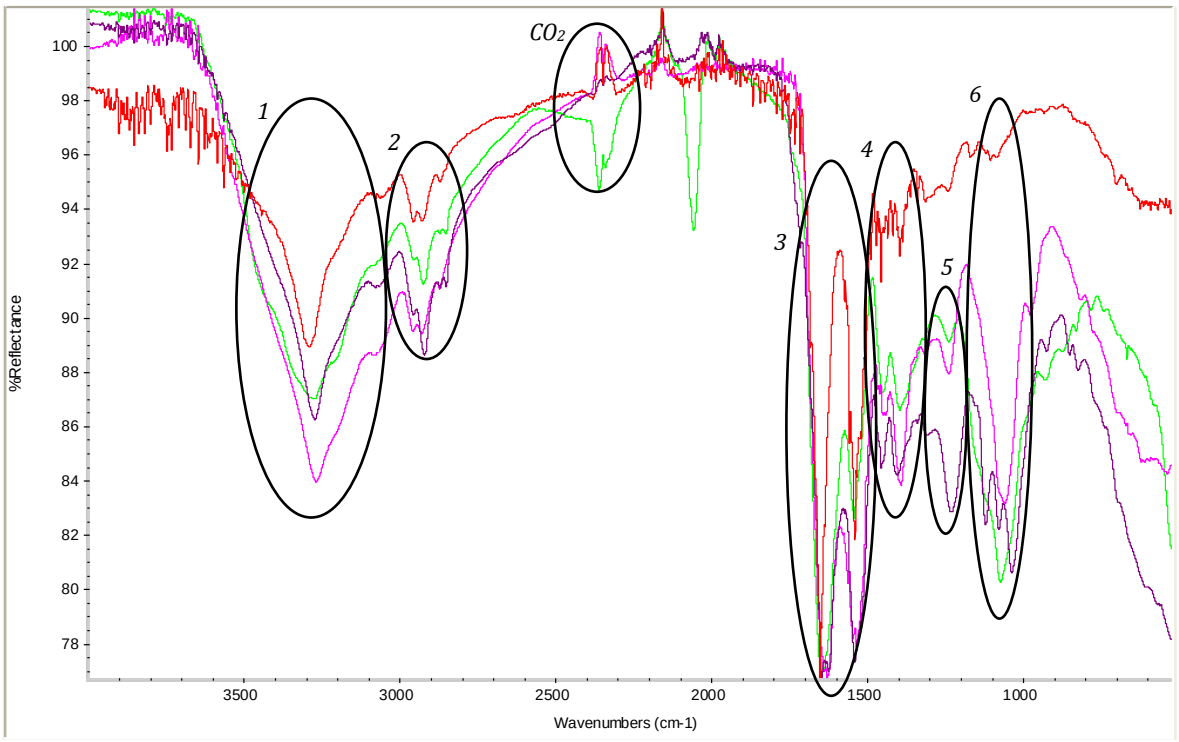

Figure 3.50: ATR-FTIR overlay of neat blood (red), saliva (green), semen (pink) & vaginal secretions (purple) spectra with the common macromolecule groups circled; [1] - amide A, [2] - CH_2/CH_3 lipids, [3] - amide I & II, [4] - CH_3 amino acid side chains of proteins, [5] - phosphate groups & [6] - sugar/sugar moieties.

There are six groupings of common biological components across the four neat body fluid spectra; namely, amide A [*1*], methyl and methylene stretching in lipids [*2*], amide I and II [*3*],

methyl and methylene bending of amino acid side chains in proteins [*4*], phosphate groups [*5*] and sugar and sugar moieties [*6*] (Figure 3.50). At the high frequency end of the spectrum lie the amide A and methyl/methylene stretching vibrations associated with lipids (Figure 3.50 [*1 & 2*]). The conformation of these peaks within the neat body fluid spectra were similar, with only small differences in the relative shape and size of the peaks observed. At the lower end of the spectrum, many observable differences were evident in the peaks within the 1660-900 cm^{-1} region of the infrared spectrum. Amide I and II correspond to proteins within the samples and can provide an indication of the secondary structure of the proteins which give rise to these peaks (Barth 2007; Hering & Harris, 2009). The most variation between the four different body fluid spectra was apparent in the amide I and II peaks. The amide I and II peaks of blood (Figure 3.51, red) exhibit strong, narrow peaks with a deep furrow, whereas the other three body fluids exhibit much shallower furrows between these peaks. Comparisons between the blood and saliva amide I and II peaks (Figure 3.51, green) demonstrate that the amide II exhibits a weaker peak strength compared to amide I, whereas in semen and vaginal secretions (Figure 3.51, pink & purple, respectively) the amide II peaks exhibit a peak strength similar to that of the amide I peaks. The furrow observed between the amide I and II peaks within these two body fluids were the shallowest and comparison of these peaks demonstrate that the peak conformation observed at amide I and II was near identical.

The methyl/methylene bending vibrations associated with amino acid side chains in proteins (Figure 3.50, [*4*]) exhibited the same general composition of weak, narrow peaks within all four body fluids. However, the relative size of each peak in relation to each other varied between the body fluids. In the blood spectra (Figure 3.52, red), the peaks were less defined and the asymmetric vibrational mode (1456 cm^{-1}) exhibited a stronger peak intensity than the symmetric vibration peak (1395 cm^{-1}) for the amino acid side chains. In contrast, the symmetric mode peak exhibited a greater peak strength than the asymmetric mode peak in both saliva and semen (Figure 3.52, green & pink). Particularly, the asymmetric mode peak in semen was much larger than the symmetric mode peak, which appears more as a shoulder to the asymmetric mode peak. These peaks within the vaginal secretion spectra exhibited a similar strength, with no distinct difference between the symmetric and asymmetric mode peaks (Figure 3.52, purple).

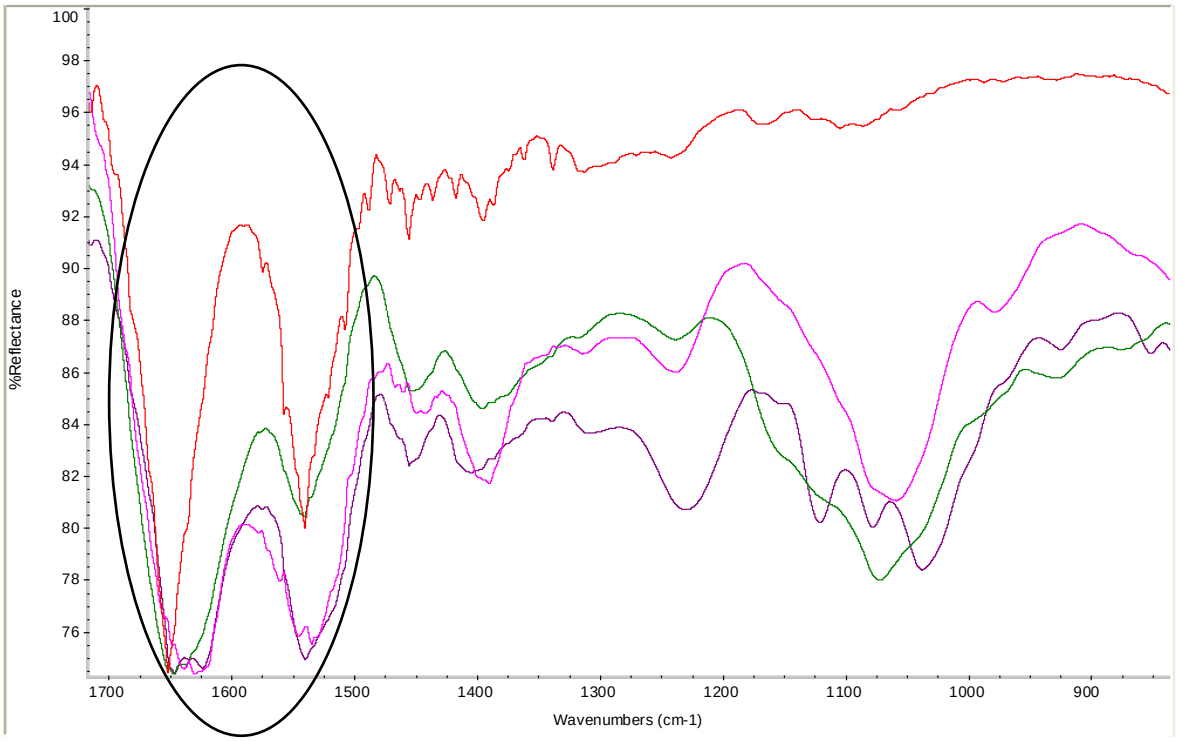

Figure 3.51: Comparison of amide I & II peaks (circled) in neat blood (red), saliva (green), semen (pink) & vaginal secretions (purple).

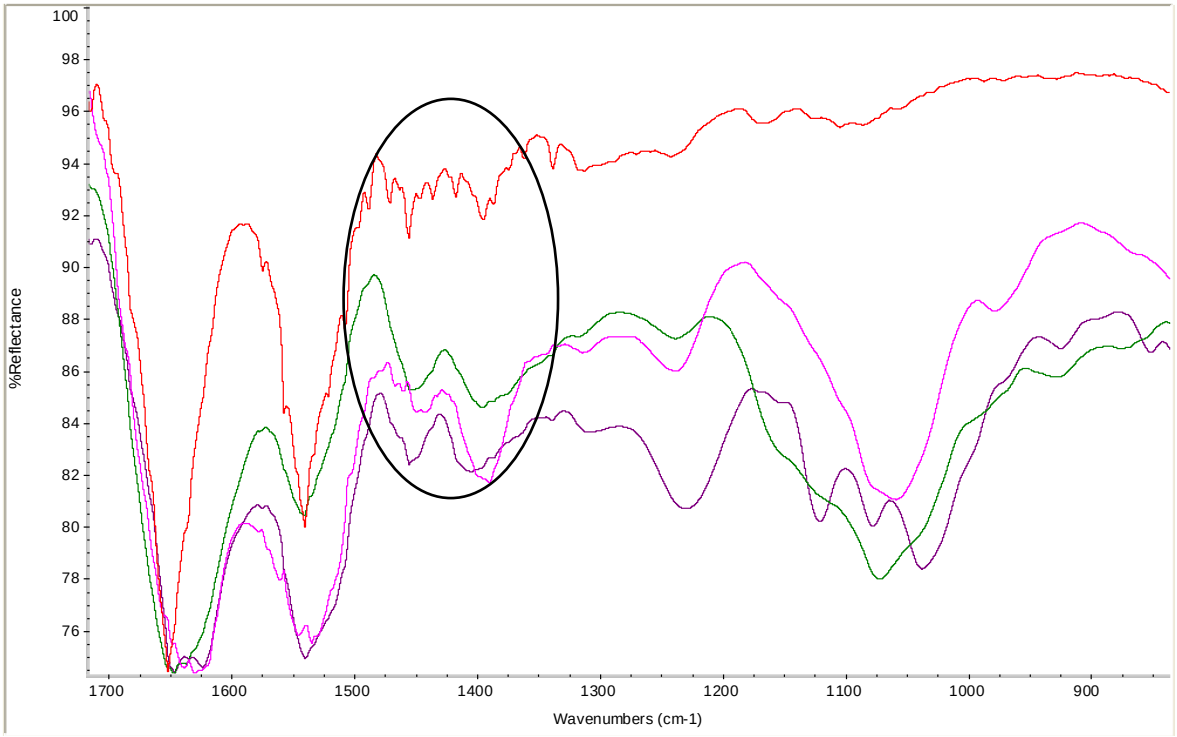

Figure 3.52: Comparison of the methyl/methylene bending vibrations of amino acid side chains in proteins (circled) in neat blood (red), saliva (green), semen (pink) & vaginal secretions (purple).

Peaks corresponding to phosphate group vibrations were observed within the saliva, semen and vaginal secretions spectra (Figure 3.50 [*5*]), but not the blood spectra. This particular region of the infrared spectrum is known to exhibit overlap between amide III and phosphate vibrations (Movasaghi et al, 2008) and in the blood spectra the peaks exhibited in the 1350-1220 cm^{-1} region were indicative of amide III, characterised by the broad, "W" peak conformation (Figure 3.6). The peak observed between 1250-1220 cm^{-1} in saliva, semen and vaginal secretion spectra were attributable to different phosphate groups; phospholipids gave rise to the peak in saliva (Figure 3.53, green), whereas nucleic acid phosphate vibrations were attributed to the peaks observed in semen and vaginal secretion spectra (Figure 3.53, pink & purple). The shape of the phosphate group peaks in these three body fluids exhibited the same, rounded apex. However, the variation in peak strength differed amongst the body fluids, with saliva exhibiting the weakest intensity and vaginal secretions exhibiting the strongest.

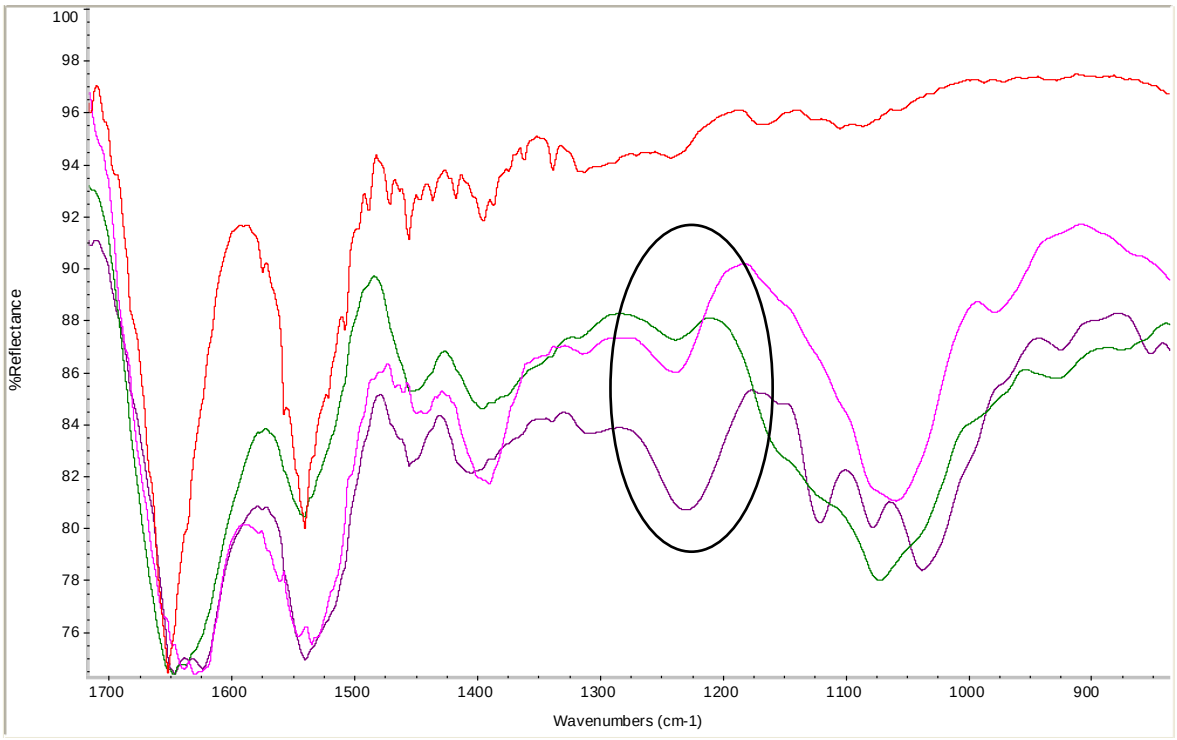

Figure 3.53: Comparison of the phosphate group vibrations (circled) in neat saliva (green), semen (pink) & vaginal secretions (purple) (neat blood spectrum in red).

At the lowest end of the spectrum, vibrations originating from sugars and sugar moieties were observed within each of the four body fluid spectra, typically ranging from 1150-950 cm^{-1}. Each body fluid exhibited individual characteristic peak conformations that allow for component identifications to be made specific to each body fluid (Figure 3.50 [*6*]). Within blood, the sugar peak corresponds to glucose, although the peak observed is very weak and

broad which varies greatly from the other three body fluids (Figure 3.54, red). The sugar and sugar moieties exhibited in saliva were from glycosylation. In semen, fructose and prostate specific antigen (PSA) were attributable to the peaks, and in vaginal secretions, glycogen from sloughed epithelia give rise to the sugar peaks. It is evident from Figure 3.54 that each of the sugar-related peaks within the body fluids exhibit very different peak conformations; saliva demonstrates a broad peak with a single apex (Figure 3.54, green), semen displays a narrower, well defined peak with a small shoulder at approximately 980 cm^{-1} (Figure 3.54, pink), and vaginal secretions exhibit a distinct peak with three apexes (Figure 3.54, purple). As discussed in Section 3.4, the sugar peak within vaginal secretion spectra vary depending on whether the samples were collected during the follicular or luteal phase of the menstrual cycle. Despite the variation in glycogen peak composition across vaginal secretion spectra, the characteristic shape of the glycogen peak differs greatly from the sugar peaks observed within blood, saliva and semen spectra (Figure 3.54, blue), and therefore each sugar/sugar moiety peak can be differentiated from one another.

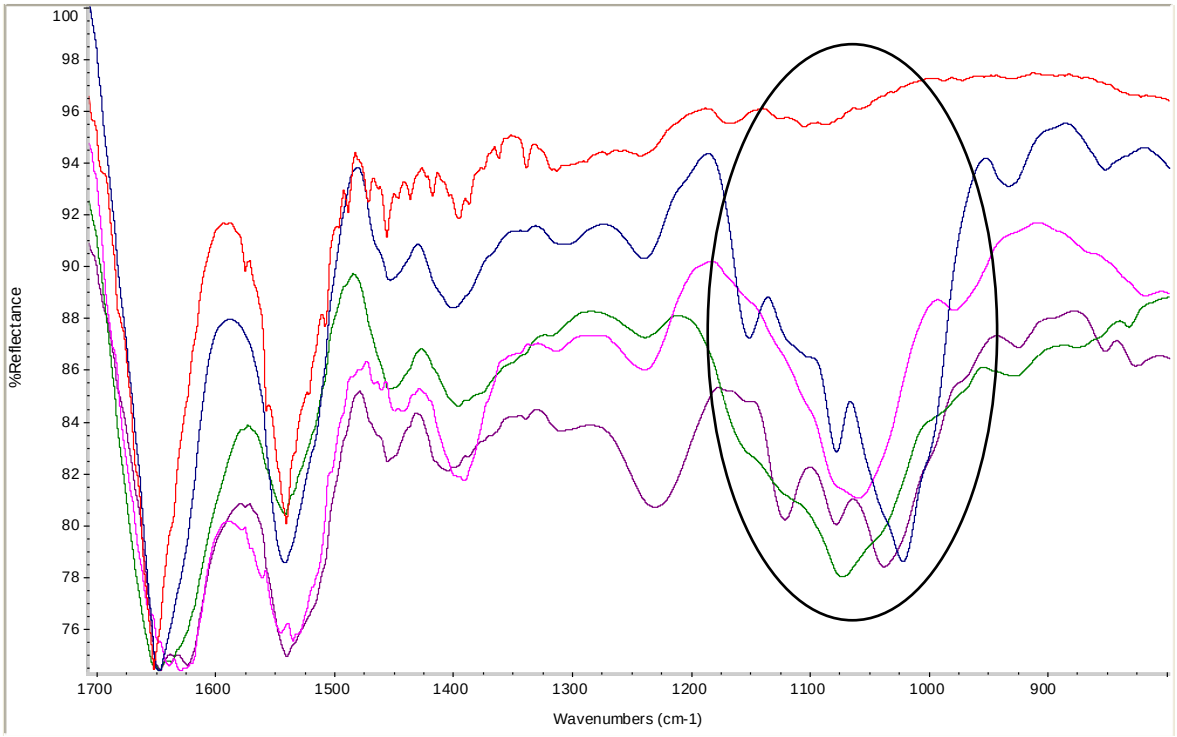

Figure 3.54: Comparison of the sugar/sugar moiety peaks in; a) neat blood (red), saliva (green), semen (pink) & vaginal secretions (purple), b) follicular (dark blue) & luteal (pink) phase vaginal secretions with blood, saliva and semen.

It was evident from the spectra obtained from all of the body fluid samples, whether in a neat, stain or extracted state, that the spectral patterns observed enabled each body fluid to be distinguished from one another. However, as there were six regions within the spectra that

corresponded to common macromolecule groups, the ratios of these peaks were examined to establish any further similarities or differences. As amide A and the methyl/methylene stretching vibrations of lipids exhibited the least variation in peak conformation across the four body fluid spectra, these peaks were not included in the ratio comparisons. The peaks within the fingerprint region of the spectrum typically exhibited peak conformations that can allow specific components to be identified. Therefore, peak ratios were compared amongst the four macromolecule groups observed in this region. Table 3.11 demonstrates the specific peak ratios examined.

The peak intensity (%) of each of the characteristic macromolecule groups was utilised in the analysis of peak ratios, rather than peak frequency (cm^{-1}), as the composition and strength of each peak varied depending on the body fluid (Figure 3.50). Peak frequency was not suitable to examine peak ratios as many of these peaks exhibited similar peak frequencies across the four body fluids, therefore, the ratios obtained would not vary enough to enable body fluid discrimination. However, the peak intensity differed for each of the common macromolecule groups due to the peak composition and relative concentration of the specific constituent in comparison to the other biological constituents within the sample. As a result, it would be expected that the peak intensities observed for the same macromolecule peaks would differ depending on the body fluid, which in turn would result in different peak ratios between the same macromolecule groups.

Table 3.11: Peak ratios examined in the discrimination of blood, saliva, semen & vaginal secretion spectra.

Ratio	Macromolecule groups
A	Amide II:Amide I
B	Asymmetric CH_2/CH_3 amino acid side chains in proteins:Amide I
C	Symmetric CH_2/CH_3 amino acid side chains in proteins:Amide I
D	Amide III/Phosphate groups:Amide I
E	Sugar:Amide I
F	Amide II: Asymmetric CH_2/CH_3 amino acid side chains in proteins
G	Symmetric CH_2/CH_3 amino acid side chains in proteins: Asymmetric CH_2/CH_3 amino acid side chains in proteins
H	Amide III/Phosphate groups:Asymmetric CH_2/CH_3 amino acid side chains in proteins
I	Sugar:Asymmetric CH_2/CH_3 amino acid side chains in proteins

The macromolecules corresponding to proteins, amino acids, phosphate groups and sugars were ratioed against the strongest peak within the body fluid spectra; amide I, and one of the weakest peaks in the spectra; asymmetric methyl/methylene groups in amino acid side chains. As the spectral patterns observed for each of the body fluids appeared reproducible, it was thought that the ratios observed for each of the peak combinations (Table 3.11) would be consistent for each sample type of each body fluid, which could potentially allow for unknown samples to be definitively identified.

Initially, the peak ratios were compared between the spectra of each of the body fluid states (neat, stain and extracted) for each body fluid. Figure 3.55 demonstrates the ratios obtained across the blood (a), saliva (b), semen (c) and vaginal secretions (d) spectra for all sample types.

It is evident that the same peak ratios were not obtained for all of the macromolecule groups examined within each body fluid and the different sample states, although the majority of the peak ratio values fell within the range of 0.60-1.60. Ratio comparisons within the blood samples demonstrate that the ratios against amide I (A-E) exhibited the greatest difference between the neat, stain and extract samples. The extracted blood samples demonstrated the greatest difference in ratio compared to the neat and stain samples, with only overlap in variation exhibited at combination B. The neat and stain samples exhibited closer ratio values with strong overlap in variation amongst the combinations A-E. In contrast, ratio combinations F-I demonstrated more similar ratio values, with tight clusters forming between the different blood samples at combinations G and H. Typically, the peak ratios of the blood extract spectra were higher, except at combinations B and F, than those observed in neat blood and bloodstains. This was due to the peak intensities of extracted blood exhibiting a greater average intensity in comparison to the other blood sample states, which demonstrated comparable peak intensities with one another (Figure 3.9). The weaker average peak intensities observed in the neat and stained blood were due to background interference from the atmosphere (neat) and cotton substrate (stain) during analysis. As the extract samples were analysed up to only one hour rather than five, very little, to no atmospheric interference was observed in the extract spectra and thus stronger peak intensities were observed, resulting in larger ratio values.

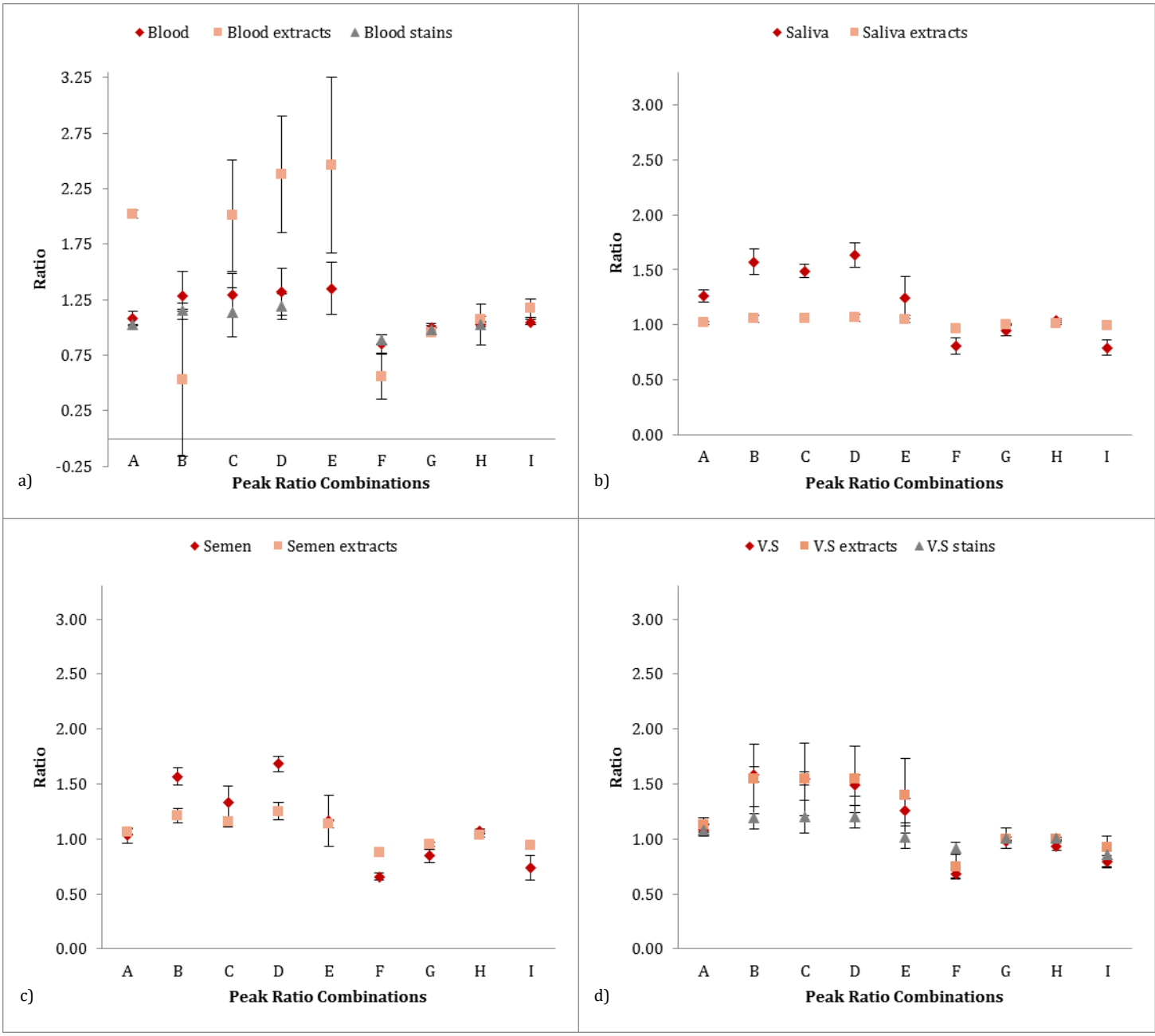

Figure 3.55: Scatter graphs demonstrating the ratios of the protein, lipid, phosphate & sugar groups across the spectra of neat, stains & extracted; a) blood, b) saliva, c) semen & d) vaginal secretions.

The peak ratios from the neat and extracted saliva spectra (Figure 3.55b) only exhibited overlap at ratio combinations G and H, and overall the variation exhibited in the ratios was small. The ratios exhibited by the neat saliva followed a similar pattern as those observed in the extracted blood, whereby the values obtained from amide I ratio combinations (A-E) were higher than those obtained from ratios against asymmetric methylene groups of amino acids (F-I). Little variation was observed in the neat saliva ratios, with the exception of combination E, where some overlap was observed between the neat and extracted saliva. In

contrast, extracted saliva demonstrated little fluctuation in the peak ratios across the nine different peak combinations. This was a result of the weak peak intensities in the extracted spectra, with an average intensity of 91% for the strongest peak (amide I) and 98% for the weakest peak (phospholipids). Due to the similarity of the peak intensities, the peak ratios exhibited a small range (0.97-1.07) which gave a linear appearance across all of the peak ratio combinations within the graph.

The ratio comparisons of the semen samples (Figure 3.55c) demonstrated no particular trend amongst the combinations examined. Overlap in peak ratios for neat and extracted semen was observed at combinations A, E and H; whereas at the remaining combinations differences in ratio values were evident as no overlap in variation was present. The differences in peak ratio observed at each combination was not consistent across the semen sample types, with a range of 0.66-1.57 evident across the combinations, and as a result, there appears to be no correlation between the type of semen sample and ratio value.

The peak ratios of the neat, stain and extracted vaginal secretion samples (Figure 3.55d) did not exhibit a large difference in ratio value in comparison to the blood ratios. Overlap between the three sample states was observed at ratio combinations A, G-I. However, the ratios exhibited for the stain samples demonstrated a relative consistency in the ratio values obtained at each combination in comparison to the neat and extracted vaginal secretion spectra. This was due to the reduced peak intensity observed across the stain spectra, which can be associated with the substrate upon which the stain was deposited. An interesting observation was that the peak ratios obtained for the neat and extracted vaginal secretion spectra were very similar, if not overlapping, at most of the peak combinations. Of all the body fluid samples, the consistency in peak ratio between neat and extracted samples was only observed within the vaginal secretion spectra. However, the variation in peak ratios across the combinations was overlapping. The largest variation was exhibited at combinations B-E, whereas the remaining combinations demonstrated very small variation.

Based on the peak ratios observed for each individual body fluid, whether in neat, stain or extract state, it is evident that the ratios were not consistent across the samples and there was great intra-sample variability exhibited. A comparison of all the saliva, semen and vaginal secretion samples, and the neat blood and bloodstain samples demonstrated that the range in which the peak ratios typically fell was 0.65-1.65. Within this range there was clear overlap not only in the peak ratio values, but also the variation of each peak ratio. This demonstrates high inter-sample variability, which is evident in Figure 3.56. However, the extracted blood samples typically gave ratio values outside of the range demonstrated by the other body fluid

samples (0.55-2.46). Therefore, it could be suggested that a peak ratio value greater than 1.65 could indicate blood, if the sample under analysis had been extracted. However, such a difference in the ratio value is likely to be due to the peak intensities exhibited by the extracted bloodstain spectra, which were much greater than those obtained from the other body fluids and sample states analysed and thus resulted in higher ratio values.

The peak intensities observed within an ATR-FTIR spectra can vary from sample to sample and depend on the sample type. A liquid sample that has dried *in situ* on the ATR-FTIR analysis stage will typically yield stronger peak intensities than a sample on a piece of cotton due to the type of contact between the sample and internal reflective element (IRE). Once the liquid component of a sample has evaporated, the remaining cellular material adheres tightly to the IRE and therefore complete surface contact is maintained between the sample and the IRE during analysis (Shimadzu Corporation, 2014a). This would result in strong peak intensities for the dominant detectable components within the sample, as demonstrated by the high peak ratios. The contact that would be achieved between a solid sample, such as the body fluid stains on cotton, and the IRE would be different, as the sample needs to be secured in place with an anvil. If there is insufficient pressure or the sample does not completely cover the IRE, interference from the atmosphere and the substrate containing the stain can affect the intensity of the resulting peaks as complete contact is not maintained between the sample and the IRE (Shimadzu Corporation, 2014b). This was clearly demonstrated in the lower peak ratio values which indicate a similarity in peak intensity.

All of the neat and extracted samples were in a liquid state upon deposition on to the ATR-FTIR analysis stage, therefore it would be expected that similar peak intensities would be exhibited by the characteristic peaks in these spectra. However, there were differences in the peak ratios exhibited by the neat and extracted body fluid samples as a result of differences in peak intensity. According to Beer-Lambert's Law (Equation 2.7), absorption peak intensity is proportional to sample concentration when the absorption coefficient and cell path length remain constant (Griffiths & De Haseth, 2007; Housecroft & Constable, 2006). Within ATR-FTIR spectroscopy, the cell path length refers to the coupling of the penetration depth of the evanescent wave of infrared radiation and the IRE (Shimadzu Corporation, 2014b). Therefore, provided the same instrument was utilised to examine different samples, the cell path length and absorption coefficient would be constant, and the peak intensity exhibited in spectra would be indicative of component concentration within a sample. As the extracted samples were removed from the cotton substrate, the body fluid was effectively diluted with water. Additionally, it was not known how much of the stain was successfully extracted from the cotton and subsequently, the concentrations of body fluid components present within the

extract aliquots would be lower than those in the neat body fluids. This correlates with the decreased peak intensities observed, although this was not reflected in the peak ratios as there appeared to be no correlation between the sample type and ratio value obtained, with the exception of blood samples.

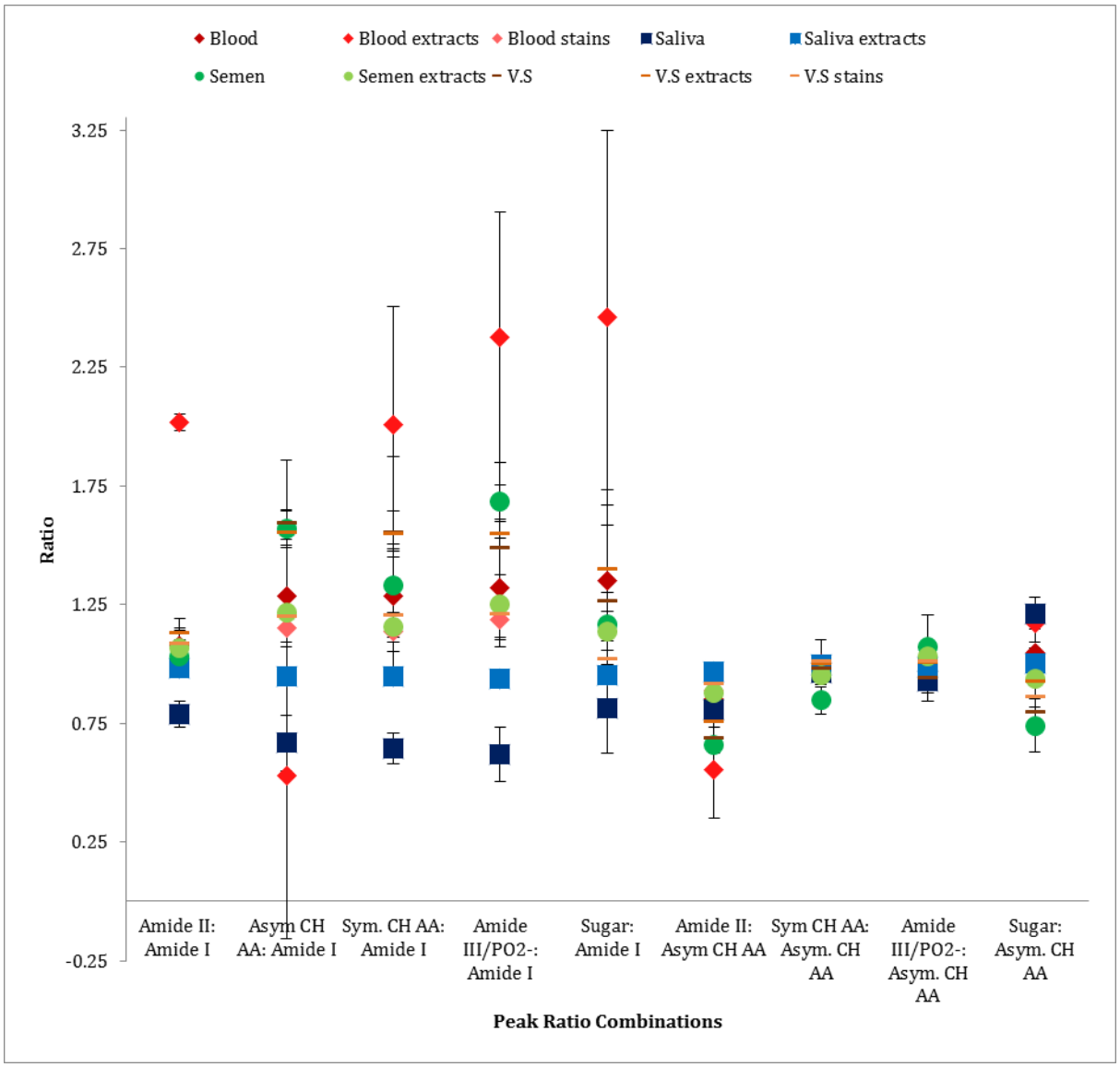

Figure 3.56: Scatter graph demonstrating the average peak ratios exhibited across the macromolecule groups within the spectra of blood, saliva, semen & vaginal secretions.

Figure 3.56 demonstrates the comparison of the peak ratio values obtained for all four body fluids in their neat, stain and extract states. Overlap between the various sample types at ratio combinations A and F-I demonstrate that it would not be possible to distinguish between blood, saliva, semen and vaginal secretions due to the tight clusters formed as a result of ratio values obtained within the same range. However, at combination A it was evident that the neat saliva and extracted blood demonstrated clear separation from the

overlapping cluster, in addition to no overlap in the variation associated with these samples. This suggests that neat saliva and extracted blood could be identified based on the value obtained from the ratio of amide II to amide I. Conversely, it is demonstrated that the ratio examination of macromolecule peaks which exhibit similar peak strengths is not appropriate to distinguish between body fluids due to the comparable peak ratio values obtained.

At combinations B-E, very little overlap was observed amongst the body fluid sample types which could potentially enable discrimination of body fluids based on peak ratios. However, the associated variation with the ratios at these combinations demonstrated overlap for all samples, with the exception of neat and extracted saliva at combinations C and D. To confidently determine the identification of a body fluid based on peak ratios, there ideally should be no overlap observed in the peak ratios corresponding to the macromolecule groups of the ATR-FTIR spectra. As a result, it can be stated that the examination of ratios from the peaks exhibited within a spectrum pertaining to a body fluid is not a suitable method to distinguish between blood, saliva, semen or vaginal secretions.

The results obtained throughout this research have demonstrated the reproducibility of ATR-FTIR spectroscopy as a method to identify blood, saliva, semen and vaginal secretions from neat, stained and extracted samples. Based on the findings presented here, it is possible to state that the comparison of peak ratios pertaining to body fluid specific macromolecules is not a suitable method to enable discrimination between spectra originating from these body fluids. However, the specific peak frequencies and peak conformations within the spectra, which arise from functional groups within common macromolecules, can be attributed to biological and chemical components specific to each body fluid. The complex mixture of constituents provides an overall spectral pattern that represents the biochemical fingerprint (Naumann et al. 2009) of blood, saliva, semen and vaginal secretions individually, which can be utilised to as an alternative method to definitively identify and distinguish between these four body fluids.

4. FOURIER TRANSFORM INFRARED SPECTROSCOPY III:

BODY FLUID AGE DETERMINATION RESULTS & DISCUSSION

Establishing the approximate age since deposition of body fluid stains is highly sought after within the forensic science community. To date there have been many techniques investigated in the age determination of body fluids (Anderson et al. 2011; Edelman et al. 2012a; Li et al. 2013; Simard et al. 2012; Strasser et al. 2007), although there has been no successful development of an age determination technique that is robust enough for routine forensic application. ATR-FTIR spectroscopy has successfully demonstrated that blood, saliva, semen and vaginal secretion samples as old as 18 months can be detected and distinguished from one another. As a result, ATR-FTIR spectroscopy as a potential method for body fluid stain age determination was explored. Blood, saliva, semen and vaginal secretion samples were deposited on to cotton and aged for varying lengths of time (Table 2.2). Once the desired age had been reached, the samples were analysed as stains and extracts.

4.1 BLOOD

4.1.1 BLOODSTAINS

Blood samples deposited on cotton were placed into storage, in accordance with the Human Tissue Act (2004), for short term, up to seven days, and long term, up to 18 months, ageing. Across 163 bloodstains, 649 measurements were taken over the ageing period. Figure 4.1 demonstrates the overlay of the typical spectra obtained from bloodstains on cotton aged from 24 hours to 7 days (a) and 14 days to 18 months (b).

Initial observations demonstrate that the spectra produced from samples of each age exhibit the same characteristic peaks observed within neat blood. It was only within the 1200-800 cm^{-1} region of the infrared spectrum that the interference of peaks pertaining to the cotton substrate were observed, as previously demonstrated in Section 3.1.1.

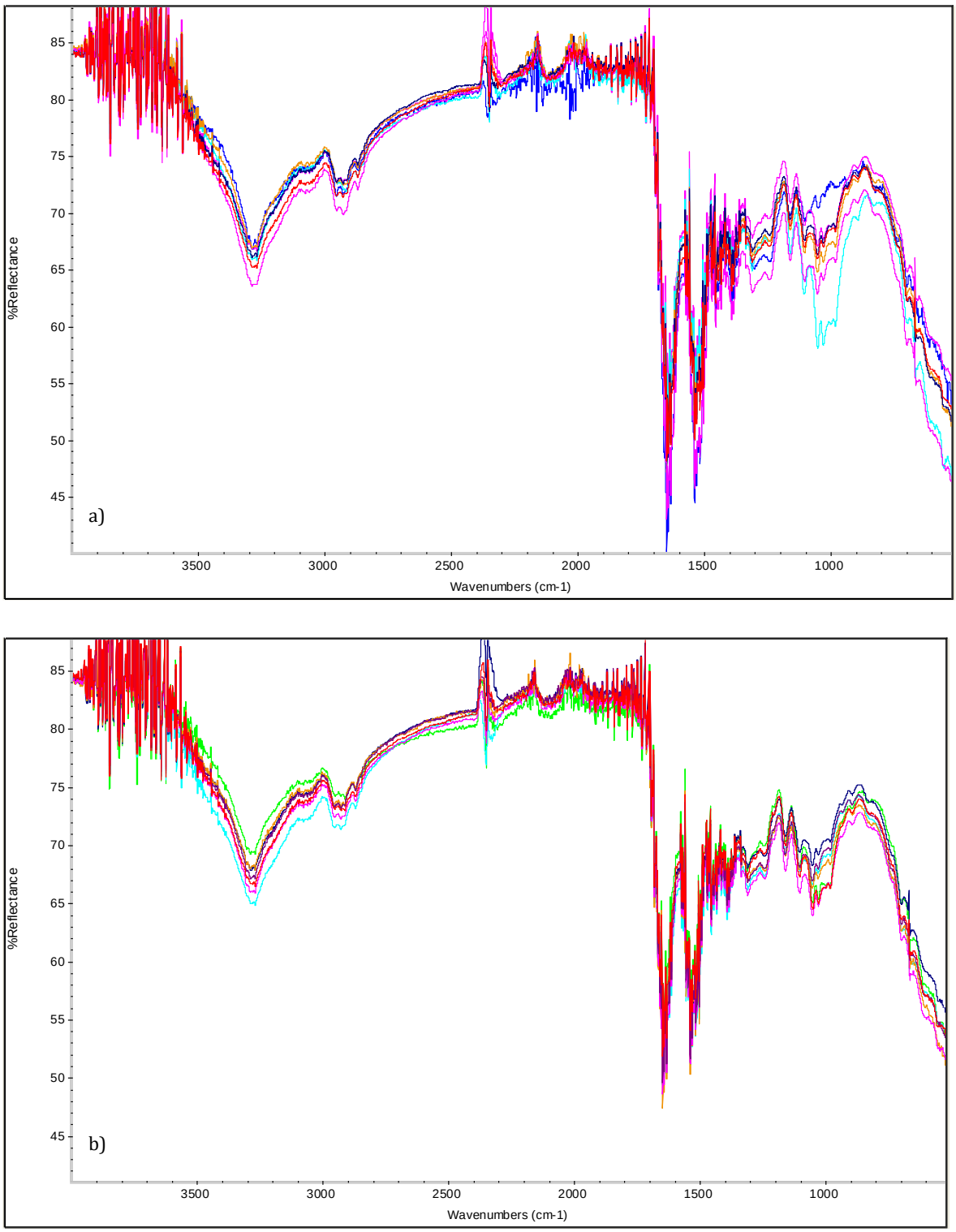

Figure 4.1: Overlay of bloodstain spectra; a) short term aged to 24 hours (blue), 48 hours (purple), 3 days (red), 4 days (turquoise), 5 days (orange), 6 days (dark blue) & 7 days (pink); b) long term aged to 14 days (green), 1 month (turquoise), 2 months (dark blue), 3 months (red), 6 months (orange), 12 months (pink) & 18 months (purple).

Upon inspection of the overlay spectra of the short term aged bloodstains (Figure 4.1a), it appeared as though there were no apparent distinct changes that could be due to differences in sample age. However, examination of the fingerprint region, excluding the 1200-800 cm^{-1} region, demonstrated variation in peak intensity amongst the seven different ages. In particular, the amide I (~1650 cm^{-1}) and amide II (~1541 cm^{-1}) peaks demonstrate a decrease in a peak intensity after 24 hours (Figure 4.1a, blue). The amide III (~1306 cm^{-1}) characteristic "W" conformation exhibits different peak intensities for each sample age as there is little overlap of the spectra in that region. Additionally, the methyl bending vibrations of amino acid side chains/fibrinogen peaks (~1456 & 1395 cm^{-1}), situated between the amide II and amide III peaks, appear to vary in peak intensity over time. However, due to the lack of peak definition, as a result of substrate interference, the extent of the variation was difficult to determine from the spectra alone. Similar observations were evident in the spectra of long term aged blood samples from 14 days to 18 months (Figure 4.1b), although the amount of variation in peak intensity observed across the aged bloodstain spectra did not appear to be as great as that observed within the short term aged spectra.

In order to identify any potential variation that could be attributed to bloodstain age, the specific intensities of all the blood characteristic peaks, excluding glucose due to cotton overlap, were examined. Additionally, the ratios of the peaks within the fingerprint region, excluding glucose, were also examined; namely, the amide I, amide II, the methyl bending vibrations of amino acid side chains/fibrinogen and amide III peaks. The peak combinations utilised were the same of those studied in the comparison of body fluid spectra detailed in Section 3.5 (Table 3.11).

4.1.1.1 PEAK INTENSITIES

The bloodstains utilised for short term ageing originated from one donor. A total of 35 bloodstains, five per sample age, were deposited on to cotton and aged for 24 hour to 7 days. The bloodstains utilised for long term ageing originated from three donors. A total of 128 bloodstains, four per sample age, were deposited on to cotton and aged for 24 hour to 18 months. As there was no evidence of spectral variation in bloodstains obtained from different donors (Section 3.1.1), the peak intensity data was pooled for analysis, rather than grouped according to donor. Direct ATR-FTIR spectroscopic analysis of the bloodstains was utilised in the first instance for all of the aged samples. As blood characteristic spectra could be obtained from the direct analysis of the bloodstains, the peak intensities and ratios were examined with no spectral manipulation. Figure 4.2 demonstrates the average peak intensities observed in the spectra of bloodstains aged from 24 hours to 7 days.

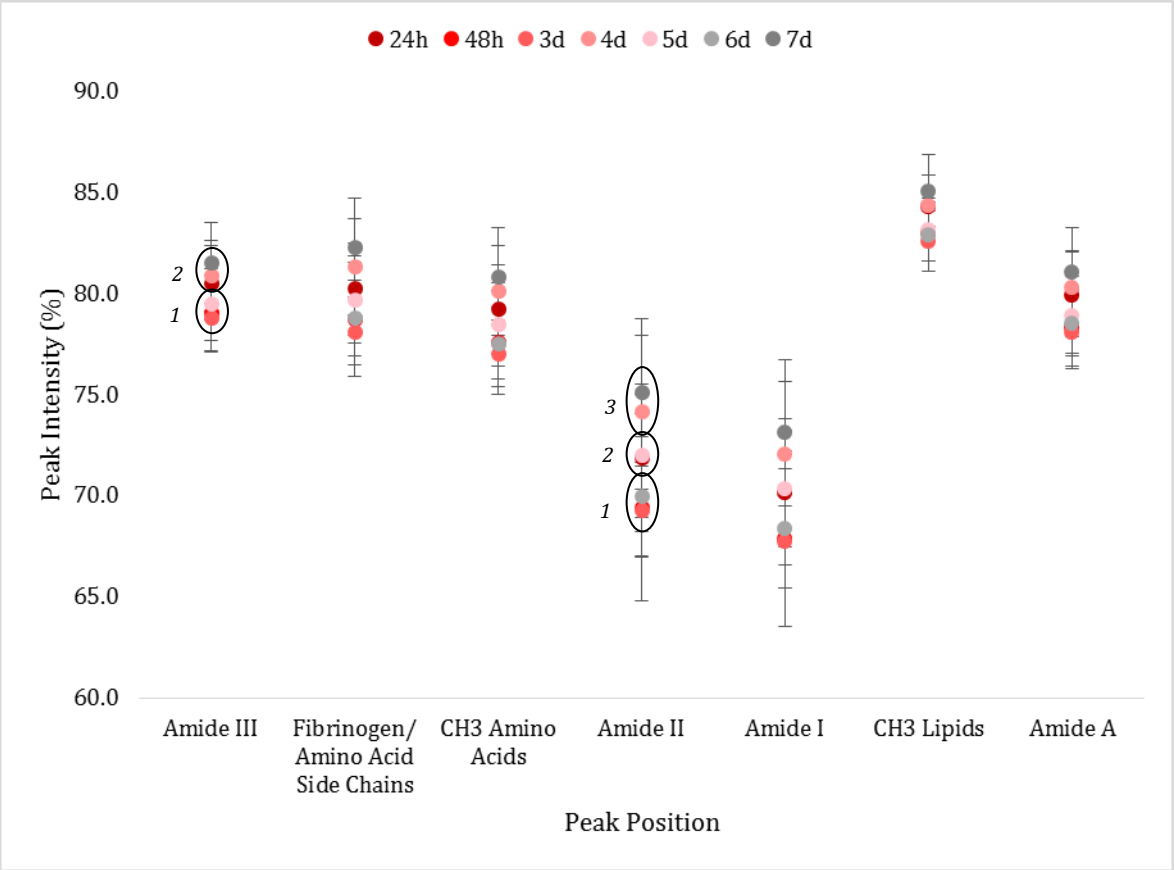

Figure 4.2: Scatter graph demonstrating the average peak intensities exhibited by the characteristic peaks of blood in the spectra of bloodstains aged from 24 hours to 7 days, with clusters 1-3 circled.

Initial observations of the short term aged bloodstain average peak intensities (Figure 4.2) demonstrate that there was some overlap in peak intensity between some of the sample ages, but not all. In particular, there appeared to be two groups, or clusters, of sample ages that exhibited the same or similar peak intensities at the high frequency peaks; amide A, methyl stretches in lipids, and at the low frequency peak amide III (highlighted as cluster [*1*] & [*2*] at amide III on Figure 4.2). At the mid-frequency range of peaks; namely, amide I and II, asymmetric methyl bending of amino acids and symmetric bending of amino acids/fibrinogen, three clusters of sample ages with the same or similar peak intensities were evident. Each of the clusters comprised of the same overlapping sample ages across all the peaks (highlighted as cluster [*1*] [*2*] & [*3*] at amide II on Figure 4.2). The bloodstains aged to 48 hours, 3 days and 6 days form cluster one (in both cluster sets) representing the strongest peak intensities across the age range, with 3 days exhibiting the strongest intensity at all peaks.

The 6 day old bloodstains demonstrated the weaker peak intensities of this cluster, whereas 48 hours overlapped between both 3 and 6 day old intensities. At the amide A, methyl

stretches in lipids, and amide III peaks, this cluster of sample ages also included the 5 day aged bloodstains. In comparison with the mid-range frequency peaks, the average peak intensities observed from 5 day aged bloodstains did not overlap with the strong peak intensity cluster, cluster one, at all and were clearly separate from the peak intensities of 48 hour, 3 day and 6 day aged bloodstains. However, at these peaks, overlap was observed between 5 day and 24 hour aged bloodstain intensities (cluster [*2*]). The degree of overlap between these two sample ages varied across these peaks, with clear overlap exhibited at the amide I and II peaks, but very little overlap observed at the asymmetric methyl bending of amino acids and symmetric bending of amino acids/fibrinogen peaks. In contrast, at the amide A, methyl stretches in lipids, and amide III peaks the 24 hour aged bloodstains intensities demonstrated overlap with the 4 day aged intensities, which in turn, the 4 day aged bloodstains formed a cluster (cluster [*3*] at the mid-frequency peaks) with the 7 day aged intensities across all seven peaks. This cluster represented the weakest peak intensities observed from all the short term aged bloodstains, with 24 hours exhibiting the strongest intensities of the cluster and 7 days exhibiting the weakest. The 7 day aged bloodstains consistently yielded the weakest peak intensities across the aged samples, and overall there was very little, to no overlap observed between the 7 day aged and 4 day aged bloodstain intensities.

Figure 4.3 demonstrates the average peak intensities observed in the spectra of bloodstains aged from 24 hours to 18 months. Initial observations of the long term aged bloodstain average peak intensities demonstrate that there was some overlap of the peak intensities of some of the bloodstain ages, but not all. Across all seven peaks, the distribution of the average peak intensities per age could be categorised into four consistent clusters. Cluster one comprised of two bloodstain ages, 48 hours and 3 months, which exhibited the strongest average peak intensities. The 48 hour aged bloodstains demonstrated the strongest peak intensity at all peaks examined and small overlap was observed between the 48 hour and 3 month peak intensities, although this was only minor and both ages could be clearly differentiated from one another. Cluster two consisted of 24 hour, 21 day and 1 month aged bloodstain average intensities, which exhibited overlap of all three ages. In particular, there was strong overlap between 24 hours and 1 month at peaks amide III, symmetric methyl bends of amino acids/fibrinogen, asymmetric methyl bends of amino acids, methyl stretches of lipids and amide A. At these same peaks, a slight overlap was observed between the 21 days and 1 months intensities, although both ages could still be distinguished from one another. At the amide II and I peaks, the strong overlap was exhibited in the 21 days and 1 month ages, with only slight overlap with 24 hours.

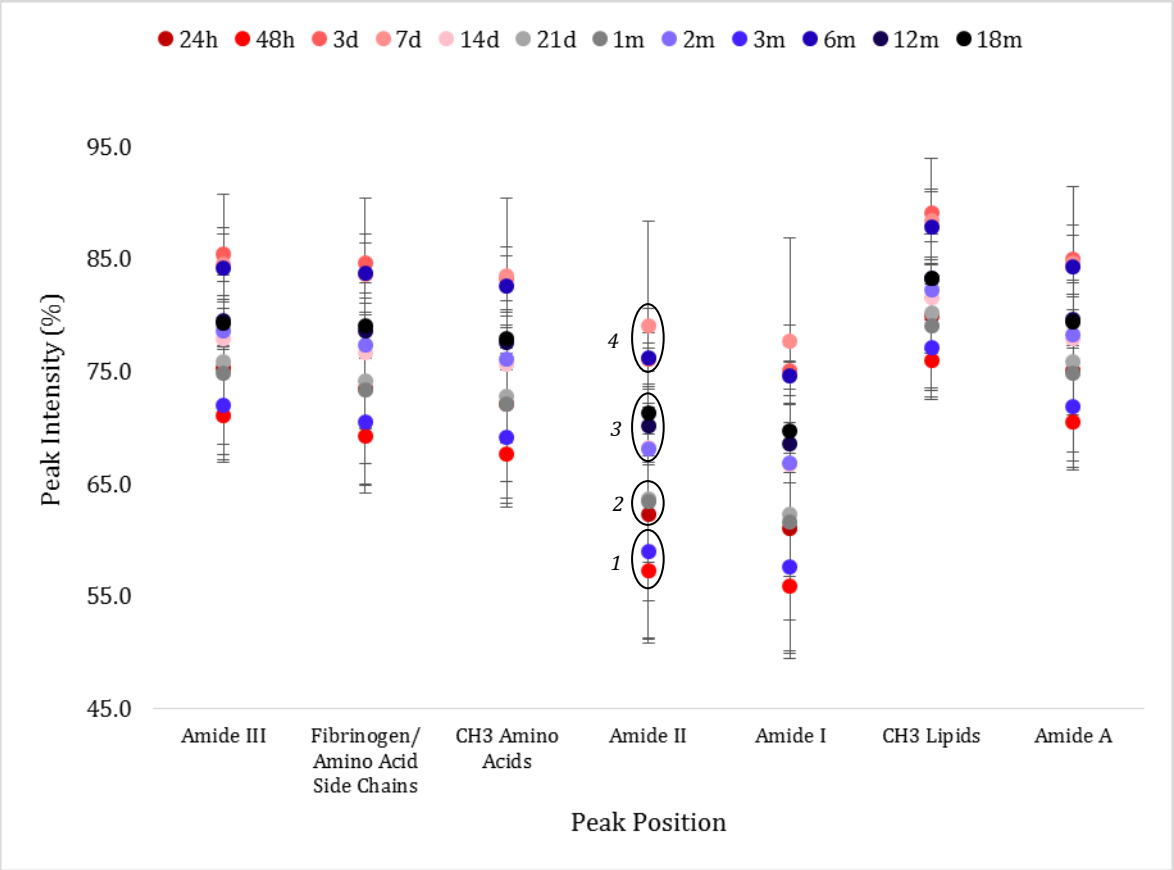

Figure 4.3: Scatter graph demonstrating the average peak intensities exhibited in the spectra of bloodstains aged from 24 hours to 18 months, with clusters 1-4 circled.

Cluster three was the largest cluster within Figure 4.3 which comprised of the peak intensities yielded by 14 day, 2, 12 and 18 month aged bloodstains. The 14 day and 2 month aged intensities were stronger than the 12 and 18 month aged intensities. Considerable overlap was exhibited between the 14 day and 2 month and the 12 and 18 month intensities, independently. However, at the amide I and II peaks, the overlap of 12 and 18 months was reduced and the two bloodstain ages could be differentiated from one another. Additionally at the amide I and II peaks, no overlap was exhibited between the 2 and 12 month intensities, whereas at all other peaks slight overlap between these bloodstain ages was observed. The final cluster, cluster four, demonstrated the bloodstain ages that exhibited the weakest peak intensities across all the ages examined. This cluster consisted of bloodstain ages 3 days, 7 days, and 6 months. Overlap between the three ages was observed across all the peaks examined, with the exception of amide I and II, whereby the 7 day intensities were completely separated from the 3 day and 6 month intensities. Of the three ages, 6 month aged bloodstains exhibited the strongest intensities within the cluster. The weakest intensity was exhibited by 3 day aged bloodstains at the amide III, symmetric methyl bends of amino acids/fibrinogen, methyl stretches of lipids and amide A peaks, whereas at peaks asymmetric

methyl bends of amino acids, amide I and II, the weakest intensity was exhibited by the 7 day aged bloodstains.

It is evident from Figure 4.2 and Figure 4.3 that the differing sample ages could be distinguished from one another based on the average peak intensities of bloodstains aged for short periods of time, 24 hours to 7 days, and long periods of time, 24 hours to 18 months. These results suggest that ATR-FTIR spectroscopy has the potential to be utilised as a technique to determine bloodstain age. However, the peak intensity variation exhibited across each bloodstain age, both in short (~±2%) and long term (~±5%) ageing, demonstrates that all the age's exhibited overlap, as demonstrated by the error bars in Figure 4.2 and Figure 4.3.

4.1.1.2 PEAK RATIOS

In addition to the examination of peak intensity as a variable to determine bloodstain age, the ratios of the characteristic peaks associated with macromolecules (Table 3.11, Section 3.5) were also assessed. Figure 4.4a demonstrates the average peak ratios observed in the spectra of bloodstains aged from 24 hours to 7 days. Figure 4.4b demonstrates the average peak ratios observed in the spectra of bloodstains aged from 24 hours to 18 months. Initial observations of the short term aged bloodstain peak ratios (Figure 4.4a) demonstrate that there was clear overlap of all the bloodstain ages at ratio combinations; amide II:amide I (A), symmetric bending of amino acids/fibrinogen:asymmetric methyl bending of amino acids (G), and amide III:asymmetric methyl bending of amino acids (H). At each of these ratios, dense clusters containing all seven bloodstain ages were observed. As a result, differentiation of age overlap was not possible. A similar cluster was observed at ratio F, amide III:asymmetric methyl bending of amino acids, although the distribution of the seven bloodstain ages was not as concentrated and therefore overlap was not exhibited by all of the sample ages. The bloodstain ages that exhibited the lowest and highest ratios at ratio F were 3 days and 7 days, respectively.

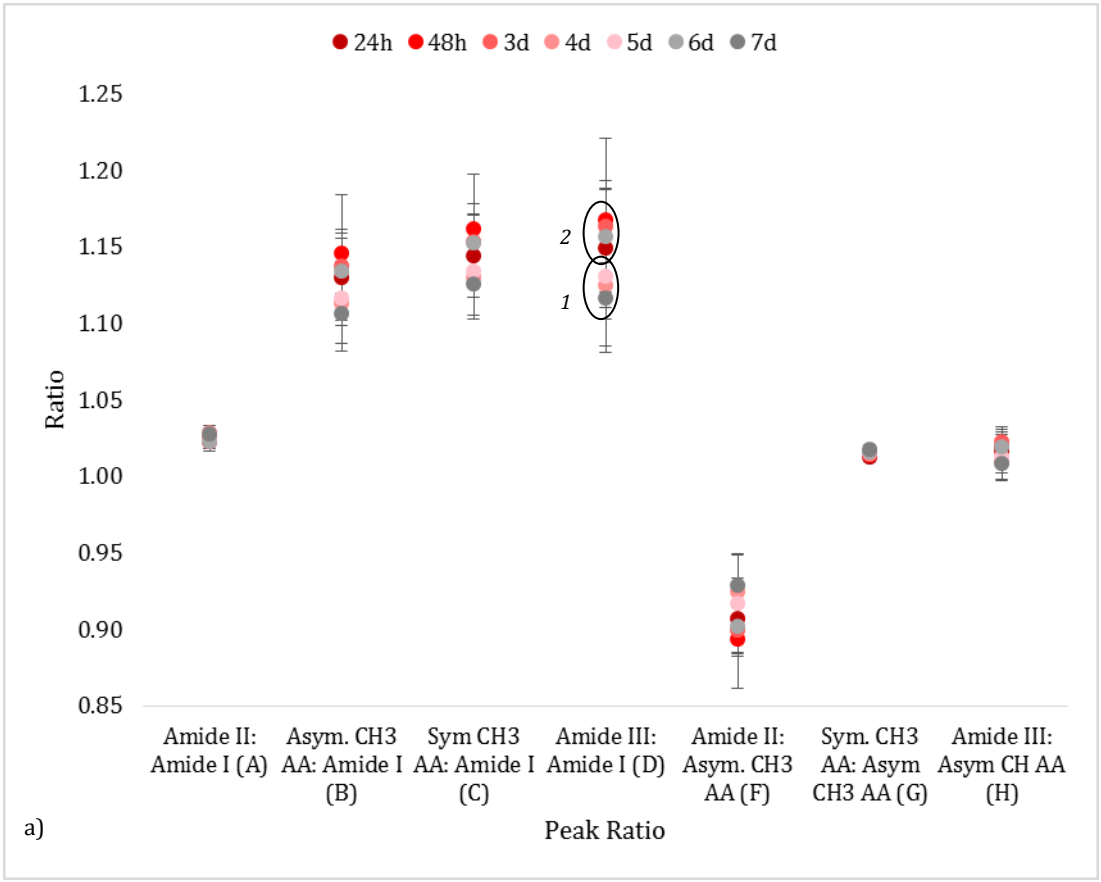

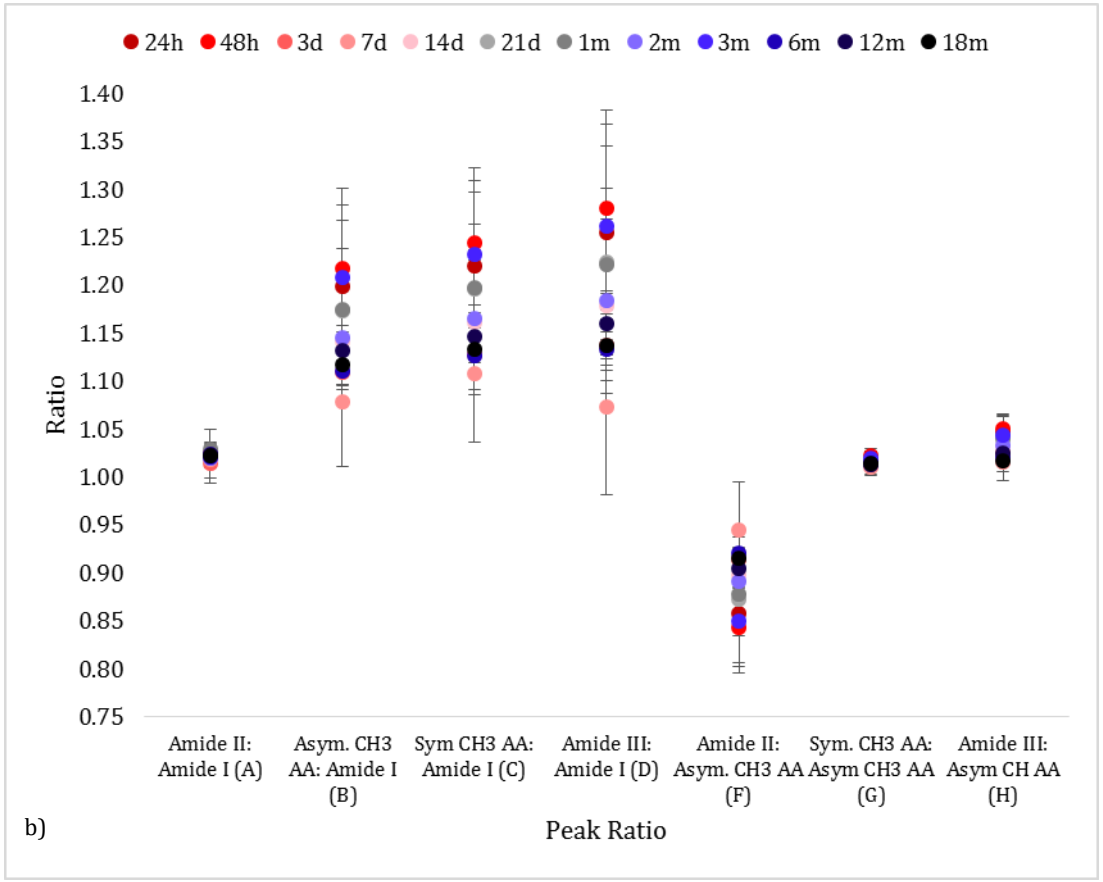

Figure 4.4: Scatter graph demonstrating the average peak ratios exhibited by the characteristic peaks of blood in the spectra of bloodstains aged from; a) 24 hours to 7 days, with clusters 1 & 2 circled, b) 24 hours to 18 months.

The distribution of average peak ratios at peak combinations B-D (asymmetric methyl bending of amino acids:amide I, symmetric methyl bending of amino acids/fibrinogen:amide I and amide III:amide I, respectively) was more wide spread, with distinct separation of some of the bloodstain ages. Specifically, across these three ratio combinations two clusters were evident which could be categorised as 'low' and 'high' ratios. Within the 'low' cluster bloodstain ages 7, 4 and 5 days were consistently observed. The lowest ratio in this cluster, and subsequently across the dataset, was demonstrated by 7 day aged bloodstains, whereas the highest ratio in the cluster was exhibited by bloodstains aged to 5 days.

Situated between these ages was 4 day aged bloodstains, which demonstrated a clear overlap with both 7 and 5 days in the average peak ratio at combinations B-D. The 'high' ratio cluster, cluster two, comprised of average peak ratios for bloodstains aged to 24 hours, 6 and 3 days and 48 hours (in ascending order). The lowest ratio within this cluster was exhibited by the 24 hour aged bloodstains, and the highest exhibited by the 48 hour aged bloodstains. The average peak ratios corresponding to 6 and 3 day aged bloodstains were observed in between the 24 and 48 hour ratios. Two clusters of aged bloodstain ratios was also observed at ratio combination amide II:asymmetric methyl bending of amino acids (F), whereby the clusters consisted of the same groups of bloodstain ages as those at ratios B-D but the distribution order was reversed. The aged bloodstains with the lower ratio values were those observed in cluster two at B-D, and those with the higher value at combination F were the aged bloodstains grouped in cluster one.

Initial observations of the long term aged bloodstain peak ratios (Figure 4.4b) mirror those observed in the peak ratios exhibited in Figure 4.4a, whereby there was clear overlap of all the bloodstain ages at ratio combinations A, G and H. At each of these ratios, dense clusters containing all twelve bloodstain ages were observed. As a result, differentiation of age overlap was not possible. The distribution of average peak ratios at combinations B-D was more wide spread, with distinct separation of most of the bloodstain ages. Unlike the average distributions observed within Figure 4.4a, there were no clusters of overlapping average ratios across the twelve bloodstain ages. Overlap of ratio values for aged bloodstains were evident between, in ascending order, 6 months, 3 days and 18 months, 14 days and 2 months, 21 days and 1 month and 24 hours and 3 months. The overlap observed varied amongst the small groupings, with mostly only slight overlap observed, although 21 days and 1 month were the least distinguishable from one another. Despite overlap, most of the aged ratios could be distinguished from one another. At ratio combination F, the distribution order of the ratio values corresponding to each bloodstain age was reversed as seen in the short term aged bloodstains (Figure 4.4a).

Amongst the aged bloodstains, the 7 day ratios consistently demonstrated the lowest ratio and the 48 hour ratios demonstrated the highest, except at combination F where this order was reversed. This correlates with the strongest intensity/lowest ratio and weakest peak/highest ratio distribution observed in Figure 4.4a.

The examination of average peak ratio values of aged bloodstains demonstrated that bloodstains aged to 7 days could be differentiated from the remaining sample ages, both older and younger, due to its consistently lower ratio values at combinations B-D, and its higher value at combination F. These results mirror those found in the examination of average peak intensity (Section 4.1.1.1), which suggest that ATR-FTIR spectroscopy has the potential to be utilised as a technique to determine between bloodstain ages. However, the variation exhibited by each peak ratio across each bloodstain age demonstrates that all the ages (~ ±0.25% short term aged, ~ ±0.03% long term aged) exhibited overlap, as demonstrated by the error bars in Figure 4.4.

Comparison of the average peak intensities and average peak ratios of the short term aged bloodstains demonstrated that the sample age distribution from strongest intensity/highest ratio to weakest intensity/lowest ratio was 48 hours, 3 days, 6 days, 24 hours, 5 days, 4 days and 7 days. Comparable distribution patterns were also observed within the average peak intensities and average peak ratios of the long term aged bloodstains (Figure 4.3 & Figure 4.4b). Specifically, the distribution pattern observed in both scatter graphs from strongest intensity/highest ratio to weakest intensity/lowest ratio was 48 hours, 3 months, 24 hours, 1 month, 21 days, 2 months, 14 days, 12 months, 18 months, 6 months, 3 days and 7 days.

The examination of the average peak intensities and their respective ratios from spectra obtained from bloodstains aged from 24 hours to 18 months have demonstrated that these values vary across each of the ages analysed. However, there appears to be no in decrease in peak intensity, or increase in peak ratio that correlates with the increase in bloodstain age. Additionally, the variation in peak intensity and ratio exhibited within each age means that the different bloodstain ages could not be distinguished from one another. Therefore, it can be stated that ATR-FTIR spectroscopy is not an appropriate technique to determine the age of bloodstains when analysed directly from cotton.

4.1.2 EXTRACTED BLOOD

The age determination of extracted bloodstains was carried out with the same samples prepared for short term ageing analysis (Section 4.1.1). As spectra consisting of the key characteristic peaks of neat blood were observed when bloodstains on cotton were analysed directly, only samples aged from 24 hours to 7 days, 12 and 18 months were extracted and subsequently analysed. Across 55 bloodstains, 330 measurements were taken, of which 220 spectra represented a wet spectrum (Figure 3.2a) and 110 represented a dry spectrum (Figure 3.3a). Figure 4.5 demonstrates the overlay of the typical spectra obtained from extracted bloodstains from 24 hours to 7 days (a) and 24 hours to 7days, 12 and 18 months (b).

Initial observations demonstrate that the ATR-FTIR spectra of extracted aged bloodstains were comparable to the spectra obtained from neat blood. The same characteristic peaks were observed, with little to no interference from the cotton or any contaminants. Upon inspection of the overlay spectra of the short term aged bloodstain extracts, distinct overlap, with little variation was evident in the amide A (~3285 cm^{-1}), methyl stretches of lipids (~2597 cm^{-1}), amide I (~1645 cm^{-1}) and amide II peaks (~1537 cm^{-1}). However, examination of the fingerprint region demonstrated that the peak intensities differed amongst the different ages. Particularly, the methyl bending vibrations of amino acid side chains/fibrinogen (~1453 & 1395 cm^{-1}), amide III (~1304 cm^{-1}) and carbohydrate (~1168 & 1104 cm^{-1}) peaks appear to vary in peak intensity over time. Comparison of the extracted 12 and 18 month aged bloodstain spectra demonstrate further differences in the peak intensities observed (Figure 4.5b). The 12 month extracted spectra was comparable to those obtained by the younger bloodstain extracts, although the peak intensities across the whole of the spectrum appear to be dramatically weaker. In contrast, the spectra obtained from the extracted 18 month old bloodstain exhibits different peak conformations across the spectrum, as discussed in Section 3.1.2.

In order to identify any potential variation that could be attributed to bloodstain age, the specific intensities of all the blood characteristic peaks were examined. Additionally, the peak ratios of the peaks within the fingerprint region were examined. Namely, the amide I, amide II, the methyl bending vibrations of amino acid side chains/fibrinogen, amide III and glucose peaks. The peak combinations utilised were the same as those studied in the comparison of body fluid spectra detailed in Section 3.5 (Table 3.11).

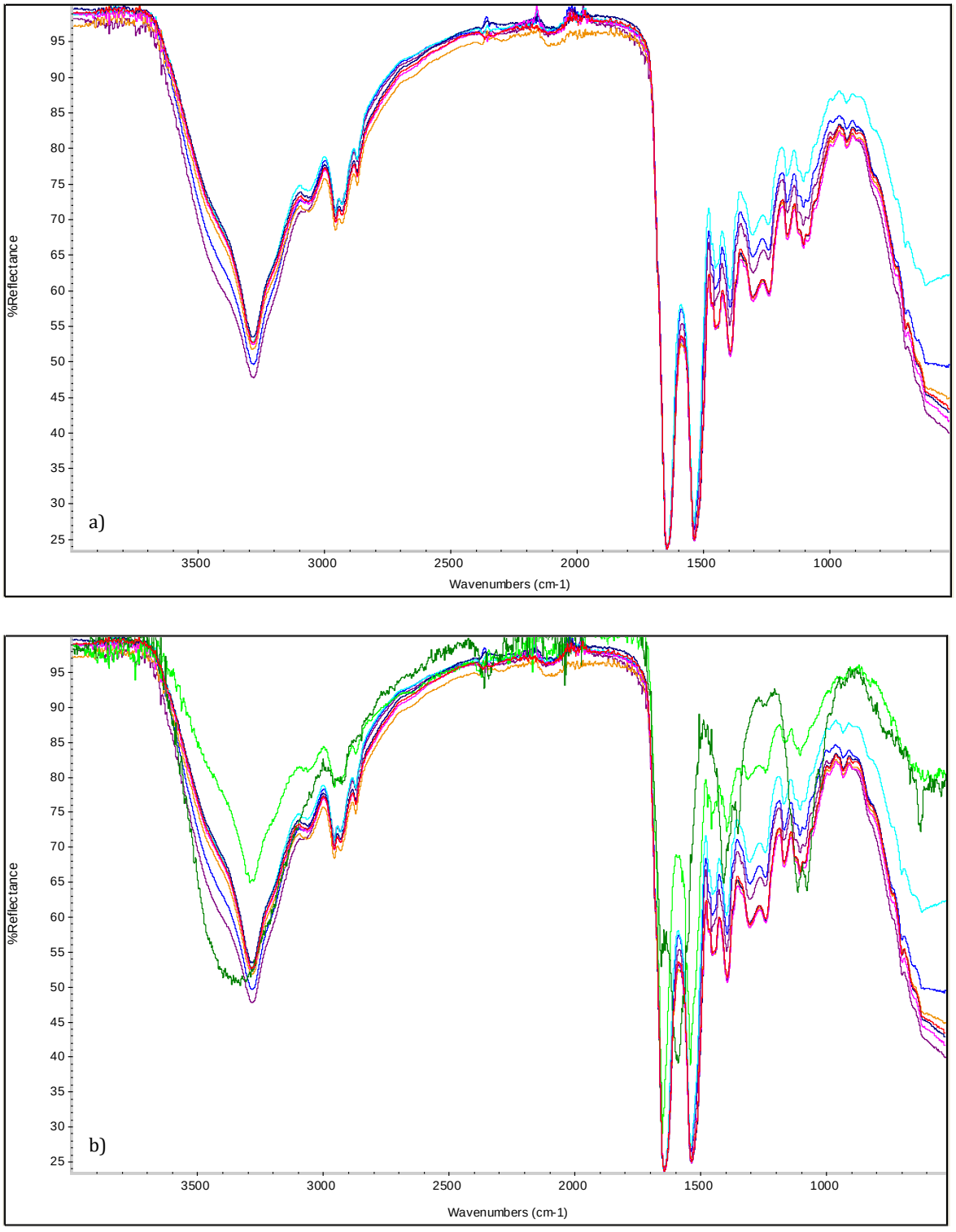

Figure 4.5: Overlay of extracted bloodstain spectra; a) short term aged to 24 hours (blue), 48 hours (purple), 3 days (red), 4 days (turquoise), 5 days (orange), 6 days (dark blue) & 7 days (pink); b) short term aged (24 hours to 7 days) including 12 month (green) & 18 month (dark green) aged bloodstain extracts.

4.1.2.1 PEAK INTENSITIES

The bloodstain extracts were in a liquid form, thus ATR-FTIR spectroscopic analysis was conducted via the "wet-to-dry" approach utilised in the analysis of neat body fluids (Section 2.2.2.1). Figure 4.6 demonstrates the average peak intensities observed in the spectra of extracted bloodstains that were aged from 24 hours to 7 days and 12 months. The data from the 18 months bloodstain extracts was not included due to the dissimilarities in spectral peaks compared to the younger extracted bloodstains.

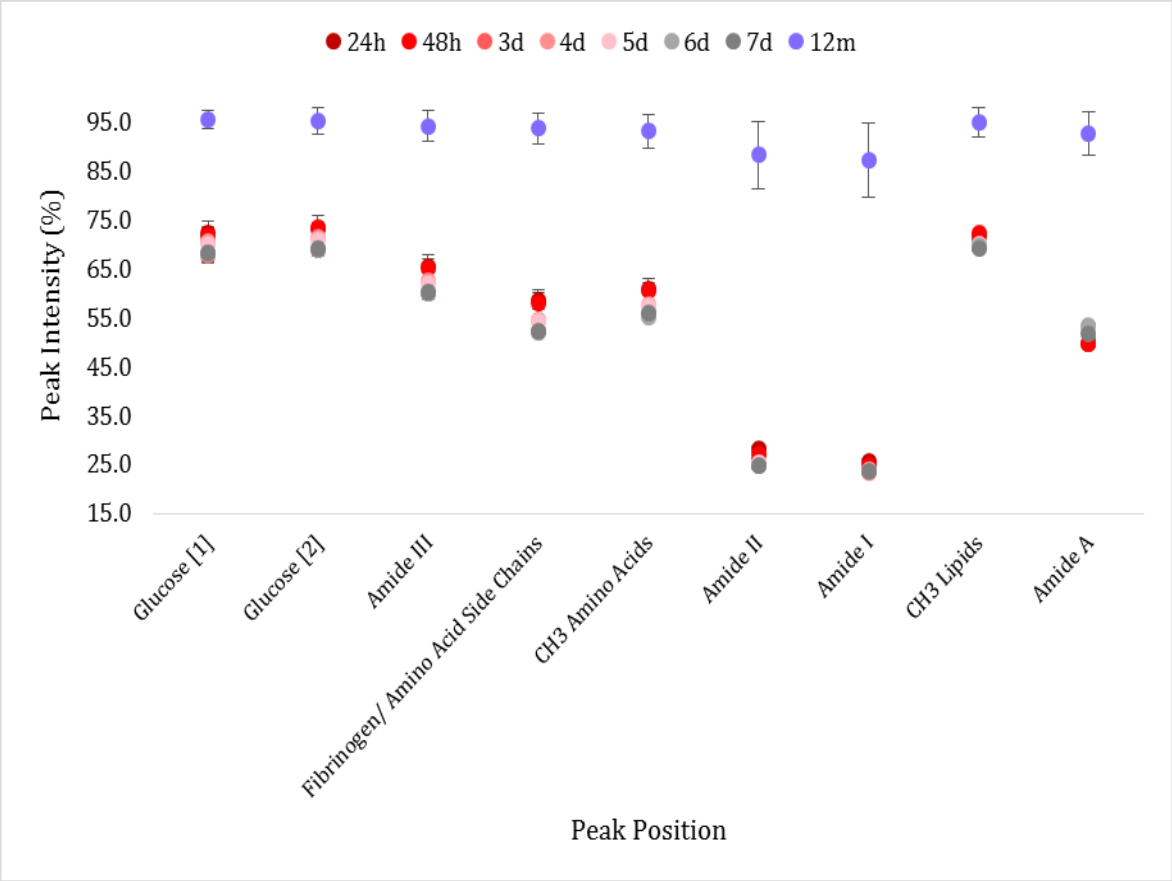

Figure 4.6: Scatter graph demonstrating the average peak intensities exhibited by the characteristic peaks of blood in the spectra of extracted bloodstains aged from 24 hours to 7 days & 12 months.

Initial observations of the average peak intensities (Figure 4.6) demonstrate that the intensities exhibited by the extracted 12 month aged bloodstains were clearly distinguishable from the average peak intensities of the extracted 24 hours to 7 day aged bloodstains. The extracted 12 month aged bloodstains exhibited the weakest peak intensities amongst the extracted aged bloodstains, with a maximum peak intensity of approximately 85%. No overlap in peak intensity variation across the extracted 12 month aged bloodstains was observed with the variation exhibited by the younger extracted samples. The striking difference in average peak intensity between the extracted 12 month aged bloodstains and

the extracted 24 hour to 7 day aged bloodstains is likely to be as a result of the difficulty in extracting the bloodstains from the cotton substrate. As stated in Section 3.1.2, the 12 and 18 month aged bloodstains did not appear to physically wash away from the cotton, unlike the extracted bloodstains aged for 24 hours to 7 days. As a result, the amount of cellular material recovered from the cotton would have been reduced, resulting in weaker peak intensities in ATR-FTIR spectra compared to the aged bloodstains that appeared to wash from the cotton into the extraction solute.

Inspection of the average peak intensities of the extracted 24 hour to 7 day aged bloodstains demonstrates that tight clusters were formed due to the overlap between the short term ages. There was little variation exhibited in the peak intensities across the extracted 24 hour to 7 day aged bloodstains, which is evident by the apparent lack of error bars in Figure 4.6. The extracted 7 day aged bloodstains yielded the strongest peak intensities at all the peaks, except at amide A, where the strongest peak intensity was exhibited by extracted 48 hour aged bloodstains. The weakest average peak intensity of the 24 hour to 7 day cluster was observed in the extracted 48 hour aged bloodstains, although at amide A the weakest intensity was exhibited by extracted 6 day aged bloodstains.

It is evident from Figure 4.6 that due to the tight cluster and overlap in variation, it was not possible to differentiate between each short term age examined in the extracted bloodstains. However, the extracted 12 month aged bloodstains could clearly be differentiated from the extracted short term aged bloodstains. These results suggest that ATR-FTIR spectroscopy has the potential to be utilised as a technique to distinguish between bloodstains aged 12 months and those aged 7 days or younger when the stains are extracted. The peak intensity variation exhibited across the extracted bloodstains aged between 24 hours and 7 days does not enable differentiation of bloodstain age. However, no bloodstains were extracted that were aged between 7 days and 12 months, therefore in order to determine whether extracted bloodstains aged older than 7 days, but younger than 12 months, could be differentiated from one another, these sample ages would need to be examined.

4.1.2.2 PEAK RATIOS

Figure 4.7 demonstrates the average peak ratios observed in the spectra of extracted bloodstains aged from 24 hours to 7 days and 12 months. Initial observations of the average peak ratios exhibited by extracted bloodstains demonstrate that the 12 month aged bloodstains could be clearly distinguished from the 24 hour to 7 day aged bloodstains, with the exception of ratio combinations A, G and H. At these combinations a tight cluster of all the extracted bloodstain ages was evident and differentiation between the ages was not possible.

The extracted 12 month aged bloodstains typically exhibited a consistent peak ratio, approximately 1.0, across the ratio combinations examined. In contrast, the extracted 24 hour to 7 day aged bloodstains exhibited much higher average peak ratios (approximately 2.2-2.9) at combinations B-E and a much lower ratio value at combination F (approximately 0.45). There was clear overlap of all the short term aged extracted bloodstains ages at all the ratio combinations examined, whereby dense clusters containing the seven short term ages were observed. As a result, differentiation of the extracted 24 hour to 7 day aged bloodstains was not possible. The extracted bloodstain age that typically exhibited the lowest average ratios was 7 days and 4 days was the highest average ratio amongst the 24 hour to 7 day cluster.

The distribution and overlap observed in the average peak ratios exhibited by the extracted aged bloodstains was similar to those exhibited in the average peak intensities, in that the 12 month aged extracts could be clearly differentiated from the 24 hour to 7 day aged extracts, except at ratio combinations A, G and H (Figure 4.7). Very little variation as observed in the peak ratios per extracted bloodstain age, which enabled the 12 month aged ratios to still be distinguished from the short term aged ratios even when the separation was minimal.

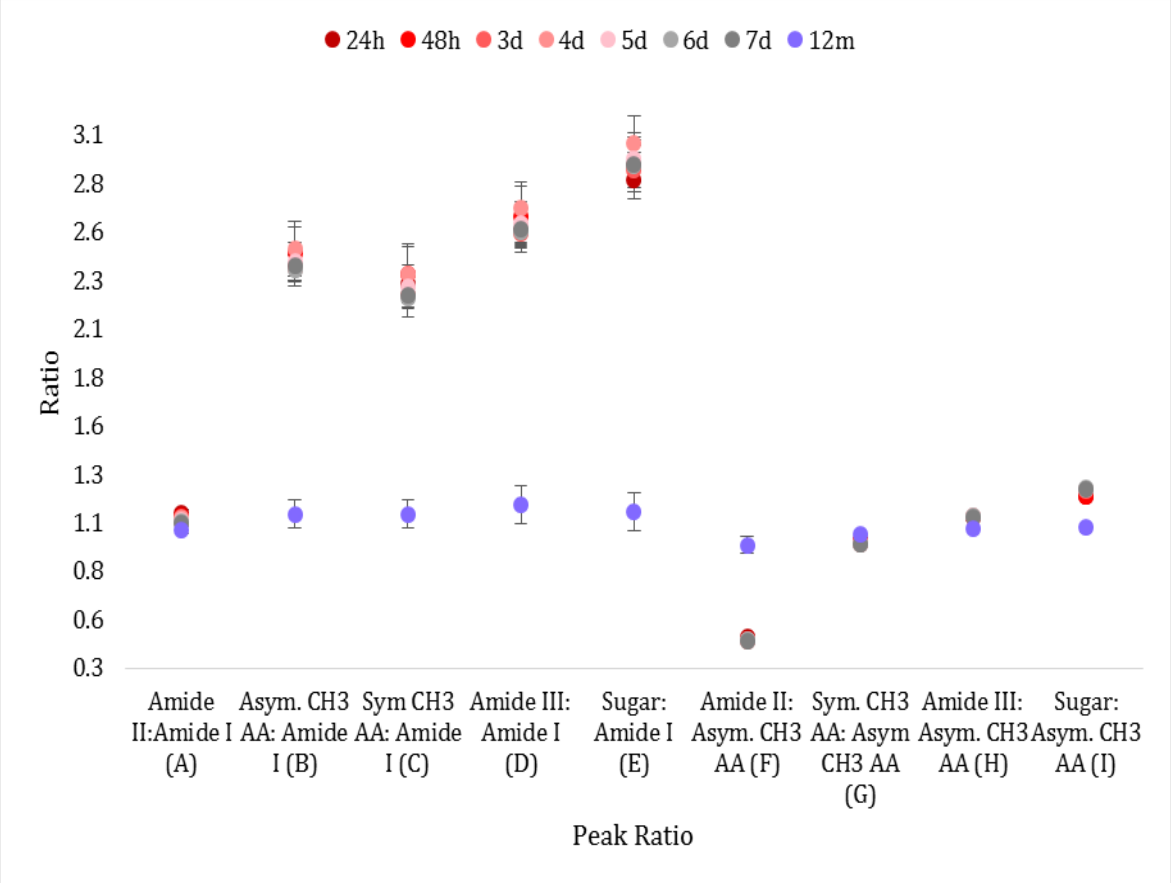

Figure 4.7: Scatter graph demonstrating the average peak ratios exhibited by the characteristic peaks of blood in the spectra of extracted bloodstains aged from 24 hours to 7 days & 12 months.

These results further supports the similarity of the average peak ratios with the average peak intensities obtained from the extracted 24 hour to 7 days and 12 month aged bloodstains. The results provide additional support to the suggestion that ATR-FTIR spectroscopy has the potential to be utilised as a technique to distinguish between bloodstains aged 12 months and those aged 7 days or younger when the stains are extracted. The peak ratio variation exhibited across the extracted bloodstains aged between 24 hours and 7 days did not enable differentiation of bloodstain age. However, as stated in Section 4.1.2.1, no bloodstains aged from 7 days up to 12 months were extracted, therefore it is not known whether there is any overlap in the peak intensities or ratios of extracted aged bloodstains between these ages.

Comparison of the average peak intensities and average peak ratios of the 24 hour to 7 day and 12 month aged bloodstains demonstrated similarities in the distribution patterns exhibited by the eight bloodstain ages. Due to the dense clustering of the aged extracted bloodstain intensities and ratios, it was not possible to differentiate confidently between the 24 hour to 7 day aged samples, although the 12 month aged extracts could be clearly distinguished. As a result, the sample age distribution could not be determined for all the ages examined. The examination of the average peak intensities and their respective ratios from spectra obtained from extracted bloodstains aged from 24 hours to 7 days and 12 months have demonstrated that these values vary across each of the ages analysed. However, there appears to be no in decrease in peak intensity, or increase in peak ratio that correlates with the increase in bloodstain age. Additionally, the variation in peak intensity and ratio exhibited within each age illustrates that the different bloodstain ages could not distinguished from one another. Therefore, it can be stated that ATR-FTIR spectroscopy is not an appropriate technique to determine the age of bloodstains when analysed as extracts from cotton.

4.2 SALIVA

4.2.1 EXTRACTED SALIVA

Saliva samples of 100 µl aliquots were deposited on to cotton and placed into storage, in accordance with the Human Tissue Act (2004), for short term, up to 7 days, and long term ageing, up to 18 months. Across 92 saliva stains, 460 measurements were taken across the ageing period. However, as saliva stains on cotton were undetectable when analysed with ATR-FTIR spectroscopy (Section 3.2.1), only extracted saliva stains were examined to identify any potential variation that could be attributed to saliva stain age. Sixty three of the aged saliva stains were extracted and a total of 378 measurements were taken, of which 240 spectra represented a wet spectrum (Figure 3.2b) and 138 represented a dry spectrum (Figure 3.3b). Figure 4.8 demonstrates the overlay of the typical extracted spectra obtained from 24 hours to 7 days (a) and 24 hours to 18 months (b).

Initial observations of the short term aged extracted saliva stains (Figure 4.8a) demonstrate that the spectra produced from samples of each age exhibit the characteristic peaks of neat saliva, although there was variation in the peak definition and their relative proportions. In particular, the amide A (~3282 cm^{-1}) peak varied from a defined, medium/weak peak to a broad, strong/medium peak. The asymmetric and symmetric methylene stretches in oral mucosa lipids (~2926 & 2850 cm^{-1}) exhibited a distinct difference in the intensity strength, which varied from typically weak, as in the neat spectra, to the same strength as the amide A and sugar moiety peaks. The asymmetric and symmetric methylene bends of amino acids (~1452 & 1393 cm^{1}) and the sugar moiety peaks also varied amongst the different extracted saliva stain ages. Similar observations were evident in the overlay of the extracted 24 hour to 18 month aged saliva spectra; the amide A, asymmetric and symmetric methylene stretches of lipids and the sugar moiety peaks exhibited a similar variation across the sample ages. However, the amide I and II peaks (~1644 & 1545 cm^{-1}) demonstrated extensive interference, resulting in very poor definition of the peaks. The extracted saliva samples aged from 24 hours to 18 months (Figure 4.8b) exhibited great variation in spectral quality compared to the short term aged extracted samples. Due to the variation in spectral quality (Section 3.2.2), only extracted aged saliva stain spectra comprising of the characteristic peaks associated with neat saliva were included in age determination analysis. As a result, a total of 82 spectra (59%) of reasonable or good quality pertaining to saliva stains aged from 24 hours to 14 days were examined.

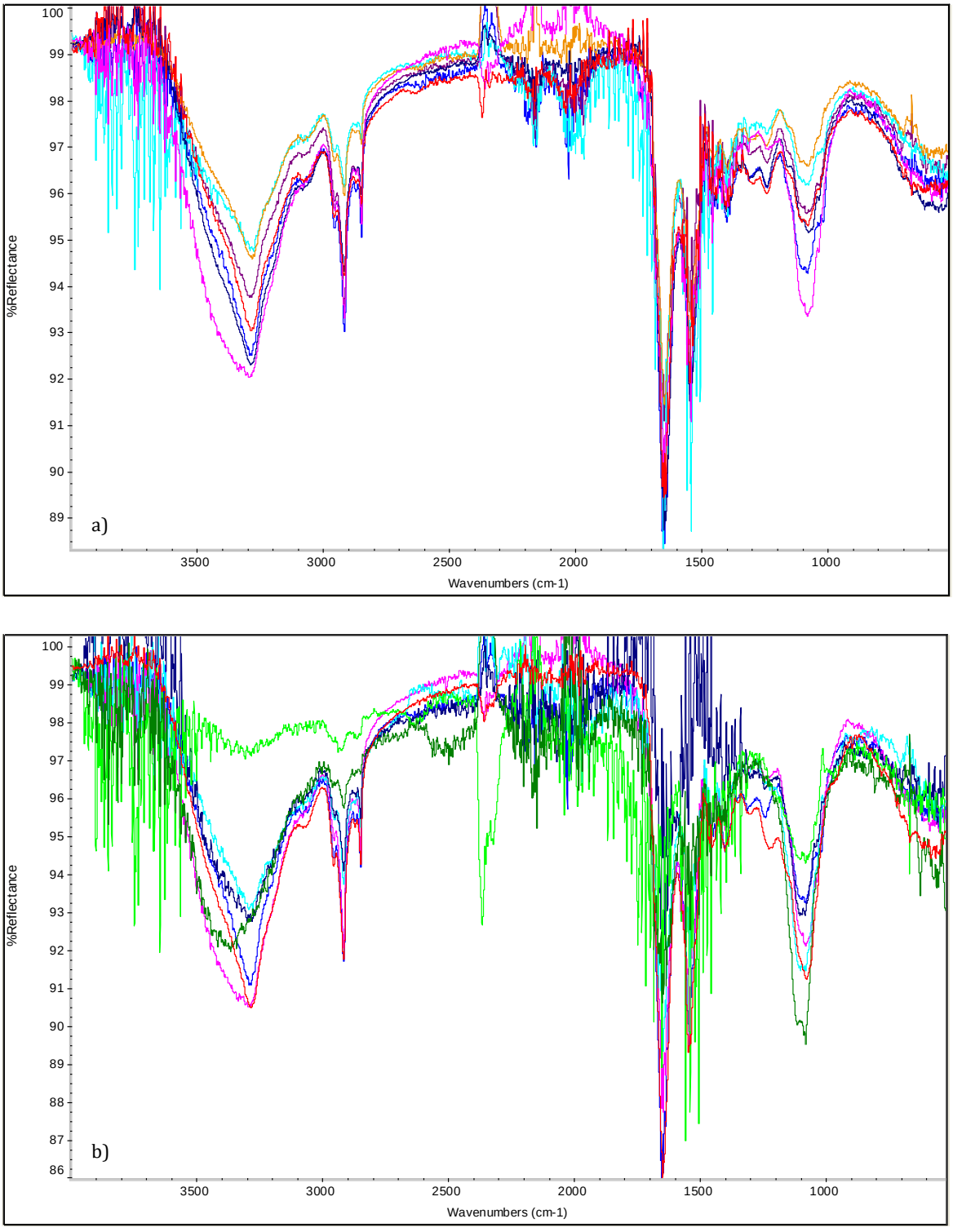

Figure 4.8: Overlay of extracted saliva stain spectra; a) short term aged to 24 hours (blue), 48 hours (purple), 3 days (red), 4 days (turquoise), 5 days (orange), 6 days (dark blue) & 7 days (pink); b) long term aged to 24 hours (blue), 7 days (pink), 1 month (turquoise), 2 months, (dark blue), 3 months (red), 12 months (green) & 18 months (dark green).

In order to identify any potential variation that could be attributed to saliva stain age, the specific intensities of all the saliva characteristic peaks were examined. Additionally, the

ratios of the peaks within the fingerprint region were examined. Namely, the amide I, amide II, the asymmetric and asymmetric methyl bending vibrations of amino acid side chains, amide III and sugar moiety peaks. The peak combinations utilised were the same as those studied in the comparison of body fluid spectra detailed in Section 3.5 (Table 3.11).

4.2.1.1 PEAK INTENSITIES

The saliva stain extracts were in a liquid form, thus ATR-FTIR spectroscopic analysis was conducted via the "wet-to-dry" approach utilised in the analysis of neat body fluids (Section 2.2.2.1). Figure 4.9 demonstrates the average peak intensities observed in the spectra of extracted saliva stains that were aged from 24 hours to 7 days and 14 days.

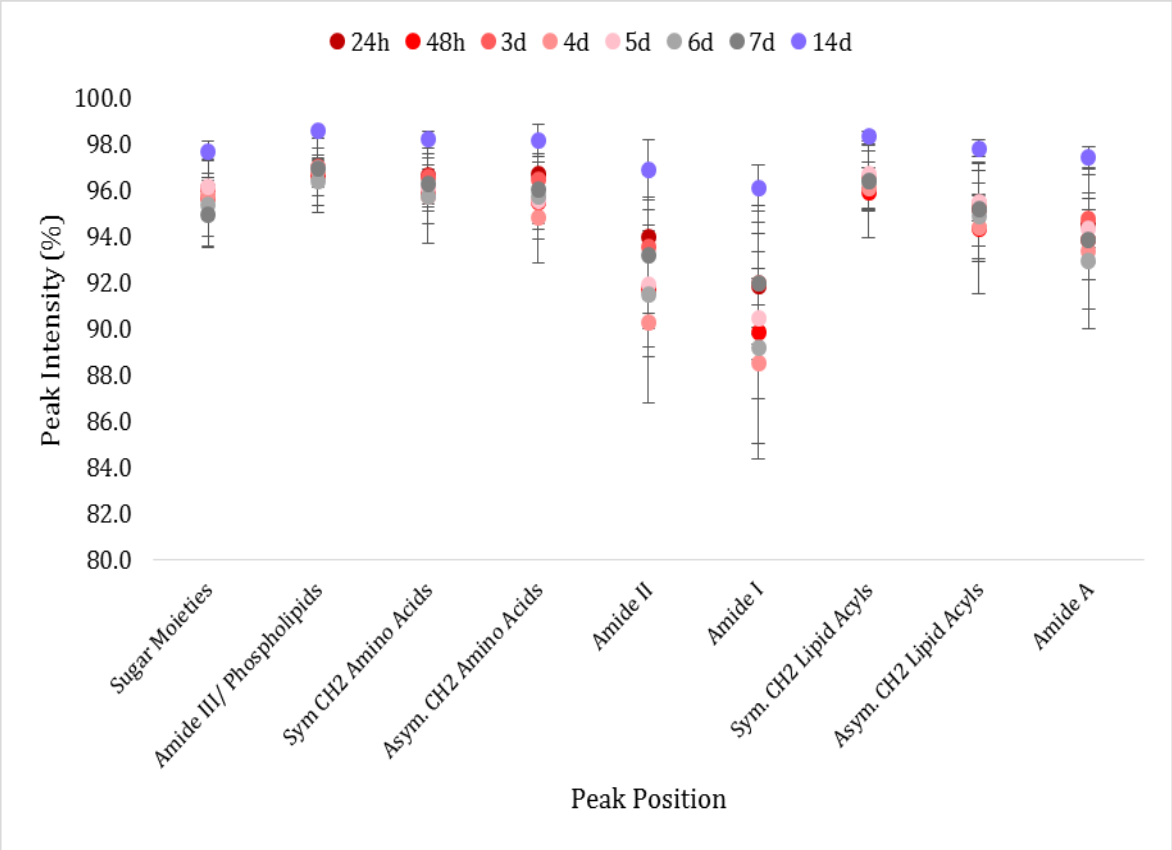

Figure 4.9: Scatter graph demonstrating the average peak intensities exhibited by the characteristic peaks of saliva in the spectra of extracted saliva stains aged from 24 hours to 14 days.

Initial observations of the average peak intensities demonstrate that the intensities obtained by 14 days aged saliva stains were distinguishable from the younger extracted saliva stains, as they exhibited the weakest intensities at all the characteristic peaks of saliva. The maximum peak intensity exhibited by the 14 day aged extracted saliva stains was approximately 96%, which indicates very low detection. The variation in peak intensity for the extracted 14 day aged samples demonstrated an overlap with the younger extracted

samples across all peaks. Therefore it would not be possible to distinguish 14 day aged saliva stains extracts from 24 hour to 7 day aged saliva stain extracts. Inspection of the average peak intensities of the extracted 24 hours to 7 day aged saliva stains demonstrates that tight clusters of overlapping intensities were exhibited at all peaks, except amide I and II. The maximum peak intensity observed across the peaks was approximately 95%, which was not greatly different from those exhibited by the extracted 14 day aged saliva stains. Due to the clustering of peak intensities, it was not possible to differentiate between the various sample ages examined. However, the extracted saliva stain ages that exhibited the strongest and weakest peak intensities could be determined. Table 4.1 demonstrates that there was no apparent consistency in yielding the strongest or weakest peak intensity amongst the cluster of 24 hours to 7 days.

Table 4.1: Extracted saliva stain ages that exhibited the strongest and weakest peak intensities within the 24 hour to 7 day aged cluster.

Peak	Strongest Peak Intensity	Weakest Peak Intensity
Sugar Moiety	7 days	5 days
Amide III/Phospholipids	6 days	7 days
Symmetric CH_2 Amino Acids	6 days	24 hours/3 days
Asymmetric CH_2 Amino Acids	4 days	24 hours
Amide II	4 days	24 hours
Amide I	4 days	7 days
Symmetric CH_2 Lipids	48 hours	5 days/7 days
Asymmetric CH_2 Lipids	3 days/4 days	5 days/7 days
Amide A	6 days	3 days

At the amide I and II peaks, the distribution of the extracted saliva stain ages was more wide-spread which allowed for some of the sample ages to be distinguished from one another. In particular, the extracted 4 day aged saliva stains, which exhibited the strongest intensity at these peaks, were clearly separated from the remaining ages. Overlap between 6 days, 48 hours and 5 days formed a small cluster situated above 4 days, demonstrating weaker average peak intensities. The weakest average intensities amongst the 24 hour to 7 day aged extracts also formed a small cluster of overlap. This cluster comprised of extracted 7 day, 3 day and 24 hour aged saliva stains. These ages were clearly separated from the other four ages examined, which could allow for differentiation between these extracted aged saliva

stains. However, the variation in peak intensity across the extracted 24 hour to 7 day aged saliva stains demonstrates overlap with all the sample ages, including 14 days.

It is evident from Figure 4.9 that due to the distribution and overlap in variation, it was not possible to differentiate between the 24 hour to 7 day aged extracted saliva stains examined at all peaks. However, the extracted 14 day aged saliva stains could clearly be differentiated from the younger extracted aged saliva stains. These results suggest that ATR-FTIR spectroscopy has the potential to be utilised as a technique to distinguish between saliva stains aged 14 days and those aged 7 days or younger when the stains are extracted. However, the variation in peak intensity exhibited across all of the extracted saliva stains examined does not enable differentiation between saliva stain ages.

4.2.1.2 PEAK RATIOS

Figure 4.10 demonstrates the average peak ratios (Table 3.11) observed in the spectra of extracted saliva stains aged from 24 hours to 7 days and 14 days. Initial observations demonstrate that the 14 day aged extracts could clearly be distinguished from the 24 hour to 7 day aged extracted, except at ratio combinations A, G-I. At these particular combinations all of the aged saliva extracts formed a cluster overlapping one another, therefore it was not possible to differentiate between the extract ages.

At ratio combinations B-F the distribution of the average peak ratio values per extracted saliva stain age were more wide spread, enabling some age differentiation. The distribution pattern observed at these peak ratios was also consistent, unlike the distribution patterns observed in the average peak intensities (Figure 4.9), although the distribution order was reversed and less clearly separated at combination F. The extracted 14 day aged saliva stains exhibited the lowest ratio value across combinations B-E, with no overlap observed. Overlap was exhibited between 7 and 3 days, 3 days and 24 hours, 5 days and 48 hours (only at E and F), and 48 hours and 6 days. The highest average peak ratio value was typically observed in the extracted 4 day aged saliva stains, except at combination F where it was the lowest ratio.

As demonstrated in Figure 4.10, these results suggest that ATR-FTIR spectroscopy has the potential to be utilised as a technique to distinguish between aged extracted saliva stains. However, due to the large overlap in peak ratio variation exhibited across all of the extracted saliva stains examined, it was not possible to differentiate saliva stain age. This is likely due to the very weak peak intensities yielded for all of the characteristic saliva peaks within the extracted spectra.

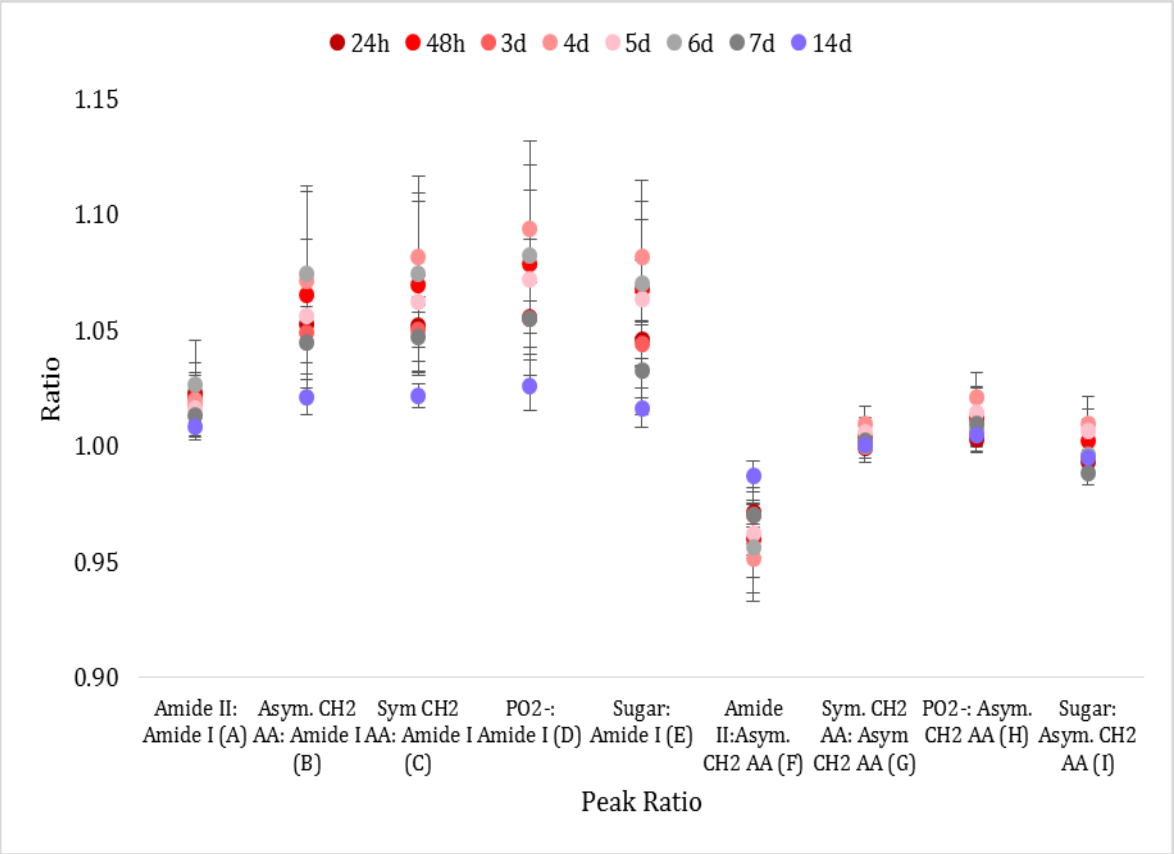

Figure 4.10: Scatter graph demonstrating the average peak ratios exhibited by the characteristic peaks of saliva in the spectra of extracted saliva stains aged from 24 hours to 7 days & 14 days.

Comparison of the average peak intensities and average peak ratios of the short term aged extracted saliva stains demonstrated similarities in the distribution patterns exhibited by the eight extracted saliva stain ages. In particular, the sample age distribution from strongest intensity/highest ratio to weakest intensity/lowest ratio was 4 days followed by 6 days, 48 hours, 5 days and a cluster of 7 days, 3 days and 24 hours, followed by 14 days. The examination of the average peak intensities and their respective ratios from spectra obtained from extracted saliva stains aged from 24 hours to 14 days has demonstrated that these values vary across each of the ages analysed. However, there appears to be no in decrease in peak intensity, or increase in peak ratio that correlates with the increase in saliva stain age. Additionally, the variation in peak intensity and ratio exhibited within each age means that the different extracted saliva stain ages could not be distinguished from one another. Therefore, it can be stated that ATR-FTIR spectroscopy is not an appropriate technique to determine the age of saliva stains when analysed as extracts from cotton.

4.3 SEMEN

4.3.1 EXTRACTED SEMEN

Semen samples deposited on cotton were placed in to storage for short term, up to 7 days, and long term ageing, up to 9 months. As semen stains were undetectable when analysed with ATR-FTIR spectroscopy directly, only extracted semen stains were examined to identify any potential variation in the spectra that could be attributed to semen stain age. A total of 99 semen stains were deposited for ageing analysis, all of which were extracted and examined with ATR-FTIR spectroscopy. The total number of measurements taken from the extracted semen stains was 594, of which 396 represented a wet spectrum (Figure 3.2c) and 198 represented a dry spectrum (Figure 3.3c). Figure 4.11 demonstrates an overlay of the typical extracted spectra obtained from semen stains aged from 24 hours to 7 days (a) and 24 hours to 9 months (b).

Initial observations of the short term aged extracted semen stain ATR-FTIR spectra (Figure 4.11a) demonstrate that the spectra produced from samples of each age exhibit the characteristic peaks of semen. The notable difference between the neat and extracted semen spectra is the lack of definition in the amide II peak; within the extracted semen spectra this peak appears more as a shoulder to the amide I peak, rather than a distinctly independent peak (Section 3.3.2). Upon inspection of the overlay spectra, distinct overlap was evident amongst the amide A (~3268 cm^{-1}), methyl stretches of lipids (~2950 cm^{-1}), amide I (~1625 cm^{-1}), amide II (~1540 cm^{-1}), asymmetric and symmetric bending of amino acid side chains (~1450 cm^{-1} & 1393 cm^{-1}), nucleic acid phosphates (~1240 cm^{-1}) and fructose/prostate specific antigen (PSA) (~1059 & 980 cm^{-1}) peaks. Variation in the intensities of the amide A, methyl stretches of lipids, asymmetric and symmetric bending of amino acid side chains, nucleic acid phosphates and fructose/PSA peaks was observed amongst the different ages. In contrast, very little variation was observed in the dominant protein peaks, amide I and II, across the different extracted semen stain ages. Comparison of the long term aged extracted semen spectra (Figure 4.11b) demonstrate similar differences in peak intensity variation, with the most distinct difference observable in the conformation of the amide II peak, which appeared to have diminished and formed part of the amide I peak.

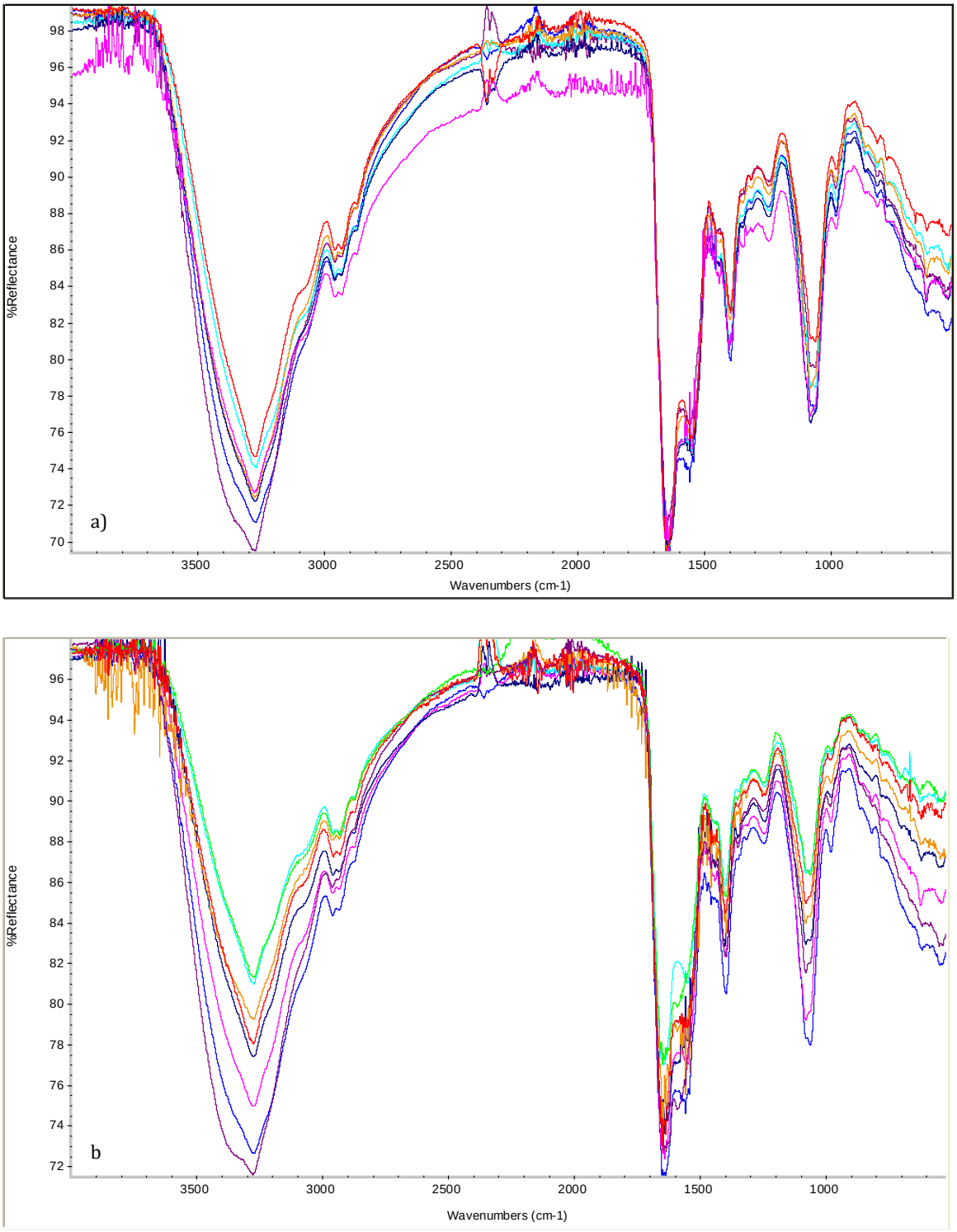

Figure 4.11: Overlay of extracted semen stain spectra; a) short term aged to 24 hours (blue), 48 hours (purple), 3 days (red), 4 days (turquoise), 5 days (orange), 6 days (dark blue) & 7 days (pink); b) long term aged to 24 hours (blue), 7 days (pink), 1 month (turquoise), 2 months, (dark blue), 3 months (red), 6 months (orange), 8 months (purple) & 9 months (green).

In order to identify any potential variation that could be attributed to extracted semen stain age, the specific intensities of all the semen characteristic peaks were examined. Additionally,

the peak ratios of the peaks within the fingerprint region were also examined. Namely, the amide I, amide II, the methyl bending vibrations of amino acid side chains, nucleic acid phosphates and fructose/PSA peaks. The peak combinations utilised were the same as those studied in the comparison of body fluid spectra detailed in Section 3.5 (Table 3.11).

4.3.1.1 PEAK INTENSITIES

The semen stain extracts were in a liquid form, thus ATR-FTIR spectroscopic analysis was conducted via the "wet-to-dry" approach utilised in the analysis of neat body fluids (Section 2.2.2.1). Figure 4.12 demonstrates the average peak intensities observed in the spectra of extracted semen stains that were aged from 24 hours to 9 months.

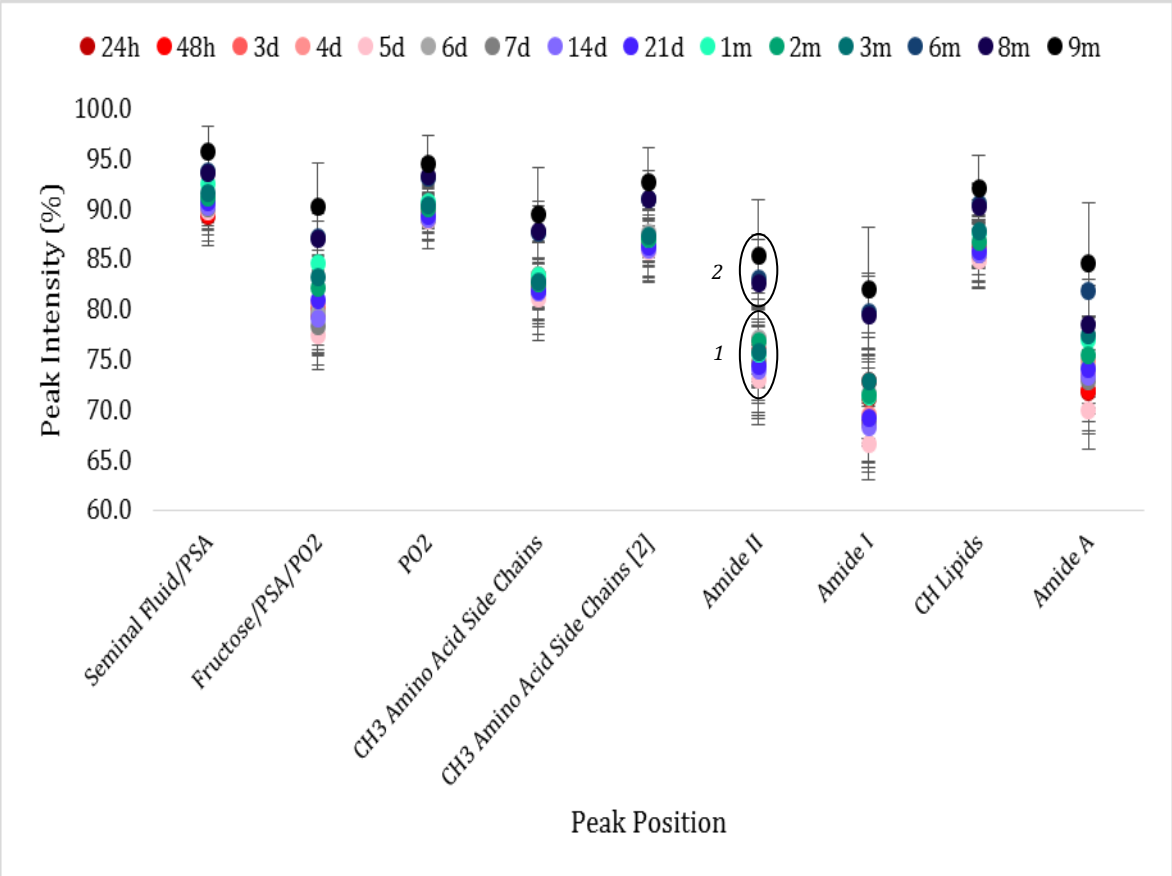

Figure 4.12: Scatter graph demonstrating the average peak intensities exhibited by the characteristic peaks of semen in the spectra of extracted semen stains aged from 24 hours to 9 months, with clusters 1 & 2 circled.

Initial observations of the average peak intensities demonstrate that there was considerable overlap amongst the majority of the aged extracted semen stains. The overlap exhibited formed a dense cluster (cluster [*1*]) of the 24 hours to 3 month aged samples which corresponded with the strongest peak intensities exhibited, approximately 60-90%. Due to

the degree of overlap between these extracted semen stain ages, specific sample differentiation was difficult. In particular, the 24 hour to 7 day average peak intensities were not visible as a result of the strong overlap with the 21 day to 3 month average peak intensities.

At the amide I, II and fructose/PSA peaks the density of the cluster was reduced as the extracted semen stain intensities appeared more separated. Therefore, it was possible to distinguish between the overlap of the 14 day to 3 month aged samples. The 6 and 8 month aged extracted semen stains exhibited weaker peak intensities than the younger samples. These particular ages exhibited strong overlap at all of the peaks examined and formed part of cluster two, which also comprised of the 9 month aged extracted semen stains. The 9 month samples exhibited the weakest peak intensity (~90%) amongst all the ages examined and was clearly separated from all the other extracted semen stains.

It is evident from Figure 4.12 that due to the distribution and overlap in variation, it was not possible to confidently differentiate between the 24 hour to 3 month aged extracted semen stains examined at all peaks. In contrast, the 6, 8 and 9 month aged extracted semen stains could be differentiated from the younger extracted stains, and the 9 month aged samples could be differentiated from all the other aged extracted semen stains. These results suggest that ATR-FTIR spectroscopy has the potential to be utilised as a technique to distinguish between semen stains aged 6 months and older from those aged 3 months or younger when the stains are extracted. However, the peak intensity variation exhibited across all of the extracted semen stains examined does not enable differentiation between semen stain ages.

4.3.1.2 PEAK RATIOS

Figure 4.13 demonstrates the average peak ratios (Table 3.11) observed in the spectra of extracted semen stains aged from 24 hours to 9 months. Initial observations demonstrate that different distribution patterns of the average peak ratios were obtained depending on the ratio combination. In particular, combinations A, G-I exhibited one cluster for all the ratio values of the aged extracted semen stains. Due to the strong overlap exhibited within these clusters, confident differentiation was not possible. In contrast, combinations B-E exhibited the same distribution pattern, with clearer separation between the ratio values of the aged extracted semen stains, although overlap was still evident. The aged extracts that demonstrated the lowest ratio values at these combinations were 6, 8 and 9 months, which formed a small cluster that was distinguishable from the other extract ages. A large cluster was apparent for the majority of the semen extract ages, consisting of the 24 hour to 4 day, 6 day to 3 month ratio values. The 24 hour to 4 day aged extracts were not clearly visible

within the distribution due to overlap with 6 and 7 day, and 1-3 months, whereas the 14 and 21 day extracts could be distinguished from the remaining ages as these exhibited a higher ratio value. In contrast, the 5 day aged extracts were completely separate from all the other aged extracts at combinations B-D as these samples exhibited the highest ratio value.

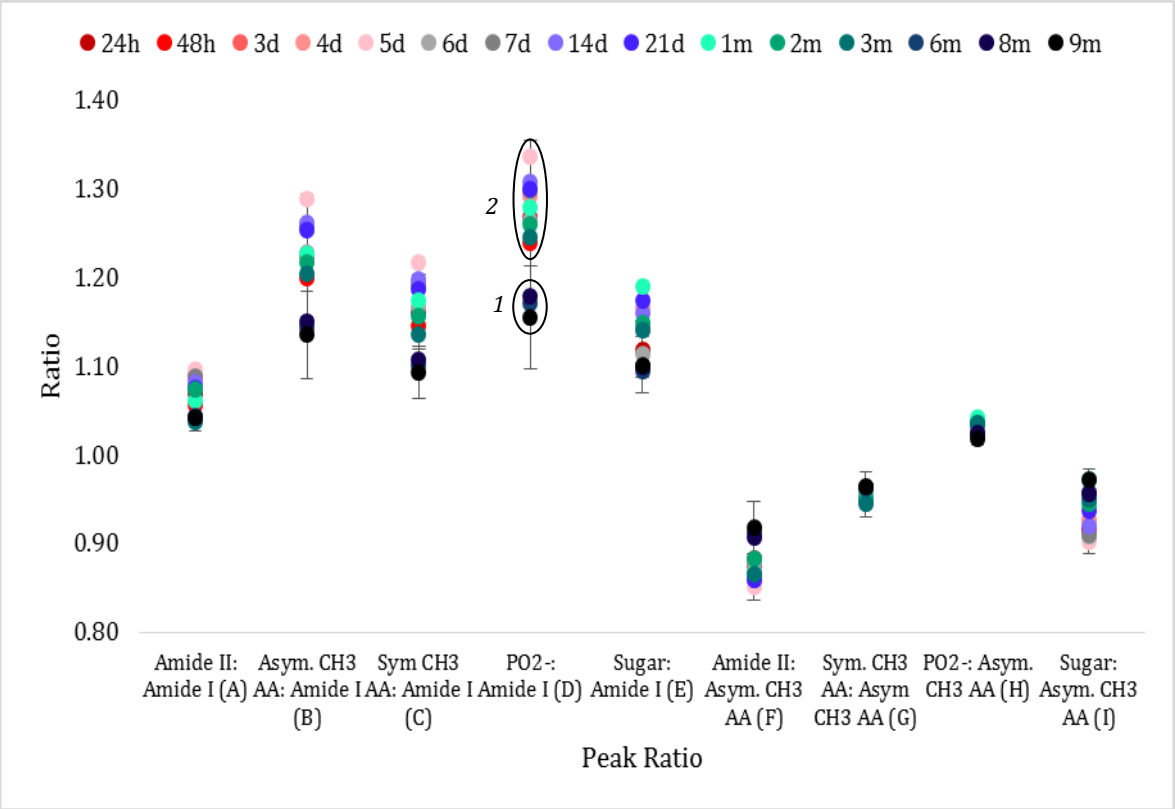

Figure 4.13: Scatter graph demonstrating the average peak ratios exhibited by the characteristic peaks of semen in the spectra of extracted semen stains aged from 24 hours to 9 months, clusters 1 & 2 circled.

The distribution pattern observed at combination F exhibited two distinct clusters which comprised of the reverse distribution to that demonstrated at ratio combinations B-E. A dense cluster of the 24 hour to 3 month aged extracts exhibited the low ratio values and due to the overlap it was not possible to differentiate between each of the semen extract ages. At the higher ratio value for the F combination, the 6-9 month aged extracted formed a small cluster that was clearly separated from the younger aged extracts, although overlap between these ages meant that age differentiation was not possible.

It is evident from Figure 4.13 that due to the distribution and overlap in variation, it was not possible to confidently differentiate between the 24 hour to 8 month aged extracted semen stains examined at ratio combinations A, E-I. Whereas, at combinations B-D, the distribution was not as dense and some age differentiation was possible. The 9 month aged extracted semen stains could be differentiated from the younger extracted stains at almost all of the

peak ratios examined. These results suggest that ATR-FTIR spectroscopy has the potential to be utilised as a technique to distinguish between some aged semen stains aged when the stains are extracted. However, the peak intensity variation exhibited across all of the extracted semen stains examined does not enable differentiation between semen stain ages.

Comparison of the average peak intensities and average peak ratios of the aged extracted semen stains demonstrated similarities in the distribution patterns exhibited by the fifteen sample ages, although the distribution appeared opposite to one another. However, due to the dense clustering apparent in both the average peak intensities and average peak ratios, it was not possible to determine the distribution of sample age from strongest intensity/highest ratio to weakest intensity/lowest ratio. The examination of the average peak intensities and their respective ratios from spectra obtained from extracted semen stains aged from 24 hours to 9 months have demonstrated that these values exhibit slight variation across each of the ages analysed. Additionally, at ratio combinations B-D it was possible to distinguish between aged extracted semen stains that were younger than 6 months old. However, there appears to be no decrease in peak intensity, or increase in peak ratio that correlates with the increase in semen stain age. Additionally, the variation in peak intensity and ratio exhibited within each age illustrates that the different extracted semen stain ages could not be distinguished from one another. Therefore, it can be stated that ATR-FTIR spectroscopy is not an appropriate technique to determine the age of semen stains when analysed as extracts from cotton.

4.4 VAGINAL SECRETIONS

4.4.1 VAGINAL SECRETION STAINS

Vaginal secretion samples deposited on cotton were place into storage, in accordance with the Human Tissue Act (2004), for short term, 24 hours to 7 days, and long term ageing, up to 6 months. Across 63 samples, 315 measurements were taken over the ageing period. Figure 4.14 demonstrates the overlay of the typical spectra obtained from vaginal secretions stains on cotton aged from 24 hours to 7 days (a) and 1 month to 6 months (b).

Initial observation of the short term aged vaginal secretion stain spectra demonstrate that each of the sample ages produced spectra exhibiting the characteristic peaks of vaginal secretions within the follicular phase. It is evident that there was very little variation in peak conformation and intensity over the seven ages. In contrast, the long term aged vaginal secretion stain spectra appear to exhibit differences in peak intensity. In particular, the amide A (~3274 cm^{-1}) and the methylene stretches of lipids (~2923 cm^{-1}) appeared to vary over time. The amide I and II peaks (~1641 & 1542 cm^{-1}) demonstrated concise overlap amongst the different sample ages, although the intensity of the peaks demonstrated a decrease. Variation in peak intensity was also exhibited in the asymmetric and symmetric bending of amino acid side chains (~1454 & 1406 cm^{-1}), nucleic acid phosphate (~1233 cm^{-1}) and the glycogen peaks (~1127-1030 cm^{-1}).

In order to identify any potential variation that could be attributed to vaginal secretion stain age, the specific intensities of all the vaginal secretion characteristic peaks were examined. Additionally, the ratios of the peaks within the fingerprint region were examined. Namely, the amide I, amide II, the methyl bending vibrations of amino acid side chains, nucleic acid phosphate and glycogen peaks. The peak combinations utilised were the same as those studied in the comparison of body fluid spectra detailed in Section 3.5 (Table 3.11).

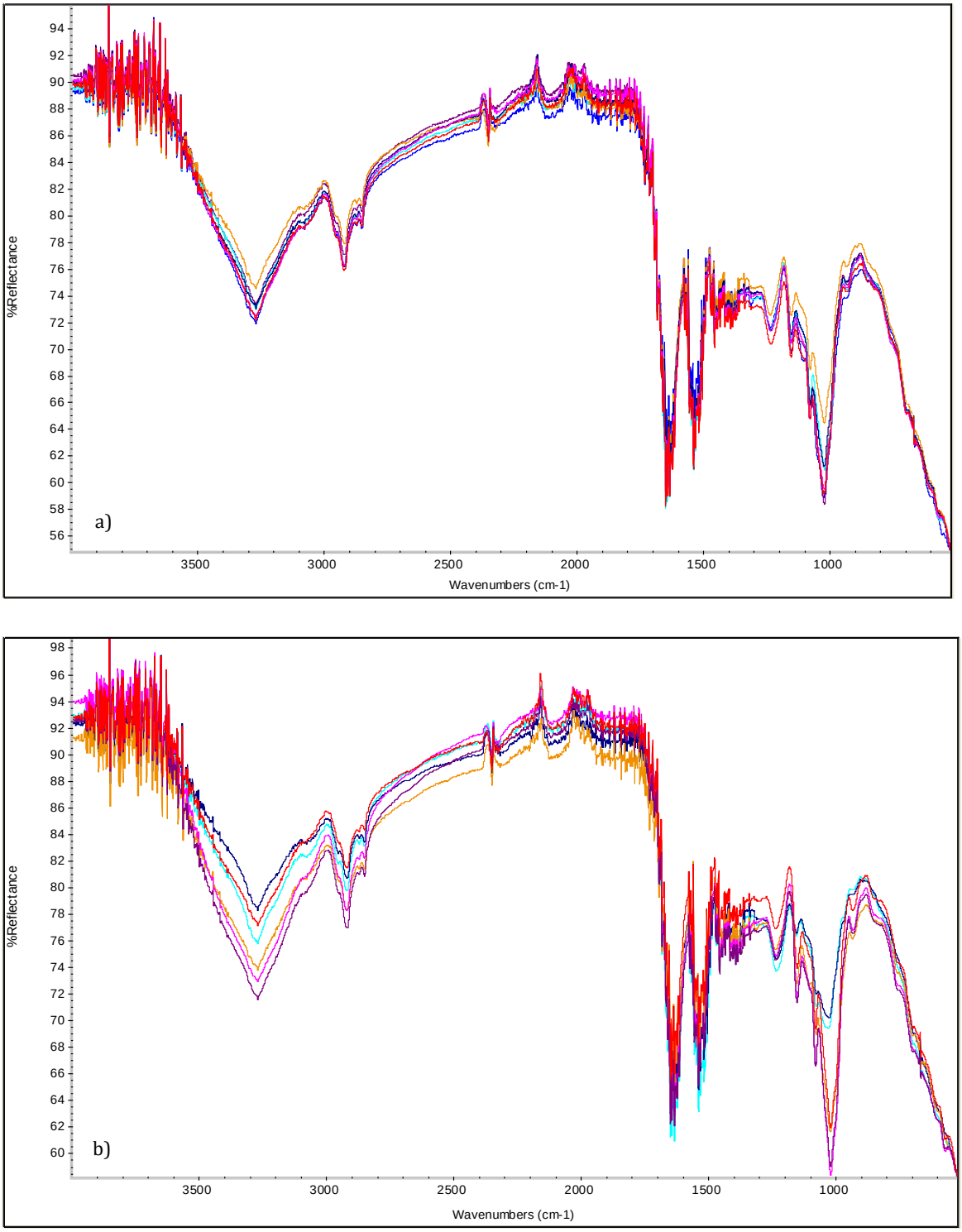

Figure 4.14: Overlay of vaginal secretion stain spectra; a) short term aged to 24 hours (blue), 48 hours (purple), 3 days (red), 4 days (turquoise), 5 days (orange), 6 days (dark blue) & 7 days (pink); b) long term aged to 1 month (turquoise), 2 months (dark blue), 3 months (red), 4 months (orange), 5 months (pink) & 6 months (purple).

4.4.1.1 PEAK INTENSITIES

Direct ATR-FTIR spectroscopic analysis of the vaginal secretion stains was utilised in the first instance for all of the aged samples. As vaginal secretion characteristic spectra could be obtained from the direct analysis of the vaginal secretion stains, the peak intensities and ratios were examined with no manipulation. Figure 4.15 demonstrates the average peak intensities observed in the spectra of vaginal secretion stains aged from 24 hours to 6 months.

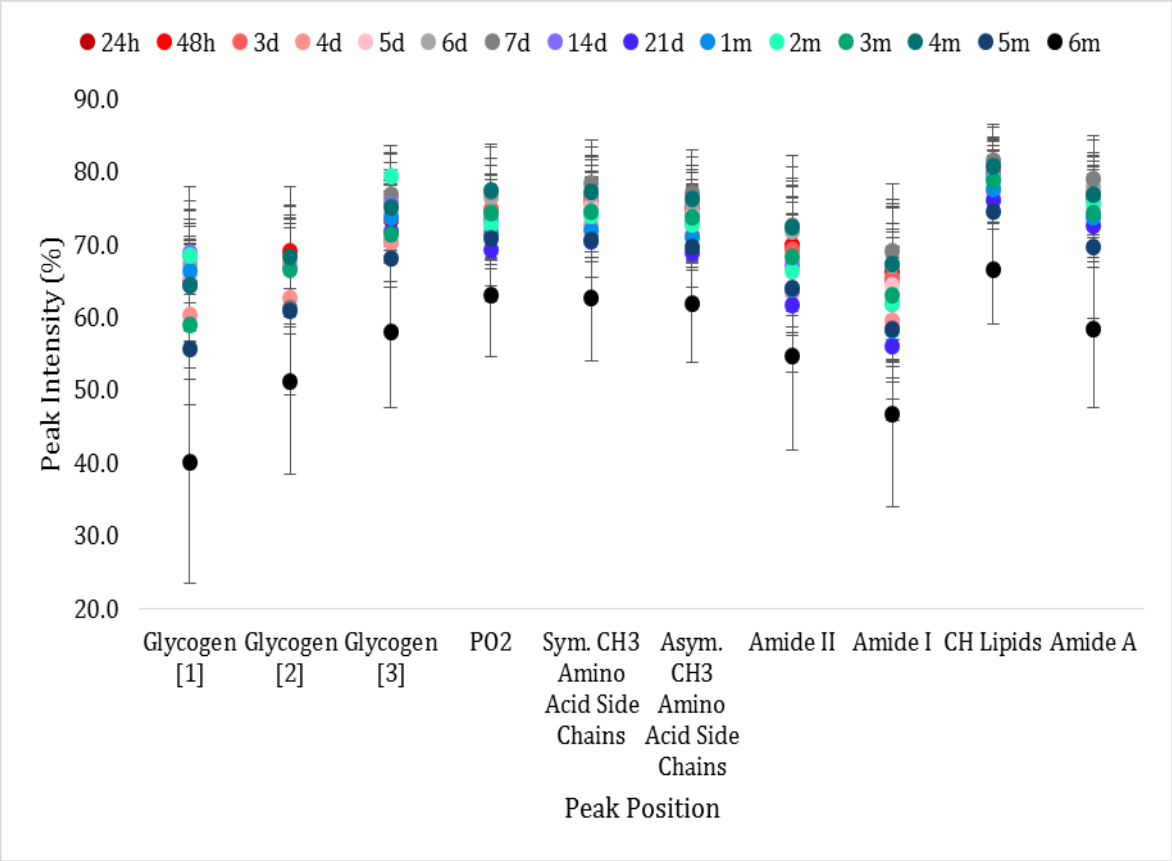

Figure 4.15: Scatter graph demonstrating the average peak intensities exhibited by the characteristic peaks of vaginal secretions in the spectra of vaginal secretion stains aged from 24 hours to 6 months.

Initial observations of the average peak intensities demonstrate that there was considerable overlap amongst the majority of the vaginal secretion stain ages. The 6 month aged vaginal secretion stains were clearly distinguishable from the remaining sample ages due to exhibiting the strongest average peak intensity, approximately 40%. A dense cluster of overlapping vaginal secretion stain ages made it difficult to differentiate between the sample ages, particularly the 24 hour to 5 day aged vaginal secretion stains which were predominantly overlapped by the 14 day to 5 month aged samples. The 14 days to 5 month aged samples were clearly observed amongst the cluster in contrast to the 24 hour to 5 day

aged vaginal secretion stains which were barely visible. The vaginal secretion stain age that exhibited the weakest average peak intensity varied dependent on the peak; at the glycogen peaks, the weakest intensities were exhibited by 14 days [1], 48 hours with overlap from 4 months [2] and 2 months [3]; at the nucleic acid phosphate peak, the weakest intensity was demonstrated by 4 months. At all the remaining peaks the 7 day aged vaginal secretion stains exhibited the weakest peak intensity, with some overlap with 4 months and 6 days observed.

The distribution of the vaginal secretion stain ages was comparable throughout the peaks examined, which could enable some differentiation between non-overlapping ages. For example, the 6 month aged vaginal secretion stains could be differentiated from all of the younger aged stains due to the consistently strong peak intensity observed at all the peaks examined. These results suggest that ATR-FTIR spectroscopy has the potential to be utilised as a technique to determine vaginal secretion stain age. However, the peak intensity variation exhibited across each vaginal secretion stain age, demonstrates that all the ages exhibited overlap, as demonstrated by the error bars in Figure 4.15.

4.4.1.2 PEAK RATIOS

Figure 4.16 demonstrates the average peak ratios (Table 3.11) observed in the spectra of vaginal secretion stains aged from 24 hours to 6 months.

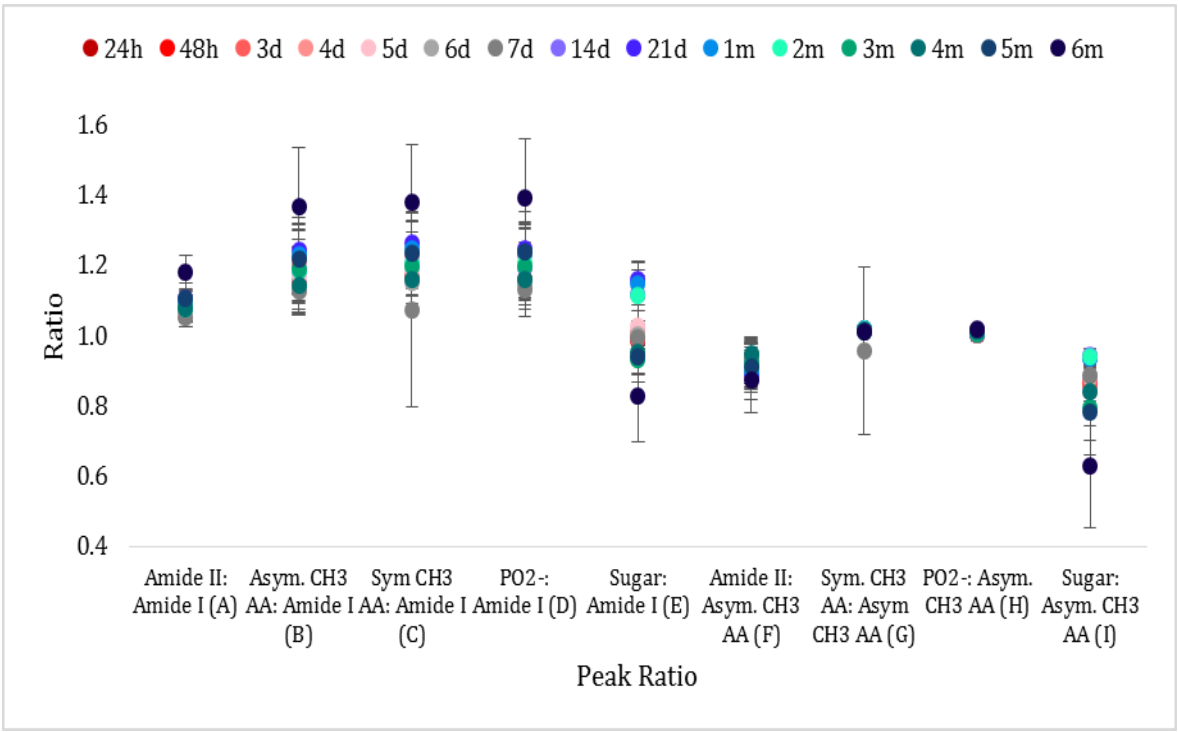

Figure 4.16: Scatter graph demonstrating the average peak ratios exhibited by the characteristic peaks of vaginal secretions in the spectra of vaginal secretion stains aged from 24 hours to 6 months.

Initial observations demonstrate that there was distinct overlap of all the sample ages, except 6 months, at ratio combinations A-D and F-I. These combinations refer to ratios amide II:amide I (A), asymmetric methyl bending of amino acid side chains:amide I (B), symmetric methyl bending of amino acid side chains:amide I (C), nucleic acid phosphate:amide I (D), amide II:asymmetric methyl bending of amino acid side chains (F), symmetric methyl bending of amino acid side chains:asymmetric methyl bending of amino acid side chains (G), nucleic acid phosphate:asymmetric methyl bending of amino acid side chains (H) and sugar:asymmetric methyl bending of amino acid side chains (I), respectively. At each of these ratios a dense cluster of the vaginal secretion stain ages was observed, particularly at combinations G and H, where all of the ages were concentrated to the same ratio value. As a result, differentiation between the vaginal secretion stain ages was not possible at these ratio combinations, based on ratio values.

The distribution of the vaginal secretion stain ages was more wide spread at combinations E, glycogen:amide I and glycogen:asymmetric methyl bending of amino acid side chains. At these ratios, some of the sample ages could be differentiated from one another based on their average peak ratio values. Specifically, at the high ratio end of combination E a small cluster comprising of 14 day to 2 month aged vaginal secretion stains was evident above a large cluster of 24 hour to 7 day and 3 to 5 month aged samples overlapping tightly. The 6 month aged vaginal section stain was clearly distinguishable from the two clusters due to its low ratio value. At combination I, differentiation was only possible between the 6 months and younger aged vaginal secretion stains.

It is evident from Figure 4.16 that due to the concentrated overlap in the average peak ratios for each of the different ages, it was not possible to differentiate between the vaginal secretion stain ages examined. This was also evident in the overlap in variation exhibited at each ratio combination. Differentiation based on the average peak ratio values could be possible only for the 6 month aged vaginal secretion stains at ratio combinations A-E and I. However, the associated variation with each of the aged samples at these peak ratios was large and overlapping, therefore differentiation of the aged vaginal secretion stains was not possible. As a result, the examination of peak ratios with ATR-FTIR spectroscopy has been demonstrated to not be an appropriate technique for distinguishing between aged samples of vaginal secretion stains.

Comparison of the average peak intensities and average peak ratios of the aged vaginal secretion stains demonstrated some similarities in the distribution patterns exhibited by the fifteen sample ages. However, due to the dense clustering apparent in both the average peak

intensities and average peak ratios, it was not possible to confidently determine the distribution of sample age from strongest intensity/highest ratio to weakest intensity/lowest ratio. The examination of the average peak intensities and their respective ratios from spectra obtained from vaginal secretion stains aged from 24 hours to 6 months have demonstrated that these values exhibit slight variation across each of the ages analysed. However, there appears to be no apparent decrease in peak intensity, or increase in peak ratio that correlates with the increase in vaginal secretion stain age. Additionally, the variation in peak intensity and ratio exhibited within each age illustrates that the different vaginal secretion stain ages could not be distinguished from one another. Therefore, it can be stated that ATR-FTIR spectroscopy is not an appropriate technique to determine the age of vaginal secretion stains when analysed directly from cotton.

4.4.2 EXTRACTED VAGINAL SECRETION STAINS

The age determination of extracted vaginal secretion stains was carried out with the same samples utilised for direct ATR-FTIR spectroscopic analysis of vaginal secretion stains (Section 4.4.1). As spectra consisting of the key characteristic peaks of neat vaginal secretions were observed when vaginal secretion stains on cotton were analysed directly, samples aged from 24 hours to 6 months were extracted and subsequently analysed. Across 63 vaginal secretion stains, 378 measurements were taken, of which 252 spectra represented a wet spectrum (Figure 3.2d) and 126 represented a dry spectrum (Figure 3.3d). Figure 4.17 demonstrates the overlay of the typical spectra obtained from extracted vaginal secretion stains from 24 hours to 7 days (a) and 1 to 6 months (b).

Initial observations of the short term aged spectra demonstrated that extracted vaginal secretions of varying ages yielded spectra exhibiting the characteristic peaks of vaginal secretions within the follicular phase of the menstrual cycle. It was evident within the overlay spectra that there were differences in peak intensity for most of the peaks amongst the seven sample ages. In particular, decreases in peak intensity were exhibited for the amide A (~3274 cm^{-1}), methylene stretches in lipids (~2923 cm^{-1}), amide I and II (~1641 & 1542 cm^{-1}), nucleic acid phosphate (~1233 cm^{-1}) and glycogen peaks (~1127-1030 cm^{-1}). Peak intensity decrease was also observed in asymmetric and symmetric methyl bends of amino acid side chains (~1454 & 1406 cm^{-1}), although there appeared to be more of an overlap between the sample ages than a clear decrease. Comparable observations were evident in the long term aged spectra (Figure 4.17b), with greater variation in peak intensity exhibited in

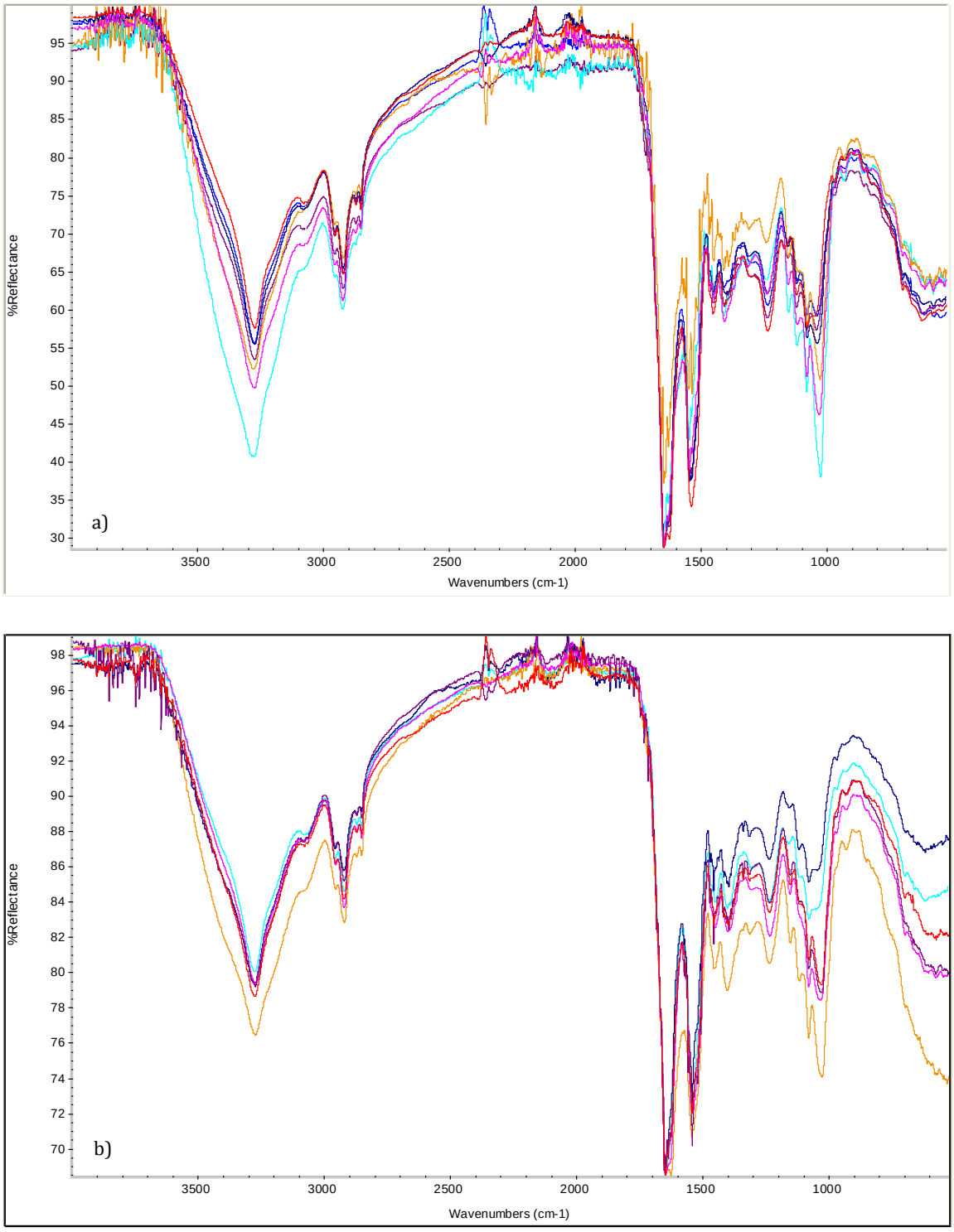

Figure 4.17: Overlay of extracted vaginal secretion stain spectra; a) short term aged to 24 hours (blue), 48 hours (purple), 3 days (red), 4 days (turquoise), 5 days (orange), 6 days (dark blue) & 7 days (pink); b) long term aged to 1 month (turquoise), 2 months (dark blue), 3 months (red), 4 months (orange), 5 months (pink) & 6 months (purple).

the peaks of the fingerprint region; asymmetric and symmetric methyl bends of amino acid side chains, nucleic acid phosphate and glycogen. The amide A, methylene stretches in lipids, amide I and II peaks appeared to exhibit more overlap in their intensities than increases or decreases.

In order to identify any potential variation that could be attributed to extracted vaginal secretion stain age, the specific intensities of all the extracted vaginal secretion characteristic peaks were examined. Additionally, the ratios of the peaks within the fingerprint region were examined; namely, the amide I, amide II, the methyl bending vibrations of amino acid side chains, nucleic acid phosphate and glycogen peaks. The peak combinations utilised were the same as those studied in the comparison of body fluid spectra detailed in Section 3.5 (Table 3.11).

4.4.2.1 PEAK INTENSITY

The vaginal stain extracts were in a liquid form, thus ATR-FTIR spectroscopic analysis was conducted via the "wet-to-dry" approach utilised in the analysis of neat body fluids (Section 2.2.2.1). Figure 4.18 demonstrates the average peak intensities observed in the spectra of extracted vaginal secretion stains that were aged from 24 hours to 6 months.

Initial observations of the average peak intensities demonstrate that there was overlap between some of the sample ages, but not all. In particular, the distribution and overlap of the extracted vaginal secretion stain ages could be categorised into small clusters. The extracted vaginal secretion stains that exhibited the strongest peak intensities were typically the 24 hour to 3 day aged samples, which formed a small, overlapping cluster. Overlap of these ages with 4 and 6 month aged extracted samples was seen at the glycogen [1], [2] and amide A peaks. The 6 month extracted vaginal secretion stain age formed a small cluster with 4 months at the majority of the peaks, with very little overlap with other sample ages exhibited. The clusters that followed, decreasing in peak intensity, consisted of 14 days and 5 months, with overlap from 4 months at glycogen [1] and amide I peaks, and 6, 7 and 21 days, with some overlap from various different extracted samples ages. The cluster that was most distinct, comprised of many overlapping extracted vaginal secretion stain ages, although differentiation was still possible. This cluster comprised of ages 4 and 5 days and 1 to 3 months and these ages typically gave the weakest peak intensities within their spectra.

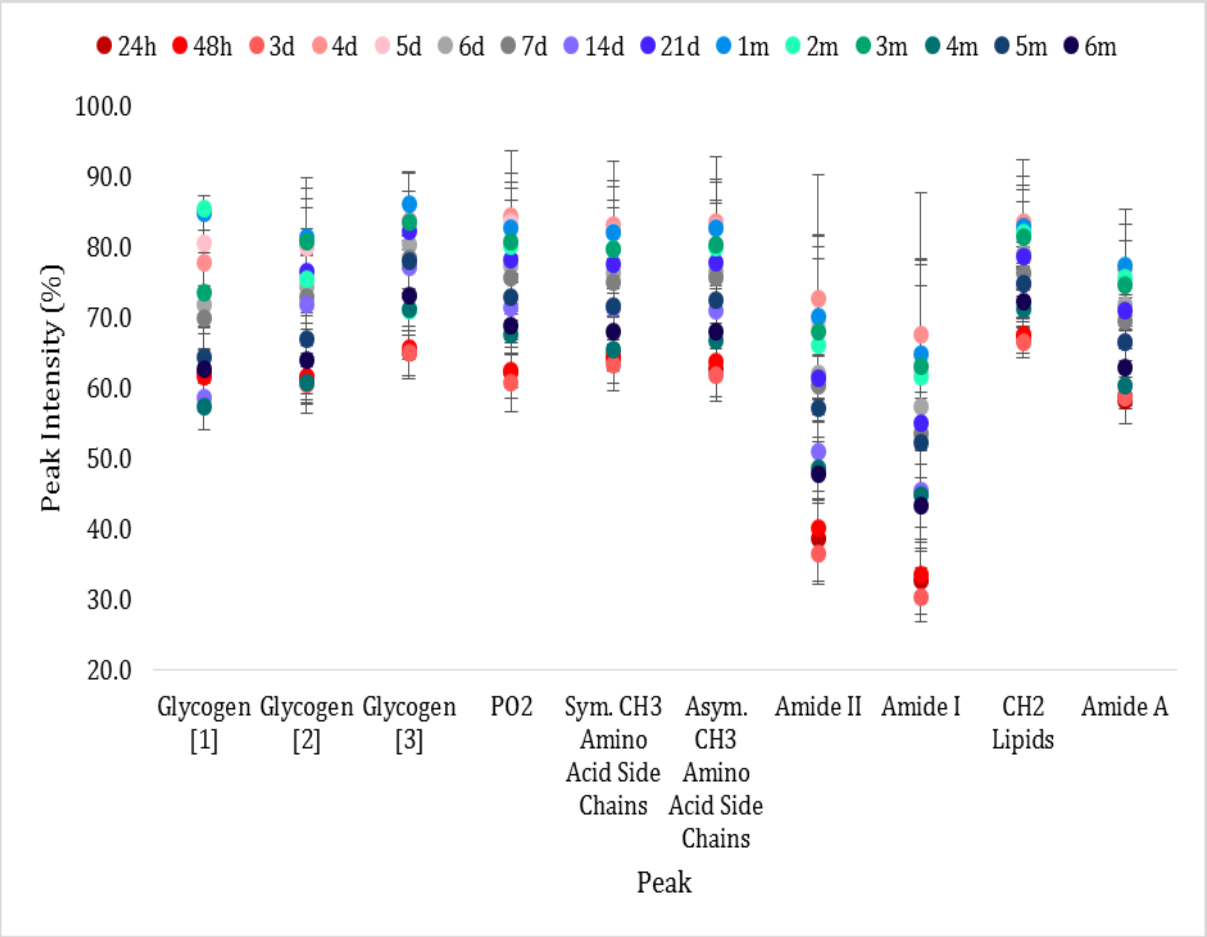

Figure 4.18: Scatter graph demonstrating the average peak intensities exhibited by the characteristic peaks of vaginal secretions in the spectra of extracted vaginal secretion stains aged from 24 hours to 6 months.

The distribution of the extracted vaginal secretion stain ages was comparable throughout the peaks examined, which could enable differentiation between the majority of the ages due to the more wide spread distribution. It is worthy of note that most of the overlap observed across the extracted vaginal secretion stain ages was not observed at all the peaks examined. Where overlap was observed at all or most of the peaks, the ages within the overlapping cluster were consistently observed in the relevant cluster. These results suggest that ATR-FTIR spectroscopy has the potential to be utilised as a technique to determine vaginal secretion stain age. However, the peak intensity variation exhibited across each extracted vaginal secretion stain age, demonstrates that all the ages exhibited overlap, as demonstrated by the error bars in Figure 4.18.

4.4.2.2 PEAK RATIOS

Figure 4.19 demonstrates the average peak ratios (Table 3.11) observed in the spectra of extracted vaginal secretion stains aged from 24 hours to 6 months.

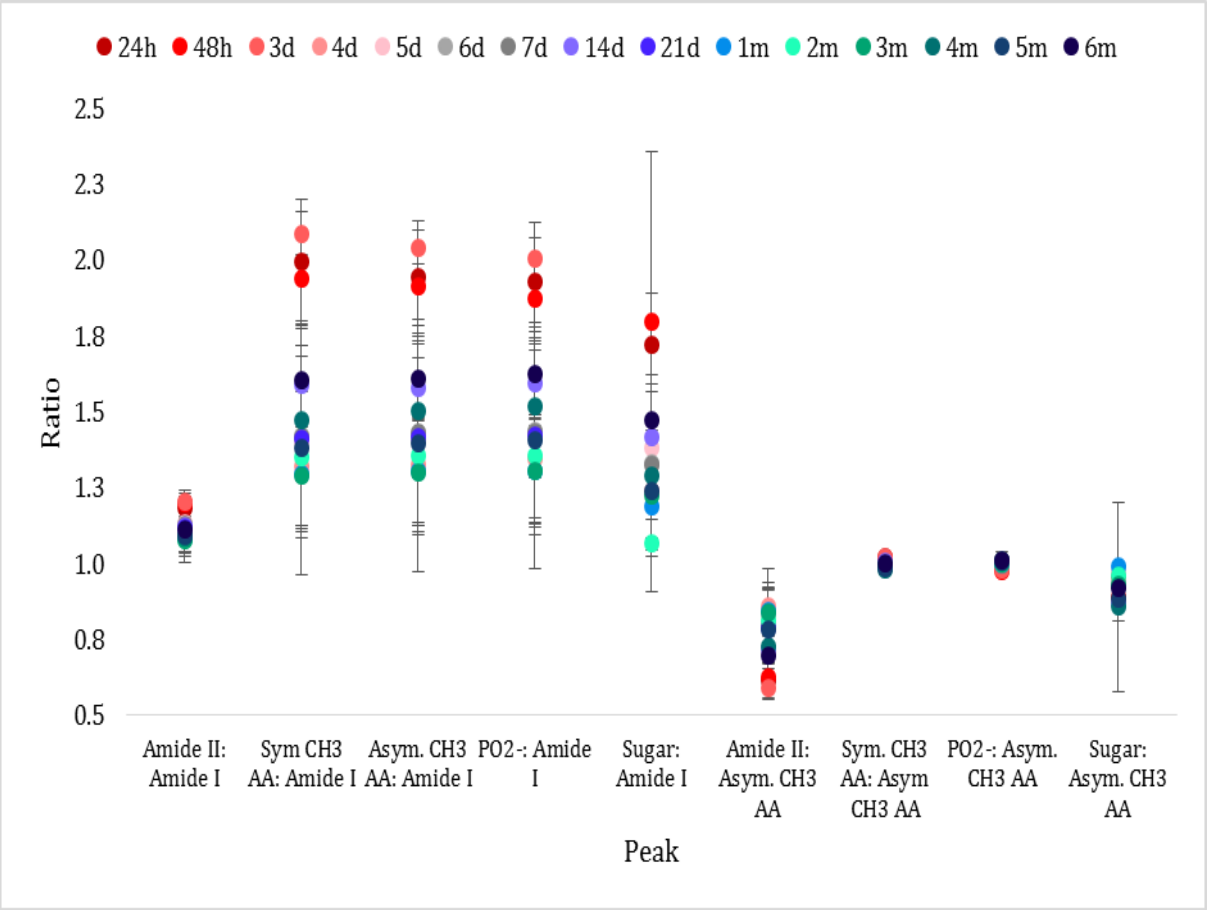

Figure 4.19: Scatter graph demonstrating the average peak ratios exhibited by the characteristic peaks of vaginal secretions in the spectra of extracted vaginal secretion stains aged from 24 hours to 6 months.

Initial observations of the average peak ratios exhibited by the various aged extracted vaginal secretion stains demonstrates that there were very dense clusters of overlap at ratio combinations; A, amide II:amide I; G, symmetric methyl bends of amino acid side chains:asymmetric methyl bends of amino acid side chains; H, nucleic acid phosphate:asymmetric methyl bends of amino acid side chains; and I, glycogen:asymmetric methyl bends of amino acid side chains. At combination F there was considerable overlap evident amongst the aged extracted vaginal secretion stains, although differentiation was possible for the 24 hour to 3 day, and 4 and 6 month extracts compared to the other extracted ages.

At ratio combinations B-D (asymmetric methyl bending of amino acid side chains:amide I, symmetric methyl bending of amino acid side chains:amide I, nucleic acid phosphate:amide I, respectively), the ratio value distribution of the extracted vaginal secretion stains ages was much more wide spread and differentiation between each of the ages could be determined. In particular, the distribution order from lowest to highest ratio value was observed as; 3

months, 4 days, 1, 2 and 5 months, 21, 7 and 6 days as a large cluster exhibited some overlap between the ratio values, 4 months, overlap of 14 days and 6 months, 48 hours, 24 hours and 3 days. A similar distribution pattern was evident at combination E, sugar:amide I, although the lowest ratio value was 2 months and the highest was 48 hours. Ratio combination F, amide II:asymmetric methyl bending of amino acid side chains, exhibited a more dense cluster that appeared to form three groups, at the lowest ratio value for the combination were the 24 hour to 3 day aged extracted vaginal secretions, followed by 4 and 6 months and then a tight overlap of all the remaining extract ages. The sample ages within this tight overlapping group could not differentiated from one another.

It is evident from ratio combinations B-E that it was possible to differentiate between the extracted vaginal secretion stain ages based on the average peak ratios. However, differentiation was not possible at combinations A, G-I due to the dense overlapping clusters of all the samples ages. Inspection of the associated variation with each of the aged samples at all the peak ratios demonstrates there is large overlap across all of the extracted vaginal secretion stain ages. As a result, the examination of peak ratios with ATR-FTIR spectroscopy has been demonstrated to not be an appropriate technique to distinguish between aged samples of extracted vaginal secretion stains.

Comparison of the average peak intensities and average peak ratios of the aged extracted vaginal secretion stains demonstrated similarities in the distribution patterns exhibited by the fifteen sample ages. The approximate sample age distribution from strongest intensity/highest ratio to weakest intensity/lowest ratio was 3 days, 24 hours, 48 hours, 6 months, 14 days, 4 months, 21 days, 5 months, 6 days, 7 days, 5 days, 2 months, 3 months, 1 month and 4 days. The examination of the average peak intensities and their respective ratios from spectra obtained from extracted vaginal secretion stains aged from 24 hours to 6 months have demonstrated that these values exhibit slight variation across each of the ages analysed. However, there appears to be no apparent decrease in peak intensity, or increase in peak ratio that correlates with the increase in vaginal secretion stain age. Additionally, the variation in peak intensity and ratio exhibited within each age illustrates that the different vaginal secretion stain ages could not be distinguished from one another. Therefore, it can be stated that ATR-FTIR spectroscopy is not an appropriate technique to determine the age of vaginal secretion stains when analysed as extracts from cotton.

4.5 CONCLUDING SUMMARY

The examination of blood, saliva, semen and vaginal secretions with ATR-FTIR spectroscopy was explored to ascertain whether this technique could be successfully utilised in the application of body fluid identification and age determination (Sections 3 & 4). All four body fluids have demonstrated that unique spectra can be reproducibly obtained from each body fluid type. The body fluid spectra consist of a complex mixture of common macromolecules typically found within biological materials, although the specific peak frequencies and overall spectral pattern enable these body fluids to be discriminated from one another. To ensure that this method was appropriate for forensic application, stains of each body fluid were prepared and aged up to 18 months to establish whether ATR-FTIR spectroscopy could still produce a spectrum that represented the respective body fluid. Blood and vaginal secretion stains could successfully be detected and produce the characteristic spectra associated with these body fluids, although saliva and semen stains were undetectable. The extraction of the body fluid stains from the cotton substrate with a simple water extraction method enabled all four body fluids to be detected, with excellent quality spectra obtained for blood, semen and vaginal secretions which were comparable to the spectra of the neat body fluids. The quality of the saliva extracted samples varied considerably due to the dilute nature of the body fluid.

The age of a body fluid stain appeared to have no correlation with spectral quality and stains as old as 18 months could be identified. Comparisons between the body fluid spectra demonstrated that blood, saliva, semen and vaginal secretion samples exhibited different peak compositions and strengths for common macromolecule functional groups and therefore the spectral pattern and specific peak frequencies can be utilised to distinguish between these four body fluids. Examination of the ratios between the common macromolecule peaks demonstrated that the ratios overlapped across nine different peak combinations for all body fluids and body fluid states. Therefore, peak ratios comparisons were not a suitable method to discriminate between the spectra blood, saliva, semen and vaginal secretions.

The peak intensities of the characteristic macromolecule groups and the peak ratios were compared over the varying body fluid ages to determine whether any variation in these measurements could be correlated with sample age. Examination of the average peak intensities and ratios over time demonstrated that it was not possible to distinguish between the different body fluid ages, with the exception of the peak intensities exhibited by extracted

bloodstains. The 12 month aged extracted bloodstains yielded much weaker peak intensities than those obtained from the 24 hour to 7 day aged extracts. However, the analysis of extracted bloodstains aged from 7 days up to 12 months needs to be examined to determine whether discrimination can still be achieved. Typically, the overlap in variation exhibited across all the ages examined for all the body fluids suggests that the variation overlap will prevent such differentiation between younger and older samples.

Overall, it can be stated that ATR-FTIR spectroscopy can be used to successfully identify and distinguish between body fluids when in their neat state, or as stains on cotton that are as old as 18 months. Additionally, the peak intensities and ratios obtained from ATR-FTIR spectra are not suitable to determine the age of saliva, semen or vaginal secretion stains; although it has the potential to determine the age of bloodstains when samples are extracted.

5. PROTEIN ANALYSIS: SEPARATION & QUANTIFICATION

5.1 INTRODUCTION

The analysis of proteins within forensic science is seldom documented outside of its application in presumptive testing, whereby the presence of particular enzymes, proteins or antibodies produces a colour change, which then indicates the presence of a particular body fluid (Li, 2008). However, presumptive tests are not powerful forensic tests and are limited by their cross-reactivity and subjectivity. This chapter addresses the application of protein analyses that are more sophisticated and sensitive than those currently utilised within forensic science. The introduction provides a background into the chemistries and techniques involved in protein analysis and the previous applications of proteins analyses with body fluid samples. Additionally, the methodology utilised within this research, the results obtained and a discussion of the research findings are included.

5.1.1 SEPARATION

5.1.1.1 PRINCIPLES OF ELECTROPHORESIS

Electrophoresis is a separation technique that involves the migration of charged macromolecule particles under the influence of an electric field (Gaál et al. 1980; Walker, 2010). All proteins, peptides, amino acids and nucleic acids possess an electrical charge due to the ionisation of amino and carboxyl groups when in solution (Crowe & Bradshaw, 2010). When these molecules are in solution of any given pH, the nature of their charge renders the species as cations, if positively charged, or anions, if negatively charged. Therefore, the species have become ionised. The introduction of an electric field to the solution enables the charged particles, or ions, to migrate towards the electrode of the same charge as that of the ions' net charge, with cations migrating toward the cathode, which is negatively charged in electrophoresis, and anions migrating toward to the anode which is positively charged (Figure 5.1). As the ions migrate they begin to separate from one another based on their

electrical charge, size or shape, which enables species characterisation based on the migration distance travelled by each ion, or group of ions (Walker, 2010).

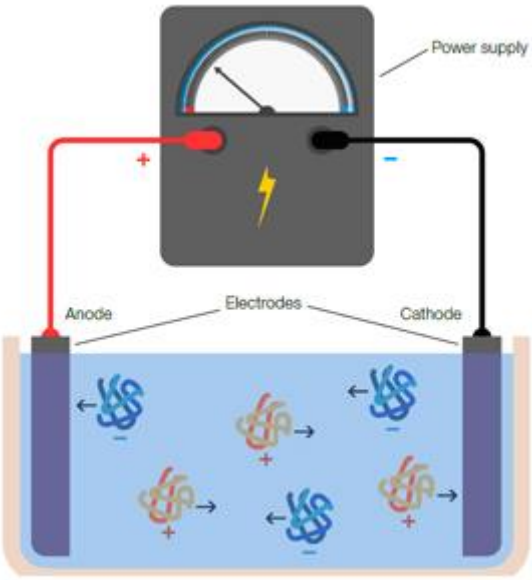

Figure 5.1: Example of ion migration during electrophoresis (Bio-Rad, 2014d).

To better understand the ways in which ions separate under electrophoretic conditions, a better knowledge of the underlying principles of electrophoresis is required. The electrical field applied in electrophoresis is often in volts and this creates what is known as a potential gradient, whereby a force is put upon the ions which causes their migration toward the electrodes (Walker, 2010). The potential gradient can be calculated as the applied voltage divided by the distance between the electrodes. As the ions migrate due to the force applied to them, there is a frictional resistance present which retards the ions migration. The frictional resistance is caused by a number of factors, including the hydrodynamic shape and size of the ions, the viscosity of the buffer and the relative pore size of the medium which the ions are travelling through (Gaál et al. 1980; Walker, 2010). The rate at which the ions migrate through the electrophoretic medium when an electrical field is applied is termed the electrophoretic mobility, which can be determined by the ratio of the ion velocity to the strength of the electric field. The combination of all these factors enable the separation of the ions based on their differences in electrophoretic mobility, which allows ions with similar charges to be separated if they vary in molecular size. This is due to each ion experiencing different frictional resistance (Walker, 2010).

The separation of ions via electrophoresis can be accelerated when the voltage of the electrical field is increased, which results in an increase in the flow of electrical current through the electrophoretic medium (Gaál et al. 1980; Walker, 2010). However, the increase

in voltage also results in the generation of heat which can have damaging effects on the ion separation. For example, increased heat can denature the sample being analysed, resulting in a broadening of separated ions and a reduction in the frictional resistance exhibited by the electrophoretic medium (Walker, 2010). When applying an electrical field to electrophorese ions it is important to ensure that the current of the voltage applied is constant, so that fluctuations in heat do not occur.

5.1.1.2 SODIUM DODECYL SULPHATE POLYACRYLAMIDE GEL ELECTROPHORESIS

The most commonly utilised method of electrophoresis in the analysis of proteins is sodium dodecyl sulphate polyacrylamide gel electrophoresis (SDS-PAGE), which separates complex mixtures of proteins based on their size (Bio-Rad, 2014d). This then enables molecular weight determination of proteins based on the migration distance and protein purification to be carried out. SDS is an anionic detergent which binds to and denatures proteins, giving them a net negative charge. The detergent breaks down the secondary and tertiary structures of the proteins by coating them, which results in the proteins opening up and forming a rod-like shape where the SDS molecules appear bound to the polypeptide chains (Figure 5.2) (Life Technologies, 2014; Walker, 2010). This SDS-bound protein is known as a SDS-protein complex.

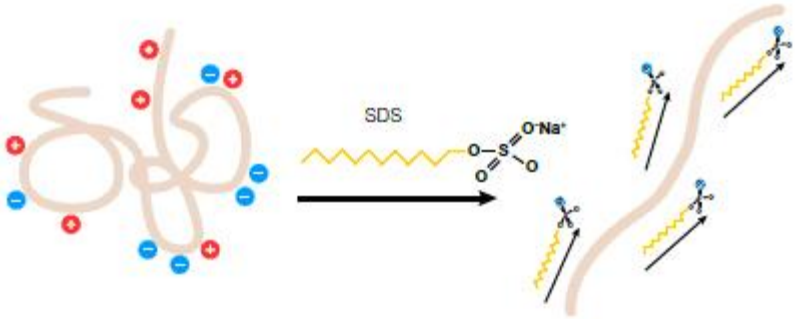

Figure 5.2: Break down of secondary and tertiary protein structures by SDS to form a rod-like shape protein-SDS complex (Bio-Rad, 2014d).

The SDS is added to the protein-containing sample in the form of a buffer, which is heated for approximately five minutes to fully denature the proteins. Often a reducing agent, such as β-mercaptoethanol, is added to the buffer to ensure all tertiary structures are broken by reducing any disulphide bonds that may be present (Walker, 2010). SDS molecules bind to proteins at an average of one SDS molecule to two amino acid residues, which equates approximately to 1.4 g of SDS to 1 g of protein. As a result, the charge-to-mass ratio of all the proteins within the sample is similar, therefore the distance migrated by each protein is based solely on the size of the molecules (Bio-Rad, 2014b; Walker, 2010). The sample buffer

also contains a tracking dye, such as bromophenol blue, to visualise the monitoring of the electrophoretic run, and glycerol or sucrose to give the overall sample enough density for it to settle into the base of the loading wells of the electrophoresis gel.

The electrophoretic medium utilised within SDS-PAGE is polyacrylamide gel which is formed by the polymerisation of acrylamide with small concentrations of N-N'-methylene-bisacrylamide (bis-acrylamide) in the presence of ammonium persulphate (APS) and catalyst N,N,N,N'-tetramethylenediamine (TEMED). As the name suggests, bis-acrylamide is two molecules of acrylamide linked by a methylene group and it is included in the gel to enable cross linking for polymerisation (Figure 5.3). The cross linking of bis-acrylamide and acrylamide produces a matrix that contains pores which allow the proteins to migrate through (Walker, 2010).

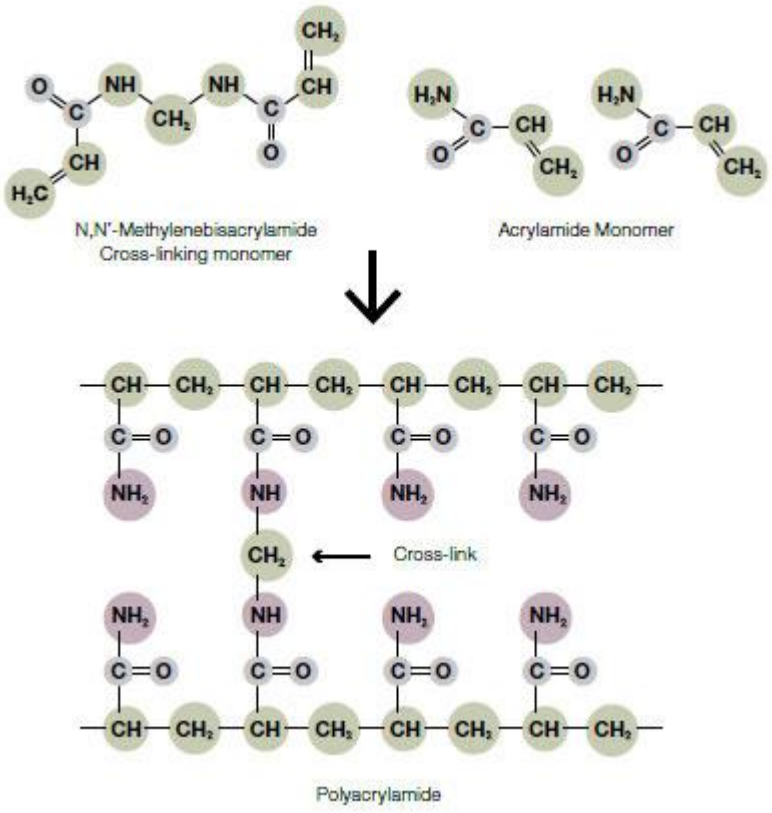

Figure 5.3: Cross linking of acrylamide and bis-acrylamide molecules to allow polymerisation (Bio-Rad, 2014c).

The size of the pores within a polyacrylamide gel depends on the percentage of acrylamide used. Higher percentages of acrylamide (e.g. 12%) produce gels containing smaller pores which are ideal for separating proteins of small molecular weights, whereas lower

percentages of acrylamide (e.g. 4%) produce larger pores in gels which are more appropriate to analyse proteins of larger molecular weights (Hayworth, 2014a). As proteins migrate through polyacrylamide gels, a sieving effect takes place whereby the smaller proteins that can pass through the pores easily will have a faster electrophoretic mobility than large proteins which cannot pass through the pores as easily (Walker, 2010).

Traditional polyacrylamide gels for SDS-PAGE are formed by pouring the polyacrylamide solution into a cassette consisting of two glass plates and a well comb, which can make up to 20 wells within the gel, depending on the size prepared (Bio-Rad, 2014b; Walker, 2010). To enable optimum separation of proteins, the polyacrylamide gel usually comprises of a stacking gel on top of a separating gel. The stacking gel has a lower acrylamide percentage than the separation gel, typically 7% acrylamide, as well as a lower pH and different ionic content. This enables the proteins to concentrate in to a tight band before entering the separation gel when under the influence of the electric field (Hayworth, 2014a). The tight band of protein-SDS complexes is formed due to the presence of glycinate ions in the electrophoresis buffer and chloride ions in the sample loading buffer and stacking gel buffer. An interface is created where the protein-SDS complexes lie in the middle. Glycinate ions have a lower electrophoretic mobility than the protein-SDS complexes, whereas the chloride ions have a higher electrophoretic mobility (Walker, 2010). However, in order for the current not to be broken, all the molecules must migrate at the same speed. This results in an adjustment of concentration across the three ionic species, whereby the chloride ion concentration is greater than the protein-SDS complex concentration, which in turn is greater than the glycinate ion concentration. As the interface migrates from the stacking gel into the separation gel, the higher pH causes the glycinate ions to become more ionised which increases their electrophoretic mobility (Walker, 2010). The protein-SDS complexes can then electrophorese at their own rate, separating into bands of molecules of the same size. Smaller proteins migrate faster than larger proteins due to the sieving effect and the frictional resistance of the gel (Walker, 2010).

Gradient polyacrylamide gels are an alternative electrophoresis medium that can be utilised in the separation of proteins. Instead of being composed of a separation and stacking gel of differing acrylamide percentages, gradient gels have low percentage acrylamide in the upper most part of the gel, where the sample are loaded. The lower part of the gel is composed of a higher percentage acrylamide (Hayworth, 2014a). The benefit of gradient gels is that the stacking and separation of proteins is carried out in one gel rather than two separate gels placed one on top of the other. However, gradient gels are notoriously difficult to prepare (Hayworth, 2014a). Precast gels for electrophoresis are now more routinely used than

traditional pouring gels as they can often be more cost effective and less time consuming. In addition, it also eliminates the requirement to handle acrylamide which is a suspected carcinogen and known neurotoxin (Hayworth, 2014a).

Once protein separation has been achieved by electrophoresis the proteins can be either blotted on to a membrane for Western blotting analysis, or visualised in order for further analysis, such as molecular weight determination, or protein identification to be carried out (Hayworth, 2014; Walker, 2010). Gel staining allows the proteins to be visualised based on a colour-producing chemical reaction occurring in areas containing protein. The most commonly utilised staining techniques for protein gels are Coomassie Blue, silver and fluorescent stains, although protein visualisation with stain-free technology is now a widely available alternative (Bio-Rad, 2014e). Coomassie stains are the most frequently applied protein staining technique following protein separation by gel electrophoresis (Hayworth, 2014b). Comprising of an acidic-methanol mixture, Coomassie stains fix proteins to the gel and produces a blue colour (Figure 5.4). The sensitivity of Coomassie staining is relatively good, with very faint bands of proteins visualised with Coomassie corresponding to approximately 100 ng of protein, although often, even greater sensitivity is required (Bio-Rad, 2014c; Walker, 2010).

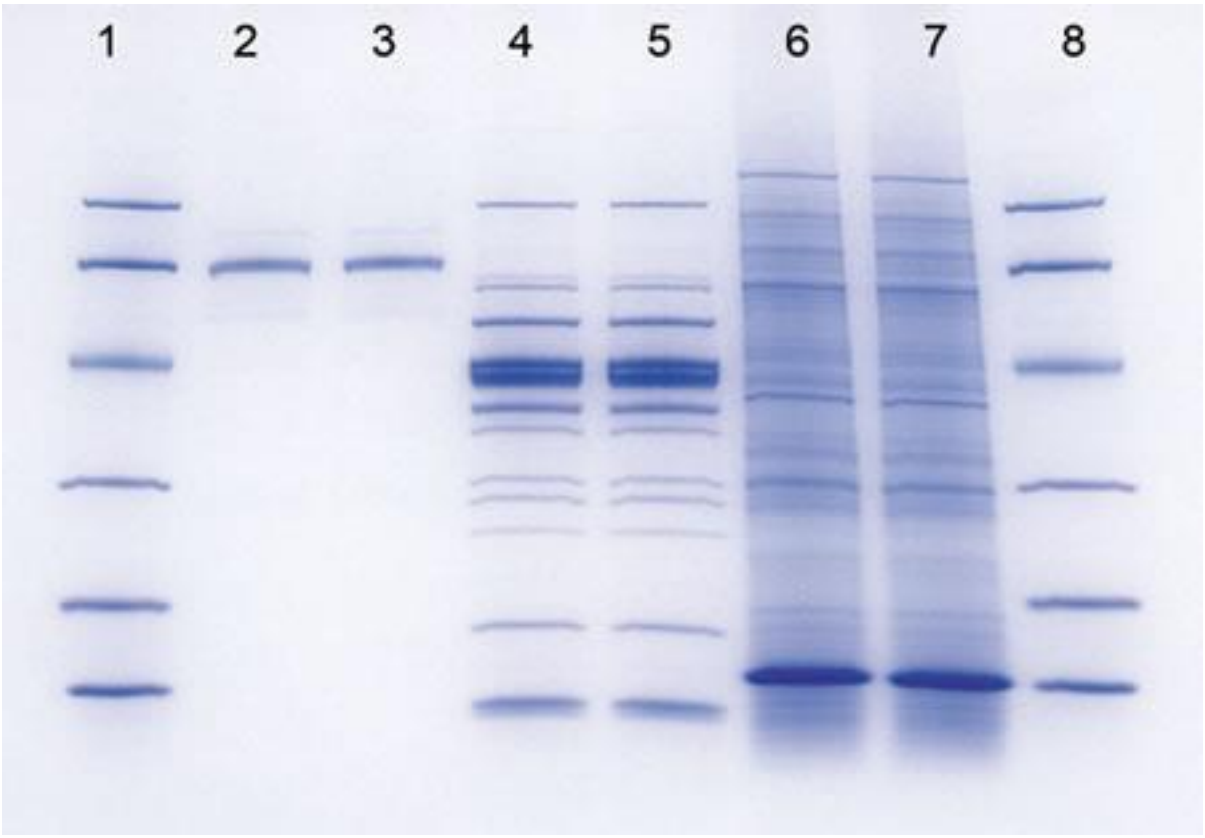

Figure 5.4: Example of separated proteins stained with a Coomassie dye (Bio-Rad, 2014b).

Silver staining offers 100-fold higher sensitivity than that of Coomassie, whereby metallic silver is deposited on to gel areas containing protein as a result of silver ions interacting with particular functional groups within the proteins (Hayworth, 2014b). This produces a dark band indicating the presence of proteins. However, silver staining protocols are more complex and time consuming than Coomassie staining techniques and frequently provide unreproducible results (Bio-Rad, 2014e). Recent technological advances in fluorescence detection have enabled the use of fluorescent staining as a technique to visualise protein patterns after electrophoretic separation. Fluorescent stains bind with proteins and offer a higher sensitivity than Coomassie stains, but lower than silver stains. However, the protocol of fluorescent staining is simple, reproducible and does not alter any of the protein constituents (Bio-Rad, 2014e; Hayworth, 2014b). Stain-free technology makes use of a trihalo compound present in stain-free precast gels which covalently binds to the tryptophan residues of proteins. The covalent bonds can then be visualised when the gel is examined under ultra-violet light with automated imaging and analysis systems (Bio-Rad, 2014e). Stain-free protein visualisation is advantageous as it is fast, has sensitivity superior to Coomassie staining and removes the requirement to destain the gel if further analysis is to be carried out. However, a major limitation of stain-free protein visualisation is that proteins that do not have tryptophan residues are subsequently not detected and therefore additional staining analysis may be required (Bio-Rad, 2014e).

5.1.1.3 ALTERNATIVE GEL ELECTROPHORETIC TECHNIQUES

SDS-PAGE is an electrophoretic technique that separates proteins based on their size. However, other variations of electrophoresis enable the separation of proteins based on their isoelectric point, mass-to-charge ratio, or a combination of isoelectric point and protein size. (Walker, 2010). Native polyacrylamide gel electrophoresis (PAGE) was the first documented technique of protein electrophoresis, which separates proteins based on their mass-to-charge ratio. Unlike SDS-PAGE, native PAGE utilises a sample buffer that contains no detergents or reducing agents, which allows the proteins to maintain their native charge in addition to preserving their biological activity, interactions and conformation (Bio-Rad, 2014d). Under the influence of an electric field, the proteins are free to migrate toward the electrode of their native charge. This is advantageous as proteins of the same molecular weight can be distinguished from one another, although unpredictable patterns of separation are produced with this analysis (Bio-Rad, 2014b; Walker, 2010).

Protein separation according to isoelectric point (p*I*), the point at which a migrating protein no longer carries an electrical charge, can be achieved with the electrophoretic technique

isoelectric focusing (IEF) (Crowe & Bradshaw, 2010). IEF differs from SDS-PAGE in that strip gels containing a pH gradient are the electrophoretic medium and only one sample can be run on each strip gel. The pH gradient of the strip gel can vary, although the most common format utilised is where one end of the gel has a high pH and the other has a low pH. When an electric field is applied to a gel containing a protein sample, the protein ions will migrate as normal towards the electrodes. However, as the proteins migrate, their electric charge adjusts according to the pH. When the proteins have reached the area of the gel where the pH matches the proteins p*I*, the protein will no longer hold an electrical charge and will therefore no longer be influenced by the electrical field and no further migration takes place (Bio-Rad, 2014b; Crowe & Bradshaw, 2010; Hayworth, 2014a). The p*I* of proteins varies, resulting in various proteins within a sample focusing at different isoelectric points across the pH gradient gel.

Once proteins have been separated by IEF, the same gel can be further separated by traditional SDS-PAGE. The combination of IEF and SDS-PAGE is termed as two-dimensional (2-D) gel electrophoresis, whereby proteins are separated by p*I* in the first dimension, followed by size separation in the second dimension (Walker, 2010). The strip gel is placed on to a polyacrylamide gel and SDS-PAGE is carried out as normal. This allows for proteins of the same p*I* but different molecular weight to be separated, providing a 2-D map corresponding to the proteins present within a sample (Bio-Rad, 2014a).

The separation of proteins by any of these gel electrophoretic techniques can then be visualised by gel staining where relative abundance and molecular weight determinations can be made, depending on the separation method. Following visualisation, proteins can then be excised from the gels to undergo further analysis such as chromatographic separation and identification with mass spectrometry, if required (Walker, 2010).

5.1.1.4 PROTEOMIC SEPARATION TECHNIQUES

Advances in technology have enabled the analysis of proteins to become more sensitive and accurate than traditional protein analysis methods. This technological advancement has led to the development of proteomics, which is the large scale, comprehensive identification of protein composition within biological materials (Tang et al. 2007). The most frequently utilised proteomic separation technique is mass spectrometry (MS) which is often coupled with chromatographic techniques such as gas chromatography (GC) or high performance liquid chromatography (HPLC) (Choudhury et al. 2013). MS is an analytical technique that separates molecules based on their mass to charge (*m/z*) ratio which can lead to protein

component identification. The fundamental components of a mass spectrometer are summarised in Figure 5.5.

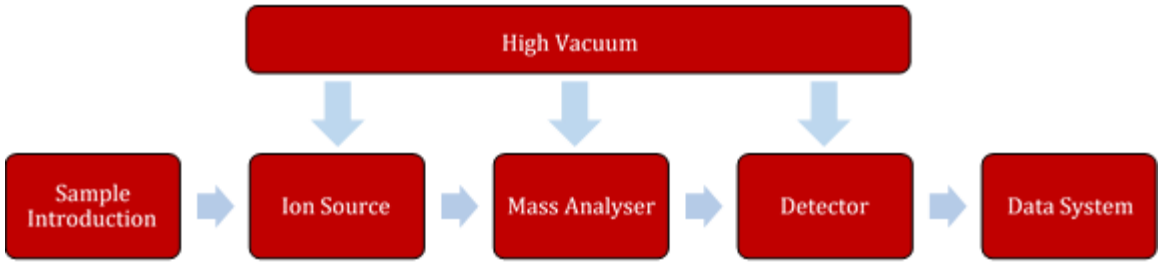

Figure 5.5: The fundamental components of a mass spectrometer.

When protein samples are introduced into the mass spectrometer, sample ionisation occurs to convert the sample into a gas phase which enables component separation and ion detection. For the analysis of proteins, two configurations of MS are commonly utilised for the ion source; namely electrospray ionisation (ESI) and matrix assisted laser desorption/ionisation (MALDI) (Aitken, 2010; Walsh, 2002). ESI ionises proteins by sampling a protein solution through a capillary-thin tube over a strong electrical field. This process generates a mist of protein solution, or spray, containing droplets of charged protein molecules, in which the solution is rapidly evaporated so that the sample can be fed through into the mass analyser (Aitken, 2010; Choudhury, 2013; Walsh, 2002). Protein ionisation with MALDI varies from ESI in that the protein sample is thoroughly mixed with a matrix consisting of UV absorbing organic acids. Upon drying, a laser is utilised to vaporise the matrix-protein complex into a gas phase. It is when the protein ions have been vaporised, either by ESI, MALDI or any other MS configuration, that the ions are accelerated towards the mass analyser. Here, the molecules are separated based on their *m/z* (Aitken, 2010; Choudhury, 2013; Walsh, 2002).

Like the ion source of the mass spectrometer, there are a number of different mass analysers available. However, for protein separation, particularly with MALDI, a time-of-flight (TOF) analyser is often adopted, which has the advantage of an almost unlimited mass range. This enables proteins to be separated with high accuracy, regardless of whether they are of low or high molecular weight (Aitken, 2010). TOF mass analysers record the time in which it takes for each ion to reach the detector. The TOF measurement is predominantly a reflection of the molecular mass of each ion as all of the protein ions have the same charge during their transition through the mass analyser to the detector. The smaller the protein ion, the less time it takes to reach the detector (Walsh, 2002). Once the ions have reached the detector, a signal is produced and retrieved by the data system to generate an output of the protein

sample composition in the form of a mass spectrum. This is a plot of the ion abundance detected at each *m/z* against time which can then be utilised to identify the protein components (Aitken, 2010; Walsh, 2002).

5.1.2 QUANTIFICATION

Quantification techniques are those that aim to determine the amount of molecules of interest that are present within a sample. In the analysis of proteins, quantification methods can be utilised to determine total protein yield or target-specific yield to ascertain the purity of a sample (Walker, 2010; Walsh, 2002). There are a number of different assays available to quantify protein samples for both total and specific protein targets, although here the focus will lie in total protein yield.

At present, there are two main techniques utilised to quantify total protein yield; namely absorption at 280 nm with UV light and the Bradford assay. The absorption of proteins at the wavelength 280 nm is performed with spectrophotometry in the ultra-violet region of the electromagnetic spectrum (Walker, 2010; Walsh, 2002). Proteins can be quantified at this wavelength based on the presence of aromatic amino acid residues tryptophan and tyrosine, which strongly absorb at 280 nm. The extinction coefficient, that is the strength of light absorption at a given wavelength by a constituent, varies amongst different proteins as the proportion of aromatic amino acids within proteins differ throughout a sample (Walker, 2010). However, it is possible to determine total protein yield as most proteins exhibit an extinction coefficient in the range of 0.4-1.5. If a sample were to produce an absorption reading of 1.0 when analysed at 280 nm with a pathlength of 1 cm, the protein concentration could be determined as being approximately 1.0 mg cm^{-3} (Walker, 2010). The main advantage of this technique is that is it non-destructive to the sample as no reagents are added when measuring the protein content under UV light. Protein concentration can be determined in yields as little as 10 µg cm^{-3}, demonstrating adequate sensitivity for most sample requirements. This sensitivity can be improved by analysing protein samples at 190 nm, where peptide bonds absorb UV light strongly. However, spectrophotometers tend to have low output when measuring at this wavelength and interference of sample buffers can occur, which are introduced to samples for protein extraction prior to quantification, as many absorb at this wavelength (Walker, 2010). A further limitation to quantification based on absorption at 280 nm is that nucleic acids also absorb at this wavelength, almost 10-fold greater than proteins. This can mask the protein concentration within a sample if high concentrations of nucleic acids are also present. It is possible to apply a correction factor,

although even relatively small numbers of nucleic acids present in a sample can mask any protein absorption (Walsh, 2002; Walker, 2010).

The Bradford assay is frequently adopted as the quantification method of choice when determining total protein yield. It is a colorimetric technique that makes use of Coomassie Brilliant Blue dye reagents to enable protein absorption measurements at 595 nm with spectrophotometry. The Bradford assay was first reported by Bradford in 1976 when it was observed that Coomassie G-250 Brilliant Blue reagent binds to proteins when exposed to acidic conditions (Bradford, 1976; Thermo Scientific, 2014). The Coomassie dye exists in three forms, each of which exhibits a different colour. Cationic Coomassie is reddish-brown in colour and has a maximum absorption at 470 nm, neutral Coomassie is green and the anionic form takes a blue colour with a maximum absorption at 610 nm (Bio-Rad, 2014b; Thermo Scientific, 2014). When the cationic Coomassie reagent binds to protein, the reagent converts to an unprotonated blue form which has a maximum absorption at 595 nm (Bio Rad, 2014). It is the basic amino acids within proteins in which the Coomassie reagent forms a bond, with the number of Coomassie molecules bound being proportional to the number of positive charges within the protein molecule (Thermo Scientific, 2014). The method itself is very simple and quick to perform. Protein concentrations are easily determined with the Bradford assay by production of a calibration curve from measurements at 595 nm of serially diluted known concentrations of a protein standard, such as bovine serum albumin (BSA) (Walsh, 2002). However, the limitations of the Bradford assay as a means of protein quantification are that interference can occur from chemical-protein and chemical-dye interactions and that low molecular weight proteins and free amino acids and peptides do not contribute to the dye colour change (Bio Rad, 2014; Thermo Scientific, 2014).

In addition to UV-light absorption at 280 nm and the Bradford assay, alternative protein quantification assays are available. These include the Lowry assay, a two-step colorimetric assay in which alkaline cupric tartrate-protein complexes are produced, which are then reduced and absorption is measured between 500-800 nm. In addition, the bicinchoninic acid (BCA) assay can also determine protein yield and works similarly to that of the Lowry assay, whereby a copper-protein complex is formed and subsequently reduced. Absorption at 562 nm is then carried out to enable protein determination (Sigma-Aldrich, 2014).

5.1.3 PREVIOUS APPLICATIONS WITH BODY FLUIDS

The analysis of proteins within biological forensic evidence does not routinely involve more than their detection with presumptive testing. However in biomedicine, large-scale analysis of the complete protein composition, or the proteome, of biological samples such as body fluids, tissues and cells has been well documented in recent years. This research has been undertaken in the quest to identify potential protein components that could act as biomarkers for disease by comparing the proteome of healthy samples with diseased samples (Haudek et al. 2009). Traditional protein analysis methods make use of separation via electrophoresis and protein identification with Western blotting or ELISA, where specific proteins can be detected. However, as technology has evolved, more sensitive and discriminatory techniques, such as MALDI-TOF MS, have been investigated which are not protein specific in their application but can identify the numerous proteins present within a sample. There is a plethora of literature spanning the proteomic analysis of cells and tissues for various different diseases (Ahram & Petricoin, 2008; Coon et al. 2008; Srinivas et al. 2002). However, in keeping with the focus of this research, the particular interest of proteomics and older protein analyses lie in their application to blood, saliva, semen and vaginal secretions.

Table 5.1 provides an overview of some of the various techniques employed to examine the protein components of human body fluids and the number of proteins identified by each research group. Blood, particularly blood serum, has been documented as an ideal body fluid to examine potential biomarkers of disease as it circulates the entire human body and therefore has contact with many different tissues (Haudek et al. 2009). It is possible that changes in protein abundance due to disease could be detectable with proteomic analyses and therefore lead to clinical diagnosis. Haudek et al. (2009) suggested that if the proteins expressed in specific fluids, tissues and cells in healthy samples were known, disease marker assignment and detection interpretation could be easier. To demonstrate this, Haudek et al. (2009) documented the comparative analysis of the most abundant proteins within whole blood using two independent methods; two dimensional (2-D) electrophoresis and mass spectrometry (MS) to identify the protein patterns and constituents respectively, and "shotgun" proteomics, which involves chromatographic separation incorporated into the mass spectrometry procedure (Haudek et al. 2009). In total, 1174 protein constituents were identified between the two techniques. However, a large number of proteins were identified as isoforms of the same protein or were present in many different constituents within blood and other cell types. This would make biomarker assignment more difficult as the specificity of detection would decrease. To overcome this, Haudek et al. (2009) compared the proteomic

profiles of all the protein constituents identified within whole blood to those of other known cell types and identified that 14 proteins were specifically expressed by neutrophils, 13 specifically by platelets, 9 specifically by erythrocytes and lymphocytes, independently, and 6 proteins expressed specifically by monocytes.

Table 5.1: Overview of proteomic research carried out with body fluids.

Body Fluid Sample	Technique Utilised	Number of Proteins Identified	Reference
Blood serum	SCX chromatography & µLC-MS/MS	341 (low molecular weight)	Tirumalai et al. (2003)
Peripheral blood mononuclear cell microsomes	SDS-PAGE & MS	361	Nicholson et al. (2005)
Blood serum	MALDI-TOF MS	Not stated	Huleihel et al. (2005)
Peripheral blood	2-D Electrophoresis & "Shotgun proteomics" with MS	1174	Haudek et al. (2009)
Saliva	SDS-PAGE	34	Schwartz, Zhu, & Sreebny (1995)
Saliva	2-D Electrophoresis & MS	101	Ghafouri, Tagesson, & Lindahl (2003)
Saliva	2-D Electrophoresis & MS	26 & 10, respectively	Huang (2004)
Saliva	2-D Electrophoresis & MALDI-TOF-TOF MS/MS	90	Vitorino et al. (2004)
Saliva	SDS-PAGE & LC-MS/MS & SELDI-TOF MS	218	Esser et al. (2008)
Seminal fluid	2-D Electrophoresis	Not stated	Edwards, Tollaksen, & Anderson (1981)
Seminal fluid	SDS-PAGE & 2-D Electrophoresis, MALDI-TOF MS & LC-MS/MS	100+	Fung et al. (2004)
Seminal fluid	SDS-PAGE & LC-MS/MS/MS	923	Pilch & Mann (2006)
Vaginal secretions	SDS-PAGE	4	Itoh & Manaka (1988)
Cervico-vaginal fluid	2-D Electrophoresis, MALDI-TOF MS & capillary LC-ESI MS/MS	15	Di Quinzio et al. (2007)
Cervico-vaginal fluid	SDS-PAGE, SCX chromatography, MS & ELISA	685	Shaw, Smith, & Diamandis (2007)
Cervico-vaginal fluid	2-D Electrophoresis & MALDI-TOF MS	147	Tang et al. (2007)

The identification of blood cell specific proteins highlights their usefulness as biomarkers which could enable protein abundance monitoring in relation to disease (Haudek et al. 2009). Of the two techniques explored, shotgun proteomics yielded higher sensitivity and specificity in protein detection and identification than separation with 2-D electrophoresis followed by MS. This is due to many of the protein spots separated with 2-D electrophoresis belonging to the same constituent, therefore only a limited number of differentially expressed proteins were identified (Haudek et al. 2009).

Tirumalai et al. (2003) also investigated the protein composition of blood, but to a much more specific scale. The low molecular weight proteins present in blood serum were determined by strong cation exchange chromatography (SCX) with micro-capillary reversed phase liquid chromatography coupled to on-line electrospray ionisation tandem MS (μLC-MS/MS). By removing the high molecular weight proteins, such as albumin and the immunoglobulins, Tirumalai et al. (2003) suggested that protein composition of serum could hold important histological information that could be utilised in the diagnosis of disease. The ultrafiltration of the high molecular weight proteins in blood serum demonstrated that 341 low molecular weight proteins could be identified and categorised based on their functional class. This large number of low molecular weight proteins contributes only 1% of the entire protein content of blood serum and demonstrates the potential biomarkers that may have been masked in previous methods (Tirumalai et al. 2003). The sensitivity of the proteomic techniques applied by Tirumalai et al. (2003) is evident in the number of low molecular weight proteins identified, but also in that no albumin peptides or isoforms were detected. As albumin contributes to approximately 50% of the protein content in serum, these findings demonstrate the accuracy of the proteomic methods adopted.

As stated in Section 2.1.2, saliva is often sought after as an alternative body fluid to clinically test for the detection and diagnosis of disease. Therefore, it is not surprising that extensive proteomic analysis has been conducted on saliva as a means to characterise the protein content and determine biomarkers appropriate for the monitoring of disease. As saliva is typically comprised of 99% water, highly sensitive methods are required to determine the protein constituents. Vitorino et al. (2004) examined the protein composition of whole saliva with 2-D electrophoresis separation followed by MALDI-TOF-TOF MS/MS identification. Over 200 proteins spots were obtained from 2-D electrophoresis, of which 100 were excised for MALDI-TOF-TOF MS/MS analysis. Ninety five percent of the excised proteins were successfully identified, including twelve proteins that had not been formally identified in saliva previously (Vitorino et al. 2004). As seen in the blood protein identification findings, a number of the excised protein spots identified were attributed to the same protein due to the

various isoforms present as a result of post-translational modifications (Vitorino et al. 2004). This was also reported by Huang (2004), whereby of 202 protein spots separated by 2-D electrophoresis, 54 were excised and analysed by MS only and these could be attributed to just 26 individual proteins.

Esser et al. (2008) developed on the findings of Huang (2004) and Vitorino et al. (2004) by examining the protein composition of saliva and assessing the stability of salivary proteins at room temperature over four hours. The techniques employed were surface-enhanced laser desorption/ionisation time of flight MS (SELDI-TOF MS), which enabled comparative protein profiling to be conducted, and traditional SDS-PAGE with LC MS/MS. The findings reported that over 200 proteins were identified, all of which were successfully identified with at least 95% confidence (Esser et al. 2008). Additionally, differences in protein abundance were observed in the MS spectra between samples of zero hours up to four hours. In particular, 11 peptides were seen to decrease in intensity across the spectra spanning 0-4 hours and is thought to be a result of protein degradation. Three peptides were observed to increase over the 4 hour period, suggesting these are breakdown products of protein degradation (Esser et al. 2008). It is evident that the more sensitive MS method utilised, the more proteins can be successfully identified and characterised. Additionally, fluctuations in protein abundance can also be detected in the protein profile of saliva sample. The similarity in the findings reported by Esser et al. (2008), Huang (2004) and Vitorino et al. (2004) demonstrates the reproducibility and reliability in the 2-D electrophoresis and MS techniques in the proteomic analysis of saliva.

The proteomic composition of semen is often examined to identify any reproductive organ specific diseases or fertility issues. The importance of understanding the proteome of healthy semen, or seminal fluid is demonstrated by Fung et al. (2004) and Pilch & Mann (2006), who both reported comprehensive protein characterisations of human seminal fluid. Fung et al. (2004) explored the proteome of seminal fluid to identify potential biomarkers specific to prostate cancer. The analytical techniques employed were separation with 2-D electrophoresis and MALDI-MS, and 1-D electrophoresis and electrospray ionisation (ESI) MS for the detection of proteins that could not be resolved with 2-D electrophoresis. The results obtained from both methods demonstrate that over 100 unique protein constituents, including isoforms were identified in seminal plasma. This allows for future biomarkers to be established based on the proteomic map of seminal plasma. The results documented by Pilch & Mann (2006) vary significantly, as over 900 seminal fluid proteins were identified and their relative abundance indicated by the number of peptides identifying particular proteins. The techniques utilised by Pilch & Mann (2006) were 1-D electrophoresis followed by LC-

MS/MS/MS. In addition to the large number of proteins identified, the subcellular location could be determined in 52% of the known proteins, of which 78% were assigned as cellular proteins and 25% as secreted proteins. Alongside this, the identified proteins could also be characterised by their function within seminal plasma. The depth of seminal proteome characterisation reported by Pilch & Mann (2006) demonstrates the high sensitivity of proteomic techniques and how it is possible to identify not just the proteins present within a sample, but also the functions and subcellular locations of these proteins. In comparison to the data obtained by Fung et al. (2004), Pilch & Mann (2006) identified many more proteins within seminal fluid, although direct comparisons cannot be made as different MS techniques were adopted by each research group. However, these articles do demonstrate the lack of consistency in the way in which proteomic analyses are carried out.

As mirrored by the proteomic analysis of blood, saliva and seminal fluid, the techniques employed to characterise human cervico-vaginal fluid (CVF) proteins and the number of successful protein identifications also vary between research groups. Di Quinzio et al. (2007) investigated the proteomic map of CVF in pregnant women and observed variation in the proteins maps produced with 2-D electrophoresis. A total of 157 protein spots were observed as being common to all the CVF samples obtained and only a proportion of the most abundant proteins were analysed further with MALDI-TOF MS and capillary LC-ESI-MS/MS (Di Quinzio et al. 2007). Proteomic analysis successfully identified 21 proteins, 6 of which were protein isoforms, which represented various functions and subcellular locations. Tang et al. (2007) took a different approach to Di Quinzio et al. (2007) by comparing the proteome of the CVF from healthy, non-pregnant women and CVF from women infected with the yeast infection, *Candidiasis*. Two-dimensional electrophoresis and MALDI-TOF MS yielded 147 successful protein identifications from 192 protein spots in CVF from healthy women. A total of 59 distinct proteins were established from this analysis (Tang et al. 2007). When the protein maps were compared to the maps produced from CVF samples of infected women, no observable differences were found, which suggests that *Candidiasis* did not cause a change in protein abundance in CVF. Based on the findings reported by Tang et al. (2007), the knowledge of the proteome of CVF is better understood and clinicians are aware that diagnosis of *Candidiasis* is not appropriate by proteomics. Again, it can be seen that different proteomic techniques yield different results in the number of proteins visualised and identified.

Based on the literature discussed and the information in Table 5.1, it can be seen that the initial technique utilised to separate the samples is electrophoresis. Predominately, 2-D gel electrophoresis is utilised to enable the separation of proteins by isoelectric focusing in the

first dimension, followed by molecular weight in the second dimension. However, many authors have stated that 2-D electrophoresis is not always appropriate as proteins that are too basic, too acidic or hydrophobic are often not resolved and therefore not detected, preventing further analysis being carried out on these proteins (Fung et al. 2004; Pilch & Mann, 2006). In these instances traditional SDS-PAGE, which is often referred to as 1-D electrophoresis, is utilised and is able to yield large numbers of proteins which can be taken on for further analysis. The incorporation of further analytical techniques, such as MALDI-TOF MS and LC-MS/MS, often requires elaborate purification and sample preparation methods before the proteins can be specifically identified. Fortunately, the purification and sample preparation is carried out directly on excised gel fragments, therefore the original sample may not be exhausted by this type of analysis.

However, proteomic analyses are expensive and time consuming to carry out. Additionally, there is no standard method to ensure reproducible and accurate results from the same sample type. There is a clear lack of consistency in proteomic methodology to enable its implementation into routine operating procedures for biomedicine or indeed forensic investigations. From a forensic perspective, the level of sensitivity required to differentiate between body fluid samples does not need to be at the same level as that required for diagnostic purposes, as the differentiation of individual isoforms of all the proteins present are not necessary. In fact, as many proteins are common between blood, saliva, semen and vaginal secretions, the degree of sensitivity exhibited by techniques such as MALDI-TOF MS could lead to false positive results during attempted identification. A method that can be utilised to identify body fluids from one another and has the potential to determine the age, or time since deposition, of body fluid stains ideally should be as straightforward and cost effective as possible. Electrophoretic analysis by gel has demonstrated these characteristics, in addition to providing the essential first step to enable proteomic analysis to be carried. Therefore, it has the potential for appropriate application within the forensic analysis of body fluids in order to establish the body fluid source or sample age.

5.2 MATERIALS & METHODS

Samples of human blood, saliva, semen and vaginal secretions were utilised within this aspect of the research. The sample collection and storage methods were carried out in the same manner as samples utilised within the FTIR spectroscopic analysis (Section 2.2.1).

5.2.1 SDS-PAGE

Protein extraction was carried out directly on neat body fluid samples or on the water-extracted body fluid samples, from the FTIR spectroscopy analysis with 1% sodium dodecyl sulphate (SDS). Three hundred microliters of 1% SDS was added to each sample which were then vortexed for one minute, followed by incubation at 90°C for five minutes. Micro-centrifugation was then carried out at 14,000 rotations per minute (rpm) for 15 minutes, where the supernatant from each sample was aliquoted into a fresh, sterile Eppendorf tube and the pellet discarded.

In fresh Eppendorf tubes, 5 µl of Laemlli 2x SDS-PAGE buffer with 5% β-mercaptoethanol was aliquoted and 5 µl of sample extract was added then mixed thoroughly with a pipette. All samples were then micro-centrifuged at 14,000 rpm for thirty seconds.

Gel electrophoresis was carried out utilising the Mini-PROTEAN® Tetra System (BioRad, California) and PowerPac™ Basic Power Supply (BioRad, California). Precast Mini-PROTEAN® TGX Stain-Free™ 12 well, any kDA, polyacrylamide gels (BioRad, California) were placed into the analysis chamber prior to sample loading on the gels. The analysis chamber was filled with 1x running buffer, ensuring that the buffer was poured directly over the gels, washing them *in situ* until the chamber was full. The Mini-PROTEAN® Tetra System tank was then filled to the desired marker, depending on whether one-two gels, or three-four gels were to be run.

Eight microliters of prepared sample were loaded on to the precast gels alongside unstained Precision Plus Protein™ molecular weight size standards (BioRad, California). All samples were run at 100 volts for one hour and 10 minutes and then visualised on a stain free sample imaging tray with the Gel Doc EZ Imager and Image Lab v4.0 software (BioRad, California).

5.2.2 BRADFORD ASSAY

Total protein yield from each extracted sample was determined with the Coomassie Plus protein (Bradford) assay kit and spectrophotometry. Bovine serum albumin (BSA) standard protein was utilised to prepare standard (Table 5.2) and micro (Table 5.3) dilution series tests in order to measure the protein absorption at 595 nm with a BioChrom WPA BioWave II UV/Vis spectrophotometry (BioChrom, Massachusetts).

Table 5.2: Bradford assay standard test BSA dilutions.

Tube	DiH_2O Volume (µl)	Volume & Source of BSA (µl)	Final BSA Concentration (µg/ml)
A	0	300 – stock	2000
B	125	375 – stock	1500
C	325	325 – stock	1000
D	175	175 – tube B	750
E	325	325 – tube C	500
F	325	325 – tube E	250
G	325	325 – tube F	125
H	400	100 – tube G	25
I	400	0	0

Table 5.3: Bradford assay micro test BSA dilutions.

Tube	DiH_2O Volume (µl)	Volume & Source of BSA (µl)	Final BSA Concentration (µg/ml)
A	2370	30 – stock	25
B	4950	50 – stock	20
C	3970	30 – stock	15
D	2500	2500 – tube B	10
E	2000	2000 – tube D	5
F	1500	1500 – tube E	2.5
G	5000	0	0

The Bradford assay standard test was utilised for blood samples and the micro test was utilised for saliva, semen and vaginal secretions samples. A ten-fold dilution of 100 µl sample extract to 900 µl diH_2O was first prepared for each SDS-extracted sample. For the standard test, 50 µl of prepared standard or sample was aliquoted into individual sterile test tubes, followed by 1.5 ml of Coomassie Plus reagent which was thoroughly mixed with a pipette. For the micro test, 1.0 ml of standard or sample was aliquoted into individual sterile test tubes with 1.0 ml of Coomassie Plus reagent. All standards and samples were then incubated at room temperature for ten minutes. One millilitre of each standard and sample was aliquoted into sterile plastic cuvettes, ready for spectrophotometric measurement. An initial blank measurement was carried out with a water filled cuvette at the protein absorption wavelength (595 nm). All standards and samples were measured in replicates of three at this wavelength and the measurement reading recorded.

5.2.3 STATISTICAL TOOLS

All statistical analysis of data was carried out with Microsoft Excel. Linear regression analysis was utilised in order to establish whether there was a correlation between body fluid stain age and protein concentration.

5.3 RESULTS & DISCUSSION

5.3.1 SDS-PAGE

FORENSIC BODY FLUID IDENTIFICATION & AGE DETERMINATION

Sodium dodecyl sulphate polyacrylamide gel electrophoresis (SDS-PAGE) is a well-established analytical method utilised for the denaturation and separation of proteins. As separation occurs purely on a molecular weight basis, lanes of bands are detectable which indicate the relative molecular weight and abundance of the proteins within each band (Hayworth, 2014).

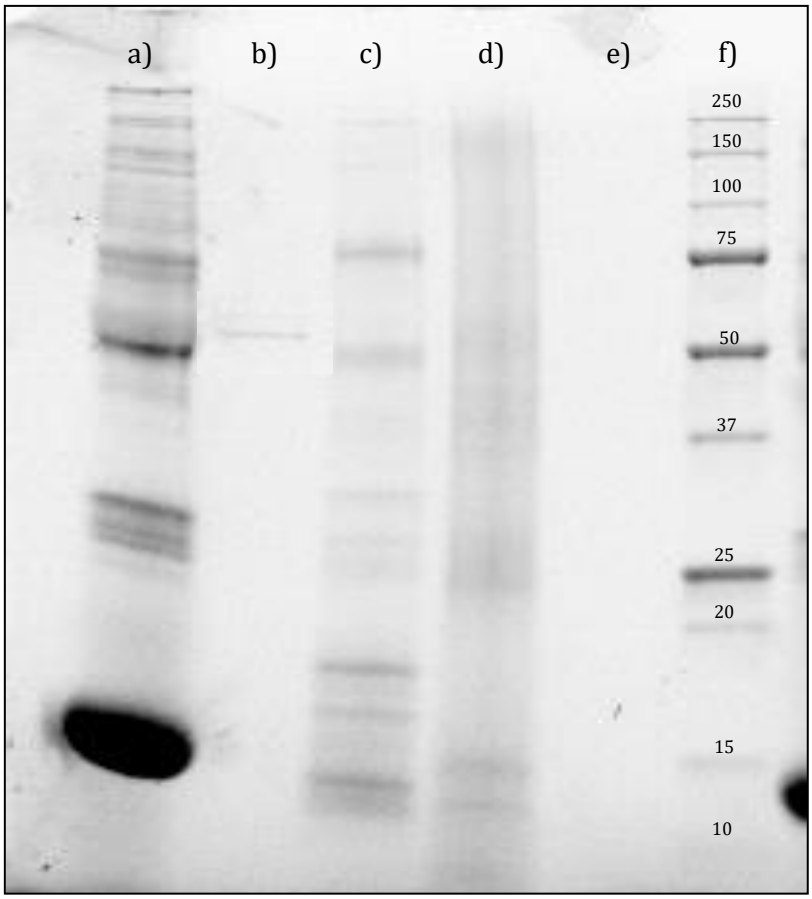

Figure 5.6: SDS-PAGE separation of neat body fluids; a) blood, b) saliva, c) semen, d) vaginal secretions, e) negative control, f) protein size standard with molecular weights (kDa).

Analysis of blood, saliva, semen and vaginal secretions utilising protein separation by SDS-PAGE was conducted in order to determine whether the separation patterns enabled differentiation between each body fluid. Visualisation of the electrophoresed gels with stain-free technology enabled the detection and identification of proteins present within each body fluid based on the distance migrated by each protein band. Figure 5.6 demonstrates the

separation patterns observed for the four body fluids examined and it is evident that each of the body fluid samples produced very different separation patterns.

Of the four body fluids, blood exhibited the most detailed and distinct separation of proteins, with approximately 13 individual bands detected, whereas only two very faint bands were observed in saliva. The neat semen exhibited more visible bands than saliva, with approximately seven bands that appeared faint with some smearing. In contrast, the vaginal secretions separation appears as one large smear, with only two distinct, but faint bands observed at the bottom of the gel. It is evident from the electrophoretic separation that each of the body fluids exhibited different protein separation patterns and as a result, it was possible to differentiate between blood, saliva, semen and vaginal secretions. The distance travelled by each of the bands enabled the molecular weight (kDa) of each protein band to be determined, which were then compared with the molecular weights of proteins specific to, and/or abundant within each of the body fluids (Osborne & Brooks, 2006). Table 5.4 demonstrates the approximate molecular weights determined for each of the bands observed within the four body fluids.

Table 5.4: Approximate molecular weights of the protein bands separated in blood, saliva, semen & vaginal secretions by SDS-PAGE.

Band No.	Blood (kDa)	Saliva (kDa)	Semen (kDa)	Vaginal Secretions (kDa)
1	150	72	94	13
2	137	70	62	10
3	133	-	36	-
4	115	-	31	-
5	109	-	17	-
6	74	-	14	-
7	68	-	11	-
8	51	-	-	-
9	44	-	-	-
10	28	-	-	-
11	24	-	-	-
12	23	-	-	-
13	9	-	-	-

5.3.1.1 BLOOD

The most abundant proteins present in blood are typically haemoglobin and albumin, although there are a plethora of other proteins that contribute to the plasma and cellular composition of blood (Moore et al. 2010). Upon inspection of the blood separation in Figure 5.6a, the position of bands from the top of the gel demonstrated a smaller migration than the largest molecular weight (250 kDa) of the protein size standard (Figure 5.6f). This would ordinarily suggest that the molecular weights of these bands were likely to be approximately ≥200 kDa, therefore, bands 1-5 (Figure 5.6 & Figure 5.7) could be attributed to proteins fibrinogen (340 kDa), spectrin (220-240 kDa) and ankyrin (200 kDa) (Mordacq & Ellington, 1994). However, the blood separation observed in this gel (Figure 5.6a & 5.7) exhibited a curve on the bands which caused the migration distance to be shorter than typically observed in the separation of blood. Comparisons with blood separations that did not exhibit this "smile" effect on other gels demonstrated that the overall distance migrated between the first and last bands was consistent (9.5 cm). Consequently, the molecular weights exhibited by bands 1-5 of the blood can confidently be identified as those stated in Table 5.4.

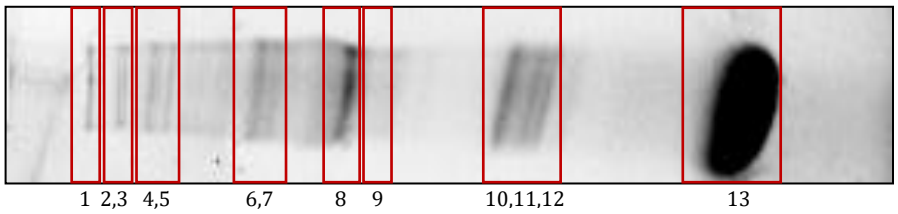

Figure 5.7: Band assignment of the protein separation pattern observed in neat blood.

The molecular weight of band 1 was consistent with that of immunoglobulins, which have molecular weights ranging from 150-190 kDa (Mordacq & Ellington, 1994). Bands 2, 3 and 5 of the blood separation pattern, with molecular weights of 137, 133 and 109 kDa could not be identified. Band 4 was identified as erythrocyte cytoplasmic protein ubiquitin-activating enzyme, which has an approximate molecular weight of 117 kDa (Kakhniashvili et al. 2004). In between bands 5 and 6 there appeared to be a smear in the gel lane, although no distinct bands were observed. This could be due to unseparated proteins present or an overload of protein within the sample (Vincini, 2010). Bands 6 and 7 were representative of molecular weights 74 and 68 kDa, which correlate with the molecular weights of prothrombin and transferrin (band 6) and albumin (band 7), all of which are key proteins within human serum (Mordacq & Ellington, 1994). Band 8 was one of the most distinct bands within the blood separation, representing a molecular weight of 51 kDa. This band was also identified as a plasma protein involved in the coagulation of blood and known as coagulation factor IX, or Christmas factor (Schenk et al. 2008).

The molecular weight of band 9 was 44 kDa and was the least observable across the blood protein separation due to consistently weak band intensity. This band could be identified as actin, a key protein in the cytoskeleton of erythrocytes (Mordacq & Ellington, 1994). Band 10 was representative of glycophorin (28 kDa), a main erythrocyte membrane protein (Mordacq & Ellington, 1994; Tayyab & Qasim, 1988). It has also been reported that albumin has an isoform with a molecular weight of 28 kDa, therefore band 10 may also comprise of this plasma abundant protein (Kshirsagar et al. 1984). The molecular weight of bands 11-13 were 24, 23 and 9 kDa, which could not be identified based on the literature of known proteins within blood. Haemoglobin (Hb) has a total molecular weight of approximately 65 kDa, although its alpha and beta chains have individual molecular weights of approximately 15 kDa each (Hill et al. 1962; Sun & Palmer, 2008). Therefore it was anticipated that a distinct band within the low molecular weight end of the gels would be detected as haemoglobin accounts for 75% of erythrocyte cytoplasmic protein (Kakhniashvili et al. 2004; Mordacq & Ellington, 1994). However, no such band was observed that corresponds with the Hb protein molecular weight. Band 13 was the most distinct and broad of all the bands and comprises of the low molecular weight proteins (≤10 kDa) present within blood. Due to the density and broadness of the band, identification of specific proteins was not possible.

The electrophoretic pattern observed within the neat blood was similar to that reported by Mordacq & Ellington (1994) who stated that approximately 10 protein bands were observed in the SDS-PAGE analysis of erythrocytes. A total of 13 bands were observed across the blood separations, which exhibited similarities in identification from both plasma and membrane proteins reported by Mordacq & Ellington (1994) with SDS-PAGE, but also with more in depth proteomic studies (Schenk et al. 2008).

As body fluids encountered at crime scenes are often recovered as stains, it was necessary to determine whether SDS-PAGE could be applied to bloodstains on cotton. A total of 35 bloodstains on cotton aged from 24 hours to 7 days were analysed with SDS-PAGE and the electrophoretic patterns observed were comparable with those obtained from blood samples (Figure 5.8). The aged bloodstain samples were extracted from the cotton substrate with the water extraction method stated in Section 2.2.2.1 prior to SDS-PAGE. The most noticeable difference in the protein separation of the extracted aged bloodstains was the decrease in band distinction compared to the blood separation. This was anticipated due to the bloodstain being recovered and effectively diluted as a result of the extraction, therefore the samples were not of the same purity or concentration as blood samples. However, it was evident that the overall separation pattern expected from blood was produced. Smearing across the sample lanes contributed to the decrease in band distinction which made band

identification more difficult. As a result, only nine protein bands could be distinguished. Comparison of the molecular weights determined from the extracted bloodstains and the blood demonstrated that six of the bands could be attributed to the same proteins; namely immunoglobulins (highlighted in dark red), fibrinogen (dark blue) (Schenk et al. 2008), albumin (blue), glycophorin/albumin isoform (light green) and the low molecular weight proteins (yellow). Bands corresponding to molecular weights of 150, 133, 115, 109, 74, 68, 51 and 44 kDa were not observed within the extracted bloodstains samples, but were in the blood. This may be a result of protein degradation, causing a change in the protein molecular weight due to amino acid and peptide chain breakdown (Cooper, 2000).

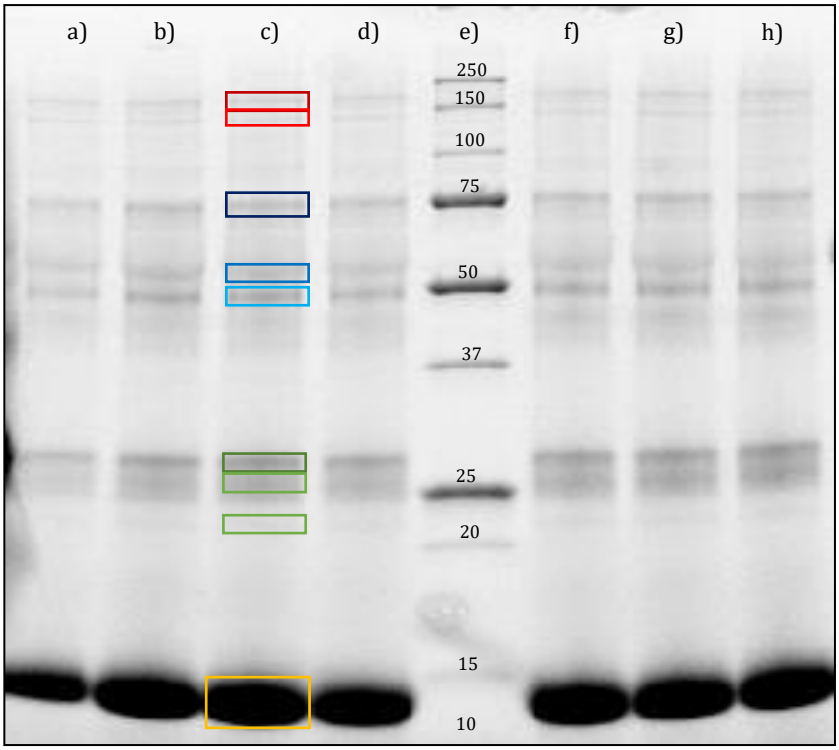

Figure 5.8: Example of the electrophoretic pattern produced from bloodstain extracts from stains aged 24 hours to 7 days when analysed with SDS-PAGE with specific protein bands highlighted; a) 24 hours, b) 48 hours, c) 3 days, d) 4 days, e) size standard with molecular weights (kDa), f) 5 days, g) 6 days & h) 7 days.

Despite the small differences in molecular weights within the protein bands, the separation pattern exhibited by SDS-PAGE analysis was similar to that of blood and therefore it was possible to determine the extracted bloodstain samples as blood. It was anticipated that differences in molecular weight were observed between the blood and extracted bloodstains, particularly within the high molecular weight proteins, which migrate much slower through the polyacrylamide gel that those of a lower molecular weight. If electrophoretic running time, gel porosity and voltage were not constant for all gels analysed, the migration, and

subsequent separation and resolution of proteins bands will vary between gels, giving rise to differences in distance migration and molecular weight calculations.

Despite the variation in molecular weight amongst the neat and extracted bloodstains, the protein separation patterns observed amongst the different aged samples were consistent for the 24 hours to 7 day aged bloodstains (Figure 5.8). The only observable difference amongst the aged samples was evident in the 24 hour samples, which demonstrated the least visibly distinct separation pattern in comparison to the other aged bloodstains. Little variation was exhibited in the separation patterns of the aged bloodstains, and as a result it was not possible to distinguish between the seven different bloodstain ages examined. However, the consistency in the bloodstain protein separation pattern demonstrates the reproducibility of SDS-PAGE as a method to enable the identification of blood.

5.3.1.2 SALIVA

The protein separation of saliva exhibited the least amount of protein bands amongst the four body fluids analysed, as only two bands were evident in the saliva samples (Figure 5.6b). The distinction of these bands varied dependent on the volume of saliva utilised for SDS-PAGE analysis; the greater volume of saliva analysed, the more distinct the bands appeared to be (Figure 5.9). Samples of varying volumes of neat saliva (20 µl to 1 ml) were SDS extracted and then analysed to determine the limit of detection in obtaining protein separation that was clearly visible. Clear band distinction was achieved for all volumes of saliva analysed in this instance, whereby two very distinct protein bands and a third faint band were observed within the SDS-PAGE gels (highlighted in Figure 5.9). The molecular weights of the two distinct bands observed were 72 and 70 kDa, which do not compare to the molecular weights of the most abundant proteins predominantly found in saliva; α-amylase and lysozyme. These proteins in saliva that are frequently utilised in saliva detection, have molecular weights of 46-60 and 14 kDa, respectively (Huang, 2004; Schenkels et al. 1995; Silletti et al. 2010), which vary greatly from the bands observed in the saliva separation. Comparisons with the molecular weights of other saliva abundant proteins, such as extra parotid glycoprotein (18-20 kDa), also confirmed that the two distinct bands observed in saliva samples were not attributable to the most common proteins within saliva (Schenkels et al. 1995). However, the 72 and 70 kDa protein band doublet was identified as heat shock protein 70 (HSP70/HSPA) and secretory IgA, which have molecular weights within this small range and both have roles within the immunity defence of the oral cavity (Fábián et al. 2012; Schenkels et al. 1995).

The faint band observed at the bottom of the gel had a molecular weight of 11 kDa and comparisons with literature demonstrate that this molecular weight is consistent with

cystatins, particularly Stefins A and B within saliva (Castagnola et al. 2011; Tang et al. 2007). These proteins acts as inhibitors to cysteine proteases within a number of human body fluids, and within saliva these proteins specifically inhibit lysozymal proteases (Baron et al. 1999). The protein composition of saliva has been reported by a number of research groups, of whom have stated that many proteins are detectable with protein-based analyses (Ghafouri et al. 2003; Huang, 2004; Schenkels et al. 1995; Silletti et al. 2010; Vitorino et al. 2004). The protein separation patterns exhibited here do not correlate with these findings and a possible explanation for this is that glycoproteins and mucins, particularly of high molecular weights, precipitate and create a blockage in the gel lane of one dimensional SDS-PAGE (Lamy et al. 2012; Vitorino et al. 2004). This then prevents protein migration and only proteins of relatively small molecular weights and with no glycosylation can migrate through the blockade and separate appropriately.

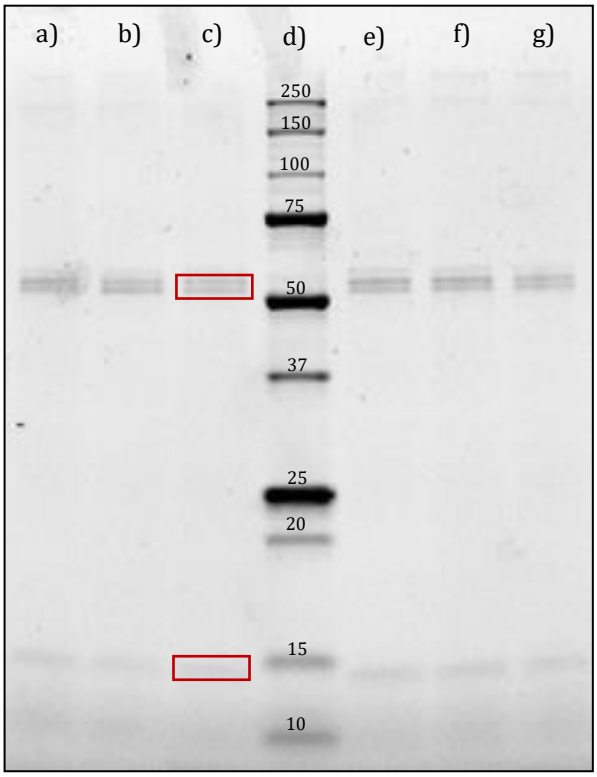

Figure 5.9: SDS-PAGE separation of neat saliva demonstrating the bands observed for different volumes with protein bands highlighted; a) 20 µl, b) 50 µl, c) 100 µl, d) protein size standard with molecular weights (kDa), e) 250 µl, f) 500 µl, g) 1 ml.

Large volumes of saliva at 250 µl or greater are less likely to be encountered on evidence or at crime scenes, and as a result saliva stains were deposited in volumes of 100 µl. A total of 35 saliva stains were aged from 24 hours to 7 days and then extracted (as per the method utilised in Section 2.2.2.1) prior to SDS-PAGE analysis. The electrophoretic patterns observed within the gels of aged extracted saliva stains demonstrate that one very faint band (71 kDa,

highlighted in dark red), which was barely visible, and two more distinct bands (53 (red) & 10 kDa (dark blue), respectively) were detected on the gels (Figure 5.10). The bands of molecular weights 71 and 10 kDa correspond with those observed within the saliva separation pattern, although the 53 kDa band did not. Due to the dilute nature of saliva, it was not unexpected for saliva stain extracts to exhibit much less visible protein bands. However, it was evident within the aged extracted saliva stain gels that very little protein material was detected at all. A cotton blank sample was subjected to SDS-PAGE analysis (Figure 5.10i) which demonstrated two bands, one with a molecular weight of 55 kDa and one of 10 kDa (highlighted in green). The two distinct bands observed within the saliva stain samples therefore can be attributed to contamination from the cotton substrate, rather than salivary proteins.

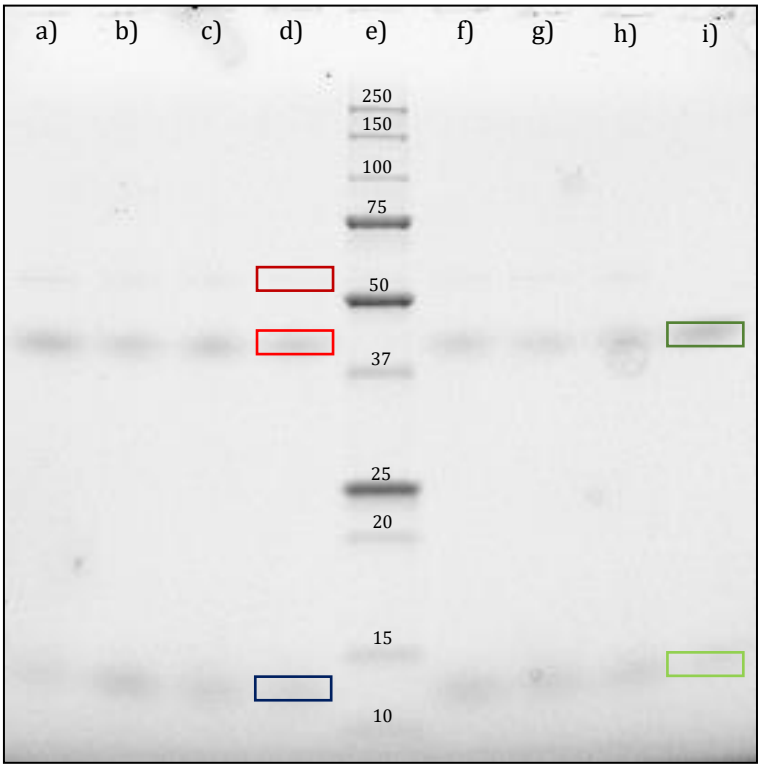

Figure 5.10: Example of the electrophoretic pattern produced from saliva stain extracts from stains aged 24 hours to 7 days when analysed with SDS-PAGE with specific protein bands highlighted; a) 24 hours, b) 48 hours, c) 3 days, d) 4 days, e) size standard with molecular weights (kDa), f) 5 days, g) 6 days, h) 7 days & i) cotton blank.

Though the salivary proteins were barely detectable in the aged extracted saliva stains, the molecular weight (71 kDa) of the protein band specifically attributed to saliva was consistent across the seven saliva stain ages examined. This highlights the reproducibility of the method, even when working with low concentrations of sample proteins. Additionally, it has been demonstrated that potential protein degradation does not appear to hinder the ability to

detect saliva from stains as old as seven days. The predominate absence of proteins, and the specific presence of a protein with a molecular weight of approximately 71 kDa band could potentially enable saliva identification. However, due to the very faint detection of proteins attributed to only saliva, SDS-PAGE was not appropriate to distinguish between saliva stains aged from 24 hours to 7 days.

5.3.1.3 SEMEN

Semen is a complex body fluid, comprised of spermatozoa and protein-rich seminal fluid. Proteins are present within seminal fluid from the various reproductive gland secretions, therefore it was anticipated that a plethora of proteins would be detected with SDS-PAGE analysis. However, the SDS-PAGE separation patterns observed from semen demonstrated more protein bands than saliva, but less band distinction and more smearing than those observed within blood (Figure 5.6c). A maximum of seven bands could successfully be detected from the separation pattern, most of which were detected towards the low molecular weight end of the gels (Figure 5.11). This correlates with the findings reported in literature, whereby most proteins within seminal fluid are found in the region typical of 30 kDa or less (Edwards et al. 1981; Pilch & Mann, 2006). The bands detected at the higher molecular weight end of the gels, namely bands 1 and 2, exhibited molecular weights of 94 and 62 kDa, respectively. Comparisons with comprehensive characterisations of proteins within semen demonstrated that specific protein identification was not possible for band 1. However, band 2 of 62 kDa was identified as semenogelin II, one of the key proteins in the coagulation of semen upon ejaculation (Fung et al. 2004; Lundwall et al. 2002).

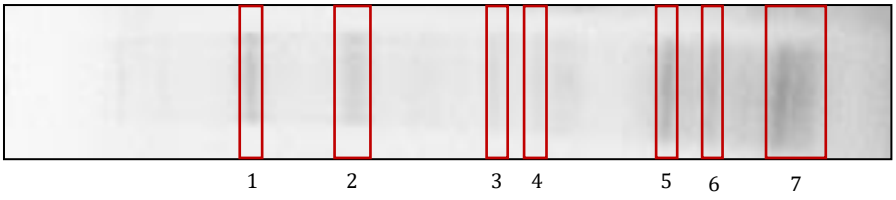

Figure 5.11: Band assignment of the protein separation pattern observed in neat semen.

The protein bands evident at the low molecular weight end of the gel were more difficult to identify, with only two of five bands indicative of specific proteins within semen. In particular, band 5 was identified as prolactin induced protein and epididymal secretory protein of 17 kDa, and band 6 corresponds with the molecular weight of prostate specific protein (PSP 94) at 14 kDa (Duncan & Thompson, 2007; Fung et al. 2004). The remaining bands of molecular weights 36, 31 and 11 kDa that were detected with SDS-PAGE could not be specifically identified. It may be possible to attribute bands 3 and 4 of 36 and 31 kDa,

respectively, to zinc-α2-glycoprotein, which has a molecular weight range of 30-40 kDa (Duncan & Thompson, 2007; Fung et al. 2004; Hassan et al. 2008). However, this identification was not definite as this particular protein is not specific to semen and is found in many different body fluids due to its role in fatty acid depletion (Hassan et al. 2008). Comparisons with the protein separation patterns of blood, saliva and vaginal secretions demonstrate that this protein was not detected by SDS-PAGE in these other body fluids, therefore its detection within semen samples could potentially be utilised as a factor in semen identification with this method.

As smearing was present amongst the proteins bands for the semen samples, it is likely that more semen specific/abundant proteins were detected with SDS-PAGE, although no distinct bands were actually formed which hindered identification. There have been a number of reports detailing more comprehensive protein separation patterns with SDS-PAGE and it has been documented that the majority of the proteins within semen exhibit molecular weights of less than 80 kDa (Fung et al. 2004). The gels utilised in this investigation were of approximately 10-20% acrylamide, which were suitable for analysis of proteins of any molecular weight. Consequently, the low molecular weight proteins observed within the semen samples were concentrated towards to the bottom end of the gel and protein identification was seldom specific, if possible at all, which demonstrated a reduction in sensitivity and specificity. To improve separation of low molecular weight proteins within semen, a higher concentration of polyacrylamide gel would be required, which could allow for better band resolution and identification.

Semen is one of the most important biological evidence types that can be recovered from crime scenes and often the body fluid is deposited on to a substrate. Therefore, it was essential to determine whether SDS-PAGE could be utilised to detect semen stains that had been aged and extracted from a cotton substrate. A total of 35 semen stains were aged from 24 hours to 7 days and then extracted prior to SDS-PAGE analysis and the electrophoretic separation patterns were comparable with the neat semen (Figure 5.12). The most observable difference within the separation patterns of the extracted aged semen stains was the decrease in band distinction for the proteins with higher molecular weights, namely those of approximately 96 (highlighted dark red) and 65 kDa (red). These bands were barely visible, whereas the zinc-α2-glycoprotein band (dark blue) was much more distinct and the low molecular weight bands (blue) were clearly observed at the bottom end of the gel. An additional protein band with a molecular weight of approximately 50 kDa (green) was observed within all seven semen stain ages. A protein of this molecular weight was not

detected within semen and comparisons with a cotton blank sample demonstrate that this band arises from the cotton substrate upon which the stains were deposited.

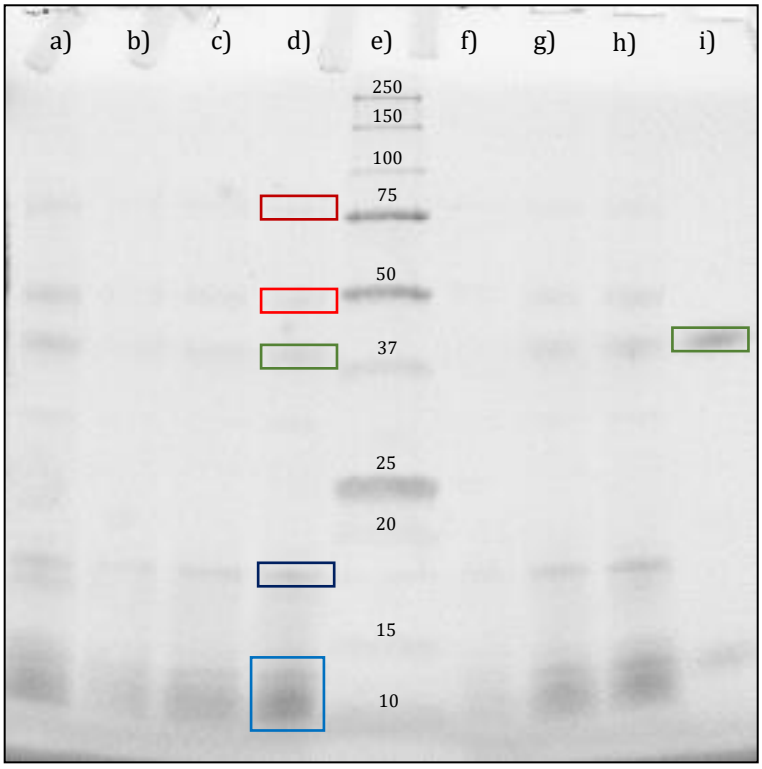

Figure 5.12: Example of the electrophoretic pattern produced from semen stain extracts from stains aged 24 hours to 7 days when analysed with SDS-PAGE with specific protein bands highlighted; a) 24 hours, b) 48 hours, c) 3 days, d) 4 days, e) size standard with molecular weights (kDa), f) 5 days, g) 6 days, h) 7 days & i) cotton blank.

The protein separation patterns observed within the aged extracted semen stains were comparable to the separation pattern of semen, despite the decrease in band distinction, particularly at the high molecular weight end of the gel. Reduced detection of all the expected semen bands was only observed within the 48 hour and 5 day aged samples, which may be due to the recovery of the semen stains from the cotton substrate during the extraction procedure. The consistency in the overall protein separation pattern of the semen stains demonstrates that sample age does not appear to effect the detection and pattern of proteins within semen. However, it is does highlight that SDS-PAGE is not appropriate to differentiate between semen stains of different ages. The specific separation pattern of proteins from semen and aged extracted semen stain samples has been demonstrated as reproducible amongst all the semen samples analysed. As a result, this specific separation pattern could be utilised to distinguish semen from blood, saliva or vaginal secretions.

5.3.1.4 VAGINAL SECRETIONS

The protein separation yielded by vaginal secretions appeared predominantly as one large smear, with very few distinct protein bands detected (Figure 5.6d). Vaginal secretions are a diverse and complex mixture of proteins and biological components that are seldom specific to this secretion. It is the abundance and combination of such components that enables vaginal secretions to be distinguished from other body fluids. Observation of the separation pattern exhibited by vaginal secretions demonstrates that only two bands could be distinguished within the smear at the low molecular weight end of the gels (Figure 5.13). The molecular weights of the these bands were 13 and 10 kDa, both of which could potentially be attributed to cystatins, which are known to be abundantly expressed within epithelia of the vagina (Di Quinzio et al. 2007; Tang et al. 2007).

Figure 5.13: Band assignment of the protein separation pattern observed in neat vaginal secretions.

The smear observed in the gel lane of neat vaginal secretions suggest that proteins were detected within the samples, although no band formation corresponding to molecular weight was possible. This may be due to the protein extraction method utilised, whereby the reagents were not suitable to enable optimal separation of the plethora of proteins within vaginal secretions. Development of the protein extraction method applied prior to PAGE separation may provide greater band resolution and subsequently greater protein identifications. The smear observed may also be due to the abundance of high molecular weight glycoproteins and mucins within vaginal secretions. It is known that these large molecules do not migrate successfully when analysed with SDS-PAGE, which could therefore result in a smear observed across the gel lanes that is comparable to what is observed in sample overloading (Andersch-Björkman et al. 2007; Lamy et al. 2012).

Of the four most commonly encountered body fluids at crime scenes, vaginal secretions is the only body fluid that has no specific presumptive test currently available to indicate its presence. Therefore, it was necessary to determine whether stains of vaginal secretions could be detected with SDS-PAGE. A total of 35 vaginal secretion stains that had been aged from 24 hours to 7 days were extracted (method as per Section 2.2.2.1) and analysed with SDS-PAGE.

The electrophoretic patterns observed amongst all 35 of aged extracted vaginal secretion stains was that the characteristic smearing, as detected in the neat vaginal secretions, was evident for all samples (Figure 5.14). Only one band within each sample could be distinguished within the smear and this had a molecular weight of 44 kDa (highlighted green). Comparisons with the protein band molecular weights identified in vaginal secretions demonstrates that this band was unlikely to have arisen from the body fluid, but rather the cotton substrate from which the vaginal secretions were extracted. A cotton blank sample was also run alongside the aged extracted vaginal secretion stains and the molecular weight associated with the band observed was 48 kDa, which corresponds with the molecular weight of the distinct band observed in the vaginal secretion stains (green).

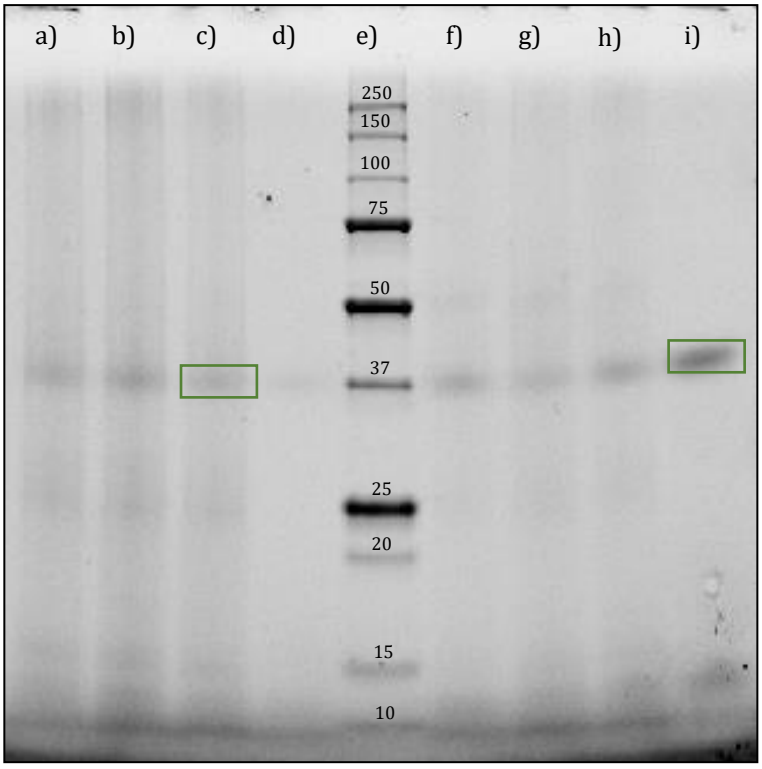

Figure 5.14: Example of the electrophoretic pattern produced from vaginal secretion stain extracts from stains aged 24 hours to 7 days when analysed with SDS-PAGE with specific protein bands highlighted; a) 24 hours, b) 48 hours, c) 3 days, d) 4 days, e) size standard with molecular weights (kDa), f) 5 days, g) 6 days, h) 7 days & i) cotton blank.

The separation patterns exhibited by each of the sample ages were consistent and reproducible, with only variation in the visible strength of the smear and band distinction. Figure 5.14 demonstrates that the separation patterns observed for the 24 hour to 3 day aged extracted vaginal secretion stains exhibited the most intense smearing. The intensity decreased as sample age increased, with the 4 and 5 day samples demonstrating barely any smearing. However, the smearing of the samples were more apparent in the 6 and 7 day aged

extracted vaginal secretion stains. This then suggests that the variation in protein intensity strength is likely to be impacted by the initial extraction of the vaginal secretion stains from the cotton, rather than the sample age. If sample recovery is poor, fewer proteins would be present in the sample, which would be reflected within the separation and detection of proteins with SDS-PAGE. Amongst all the sample ages analysed, there was no apparent variation in the presence or absence of protein bands, therefore it was not possible to differentiate between vaginal secretion stains of different ages.

5.3.1.5 BODY FLUID COMPARISON

The results discussed in the previous Sections (5.3.1.1-5.3.1.4) demonstrate that SDS-PAGE can successfully detect proteins within each of the four body fluids examined and that the separation patterns produced by each of these body fluids were different. Very little overlap in protein bands was observed amongst the blood, saliva, semen and vaginal secretion samples, which was surprising due to the documented ubiquity of proteins such as zinc-α2-glycoprotein, lysozyme, albumin and immunoglobulins (Fung et al. 2004; Mordacq & Ellington, 1994; Schenkels et al. 1995; Tang et al. 2007). The only protein overlap found was cystatins within both semen and vaginal secretions. However, the overall separation pattern observed and the combination of bands detected enable the cystatin bands to be attributed to either semen or vaginal secretions. This approach can be taken to distinguish between each of the four body fluids, as all produced very different, but reproducible separation patterns.

The SDS-PAGE analysis of aged body fluid stains demonstrated that when samples had been recovered by water extraction prior to analysis, separation patterns comparable to those of the body fluids could still be achieved for blood and semen. However, the protein bands exhibited in saliva and vaginal secretions were not detectable in the extracted aged saliva and vaginal secretion stains. The protein separation patterns of extracted aged blood and semen stains did not appear to vary as sample age increased, though a decrease in band distinction and appearance was observed in the aged samples compared to the body fluids which was consistent. This demonstrates the overall robustness and reproducibility of the technique and highlights its potential to be utilised as an identification screening method that can be applied to samples of unknown origin and age.

5.3.2 BRADFORD ASSAY

FORENSIC BODY FLUID AGE DETERMINATION

The Bradford assay enables the quantification of total protein yield from a sample extract that can be utilised for separation with SDS-PAGE or other protein separation techniques. Proteins are known to absorb strongly at 595 nm when analysed with the Bradford assay and the resulting measurement can be utilised to determine the total protein yield from a sample (Walker, 2010). A total of 144 body fluid samples were analysed with the Bradford assay to determine protein concentration. The concentration of proteins within the body fluids and extracted body fluid stains was examined to determine whether total protein concentration varied in relation to sample age. The blood, saliva, semen and vaginal secretion samples quantified had undergone two extractions prior to Bradford assay analysis; recovery from the cotton substrate with a water extraction (Section 2.2.2.1), followed by 1% SDS extraction (Section 5.2.1). As detergents react with the Bradford assay reagents (Thermo Scientific, 2014), a dilution of the body fluid extracts was required in order to obtain measurements that were representative of the sample protein content only. Protein extraction of the samples was conducted with 1% SDS, therefore only a 10-fold dilution was required for all of the body fluid samples analysed. Table 5.5 demonstrates the average total protein yield, with dilution factor corrected, of the body fluids and aged body fluid stains examined.

Table 5.5: The average total protein yields from blood, saliva, semen and vaginal secretions & extracted aged stains (24 hours to 7 days).

Age (days)	Blood (µg/mL)	Saliva (µg/mL)	Semen (µg/mL)	Vaginal Secretions (µg/mL)
Fluid	4690 ± 0.07	266.5 ± 0.01	189.4± 0.00	273.3 ± 0.00
1	1417.3 ± 53.09	138.7 ± 0.51	155.6 ± 0.85	162.4 ± 0.47
2	2521.3 ± 68.09	145.2 ± 0.3	156.4 ± 0.62	161.2 ± 0.95
3	2774.7 ± 41.45	140 ± 0.48	161.9 ± 0.41	162.2 ± 0.71
4	2445.3 ± 53.34	144.7 ± 0.2	167 ± 0.52	133.6 ± 0.11
5	2246.7 ± 86.49	138.1 ± 0.33	164 ± 0.34	137.8 ± 0.22
6	2348 ± 67.53	146.3 ± 0.74	160.5 ± 0.2	147 ± 0.16
7	2330.7 ± 112.43	143 ± 0.09	160.8 ± 0.6	147.6 ± 0.44

Comparisons were made between the total protein yield from the body fluids and the total protein yields from each stain age to establish the difference in concentrations that could be

attributable to sample age. It was not surprising that the body fluids yielded greater concentrations of protein when compared to the extracted stains. Blood yielded the greatest concentration amongst the body fluids, with an average concentration of over 4.5 mg/mL, which was approximately 20 times greater than the total protein yield of saliva, semen and vaginal secretions. However, when compared to the extracted aged bloodstains, there was only approximately a 50% decrease in protein yield. Examination of the total protein yields for the 24 hour to 7 day aged extracted bloodstains indicates that there was no apparent variation in protein concentration that corresponded with the age of the bloodstains. However, of all the body fluid stains examined, the bloodstains exhibited the largest variation (± 768.5 µg/mL on average).

Surprisingly, semen yielded the lowest protein concentration of the four body fluids, with an average yield of 189.4 µg/mL; whereas the average protein yields of saliva and vaginal secretions were very similar, 266.5 and 273.3 µg/mL, respectively. This was likely as a result of the similarities in biological composition of saliva and vaginal secretions (Gomes et al. 2011; Zubakov et al. 2009). The difference in total protein yield between the saliva and vaginal secretions and saliva and vaginal secretion extracted stains were comparable and appeared to decrease by approximately 45%, much like the blood yields. However, the difference in total protein yield between semen and extracted semen stains was much smaller, with only a 15% decrease observed. This may be due to a high abundance of spermatozoa within the semen stains, which could have been recovered more effectively during the initial extraction process, compared to other proteins and cellular material. Examination of the average total protein yield from the extracted aged saliva, semen and vaginal secretion stains demonstrates that there was no apparent variation in protein concentration over the seven sample ages examined. These results correspond with those obtained from the aged bloodstains, although the variation in protein concentration for saliva, semen and vaginal secretion stains was negligible compared to the variation of the aged bloodstains.

5.3.2.1 LINEAR REGRESSION

In order to assess whether there was in fact a relationship evident between total protein yield and body fluid stain age, linear regression analysis was carried out. Linear regression is a statistical technique that examines the relationship between two variables in order to predict an outcome (Field, 2013). If such a relationship was present between these two variables, it would be anticipated that the protein yield would vary in a linear fashion. This would then enable predictions of sample age to be made based on the total protein yield measurements

of an unknown sample. Table 5.6 demonstrates the R^2 and p values obtained for the total protein yields of the aged extracted blood, saliva, semen and vaginal secretion stains analysed with the Bradford assay. The R^2 corresponds to the proportion of the variation within the dependent variables, in this instance the body fluid, that can be explained by the independent variable; the stain age (Hair et al. 2006). The p value indicates whether any significant differences were detected within the dataset.

Table 5.6: R^2 values from linear regression analysis of the total protein yields of extracted blood, saliva, semen & vaginal secretion stains that had been aged from 24 hours to 7 days obtained by the Bradford assay.

Extracted Body Fluid	R^2	p value
Blood	0.0309	0.312
Saliva	0.0383	0.265
Semen	0.0907	0.079
Vaginal Secretions	0.333	0.000

It is evident from the R^2 values that less than 10% of the variation observed in the total protein yield of blood, saliva and semen stains was attributable to the age of the body fluid stains. These values demonstrate that there was no apparent relationship between protein concentration and stain age. In contrast, a third of the variation (33%) observed in the protein yield of vaginal secretion stains could be correlated with stain age. Despite, the increased relationship between protein yield and sample age in vaginal secretion stains compared to the blood, saliva and semen stains, the proportion of attributable variation was still relatively low. The significance levels (p) were also obtained as part of the linear regression analysis and it was demonstrated that significant differences were only detected within the vaginal secretion stain dataset ($p = 0.000$). The p values obtained from the blood, saliva and semen stain regression were all > 0.05, and therefore no significant differences were found within these datasets. It is evident from the linear regression results that total protein yield was not a significant variable in the age determination of body fluid stains when analysed with the Bradford assay.

5.4 CONCLUDING SUMMARY

The examination of blood, saliva, semen and vaginal secretions with protein analyses, SDS-PAGE and the Bradford assay, was explored to ascertain whether these techniques could be successfully utilised in the application of body fluid identification and age determination. All four body fluids have demonstrated that individualising protein separation patterns can be reproducibly obtained for each body fluid type when analysed with SDS-PAGE. The separation patterns exhibited different bands of different molecular weights, some of which could be confidently identified as specific proteins known within each individual body fluid. To ensure that the SDS-PAGE method was appropriate for forensic application, stains of each body fluid were prepared and aged from 24 hours to 7 days to establish whether the protein separation patterns could be detected, and proteins identified. This was examined to determine whether each body fluid could be differentiated from one another. Blood and semen could successfully be detected and produce the characteristic protein separation patterns expected for these body fluids. However, as the samples were recovered from the cotton substrate prior to SDS-PAGE analysis, the strength of the protein bands were not as distinct as their neat counterparts. As a result, some protein bands were not distinguishable, although the overall separation pattern was apparent. The vaginal secretion stain samples demonstrated the characteristic smear pattern, but no distinct bands were observed that were attributable to the body fluid. Similarly, the saliva stain aged samples could not be detected with SDS-PAGE, as only cotton contamination was observed within the protein separation patterns.

The age of the blood, semen and vaginal secretion stains appeared to have no correlation with the SDS-PAGE protein separation patterns and particular bands observed, as little to no variation was demonstrated across the gels. Comparisons between the patterns indicated that the recovery of the body fluid during the initial extraction process had the greatest impact on the distinction of the protein separation patterns. However, no observable changes in the presence or absence of protein bands were evident that could indicate differences in blood, semen or vaginal secretion stain age.

Examination of the four body fluids with the Bradford assay demonstrated that each body fluid yielded different protein concentrations, although saliva and vaginal secretions yielded concentrations that were comparable. As the Bradford assay is a quantification technique for total protein yield, it was not appropriate for application in body fluid identification.

Therefore, this method was utilised to establish whether variation in protein concentration may be indicative of the age of a body fluid stain. Blood, saliva and vaginal secretion stains aged 24 hour to 7 days demonstrated a decrease in protein yield of approximately 48% compared the body fluid samples, whereas the same aged semen stains demonstrated a much smaller decrease in protein concentration of only 15% compared to its fluid counterpart. Sample age did not appear to correlate with variation in total protein concentration, which was confirmed by linear regression analysis. The results of linear regression suggested that less than 10% of the variation in protein concentration was attributable to sample age for the blood, saliva and semen stains. However, sample age accounted for approximately one third of the variation in protein concentration for the aged vaginal secretion stains.

Overall, it can be stated that SDS-PAGE can be utilised to identify and differentiate between body fluids when in their fluid state. Identification and differentiation of body fluids can also be achieved when extracted aged stains are examined, although a decrease in protein band distinction prevents clear resolution of the separated bands which can hinder identification. Furthermore, it can be stated that the Bradford assay can be utilised to provide an indication of the protein concentration within body fluid stains that have been aged up to 7 days. However, neither the Bradford assay, nor SDS-PAGE are appropriate methods to determine the age of body fluid stains in the time periods examined in this research, although longer term variation may exist.

6. SYNTHESIS & CONCLUSIONS

This research has investigated the application of two techniques that are not routinely utilised within forensic biology; ATR-FTIR spectroscopy and protein analyses for the purposes of body fluid identification and age determination. This chapter synthesises the main findings from both of these techniques reported in Sections 3, 4 and 5.3, and provides a critical analysis of the methodology. Comparisons between the two techniques will be detailed, focusing on the benefits and limitations of each technique and how the research questions have been addressed.

6.1 SYNTHESIS

The development of better methods to enable the identification and age determination of body fluids, in keeping with the recommendations of the Silverman Report (Silverman, 2011), has been the focus of this research. This has been an area of forensic science that has been at the forefront of research over the last decade with literature exploring genetic, proteomic and chemical techniques (Anderson et al. 2005; Bremmer et al. 2012; Frumkin et al. 2011; Haas et al. 2011; Hanson & Ballantyne, 2013; Li et al. 2013; Virkler & Lednev, 2008). As a result, sophisticated advances have been made although many of the methodologies have been demonstrated as not fit for routine forensic application at present due to high costs, complex and labour intensive protocols and large error margins. This research has made use of the current literature to address the challenge faced in the current "live-time" era of forensic and criminal investigation with two aims:

- To investigate the use of alternative forensic techniques in the application of body fluid identification in order to establish a robust, confirmatory and cost effective method.
- To establish a suitable technique that can be utilised to determine the age of body fluid samples, as currently there is no routinely utilised method within forensic investigation.

The various techniques previously explored in the identification and age determination of body fluids typically fell into two categories; biological or chemical techniques, which encompassed a range of different approaches. In order to address the aims of this research, two techniques were utilised that fell within the umbrellas of biological and chemical techniques, but had not been considered in the application of body fluid identification and age determination to date. The techniques utilised were attenuated total reflectance Fourier Transform infrared (ATR-FTIR) spectroscopy and protein analyses involving sodium dodecyl sulphate polyacrylamide gel electrophoresis (SDS-PAGE) and the Bradford assay.

6.1.1 EMPIRICAL FINDINGS

Human blood, saliva, semen and vaginal secretions could successfully be detected and differentiated from one another, when analysed in their neat state with both ATR-FTIR spectroscopy and SDS-PAGE. ATR-FTIR spectroscopy enabled identification based on the unique spectral pattern and combination of peaks corresponding to the macromolecule groups common within biological material, such as proteins, sugars and phosphates. Identification with SDS-PAGE was achieved by examining the separation pattern of the various proteins within each of the body fluids. As each body fluid is comprised of a myriad of proteins in differing concentrations, the separation patterns detected were unique to each body fluid, even when overlap in proteins was observed.

Comparisons between the ATR-FTIR spectra of neat body fluids and known proteins within each of the body fluids, as well as peak frequencies in literature, enabled specific peaks to be attributed to the relevant protein components. This further reinforced the discrimination and identification of each body fluid. Identification with SDS-PAGE was additionally supported by comparison of the molecular weights of proteins specific and/or abundant to each body fluid. However, it was not possible to identify all of the protein bands observed within each of the body fluids due to differences in observed molecular weights with expected molecular weights of documented proteins within each body fluid.

Direct ATR-FTIR spectroscopic examination of body fluids deposited as stains on to cotton demonstrated that blood and vaginal secretions could successfully be detected against the cotton and subsequently identified. The age of the stain appeared to have no effect on the detection of these body fluids, as stains as old as 18 months could be detected and identified. In contrast, stains of saliva and semen could not be detected when directly analysed with ATR-FTIR spectroscopy. However, when the stains were extracted from the cotton with a

simple water-based procedure, all four body fluids could be detected, although the saliva extracts were the least reproducible due to the dilute nature of the body fluid. As demonstrated with the blood and vaginal secretion stain direct analysis, the age of the stains appeared to have no effect on the detection of each body fluid when extracted, as stains aged up to 12 months prior to extraction could successfully be detected and identified.

Successful detection of blood, semen and vaginal secretion extracted stains was also achieved with SDS-PAGE analysis, although the resolution of the bands was of poorer quality compared to the body fluids. As a result, confident assignments of proteins were not possible for all the protein bands expected to be present in the separation patterns based on those observed within the neat body fluids. Saliva was not detected at all when extracted from the cotton and analysed with SDS-PAGE. The age of the extracted samples also appeared to have no impact on the detection of the proteins, as no observable changes in the separation patterns were observed amongst the 24 hour to 7 day aged samples. Therefore, SDS-PAGE was demonstrated as an inappropriate technique to distinguish between aged body fluid stains.

Age determination analysis with ATR FTIR spectroscopy demonstrated that macromolecule group peak intensities and ratios were not appropriate variables to discriminate between body fluids stains and extracts that had been aged from 24 hours to 9 months; although discrimination was observed between extracted bloodstains that were aged to 12 months compared to the 7 day aged and younger extracted bloodstains, which provided an indication of the sample age. Furthermore, comparison of the average total protein yield obtained with the Bradford assay from aged extracted body fluid stains demonstrated that there was no correlation with protein concentration and sample age for any of the body fluids examined.

6.1.2 CRITIQUE & IMPLICATIONS

6.1.2.1 COMPARISON OF THE TECHNIQUES

ATR-FTIR spectroscopy and protein analyses, SDS-PAGE and the Bradford assay, are techniques that are well documented in their application to body fluid analysis (Sections 2.1.2 & 5.1.3). These techniques are efficient and user-friendly, which are desirable characteristics in the development of a new application for routine utilisation within forensic investigations. ATR-FTIR spectroscopy has an advantage over the protein analyses in that little, to no sample preparation is required to conduct analysis. The methodology utilised in the analysis of body fluids was optimised to be as non-destructive as possible to maintain the integrity of the samples. Therefore no reagents, chemicals or complicated extraction procedures were

required to obtain spectra representative of each body fluid type. Where possible, direct analysis of the body fluid samples was conducted as this enabled the potential for further forensic testing, such as DNA profiling, to be carried out on the same samples. However, where direct analysis was not possible, a simple water extraction procedure enabled detection and identification of the body fluids from stains. The water extraction provided sufficient recovery of the biological material whilst not altering the biochemical composition of the body fluids.

In contrast, both SDS-PAGE and the Bradford assay require a number of preparatory steps with buffers and reagents that are potentially harmful, before samples can be analysed. This typically requires the alteration of samples to extract the proteins from the remaining cellular material, or enable colourimetric analysis. This increases the analysis time and is destructive to the sample which therefore limits any further forensic analysis. However, the protein extract samples can be utilised for both SDS-PAGE and the Bradford assay as only small volumes (5 µl for SDS-PAGE & 100 µl for the Bradford assay) of the extract are required for each analysis.

The run time of each technique is relatively quick, with instantaneous measurements obtained with the Bradford assay and ATR-FTIR spectra obtained in less than one minute when analysing dry samples at 32 scans. If wet-to-dry analysis is carried out with ATR-FTIR spectroscopy, the run time is still less than one minute, although *in situ* drying of the sample needs to be taken into consideration, which can result in a waiting time of up to one hour before dry spectra can be obtained. The run time for SDS-PAGE analysis can vary depending on the voltage used during electrophoresis. For greater band resolution, a voltage of 100 (V) was utilised in this research which gave a run time of one hour and ten minutes. Compared to techniques such as DNA analysis, these analysis times are very quick, although for application as a screening tool in body fluid identification, a run time of less than one minute with an instantaneous output ready for interpretation is more desirable.

The outputs of each of the techniques are very different and require different interpretational skills and knowledge to ensure that correct component assignments and calculations are made. Following ATR-FTIR spectroscopic analysis, a spectrum consisting of peaks and troughs at different wavenumber frequencies is produced. The frequencies and peak intensities are utilised to identify the components under analysis and can be generated by the analytical software package associated within the instrument. The spectra can be then compared with a spectral library to identify the most probable match. This is advantageous as it is a relatively objective process and does not require specific interpretational skills.

The interpretation of SDS-PAGE separation patterns require visualisation before interpretation and identification can be carried out. A stain-free detection system and software package (Image Lab v.4.0, Bio-Rad, California) were utilised in this research which removed the time consuming process of staining and destaining the gels to visualise the protein bands. However, the stain-free detection system only detects proteins containing tryptophan (Bio-Rad, 2014), therefore it is possible that many more proteins were successfully extracted from the samples, but were not detected after SDS-PAGE due to the detection system utilised. The protein bands that are detectable with the stain-free technology can be automatically detected with the Image Lab (v.4.0) software, although often the band assignment by the software is incorrect. Therefore, manual band assignment is required which relies on the subjectivity of determining the correct number of bands. When poor resolution or smearing is present within the separation patterns, an over or under interpretation of protein bands may occur. It is only once manual interpretation of the protein bands has been completed that comparisons can be made with proteins of known molecular weights, although often, many of the bands detected with SDS-PAGE cannot be identified.

The interpretation of the Bradford assay measurements is more robust than that of SDS-PAGE, as absorbance measurements from calibration standards and unknown samples allow for a calibration curve to be utilised to determine the total protein yield. As the absorbance measurements are automated, there is little subjectivity in the interpretation of protein concentrations. When introducing a new method of analysis within a forensic context, the production of results should be easily interpretable and objective, as it is not time consuming for the practitioner, nor does it require complex calculations in order to obtain an identification.

ATR-FTIR spectroscopy has been criticised in the past for its reduced sensitivity and specificity in comparison to traditional transmission spectroscopy and other FTIR spectroscopy configurations (De Wael et al. 2008; Kazarian & Chan, 2013). The sensitivity demonstrated by the technique within this research was not sufficient to detect changes in macromolecules over time, which could provide an indication of sample age. However, for the purposes of body fluid identification, ATR-FTIR spectroscopy has demonstrated sufficient sensitivity and specificity to enable characterisation of biological macromolecules and variation between macromolecule group components, and their resulting peaks, to allow for the discrimination of blood, saliva, semen and vaginal secretions. Furthermore, the ATR-FTIR spectroscopic methodology utilised within this research has the potential to be adapted to more advanced configurations, such as FTIR microspectroscopic imaging which could

increase the sensitivity and specificity of the technique and its application to body fluid identification.

In contrast, SDS-PAGE analysis demonstrated sufficient sensitivity to provide a representation of the various proteins and characteristic separation patterns of blood, saliva, semen and vaginal secretions when extracted with 1% SDS. This enabled the differentiation of each of the body fluids, although the specificity of the technique was poor as it was not possible to identify a number of the protein bands detected with SDS-PAGE. It is well documented that SDS-PAGE has reduced specificity in comparison to more sophisticated and advanced methods of protein analysis, such as two-dimensional (2-D) electrophoresis and proteomics with mass spectrometry (Beranova-Giorgianni, 2003; Lamy et al. 2012).

The Bradford assay demonstrated good sensitivity and has a working range of 1-1500 µg/mL, which enabled an indication of the total protein yield even in samples that did not demonstrate any protein bands when analysed with SDS-PAGE. However, as the Bradford assay only provides quantification of the total protein concentration within a sample, it cannot identify proteins or enable quantification of specific proteins. As a result, this technique is only appropriate when utilised in conjunction with SDS-PAGE.

6.1.2.2 REAL WORLD IMPLICATIONS OF THE RESEARCH

The development of well-established techniques for application within forensic biology has proved challenging. However, the findings from this research have demonstrated that two new methods of body fluid screening have been identified, which have the potential to be adopted into routine forensic biological analysis. SDS-PAGE has demonstrated proof-of-concept within this research, although, compared to ATR-FTIR spectroscopy, it is unlikely to be utilised by scenes of crime officers or forensic practitioners for routine analysis when more discriminatory, sensitive and time-effective techniques exist.

ATR-FTIR spectroscopy has demonstrated results, benefits and limitations similar to spectroscopic methods previously reported, although many of these reports have focused solely on the identification and age determination of bloodstains (Bremmer et al. 2011; Edelman et al. 2012b; Li et al. 2013). The findings obtained from ATR-FTIR spectroscopy in this research can be seen to address the body fluid analysis challenges stated by the Forensic Science Special Interest Group (ForSci SIG) (Section 1.4.1). It has been demonstrated how a well-established technique that is routinely utilised for forensic chemical analysis, can provide a non-destructive screening method appropriate for all four key body fluids which has the specificity to discriminate between each type. This has potential for adoption for use

at crime scenes with portable ATR-FTIR instruments, as well as traditional analysis within the laboratory by forensic practitioners.

6.1.3 RECOMMENDATIONS FOR FURTHER WORK

The application of ATR-FTIR spectroscopy for the identification of body fluids has scope for further development to support its potential introduction into routine forensic biological analysis. Though blood, saliva, semen and vaginal secretions are predominantly the most important body fluids encountered at crimes scenes, it is not unusual for menstrual blood, urine or sweat to be recovered. A main consideration of further work would be to determine whether these body fluids can be detected and discriminated from one another and the four key body fluids with this technique.

Another recommendation for further work for body fluid identification is to explore body fluid stains deposited on a variety of different substrates, such as polyester, denim, nylon. These materials are often utilised in the production of clothing, upon which forensic biological evidence is often found. The examination of body fluid stains, both directly from the substrate and extracted from the substrate could be conducted to determine whether body fluid detection and identification with ATR-FTIR spectroscopy is achievable.

Further to the body fluid identification, the age determination of extracted aged bloodstains with ATR-FTIR spectroscopy requires further investigation. Aged bloodstains older than 7 days, but younger than 12 months were not examined during this investigation, leaving a gap in the data. To address this gap, bloodstains aged from 7 days up to 12 months could be extracted and examined, as per the method utilised within this investigation, to determine whether average peak intensities and ratios could distinguish between the different ages.

Another key consideration for further development of the application of ATR-FTIR spectroscopy for forensic biological analysis is the examination of body fluid mixtures to determine whether detection of different body fluid components is possible with this technique. In particular, differing ratios of body fluid mixtures could be explored to investigate the limit of detection of each known volume per body fluid component within a mixture. This would be of great use in investigations where mixed DNA profiles have been obtained and the source of each donors DNA could provide intelligence information to an investigation.

The limit of detection of individual body fluids is another aspect of further work that would be beneficial. Body fluids may be diluted as a result of cleaning crime scenes or pieces of evidence on which biological evidence may be present. The examination of various dilutions of neat body fluids and extracted body fluid stains would provide an indication of the sensitivity of ATR-FTIR spectroscopy. This can then be compared with the limit of detection of current presumptive tests and recommendations of detection limits can be suggested to users.

A final suggestion of further work in the utilisation of ATR-FTIR spectroscopy for forensic biological analysis is the examination of the effects that temperature and humidity have on body fluid identification. The samples analysed within this research were stored at room temperature, in darkness with no control of humidity. Exposure of body fluid samples to lower and higher temperatures with varying levels of humidity prior to ATR-FTIR spectroscopic analysis would determine whether confident identification was still achievable. This could potentially provide investigators with viable options of the appropriate forensic analyses to be applied to biological evidence recovered from crime scenes exposed to various environmental conditions.

6.1.4 LIMITATIONS

During this research limitations were faced that potentially impacted the findings presented; namely the consideration of the extraction method, the number of donors used per body fluid, and the collection method of vaginal secretion samples. One of the main findings within this research was that saliva and semen stains could not be detected when analysed directly from cotton with ATR-FTIR spectroscopy. This was overcome with the introduction of an extraction procedure to recover the biological material from the cotton substrate so that wet-to-dry analysis could be carried out on the aged saliva or semen samples. As a result, none of the aged body fluids were examined as extracted stains for the same sample ages. This had a particular impact on the aged bloodstains; whereby as the stains were detectable when analysed directly, extraction of the stains was not considered as vital compared to the saliva and semen stains. This then resulted in only short term aged bloodstains (24 hours to 7 days) and two groups of long term aged bloodstains (12 & 18 months) being examined as extracts, leaving a gap in the data. If the significance of producing spectra from extracted bloodstains was comparable to those of the neat blood had been explored further, this gap in the data would not observed and it may have been possible to provide a definitive conclusion on the utilisation of ATR-FTIR spectroscopy in the age determination of extracted aged bloodstains.

Throughout the research only a small number of different donors were utilised, with three donors utilised in the collection of blood samples and one individual donor per body fluid utilised for saliva, semen and vaginal secretion samples. Due to the nature of saliva, semen and vaginal secretions, it was more difficult to recruit volunteer donors for these body fluids and as a result, no inter-person variation could be explored for these samples. This potentially impacted the findings obtained from this research, as generalisations to the population and statistical comparisons of different donors were not possible. However, support from literature had demonstrated that the overall characteristics of the spectra produced from each of the body fluids examined were consistent. Therefore, it was anticipated that there would be very few detectable differences between donors in the ATR-FTIR spectra of these body fluids.

Of all the body fluid types examined, the collection of the vaginal secretion samples was the most difficult. Preliminary studies involved the collection of vaginal secretions with a sterile cotton swab, of which the vaginal cellular material was extracted with phosphate buffered saline (PBS) prior to deposition for ageing. However, the preliminary results demonstrated that no vaginal material was detectable with ATR-FTIR spectroscopy. Vaginal secretions encountered at crime scenes are likely to be in their neat state or deposited neat on to a substrate. Therefore it was felt that the collection, extraction and subsequent deposition of the body fluid did not reflect how vaginal secretions would be present on forensic evidence. Extensive research into appropriate collection methods impacted the utilisation of this body fluid within this investigation, which resulted in vaginal secretion stains being aged for the least amount of time in comparison to the remaining three body fluids. However, once an appropriate collection method had been identified and tested, vaginal secretion stains were deposited for the longest ageing period possible within the remaining timeframe of the research.

The experimental challenges faced during this research have affected the results obtained, although overall this affect has been minor. To overcome such experimental challenges in the future, the introduction of a risk register could enable any potential risks to be identified that may prevent aspects of the research moving forward at the anticipated pace. This would help to strengthen the structure the research design prior to any experimental work, and implement a strategy to address any risks if they were encountered during the research.

6.2 CONCLUSION

In the quest to determine a method that is robust, confirmatory and cost effective for application in the forensic identification and age determination of body fluids, this research has demonstrated the benefits and limitations of ATR-FTIR spectroscopy and protein analyses. Age determination analysis has not been possible with these techniques and can therefore be recommended as inappropriate. However, the overall significance of this research lies in the application of both ATR-FTIR spectroscopy and SDS-PAGE for the identification of human body fluids. ATR-FTIR spectroscopy in particular has reproducibly demonstrated successful detection and identification of blood, saliva, semen and vaginal secretions when neat, as stains and when extracted from stains, which has the potential to be adopted into routine forensic biological analysis.

7. REFERENCES

Adams, E.G. & Wraxall, B.G. (1974). Phosphatases in body fluids: The differentiation of semen and vaginal secretion. *Forensic Science*. 3. p.pp. 57–62.

Ahmed, M.K. & Mantsch, H.H. (1994). Fourier transform infrared spectroscopy of human saliva. *Proceeding of SPIE 2089*, 9th International Conference on Fourier Transform Spectroscopy, 520.

Ahram, M. & Petricoin, E.F., (2008). Proteomics Discovery of Disease Biomarkers. *Biomarker insights*. 3 (703). p.pp. 325–333.

Aitken, A. (2010) Mass Spectrometric Techniques. In: Wilson, K. & Walker, J. (eds) Principles and Techniques of Biochemistry and Molecular Biology, 7th Ed. Cambridge, Cambridge University Press.

Al-Garawi, Z.S.M., Tomi, I.H.R. & Al-Daraji, A.H.R. (2012). Synthesis and characterization of new amino acid-schiff bases and studies their effects on the activity of ACP, PAP and NPA enzymes (in vitro). *E-Journal of Chemistry*. 9 (2). p.pp. 962–969.

De Almeida, P.D.V., Gregio, A.M.T., Machado, M.A.N., de Lima, A.A.S. & Azevedo, L.R. (2008). Saliva composition and functions: A comprehensive review. *The Journal of Contemporary Dental Practice*. 9 (3). p.pp. 72–80.

Altuntaş, E., Kempe, K., Crecelius, A., Hoogenboom, R. & Schubert, U.S. (2010). ESI-MS & MS/MS Analysis of Poly(2-oxazoline)s with Different Side Groups. *Macromolecular Chemistry and Physics*. 211 (21). p.pp. 2312–2322.

Andersch-Björkman, Y., Thomsson, K.A., Holmén Larsson, J.M., Ekerhovd, E. & Hansson, G.C. (2007). Large scale identification of proteins, mucins, and their O-glycosylation in the endocervical mucus during the menstrual cycle. *Molecular & Cellular Proteomics*. 6 (4). p.pp. 708–716.

Anderson, S., Howard, B., Hobbs, G.R. & Bishop, C.P. (2005). A method for determining the age of a bloodstain. *Forensic Science International*. 148. p.pp. 37–45.

Anderson, S.E., Hobbs, G.R. & Bishop, C.P. (2011). Multivariate analysis for estimating the age of a bloodstain. *Journal of Forensic Sciences*. 56 (1). p.pp. 186–193.

Andrasko, J. (1997) The estimation of age of bloodstains by HPLC analysis. *Journal of Forensic Sciences*. 42 (4). p.pp 601-604.

Arany, S. & Ohtani, S., (2011). Age estimation of bloodstains: a preliminary report based on aspartic acid racemization rate. *Forensic science international*. 212 (1-3). p.pp. e36–9.

Arrondo, J.L. & Goñi, F.M. (1998). Infrared studies of protein-induced perturbation of lipids in lipoproteins and membranes. *Chemistry and Physics of Lipids*. 96. p.pp. 53–68.

Arrowsmith, M.I. (2013) *FTIR Smart Orbit vs. Golden Gate*, [Email] Message to: Orphanou, C.M. 18th October 2013.

Association of Chief Police Officers. (2013). *Live-time Forensics*. Harrogate, Great Britain.

Banwell, C.N. & McCash, E.M. (1994) *Fundamentals of Molecular Spectroscopy*. 4th Edition. England, McGraw-Hill Publishing Company.

Barcot, O., Balarin, M., Gamulin, O., Jezek, D., Romac, P. & Brnjas-Kraljevic, J. (2007). Investigation of spermatozoa and seminal plasma by Fourier Transform infrared spectroscopy. *Applied Spectroscopy*. 61 (3). p.pp. 1–5.

Baron, A.C., DeCarlo, A.A. & Featherstone, J.D.B. (1999). Functional aspects of the human salivary cystatins in the oral environment. *Oral Diseases*. 5. p.pp. 234–240.

Barth, A. (2007). Infrared spectroscopy of proteins. *Biochimica et Biophysica Acta*. 1767 (9). p.pp. 1073–1101.

Barth, A. & Haris, P.I. (Eds.) (2009). *Biological & Biomedical Infrared Spectroscopy: Advances in Biomedical Spectroscopy, Volume 2*, Netherlands, IOS Press.

Bartick, E.G., (2002). Applications of Vibrational Spectroscopy in Criminal Forensic Analysis. In: J. M. Chalmers & P. R. Griffiths (eds.). *Handbook of Vibrational Spectroscopy*. Chichester: John Wiley & Sons Ltd., pp. 1–13.

Bartlett, J., Gakhar, L., Penterman, J., Singh, P., Mallampalli, R., Porter, E. & McCray, P., (2013). PLUNC: A multifunctional surfactant of the airways. *Biochemical Society Transactions*. 39 (4). p.pp. 1012–1016.

Bauer, M., Polzin, S. & Patzelt, D. (2003). Quantification of RNA degradation by semi-quantitative duplex and competitive RT-PCR: a possible indicator of the age of bloodstains? *Forensic Science International*. 138 (1-3). p.pp. 94–103.

Bem, S. & Ostrowski, W.S. (2001). Effect of tartaric acid on conformation and stability of human prostatic phosphatase: An infrared spectroscopic and calorimetric study. *Acta Biochimica Polonica*. 48 (3). p.pp. 755–762.

Beranova-Giorgianni, S. (2003). Proteome analysis by two-dimensional gel electrophoresis and mass spectrometry: Strengths and limitations. *Trends in Analytical Chemistry*. 22 (5). p.pp. 273–281.

Van der Bijl, P., Thompson, I.O. & Squier, C.A. (1997). Comparative permeability of human vaginal and buccal mucosa to water. *European Journal of Oral Sciences*. 105 (6). p.pp. 571–575.

Van den Berge, M., Carracedo, A, Gomes, I., Graham, E. A M., Haas, C., Hjort, B., Hoff-Olsen, P., Maroñas, O., Mevåg, B., Morling, N., Niederstätter, H., Parson, W., Schneider, P.M., Court, D.S., Vidaki, a & Sijen, T. (2014a). A collaborative European exercise on mRNA-based body fluid/skin typing and interpretation of DNA and RNA results. *Forensic Science International. Genetics*. 10. p.pp. 40–8.

Bio Rad (2014). *Quick Start Bradford Instruction Manual*. p.pp. 1–35.

Bio-Rad (2014a). *2D Protein Electrophoresis | Applications & Technologies | Bio-Rad*. [Online]. 2014. Available from: http://www.bio-rad.com/en-uk/applications-technologies/2-d-electrophoresis. [Accessed: 29 July 2014].

Bio-Rad (2014b). *Coomassie Stains | Life Science Research | Bio-Rad*. [Online]. 2014. Available from: http://www.bio-rad.com/en-uk/product/coomassie-stains?pcp_loc=lnav. [Accessed: 4 August 2014].

Bio-Rad (2014c). *Polyacrylamide Gels | Applications & Technologies | Bio-Rad*. [Online]. 2014. Available from: http://www.bio-rad.com/en-uk/applications-technologies/polyacrylamide-gels. [Accessed: 2 August 2014].

Bio-Rad (2014d). *Protein Electrophoresis Methods | Applications & Technologies | Bio-Rad*. [Online]. 2014. Available from: http://www.bio-rad.com/en-uk/applications-technologies/protein-electrophoresis-methods#two-d_electrophoresis. [Accessed: 29 July 2014].

Bio-Rad (2014e). *Protein Staining | Applications & Technologies | Bio-Rad*. [Online]. 2014. Available from: http://www.bio-rad.com/en-uk/applications-technologies/protein-staining. [Accessed: 29 July 2014].

Blanchard, C.R. (1996). Atomic force microscopy. *The Chemical Editor*. 1 (5). p.pp 1-8.

Botonjic-Sehic, E. Brown, C.W. Lamontagne, M. & Tsaparikos, M. (2009). Forensic application of near-infrared spectroscopy: Ageing of bloodstains. *Spectroscopy*. 24 (2). p.pp 42-48.

Boyd, S., Bertino, M.F. & Seashols, S.J. (2011). Raman spectroscopy of blood samples for forensic applications. *Forensic Science International*. 208. p.pp. 124–128.

Bradford, M.M. (1976). A rapid and sensitive method for the quantitation of microgram quantities of protein utilizing the principle of protein-dye binding. *Analytical biochemistry*. 72. p.pp. 248–54.

Branden, C. & Tooze, J. (1991). *Introduction to Protein Structure*. United States of America, Garland Publishing Inc.

Bremmer, R.H., de Bruin, K.G., van Gemert, M.J.C., van Leeuwen, T.G. & Aalders, M.C.G. (2012). Forensic quest for age determination of bloodstains. *Forensic Science International*. 216 (1-3). p.pp. 1–11.

Bremmer, R.H.R., Nadort, A., van Leeuwen, T.G., van Gemert, M.J.C. & Aalders, M.C.G. (2011). Age estimation of blood stains by hemoglobin derivative determination using reflectance spectroscopy. *Forensic Science International*. 206. p.pp. 166–171.

Butler, J.M. (2010). *Fundamentals of Forensic DNA Typing*. United States of America, Elsevier Inc.

Calabrò, E. & Magazù, S. (2012). Electromagnetic fields effects on the secondary structure of lysozyme and bioprotective effectiveness of trehalose. *Advances in Physical Chemistry*. p.pp. 1–6.

Carboni, I., Rapi, S. & Ricci, U. (2014). Stability of human α-salivary amylase in aged forensic samples. *Legal Medicine*. 16 (4). p.pp. 214–217.

Castagnola, M., Inzitari, R., Fanali, C., Iavarone, F., Vitali, A., Desiderio, C., Vento, G., Tirone, C., Romagnoli, C., Cabras, T., Manconi, B., Sanna, M.T., Boi, R., Pisano, E., Olianas, A., Pellegrini, M., Nemolato, S., Heizmann, C.W., Faa, G. & Messana, I. (2011). The surprising composition of the salivary proteome of preterm human newborn. *Molecular & Cellular Proteomics*. 10 (1). p.pp. 1–14.

Chiriboga, L., Xie, P., Yee, H., Vigorita, V., Zarou, D., Zakim, D. & Diem, M. (1998b). Infrared spectroscopy of human tissue. I. Differentiation and maturation of epithelial cells in the human cervix. *Biospectroscopy*. 4. p.pp. 47–53.

Chiriboga, L., Xie, P., Vigorita, V., Zarou, D., Zakim, D. & Diem, M. (1998a). Infrared spectroscopy of human tissue. II. A comparative study of spectra of biopsies of cervical squamous epithelium and of exfoliated cervical cells. *Biospectroscopy*. 4 (1). p.pp. 55–9.

Chiriboga, L., Xie, P., Zhang, W. & Diem, M. (1997). Infrared spectroscopy of human tissue. III. Spectral differences between squamous and columnar tissue and cells from the human cervix. *Biospectroscopy*. 3. p.pp. 253–257.

Chittur, K.K. (1998). FTIR/ATR for protein adsorption to biomaterial surfaces. *Biomaterials*. 19 (4-5). p.pp. 357–69.

Choudhury, H.K. Banwell, C.N. & McCash, E.M. (2013). *Fundamentals of Molecular Spectroscopy*. 5th Edition, New Delhi, McGraw-Hill Education (India) Private Ltd.

Chung, C., Lee, M. & Choe, E. (2004). Characterization of cotton fabric scouring by FT-IR ATR spectroscopy. *Carbohydrate Polymers*. 58 (4). p.pp. 417–420.

Chung, M.C.-M. (1984). Structure and Function of Transferrin. *Biochemical Education*. 12 (4). p.pp. 146–154.

Coates, J. (2000). Interpretation of infrared spectra, a practical approach. In: R. A. Meyers (ed.). *Encyclopedia of Analytical Chemistry*. Chichester: John Wiley & Sons Ltd., pp. 10815–10837.

Coolidge, F.L. (2013). *Statistics, A General Introduction*, 3rd Edition. United States of America, SAGE Publications, Inc.

Coon, J.J., Zürbig, P., Dakna, M., Dominiczak, A.F., Decramer, S., Fliser, D., Frommberger, M., Golovko, I., Good, D.M., Herget-Rosenthal, S., Jankowski, J., Julian, B. a, Kellmann, M., Kolch, W., Massy, Z., Novak, J., Rossing, K., Schanstra, J.P., Schiffer, E., Theodorescu, D., Vanholder, R., Weissinger, E.M., Mischak, H. & Schmitt-Kopplin, P., (2008). CE-MS analysis of the human urinary proteome for biomarker discovery and disease diagnostics. *Proteomics. Clinical applications*. 2 (7-8). p.p. 964.

Cooper, G.M. (2000). *Protein Degradation*. [Online]. 2000. The Cell: A Molecular Approach 2nd Edition. Available from: http://www.ncbi.nlm.nih.gov/books/NBK9957/. [Accessed: 17 November 2014].

Coutts-Lendon, C. A, Wright, N. A, Mieso, E. V & Koenig, J.L., (2003). The use of FT-IR imageing as an analytical tool for the characterization of drug delivery systems. *Journal of Controlled Release*. 93 (3). p.pp. 223–248.

Crowe, J. & Bradshaw, T. (2010). *Chemistry for the Biosciences – The Essential Concepts*, 2nd Edition. Oxford, Oxford University Press.

Defagó, M., Valentich, M.A. & Actis, A.B. (2011). Lipid characterization of human saliva. *Journal of the California Dental Association*. 39 (12). p.pp. 874–881.

Dong, A., Huang, P. & Caughey, W.S. (1990). Protein secondary structures in water from second-derivative amide I infrared spectra. *Biochemistry*. 29. p.pp. 3303–3308.

Duncan, M.W. & Thompson, H.S. (2007). Proteomics of semen and its constituents. *Proteomics Clinical Applications*. 1. p.pp. 861–875.

Edelman, G., van Leeuwen, T.G. & Aalders, M.C.G. (2012a). Hyperspectral imaging for the age estimation of blood stains at the crime scene. *Forensic Science International*. 223. p.pp. 72–77.

Edelman, G., Manti, V., van Ruth, S.M., van Leeuwen, T. & Aalders, M. (2012b). Identification and age estimation of blood stains on colored backgrounds by near infrared spectroscopy. *Forensic Science International*. 220. p.pp. 239–244.

Edwards, J.J., Tollaksen, S.L. & Anderson, N.G. (1981). Proteins of human semen. I. Two-dimensional mapping of human seminal fluid. *Clinical Chemistry*. 27 (8). p.pp. 1335–1340.

Elangovan, S., Margolis, H.C., Oppenheim, F.G. & Beniash, E. (2007). Conformational changes in salivary proline-rich protein 1 upon adsorption to calcium phosphate crystals. *Langmuir: The ACS Journal of Surfaces and Colloids*. 23. p.pp. 11200–11205.

Eliasson, R. (1965). Effect of frequent ejaculations on the composition of human seminal plasma. *Journal of Reproduction and Fertility*. 9. p.pp. 331–336.

Elkins, K.M. (2011). Rapid presumptive "fingerprinting" of body fluids and materials by ATR FT-IR spectroscopy. *Journal of Forensic Sciences*. 56 (6). p.pp. 1580–1587.

Ernest, V., Nirmala, M.J., Gajalakshmi, S., Mukherjee, A. & Chandrasekaran, N. (2013). Biophysical investigation of α-amylase conjugated silver nanoparticles proves structural changes besides increasing its enzyme activity. *Journal of Bionanoscience*. 7 (1-5). p.pp. 271–275.

Esser, D., Alvarez-Llamas, G., de Vries, M.P., Weening, D., Vonk, R.J. & Roelofsen, H. (2008). Sample Stability and Protein Composition of Saliva: Implications for Its Use as a Diagnostic Fluid. *Biomarker insights*. 3. p.pp. 25–37.

Etherington, D. (2014). *Apple's 51M iPhones, 26M iPads And 4.8M Macs In Q1 2014 Set A Record, But Growth Slows | TechCrunch*. [Online]. 2014. TechCrunch. Available from: http://techcrunch.com/2014/01/27/apple-q1-2014-iphone-ipad-mac/. [Accessed: 12 March 2014].

European Molecular Biology Laboratory - European Bioinformatics Informatics (2014). *Involucrin (IPR002360)*. [Online]. 2014. Available from: http://www.ebi.ac.uk/interpro/entry/IPR002360?q=involucrin. [Accessed: 28 April 2014].

European Molecular Biology Laboratory - European Bioinformatics Institute (2014a). *Cornifin (SPRR1) (IPR003302)*. [Online]. 2014. Available from: http://www.ebi.ac.uk/interpro/entry/IPR003302. [Accessed: 28 April 2014].

European Molecular Biology Laboratory - European Bioinformatics Institute (2014b). *Cornulin (IPR026792)*. [Online]. 2014. Available from: http://www.ebi.ac.uk/interpro/entry/IPR026792?q=cornulin. [Accessed: 28 April 2014].

Fábián, T.K., Hermann, P., Beck, A., Fejérdy, P. & Fábián, G. (2012). Salivary defense proteins: Their network and role in innate and acquired oral immunity. *International Journal of Molecular Sciences*. 13 (4). p.pp. 4295–4320.

Fang, R., Manohar, C.F., Shulse, C., Brevnov, M., Wong, A., Petrauskene, O.V., Brzoska, P. & Furtado, M.R. (2006). Real-time PCR assays for the detection of tissue and body fluid specific mRNAs. *International Congress Series*. 1288. p.pp. 685–687.

Field, A. (2013). *Discovering Statistics Using IBM SPSS Statistics*, 4th Edition. London, SAGE Publications, Inc.

Frumkin, D., Wasserstrom, A., Budowle, B. & Davidson, A. (2011). DNA methylation-based forensic tissue identification. *Forensic Science International: Genetics*. 5. p.pp. 517–524.

Fujita, Y., Tsuchiya, K., Abe, S., Takiguchi, Y., Kubo, S. & Sakurai, H. (2005). Estimation of the age of human bloodstains by electron paramagnetic resonance spectroscopy: long-term controlled experiment on the effects of environmental factors. *Forensic science international*. 152 (1). pp. 39–43.

Fung, K.Y.C., Glode, L.M., Green, S. & Duncan, M.W. (2004). A comprehensive characterization of the peptide and protein constituents of human seminal fluid. *The Prostate*. 61. p.pp. 171–181.

Gaál, Ö, Medgyesi, G.A. & Vereczkey, L. (1980). *Electrophoresis in the Separation of Biological Macromolecules*. Chichester, John Wiley & Sons.

Gajjar, K., Trevisan, J., Owens, G., Keating, P.J., Wood, N.J., Stringfellow, H.F., Martin-Hirsch, P.L. & Martin, F.L. (2013). Fourier-transform infrared spectroscopy coupled with a classification machine for the analysis of blood plasma or serum: A novel diagnostic approach for ovarian cancer. *The Analyst*. 138 (14). p.pp. 3917–26.

Garidel, P. & Schott, H. (2006a). Fourier-Transform midinfrared spectroscopy for analysis and screening of liquid protein formulations part 1: Understanding infrared spectroscopy of proteins. *BioProcess International*. p.pp. 40–46.

Garidel, P. & Schott, H. (2006b). Fourier-Transform midinfrared spectroscopy for analysis and screening of liquid protein formulations part 2: Details, analysis and applications. *BioProcess International*. 1. p.pp. 48–55.

Gazi, E., Dwyer, J., Gardner, P., Ghanbari-Siahkali, A., Wade, A.P., Miyan, J., Lockyer, N.P., Vickerman, J.C., Clarke, N.W., Shanks, J.H., Scott, L.J., Hart, C.A. & Brown, M. (2003). Applications of Fourier transform infrared microspectroscopy in studies of benign prostate and prostate cancer. A pilot study. *The Journal of Pathology*. 201 (1). p.pp. 99–108.

Gerakines, P.A., Schutte, W.A., Greenberg, J.M. & Dishoeck, E.F. Van (1995). The infrared band strengths of H2O, CO and CO2 in laboratory simulations of astrophysical ice mixtures. *Astronomy & Astrophysics*. 296. p.pp. 810–818.

Ghafouri, B., Tagesson, C. & Lindahl, M. (2003). Mapping of proteins in human saliva using two-dimensional gel electrophoresis and peptide mass fingerprinting. *Proteomics*. 3 (6). p.pp. 1003–1015.

Gilany, K., Pouracil, R.S.M. & Sadeghi, M.R. (2014). Fourier transform infrared spectroscopy: a potential technique for noninvasive detection of spermatogenesis. *Avicenna journal of medical biotechnology*. 6 (1). p.pp. 47–52.

Glatz, Z., Nováková, S. & Štěrbová, H. (2001). Analysis of thiocyanate in biological fluids by capillary zone electrophoresis. *Journal of Chromatography A*. 916. p.pp. 273–277.

Gomes, I., Kohlmeier, F. & Schneider, P.M. (2011). Genetic markers for body fluid and tissue identification in forensics. *Forensic Science International: Genetics Supplement Series*. 3 (1). p.pp. e469–e470.

Gray, D., Frascione, N. & Daniel, B., (2012). Development of an immunoassay for the differentiation of menstrual blood from peripheral blood. *Forensic Science International*. 220. p.pp. 12–18.

Great Britain, *Human Tissue Act 2004: Elizabeth II. Chapter 30*. (2004) London: The Stationary Office.

Great Britain, Office of National Statistics (2014) *Crime in England & Wales, Year Ending March 2014*, United Kingdom, Office of National Statistics.

Griffiths, P.R. & de Haseth, J.A. (2007). *Fourier Transform Infrared Spectrometry*, 2nd Edition. New Jersey, Wiley & Sons, Inc.

Gunasekaran, S. & Sankari, G., (2004). FTIR and UV-Visible spectral study on normal and diseased blood samples. *Asian Journal of Chemistry*. 16 (3-4). p.pp. 1779–1786.

Gunn, A. (2013). *Essential Forensic Biology*, 2nd Edition. Singapore, Wiley-Blackwell.

Haas, C., Klesser, B., Kratzer, A. & Bär, W., (2008). mRNA profiling for body fluid identification. *Forensic Science International: Genetics Supplement Series*. 1 (1). pp. 37–38.

Haas, C., Klesser, B., Maake, C., Bär, W. & Kratzer, A., (2009). mRNA profiling for body fluid identification by reverse transcription endpoint PCR and realtime PCR. *Forensic science international. Genetics*. 3 (2). pp. 80–8.

Haas, C., Hanson, E., Kratzer, A., Bär, W. & Ballantyne, J. (2011a). Selection of highly specific and sensitive mRNA biomarkers for the identification of blood. *Forensic Science International: Genetics*. 5. p.pp. 449–458.

Haas, C., Hanson, E., Bär, W., Banemann, R., Bento, a M., Berti, A., Borges, E., Bouakaze, C., Carracedo, A., Carvalho, M., Choma, A., Dötsch, M., Durianciková, M., Hoff-Olsen, P., Hohoff, C., Johansen, P., Lindenbergh, P. a, Loddenkötter, B., Ludes, B., Maroñas, O., Morling, N., Niederstätter, H., Parson, W., Patel, G., Popielarz, C., Salata, E., Schneider, P.M., Sijen, T., Sviezená, B., Zatkalíková, L. & Ballantyne, J. (2011b). mRNA profiling for the identification of blood: Results of a collaborative EDNAP exercise. Forensic Science International: Genetics. 5 (1). p.pp. 21–26.

Haas, C., Hanson, E., Anjos, M.J., Bär, W., Banemann, R., Berti, A., Borges, E., Bouakaze, C., Carracedo, A., Carvalho, M., Castella, V., Choma, A., De Cock, G., Dötsch, M., Hoff-Olsen, P., Johansen, P., Kohlmeier, F., Lindenbergh, P. a, Ludes, B., Maroñas, O., Moore, D., Morerod, M.-L., Morling, N., Niederstätter, H., Noel, F., Parson, W., Patel, G., Popielarz, C., Salata, E., Schneider, P.M., Sijen, T., Sviežena, B., Turanská, M., Zatkalíková, L. & Ballantyne, J. (2012). RNA/DNA co-analysis from blood stains: Results of a second collaborative EDNAP exercise. Forensic Science International: Genetics. 6 (1). p.pp. 70–80.

Haas, C., Hanson, E., Anjos, M.J., Banemann, R., Berti, A., Borges, E., Carracedo, A., Carvalho, M., Courts, C., De Cock, G., Dötsch, M., Flynn, S., Gomes, I., Hollard, C., Hjort, B., Hoff-Olsen, P., Hríbiková, K., Lindenbergh, A., Ludes, B., Maroñas, O., McCallum, N., Moore, D., Morling, N., Niederstätter, H., Noel, F., Parson, W., Popielarz, C., Rapone, C., Roeder, a D., Ruiz, Y., Sauer, E., Schneider, P.M., Sijen, T., Court, D.S., Sviežená, B., Turanská, M., Vidaki, A., Zatkalíková, L. & Ballantyne, J. (2013). RNA/DNA co-analysis from human saliva and semen stains: Results of a third collaborative EDNAP exercise. Forensic Science International: Genetics. 7 (2). p.pp. 230–239.

Haas, C., Hanson, E., Anjos, M.J., Ballantyne, K.N., Banemann, R., Bhoelai, B., Borges, E., Carvalho, M., Courts, C., De Cock, G., Drobnic, K., Dötsch, M., Fleming, R., Franchi, C., Gomes, I., Hadzic, G., Harbison, S. a, Harteveld, J., Hjort, B., Hollard, C., Hoff-Olsen, P., Hüls, C., Keyser, C., Maroñas, O., McCallum, N., Moore, D., Morling, N., Niederstätter, H., Noël, F., Parson, W., Phillips, C., Popielarz, C., Roeder, a D., Salvaderi, L., Sauer, E., Schneider, P.M., Shanthan, G., Court, D.S., Turanská, M., van Oorschot, R. a H., Vennemann, M., Vidaki, A., Zatkalíková, L. & Ballantyne, J. (2014). RNA/DNA co-analysis from human menstrual blood and vaginal secretion stains: Results of a fourth and fifth collaborative EDNAP exercise. Forensic Science International: Genetics. 8 (1). p.pp. 203–212.

Hampson, C., Louhelainen, J. & McColl, S. (2011). An RNA expression method for aging forensic hair samples. *Journal of Forensic Sciences*. 56 (2). p.pp. 359–365.

Hankins, J. (2006). The Role of Albumin in Fluid and Electrolyte Balance. *Journal of Infusion Nursing*. 29 (5). p.pp. 260–265.

Hanson, E.K., Lubenow, H. & Ballantyne, J. (2009). Identification of forensically relevant body fluids using a panel of differentially expressed microRNAs. *Analytical Biochemistry*. 387 (2). p.pp. 303–14.

Hanson, E.K. & Ballantyne, J. (2010). A blue spectral shift of the hemoglobin soret band correlates with the age (time since deposition) of dried bloodstains. *PloS One*. 5 (9). p.pp. e12830 1–11.

Hanson, E., Albornoz, a. & Ballantyne, J. (2011). Validation of the hemoglobin (Hb) hypsochromic shift assay for determination of the time since deposition (TSD) of dried bloodstains. *Forensic Science International: Genetics Supplement Series*. 3 (1). p.pp. e307–e308.

Hanson, E., Haas, C., Jucker, R. & Ballantyne, J. (2012). Specific and sensitive mRNA biomarkers for the identification of skin in "touch DNA" evidence. *Forensic Science International: Genetics*. 6 (5). p.pp. 548–58.

Hanson, E.K. & Ballantyne, J. (2013). Multiplex high resolution melt (HRM) messenger RNA profiling assays for body fluid identification. *Forensic Science International: Genetics Supplement Series*. 4 (1). p.pp. e125–e126.

Hardinge, P., Allard, J., Wain, A. & Watson, S. (2013). Optimisation of choline testing using Florence Iodine reagent, including comparative sensitivity and specificity with PSA and AP tests. *Science & Justice*. 53 (1). p.pp. 34–40.

Hassan, I., Waheed, A., Yadav, S., Singh, T.P. & Ahmad, F. (2008). Zinc alpha 2-glycoprotein: A multidisciplinary protein. *Molecular Cancer Research*. 6 (6). p.pp. 892–906.

Hassler, N., Baurecht, D., Reiter, G. & Fringeli, U.P. (2011). In situ FTIR ATR spectroscopic study of the interaction of immobilized human serum albumin with cholate in aqueous environment. *The Journal of Physical Chemistry C*. 115 (4). p.pp. 1064–1072.

Haudek, V.J., Slany, A., Gundacker, N.C., Wimmer, H., Drach, J. & Gerner, C. (2009). Proteome Maps of the Main Human Peripheral Blood Constituents research articles. *The Journal of Proteome Research*. 8. p.pp. 3834–3843.

Hawkins, W.W., Speck, E. & Leonard, V.G. (1954). Variation of the hemoglobin level with age and sex. *Blood*. 9. p.pp. 999–1007.

Hayworth, D. (2014). *Overview of Protein Assays*. [Online]. 2014. Available from: http://www.piercenet.com/method/overview-protein-assays. [Accessed: 3 August 2014].

Hayworth, D. (2014a). *Overview of Electrophoresis*. [Online]. 2014. Available from: http://www.piercenet.com/method/overview-electrophoresis. [Accessed: 29 July 2014].

Hayworth, D. (2014b). *Protein Gel Stains*. [Online]. 2014. Available from: http://www.piercenet.com/method/protein-gel-stains. [Accessed: 3 August 2014].

Hedman, J., Gustavsson, K. & Ansell, R. (2008). Using the new Phadebas® Forensic Press test to find crime scene saliva stains suitable for DNA analysis. *Forensic Science International: Genetics Supplement Series*. 1. p.pp. 430–432.

Hedman, J., Dalin, E., Rasmusson, B. & Ansell, R. (2011). Evaluation of amylase testing as a tool for saliva screening of crime scene trace swabs. *Forensic Science International: Genetics*. 5 (3). p.pp. 194–198.

Heggestuen, J. (2013). *One In Every 5 People In The World Own A Smartphone, One In Every 17 Own A Tablet*. [Online]. 2013. Business Insider. Available from:

http://www.businessinsider.com/smartphone-and-tablet-penetration-2013-10. [Accessed: 12 March 2014].

Hering, J.A. & Haris, P.I. (2009). FTIR Spectroscopy for Analysis of Protein Secondary Structure. In: Barth, A. & Haris, P.I. (Eds.) (2009). *Biological & Biomedical Infrared Spectroscopy: Advances in Biomedical Spectroscopy, Volume 2*. Netherlands, IOS Press.

Hill, R.J., Konigsberg, W., Guidotti, G. & Craig, L.C. (1962). The structure of human hemoglobin. I. The separation of the alpha and beta chains and their amino acid composition. *The Journal of Biological Chemistry*. 237 (5). p.pp. 1549–1554.

Ho, R. (2014). *Handbook of Univariate & Multivariate Data Analysis with IBM SPSS*, 2nd Edition. Baco Raton, CRC Press.

Hochmeister, M.N., Budowle, B., Rudin, O., Gehrig, C., Borer, U., Thali, M. & Dirnhofer, R. (1999). Evaluation of prostate-specific antigen (PSA) membrane test assays for the forensic identification of seminal fluid. *Journal of Forensic Sciences*. 44 (5). p.pp. 1057–1060.

Housecroft, C.E. & Constable, E.C. (2006). *Chemistry*, 3rd Edition. Essex, Pearson Education Ltd.

Huang, C.-M. (2004). Comparative proteomic analysis of human whole saliva. *Archives of Oral Biology*. 49. p.pp. 951–962.

Huang, Z., Chen, X., Chen, Y., Chen, J., Dou, M., Feng, S., Zeng, H. & Chen, R. (2011). Raman spectroscopic characterization and differentiation of seminal plasma. *Journal of biomedical optics*. 16 (11). p.p. 110501.

Hughes, C., Brown, M., Clemens, G., Henderson, A., Monjardez, G., Clarke, N.W. & Gardner, P. (2014). Assessing the challenges of Fourier transform infrared spectroscopic analysis of blood serum. *Journal of Biophotonics*. 9. p.pp. 1–9.

Huleihel, M., Karpasas, M., Talyshansky, M., Souprun, Y., Doubijanski, Y. & Erukhimovitch, V. (2005). MALDI–TOF and FTIR microscopy analysis of blood serum from diarrhea patients. *Spectroscopy*. 19 (2). p.pp. 101–108.

Humphrey, S.P. & Williamson, R.T. (2001). A review of saliva: Normal composition, flow and function. *The Journal of Prosthetic Dentistry*. 85 (2). p.pp. 162–169.

Inoue, H. Takabe, F. Iwasa, M. Maeno, Y. & Seko, Y. (1992). A new marker for estimation of bloodstain age by high performance liquid chromatography. *Forensic Science International*. 57. p.pp 17-27.

Jackson, A.R.W. & Jackson, J.M. (2010). *Forensic Science*, 3rd Edition. Essex, Pearson Education Ltd.

Jackson, M. & Mantsch, H.H. (1995). The use and misuse of FTIR spectroscopy in the determination of protein structure. *Critical Reviews in Biochemistry and Molecular Biology*. 30 (2). p.pp. 95–120.

Jackson, M., Sowa, M.G. & Mantsch, H.H. (1997). Infrared spectroscopy: a new frontier in medicine. *Biophysical Chemistry*. 68 (1-3) p.pp. 109–25.

James, P.S., Wolfe, C.A., Mackie, A., Ladha, S., Prentice, A. & Jones, R. (1999). Lipid dynamics in the plasma membrane of fresh and cryopreserved human spermatozoa. *Human Reproduction*. 14 (7). p.pp. 1827–1832.

JPK Instruments (2014). A practical guide to AFM force spectroscopy and data analysis, *Technical Note*. p.pp 1-8.

Juusola, J. & Ballantyne, J. (2003). Messenger RNA profiling: a prototype method to supplant conventional methods for body fluid identification. *Forensic Science International*. 135 (2). p.pp. 85–96

Kakhniashvili, D.G., Bulla, L. a & Goodman, S.R. (2004). The human erythrocyte proteome: Analysis by ion trap mass spectrometry. *Molecular & Cellular Proteomics: MCP*. 3 (5). p.pp. 501–509.

Kanagathara, N., Thirunavukkarasu, M., Jeyanthi, E.C. & Shenbagarajan, P. (2011). FTIR and UV-Visible spectral study on normal blood samples. *International Journal of Pharmacy and Biological Science*. 1 (2). p.pp. 74–81.

Kazarian, S.G. & Chan, K.L. a (2006). Applications of ATR-FTIR spectroscopic imageing to biomedical samples. *Biochimica et Biophysica Acta*. 1758 (7). p.pp. 858–67.

Kazarian, S.G. & Chan, K.L.A. (2013). ATR-FTIR spectroscopic imaging: Recent advances and applications to biological systems. *The Analyst*. 138 (7). p.pp. 1940–1951.

Kemp, W. (1991). *Organic Spectroscopy*, 3rd Edition. Hampshire, Palgrave.

Khaustova, S., Shkurnikov, M., Tonevitsky, E., Artyushenko, V. & Tonevitsky, A. (2010). Noninvasive biochemical monitoring of physiological stress by Fourier transform infrared saliva spectroscopy. *The Analyst*. 135 (12). p.pp. 3183–3192.

Knight, R. (Ed.) (2013). *Transfusion and Transplantation Science*, Fundamentals of Biomedical Science. Oxford, Oxford University Press.

Kohlmeier, F. & Schneider, P.M. (2012). Successful mRNA profiling of 23 years old blood stains. *Forensic Science International: Genetics*. 6 (2). p.pp. 274–276.

Kong, J. & Yu, S. (2007). Fourier transform infrared spectroscopic analysis of protein secondary structures. *Acta Biochimica et Biophysica Sinica*. 39 (8). p.pp. 549–559.

Krebs, H.A. (1950). Chemical composition of blood plasma and serum. *Annual Review of Biochemistry*. (12). p.pp. 409–430.

Kshirsagar, B., Wilson, B. & Wiggins, R.C. (1984). Polymeric complexes and fragments of albumin in normal human plasma. *Clinica Chimica Acta; International Journal of Clinical Chemistry*. 143 (3). p.pp. 265–273.

Lamy, E., Costa, A.R., Antunes, C.M., Vitorino, R. & Amado, F. (2012). Protein electrophoresis in saliva study. In: K. Ghowski (ed.). *Electrophoresis*. InTech, pp. 63–83.

Langford, A. Dean, J. Reed, R. Holmes, D, Weyers, J. & Jones, A. (2005). *Practical Skills in Forensic Science*. Essex, Pearson Education Limited.

Larson, D. (2013). *Infrared: Interpretation - UC Davis Chemwiki*. [Online]. 2013. Available from: http://chemwiki.ucdavis.edu/Physical_Chemistry/Spectroscopy/Vibrational_Spectroscopy/Infrared_Spectroscopy/Infrared:_Interpretation. [Accessed: 3 September 2014].

Lehmann, H. & Carrell, R.W. (1969). Variations in the structure of human haemoglobin. With particular reference to the unstable haemoglobins. *British Medical Bulletin*. 25 (1). p.pp. 14–23.

Lenzi, A., Picardo, M., Gandini, L. & Dondero, F. (1996). Lipids of the sperm plasma membrane: From polyunsaturated fatty acids considered as markers of sperm function to possible scavenger therapy. *Human Reproduction Update*. 2 (3). p.pp. 246–256.

Lerner, E. (2014). *University of Pennsylvania: Penn Physicists Conquer the "Coffee Ring Effect."* [Online]. 2014. Available from: http://www.upenn.edu/spotlights/penn-physicists-conquer-coffee-ring-effect. [Accessed: 11 September 2014].

Li, L., Frey, M. & Browning, K.J. (2010). Biodegradability Study on Cotton and Polyester Fabrics. *Journal of Engineered Fibres and Fabrics*. 5 (4). p.pp. 42–53.

Li, R. (2008). *Forensic Biology.* United States of America, CRC Press.

Li, B., Beveridge, P., O'Hare, W.T. & Islam, M. (2011). The estimation of the age of a blood stain using reflectance spectroscopy with a microspectrophotometer, spectral pre-processing and linear discriminant analysis. *Forensic Science International*. 212 (1-3). p.pp. 198–204.

Li, B., Beveridge, P., O'Hare, W.T. & Islam, M. (2013). The age estimation of blood stains up to 30 days old using visible wavelength hyperspectral image analysis and linear discriminant analysis. *Science & Justice*. 53 (3). p.pp. 270–277.

Life Technologies (2014). *SDS PAGE, Protein Gel Electrophoresis Solutions*. [Online]. 2014. Available from: http://www.lifetechnologies.com/uk/en/home/life-science/protein-expression-and-analysis/protein-gel-electrophoresis/sds-page.html. [Accessed: 3 February 2014].

Lindenbergh, A., Maaskant, P. & Sijen, T. (2013). Implementation of RNA profiling in forensic casework. *Forensic science international. Genetics*. 7 (1). p.pp. 159–66.

Lundwall, Å., Bjartell, A., Olsson, A.Y. & Malm, J. (2002). Semenogelin I and II, the predominant human seminal plasma proteins, are also expressed in non-genital tissues. *Molecular Human Reproduction*. 8 (9). p.pp. 805–810.

Ma, L.L., Yi, S.H., Huang, D.X., Mei, K. & Yang, R.Z. (2013). Screening and identification of tissue-specific methylation for body fluid identification. *Forensic Science International: Genetics Supplement Series*. 4 (1). p.pp. e37–e38.

Malm, J., Jonsson, M., Frohm, B. & Linse, S. (2007). Structural properties of semenogelin I. *The FEBS journal*. 274 (17). p.pp. 4503–4510.

Marques, M.R.C., Loebenberg, R. & Almukainzi, M. (2011). *Simulated Biological Fluids with Possible Application in Dissolution Testing*. (August). p.pp. 15–28.

Marrone, A. & Ballantyne, J. (2009). Changes in dry state hemoglobin over time do not increase the potential for oxidative DNA damage in dried blood. *PloS One*. 4 (4). p.pp. e5110.

McLaughlin, G., Sikirzhytski, V. & Lednev, I.K. (2013). Circumventing substrate interference in the Raman spectroscopic identification of blood stains. *Forensic Science International*. 231 (1-3). p.pp. 157–166.

McLaughlin, G. & Lednev, I.K. (2014). A modified Raman multidimensional spectroscopic signature of blood to account for the effect of laser power. *Forensic Science International*. 240. p.pp. 88–94.

Merck Sharp & Dohme Corporation (2014). *Female Reproductive Endocrinology: Merck Manual Professional*. [Online]. 2014. Available from: http://www.merckmanuals.com/professional/gynecology_and_obstetrics/female_reproductive_endocrinology/female_reproductive_endocrinology.html. [Accessed: 7 October 2014].

Mirmonsef, P., Hotton, A.L., Gilbert, D., Burgad, D., Landay, A., Weber, K.M., Cohen, M., Ravel, J. & Spear, G.T. (2014). Free glycogen in vaginal fluids is associated with Lactobacillus colonization and low vaginal pH. *PloS One*. 9 (7). p.p. e102467 1–11.

Mordacq, J.C. & Ellington, R.W. (1994). Polyacrylamide Gel Electrophoresis (PAGE) of Blood Proteins. In: C. A. Goldman (ed.). *Tested Studies for Laboratory Teaching, Volume 15*. pp. 15–44.

Moore, W.S. (1968). Electron paramagnetic resonance. *Physics Education*. 3. p.pp. 11–16.

Moore, G. Knight, G. & Blann, A. (2010). *Haematology.* Fundamentals of Biomedical Science, Oxford, Oxford University Press.

Mostaço-Guidolin, L.B. & Bachmann, L. (2011). Application of FTIR spectroscopy for identification of blood and leukemia biomarkers: A review over the past 15 years. *Applied Spectroscopy Reviews*. 46 (5) p.pp. 388–404.

Movasaghi, Z. Rehman, S. & ur Rehman, I. (2008). Fourier Transform Infrared (FTIR) Spectroscopy of Biological Tissues. *Applied Spectroscopy Reviews*. 43. p.pp 134-179.

National Centre for Biotechnology Information (2014). *AMBP alpha-1-microglobulin/bikunin precursor [Homo sapiens (human)] - Gene - NCBI*. [Online]. 2014. Available from: http://www.ncbi.nlm.nih.gov/gene/259. [Accessed: 28 April 2014].

National Forensic Science Technology Centre (2007). *Leucomalachite Green Presumptive Test for Blood*.

Naumann, D. Fabian, H. & Lasch, P. (2009). FTIR Spectroscopy of Cells, Tissues & Body Fluids. In: Barth, A. & Haris, P.I. (Eds.) (2009). *Biological & Biomedical Infrared Spectroscopy: Advances in Biomedical Spectroscopy, Volume 2*. Netherlands, IOS Press.

Nicholson, I.C., Mavrangelos, C., Fung, K., Ayhan, M., Levichkin, I., Johnston, A., Zola, H. & Hoogenraad, N.J. (2005). Characterisation of the protein composition of peripheral blood mononuclear cell microsomes by SDS-PAGE and mass spectrometry. *Journal of immunological methods*. 305 (1). p.pp. 84–93.

Nussbaumer, C., Gharehbaghi-Schnell, E. & Korschineck, I. (2006). Messenger RNA profiling: a novel method for body fluid identification by real-time PCR. *Forensic science international*. 157 (2-3). p.pp. 181–6.

Ollesch, J., Drees, S.L., Heise, H.M., Behrens, T., Brüning, T. & Gerwert, K. (2013). FTIR spectroscopy of biofluids revisited: an automated approach to spectral biomarker identification. *The Analyst*. 138 (14). p.pp. 4092–102.

Olsén, E.-L., Edenberger, E., Mattsson, M. & Ansell, R. (2011). Phadebas® Forensic Press test and the presence of amylases in body fluids naturally deposited on textile. *Forensic Science International: Genetics Supplement Series*. 3 (1). p.pp. e155–e156.

Olsztynska-Janus, S., Szymborska-Malek, K., Gasior-Glogowska, M., Walski, T., Komorowska, M., Witkeiwicz, W., Pezowics, C., Kobielarz, M. & Szotek, S. (2012). Spectroscopic techniques in the study of human tissues and their components. Part I: IR spectroscopy. *Acta of Bioengineering & Biomechanics*. 14 (3). p.pp. 101–115.

Omaha Police Department Crime Laboratory (2003). *Luminol processing for hidden blood*. p.pp. 1–5.

Omelia, E.J., Uchimoto, M.L. & Williams, G. (2013). Quantitative PCR analysis of blood- and saliva-specific microRNA markers following solid-phase DNA extraction. *Analytical biochemistry*. 435 (2). p.pp. 120–2.

Osborne, C. & Brooks, S. a (2006). SDS-PAGE and Western blotting to detect proteins and glycoproteins of interest in breast cancer research. *Methods in Molecular Medicine*. 120. p.pp. 217–229.

Owen, D.H. & Katz, D.F. (2005). A review of the physical and chemical properties of human semen and the formulation of semen simulant. *Journal of Andrology*. 26 (4). p.pp. 459–469.

Pallister, C. (1994). *Blood: Physiology & Pathophysiology*. Oxford, Butterworth & Heinemann Ltd.

Pelton, J.T. & McLean, L.R. (2000). Spectroscopic methods for analysis of protein secondary structure. *Analytical biochemistry*. 277 (2). p.pp. 167–76.

Petibois, C., Rigalleau, V., Melin, A.M., Perromat, A., Cazorla, G., Gin, H. & Déléris, G. (1999). Determination of glucose in dried serum samples by Fourier-transform infrared spectroscopy. *Clinical Chemistry*. 45 (9). p.pp. 1530–5.

Petibois, C., Cazorla, G., Cassaigne, a & Déléris, G. (2001a). Plasma protein contents determined by Fourier-transform infrared spectrometry. *Clinical Chemistry*. 47 (4). p.pp. 730–8.

Petibois, C., Cazorla, G., Gin, H. & Déléris, G. (2001b). Differentiation of populations with different physiologic profiles by plasma Fourier-transform infrared spectra classification. *The Journal of Laboratory and Clinical Medicine*. 137 (3). p.pp. 184–90.

Pfeiffer, H. Mörnstad, H. & Teivens, A. (1995). Estimation of chronological age using the aspartic acid racemization method. I. On human rib cartilage. *International Journal of Legal Medicine*. 108. p.pp 19-23.

Pilch, B. & Mann, M. (2006). Large-scale and high-confidence proteomic analysis of human seminal plasma. *Genome Biology*. 7 (5). p.pp. R40:1–10.

Qi, B., Kong, L. & Lu, Y. (2013). Gender-related difference in bloodstain RNA ratio stored under uncontrolled room conditions for 28 days. *Journal of Forensic and Legal Medicine*. 20 (4). p.pp. 321–325.

Di Quinzio, M.K.W., Oliva, K., Holdsworth, S.J., Ayhan, M., Walker, S.P., Rice, G.E., Georgiou, H.M. & Permezel, M. (2007). Proteomic analysis and characterisation of human cervico-vaginal fluid proteins. *The Australian & New Zealand Journal of Obstetrics & Gynaecology*. 47. p.pp. 9–15.

Raju, P.S. & Iyengar, N.K. (1964). Acid phosphatase reaction as a specific test for the identification of seminal stains. *The Journal of Criminal Law and Criminology*. 55 (4). p.pp. 522–525.

Ramasubbu, N., Paloth, V., Luo, Y., Brayer, G.D. & Levine, M.J. (1996). Structure of human salivary alpha-amylase at 1.6 A resolution: Implications for its role in the oral cavity. *Acta Crystallographica. Section D, Biological Crystallography*. 52 (3). p.pp. 435–446.

Ramasubbu, N., Ragunath, C., Sundar, K., Mishra, P.J. & Kandra, L. (2005). Structure-function relationships in human salivary α-amylase: Role of aromatic residues. *Biologia*. 60 (16). p.pp. 47–56.

Richard, M.L.L., Harper, K. a, Craig, R.L., Onorato, A.J., Robertson, J.M. & Donfack, J. (2012). Evaluation of mRNA marker specificity for the identification of five human body fluids by capillary electrophoresis. *Forensic Science International: Genetics*. 6 (4). p.pp. 452–60.

Sahu, K.C. (2007). *Textbook of Remote Sensing & Geographical Information Systems*. New Delhi, Atlantic Publishers & Distributors Ltd.

cenesafe (2010). *Kastle Meyer Presumptive Blood Testing Kit*. [Online]. 2010. Available from: https://www.scenesafe.co.uk/index.php?route=product/product&product_id=161. [Accessed: 17 September 2014].

Schenk, S., Schoenhals, G.J., de Souza, G. & Mann, M. (2008). A high confidence, manually validated human blood plasma protein reference set. *BMC Medical Genomics*. 1 (41). p.pp. 1–28.

Schenkels, L.C.P.M., Veerman, E.C.I. & Nieuw Amerongen, a. V. (1995). Biochemical composition of human saliva in relation to other mucosal fluids. *Critical Reviews in Oral Biology & Medicine*. 6 (2). p.pp. 161–175.

Schultz, C.P., Ahmed, M.K., Dawes, C. & Mantsch, H.H. (1996). Thiocyanate levels in human saliva: Quantitation by Fourier transform infrared spectroscopy. *Analytical Biochemistry*. 240 (1). p.pp. 7–12.

Schwartz, S.S., Zhu, W.X. & Sreebny, L.M. (1995). Sodium dodecyl sulphate-polyacrylamide gel electrophoresis of human whole saliva. *Archives of Oral Biology*. 40 (10). p.pp. 949–58.

Scott, D.A., Renaud, D.E., Krishnasamy, S., Meriç, P., Buduneli, N., Cetinkalp, S. & Liu, K.-Z. (2010). Diabetes-related molecular signatures in infrared spectra of human saliva. *Diabetology & Metabolic Syndrome*. 2 (48). p.pp. 1–9.

Setzer, M., Juusola, J. & Ballantyne, J. (2008). Recovery and stability of RNA in vaginal swabs and blood, semen, and saliva stains. *Journal of Forensic Sciences*. 53 (2). p.pp. 296–305.

Shaw, R.A. & Mantsch, H.H. (2006). Infrared Spectroscopy in Clinical and Diagnostic Analysis. In: R. A. Meyers (ed.). *Encyclopedia of Analytical Chemistry*. Chichester: John Wiley & Sons Ltd., pp. 1–20.

Shen, Y., Davies, A. & Linfield, E. (2003). Determination of glucose concentration in whole blood using Fourier-transform infrared spectroscopy. *Journal of Biological Physics*. 29. p.pp. 129–133.

Shimadzu (2014). *Principles of MALDI-TOF Mass Spectrometry*. [Online]. 2014. Available from: http://www.shimadzu.com/an/lifescience/maldi/princpl1.html. [Accessed: 28 April 2014].

Shimadzu Corporation (2014a). *ATR Precautions: Part One*. [Online]. 2014. Available from: http://www.shimadzu.com/an/ftir/support/ftirtalk/letter1/atr1.html. [Accessed: 22 October 2014].

Shimadzu Corporation (2014b). *ATR Precautions: Part Two*. [Online]. 2014. Available from: http://www.shimadzu.com/an/ftir/support/ftirtalk/letter2/atr2.html. [Accessed: 22 October 2014].

Sigma-Aldrich (2001). *Ethylenediaminetetraacetic acid disodium salt dehydrate - Product Information*. [Online]. 2001. Available from: http://www.sigmaaldrich.com/content/dam/sigma-aldrich/docs/Sigma/Product_Information_Sheet/e5134pis.pdf. [Accessed: 26 April 2014].

Sigma-Aldrich (2014). *Tools for Protein Quantitation* /. [Online]. 2014. Available from: http://www.sigmaaldrich.com/life-science/proteomics/protein-quantitation/tools-for-protein.html. [Accessed: 4 August 2014].

Sikirzhytskaya, A., Sikirzhytski, V. & Lednev, I.K. (2012). Raman spectroscopic signature of vaginal fluid and its potential application in forensic body fluid identification. *Forensic Science International*. 216 (1-3). p.pp. 44–8.

Sikirzhytski, V., Virkler, K. & Lednev, I.K. (2010). Discriminant analysis of Raman spectra for body fluid identification for forensic purposes. *Sensors (Basel, Switzerland)*. 10 (4). p.pp. 2869–84.

Sikirzhytski, V., Sikirzhytskaya, A. & Lednev, I.K. (2012). Advanced statistical analysis of Raman spectroscopic data for the identification of body fluid traces: Semen and blood mixtures. *Forensic Science International*. 222 (1-3). p.pp. 259–265.

Silletti, E., Vitorino, R.M.P., Schipper, R., Amado, F.M.L. & Vingerhoeds, M.H. (2010). Identification of salivary proteins at oil-water interfaces stabilized by lysozyme and beta-lactoglobulin. *Archives of Oral Biology*. 55 (4). p.pp. 268–278.

Silverman, B. (2011). *Research and Development in Forensic Science: a Review*.

Simard, A.-M., DesGroseillers, L. & Sarafian, V. (2012). Assessment of RNA stability for age determination of body fluid stains. *Canadian Society of Forensic Science Journal*. 45 (4). p.pp. 179–194.

Sitole, L., Steffens, F., Krüger, T.P.J. & Meyer, D. (2014). Mid-ATR-FTIR spectroscopic profiling of HIV/AIDS sera for novel systems diagnostics in global health. *Omics: A Journal of Integrative Biology*. 18 (8). p.pp. 513–523.

Smith, K.R. & Olson, L.A. (2002). *Removal of Blood Stains*. 2 (12). p.pp. 1–7.

Snider, J. (2014). *Protein Glycosylation*. [Online]. 2014. Available from: http://www.piercenet.com/method/protein-glycosylation. [Accessed: 22 September 2014].

Squier, C. & Brogden, K. (2011). *Human Oral Mucosa: Development, Structure & Function*. Chichester, John Wiley & Sons Ltd.

Srinivas, P.R., Verma, M., Zhao, Y. & Srivastava, S. (2002). Proteomics for cancer biomarker discovery. *Clinical Chemistry*. 48 (8). p.pp. 1160–9.

Van Steendam, K., De Ceuleneer, M., Dhaenens, M., Van Hoofstat, D. & Deforce, D. (2013). Mass spectrometry-based proteomics as a tool to identify biological matrices in forensic science. *International Journal of Legal Medicine*. 127 (2). p.pp. 287–98.

Strasser, S., Zink, A., Kada, G., Hinterdorfer, P., Peschel, O., Heckl, W.M., Nerlich, A.G. & Thalhammer, S. (2007). Age determination of blood spots in forensic medicine by force spectroscopy. *Forensic Science International*. 170 (1). p.pp. 8–14.

Strachan, T. & Read, A. (2011). *Human Molecular Genetics*, 4th Edition. Garland Science, United States of America, Taylor & Francis Group.

Sultana, R.R., Zafarullah, S.N. & Kirubamani, N.H. (2011). Utility of FTIR spectroscopic analysis of saliva of diabetic pregnant women in each trimester. *Indian Journal of Science & Technology*. 4 (8). p.pp. 967–970.

Sun, G. & Palmer, A.F. (2008). Preparation of ultrapure bovine and human hemoglobin by anion exchange chromatography. *Journal of Chromatography B*. 867 (1). p.pp. 1–14.

Swinburne University of Technology (2014). *Electromagnetic Radiation | COSMOS*. [Online]. 2014. Available from: http://astronomy.swin.edu.au/cosmos/E/electromagnetic+radiation. [Accessed: 3 July 2014].

Szafarska, M., Woźniakiewicz, M., Pilch, M., Zięba-Palus, J. & Kościelniak, P. (2009). Computer analysis of ATR-FTIR spectra of paint samples for forensic purposes. *Journal of Molecular Structure*. 924-926. p.pp. 504–513.

Tang, L.-J., De Seta, F., Odreman, F., Venge, P., Piva, C., Guaschino, S. & Garcia, R.C. (2007). Proteomic analysis of human cervical-vaginal fluids. *Journal of Proteome Research*. 6 (7). p.pp. 2874–2883.

Taylor, S.E., Cheung, K.T., Patel, I.I., Trevisan, J., Stringfellow, H.F., Ashton, K.M., Wood, N.J., Keating, P.J., Martin-Hirsch, P.L. & Martin, F.L. (2011). Infrared spectroscopy with multivariate analysis to interrogate endometrial tissue: A novel and objective diagnostic approach. *British Journal of Cancer*. 104 (5). p.pp. 790–797.

Tayyab, S. & Qasim, M.A. (1988). Biochemistry and roles of glycophorin A. *Biochemical Education*. 16 (2). p.pp. 63–66.

Technologies, C. (2012). *What is a Microspectrophotometer?* [Online]. 2012. Available from: http://www.craictechnologies.com/products/what-is-a-microspectrophotometer. [Accessed: 12 March 2014].

Technology Strategy Board (2011). *Forensic Challenges Catalogue*. [Online]. 2011. Forensic Science - innovateuk. Available from: https://connect.innovateuk.org/web/forensics/research-challenges-catalogue. [Accessed: 8 July 2014].

Thanakiatkrai, P., Yaodam, A. & Kitpipit, T. (2013). Age estimation of bloodstains using smartphones and digital image analysis. *Forensic science international*. 233 (1-3). p.pp. 288–97.

The Pennsylvania State University (2014). *7.2 Electromagnetic Radiation | Mapping our Changing World*. [Online]. 2014. Available from: https://www.e-education.psu.edu/geog160/node/1958. [Accessed: 30 June 2014].

Thermo Scientific (2014). *Coomassie (Bradford) Protein Assay*. [Online]. 2014. Available from: http://www.piercenet.com/product/coomassie-bradford-protein-assay. [Accessed: 4 August 2014].

Thummalapalli, R. (2010). *Fourier Transform: Nature's Way of Analyzing Data*. [Online]. 2010. Yale Scientific Magazine. Available from: http://www.yalescientific.org/2010/12/fourier-transform-natures-way-of-analyzing-data/. [Accessed: 2 July 2014].

Tirumalai, R.S., Chan, K.C., Prieto, D. a, Issaq, H.J., Conrads, T.P. & Veenstra, T.D. (2003). Characterization of the low molecular weight human serum proteome. *Molecular & Cellular Proteomics*. 2 (10). p.pp. 1096–103.

Tobe, S.S., Watson, N. & Daéid, N.N. (2007). Evaluation of six presumptive tests for blood, their specificity, sensitivity, and effect on high molecular-weight DNA. *Journal of Forensic Sciences*. 52 (1). p.pp. 102–109.

Tsuge, K., Kataoka, M. & Seto, Y. (2000). Cyanide and thiocyanate levels in blood and saliva of healthy adult volunteers. *Journal of Health Science*. 46 (5). p.pp. 343–350.

UniProt (2014). *AMY1A - Alpha-amylase 1 precursor - Homo sapiens (Human)*. [Online]. 2014. Available from: http://www.uniprot.org/uniprot/P04745. [Accessed: 22 September 2014].

University College London (2010). *MADLI-QTOF MS / ESI-QTOF MS*. [Online]. 2010. Available from: http://www.ucl.ac.uk/ich/services/lab-services/mass_spectrometry/proteomics/technologies/madli. [Accessed: 28 April 2014].

University of Leeds (2013). *Histology Guide | Blood*. [Online]. 2013. Available from: http://www.histology.leeds.ac.uk/blood/blood_wbc.php. [Accessed: 13 December 2013].

University of Liverpool (2013). *Vibrational Spectroscopy: ChemTube 3D*. [Online]. 2013. Available from: http://osxs.ch.liv.ac.uk/java/spectrovibcd1-CE-final.html. [Accessed: 18 August 2014].

Vandenberg, N. & van Oorschot, R. a H. (2006). The use of Polilight in the detection of seminal fluid, saliva, and bloodstains and comparison with conventional chemical-based screening tests. *Journal of Forensic Sciences*. 51 (2). p.pp. 361–370.

Venkataraman, N., Cole, A.L., Svoboda, P., Pohl, J. & Cole, A.M. (2005). Cationic polypeptides are required for anti-HIV-1 activity of human vaginal fluid. *The Journal of Immunology*. 175. p.pp. 7560–7567.

Vermassen, T., Speeckaert, M.M., Lumen, N., Rottey, S. & Delanghe, J.R. (2012). Glycosylation of prostate specific antigen and its potential diagnostic applications. *Clinica Chimica Acta: International Journal of Clinical Chemistry*. 413 (19-20). p.pp. 1500–1505.

Vincini, L. (2010). *The Characterisation and Identification of Body Fluid Proteins for Forensic Purposes*. Robert Gordon University.

Virkler, K. & Lednev, I.K. (2008). Raman spectroscopy offers great potential for the nondestructive confirmatory identification of body fluids. *Forensic Science International*. 181 (1-3). p.pp. e1–5.

Virkler, K. & Lednev, I.K. (2009a). Analysis of body fluids for forensic purposes: From laboratory testing to non-destructive rapid confirmatory identification at a crime scene. *Forensic Science International*. 188. p.pp. 1–17.

Virkler, K. & Lednev, I.K. (2009b). Blood species identification for forensic purposes using Raman spectroscopy combined with advanced statistical analysis. *Analytical chemistry*. 81 (18). p.pp. 7773–7.

Virkler, K. & Lednev, I.K. (2009c). Raman spectroscopic signature of semen and its potential application to forensic body fluid identification. *Forensic science international*. 193 (1-3). p.pp. 56–62.

Virkler, K. & Lednev, I.K. (2010a). Forensic body fluid identification: the Raman spectroscopic signature of saliva. *The Analyst*. 135 (3). p.pp. 512–7.

Virkler, K. & Lednev, I.K. (2010b). Raman spectroscopic signature of blood and its potential application to forensic body fluid identification. *Analytical and bioanalytical chemistry*. 396 (1). p.pp. 525–34.

Vitorino, R., Lobo, M.J.C., Ferrer-Correira, A.J., Dubin, J.R., Tomer, K.B., Domingues, P.M. & Amado, F.M.L. (2004). Identification of human whole saliva protein components using proteomics. *Proteomics*. 4 (4). p.pp. 1109–1115.

De Wael, K., Lepot, L., Gason, F. & Gilbert, B. (2008). In search of blood - Detection of minute particles using spectroscopic methods. *Forensic Science International*. 180. p.pp. 37–42.

Walker, J. (2010). Electrophoretic Techniques. In: Wilson, K. & Walker, J. (Eds.) *Principles and Techniques of Biochemistry and Molecular Biology*, 7th Edition. Cambridge, Cambridge University Press.

Walsh, G. (2002). *Proteins Biochemistry and Biotechnology*. Chichester, John Wiley & Sons Ltd.

Wang, Z., Luo, H., Pan, X., Liao, M. & Hou, Y. (2012). A model for data analysis of microRNA expression in forensic body fluid identification. *Forensic science international. Genetics*. 6 (3). p.pp. 419–23.

Wang, Z., Zhang, J., Luo, H., Ye, Y., Yan, J. & Hou, Y. (2013). Screening and confirmation of microRNA markers for forensic body fluid identification. *Forensic science international. Genetics*. 7 (1). p.pp. 116–23.

Wartewig, S. & Neubert, R.H.H. (2005). Pharmaceutical applications of Mid-IR and Raman spectroscopy. *Advanced drug delivery reviews*. 57 (8). p.pp. 1144–70.

Wasserstrom, A., Frumkin, D., Davidson, A., Shpitzen, M., Herman, Y. & Gafny, R. (2013). Demonstration of DSI-semen--A novel DNA methylation-based forensic semen identification assay. *Forensic science international. Genetics*. 7 (1). p.pp. 136–42.

Wong, P.T., Wong, R.K., Caputo, T. a, Godwin, T. a & Rigas, B. (1991). Infrared spectroscopy of exfoliated human cervical cells: Evidence of extensive structural changes during carcinogenesis. *Proceedings of the National Academy of Sciences of the United States of America*. 88 (24). p.pp. 10988–10992.

Wood, B.R., Quinn, M. a, Tait, B., Ashdown, M., Hislop, T., Romeo, M. & McNaughton, D. (1998). FTIR microspectroscopic study of cell types and potential confounding variables in screening for cervical malignancies. *Biospectroscopy*. 4 (2). p.pp. 75–91.

Wood, B.R., Chiriboga, L., Yee, H., Quinn, M. a, McNaughton, D. & Diem, M. (2004). Fourier transform infrared (FTIR) spectral mapping of the cervical transformation zone, and dysplastic squamous epithelium. *Gynecologic Oncology*. 93 (1). p.pp. 59–68.

Workman, J.J. (2005). *An Introduction to Near Infrared Spectroscopy*. [Online]. 2005. spectroscopyNOW.com. Available from: http://www.spectroscopynow.com/details/education/sepspec1881education/An-Introduction-to-Near-Infrared-Spectroscopy.html?tzcheck=1. [Accessed: 6 March 2014].

World Health Organisation (2010). *WHO Laboratory Manual for the Examination and Processing of Human Semen*. 5th Ed. Switzerland: WHO Library Cataloguing-in-Publication Data.

WWF (2014). *Cotton Farming*. [Online]. 2014. Available from: http://wwf.panda.org/about_our_earth/about_freshwater/freshwater_problems/thirsty_crops/cotton/. [Accessed: 10 September 2014].

Yang, H., Zhou, B., Deng, H., Prinz, M. & Siegel, D. (2013). Body fluid identification by mass spectrometry. *International Journal of Legal Medicine*. 127. p.pp. 1065–1077.

Yang, Y., Xie, B. & Yan, J. (2014). Application of next-generation sequencing technology in forensic science. *Genomics, Proteomics & Bioinformatics*. 12 (5). p.pp. 190–197.

Yekkala, R., Meers, C., Van Schepdael, A., Hoogmartens, J., Lambrichts, I. & Willems, G. (2006). Racemization of aspartic acid from human dentin in the estimation of chronological age. *Forensic Science International*. 159 Suppl . p.pp. S89–94.

Yoon, M.-S., Jankowski, V., Montag, S., Zidek, W., Henning, L., Schlüter, H., Tepel, M. & Jankowski, J. (2004). Characterisation of advanced glycation endproducts in saliva from patients with diabetes mellitus. *Biochemical and Biophysical Research Communications*. 323 (2). p.pp. 377–81.

Yoshida, S. & Yoshida, H. (2004). Noninvasive analyses of polyunsaturated fatty acids in human oral mucosa in vivo by Fourier-transform infrared spectroscopy. *Biopolymers*. 74 (5). p.pp. 403–412.

Zegels, G., Van Raemdonck, G. a a, Coen, E.P., Tjalma, W. a a & Van Ostade, X.W.M. (2009). Comprehensive proteomic analysis of human cervical-vaginal fluid using colposcopy samples. *Proteome Science*. 7 (17). p.pp. 1–16.

Zeng, G., Kelley, J., Kish, J.D. & Liu, Y. (2014). Temperature-dependent deliquescent and efflorescent properties of methanesulfonate sodium studied by ATR-FTIR spectroscopy. *The journal of physical chemistry. A*. 118 (3). p.pp. 583–91.

Zubakov, D., Kokshoorn, M., Kloosterman, A. & Kayser, M. (2009). New markers for old stains: Stable mRNA markers for blood and saliva identification from up to 16-year-old stains. *International Journal of Legal Medicine*. 123 (1). p.pp. 71–74.

8. APPENDICES

Appendix One

ATR-FTIR spectra of aged bloodstains, blood extracts, saliva extracts, semen extracts, vaginal secretion stains & vaginal secretion extracts.

Appendix Two

Linear regression graphs of Bradford assay total protein yields over time.

8.1 APPENDIX ONE

Bloodstains

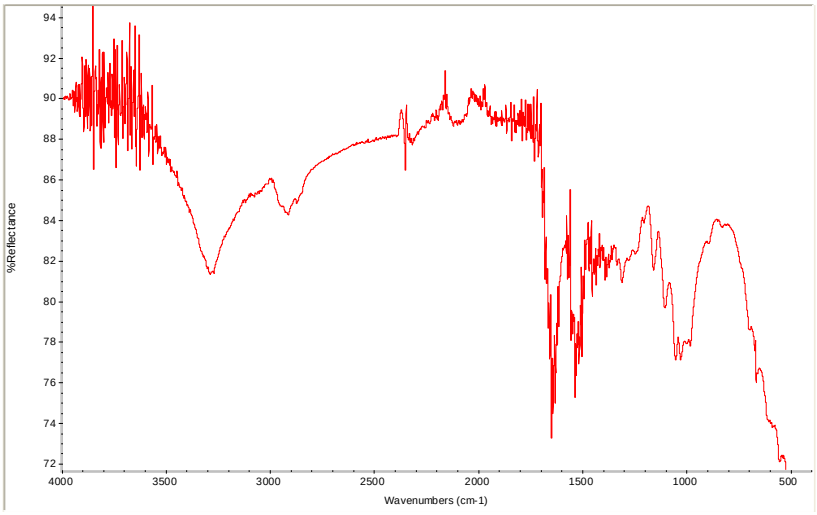

24 hours

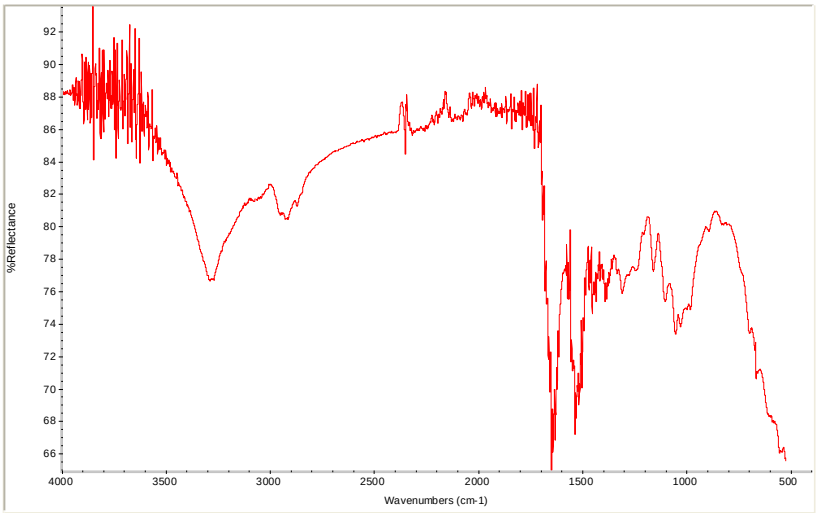

48 hours

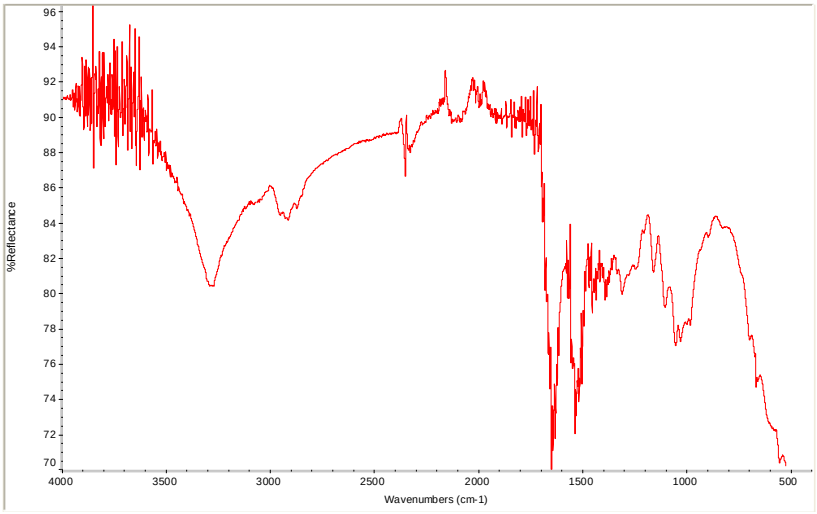

3 days

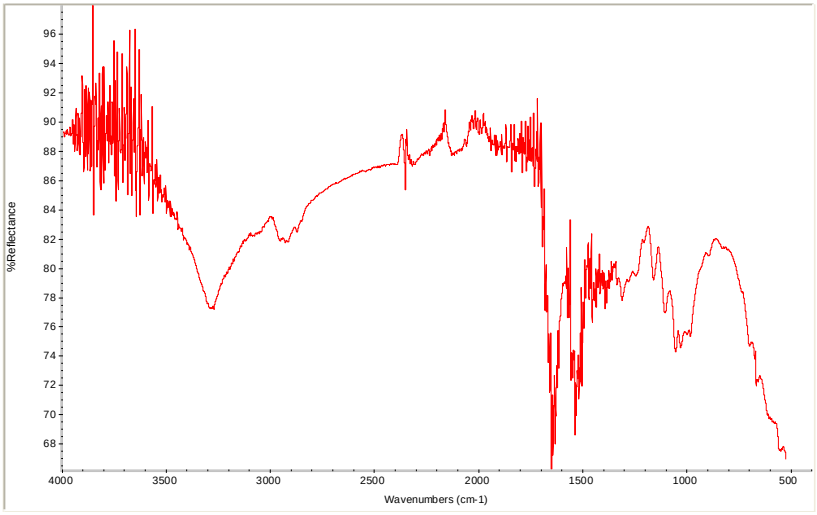

4 days

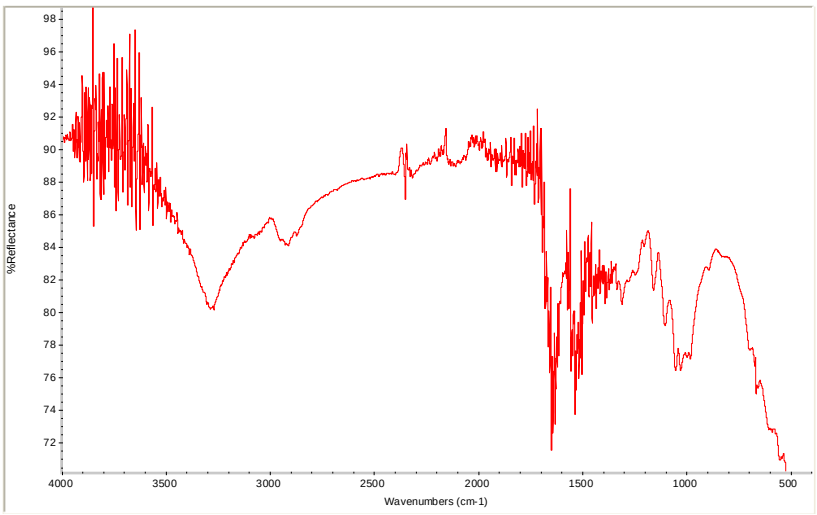

5 days

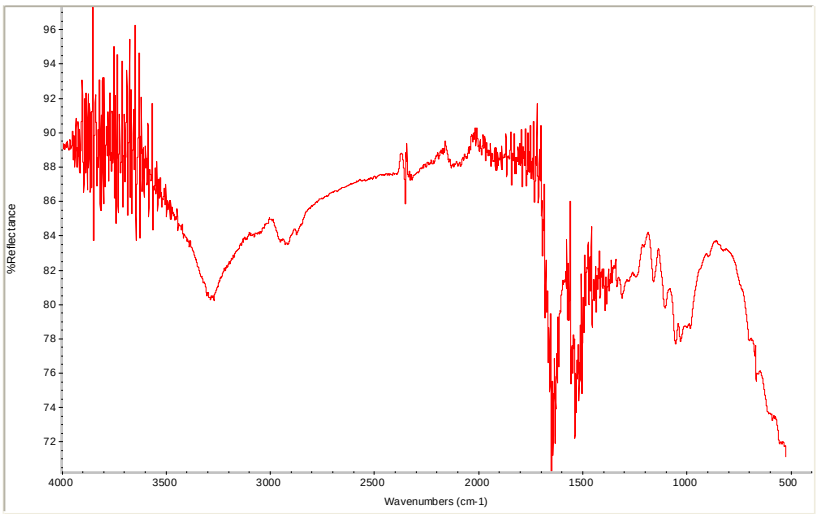

6 days

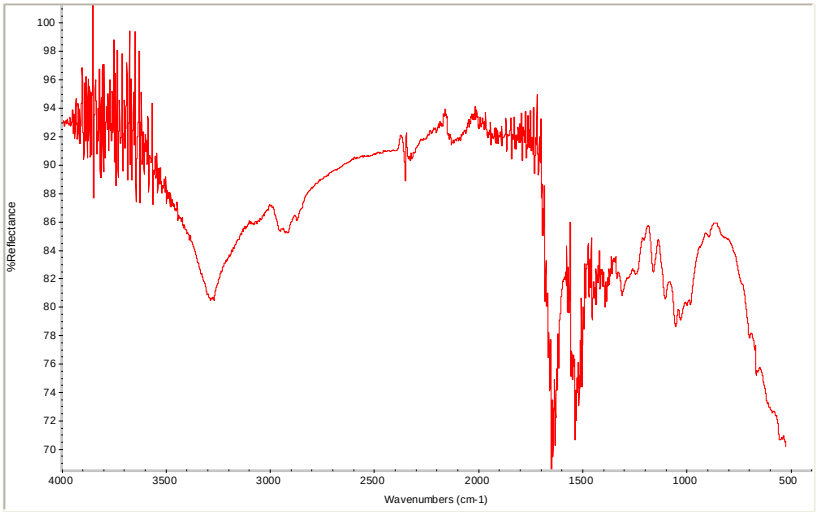

7 days

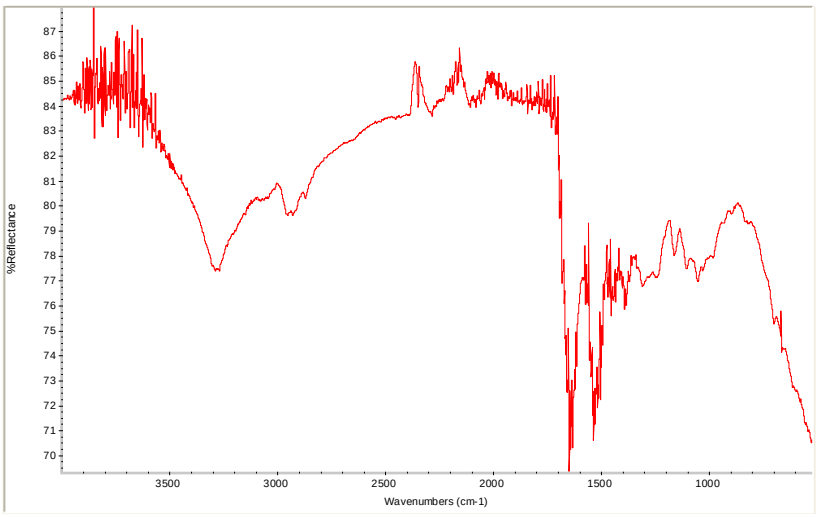

14 days

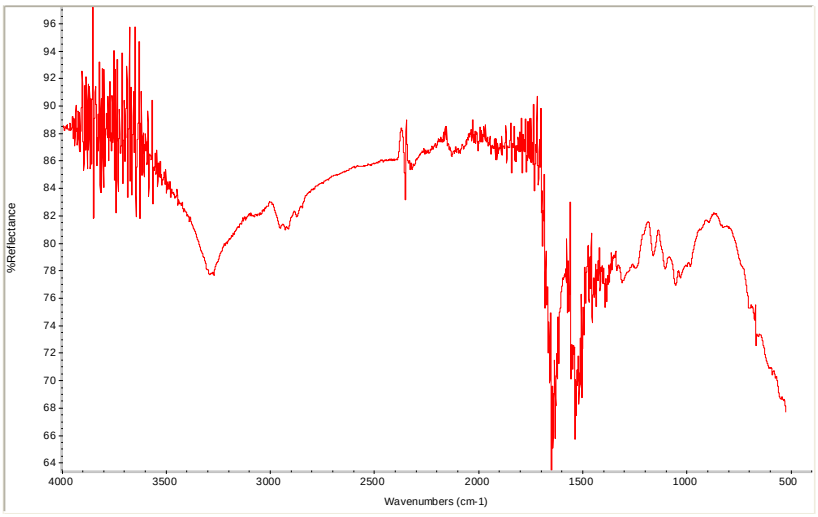

21 days

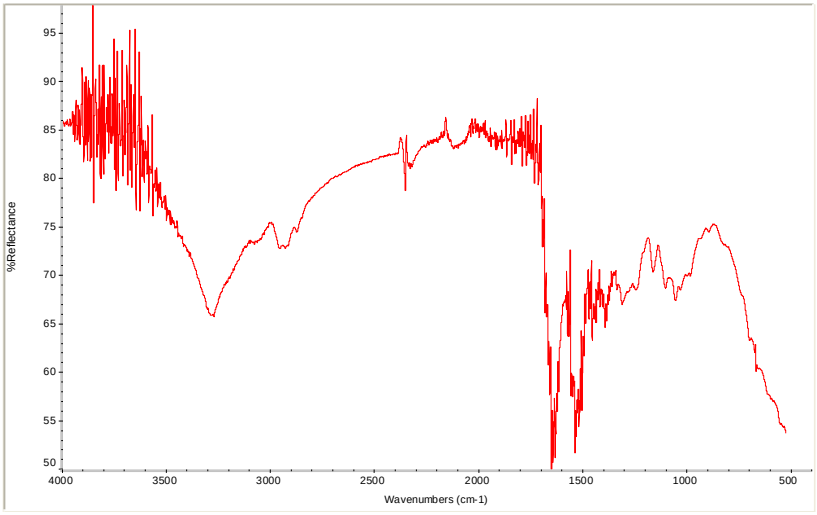

1 month

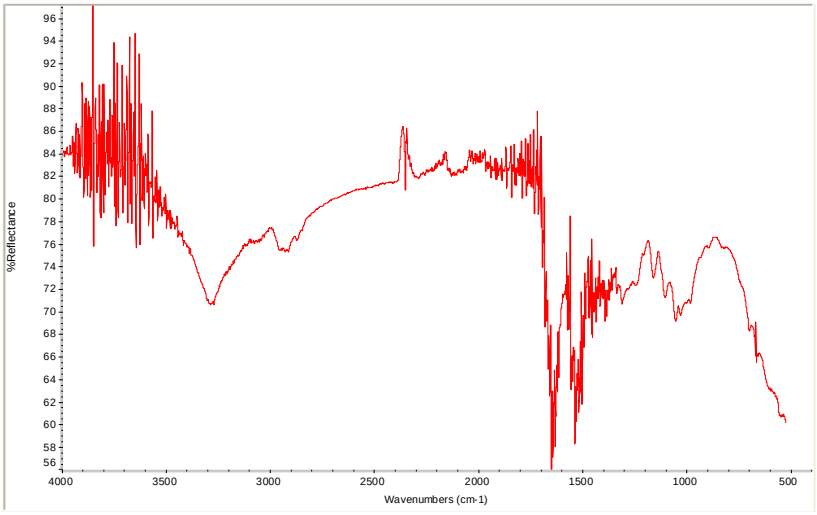

2 months

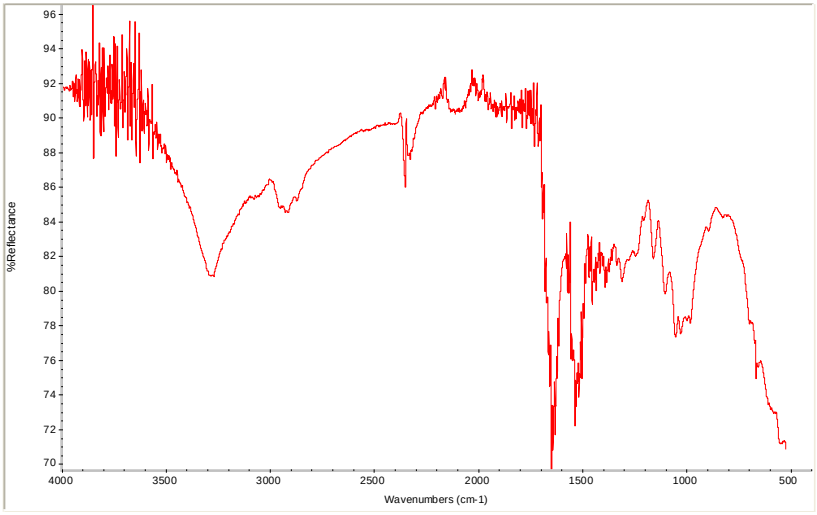

3 months

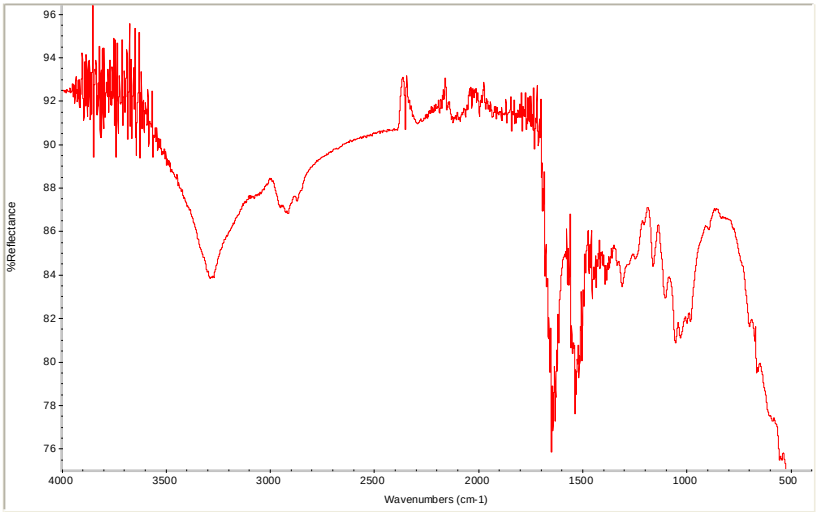

6 months

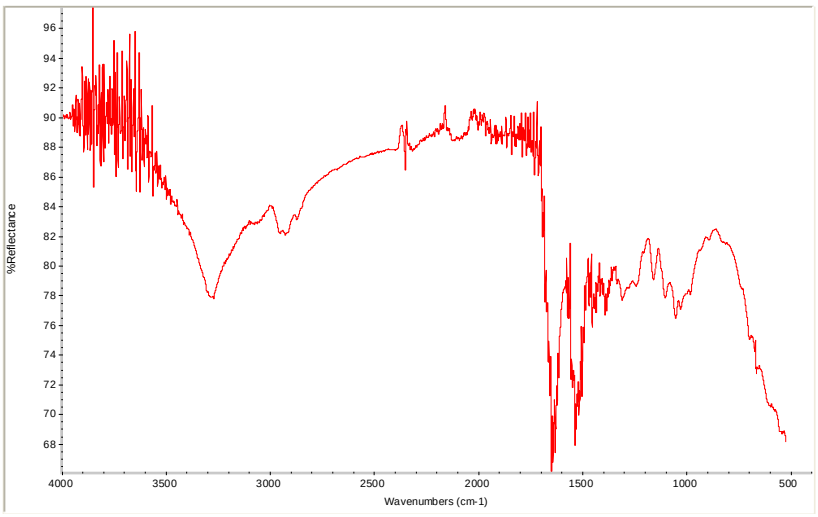

12 months

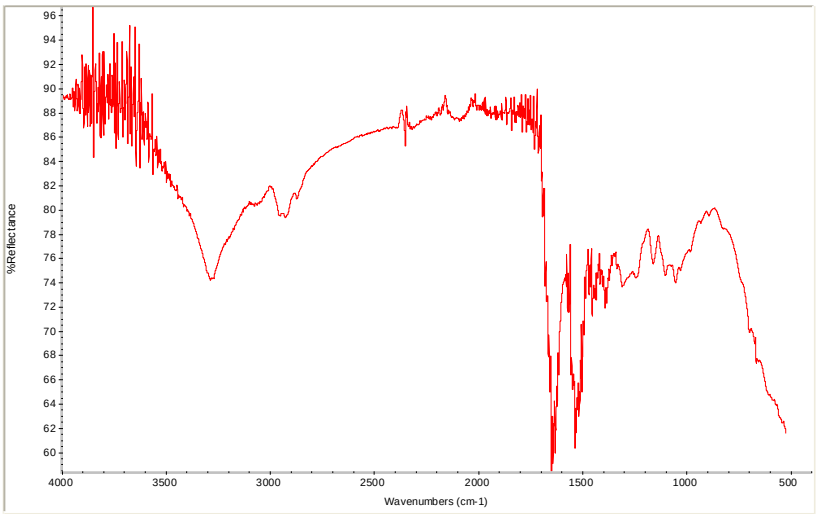

18 months

Bloodstains: Extracted

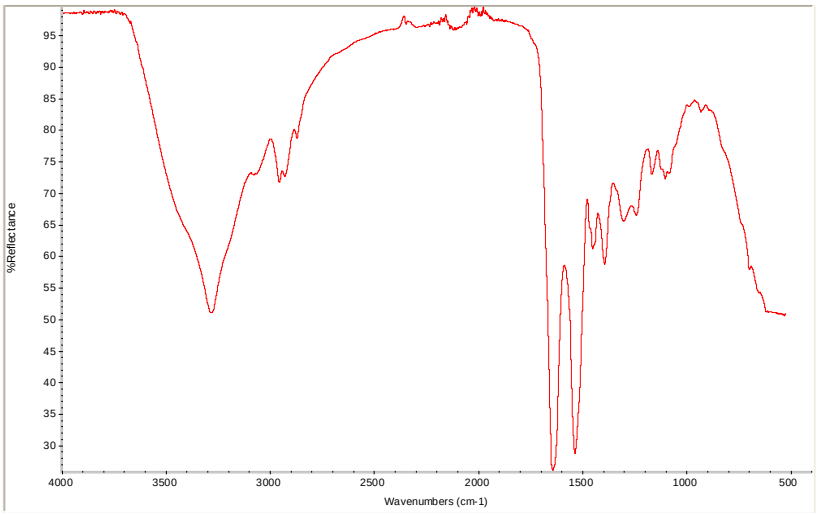

24 hours

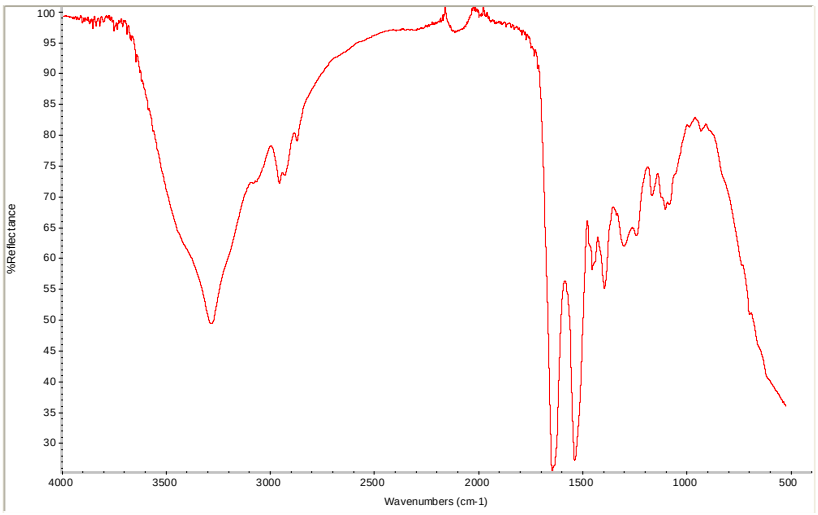

48 hours

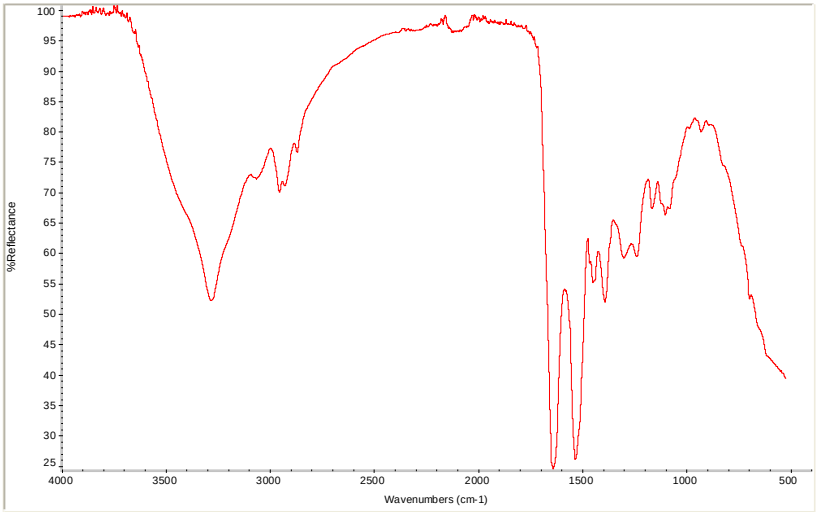

3 days

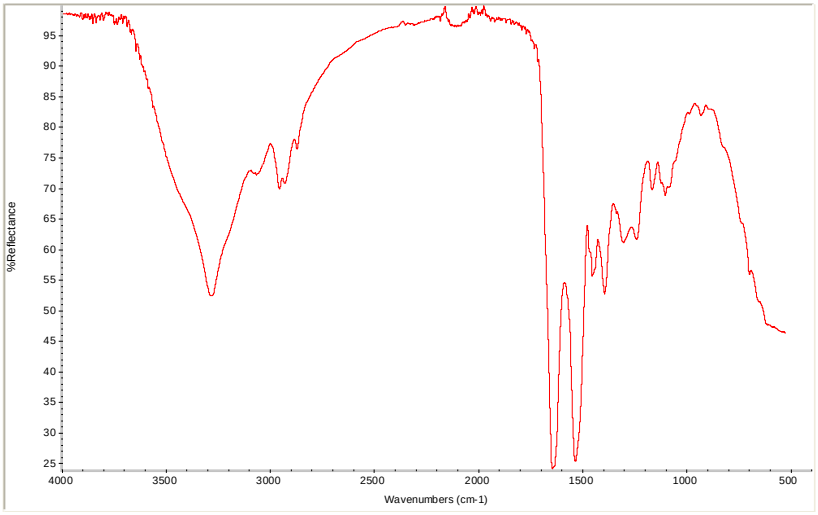

4 days

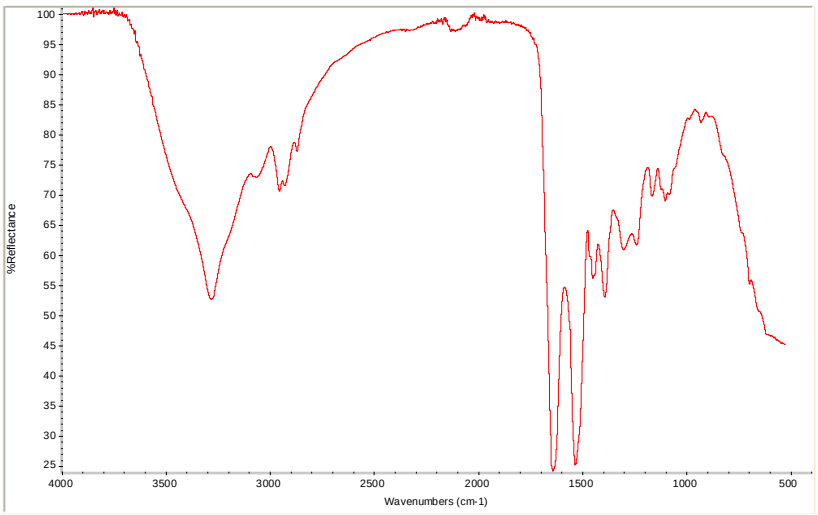

5 days

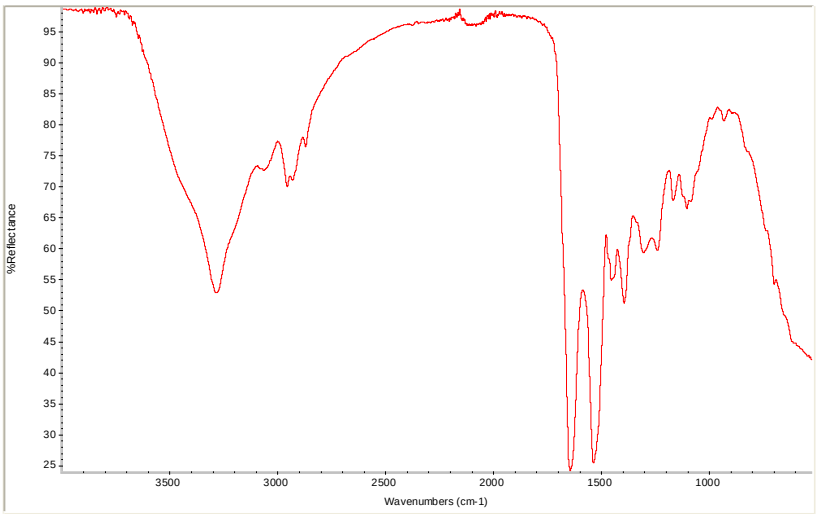

6 days

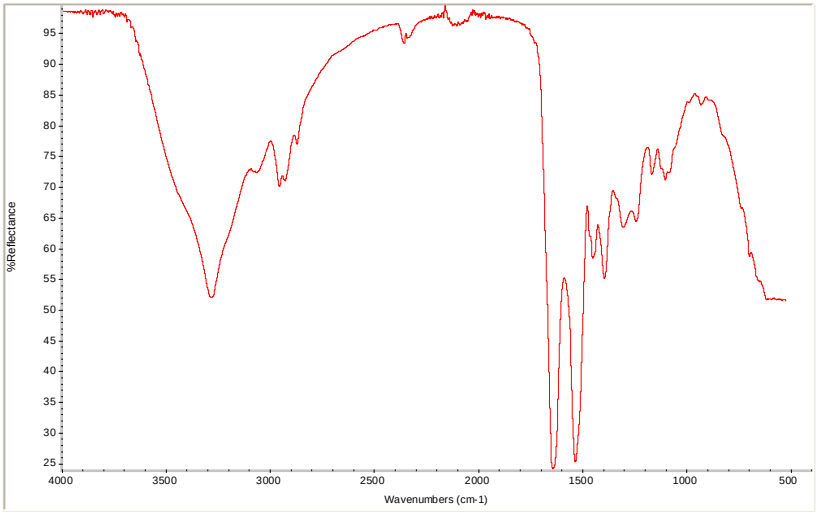

7 days

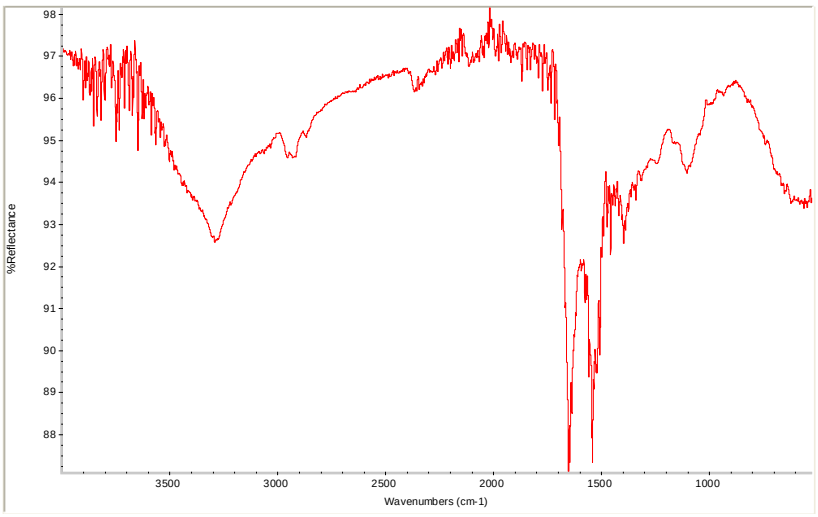

12 months

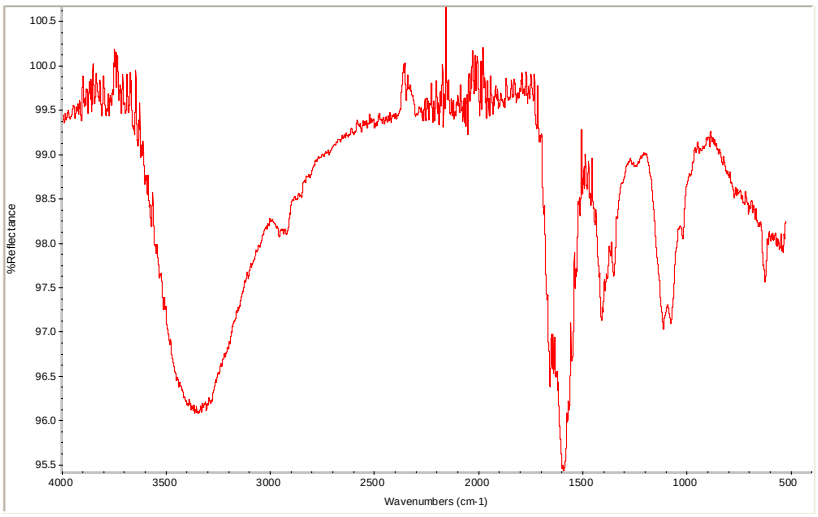

18 months

Saliva stains: Extracted

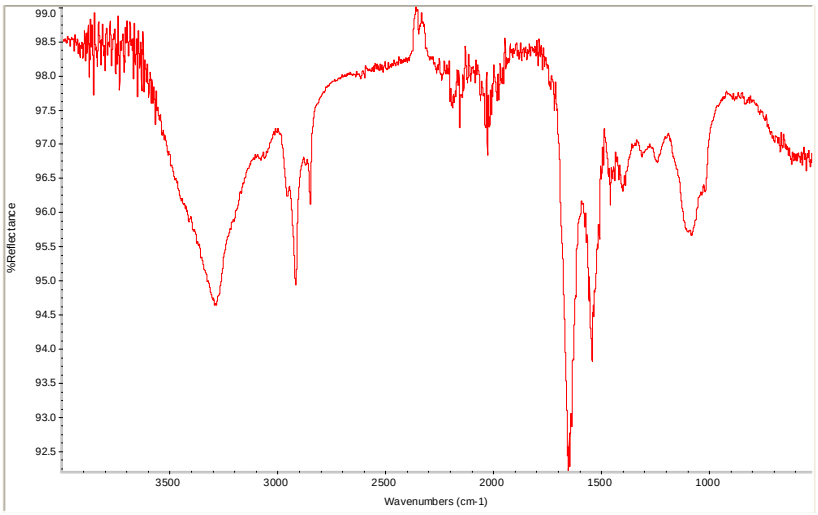

24 hours

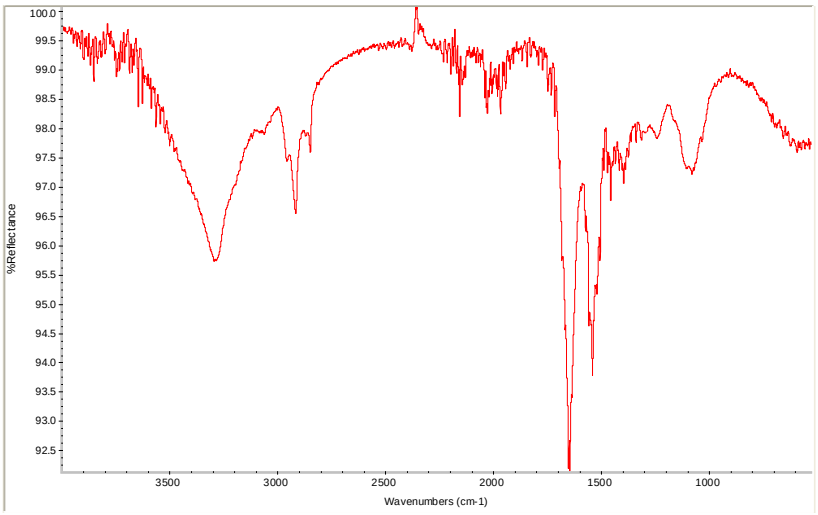

48 hours

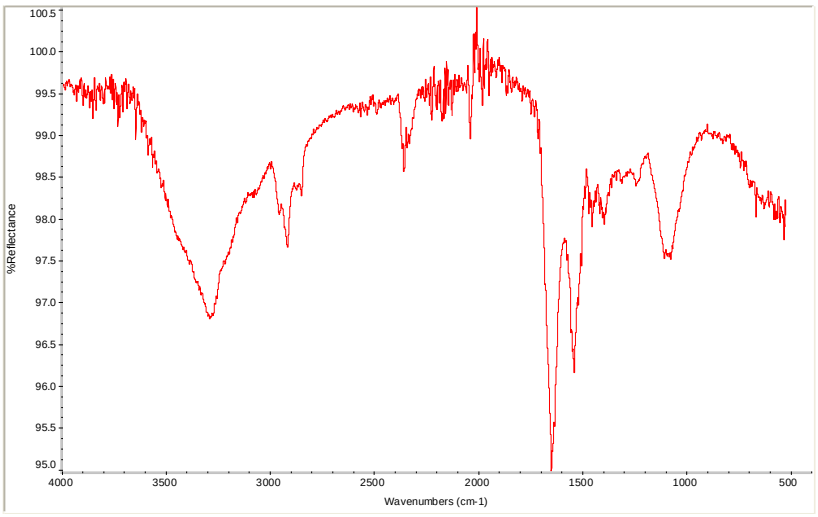

3 days

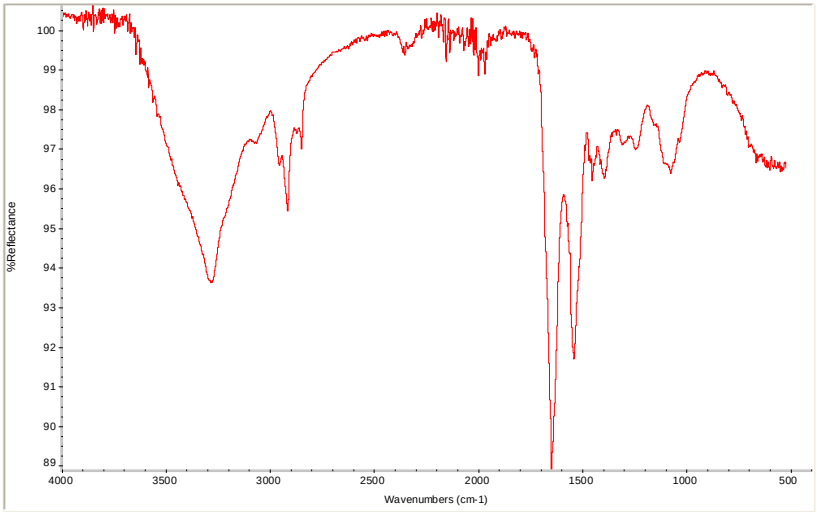

4 days

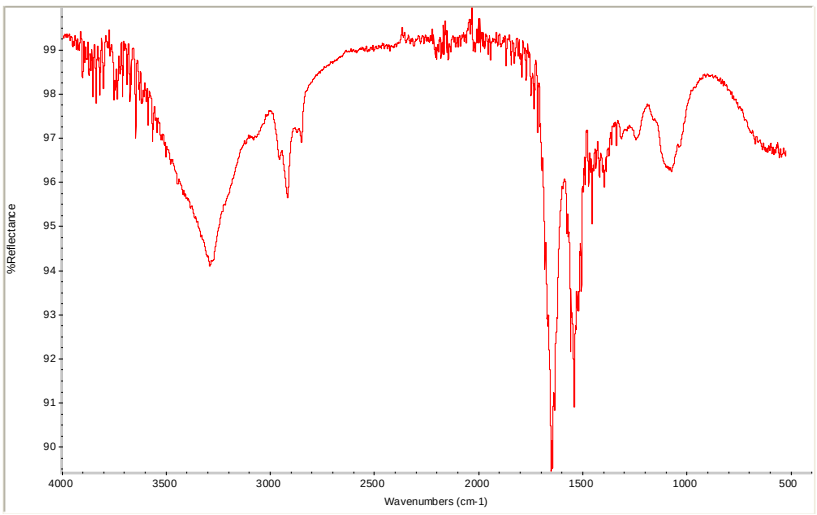

5 days

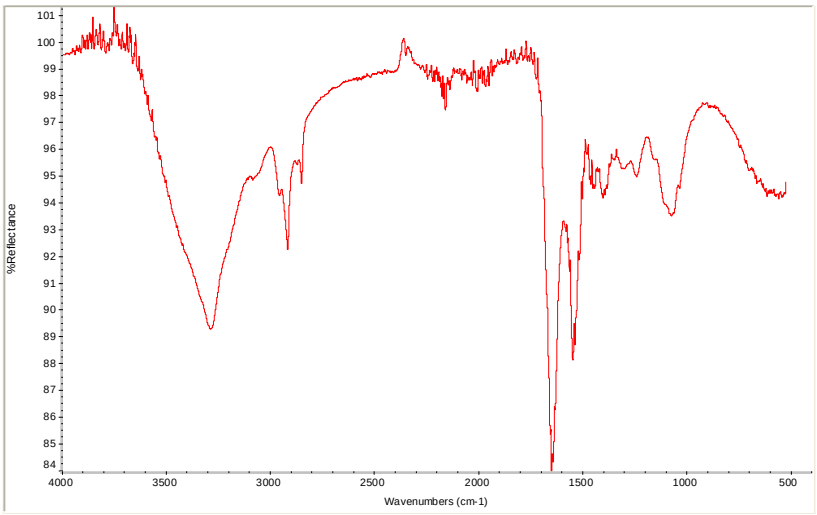

6 days

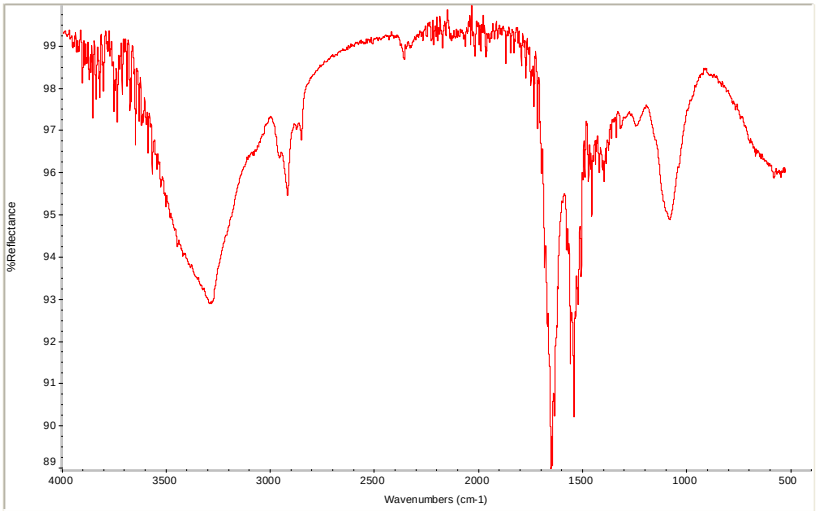

7 days

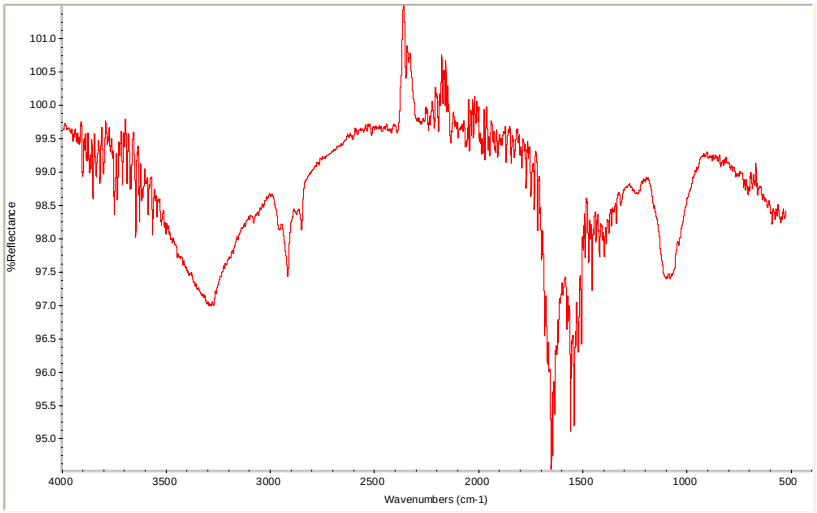

14 days

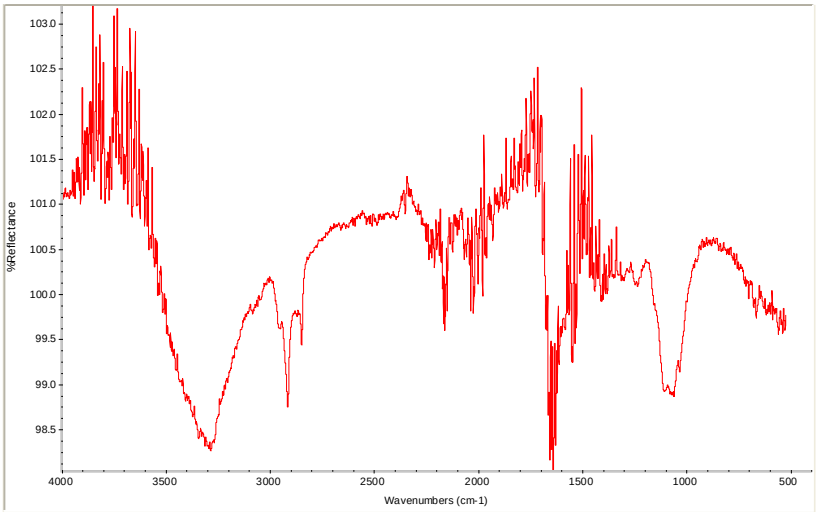

21 days

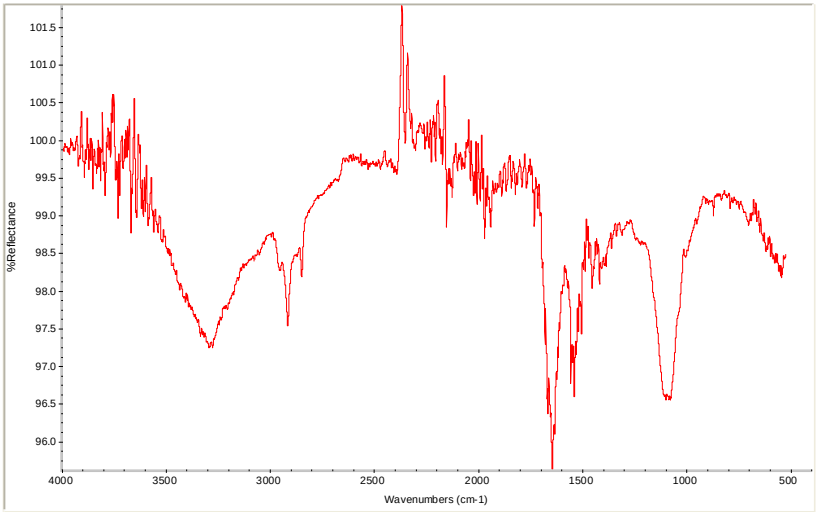

1 month

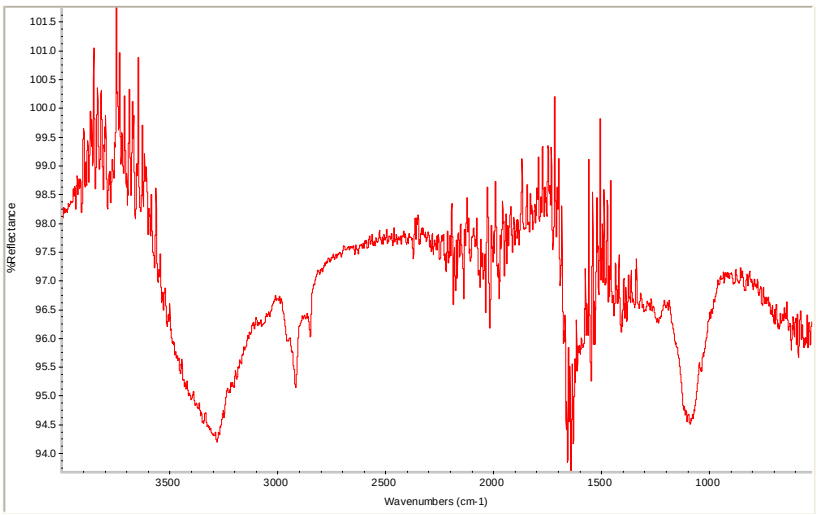

2 months

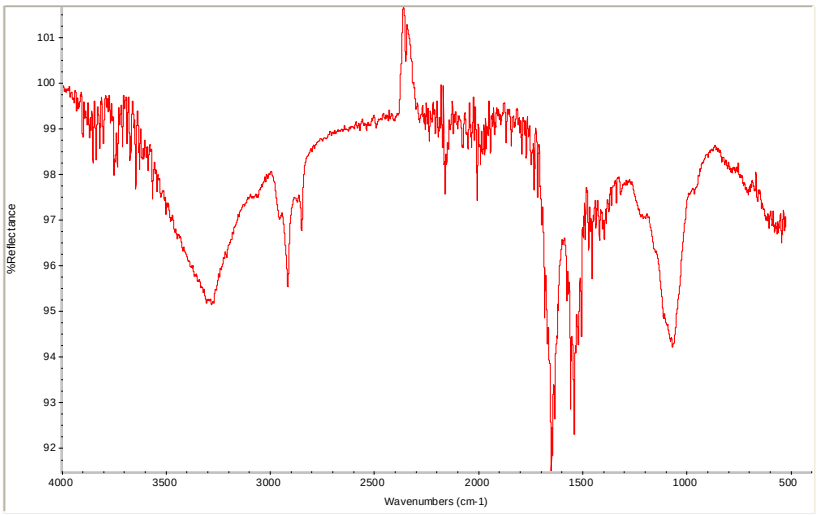

3 months

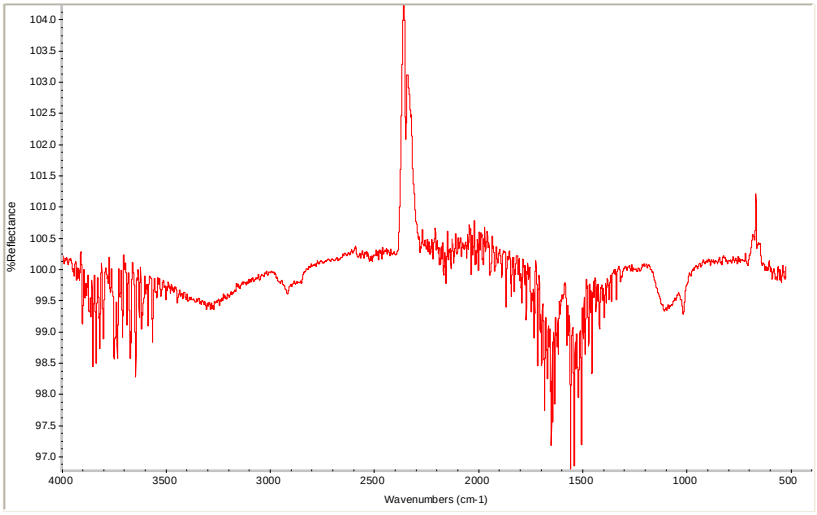

6 months

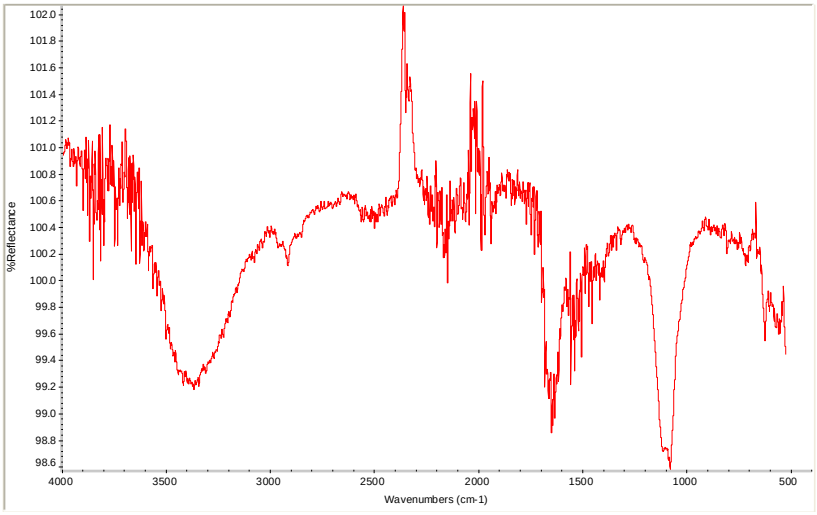

18 months

Semen stains: Extracted

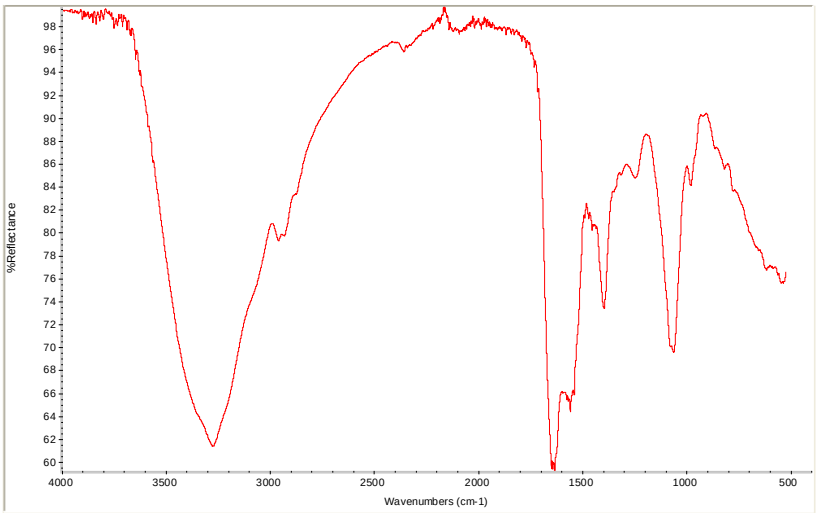

24 hours

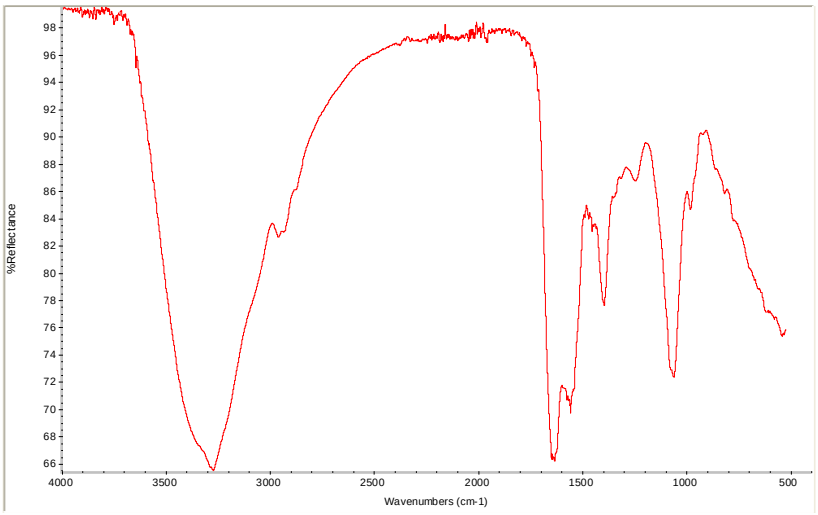

48 hours

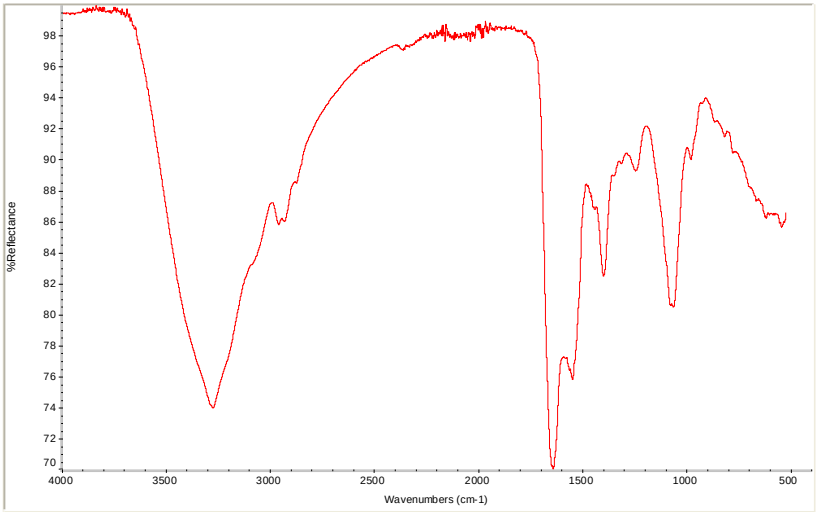

3 days

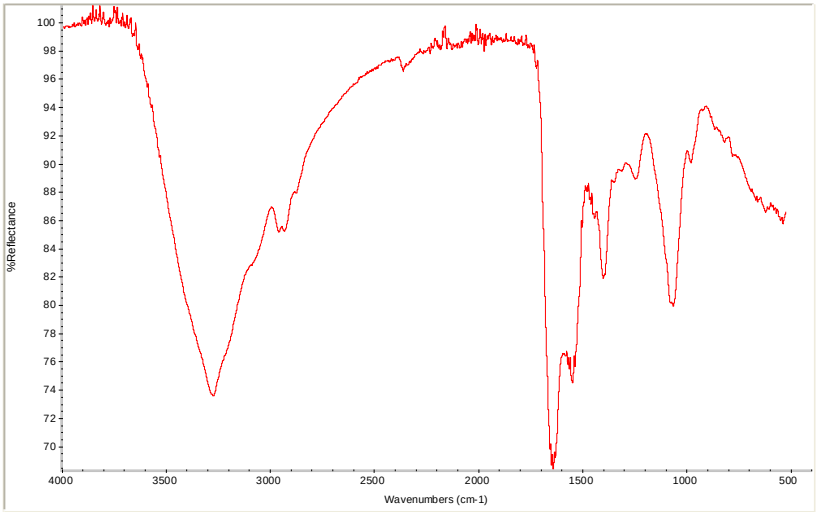

4 days

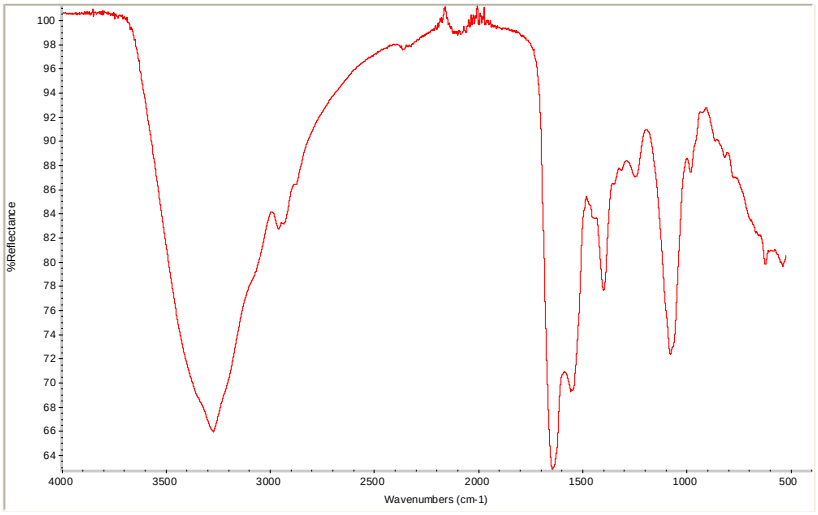

5 days

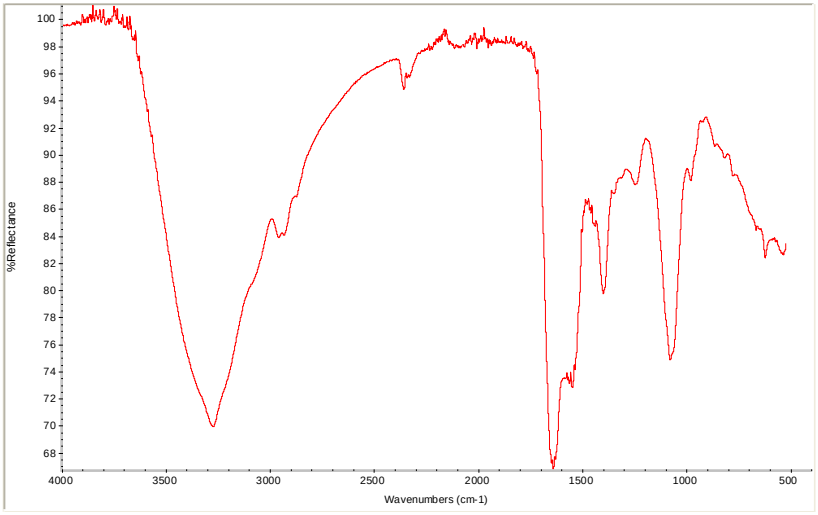

6 days

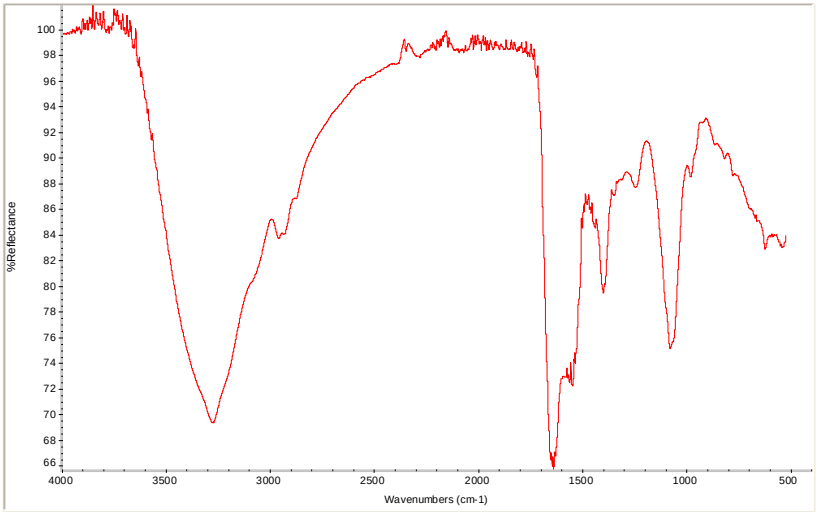

7 days

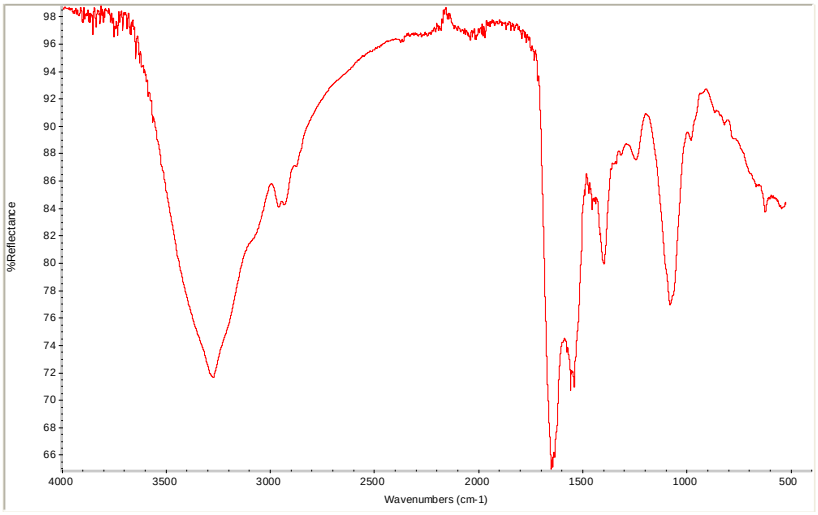

14 days

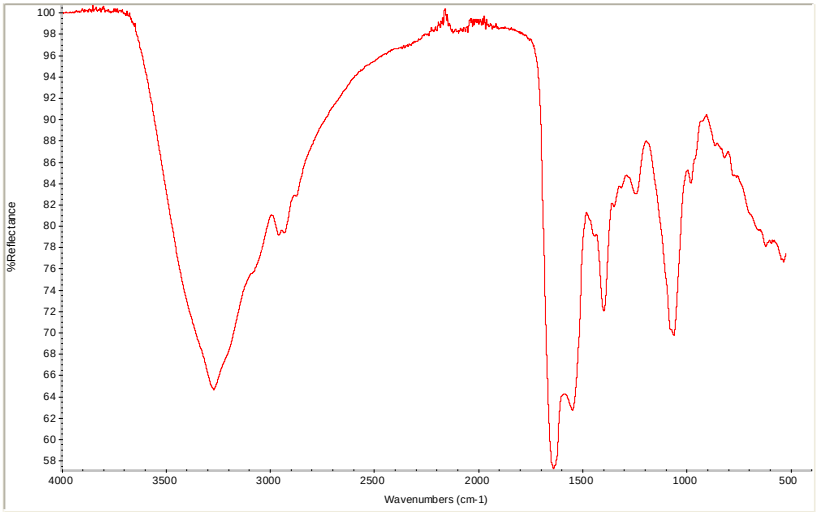

21 days

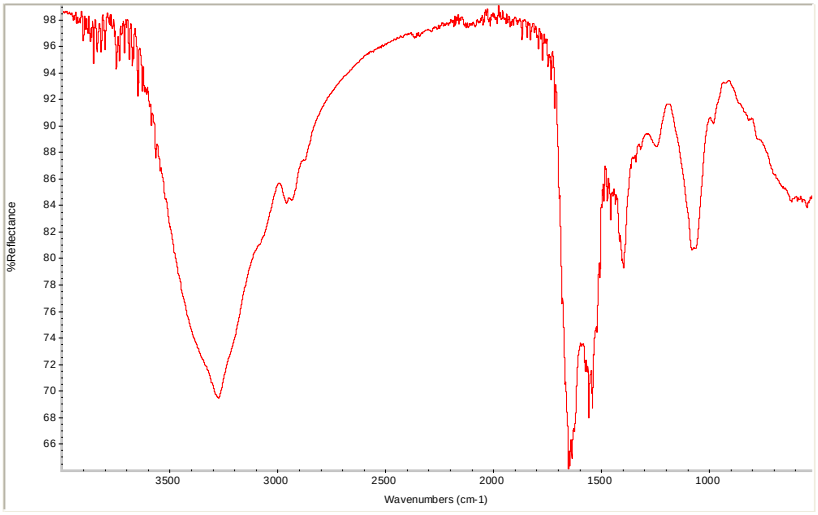

1 month

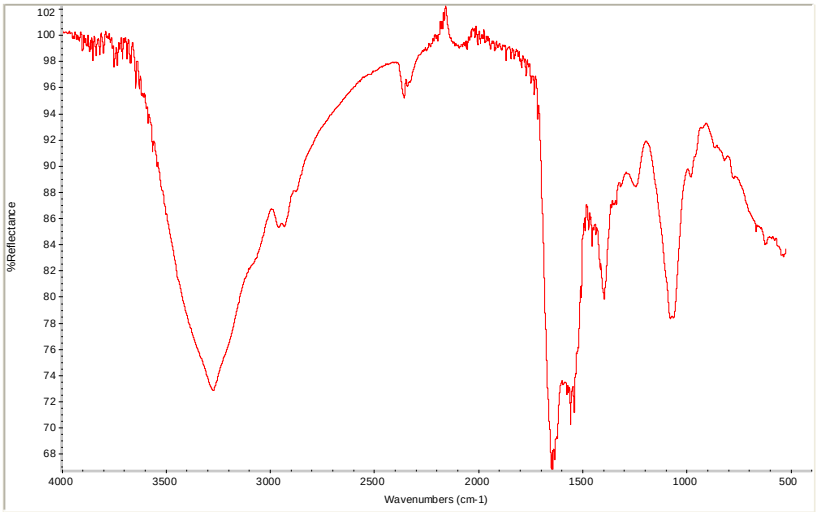

2 months

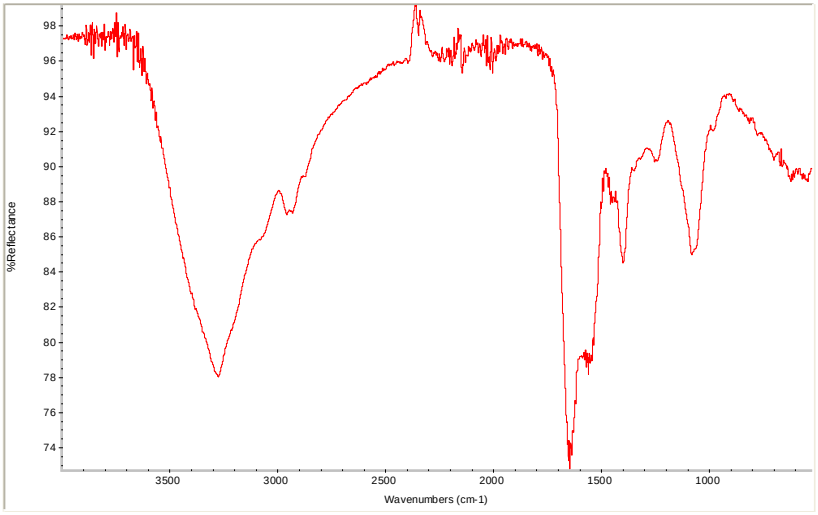

3 months

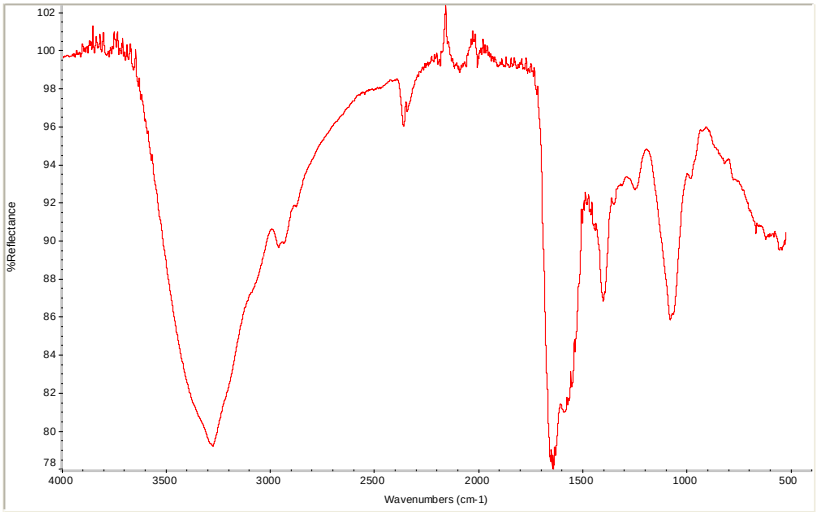

6 months

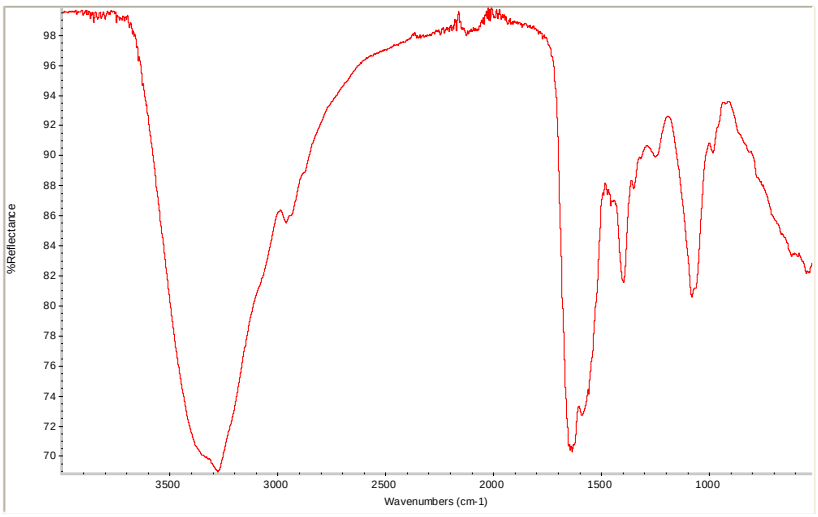

8 months

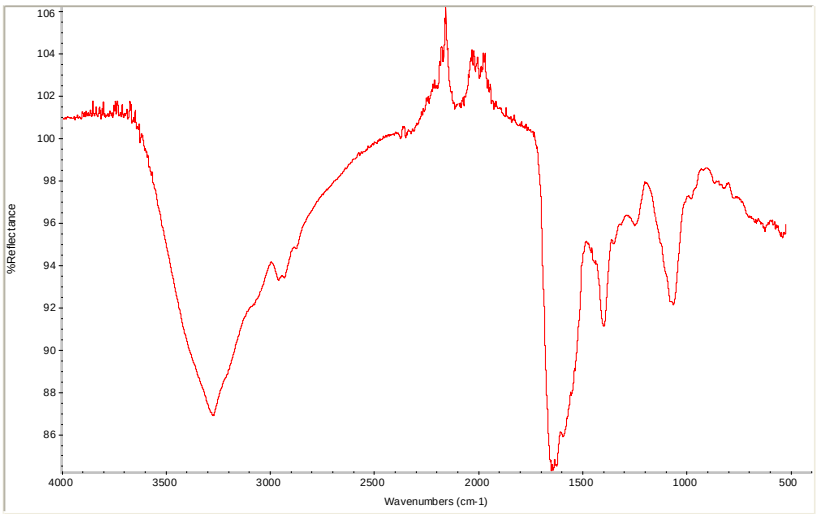

9 months

Vaginal secretion stains

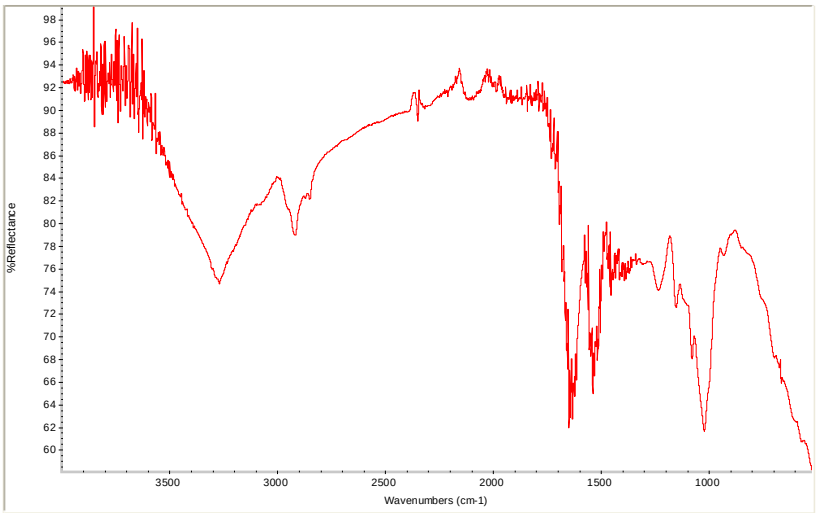

24 hours

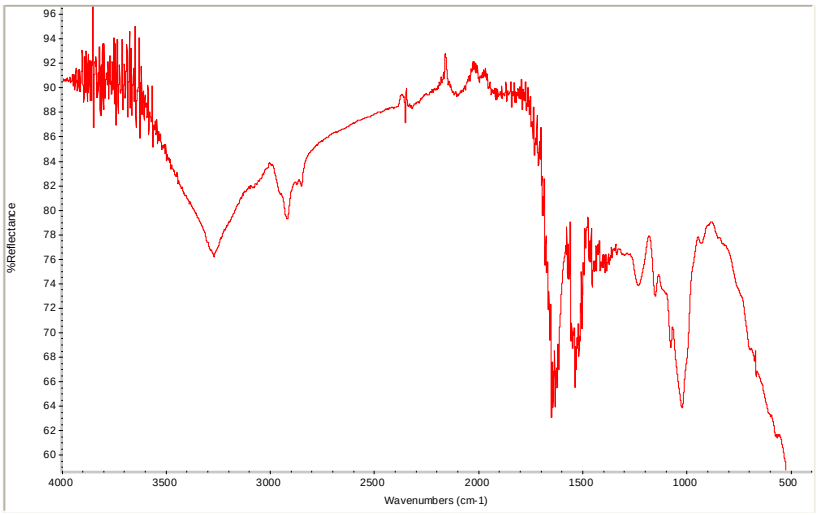

48 hours

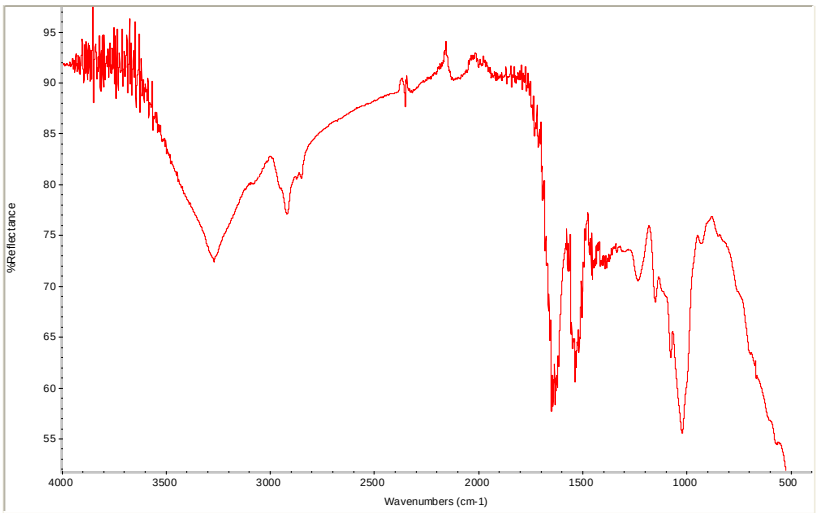

3 days

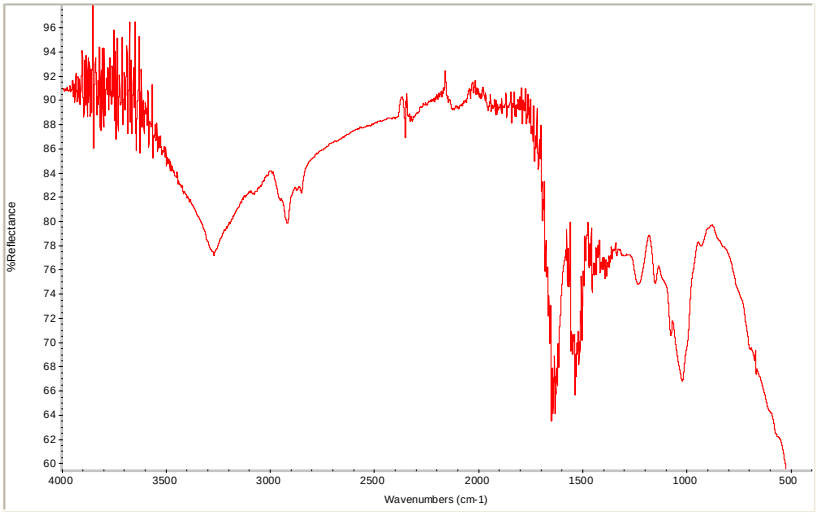

4 days

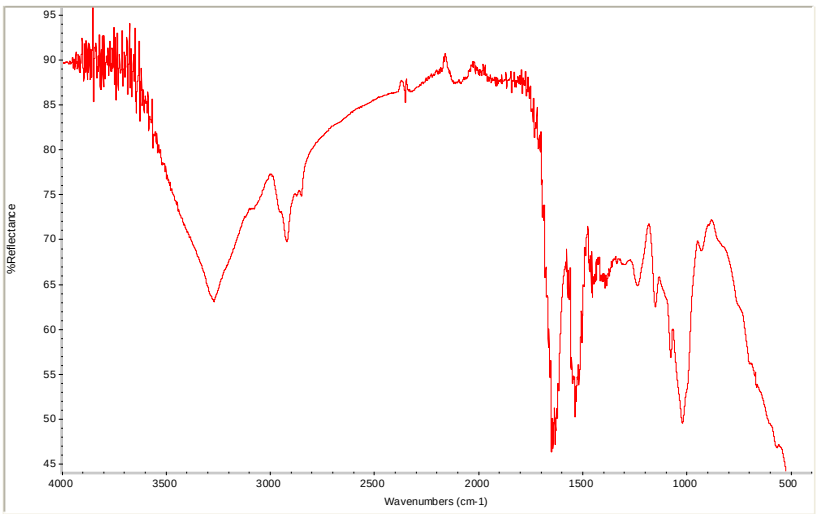

5 days

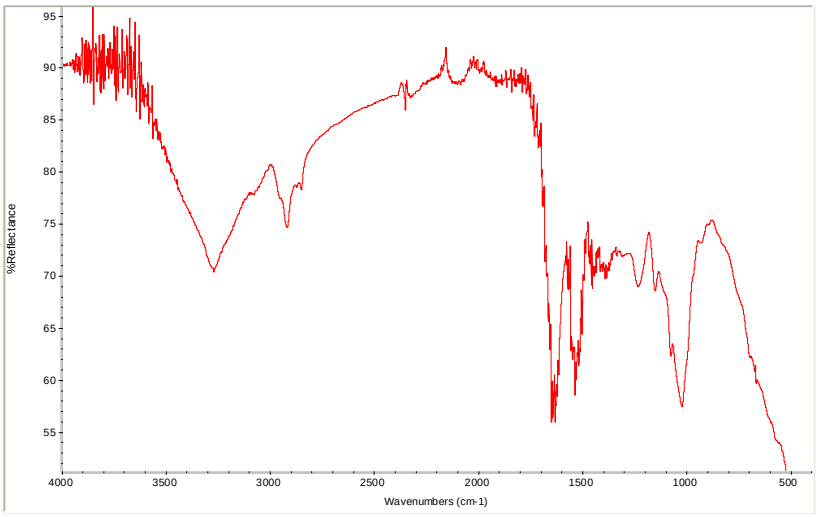

6 days

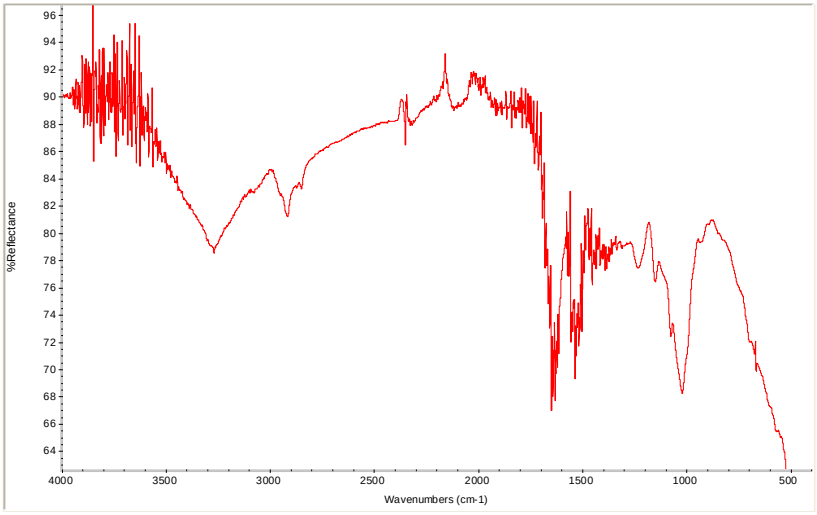

7 days

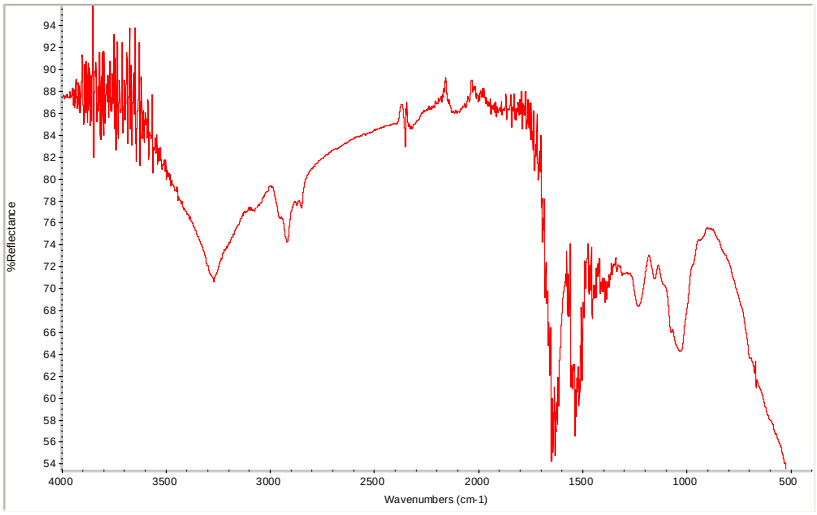

14 days

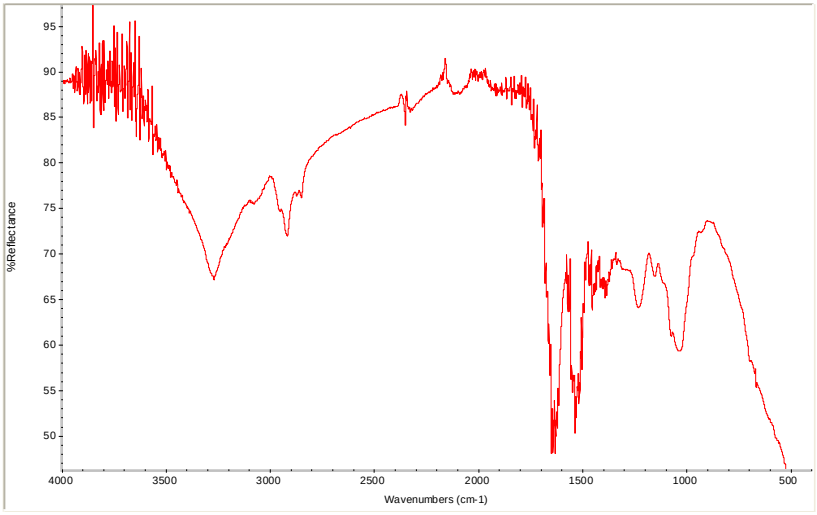

21 days

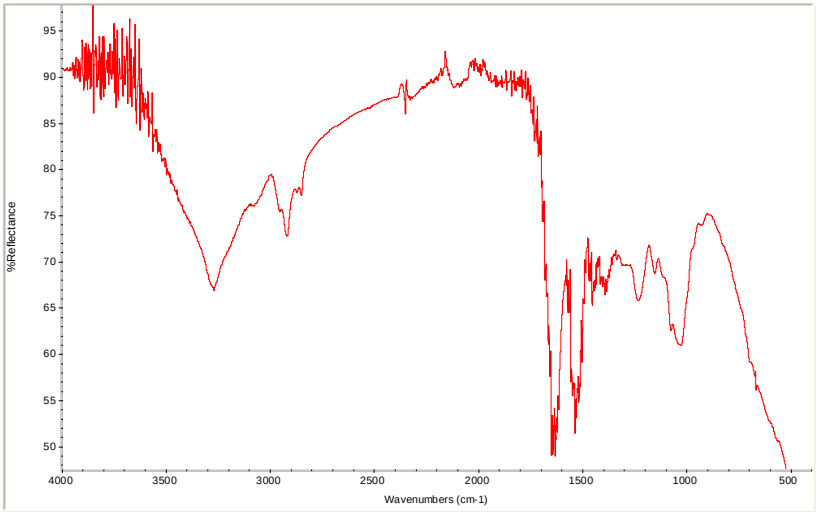

1 month

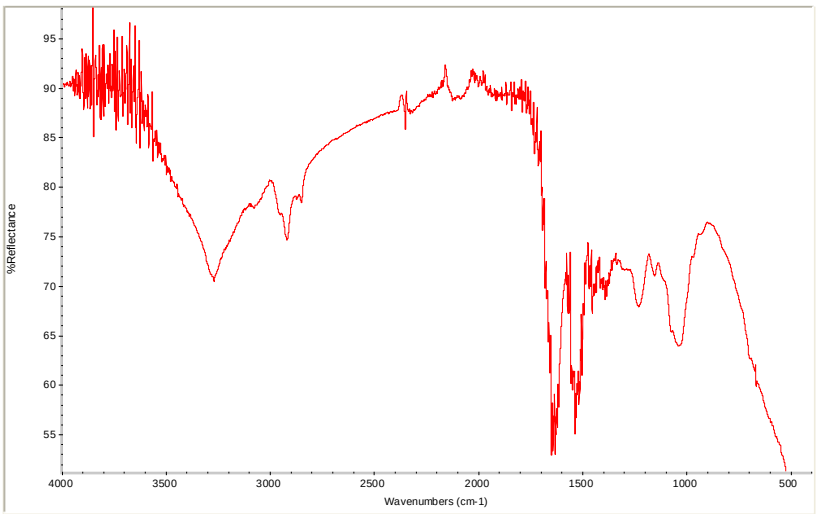

2 months

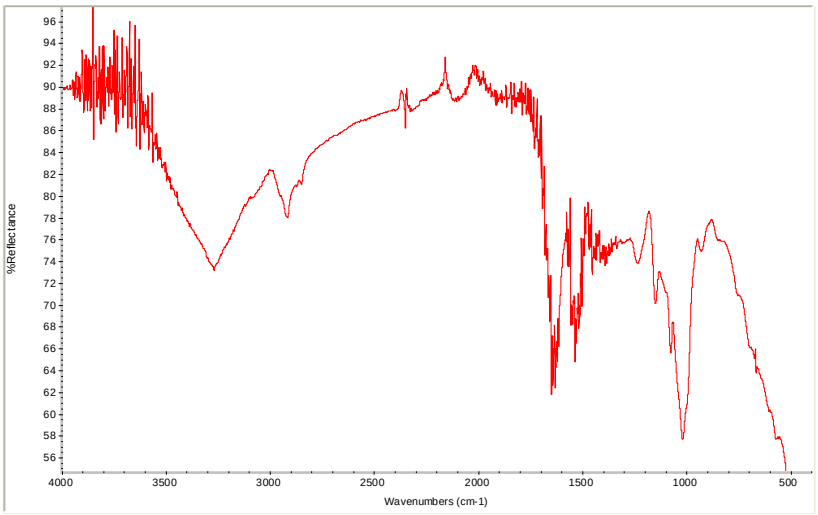

3 months

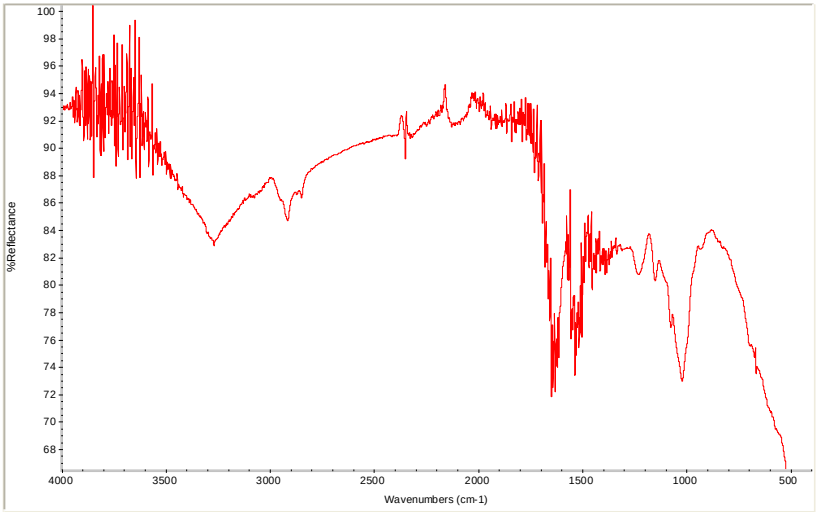

4 months

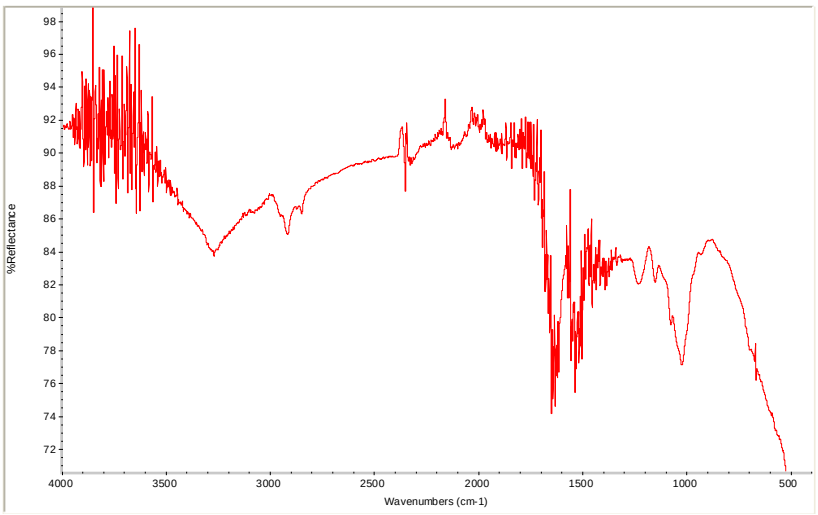

5 months

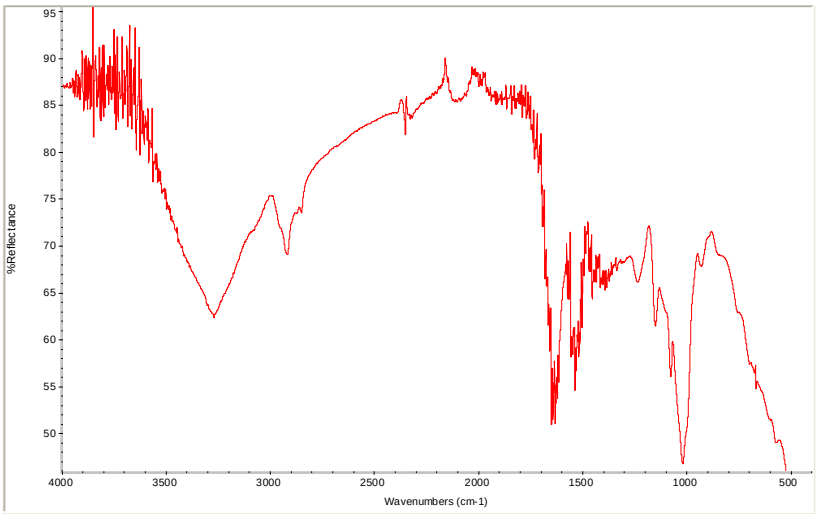

6 months

Vaginal secretion stains: Extracted

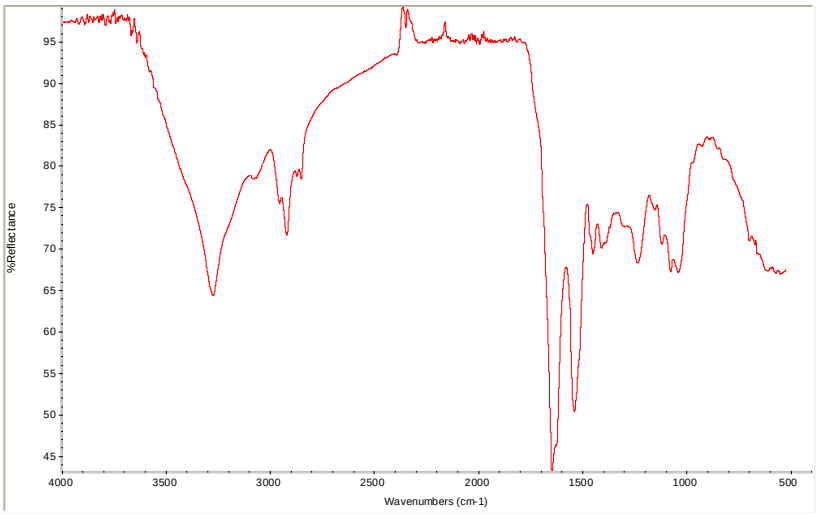

24 hours

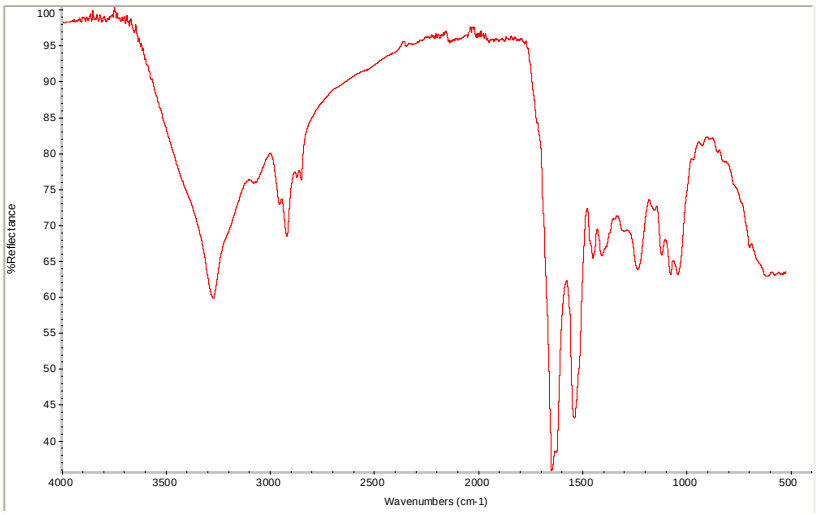

48 hours

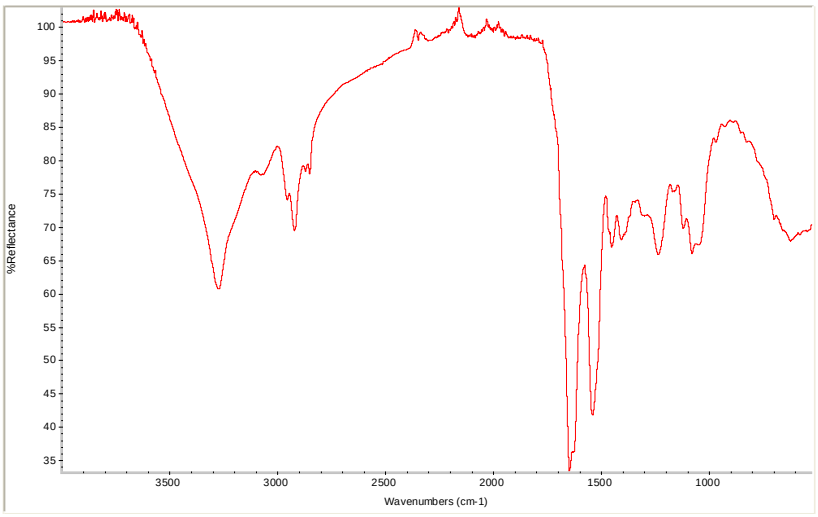

3 days

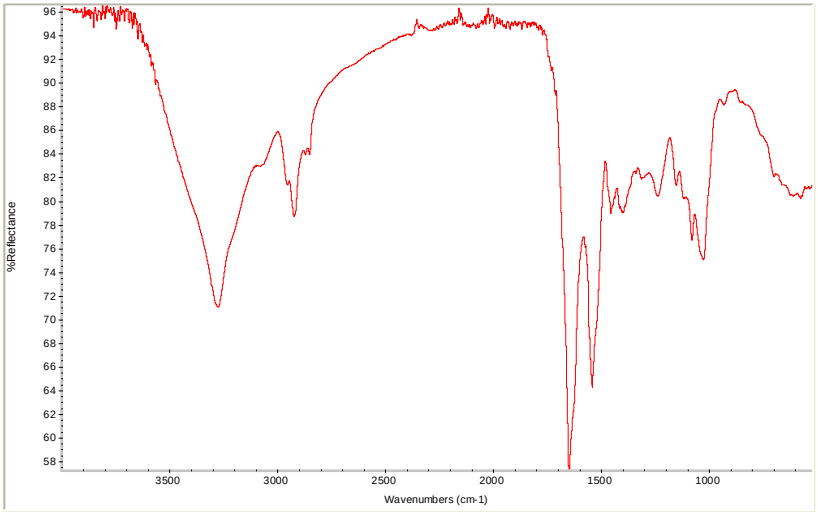

4 days

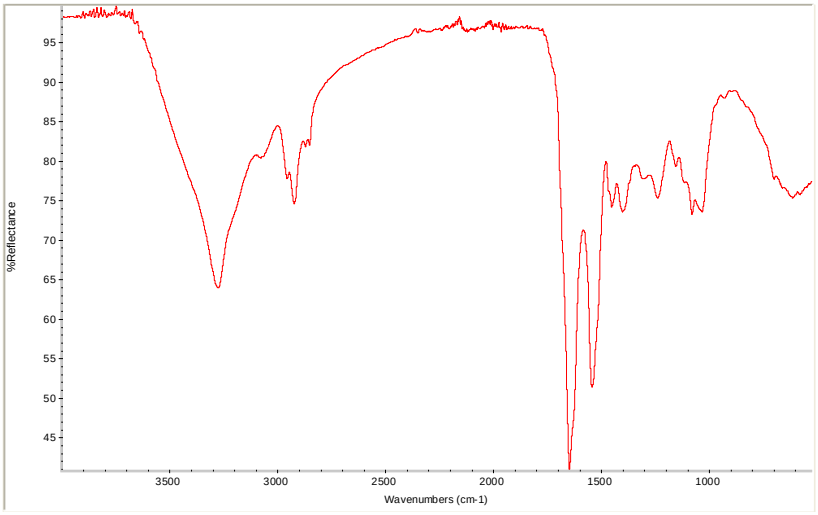

5 days

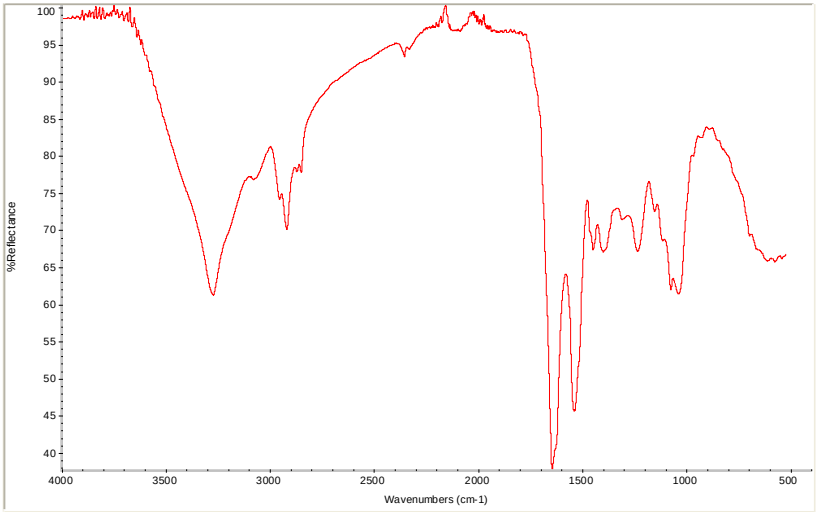

6 days

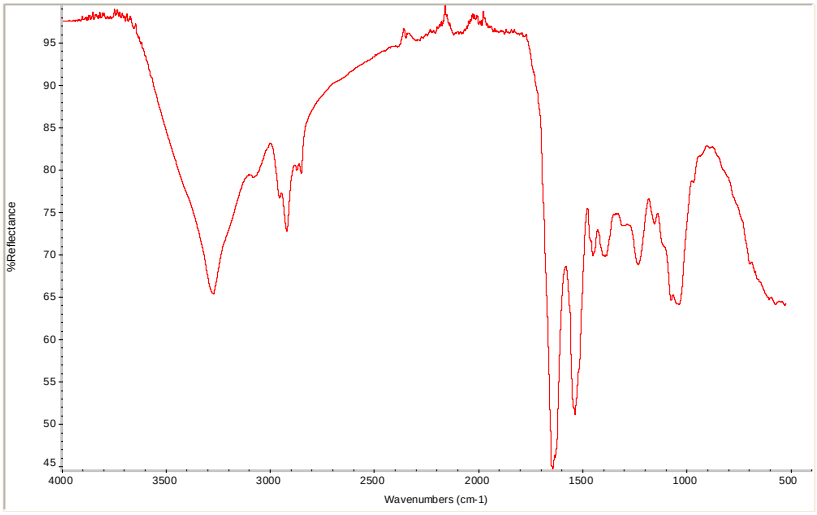

7 days

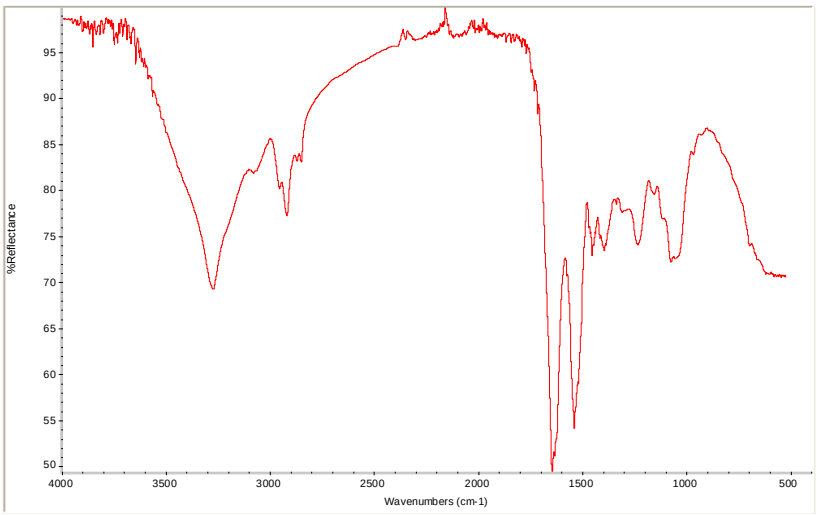

14 days

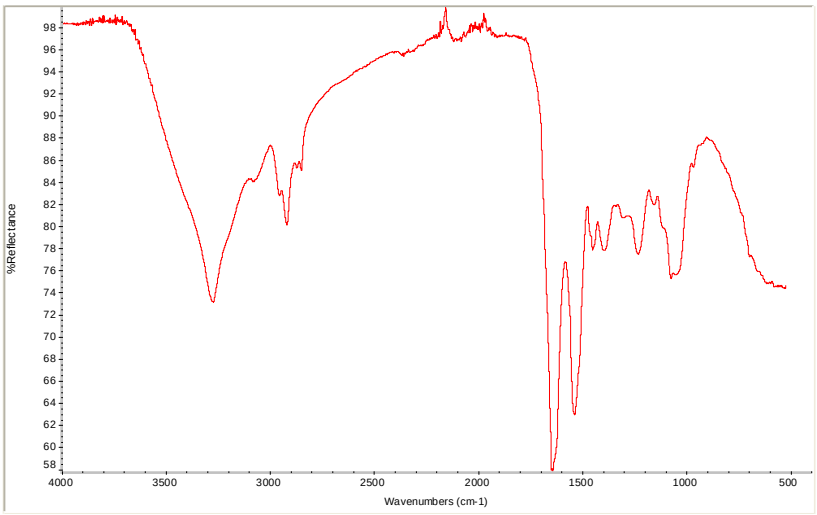

21 days

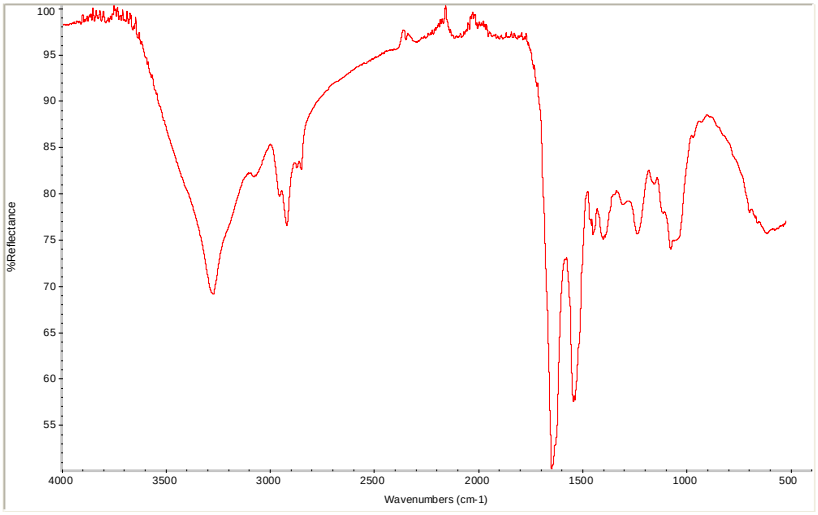

1 month

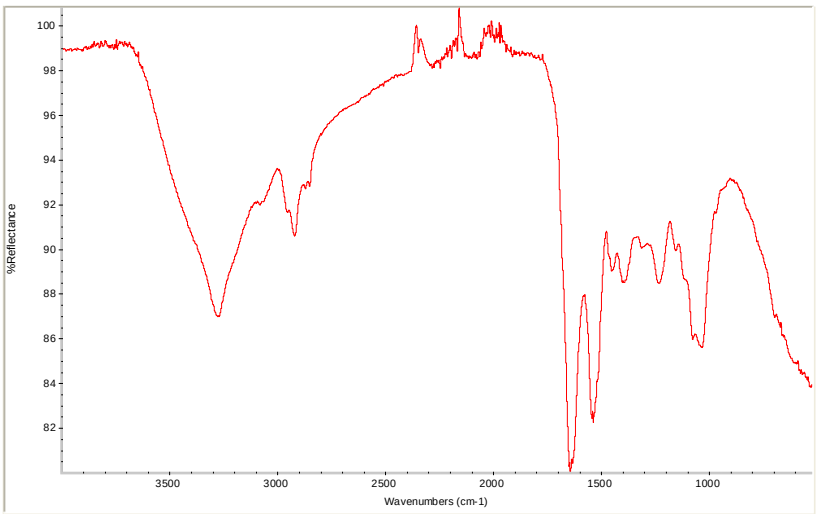

2 months

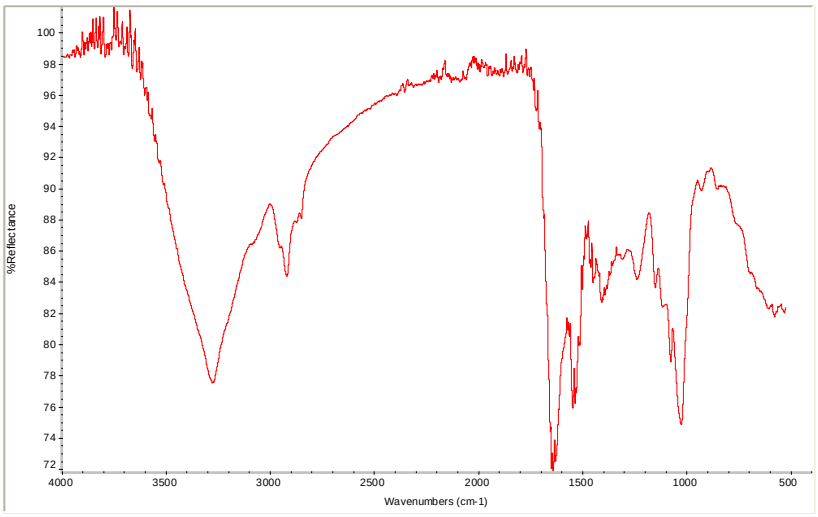

3 months

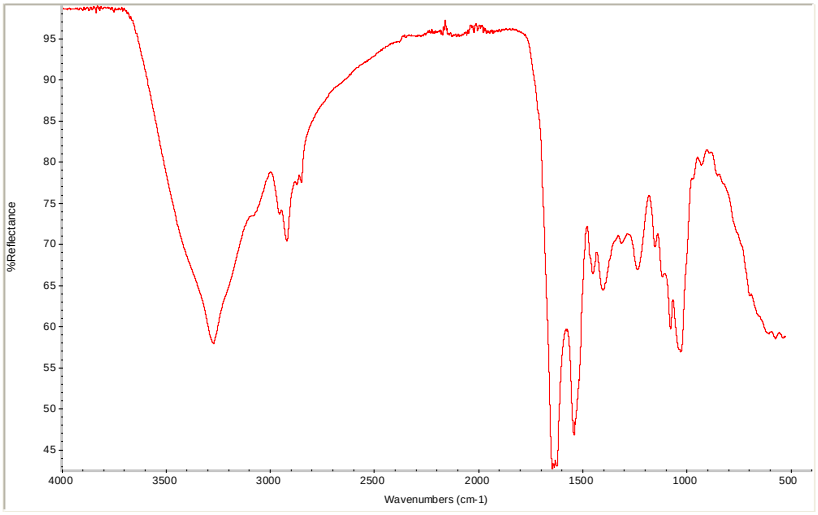

4 months

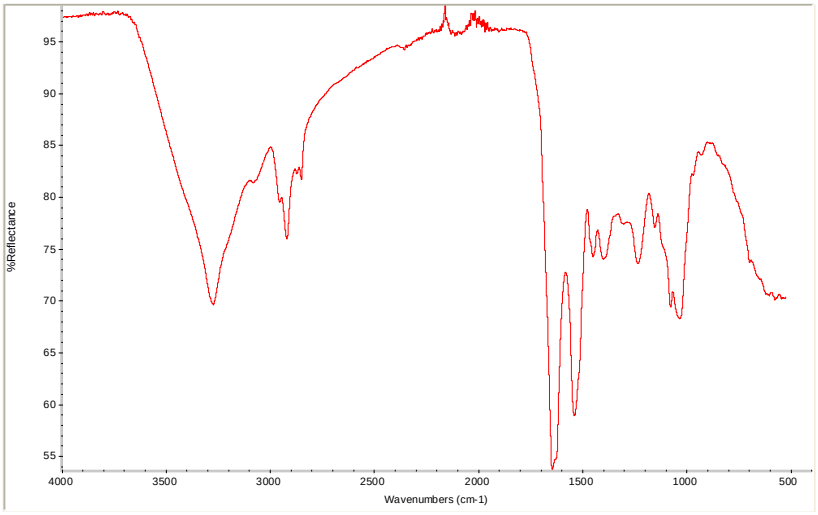

5 months

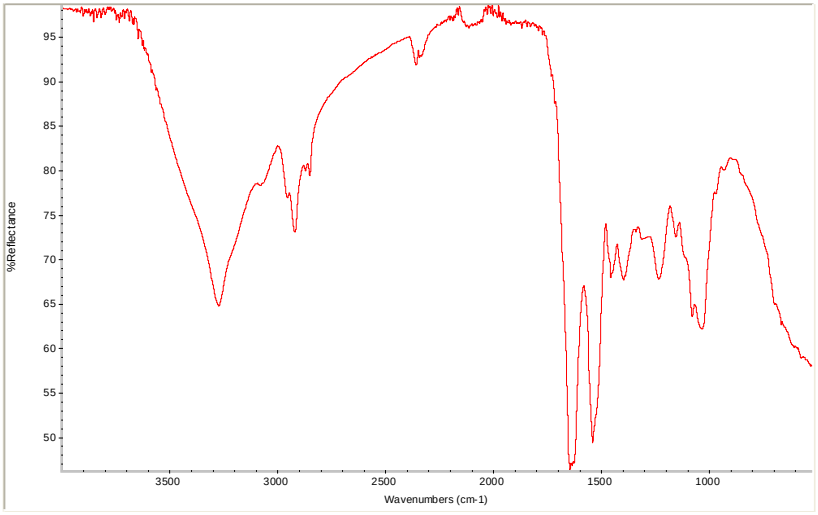

6 months

8.2 APPENDIX TWO